frontiers | Research Topics

Molecular architecture and dynamics of meiotic chromosomes

Edited by
Ricardo Benavente, Mónica Pradillo and Pedro A. San-Segundo

Published in
Frontiers in Cell and Developmental Biology

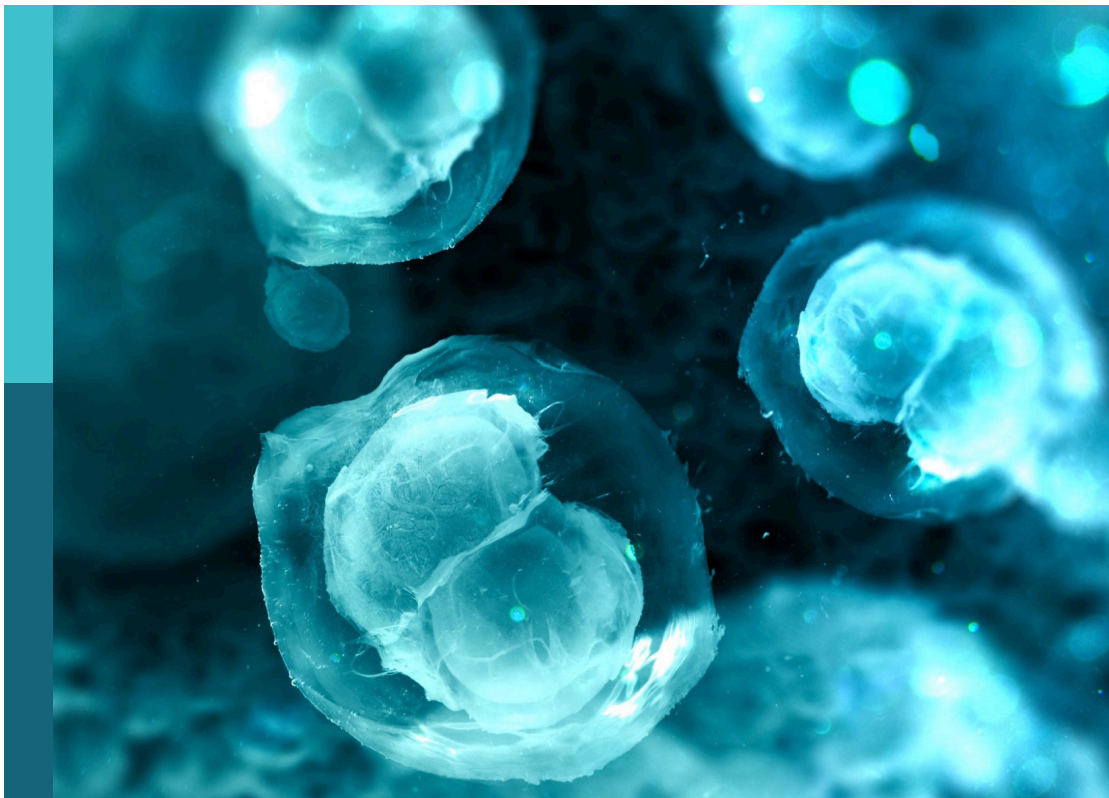

ISSN 1664-8714
ISBN 978-2-8325-4602-4
DOI 10.3389/978-2-8325-4602-4

About Frontiers

Frontiers is more than just an open access publisher of scholarly articles: it is a pioneering approach to the world of academia, radically improving the way scholarly research is managed. The grand vision of Frontiers is a world where all people have an equal opportunity to seek, share and generate knowledge. Frontiers provides immediate and permanent online open access to all its publications, but this alone is not enough to realize our grand goals.

Frontiers journal series

The Frontiers journal series is a multi-tier and interdisciplinary set of open-access, online journals, promising a paradigm shift from the current review, selection and dissemination processes in academic publishing. All Frontiers journals are driven by researchers for researchers; therefore, they constitute a service to the scholarly community. At the same time, the *Frontiers journal series* operates on a revolutionary invention, the tiered publishing system, initially addressing specific communities of scholars, and gradually climbing up to broader public understanding, thus serving the interests of the lay society, too.

Dedication to quality

Each Frontiers article is a landmark of the highest quality, thanks to genuinely collaborative interactions between authors and review editors, who include some of the world's best academicians. Research must be certified by peers before entering a stream of knowledge that may eventually reach the public - and shape society; therefore, Frontiers only applies the most rigorous and unbiased reviews. Frontiers revolutionizes research publishing by freely delivering the most outstanding research, evaluated with no bias from both the academic and social point of view. By applying the most advanced information technologies, Frontiers is catapulting scholarly publishing into a new generation.

What are Frontiers Research Topics?

Frontiers Research Topics are very popular trademarks of the *Frontiers journals series*: they are collections of at least ten articles, all centered on a particular subject. With their unique mix of varied contributions from Original Research to Review Articles, Frontiers Research Topics unify the most influential researchers, the latest key findings and historical advances in a hot research area.

Find out more on how to host your own Frontiers Research Topic or contribute to one as an author by contacting the Frontiers editorial office: frontiersin.org/about/contact

Molecular architecture and dynamics of meiotic chromosomes

Topic editors

Ricardo Benavente — Julius Maximilian University of Würzburg, Germany

Mónica Pradillo — Complutense University of Madrid, Spain

Pedro A. San-Segundo — CSIC-University of Salamanca, Spain

Citation

Benavente, R., Pradillo, M., San-Segundo, P. A., eds. (2024). *Molecular architecture and dynamics of meiotic chromosomes*. Lausanne: Frontiers Media SA.

doi: 10.3389/978-2-8325-4602-4

Table of contents

frontiers | Frontiers in Cell and Developmental Biology

TYPE Editorial
PUBLISHED 04 March 2024
DOI 10.3389/fcell.2024.1386038

OPEN ACCESS

EDITED AND REVIEWED BY
Eric C. Schirmer,
University of Edinburgh, United Kingdom

*CORRESPONDENCE
Ricardo Benavente,
ricardo.benavente@uni-wuerzburg.de
Mónica Pradillo,
pradillo@bio.ucm.es
Pedro A. San-Segundo,
pedross@usal.es

RECEIVED 14 February 2024
ACCEPTED 26 February 2024
PUBLISHED 04 March 2024

CITATION
Benavente R, Pradillo M and San-Segundo PA (2024), Editorial: Molecular architecture and dynamics of meiotic chromosomes. *Front. Cell Dev. Biol.* 12:1386038. doi: 10.3389/fcell.2024.1386038

Editorial: Molecular architecture and dynamics of meiotic chromosomes

Ricardo Benavente[1,2]*, Mónica Pradillo[3]* and Pedro A. San-Segundo[4]*

[1]Department of Cell and Developmental Biology, Biocenter, University of Würzburg, Würzburg, Germany, [2]Department of Molecular Biology, Instituto de Investigaciones Biológicas Clemente Estable, Montevideo, Uruguay, [3]Department of Genetics, Physiology and Microbiology, Faculty of Biological Sciences, Universidad Complutense de Madrid, Madrid, Spain, [4]Instituto de Biología Funcional y Genómica (IBFG), Consejo Superior de Investigaciones Científicas-Universidad de Salamanca (CSIC-USAL), Salamanca, Spain

KEYWORDS

meiosis, chromosome, pairing, synapsis, meiotic recombination, checkpoints, nuclear envelope

Editorial on the Research Topic
Molecular architecture and dynamics of meiotic chromosomes

Introduction

Meiosis is a special type of cell division that allows the generation of haploid gametes and is a key process for sexual reproduction of animals, plants and fungi. Haploidization requires that meiotic cells undergo a series of unique processes; namely, pairing, synapsis, recombination and segregation of homologous chromosomes. This involves profound meiosis-specific changes in the protein composition and architecture of homologous chromosomes as well as of the condensation and folding of chromatin that require a critical timing and regulation. The details of these changes may vary among different species. Nevertheless, the essential nature of meiosis has remained highly conserved throughout evolution.

A major goal of the present Research Topic of *Frontiers in Cell and Developmental Biology* is to provide an overview of how meiotic chromosomes and their components are critically involved in the mechanisms of haploidization and how dynamic protein complexes yield important structural intermediates and temporal regulation to this process. To this end, this special Topic contains selected original research and review articles dealing with the composition, architecture, function and regulation of meiotic chromosomes of animals, plants and fungi using microscopic, biochemical, molecular and/or genetic techniques.

This Research Topic comprises 15 articles covering different aspects of Meiosis. For clarity, we have divided them into four main themes: Architecture and recombination, Pairing and chromosome dynamics, Regulation of meiotic progression, and Nuclear envelope functions.

Architecture and recombination

In recent years, substantial progress has been achieved demonstrating the outstanding role of the chromosome axis in meiosis-specific processes, i.e., pairing, synapsis and recombination (Zickler and Kleckner, 2023). In their article, Ito and Shinohara provide an up-to-date overview on the peculiarities and roles of meiotic axial structures and their role in double-strand break (DSB) generation and regulation, as well as in crossover (CO) formation.

The mini review by Rafiei and Ronceret deals with a still intriguing aspect of meiosis, namely, CO interference (Zickler and Kleckner, 2023). Although this phenomenon has been known for decades, the mechanisms involved have remained elusive. In their article, the authors summarize the data of the literature, particularly in plants, and propose an integrative model for CO interference regulation that involves the synaptonemal complex (SC) as a structure that would allow the diffusion of a CO limiting factor. For their part, Shinohara and Shinohara have also investigated the mechanisms of CO control in budding yeast using cytological and genetic tools. They have explored the relationship between DSB frequencies and the localization of the Msh5 complex in selected strains and concluded that the complex would play an important role in CO homeostasis.

Localization and number of COs are important parameters in meiotic recombination studies. However, the quantitative manual analysis of these events is time consuming. To overcome this limitation, Soriano et al. have developed an ImageJ macro routine that allows for a faster, reproducible, and more rigorous investigation of the mentioned CO parameters in meiotic chromosome spreads of vertebrates. This tool will greatly facilitate the analysis of meiotic COs in the context of the SC, even considering overlapping chromosomes.

The SC is a meiosis-specific nuclear structure that mediates synapsis between homologous chromosomes (Page and Hawley, 2004). Very little is known about the assembly/disassembly process at the molecular level. Pollard et al. have investigated aspects of this process by live-cell imaging in budding yeast using a GFP-tagged Zip1 protein, and they have obtained highly interesting new data on SC kinetics. Notably, while SC assembly occurs with both monophasic and biphasic kinetics, final disassembly takes place rapidly due to Zip1 degradation. In addition, the authors describe a novel type of event, termed "abortive disassembly", that differs from the final disassembly in various mechanistical aspects.

Pairing and chromosome dynamics

Traditionally, meiosis has been studied in only a few model organisms. However, the emergence of new tools is enabling researchers to expand the set of model species to include less studied and more unusual systems (Grusz et al., 2017). Studies in these species are really promising and could help answer long-standing questions and provide insight into different strategies for solving meiotic problems. In this context, Marín-Gual et al. analyzed meiotic progression in four reptile species (the Australian central bearded dragon, two geckos and the painted turtle) and demonstrated that the bouquet is a highly conserved structure during prophase I, whereas the level of DSBs is highly variable among vertebrates. Curiously, these reptile species exhibit low recombination rates, and this feature is shared with the American marsupials *Thylamys elegans* and *Dromiciops gliorides*, where RPA and RAD51 foci show an extreme polarization towards chromosome ends, as it has been reported by Valero-Regalón et al. However, the distribution of meiotic DSBs seems to be different in the Australian marsupial *Macropus eugenii*, where DSB markers are present along the entire length of the chromosomes. In addition, bouquet polarization is incomplete and more transient in this species.

The ability of homologous chromosomes to pair is one of the most enigmatic processes that takes place during meiosis. Although there has been some progress in the understanding of this mechanism, it is still a long way from being fully understood. It seems clear that although meiotic recombination is essential to ensure recognition of homologues, there are interhomologous interactions that are not dependent on DSB formation in many organisms (Page and Hawley, 2004; Da Ines et al., 2014; Zickler and Kleckner, 2023). Solé et al. provide an overview of these recombination-independent events that involve different strategies based on chromosome clustering and movement, chromosome structures, proteins and even non-coding RNAs in five model species. Pairing of homologous chromosomes can be disrupted because of the presence of unequal sets of chromosomes, as is the case in organisms with chromosome rearrangements such as Robertsonian (Rb) translocations (Wallace et al., 2002). Ayarza et al. performed a detailed analysis of the inheritance of Rb (metacentric) chromosomes in the offspring of heterozygous males and females for eight Rb chromosomes. Their results show that the number of inherited Rb chromosomes is not a random process. In addition, they found no evidence for a preferential segregation of translocated chromosomes, i.e., segregation bias or meiotic drive.

Regulation of meiotic progression

The concept of cell-cycle checkpoints was originally introduced by Hartwell and Weinert more than 3 decades ago to define the control mechanisms enforcing the dependency in the order of cell cycle events. According with this notion, checkpoint pathways prevent the initiation of a late event if a previous one has not been successfully completed (Hartwell and Weinert, 1989). Meiosis involves tightly regulated processes such as homologous chromosome pairing, synapsis, recombination, and segregation. The precise coordination between these meiotic events and the progression of meiotic development is essential to ensure faithful distribution of the chromosomes to the gametes (Subramanian and Hochwagen, 2014). A review by Huang and Roig in this Research Topic focuses on the surveillance mechanisms, or checkpoints, monitoring pairing, synapsis and recombination during meiosis in mice. The authors discuss how studies in mouse models provide insights into genetic regulations and the link between meiotic errors and mammalian infertility, offering potential diagnostic value for human infertility.

Protein phosphorylation, resulting from the balance between the action of kinases and phosphatases, plays a paramount role in the regulatory pathways coordinating timely meiotic progression (Kar and Hochwagen, 2021). Among the numerous kinases acting in meiotic cells, cyclin-dependent kinases (CDKs) and polo-like kinases (PLKs) possess a prominent relevance

(Tsubouchi et al., 2018). In this Research Topic, Palacios-Blanco and Martín-Castellanos review the crucial role of cyclins and CDKs in orchestrating meiosis-specific events, including the establishment of unique chromosome architecture, homologous recombination, and synapsis. The authors highlight the evolutionary conservation of meiosis-specific cyclins and CDKs, and their diverse functions. They also emphasize the significance of these regulators in guaranteeing the precise transmission of genetic information. In addition, an original research article by Gómez et al. reports two roles for the polo-like kinase PLK1 during mammalian male meiosis, in particular the disassembly of SYCP3 and HORMAD1 from the lateral elements of the SC, and the assembly of the inner centromere at meiosis I. Their results underscore the importance of PLK1 as a master regulator of meiotic progression in mice spermatocytes.

Nuclear envelope functions

The nuclear envelope (NE) and its associated structures play critical mechanical and regulatory roles during meiosis. Rapid chromosome movements during meiotic prophase I are promoted by the evolutionarily conserved LINC complex composed by SUN and KASH proteins. The LINC traverses the NE connecting the telomeres (inside the nucleus) with the cytoskeleton (outside the nucleus) providing the physical forces for telomere-driven chromosome motion. These movements are critical for proper interhomologous interactions (Burke, 2018; da Cruz et al., 2020; Zetka et al., 2020). Another type of highly organized assemblies embedded in the NE are the nuclear pore complexes (NPCs). Various meiotic functions for the NPCs are beginning to emerge. In yeast, basket nucleoporins appear to mediate interactions of meiotic chromosomes with the NE (Komachi and Burgess, 2022), and these nucleoporins undergo a dynamic reorganization during meiotic divisions (King et al., 2023). NPCs also contribute to control of meiotic progression by regulation of SUMOylation (Yang et al., 2023). In addition, exportin-dependent nucleocytoplasmic trafficking via NPCs also plays important meiotic roles in yeast and mammals (Onuma et al., 2018; Herruzo et al., 2023). Three articles in this Research Topic address NE-related subjects.

A research article by Gurusaran et al. reports the crystal structure of the luminal coiled-coil domain (α1) of SUN1, which forms a parallel trimeric structure. The trimer is stabilized by zinc coordination via a central cysteine motif. The α1 domain combines with another coiled-coil domain (α2) to mutually reinforce SUN1 trimerization and sustain the interaction with KASH5. This study expands our knowledge about LINC organization and how forces are transduced across the NE to move chromosomes.

In a perspective article, Fernández-Álvarez discusses recent progress in understanding the non-canonical functions of the telomere bouquet during meiosis. High-resolution live-cell imaging techniques combined with data-mining algorithms tracking telomeres, together with advanced quantitative biology, are revealing novel complex chromosome movement patterns and structural features of chromatin. These approaches unveil the plasticity of the telomeric bouquet with higher spatial and temporal resolution.

A research article by Fernández-Jiménez et al. examined the meiotic role of nucleoporins SAR1 and SAR3, which are components of the NPC outer ring in *Arabidopsis thaliana*. Mutation of SAR1 or SAR3 results in abnormal chromatin condensation and chromosomal fragmentation in a subset of meiocytes. These defects are dependent on the formation of SPO11-induced DSBs, and they are also observed in other mutants deficient in the outer ring complex, like *hos1*. Distribution of NPCs is altered in *sar1* mutants. This research provides new insights into how NPCs contribute to meiotic chromosome behavior in plants.

Concluding remarks

Although our knowledge of meiosis and its biological functions has expanded in recent years, many facets still remain opaque. Comprehensive study of meiosis using innovative techniques will help to elucidate aspects that remain unclear in key meiotic events; namely, pairing, synapsis, and recombination. A deeper understanding of chromosome behavior, including dynamics, movement, and segregation, could also benefit from continued methodological advances. Future studies will allow not just to expand our fundamental scientific understanding, but also to provide valuable practical contributions to several areas including agriculture and healthcare.

Author contributions

RB: Conceptualization, Writing–original draft, Writing–review and editing, MP: Conceptualization, Writing–original draft, Writing–review and editing, PS-S: Conceptualization, Writing–original draft, Writing–review and editing.

Funding

The author(s) declare that financial support was received for the research, authorship, and/or publication of this article. RB is supported by the Comisión Sectorial de Investigación Científica (CSIC), Universidad de la República (Uruguay), under an I + D Groups 2022 grant. MP funding Research in PS-S lab is supported by Grant PID 2021-125830NB-I00 from Ministry of Science and Innovation of Spain (MCIN/AEI/10.13039/501100011033/) and "FEDER Una manera de hacer Europa". Research in MP lab is supported by the Ministry of Science and Innovation of Spain (PID 2020-118038GB-I00/AEI/10.13039/501100011033) and European Union (TED 2021-131852B-I00/AEI/10.13039/501100011033/ Unión Europea Next-Generation EU/PRTR).

Conflict of interest

The authors declare that the research was conducted in the absence of any commercial or financial relationships that could be construed as a potential conflict of interest.

Publisher's note

References

Burke, B. (2018). LINC complexes as regulators of meiosis. *Curr. Opin. Cell Biol.* 52, 22–29. doi:10.1016/j.ceb.2018.01.005

da Cruz, I., Brochier-Armanet, C., and Benavente, R. (2020). The TERB1-TERB2-MAJIN complex of mouse meiotic telomeres dates back to the common ancestor of metazoans. *BMC Evol. Biol.* 20 (1), 55. doi:10.1186/s12862-020-01612-9

Da Ines, O., Gallego, M. E., and White, C. I. (2014). Recombination-independent mechanisms and pairing of homologous chromosomes during meiosis in plants. *Mol. Plant* 7 (3), 492–501. doi:10.1093/mp/sst172

Grusz, A. L., Sigel, E. M., and Witherup, C. (2017). Homoeologous chromosome pairing across the eukaryote phylogeny. *Mol. Phylogenet. Evol.* 117, 83–94. doi:10.1016/j.ympev.2017.05.025

Hartwell, L. H., and Weinert, T. A. (1989). Checkpoints: controls that ensure the order of cell cycle events. *Science* 246 (4930), 629–634. doi:10.1126/science.2683079

Herruzo, E., Sanchez-Diaz, E., Gonzalez-Arranz, S., Santos, B., Carballo, J. A., and San-Segundo, P. A. (2023). Exportin-mediated nucleocytoplasmic transport maintains Pch2 homeostasis during meiosis. *PLoS Genet.* 19 (11), e1011026. doi:10.1371/journal.pgen.1011026

Kar, F. M., and Hochwagen, A. (2021). Phospho-regulation of meiotic prophase. *Front. Cell Dev. Biol.* 9, 667073. doi:10.3389/fcell.2021.667073

King, G. A., Wettstein, R., Varberg, J. M., Chetlapalli, K., Walsh, M. E., Gillet, L. C. J., et al. (2023). Meiotic nuclear pore complex remodeling provides key insights into nuclear basket organization. *J. Cell Biol.* 222 (2), e202204039. doi:10.1083/jcb.202204039

Komachi, K., and Burgess, S. M. (2022). The Nup2 meiotic-autonomous region relieves inhibition of Nup60 to promote progression of meiosis and sporulation in *Saccharomyces cerevisiae*. *Genetics* 221 (1), iyac045. doi:10.1093/genetics/iyac045

Onuma, A., Fujioka, Y. A., Fujii, W., Sugiura, K., and Naito, K. (2018). Effects of exportin 1 on nuclear transport and meiotic resumption in porcine full-grown and growing oocytes. *Biol. Reprod.* 98 (4), 501–509. doi:10.1093/biolre/iox168

Page, S. L., and Hawley, R. S. (2004). The genetics and molecular biology of the synaptonemal complex. *Annu. Rev. Cell Dev. Biol.* 20, 525–558. doi:10.1146/annurev.cellbio.19.111301.155141

Subramanian, V. V., and Hochwagen, A. (2014). The meiotic checkpoint network: step-by-step through meiotic prophase. *Cold Spring Harb. Perspect. Biol.* 6 (10), a016675. doi:10.1101/cshperspect.a016675

Tsubouchi, H., Argunhan, B., and Tsubouchi, T. (2018). Exiting prophase I: no clear boundary. *Curr. Genet.* 64 (2), 423–427. doi:10.1007/s00294-017-0771-y

Wallace, B. M. N., Searle, J. B., and Everett, C. A. (2002). The effect of multiple simple Robertsonian heterozygosity on chromosome pairing and fertility of wild-stock house mice (*Mus musculus domesticus*). *Cytogenet. Genome Res.* 96, 276–286. doi:10.1159/000063054

Yang, H. J., Asakawa, H., Li, F. A., Haraguchi, T., Shih, H. M., and Hiraoka, Y. (2023). A nuclear pore complex-associated regulation of SUMOylation in meiosis. *Genes. Cells* 28 (3), 188–201. doi:10.1111/gtc.13003

Zetka, M., Paouneskou, D., and Jantsch, V. (2020). The nuclear envelope, a meiotic jack-of-all-trades. *Curr. Opin. Cell Biol.* 64, 34–42. doi:10.1016/j.ceb.2019.12.010

Zickler, D., and Kleckner, N. (2023). Meiosis: dances between homologs. *Annu. Rev. Genet.* 57, 1–63. doi:10.1146/annurev-genet-061323-044915

frontiers | Frontiers in Cell and Developmental Biology

TYPE Original Research
PUBLISHED 12 October 2022
DOI 10.3389/fcell.2022.1009776

OPEN ACCESS

EDITED BY
Mónica Pradillo,
Complutense University of Madrid, Spain

REVIEWED BY
Miguel Angel Brieño-Enriquez,
Magee-Womens Research Institute, United States
Sean Burgess,
University of California, United States

*CORRESPONDENCE
Aurora Ruiz-Herrera,
aurora.ruizherrera@uab.cat

†These authors contributed equally to this work and share first authorship

SPECIALTY SECTION
This article was submitted to Nuclear Organization and Dynamics, a section of the journal Frontiers in Cell and Developmental Biology

RECEIVED 02 August 2022
ACCEPTED 23 September 2022
PUBLISHED 12 October 2022

CITATION
Marín-Gual L, González-Rodelas L, M. Garcias M, Kratochvíl L, Valenzuela N, Georges A, Waters PD and Ruiz-Herrera A (2022), Meiotic chromosome dynamics and double strand break formation in reptiles. *Front. Cell Dev. Biol.* 10:1009776. doi: 10.3389/fcell.2022.1009776

Meiotic chromosome dynamics and double strand break formation in reptiles

Laia Marín-Gual[1,2†], Laura González-Rodelas[1,2†], Maria M. Garcias[1,2], Lukáš Kratochvíl[3], Nicole Valenzuela[4], Arthur Georges[5], Paul D. Waters[6] and Aurora Ruiz-Herrera[1,2*]

[1]Departament de Biologia Cel·lular, Fisiologia i Immunologia, Universitat Autònoma de Barcelona, Cerdanyola del Vallès, Spain, [2]Genome Integrity and Instability Group, Institut de Biotecnologia i Biomedicina, Universitat Autònoma de Barcelona, Cerdanyola del Vallès, Spain, [3]Department of Ecology, Faculty of Science, Charles University, Prague, Czech Republic, [4]Department of Ecology, Evolution, and Organismal Biology, Iowa State University, Ames, IA, United States, [5]Institute for Applied Ecology, University of Canberra, Canberra, ACT, Australia, [6]School of Biotechnology and Biomolecular Sciences, Faculty of Science, UNSW, Sydney, NSW, Australia

During meiotic prophase I, tightly regulated processes take place, from pairing and synapsis of homologous chromosomes to recombination, which are essential for the generation of genetically variable haploid gametes. These processes have canonical meiotic features conserved across different phylogenetic groups. However, the dynamics of meiotic prophase I in non-mammalian vertebrates are poorly known. Here, we compare four species from Sauropsida to understand the regulation of meiotic prophase I in reptiles: the Australian central bearded dragon (*Pogona vitticeps*), two geckos (*Paroedura picta* and *Coleonyx variegatus*) and the painted turtle (*Chrysemys picta*). We first performed a histological characterization of the spermatogenesis process in both the bearded dragon and the painted turtle. We then analyzed prophase I dynamics, including chromosome pairing, synapsis and the formation of double strand breaks (DSBs). We show that meiosis progression is highly conserved in reptiles with telomeres clustering forming the *bouquet*, which we propose promotes homologous pairing and synapsis, along with facilitating the early pairing of micro-chromosomes during prophase I (i.e., early zygotene). Moreover, we detected low levels of meiotic DSB formation in all taxa. Our results provide new insights into reptile meiosis.

KEYWORDS

reptile, meiosis, gametogenesis, micro-chromosomes, DSBs, recombination, *bouquet*

Introduction

Meiosis is used by all sexually reproducing organisms to form haploid gametes (oocytes or sperm) *via* two consecutive cell divisions preceded by one round of genome replication. This follows a tightly regulated progression of chromosome condensation and folding, coupled with changes to the epigenome and gene expression (Hammoud et al., 2014; Alavattam et al., 2019; Patel et al., 2019; Vara et al., 2019; Vara and Ruiz-Herrera,

2022). Meiosis generates genetically variable gametes by recombination of the two parental chromosomes during prophase I. This involves faithful chromosome synapsis, the formation of double strand breaks (DSBs) and DNA exchange (crossovers, COs) between homologues.

Meiotic prophase I is commonly subdivided into four different stages (leptotene, zygotene, pachytene and diplotene) based on the dynamics of meiotic chromosomes and their telomeres (reviewed in Bolcun-Filas and Handel, 2018). The pairing of homologous chromosomes begins at leptotene with

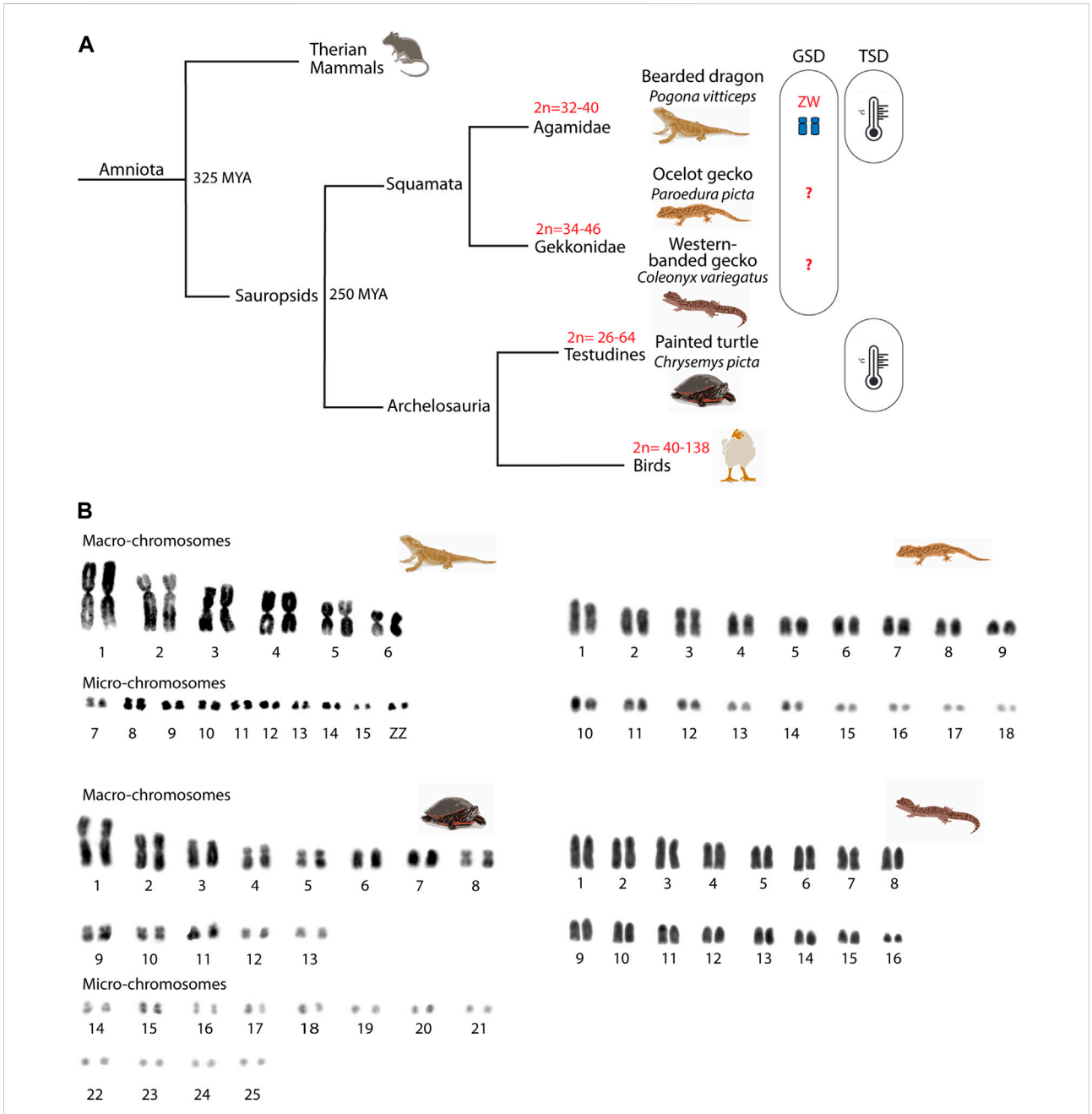

FIGURE 1
Phylogeny of the reptiles included in the study. **(A)** Phylogenetic relationships of the four reptilian species included in the study. For each phylogenetic branch, variation in diploid numbers and sex determination system are indicated. **(B)** Mitotic karyotypes of the four studied species: *Pogona vitticeps*, *Paroedura picta*, *Chrysemys picta* and *Coleonyx variegatus*. The bearded dragon (*P. vitticeps*) and the painted turtle (*C. picta*) karyotypes include macro- and micro-chromosomes, whereas the western banded gecko (*C. variegatus*) and the ocelot gecko (*P. picta*) karyotypes include chromosomes of progressively smaller size. Karyotypes correspond to mitotic metaphases from fibroblast primary cell cultures. GSD: genotypic sex determination; TSD: temperature sex determination.

the formation of a protein scaffold along chromosomes composed of cohesins and proteins specific to the synaptonemal complex (SC). This coincides with the generation of DSBs by the endonuclease protein SPO11 (Keeney et al., 1997). Telomeres play an important role during the leptotene-zygotene transition, clustering to form a structure known as the *bouquet* (Scherthan et al., 1996; Liebe et al., 2004; Reig-Viader et al., 2013). At zygotene, DSBs are repaired, leading to their resolution as either COs or non-COs (NCOs) between sister chromatids. It is not until pachytene that chromosomes are completely synapsed and COs are resolved as chiasmata (the points where genetic material is actually exchanged). The mechanisms underlying meiotic progression have been extensively studied in several model organisms, including yeast, fruit flies, nematodes, mice and zebrafish (Zickler and Kleckner, 2015; Blokhina et al., 2019; Imai et al., 2021). However, our understanding of the dynamics of meiotic prophase I and recombination among non-mammalian amniote vertebrates (i.e., sauropsids–birds/reptiles) remains incomplete (Segura et al., 2013; Marín-Gual et al., 2022).

Amniote vertebrates shared a last common ancestor approximately 325 mya (Shedlock and Edwards, 2009) (Figure 1) and are characterized by distinctive chromosome morphology and evolutionary labile sex determination. Sauropsids display variation in chromosome number, especially in birds (2n = 40–138), although this is less pronounced in reptiles (2n = 22–68) (Ruiz-Herrera et al., 2012; Montiel et al., 2016; Waters et al., 2021). The non-avian sauropsids (reptiles) are composed of Squamata (lizards and snakes), Sphenodontia (tuatara), Crocodilia (crocodiles and alligators), and Testudines (turtles). Reptiles are characterized by the presence of generally well conserved micro- and macro-chromosomes (Waters et al., 2021) and by a high variability in their sex-determining systems (i.e., ZZ/ZW, XX/XY or temperature sex determination - TSD) (Ezaz et al., 2006) (Figure 1). While meiotic progression in the chicken has been studied and mirrors eutherians (Schoenmakers et al., 2009; Guioli et al., 2012), little is known about meiosis in reptiles. The few existing reports focused on CO formation (Lisachov et al., 2017, 2019; Spangenberg et al., 2021) and formation of unreduced eggs in parthenogenetic lineages (Lutes et al., 2010), but whether meiotic progression in reptiles resembles the process described for either mammals or zebrafish (which last shared a common ancestor with amniotes approximately 400 mya) is currently unknown.

Here we provide a comparative analysis of key features of spermatogenesis and meiotic prophase I progression in previously uncharacterised reptile linages, with a focus on meiotic recombination. We examined the ocelot gecko (*Paroedura picta*) and the western-banded gecko (*Coleonyx variegatus*) as representatives of Gekkota (geckos), the Australian central bearded dragon (*Pogona vitticeps*) as a representative of Iguania (iguanas, agamids and chameleons), and the painted turtle (*Chrysemys picta*) as a representative of Testudines (turtles). These species are emerging models for thermal and reproductive physiology (Valenzuela, 2009; Starostová et al., 2013; Kubička et al., 2015), as well as developmental biology (Noro et al., 2009). The three lizards have genotypic sex determination (GSD). The bearded dragon has ZW sex chromosomes (Ezaz et al., 2005; Koubová et al., 2014), whereas the western banded gecko and the ocelot gecko GSD systems are still unknown (Rovatsos et al., 2019; Keating et al., 2022). However, the genetic sex determination of the bearded dragon can be overridden by temperature to produce viable ZZ females (Quinn et al., 2007; Holleley et al., 2015). Most turtle species have temperature-dependent sex determination (TSD, including *C. picta*), although XY and ZW systems are also present in different lineages (Bista and Valenzuela, 2020) (Figure 1).

Our study unveils shared features between bearded dragon and painted turtle spermatogenesis. We also observed that all reptiles examined here present an equivalent pattern of prophase I progression forming the *bouquet* at early stages, where homologous micro-chromosomes synapse first and cluster together. Remarkably we detected low rates of DSB formation in reptiles when compared to mammals, suggesting that low recombination rates are a distinctive feature of reptiles.

Material and methods

Samples

Male bearded dragons (n = 4, *P. vitticeps*) were obtained from captive colonies in Canberra (ACT, Australia) at the end of the breeding season (February). Male ocelot geckos (n = 3, *P. picta*) and male western banded geckos (n = 1, *C. variegatus*) were originated from breeding colonies in Charles University in Prague (Czech Republic). Male painted turtles (n = 3, *C. picta*) were wild-caught in Iowa (United States) at the end of the breeding season under appropriate permits from Iowa's DNR.

Primary fibroblast cell culture and karyotyping

Four primary fibroblast cell lines were derived from all reptile species studied. Samples of connective tissue were washed in 1xPBS supplemented with an antibiotic-antimycotic solution (100 U/ml penicillin, 100 µg/ml streptomycin, 50 µg/ml gentamicin and 0.25 µg/ml amphotericin B). Cultures were established by disaggregating tissue with a scalpel blade and resuspending cells in AmnioMAX. Cell cultures were incubated at 28°C in 5% CO_2.

For karyotyping, cells were arrested in metaphase by adding 80 µl of Colcemid (10 µg/ml) to 10 ml of medium for 2 h and

then trypsinised. Cells were centrifuged down at 600 xg for 5 min and resuspended in 5 ml of hypotonic solution (0.075M KCl) for 30 min at 37°C. Chromosomes were then fixed by addition of fixative solution (3:1 methanol/acetic acid) and metaphase spreads were obtained by dropping 15 µl of cell suspension onto a cleaned dry slide. Slides were baked at 65°C for one hour and kept at −20°C until use. Metaphases were stained homogenously with DAPI for the karyotype analysis.

Histology and testis morphometry

Testes from the bearded dragon and the painted turtle were collected for histological procedures. Briefly, testes were fixed overnight in Bouin's solution (70% saturated picric acid, 25% formaldehyde and 5% glacial acetic acid). Then, samples were dehydrated, cleared and embedded in paraffin using standard procedures. Sections (7 µm) were stained with PAS-hematoxylin.

Spermatocyte spreads and immunofluorescence

Testicular biopsies were obtained immediately after animal dissection and processed as previously described (Garcia-Cruz et al., 2011) in order to obtain spermatocyte spreads. Briefly, a piece of the testicular biopsy was carefully minced on a slide; 1% Lipsol was added and incubated for 30 min at room temperature. Then, a fixative solution containing 4% paraformaldehyde was added, and slides were kept in a humid chamber. After two hours, slides were washed in 1% photo-flo solution and further processed for immunofluorescence, or frozen at −20°C until use.

Immuno-staining of meiocytes was performed using the following primary antibodies: rabbit antibody against SYCP3 (#ab15093, Abcam, 1:100 dilution), rabbit antibody against SYCP1 (#ab15087, Abcam, 1:100 dilution), rabbit antibody against TRF2 (#NB110-57130SS, Novus Biologicals, 1:100 dilution), mouse antibody against RNA pol II (#5408, Abcam, 1:400 dilution), rabbit antibody against RAD51 (#PC130, Calbiochem, 1:50 dilution), rabbit antibody against RPA32/RPA2 (#10359, Abcam, 1:100 dilution), mouse antibody against MLH1 (#51–1327GR, BD PharmigenTM, 1:100 dilution), rabbit antibody against MLH1 (#ab47703, Abcam, 1:100 dilution) and rabbit antibody against γH2AX (#H5912, Sigma-Aldrich, 1:100 dilution).

Fluorochrome-conjugated secondary antibodies were used for detection (all from Jackson ImmunoResearch Laboratories). Antibodies were diluted in PBST (Tween 0.05% in PBS). Primary antibodies were incubated overnight at 4°C in a humid chamber and secondary antibodies for 1 h at 37°C in a humid chamber. After washing away the excess of secondary antibodies, DNA was counterstained with anti-fade solution (Vectashield) containing 8 µg/ml DAPI (4′,6′-diamidino-2-phenylindole).

Microscopy and image analysis

PAS-hematoxylin–stained tissue sections were analyzed on an Olympus CH2 microscope, and images were captured using a Zeiss Axiophot Microscope and Olympus C5060 camera. For fluorescent sample analysis and image capturing, a Zeiss Axioskop fluorescence microscope connected to a ProgRes Jenoptik camera was used. The image capture software ProgRes CapturePro was employed for image acquisition and image processing.

The accumulation of foci in the *bouquet* was analyzed as the percentage of foci per cell located in the *bouquet* region, previously delimited as the area where synaptonemal complex (i.e., SYCP3 signal) begins to assemble and SYCP3 intensity is higher. Only cells with a well-defined *bouquet* were included in the analysis.

Statistical analysis

Statistical significance for the DSB analysis as RPA and RAD51 foci, and for the analysis of the percentage of DSB foci in the *bouquet* was determined using two-sided Mann-Whitney U-tests. The critical value for statistical significance was $p < 0.05$ for all tests. Each plot or its figure legend indicates the statistical methods and corresponding *p*-values. All boxplots are represented as centre lines (median), box limits (interquartile range; 25th and 75th percentiles) and whiskers (largest and lowest data points inside the first and third quartiles plus 1.5 times the interquartile range).

Results

Spermatogenesis progression in the bearded dragon and the painted turtle

We first characterized spermatogenesis progression in the bearded dragon (*P. vitticeps*) and the painted turtle (*C. picta*) (Figure 2), following the mammalian classification of germ cell morphology (Russell et al., 1993). Both the bearded dragon (Figures 2A,B) and the painted turtle (Figures 2C,D) had a histological organisation of germ cells within the seminiferous epithelia (between the basal lamina and the lumen) that was similar to that of eutherian mammals (Russell et al., 1993) and other amniotes (Gribbins, 2011).

In both species, spermatogonia (A and B) were restricted to the basal lamina (Figures 2A,C). Type A spermatogonia presented a rounded nucleus showing one nucleolus, whereas type B spermatogonia contained densely stained chromatin

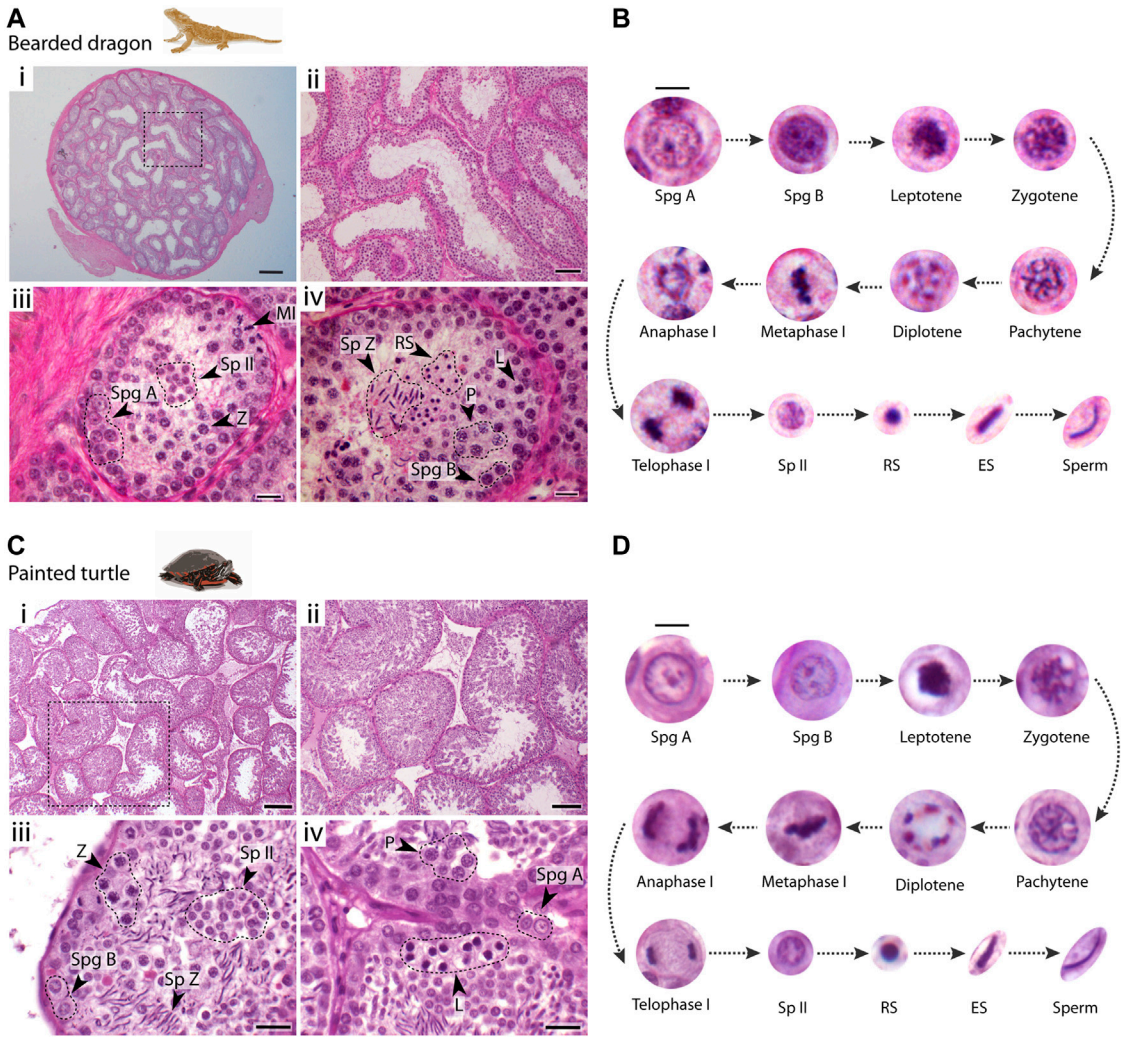

FIGURE 2
Testis histology. Histological cross-sections of seminiferous tubules of **(A)** the bearded dragon and **(C)** the painted turtle stained with PAS-hematoxylin. Dashed circles and arrowheads point clusters of different cell types. Scale bars: (i) 200 μm, (ii) 100 μm, and (iii, iv) 20 μm. Germ cell types found within the seminiferous epithelium and their progression in **(B)** the bearded dragon and **(D)** the painted turtle. Scale bar: 10 μm. Legend type: Spg A, type A spermatogonia; Spg B, type B spermatogonia; L, leptotene spermatocyte; Z, zygotene spermatocyte; P, pachytene spermatocyte; D, diplotene spermatocyte; MI, metaphase I; Sp II, secondary spermatocyte; RS, round spermatid; ES, elongating spermatid; Sp Z, spermatozoa.

and more than two nucleoli (between 2-4 nucleoli) (Figures 2B,D). Large populations of cells subsequently progress through meiosis towards the centre of the seminiferous tubule. Meiotic cells were characterized by an increase in size and condensed chromatin. This included recognizable stages of prophase I: leptotene, zygotene, pachytene and diplotene (Figure 2). Both first and second meiotic divisions and secondary spermatocyte stages occurred rapidly, as all three phases were found in low proportions in cross-sections of seminiferous tubules (Figures 2A,C). Leptotene spermatocytes were distinguished by dense filamentous chromatin at the nuclei. Zygotene spermatocytes exhibited clumps of condensed filamentous chromatin within the nucleus. Pachytene spermatocytes displayed an open nucleoplasm and their nuclei contained thick chromatin fibres. Finally, diplotene spermatocytes had chromatin fibres in a tight circle and degenerating nuclear membranes. We also distinguished meiotic cells with the chromosomes fully condensed and aligned at the metaphase plate. During the second meiotic division, secondary spermatocytes contained randomly dispersed chromatin fibres (Figures 2B,D).

Spermiogenesis (the differentiation and maturation of sperm) encompasses a longer period than previous stages as large populations of round and elongating spermatids were

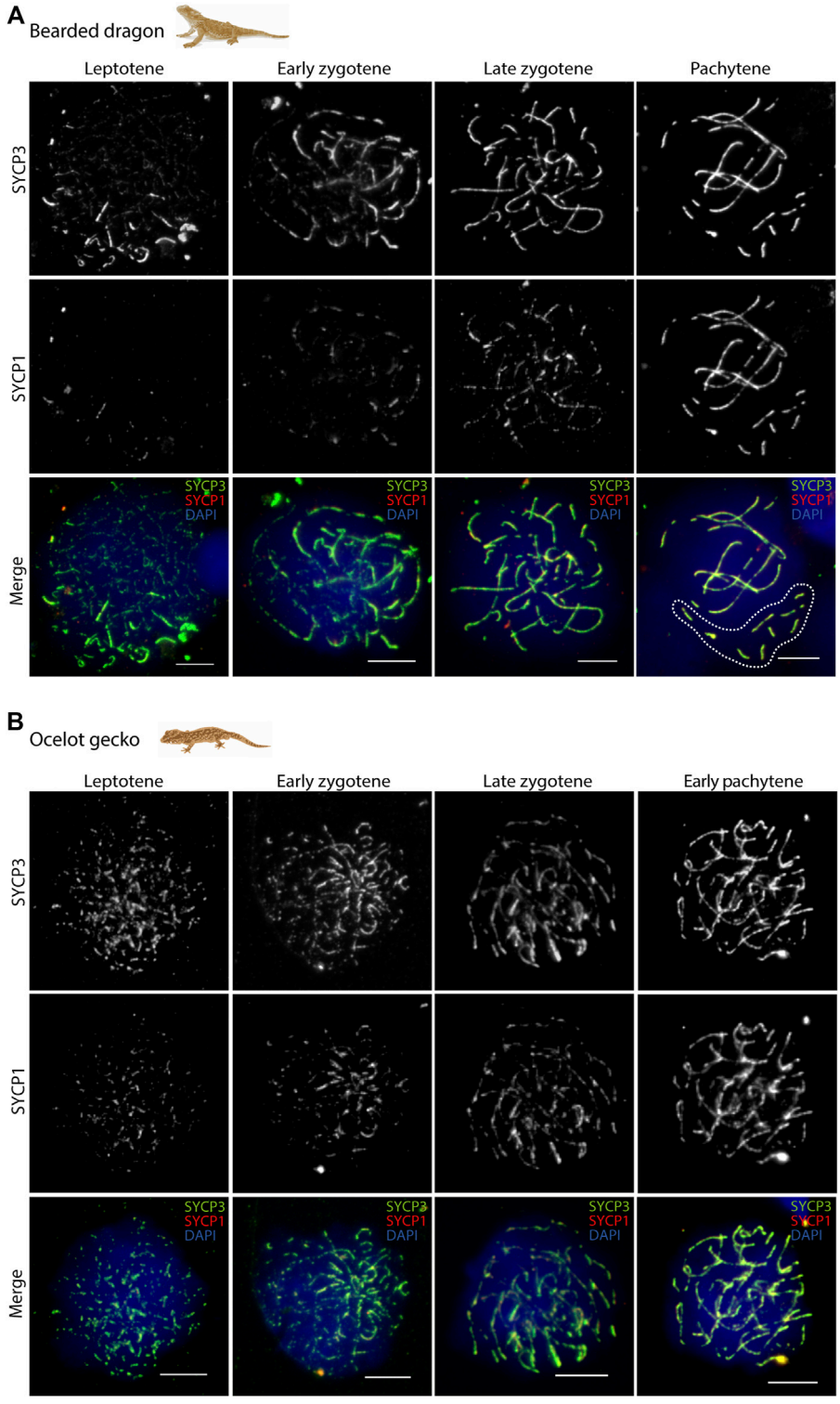

FIGURE 3
Synapsis dynamics during prophase I. Spermatocyte spreads labelled with antibodies against SYCP3 (green) and SYCP1 (red), counterstaining the DNA with DAPI (blue) for **(A)** the bearded dragon and **(B)** the ocelot gecko. Scale bar: 10 μm. White dashed circle: cluster of micro-chromosomes.

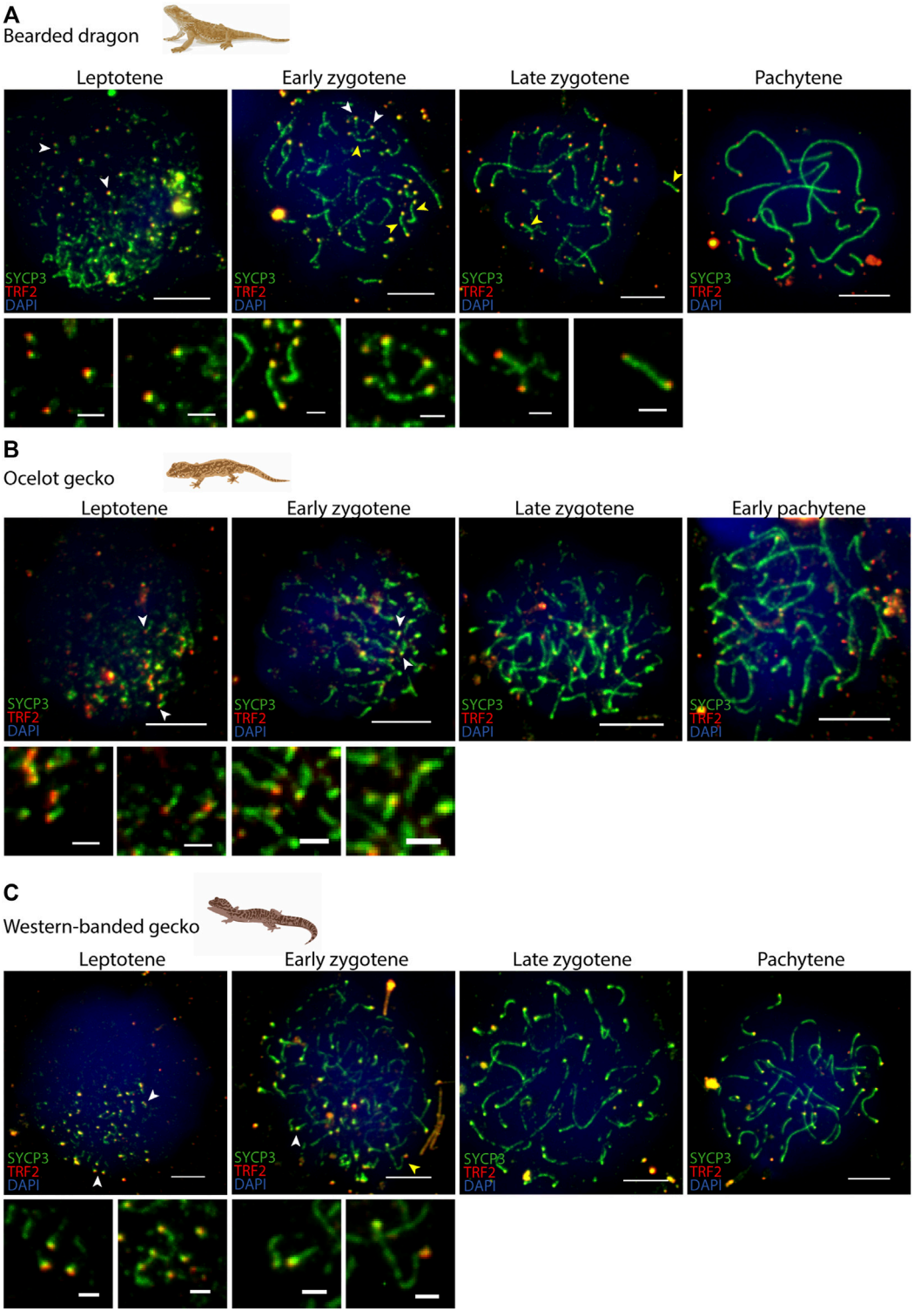

FIGURE 4
Telomere dynamics during prophase I. Spermatocyte spreads labelled with antibodies against SYCP3 (green) and TRF2 (red), counterstaining the DNA with DAPI (blue) for **(A)** the bearded dragon, **(B)** the ocelot gecko and **(C)** the western banded gecko. Scale bar: 10 μm and 2 μm (insets). White arrowheads: telomeres from which SC is beginning to assemble. Yellow arrowheads: completely associated micro-chromosomes (i.e., lateral elements of the SC completely assembled between both telomeric ends).

observed (Figure 2). Spermiogenic cells were divided into three different stages: i) round spermatids, the smallest cell type, rounded with fully condensed chromatin; ii) elongating spermatids with their round nuclei and condensed chromatin becoming elongated; iii) mature sperm after the completion of spermiogenesis and the elongation process was finalised.

Micro-chromosomes pair earlier during prophase I than macro-chromosomes

We then analyzed the meiotic chromosome pairing strategies in all four species. Chromosome pairs in all four reptile species largely differ in size (Figure 1). The chromosome complement of the reptiles herein varied: 2n = 32 chromosomes in the bearded dragon (6 pairs of macro chromosomes and 10 pairs of micros, including the sex chromosomes) (Young et al., 2013), 2n = 32 in the western-banded gecko (16 pairs of acrocentric chromosomes with continuous decreasing of size from large to small) (Pokorná et al., 2010), 2n = 36 chromosomes continuously decreasing in size in the ocelot gecko (Main et al., 2012; Koubová et al., 2014) and 2n = 50 in the painted turtle (13 pairs of macro chromosomes and 12 pairs of micros) (Badenhorst et al., 2015) (Figure 1B).

Axial elements of the synaptonemal complex labelled with anti-SYCP3 were used to classify spermatocytes into the different prophase I stages (leptotene, early zygotene, late zygotene and pachytene; Figure 3 and Supplementary Figure S1) as previously described (Alavattam et al., 2018). The proportion of thick (i.e., synapsis) and thin (i.e., unsynapsis) SYCP3 filaments were used to distinguish between earlier and later stages of zygotene spermatocytes. Zygotene spermatocytes with ≤ 50% of thick SYCP3 filaments (i.e., synapsis) were classified as "early stage", whereas zygotene spermatocytes with > 50% of synapsis, were classified as "late stage" (Alavattam et al., 2018).

In all four species we observed short filaments of SYCP3 at leptotene, which represented the forming axial elements (Figure 3; Supplementary Figure S1). The general trend in all four species was for the chromosomes to start pairing at one pole of the cell at leptotene, forming the *bouquet*, from which SYCP3-positive filaments assembled from telomeres (Figure 4; Supplementary Figure S2). As prophase I progressed, axial elements become larger at zygotene, when synapsis between homologous chromosomes takes place, as revealed by SYCP3 and SYCP1 labelling (Figure 3; Supplementary Figure S1) (Alavattam et al., 2018). At pachytene, autosomes had completed synapsis. Remarkably, we found that micro-chromosomes completed synapsis earlier than macro-chromosomes, forming a discrete cluster (Figure 3A). This previously undescribed pattern was also highlighted by TRF2 immunostaining of telomeres, which revealed that some micro-chromosomes were fully synapsed in early zygotene (Figure 4; Supplementary Figure S2).

Moreover, phosphorylated RNA polymerase II (the active form of RNA pol II) was detected in spermatocytes of all four species, with increasing signal intensity through prophase I (Supplementary Figure S3), mirroring therian mammals (Page et al., 2012; Marín-Gual et al., 2022) and insects (Viera et al., 2017). The absence of transcriptional repression of any specific pair of chromosomes during pachytene (no antibodies against γH2AX yielded any positive staining) suggested that meiotic sex chromosome inactivation (MSCI) was absent in the four reptilian species, contrasting male mammals (Turner et al., 2005; Ruiz-Herrera and Waters, 2022). The absence of MSCI is not surprising because our reptile models either do not have sex chromosomes (the painted turtle, Valenzuela et al., 2014), or because males are the homogametic sex (the bearded dragon, Ezaz et al., 2005), or because sex chromosomes are likely poorly differentiated (the ocelot gecko and the western banded gecko, Keating et al., 2022; Rovatsos et al., 2019).

DSBs dynamics in reptiles

We then analyzed the dynamics of DSB formation by immunodetection of the recombination proteins RPA (Replication Protein A) and RAD51 (Radiation Sensitive 51) (Figure 5; Supplementary Figures S4, S5) as no antibodies against MLH1 yielded any positive staining in reptile spermatocytes (data non shown). RPA binds to the 3' DNA strand following DSBs formation, and is subsequently replaced by RAD51 and/or DMC1 by early prophase I (He et al., 1995; Keeney et al., 1997). As such, the number of RPA and RAD51 sites in early prophase is a proxy for the number of DSBs, as previously described for various mammalian taxa (Segura et al., 2013; Ruiz-Herrera et al., 2017; Marín-Gual et al., 2022).

We successfully detected RPA foci in spermatocyte spreads of the western banded gecko, the ocelot gecko, and the bearded dragon (Figures 5A,B; Supplementary Figure S4; Table 1). Both geckos had equivalent numbers of RPA foci at leptotene and early zygotene (Mann-Whitney test, $p \geq 0.05$, Table 1). However, they had different RPA replacement dynamics, because the mean number of RPA foci was higher in the western banded gecko compared to the ocelot gecko by late zygotene (Mann-Whitney test, $p < 0.001$) and pachytene (Mann-Whitney test, $p < 0.01$) (Table 1). Furthermore, the RPA loading and replacement dynamics in the bearded dragon differed from both geckos, with lower RPA foci per cell at early zygotene (Mann-Whitney test, $p < 0.001$), intermediate values at late zygotene (Mann-Whitney test, $p < 0.001$) and higher RPA foci at pachytene compared to the ocelot gecko (Mann-Whitney test, $p < 0.05$) (Figure 5B; Table 1).

Similar dynamics (i.e., a decreasing numbers of foci as prophase I progressed) were detected for RAD51, which we

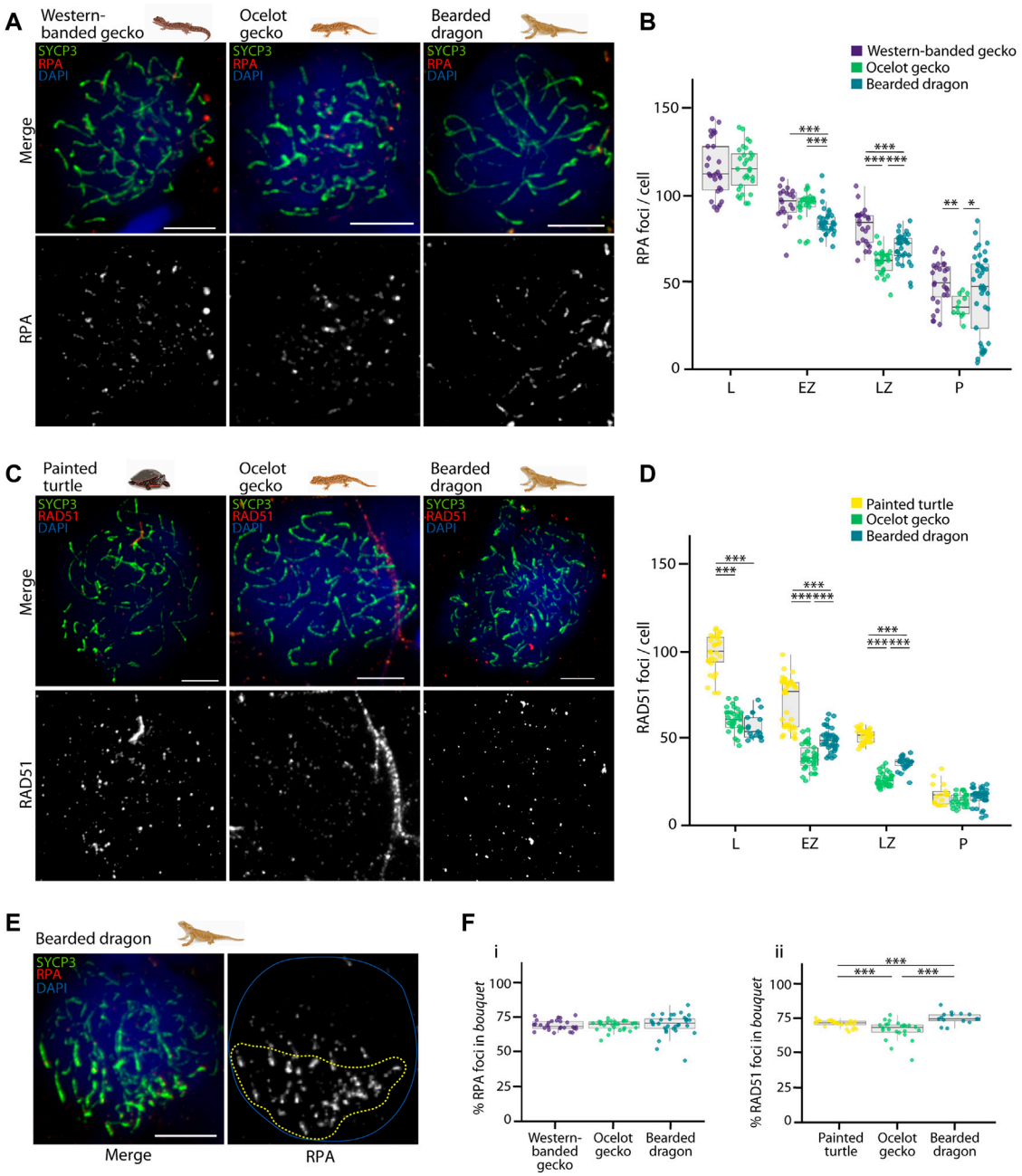

FIGURE 5
Double strand break formation dynamics during reptilian prophase I. **(A)** Late zygotene spermatocyte spreads labelled with antibodies against SYCP3 (green) and RPA (red), counterstaining the DNA with DAPI (blue) for the western banded gecko, the ocelot gecko and the bearded dragon. Scale bar: 10 μm. **(B)** Plot representing the number of RPA foci per cell detected at leptotene, early zygotene, late zygotene and pachytene. **(C)** Late zygotene spermatocyte spreads labelled with antibodies against SYCP3 (green) and RAD51 (red), counterstaining the DNA with DAPI (blue) for the painted turtle, the ocelot gecko and the bearded dragon. Scale bar: 10 μm. **(D)** Plot representing the number of RAD51 foci per cell detected at leptotene, early zygotene, late zygotene and pachytene. **(E)** Early zygotene spermatocyte spread labelled with SYCP3 (green) and RPA (red), counterstaining the DNA with DAPI (blue) in the bearded dragon. Dashed yellow circle: RPA foci detected in the *bouquet*. Blue circle: nuclei perimeter. **(F)** Plots representing the percentage of (i) RPA and (ii) RAD51 foci detected in the *bouquet* for the western banded gecko, the painted turtle, the ocelot gecko and the bearded dragon. Only cells with a well-defined *bouquet* were included in the analysis. The number of cells examined per species per stage, illustrated in panels **(B,D,F)**, are listed in Table 1. Mann-Whitney test (*$p < 0.05$, **$p < 0.01$ and ***$p < 0.001$). Legend: L, leptotene; EZ, early zygotene; LZ, late zygotene; P, pachytene.

TABLE 1 Dynamics of DSB formation during prophase I in the four reptiles included in the study. Values indicate the average number of RPA or RAD51 foci per cell immunodetected in leptotene, early zygotene, late zygotene, and pachytene, as well as the fraction of the total foci per cell detected in the *bouquet*. Values in parenthesis indicate the number of cells analyzed in each case.

		Leptotene	Early zygotene	Late zygotene	Pachytene	% foci in *bouquet*
Mean RPA foci/cell	Western-banded gecko	115 (29)	95 (20)	82 (24)	49 (17)	69 (28)
	Ocelot gecko	115 (30)	94 (25)	61 (27)	36 (11)	69 (29)
	Bearded dragon	–	85 (32)	70 (32)	44 (41)	70 (32)
Mean RAD51 foci/cell	Painted turtle	103 (29)	75 (37)	56 (37)	22 (17)	70 (26)
	Ocelot gecko	65 (31)	44 (37)	31 (35)	19 (25)	66 (24)
	Bearded dragon	61 (17)	53 (36)	40 (24)	21 (34)	75 (15)

detected in spermatocyte spreads of the painted turtle, the ocelot gecko and the bearded dragon (Figures 5C,D; Supplementary Figure S5; Table 1). Both lizards had equivalent values of RAD51 foci per cell at leptotene (Mann-Whitney test, $p \geq 0.05$), whereas the mean was higher in the bearded dragon compared to the ocelot gecko by early zygotene (Mann-Whitney test, $p < 0.001$) and late zygotene ($p < 0.001$) (Table 1). In contrast, the painted turtle showed higher mean values of RAD51 foci per cell compared to both lizards at all stages of prophase I (Man-Whitney test, $p < 0.001$) except in pachytene (Mann-Whitney test, $p \geq 0.05$) (Figure 5D; Table 1).

Remarkably, RPA and RAD51 loading followed similar dynamics, with both proteins accumulated in the *bouquet* region at early stages of prophase I (Figure 5E). Despite some variation among reptile species, between 66% and 75% of the total RPA and RAD51 foci per cell were detected in the *bouquet* (Figure 5F), indicating that DSB formation initiates at telomeres.

Discussion

Our work represents a comparative study of the dynamics of the spermatogenic cycle and prophase I progression in reptiles, with an emphasis on chromosome pairing and the formation and repair of meiotic DSBs.

Continuous spermatogenic cycle in the bearded dragon and the painted turtle

Spermatogenesis in vertebrates follows two main arrangements in the seminiferous epithelia: (i) cystic, in which developing germ cell syncytia are individually encapsulated by Sertoli cells as observed in fish and amphibians, and (ii) noncystic, where spermatogenesis takes place in seminiferous tubules (reptiles, birds, and mammals) (Schulz et al., 2010; Sousa et al., 2014). In species with noncystic spermatogenesis, the seminiferous epithelium is the building block of seminiferous tubules, which are primarily composed of Sertoli cells and germ cells. Then, germ cell differentiation takes place in a continuous manner with a species-specific time interval (e.g., 8.6 days in mice and 16 days in humans, Russell et al., 1993).

Both the histological and cytological characterization presented here for reptiles revealed that spermatogenesis progression is noncystic and highly conserved with respect to cell morphology and distribution. Analysis of the histological distribution of different germ cell types within the seminiferous epithelia revealed that both the bearded dragon and the painted turtle showed similar patters to those described in eutherian mammals (Russell et al., 1993) and other reptiles (Gribbins, 2011; Sousa et al., 2014). In fact, all amniotes described to date present similar testis structure and organization, although differences have been reported in terms of reproductive strategy and behaviour, including both continuous and seasonal breeding (Gribbins et al., 2003).

In temperate and subtropical lizards, the testicular cycle is divided in two phases: (i) the regenerative phase, which occurs in the spring, and (ii) the degenerative phase, that begins in summer (Mayhew and Wright, 1970; Amey and Whittier, 2000a). So, there is a cycle of hypertrophy and regression of reproductive organs. Previous studies in the eastern bearded dragon *Pogona barbata* classified testis as (i) regressed (only spermatogonia present), (ii) developing (spermatocytes or spermatids present), and (iii) spermiogenic (spermatogenesis and mature sperm present) (Amey and Whittier, 2000a). Consistently, the observations made here for the central bearded dragon agree with the observation of maximum spermatogenic activity in spring, followed by the cessation of spermatogenesis directly after the breeding period and testicular recrudescence in February (late summer). Both bearded dragons and the painted turtle are seasonal breeders (Gibbons, 1968; Amey and Whittier, 2000b) and since samples were collected at the end of the mating season for both species, our results showed that germ cells enter the spermatogenic cell cycle continually during the reproductive season, as all cell stages were found in the seminiferous epithelium.

Meiosis progression is highly conserved in reptiles

We found that the progression of prophase I was highly conserved among the reptiles examined. In most species, chromosomes were organized into chromosome axes but were not yet synapsed at leptotene. This was coupled with the formation of DSBs (Zickler and Kleckner, 2015). In our target reptiles, chromosome axes were detected as short stretches of SYCP3 and SYCP1 signal adjacent to the telomes, mirroring the patterns previously described in zebrafish (Blokhina et al., 2019; Imai et al., 2021). Moreover, telomeres clustered to one side of the nucleus forming the *bouquet*, presumably promoting homologous pairing and synapsis. The *bouquet* first appeared from leptotene to late zygotene, depending on the species. This feature is shared with zebrafish, suggesting that early telomere clustering is ancestral and has been retained over almost 400 million years of vertebrate evolution.

Interestingly, micro-chromosomes completed synapsis earlier than macro-chromosomes, forming discrete clusters concurrent with the *bouquet*. This suggests that the *bouquet* facilitates SYCP3 loading and synapsis of homologous chromosomes (both macro and micro-chromosomes) from the telomeres towards the central regions of the chromosomes, at the same time as micro-chromosome synapsis. Complete homologous synapsis of micro-chromosomes was observed from early zygotene to pachytene. This was coupled with a polarization of DSBs towards telomeres, a notable difference compared to some mammal species where DSBs are distributed more homogenously across the genome as the SC is being assembled (Ruiz-Herrera et al., 2017; Marín-Gual et al., 2022), although DSBs and COs have been reported to be enriched at sub-telomeric regions in human males (Barlow and Hultén, 1998; Khil and Camerini-Otero, 2010; Pratto et al., 2014).

The clustering of telomeres during early prophase I extends previous cytological and genomic studies where micro-chromosomes in reptiles tend to clump centrally in mitotic and meiotic metaphase I (Waters et al., 2021), resulting in higher inter-chromosomal genomic interactions between micro-chromosomes than for macro-chromosomes (Waters et al., 2021). This results in micro-chromosomes forming a structural and functional domain that is maintained in germ cells, probably facilitating homology search and DSBs formation. As most sauropsids are characterized by very conservative genomes (with few macro-chromosomes and up to many micro-chromosomes) (Valenzuela and Adams, 2011; Waters et al., 2021), we hypothesize that meiotic patterns described herein will apply widely in this clade.

Low meiotic DSB rates in reptiles

Remarkably, reptiles showed lower levels of DSBs than eutherian mammals. Although variable among species, between 200 and 300 DSBs per cell (mean values) occur genome-wide during leptotene in eutherian mammals (Segura et al., 2013). Marsupials show the lowest recombination rates in mammals with less than 150 RPA foci per cell in zygotene (Zenger et al., 2002; Samollow et al., 2004; Marín-Gual et al., 2022). This contrasts with our results where fewer RPA foci (from 95 to 85 per cell) and RAD51 foci (from 75 to 44 per cell) (a proxy for DSBs) were observed in early zygotene in reptiles. A closer inspection of the data revealed that squamates (geckos and the bearded dragon) showed equivalent values of DSBs in early stages of prophase I, and lower than turtles, the sister taxon to archosaurs (birds plus crocodilians). Two biological, non-mutually exclusive alternatives could explain these observations: differences in DSBs per cell observed between squamates and turtles are due to (i) contrasting chromosome number and size between the taxa examined, or (ii) these lineages differ in the genetic determinants of DSBs induction.

The first alternative agrees with previous cytological data. Specifically, studies in disparate taxa show that the total number and distribution of COs (and also initial meiotic DSBs) on a specific chromosome depends on several factors, such as chromosome size, and an individual's sex and age (Pardo-Manuel De Villena and Sapienza, 2001; Lynn et al., 2004; Garcia-Cruz et al., 2011; Ruiz-Herrera et al., 2017; Wang et al., 2019). Larger chromosomes tend to accumulate more COs (but see recent data in yeast, Murakami et al., 2021), and each chromosome arm generally presents at least one CO (the obligatory chiasmata) (Sun et al., 2017). Thus, because both geckos and the bearded dragon have lower diploid numbers (2n = 32–36) than the painted turtle (2n = 50), differences in meiotic DSBs (COs were not reported in this study) are expected among groups. This rationale would also apply to birds, which possess high chromosome numbers (typically 2n = 80, Ruiz-Herrera et al., 2012; Waters et al., 2021). In birds, cytological analyses of COs (meiotic DSBs are unreported) are restricted to species from the domesticated groups Galloanserae and Passeriformes, in which recombination rates are higher (from 1.8 cM/Mb to 2.6 cM/Mb; del Priore and Pigozzi, 2020) than those reported for mammals (from 0.18 cM/Mb to 1.78 cM/Mb; Segura et al., 2013). Moreover, birds show little variation in recombination rates between groups (del Priore and Pigozzi, 2020), and thus are not lineage-dependent (unlike mammals, Segura et al., 2013), perhaps related to high genome conservation (Waters et al., 2021).

The second hypothesis derives from the observation that recombination rates may vary by the presence of different genetic determinants of DSBs induction, such as PRDM9 (Mihola et al., 2009; Myers et al., 2010; Grey et al., 2011; Vara et al., 2019).

PRDM9 is a meiotic-specific histone (H3) methyltransferase with a C-terminal tandem repeat zinc finger (ZnF) domain that adds H3K4me3 marks at nucleosomes close to DSBs in early meiosis. This process genetically determines recombination hotspots (Mihola et al., 2009; Baudat et al., 2010; Grey et al., 2011). Experimental work has shown that PRDM9 provokes changes in local chromatin structure that tend to position nucleosomes in ways that increased overall accessibility (Yamada et al., 2020). Moreover, in the absence of PRDM9, DSBs tend to form in gene promoter regions (Brick et al., 2012; Baker et al., 2015; Lange et al., 2016). PRDM9 is present in most mammals (with the exception of canids, Muñoz-Fuentes et al., 2011), but substantial allelic variability was described in natural populations, especially in rodents (Buard et al., 2014; Capilla et al., 2014; Vara et al., 2019) contributing to speciation (Smagulova et al., 2016). Most importantly, PRDM9 gene was lost at least 13 times independently in vertebrates, including in birds, some snakes, and lizards (Cavassim et al., 2022). Although bearded dragons have a complete PRDM9 (Cavassim et al., 2022), little is known regarding geckos and turtles. It is tempting to speculate the existence of yet to be discovered genetic determinants of recombination across vertebrates, and that one (or more) of these might be responsible for reduced recombination rates observed in the species herein. Further research is needed to fully test these hypotheses.

Limitations of the study

As the use of non-model species can be challenging, future studies with a larger number of animals per species will be desirable to capture inter-individual variability in recombination rates. Additionally, here we report results obtained with two early markers of meiotic DSBs (RAD51 and RPA) in four different reptile species, but the use of direct measures of COs were precluded. Thus, future research focussed on MLH1 foci (a marker of COs) together with the analysis of chiasmata in metaphase I will provide a comprehensive view of the recombination dynamics in reptiles.

Conclusion

Overall, our findings provide new insights into meiotic chromosome dynamics and double strand break formation during reptile spermatogenesis. Shared histological patterns observed between squamates and turtles suggest that they represent the ancestral state. However, future research across more species is warranted to asses conservation of this ancestral pattern across other sauropsids. Understanding the intricacies of the mechanisms regulating chromosome synapsis, recombination and segregation during meiosis progression across vertebrates will further determine the genomic basis of biodiversity, and how it may be affected by ecotoxicological and other environmental changes.

Data availability statement

The original contributions presented in the study are included in the article/Supplementary Material, further inquiries can be directed to the corresponding author.

Ethics statement

All animals were treated, and tissues collected under appropriate permits, and experiments approved by each Universities Animal Experimentation Ethics Committees (University of Canberra, Charles University in Prague and Iowa State University) in accordance with animal ethics guidelines.

Author contributions

AR-H conceived and devised the study. LM-G, LG-R, PDW, and AR-H designed experiments and analysis. LM-G, LG-R, and MMG performed experiments and analyzed the data. LK, NV, AG, PDW, and AR-H contributed to reagents and data collection. LM-G, LG-R, PDW, and AR-H wrote the first draft of the manuscript with inputs from all authors. All authors read and approved the final version of the manuscript.

Funding

This work was supported by the Ministry of Economy, Industry and Competitiveness (CGL 2017–83802-P to AR-H), the Spanish Ministry of Science and Innovation (PID 2020–112557GGB-I00 to AR-H) and the Agència de Gestió d'Ajuts Universitaris i de Recerca, AGAUR (SGR1215 to AR-H). LM-G was supported by an FPU predoctoral fellowship from the Ministry of Science, Innovation and University (FPU18/03867). LK was supported by Czech Science Foundation (no. 20–27236J). A component of this research was supported by the Australian Research Council (DP170101147 and DP220101429 to AG and PDW), and by the National Science Foundation of the United States (NSF IOS 2127995 to NV).

Acknowledgments

The authors are grateful to Thea B. Gessler and Nicholas E. Topping for their assistance during sample collection.

Conflict of interest

The authors declare that the research was conducted in the absence of any commercial or financial relationships that could be construed as a potential conflict of interest.

Publisher's note

Supplementary material

The Supplementary Material for this article can be found online at: https://www.frontiersin.org/articles/10.3389/fcell.2022.1009776/full#supplementary-material.

SUPPLEMENTARY FIGURE 1:
Synapsis dynamics during prophase I. Spermatocyte spreads labelled with antibodies against SYCP3 (green) and SYCP1 (red), counterstaining the DNA with DAPI (blue) for **(A)** the western-banded gecko and **(B)** the painted turtle. Scale bar: 10 μm.

SUPPLEMENTARY FIGURE 2:
Telomere dynamics during prophase I. Spermatocyte spreads labelled with antibodies against SYCP3 (green), SYCP1 (red) and TRF2 (blue) for the bearded dragon. Scale bar: 10 μm and 2 μm (insets). White arrowheads: telomeres from which SC is beginning to assemble. Yellow arrowheads: completely synapsed micro-chromosomes (i.e., lateral and central elements of the SC completely assembled between both telomeric ends). Insets (bottom row panels) show micro-chromosomes completely assembled.

SUPPLEMENTARY FIGURE 3:
Transcriptional dynamics during prophase I. Spermatocyte spreads labelled with antibodies against SYCP3 (green) and RNApol II (red) for **(A)** the bearded dragon, **(B)** the ocelot gecko, **(C)** the western banded gecko and **(D)** the painted turtle. Scale bar: 10 μm.

SUPPLEMENTARY FIGURE 4:
RPA dynamics during reptilian prophase I. Spermatocyte spreads labelled with antibodies against SYCP3 (green) and RPA (red), counterstaining the DNA with DAPI (blue) for **(A)** the western banded gecko, **(B)** the ocelot gecko and **(C)** the bearded dragon. Scale bar: 10 μm.

SUPPLEMENTARY FIGURE 5:
RAD51 dynamics during reptilian prophase I. Spermatocyte spreads labelled with antibodies against SYCP3 (green) and RAD51 (red), counterstaining the DNA with DAPI (blue) for **(A)** the painted turtle, **(B)** the ocelot gecko and **(C)** the bearded dragon. Scale bar: 10 μm.

References

Alavattam, K. G., Abe, H., Sakashita, A., and Namekawa, S. H. (2018). Chromosome spread analyses of meiotic sex chromosome inactivation. *Methods Mol. Biol.* 1861, 113–129. doi:10.1007/978-1-4939-8766-5_10

Alavattam, K. G., Maezawa, S., Sakashita, A., Khoury, H., Barski, A., Kaplan, N., et al. (2019). Attenuated chromatin compartmentalization in meiosis and its maturation in sperm development. *Nat. Struct. Mol. Biol.* 26 (3), 175–184. doi:10.1038/s41594-019-0189-y

Amey, A. P., and Whittier, J. M. (2000a). Seasonal patterns of plasma steroid hormones in males and females of the bearded dragon lizard, *Pogona barbata*. *Gen. Comp. Endocrinol.* 117 (3), 335–342. doi:10.1006/gcen.2000.7426

Amey, A. P., and Whittier, J. M. (2000b). The annual reproductive cycle and sperm storage in the bearded dragon, *Pogona barbata*. *Aust. J. Zool.* 48 (4), 411–419. doi:10.1071/ZO00031

Badenhorst, D., Hillier, L. W., Literman, R., Montiel, E. E., Radhakrishnan, S., Shen, Y., et al. (2015). Physical mapping and refinement of the painted turtle genome (*Chrysemys picta*) inform amniote genome evolution and challenge turtle-bird chromosomal conservation. *Genome Biol. Evol.* 7 (7), 2038–2050. doi:10.1093/gbe/evv119

Baker, C. L., Kajita, S., Walker, M., Saxl, R. L., Raghupathy, N., Choi, K., et al. (2015). PRDM9 drives evolutionary erosion of hotspots in *Mus musculus* through haplotype-specific initiation of meiotic recombination. *PLoS Genet.* 11 (1), e1004916. doi:10.1371/journal.pgen.1004916

Barlow, A. L., and Hultén, M. A. (1998). Crossing over analysis at pachytene in man. *Eur. J. Hum. Genet.* 6 (4), 350–358. doi:10.1038/sj.ejhg.5200200

Baudat, F., Buard, J., Grey, C., and de Massy, B. (2010). Prdm9, a key control of mammalian recombination hotspots. *Med. Sci.* 26 (5), 468–470. doi:10.1051/medsci/2010265468

Bista, B., and Valenzuela, N. (2020). Turtle insights into the evolution of the reptilian karyotype and the genomic architecture of sex determination. *Genes* 11 (4), 416. doi:10.3390/genes11040416

Blokhina, Y. P., Nguyen, A. D., Draper, B. W., and Burgess, S. M. (2019). The telomere bouquet is a hub where meiotic double-strand breaks, synapsis, and stable homolog juxtaposition are coordinated in the zebrafish, *Danio rerio*. *PLoS Genet.* 15 (1), e1007730. doi:10.1371/journal.pgen.1007730

Bolcun-Filas, E., and Handel, M. A. (2018). Meiosis: The chromosomal foundation of reproduction. *Biol. Reprod.* 99 (1), 112–126. doi:10.1093/biolre/ioy021

Brick, K., Smagulova, F., Khil, P., Camerini-Otero, R. D., and Petukhova, G. v. (2012). Genetic recombination is directed away from functional genomic elements in mice. *Nature* 485 (7400), 642–645. doi:10.1038/nature11089

Buard, J., Rivals, E., Dunoyer De Segonzac, D., Garres, C., Caminade, P., de Massy, B., et al. (2014). Diversity of Prdm9 zinc finger array in wild mice unravels new facets of the evolutionary turnover of this coding minisatellite. *PLoS ONE* 9 (1), e85021. doi:10.1371/journal.pone.0085021

Capilla, L., Medarde, N., Alemany-Schmidt, A., Oliver-Bonet, M., Ventura, J., and Ruiz-Herrera, A. (2014). Genetic recombination variation in wild robertsonian mice: On the role of chromosomal fusions and Prdm9 allelic background. *Proc. Biol. Sci.* 281 (1786), 20140297. doi:10.1098/rspb.2014.0297

Cavassim, M. I. A., Baker, Z., Hoge, C., Schierup, M. H., Schumer, M., and Przeworski, M. (2022). PRDM9 losses in vertebrates are coupled to those of paralogs ZCWPW1 and ZCWPW2. *Proc. Natl. Acad. Sci. U. S. A.* 119 (9), 21144011199–e2114401211. doi:10.1073/pnas.2114401119

del Priore, L., and Pigozzi, M. I. (2020). MLH1 focus mapping in the Guinea fowl (*Numida meleagris*) give insights into the crossover landscapes in birds. *PLoS ONE* 15 (10), e0240245. doi:10.1371/journal.pone.0240245

Ezaz, T., Quinn, A. E., Miura, I., Sarre, S. D., Georges, A., and Marshall Graves, J. A. (2005). The dragon lizard *Pogona vitticeps* has ZZ/ZW micro-sex chromosomes. *Chromosome Res.* 13 (8), 763–776. doi:10.1007/s10577-005-1010-9

Ezaz, T., Stiglec, R., Veyrunes, F., and Marshall Graves, J. A. (2006). Relationships between vertebrate ZW and XY sex chromosome systems. *Curr. Biol.* 16 (17), 736–743. doi:10.1016/j.cub.2006.08.021

Garcia-Cruz, R., Pacheco, S., Brieño, M. A., Steinberg, E. R., Mudry, M. D., Ruiz-Herrera, A., et al. (2011). A comparative study of the recombination pattern in three species of Platyrrhini monkeys (primates). *Chromosoma* 120 (5), 521–530. doi:10.1007/s00412-011-0329-6

Gibbons, J. W. (1968). Reproductive potential, activity, and cycles in the painted turtle, *Chrysemys picta*. *Ecology* 49 (3), 399–409. doi:10.2307/1934106

Grey, C., Barthès, P., Friec, G., Langa, F., Baudat, F., and de Massy, B. (2011). Mouse Prdm9 DNA-binding specificity determines sites of histone H3 lysine 4 trimethylation for initiation of meiotic recombination. *PLoS Biol.* 9 (10), e1001176. doi:10.1371/journal.pbio.1001176

Gribbins, K. M., Gist, D. H., and Congdon, J. D. (2003). Cytological evaluation of spermatogenesis and organization of the germinal epithelium in the male slider turtle, *Trachemys scripta*. *J. Morphol.* 255 (3), 337–346. doi:10.1002/jmor.10069

Gribbins, K. M. (2011). Reptilian spermatogenesis: A histological and ultrastructural perspective. *Spermatogenesis* 1 (3), 250–269. doi:10.4161/spmg.1.3.18092

Guioli, S., Lovell-Badge, R., and Turner, J. M. A. (2012). Error-prone ZW pairing and no evidence for meiotic sex chromosome inactivation in the chicken germ line. *PLoS Genet.* 8 (3), e1002560. doi:10.1371/journal.pgen.1002560

Hammoud, S. S., Low, D. H. P., Yi, C., Carrell, D. T., Guccione, E., and Cairns, B. R. (2014). Chromatin and transcription transitions of mammalian adult germline stem cells and spermatogenesis. *Cell Stem Cell* 15 (2), 239–253. doi:10.1016/j.stem.2014.04.006

He, Z., Henricksen, L. A., Wold, M. S., and Ingles, C. J. (1995). RPA involvement in the damage-recognition and incision steps of nucleotide excision repair. *Nature* 374 (6522), 566–569. doi:10.1038/374566a0

Holleley, C. E., O'Meally, D., Sarre, S. D., Marshall Graves, J. A., Ezaz, T., Matsubara, K., et al. (2015). Sex reversal triggers the rapid transition from genetic to temperature-dependent sex. *Nature* 523 (7558), 79–82. doi:10.1038/nature14574

Imai, Y., Olaya, I., Sakai, N., and Burgess, S. M. (2021). Meiotic chromosome dynamics in zebrafish. *Front. Cell Dev. Biol.* 9, 757445. doi:10.3389/fcell.2021.757445

Keating, S. E., Greenbaum, E., Johnson, J. D., and Gamble, T. (2022). Identification of a cis-sex chromosome transition in banded geckos (Coleonyx, Eublepharidae, Gekkota). *J. Evol. Biol.* 00, 1–8. doi:10.1111/jeb.14022

Keeney, S., Giroux, C. N., and Kleckner, N. (1997). Meiosis-specific DNA double-strand breaks are catalyzed by Spo11, a member of a widely conserved protein family. *Cell* 88 (3), 375–384. doi:10.1016/S0092-8674(00)81876-0

Khil, P. P., and Camerini-Otero, R. D. (2010). Genetic crossovers are predicted accurately by the computed human recombination map. *PLoS Genet.* 6 (1), e1000831. doi:10.1371/journal.pgen.1000831

Koubová, M., Pokorná, M. J., Rovatsos, M., Farkačová, K., Altmanová, M., and Kratochvíl, L. (2014). Sex determination in Madagascar geckos of the genus Paroedura (Squamata: Gekkonidae): Are differentiated sex chromosomes indeed so evolutionary stable? *Chromosome Res.* 22 (4), 441–452. doi:10.1007/s10577-014-9430-z

Kubička, L., Starostová, Z., and Kratochvíl, L. (2015). Endogenous control of sexual size dimorphism: Gonadal androgens have neither direct nor indirect effect on male growth in a Madagascar ground gecko (*Paroedura picta*). *Gen. Comp. Endocrinol.* 224, 273–277. doi:10.1016/j.ygcen.2015.09.028

Lange, J., Yamada, S., Tischfield, S. E., Pan, J., Kim, S., Socci, N. D., et al. (2016). The landscape of mouse meiotic double-strand break formation, processing and repair. *Cell* 167 (3), 695–708. doi:10.1016/j.cell.2016.09.035

Liebe, B., Alsheimer, M., Höög, C., Benavente, R., and Scherthan, H. (2004). Telomere attachment, meiotic chromosome condensation, pairing, and bouquet stage duration are modified in spermatocytes lacking axial elements. *Mol. Biol. Cell* 15 (2), 827–837. doi:10.1091/mbc.E03-07-0524

Lisachov, A. P., Tishakova, K. v., Tsepilov, Y. A., and Borodin, P. M. (2019). Male meiotic recombination in the steppe agama, *Trapelus sanguinolentus* (agamidae, Iguania, reptilia). *Cytogenet. Genome Res.* 157 (1–2), 107–114. doi:10.1159/000496078

Lisachov, A. P., Trifonov, V. A., Giovannotti, M., Ferguson-Smith, M. A., and Borodin, P. M. (2017). Immunocytological analysis of meiotic recombination in two anole lizards (Squamata , Dactyloidae). *Comp. Cytogenet.* 11 (1), 129–141. doi:10.3897/CompCytogen.v11i1.10916

Lutes, A. A., Neaves, W. B., Baumann, D. P., Wiegraebe, W., and Baumann, P. (2010). Sister chromosome pairing maintains heterozygosity in parthenogenetic lizards. *Nature* 464 (7286), 283–286. doi:10.1038/nature08818

Lynn, A., Ashley, T., and Hassold, T. (2004). Variation in human meiotic recombination. *Annu. Rev. Genomics Hum. Genet.* 5, 317–349. doi:10.1146/annurev.genom.4.070802.110217

Main, H., Scantlebury, D. P., Zarkower, D., and Gamble, T. (2012). Karyotypes of two species of Malagasy ground gecko (Paroedura: Gekkonidae). *Afr. J. Herpetology* 61 (1), 81–90. doi:10.1080/21564574.2012.667837

Marín-Gual, L., González-Rodelas, L., Pujol, G., Vara, C., Martín-Ruiz, M., Berríos, S., et al. (2022). Strategies for meiotic sex chromosome dynamics and telomeric elongation in Marsupials. *PLoS Genet.* 18 (2), e1010040. doi:10.1371/journal.pgen.1010040

Mayhew, W. W., and Wright, S. J. (1970). Seasonal changes in testicular histology of three species of the lizard genus Uma. *J. Morphol.* 130 (2), 163–185. doi:10.1002/jmor.1051300205

Mihola, O., Trachtulec, Z., Vlcek, C., Schimenti, J. C., and Forejt, J. (2009). A mouse speciation gene encodes a meiotic histone H3 methyltransferase. *Science* 323 (5912), 373–375. doi:10.1126/science.1163601

Montiel, E. E., Badenhorst, D., Lee, L. S., Literman, R., Trifonov, V., and Valenzuela, N. (2016). Cytogenetic insights into the evolution of chromosomes and sex determination reveal striking homology of turtle sex chromosomes to amphibian autosomes. *Cytogenet. Genome Res.* 148 (4), 292–304. doi:10.1159/000447478

Muñoz-Fuentes, V., di Rienzo, A., and Vilà, C. (2011). Prdm9, a major determinant of meiotic recombination hotspots, is not functional in dogs and their wild relatives, wolves and coyotes. *PLoS ONE* 6 (11), e25498. doi:10.1371/journal.pone.0025498

Murakami, H., Mu, X., and Keeney, S. (2021). How do small chromosomes know they are small? Maximizing meiotic break formation on the shortest yeast chromosomes. *Curr. Genet.* 67, 431–437. doi:10.1007/s00294-021-01160-9

Myers, S., Bowden, R., Tumian, A., Bontrop, R. E., Freeman, C., MacFie, T. S., et al. (2010). Drive against hotspot motifs in primates implicates the PRDM9 gene in meiotic recombination. *Science* 327 (5967), 876–879. doi:10.1126/science.1182363

Noro, M., Uejima, A., Abe, G., Manabe, M., and Tamura, K. (2009). Normal developmental stages of the Madagascar ground gecko *Paroedura pictus* with special reference to limb morphogenesis. *Dev. Dyn.* 238 (1), 100–109. doi:10.1002/dvdy.21828

Page, J., de La Fuente, R., Manterola, M., Parra, M. T., Viera, A., Berríos, S., et al. (2012). Inactivation or non-reactivation: What accounts better for the silence of sex chromosomes during mammalian male meiosis? *Chromosoma* 121 (3), 307–326. doi:10.1007/s00412-012-0364-y

Pardo-Manuel De Villena, F., and Sapienza, C. (2001). Nonrandom segregation during meiosis: The unfairness of females. *Mamm. Genome* 12 (5), 331–339. doi:10.1007/s003350040003

Patel, L., Kang, R., Rosenberg, S. C., Qiu, Y., Raviram, R., Chee, S., et al. (2019). Dynamic reorganization of the genome shapes the recombination landscape in meiotic prophase. *Nat. Struct. Mol. Biol.* 26 (3), 164–174. doi:10.1038/s41594-019-0187-0

Pokorná, M., Rábová, M., Ráb, P., Ferguson-Smith, M. A., Rens, W., and Kratochvíl, L. (2010). Differentiation of sex chromosomes and karyotypic evolution in the eye-lid geckos (Squamata: Gekkota: Eublepharidae), a group with different modes of sex determination. *Chromosome Res.* 18 (7), 809–820. doi:10.1007/s10577-010-9154-7

Pratto, F., Brick, K., Khil, P., Smagulova, F., Petukhova, G. v., and Camerini-Otero, D. (2014). DNA recombination. Recombination initiation maps of individual human genomes.. *Science* 346 (6211). doi:10.1126/science.1256442

Quinn, A. E., Georges, A., Sarre, S. D., Guarino, F., Ezaz, T., and Graves, J. A. M. (2007). Temperature sex reversal implies sex gene dosage in a reptile. *Science* 316 (5823), 411. doi:10.1126/science.1135925

Reig-Viader, R., Brieño-Enríquez, M. A., Khoriauli, L., Toran, N., Cabero, L., Giulotto, E., et al. (2013). Telomeric repeat-containing RNA and telomerase in human fetal oocytes. *Hum. Reprod.* 28 (2), 414–422. doi:10.1093/humrep/des363

Rovatsos, M., Farkačová, K., Altmanová, M., Johnson Pokorná, M., and Kratochvíl, L. (2019). The rise and fall of differentiated sex chromosomes in geckos. *Mol. Ecol.* 28 (12), 3042–3052. doi:10.1111/mec.15126

Ruiz-Herrera, A., Farre, M., and Robinson, T. J. (2012). Molecular cytogenetic and genomic insights into chromosomal evolution. *Heredity* 108 (1), 28–36. doi:10.1038/hdy.2011.102

Ruiz-Herrera, A., Vozdova, M., Fernández, J., Sebestova, H., Capilla, L., Frohlich, J., et al. (2017). Recombination correlates with synaptonemal complex length and chromatin loop size in bovids—Insights into mammalian meiotic chromosomal organization. *Chromosoma* 126 (5), 615–631. doi:10.1007/s00412-016-0624-3

Ruiz-Herrera, A., and Waters, P. D. (2022). Fragile, unfaithful and persistent ys—On how meiosis can shape sex chromosome evolution. *Heredity* 129 (1), 22–30. doi:10.1038/s41437-022-00532-2

Russell, L. D., Ettlin, R. A., Hikim, A. P. S., and Clegg, E. D. (1993). "Histological and histopathological evaluation of the testis," in *International journal of andrology* (Florida: Cache River Press), 16, 83.

Samollow, P. B., Kammerer, C. M., Mahaney, S. M., Schneider, J. L., Westenberger, S. J., Vandeberg, J. L., et al. (2004). First-generation linkage map of the gray, short-tailed opossum, *Monodelphis domestica*, reveals genome-wide reduction in female recombination rates. *Genetics* 166 (1), 307–329. doi:10.1534/genetics.166.1.307

Scherthan, H., Weich, S., Schwegler, H., Heyting, C., Härle, M., and Cremer, T. (1996). Centromere and telomere movements during early meiotic prophase of mouse and man are associated with the onset of chromosome pairing. *J. Cell Biol.* 134 (5), 1109–1125. doi:10.1083/jcb.134.5.1109

Schoenmakers, S., Wassenaar, E., Hoogerbrugge, J. W., Laven, J. S. E., Grootegoed, J. A., and Baarends, W. M. (2009). Female meiotic sex chromosome inactivation in chicken. *PLoS Genet.* 5 (5), e1000466. doi:10.1371/journal.pgen.1000466

Schulz, R. W., de França, L. R., Lareyre, J.-J., le Gac, F., Chiarini-Garcia, H., Nobrega, R. H., et al. (2010). Spermatogenesis in fish. *Gen. Comp. Endocrinol.* 165 (3), 390–411. doi:10.1016/j.ygcen.2009.02.013

Segura, J., Ferretti, L., Ramos-Onsins, S., Capilla, L., Farré, M., Reis, F., et al. (2013). Evolution of recombination in eutherian mammals: Insights into mechanisms that affect recombination rates and crossover interference. *Proc. Biol. Sci.* 280 (1771), 20131945. doi:10.1098/rspb.2013.1945

Shedlock, A. M., and Edwards, S. v. (2009). "Amniotes (amniota)," in *The timetree of life*. Editors S. B. Hedges and S. Kumar (Oxford: Oxford University Press), 375–379.

Smagulova, F., Brick, K., Pu, Y., Camerini-Otero, R. D., and Petukhova, G. v. (2016). The evolutionary turnover of recombination hot spots contributes to speciation in mice. *Genes Dev.* 30 (3), 266–280. doi:10.1101/gad.270009.115

Sousa, A. L., Campos-Junior, P. H. A., Costa, G. M. J., and de França, L. R. (2014). Spermatogenic cycle length and sperm production in the freshwater turtle *Kinosternon scorpioides*. *Biol. Reprod.* 90 (2), 35. doi:10.1095/biolreprod.113.112391

Spangenberg, V., Arakelyan, M., Galoyan, E., Martirosyan, I., Bogomazova, A., Martynova, E., et al. (2021). Meiotic synapsis of homeologous chromosomes and mismatch repair protein detection in the parthenogenetic rock lizard *Darevskia unisexualis*. *Mol. Reprod. Dev.* 88 (2), 119–127. doi:10.1002/mrd.23450

Starostová, Z., Kubička, L., Golinski, A., and Kratochvíl, L. (2013). Neither male gonadal androgens nor female reproductive costs drive development of sexual size dimorphism in lizards. *J. Exp. Biol.* 216 (10), 1872–1880. doi:10.1242/jeb.079442

Sun, L., Wang, J., Sang, M., Jiang, L., Zhao, B., Cheng, T., et al. (2017). Landscaping crossover interference across a genome. *Trends Plant Sci.* 22 (10), 894–907. doi:10.1016/j.tplants.2017.06.008

Turner, J. M. A., Mahadevaiah, S. K., Fernandez-Capetillo, O., Nussenzweig, A., Xu, X., Deng, C. X., et al. (2005). Silencing of unsynapsed meiotic chromosomes in the mouse. *Nat. Genet.* 37 (1), 41–47. doi:10.1038/ng1484

Valenzuela, N., and Adams, D. C. (2011). Chromosome number and sex determination coevolve in turtles. *Evolution* 65 (6), 1808–1813. doi:10.1111/j.1558-5646.2011.01258.x

Valenzuela, N., Badenhorst, D., Montiel, E. E., and Literman, R. (2014). Molecular cytogenetic search for cryptic sex chromosomes in painted turtles *Chrysemys picta*. *Cytogenet. Genome Res.* 144 (1), 39–46. doi:10.1159/000366076

Valenzuela, N. (2009). The painted turtle, *Chrysemys picta*: A model system for vertebrate evolution, ecology, and human health. *Cold Spring Harb. Protoc.* 4 (7), pdb.emo124–10. doi:10.1101/pdb.emo124

Vara, C., Paytuví-Gallart, A., Cuartero, Y., le Dily, F., Garcia, F., Salvà-Castro, J., et al. (2019). Three-dimensional genomic structure and cohesin occupancy correlate with transcriptional activity during spermatogenesis. *Cell Rep.* 28 (2), 352–367.e9. doi:10.1016/j.celrep.2019.06.037

Vara, C., and Ruiz-Herrera, A. (2022). Unpacking chromatin remodelling in germ cells: Implications for development and evolution. *Trends Genet.* 38 (5), 422–425. doi:10.1016/j.tig.2021.10.007

Viera, A., Parra, M. T., Rufas, J. S., and Page, J. (2017). Transcription reactivation during the first meiotic prophase in bugs is not dependent on synapsis. *Chromosoma* 126 (1), 179–194. doi:10.1007/s00412-016-0577-6

Wang, S., Veller, C., Sun, F., Ruiz-Herrera, A., Shang, Y., Liu, H., et al. (2019). Per-nucleus crossover covariation and implications for evolution. *Cell* 177 (2), 326–338.e16. doi:10.1016/j.cell.2019.02.021

Waters, P. D., Patel, H. R., Ruiz-Herrera, A., Álvarez-González, L., Lister, N. C., Simakov, O., et al. (2021). Microchromosomes are building blocks of bird, reptile and mammal chromosomes. *Proc. Natl. Acad. Sci. U. S. A.* 118 (45), 1e2112494118–30. doi:10.1073/pnas.2112494118

Yamada, S., Hinch, A. G., Kamido, H., Zhang, Y., Edelmann, W., and Keeney, S. (2020). Molecular structures and mechanisms of DNA break processing in mouse meiosis. *Genes Dev.* 34, 806–818. doi:10.1101/gad.336032.119

Young, M. J., O'Meally, D., Sarre, S. D., Georges, A., and Ezaz, T. (2013). Molecular cytogenetic map of the central bearded dragon, *Pogona vitticeps* (Squamata: Agamidae). *Chromosome Res.* 21 (4), 361–374. doi:10.1007/s10577-013-9362-z

Zenger, K. R., McKenzie, L. M., and Cooper, D. W. (2002). The first comprehensive genetic linkage map of a marsupial: The tammar wallaby (*Macropus eugenii*). *Genetics* 162 (1), 321–330. doi:10.1093/genetics/162.1.321

Zickler, D., and Kleckner, N. (2015). Recombination, pairing, and synapsis of homologs during meiosis. *Cold Spring Harb. Perspect. Biol.* 7 (6), a016626–a016628. doi:10.1101/cshperspect.a016626

frontiers | Frontiers in Cell and Developmental Biology

TYPE Original Research
PUBLISHED 25 November 2022
DOI 10.3389/fcell.2022.1050556

OPEN ACCESS

EDITED BY
Ricardo Benavente,
Julius Maximilian University of Würzburg, Germany

REVIEWED BY
Alberto Viera,
Autonomous University of Madrid, Spain
Indrajit Nanda,
Julius Maximilian University of Würzburg, Germany

*CORRESPONDENCE
Soledad Berríos,
sberrios@med.uchile.cl

SPECIALTY SECTION
This article was submitted to Nuclear Organization and Dynamics, a section of the journal Frontiers in Cell and Developmental Biology

RECEIVED 21 September 2022
ACCEPTED 14 November 2022
PUBLISHED 25 November 2022

CITATION
Ayarza E, Cavada G, Arévalo T, Molina A and Berríos S (2022), Quantitative analysis of Robertsonian chromosomes inherited by descendants from multiple Rb heterozygotes of *Mus m. Domesticus*. *Front. Cell Dev. Biol.* 10:1050556. doi: 10.3389/fcell.2022.1050556

Quantitative analysis of Robertsonian chromosomes inherited by descendants from multiple Rb heterozygotes of *Mus m. Domesticus*

Eliana Ayarza[1], Gabriel Cavada[2], Tamara Arévalo[3], Alam Molina[3] and Soledad Berríos[3]*

[1]Departamento de Tecnología Médica, Facultad de Medicina, Universidad de Chile, Santiago, Chile, [2]Instituto de Salud Poblacional, Facultad de Medicina, Universidad de Chile, Santiago, Chile, [3]Programa Genética Humana, ICBM, Facultad de Medicina, Universidad de Chile, Santiago, Chile

Robertsonian translocation is the most common chromosomal rearrangement in mammals, and represents the type of chromosomal change that most effectively contributes to speciation in natural populations. Rb translocations involve double-strand DNA breaks at the centromere level in two telocentric chromosomes, followed by repair ligation of the respective long arms, creating a metacentric Rb chromosome. Many different chromosomal races have been described in *Mus musculus domesticus* that show reduced chromosome numbers due to the presence of Rb metacentric chromosomes. The crossroads between ancestral telocentrics and the new metacentric chromosomes should be resolved in the meiotic cells of the heterozygote individuals, which form trivalents. The preferential segregation of metacentric chromosomes to the egg during female meiosis I has been proposed to favor their fixation and eventual conversion of a telocentric karyotype to a metacentric karyotype. This biased segregation, a form of meiotic drive, explains the karyotype changes in mammalian species that have accumulated Rb fusions. We studied and compared the number of Rb chromosomes inherited by the offspring of multiple Rb heterozygous of *M. domesticus* in reciprocal crosses. We did not find that the Rb chromosomes were inherited preferentially with respect to the telocentric chromosomes; therefore, we found no evidence for the meiotic drive, nor was there a random distribution of Rb chromosomes inherited by the descendants.

KEYWORDS

Robertsonian chromosomes, meiotic drive, meiosis, heterozygotes, *Mus domesticus*

Introduction

Robertsonian (Rb) translocation is the most common chromosomal rearrangement in mammals (King 1993) and that most effectively contributes to variation or speciation in natural populations (Garagna et al., 2001a; Aniskin et al., 2006). In *Mus musculus domesticus,* many different chromosomal races have been described that show reduced chromosome numbers due to the presence of metacentric Rb chromosomes (Pialek et al., 2005). Rb translocations involve double-strand DNA breaks at the centromere level in two telocentric chromosomes, followed by fusion of the respective long arms, creating a metacentric Rb chromosome. The short arms (p) of the original telocentric chromosomes, including the proximal telomeres, part of the satellite DNA and, frequently one centromere, are lost (Nanda et al., 1995; Garagna et al., 2001a; Garagna et al., 2002). Most current models of chromosomal variation of natural populations assume that Rb chromosomes are negatively tolerated; only after a long period can the new chromosome could eventually overcome the meiotic restrictions and become established within a reproductive community (Baker and Bickham, 1986; Rieseberg 2001; Hauffe et al., 2012). However, six distinct chromosomal races of the house mice of the Madeira Island have emerged in less than 500 years. This remarkable example of chromosome evolution has been explained by reproductive chromosomal isolation and genetic drift (Britton-Davidian et al., 2000; Britton-Davidian et al., 2005). The crossroads between ancestral telocentrics and new metacentric chromosomes should be resolved in heterozygote individuals, wherein trivalents are formed during meiosis I (Wallace et al., 2002). The Mendelian distribution of metacentric/telocentric chromosomes in the heterozygote gametes will depend on the normal progression of the meiotic prophase, random arrangement of the trivalents at metaphase I, and alternate segregation between them at anaphase. The meiotic drive (also called segregation distortion) is the preferential selection of certain chromosomes or gametes that alters the gene ratio from the Mendelian expectations.

Although multiple Rb heterozygotes showed an increased loss of spermatocytes at prophase I, many of them entered meiotic divisions (Garagna et al., 2001b; Wallace et al., 2002; Manterola et al., 2009). The chromosomes of each trivalent move together into alignment at metaphase and separate from each other at anaphase I. Only gametes resulting from alternate segregation exhibit normal or balanced karyotypes. Gametes produced by adjacent segregations have unbalanced karyotypes, being nullisomic or disomic in one or more chromosomes. Selective mechanisms, such as the metaphase checkpoint, appear to be effective because spermatids resulting from alternate segregation prevail in heterozygotes (Eaker et al., 2001; Anton et al., 2004; Pylyp et al., 2013; Manieu et al., 2014; Lamotte et al., 2018). Additionally, the direction of alternate segregation during female meiosis I could potentially determine whether metacentric chromosomes are transmitted to the offspring (Yoshida and Kitano, 2012).

According to the meiotic drive hypothesis, Rb metacentrics segregated preferentially to the egg in populations that have fixed multiple different metacentrics; and preferentially segregate to the polar body in other populations that have remained telocentric (de Villena and Sapienza 2001; White et al., 2010). It is still unclear what determines the direction of the drive and how that directions can differ between populations, so that some of them retain the fusions and change karyotype, while others do not. The relative centromere strength of Rb metacentric *versus* homologous telocentrics has been proposed to determine the direction of the meiotic drive, with stronger centromeres preferentially remaining in the egg (Chmátal et al., 2014). In addition, asymmetries in the meiotic spindle orientation, tubulin and microtubule-organizing center, and associated meiotic drivers may contribute to explain the meiotic drive in oocytes (Akera et al., 2017; Wu et al., 2018; Kruger and Mueller., 2021).

In this study we attempted to determine whether the meiotic drive could be taking place during the meiosis of Robertsonian heterozygotes of *Mus musculus domesticus* who carry eight Rb chromosomes, by studying the number of Rb chromosomes (0–8), inherited by the descendants of parental males or females who are multiple heterozygous Rb.

Materials and methods

Animals and crosses

Males and females of the Rb heterozygotes 2n = 32 group of *Mus musculus domesticus* were generated by crossing the homozygote strain CD1 2n = 40, with all their chromosomes telocentric, and the homozygote Milano II race 2n = 24, with eight pairs of Rb metacentric chromosomes. The heterozygotes were crossed with homozygotes (2n = 40), to obtain offspring who could inherit between 0 and 8 Rb metacentric chromosomes (Figure 1). The eight Rb chromosomes are: Rb 2.12, 3.4, 5.15, 6.7, 8.11, 9.14, 10.13, 16.17. Numbers correspond to the 2n = 40 standard karyotype. Nineteen crosses of heterozygous females (2n = 32) and homozygous males (2n = 40) were performed with litter, with an average of 4.4 offspring in each. Ten crosses of heterozygous males (2n = 32) and homozygous females (2n = 40) were made with litter, with an average of 5.5 offspring each.

Mice were maintained at 22°C with a light/dark cycle of 12/12 h and fed *ad libitum*. The procedures involving the use of the mice were reviewed and approved by the Ethics Review Committee of the School of Medicine, Universidad de Chile (No. CBA #0441), and by the Ethics Review Committee of the Chilean National Science Foundation FONDECYT-CONICYT. The care and handling of laboratory animals was done following

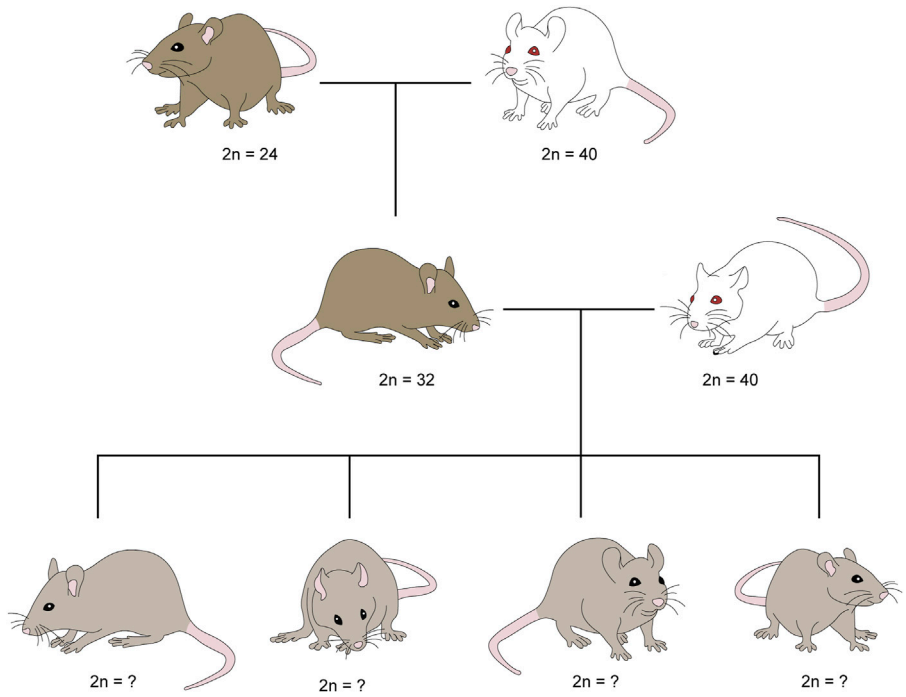

FIGURE 1
Origin of the mice under study that can inherit between 0 and 8 Rb chromosomes. Males and females of Robertsonian (Rb) heterozygotes *2n* = 32 of *Mus musculus domesticus* were generated by crossing homozygotes Milano II race *2n* = 24, with eight pairs of Rb metacentric chromosomes, and homozygote strain CD1 *2n* = 40, with all chromosomes telocentric. In turn, heterozygotes were crossed with homozygotes (*2n* = 40) to obtain offspring who could inherit between 0 and 8 Rb metacentric chromosomes.

all institutional and national guidelines (protocol CBA #0441, FMUCH).

Number of Robertsonian chromosomes and size of pericentromeric region

The number of Rb chromosomes inherited by 139 descendants of female or male Rb heterozygotes was studied in metaphase plate chromosomes obtained from bone marrow cells and stained with Giemsa or DAPI. Briefly, bone marrow cells were incubated for 10 min in 0.05 M KCl at 37°C, and the pellet was washed and fixed in 3:1 v/v methanol: acetic acid. Rb chromosomes and total chromosomes were counted in 10 metaphase plates per animal. After determining the number of Rb metacentric chromosomes, we verified that the telocentric chromosomes actually completed the corresponding diploid number.

The size of the pericentromeric region was measured in the Rb chromosomes inherited by each of the five offspring of a 2n = 32 heterozygous father and a 2n = 40 mother, which were respectively: Three, five, three, two, four, and five Rb chromosomes, respectively. Chromosomes were stained with DAPI (4′, 6-diamino-2-phenylindole), which distinguishes A-T base-rich pericentromeric heterochromatin. Metaphase plates were stained for 10 min in the dark with 10 µl DAPI (Thermo Fisher Scientific®) in 40 µl 1x PBS buffer, washed with 1x PBS buffer, and sealed with coverslips. The samples were observed under a Nikon® Optiphot fluorescence microscope and digitized using a Nikon® Digital Sight DS-5M camera.

The segmented tracing tool of the Fiji software (Just ImageJ, image processing and analysis in Java) was used to measure both chromatids and thus estimate the average total length of each chromosome (TL). The length of the centromeric region (CL) was measured in pixels and normalized with respect to the chromosomal total length (CL/TLx100), to reduce errors caused by differences in chromosome compaction. For each specimen, 20 metaphase plates were studied, and the total values were recorded according to the number of Rb chromosomes present in each metaphase plate. Hence, there were 160 values for the heterozygous parent that had eight Rb chromosomes and only 40 values for the son D that had only two Rb chromosomes. The estimated pericentromeric region length of Rb metacentric chromosomes (CL/TL) for each offspring was compared with the normalized average length of the pericentromeric regions of the eight Rb chromosomes of the parental heterozygote, which was also measured in 20 metaphase plates.

10.3389/fcell.2022.1050556

Statistical analysis

To test the null hypothesis that Rb chromosomes inherited by the offspring of multiple heterozygous parents have a random and equal distribution for the offspring of male and female heterozygous parents, a theoretical binomial distribution with probability p = 0.5 was generated, whose probability function is given as:

$$P(X = x) = \binom{8}{x} 0.5^x, X = 0, 1, 2, 3 \ldots, 8$$

Based on this distribution, the expected frequencies of the appearance of offspring with the Rb chromosome were calculated, and the Chi-2 goodness-of-fit test was used to compare the expected frequencies with those observed. The theoretical distributions, as percentages, are shown in Table 1.

TABLE 1 Expected frequencies of the appearance of offspring with the 0 to 8 Rb chromosomes, calculated on the theoretical binomial distribution with probability p = 0.5.

Descendants according Rb chromosomes inherited	Expected descendants in binomial distribution %
0	0.39
1	3.13
2	10.94
3	21.88
4	27.34
5	21.88
6	10.94
7	3.13
8	0.39
	100.00

We used the binomial proportion test to test the null hypothesis that 50% of the offspring could have a larger pericentromeric region of Rb chromosomes than the centromeric average size of 21.51 of the eight heterozygous father Rb chromosomes. The confidence interval was 95% and 5% was used for statistical significance. The data were processed using STATA v. 16.0.

Results

Number of Rb chromosomes present in the offspring of crosses between Rb heterozygous male or female parents and 2n = 40 homozygotes of ***Mus domesticus***.

We analyzed a total of 139 mice that were descended from crosses between heterozygous 2n = 32 with eight metacentric Rb chromosomes and homozygous 2n = 40 with all telocentric chromosomes were analyzed. Of these, 83 came from the cross of heterozygous females and homozygous males, and 56 from the crosses of heterozygous males and homozygous females (Table 2). In the chromosome set of offspring, 0 to 8 Rb metacentric chromosomes were found; however, in six offspring of heterozygous mothers, Rb chromosomes were absent, and no offspring showed seven Rb chromosomes (Table 2). The total number of Rb chromosomes present in the descendants of heterozygous females and males were 256 and 228, respectively. The average number of chromosomes per each descendants of heterozygous females was 3.08 (38.6%) and that of heterozygous males was 4.07 (50.7%), which shows significant difference (<0.01).

Roughly, the set of 484 Rb chromosomes inherited by the total descendants would be equivalent to approximately 44% of the maximum possible number of 1,112 metacentric Rb

TABLE 2 Number of Rb chromosomes inherited by descendants of crosses between Rb heterozygous male or female parents and homozygotes *2n* = 40, of *Mus m domesticus* mice.

Heterozygous females			Heterozygous males		
Number of Rb chromosomes per cell	**Number of descendants according Rb chromosomes**	**Total Rb chromosomes in offspring**	**Number of Rb chromosomes per cell**	**Number of descendants according Rb chromosomes**	**Total Rb chromosomes in offspring**
0act	6	0	0	2	0
1	7	7	1	1	1
2	22	44	2	5	10
3	10	30	3	14	42
4	20	80	4	14	56
5	15	75	5	10	50
6	2	12	6	5	30
7	0	0	7	1	7
8	1	8	8	4	32
TOTAL	83	256	TOTAL	56	228

TABLE 3 Observed number of descendants by inherited Rb chromosome and expected frequencies according to the binomial distribution. Heterozygous females (p-value = 0.0000); Heterozygous males (p-value = 0.0000).

Number of Rb chromosomes per cell	Heterozygous females		Heterozygous males	
	Number of descendants according Rb chromosomes (Expected)	Number of descendants according Rb chromosomes (Observed)	Number of descendants according Rb chromosomes (Expected)	Number of descendants according Rb chromosomes (Observed)
0	0.3	6	0.22	2
1	2.6	7	1.75	1
2	9.2	22	6.13	5
3	18.4	10	12.25	14
4	23.0	20	15.31	14
5	18.4	15	12.25	10
6	9.2	2	6.13	5
7	2.6	0	1.75	1
8	0.3	1	0.22	4
	83	83	56	56

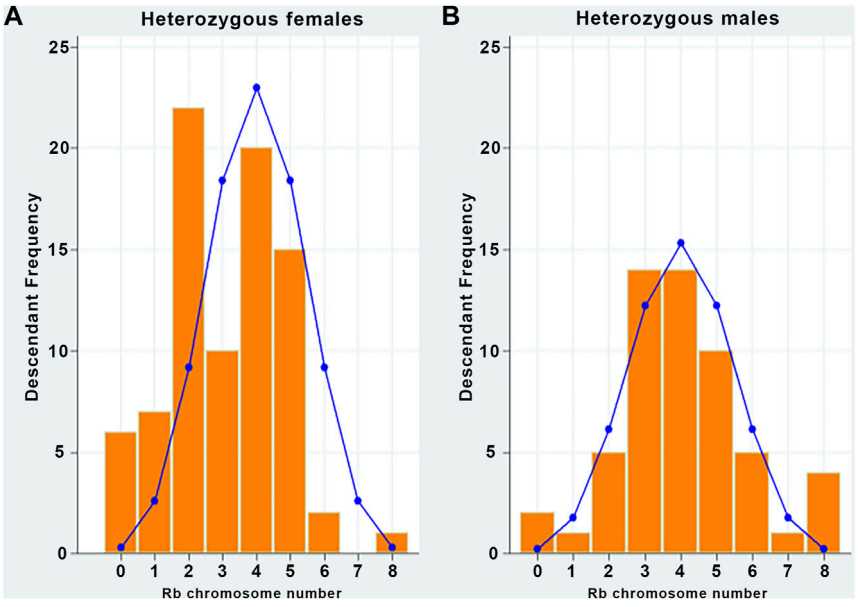

FIGURE 2
Observed frequencies do not fit the theoretical binomial distributions. **(A)** Observed (bars) descendants from heterozygous females by inherited Rb chromosome and expected (curve) frequencies according to the binomial distribution (p-value = 0.0000). **(B)** Observed (bars) descendants from heterozygous male by inherited Rb chromosome and expected (curve) frequencies according to the binomial distribution (p-value = 0.0000).

chromosomes, considering eight Rb chromosomes per 139 descendants. This suggests that although the Rb chromosomes were highly inherited, they were not preferred over telocentric chromosomes.

To assess whether the number of Rb chromosomes inherited by the offspring of multiple heterozygous parents has a random and similar distribution for offspring of male and female heterozygous parents, a theoretical binomial distribution with

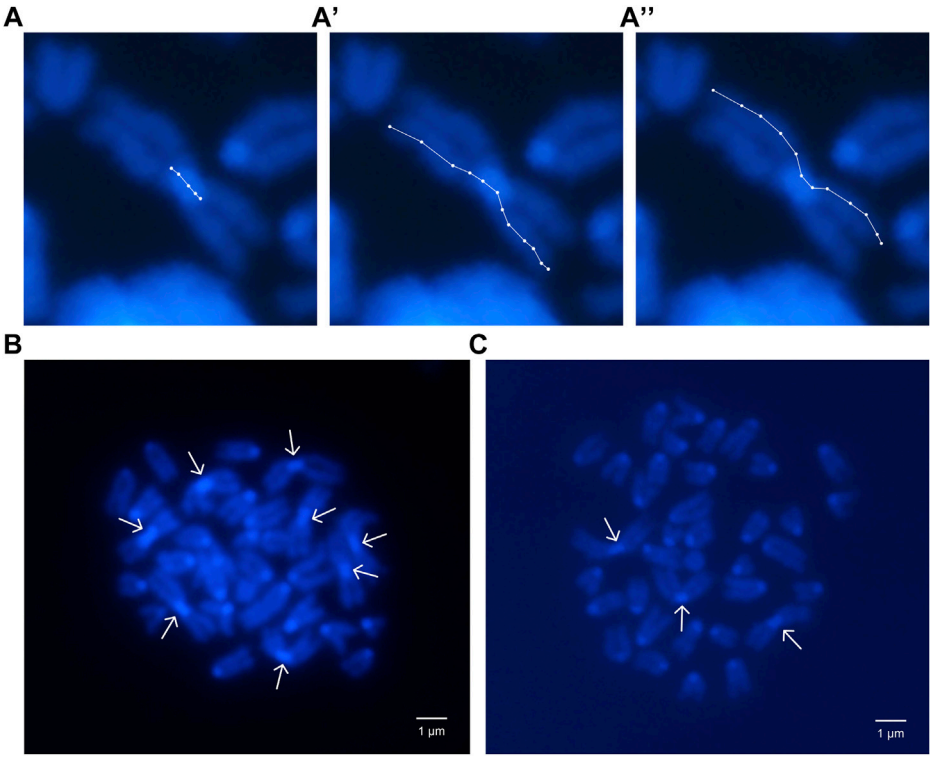

FIGURE 3
Mitotic chromosomes stained with DAPI. **(A)** Pericentromeric region length of a Rb chromosome; **(A',A")** Sister chromatid lengths of same chromosome. **(B)** Heterozygous parent *2n* = 32 metaphase plate. Arrows show 8 metacentric Rb chromosomes. **(C)** Descendent C, *2n* = 37 metaphase plate. Arrows show 3 metacentric Rb chromosomes.

probability $p = 0.5$ was generated and the observed data were compared.

In binomial distributions, the expected frequencies of descendants from heterozygous female or male parents according to the inherited Rb chromosome are shown in Table 3, and the comparison between the observed and the expected frequencies of descendants from female and male heterozygous parents is shown in Figure 2.

In both cases, the null hypothesis was rejected ($p < 0.05$), which means that the data do not follow a binomial distribution pattern; therefore, they can be associated with non-random inheritance.

Pericentromeric region size in Rb chromosomes present in the offspring of crosses between heterozygous Rb males and 2n = 40 homozygous females of ***Mus domesticus***.

The size of the pericentromeric regions of the Rb chromosomes was measured in the eight Rb chromosomes of a 2n = 32 heterozygous male, and in the Rb chromosomes inherited by his six sons (Figure 3). The descendants named A, B, C, D, E, and F presented respectively three, five, three, two, four, and five Rb chromosomes and diploid numbers of 37, 35, 37, 38, 36, and 35, respectively (Table 4).

The length of the pericentromeric regions was estimated as a percentage of CL to TL (Figure 3; Table 4). In five of the six descendants, the length of the pericentromeric region was greater than the average length of the pericentromeric regions of the Rb chromosomes of the father (Table 5). In the offspring of this family, the ratio 5/6 is greater than 0.5 (inheritance by chance) and $p = 0.0512$.

Discussion

Since the first observation of chromosome behavior during meiosis in the grasshopper *Brachystola* (Sutton 1903; Carothers 1917), the segregation of homologous chromosomes during meiosis is widely considered as being fundamentally random. However, clear examples have been described in various organisms where meiotic drive or distortion with respect to random meiotic segregation occurs (Bongiorni et al., 2004; Presgraves, 2009; Dawe et al., 2018; Malinovskaya et al., 2020; Kruger and Mueller, 2021; Pajpach et al., 2021).

In natural populations of *Mus domesticus*, a totally telocentric ancestral karyotype, Robertsonian translocations or centric mergers occur that originate from Rb metacentric

TABLE 4 Diploid number, Rb chromosomes and lengths of the pericentromeric regions of Rb chromosomes in the members of a family composed by a multiple Rb heterozygous male and a homozygous female *2n* = 40 and their six offspring. The length of the centromeric region (CL) was measured in pixels and normalized with respect to the chromosomal total length (CL/TLx100).

Animal	Diploid number	Number of Rb chromosomes	Pericentromeric length (CL/TL)%
Rb heterozygous male parent	2n = 32	8	21.51%
Descendant A	2n = 37	3	21.11%
Descendant B	2n = 35	5	25.61%
Descendant C	2n = 37	3	21.7%
Descendant D	2n = 38	2	26.28%
Descendant E	2n = 36	4	25.22%
Descendant F	2n = 35	5	22.29%
Homozygous female parent	2n = 40	0	--

TABLE 5 In 5 of the 6 descendants, the length of the pericentromeric region was verified to be greater than the average length of the pericentromeric regions of the Rb chromosomes of the father. The ratio 5/6 is greater than 0.5 (inheritance by chance) $p = 0.0512$.

Pericentromeric lengths (CL/TL) of descendants%	Father's Rb pericentromeric region length%	Descendants with greater pericentromeric region lengths
21.11	21.51	0
26.61	21.51	1
21.7	21.51	1
26.28	21.51	1
25.22	21.51	1
22.29	21.51	1

chromosomes and reduce the chromosome number (Pialek et al., 2005). Given the unusual speed with that Rb chromosomes have set in some populations, it has been proposed that Rb chromosomes can be inherited preferentially with respect to the ancestral telocentrics in the descendants of heterozygotes (Britton-Davidian et al., 2000; Britton-Davidian et al., 2005). In these cases, the meiotic drive or preferential segregation of some of the chromosomal forms were observed (de Villena and Sapienza, 2001; White et al., 2010; Clark and Akera, 2021).

Crossroads between both chromosomal forms are found in heterozygotes; in the first meiotic prophase, the metacentric Rb chromosome synapsed with the telocentrics, homologous to their arms, forming a trivalent, and subsequently, must segregate between them (Wallace et al., 2002). Although multiple Rb heterozygotes have a loss of spermatocytes at prophase I and majorly at meiotic divisions produce gametes and are fertile (Garagna et al., 2001b; Wallace et al., 2002; Manterola et al., 2009).

In Rb heterozygous males, gametes produced by alternate meiotic segregation, in which the Rb metacentric chromosome separates from the telocentric chromosomes, seem to predominate (Manieu et al., 2014). In human males heterozygous for one Robertsonian chromosome, 70%–80% of the total gametes are normal or balanced gametes (Wang et al., 2017; Lamotte et al., 2018).

In this study, we analyzed whether Rb chromosomes were preferentially inherited with respect to the telocentric chromosomes, by the offspring of heterozygous males and females for eight Rb chromosomes. Our data showed that offspring inherited between 0 and 8 Rb chromosomes and that the distribution of frequencies was not binomial. The non-binomial distribution of the descendants of any of the heterozygous parents suggests that the number of inherited Rb chromosomes would not be a random process, at least in quantitative terms, because Rb chromosomes have not been distinguished between them. We did not find that descendants of heterozygous females inherited more Rb chromosomes than those of heterozygous males. In contrast, we found that male descendants presented a significantly higher number of Rb chromosomes.

Obviously, these results were obtained from heterozygotes of crosses of the CD1 strain (2n = 40) with the Milano II race (2n = 24), and therefore cannot be directly extrapolated to all the *Mus musculus domesticus* strains/races.

The configuration of the trivalent in the meiotic prophase of Rb heterozygotes could favor the alternating segregation of the

anaphase, but this chromosomal configuration could also be relevant in the fixation of the Rb chromosomes in hybrid populations. This could be because this synaptic configuration ensures an obligatory encounter between the Rb chromosome and its telocentric homologous chromosomes, giving rise to the closeness of the abundant pericentromeric heterochromatin of the three gathered chromosomes (Berríos et al., 2014; Berríos 2017). This chromosomal conjunction, which is reiterated in thousands of cells, may also contribute to a second-centric fusion. In addition to the mentioned chromosomal configuration of first meiotic prophase, the intense DNA nicking and repair activity (Neale and Keeney 2006) and the homology of satDNA sequences shared by the mouse telocentric chromosomes create the conditions for new chromosomal rearrangements (Garagna et al., 2001a; Kalitsis et al., 2006). In this way, the concurrence of elements that could favor new chromosome-centric fusions would enhance the chance of those chromosomes regaining the homozygous condition.

The successful fixation of an Rb chromosome in natural populations is the result of the meeting of heterozygotes and the production of homozygous descendants. Any meiotic condition that favors Rb chromosomes in gametes also contributes to the fixation of Rb chromosomes.

The hypothesis that heterozygous females would transfer more Rb chromosomes to their offspring than males arises from findings in different organisms (de Villena and Sapienza, 2001; Fishman and Saunders, 2008; Presgraves, 2009; Dudka and Lampson, 2022). In addition, segregational asymmetry is difficult to explain in males, whereas in female meiosis, such asymmetry is possible because the chromosomes that eventually remain in the oocyte can be inherited, while those that remain in the polocytes are necessarily lost (Lindholm et al., 2016). In this scenario, the differences in centromere strength has been shown to predict the direction of driving. Stronger centromeres, manifested by increased kinetochore protein levels and specific interactions with spindle microtubules, would produce chromosomes that are preferentially retained in the egg (Chmatal et al., 2014; Akera et al., 2017; Wu et al., 2018).

Considering that the main cellular mechanism proposed has been focused on centromere size and its segregational advantage, we found it interesting to show what was observed in the measurement of the pericentromeric and centromeric regions of Rb chromosomes in six descendants of an Rb heterozygote. In mice, the centromeric region contains repetitive centromeric DNA sequences that are enriched in minor satellite repeats, which are prominent sites for centromeric proteins CENP-A and CENP-B assembly (Guenatri et al., 2004; Pajpach et al., 2021). The mouse pericentromeric region contains inactive chromatin and is composed of major satellite repeats, that are required for heterochromatin formation (Guenatri et al., 2004; Pajpach et al., 2021). In 5/6 of the sons, the average size of the centromeric region of the inherited Rb chromosomes was found to be significantly larger than the average size of the same region in the eight Rb chromosomes of the heterozygous male parent. The measurement made involved the centromeric DNA and the abundant pericentromeric heterochromatin located in the proximal p and q regions of the Rb chromosomes. These observations are not comparable with the cellular analyses of segregational efficiency in meiosis of the Rb chromosome according to the size and strength of its centromere because our measurements included the pericentromeric heterochromatin that we do not know how much it may contribute to the meiotic segregation of chromosomes (Chmatal et al., 2014; Iwata-Otsubo et al., 2017). On the other hand, the centromeric region sizes estimated here are on Rb chromosomes that have successfully appeared in the descendants, after overcoming meiotic segregation, gamete differentiation, fertilization, embryonic development and birth. This observation suggests that the larger size of the entire centromeric region is advantageous to the inherited Rb chromosomes.

Data availability statement

The raw data supporting the conclusion of this article will be made available by the authors, without undue reservation.

Ethics statement

The animal study was reviewed and approved by Ethics Review Committee of the School of Medicine, Universidad de Chile (No. CBA #0441), and by the Ethics Review Committee of the Chilean National Science Foundation FONDECYT-CONICYT.

Author contributions

SB wrote most of the manuscript. GC performed the statistical analyses. EA was responsible for the cross and karyotype analysis. TA made the metaphase plates and AM measured the centromeric regions. All authors have contributed to the manuscript and approved the submitted version.

Funding

This work was supported by the Comisión Superior de Investigación Científica (CONICYT-Chile) grant to SB.

Acknowledgments

Male and female specimens from the original natural populations were donated to our laboratory by Dr. Carlo Redi

and Dr. Silvia Garagna from Pavia University, Italy, as part of a collaborative research project.

Conflict of interest

The authors declare that the research was conducted in the absence of any commercial or financial relationships that could be construed as a potential conflict of interest.

Publisher's note

All claims expressed in this article are solely those of the authors and do not necessarily represent those of their affiliated organizations, or those of the publisher, the editors and the reviewers. Any product that may be evaluated in this article, or claim that may be made by its manufacturer, is not guaranteed or endorsed by the publisher.

References

Akera, T., Chmátal, L., Trimm, E., Yang, K., Aonbangkhen, C., Chenoweth, D. M., et al. (2017). Spindle asymmetry drives non-Mendelian chromosome segregation. *Science* 358, 668–672. doi:10.1126/science.aan0092

Aniskin, V. M., Benazzou, T., Biltueva, L., Dobigny, G., Granjon, L., and Volobouev, V. (2006). Unusually extensive karyotype reorganization in four congeneric Gerbillus species (Muridae: Gerbillinae). *Cytogenet. Genome Res.* 112, 131–140. doi:10.1159/000087525

Anton, E., Blanco, J., Egozcue, J., and Vidal, F. (2004). Sperm FISH studies in seven male carriers of robertsonian translocation t(13;14)(q10; q10). *Hum. Reprod.* 19, 1345–1351. doi:10.1093/humrep/deh232

Baker, R. J., and Bickham, J. W. (1986). Speciation by monobrachial centric fusions. *Proc. Natl. Acad. Sci. U. S. A.* 83 (21), 8245–8248. doi:10.1073/pnas.83.21.8245

Berríos, S. (2017). Nuclear architecture of mouse spermatocytes: Chromosome topology, heterochromatin, and nucleolus. *Cytogenet. Genome Res.* 151, 61–71. doi:10.1159/000460811

Berríos, S., Manieu, C., Page, J., Ayarza, E., Lopez-Fenner, J., Manterola, M., et al. (2014). Robertsonian chromosomes and the nuclear architecture of mouse meiotic prophase spermatocytes. *Biol. Res.* 47 (1), 16–24. doi:10.1186/0717-6287-47-16

Bongiorni, S., Fiorenzo, P., Pippoletti, D., and Prantera, G. (2004). Inverted meiosis and meiotic drive in mealybugs. *Chromosoma* 112, 331–341. doi:10.1007/s00412-004-0278-4

Britton-Davidian, J., Catalan, J., da Gracia Ramalhinho, M., Ganem, G., Auffray, J. C., Capela, R., et al. (2000). Rapid chromosomal evolution in island mice. *Nature* 403, 158. doi:10.1038/35003116

Britton-Davidian, J., Catalan, J., Ramalhinho, M. G., Auffray, J. C., Nunes, A. C., Gazave, E., et al. (2005). Chromosomal phylogeny of robertsonian races of the house mouse on the island of Madeira: Testing between alternative mutational processes. *Genet. Res.* 86, 171–183. doi:10.1017/S0016672305007809

Carothers, E. E. (1917). The segregation and recombination of homologous chromosomes as found in two genera of Acrididae (Orthoptera). *J. Morphol.* 26, 445–521. doi:10.1002/jmor.1050280205

Chmátal, L., Gabriel, S. I., Mitsainas, G. P., Martínez-Vargas, J., Ventura, J., Searle, J. B., et al. (2014). Centromere strength provides the cell biological basis for meiotic drive and karyotype evolution in mice. *Curr. Biol.* 24 (19), 2295–2300. doi:10.1016/j.cub.2014.08.017

Clark, F. E., and Akera, T. (2021). Unravelling the mystery of female meiotic drive: Where we are. *Open Biol.* 11 (9), 210074. doi:10.1098/rsob.210074

Dawe, R. K., Lowry, E. G., Gent, J. I., Harkess, A. E., Hodges, A. L., Hiatt, E. N., et al. (2018). A kinesin-14 motor activates neocentromeres to promote meiotic drive in maize. *Cell* 173, 839–850. doi:10.1016/j.cell.2018.03.009

de Villena, F. P. M., and Sapienza, C. (2001). Female meiosis drives karyotypic evolution in mammals. *Genetics* 159, 1179–1189. doi:10.1093/genetics/159.3.1179

Dudka, D., and Lampson, M. A. (2022). Centromere drive: Model systems and experimental progress. *Chromosome Res.* 30, 187–203. doi:10.1007/s10577-022-09696-3

Eaker, S., Pyle, A., Cobb, J., and Handel, M. A. (2001). Evidence for meiotic spindle checkpoint from analysis of spermatocytes from Robertsonian chromosome heterozygous mice. *J. Cell Sci.* 114, 2953–2965. doi:10.1242/jcs.114.16.2953

Fishman, L., and Saunders, A. (2008). Centromere-associated female meiotic drive entails male fitness costs in monkeyflowers. *Science* 322 (5907), 1559–1562. doi:10.1126/science.1161406

Garagna, S., Marziliano, N., Zuccotti, M., Searle, J. B., Capanna, E., and Redi, C. A. (2001a). Pericentromeric organization at the fusion point of mouse Robertsonian translocation chromosomes. *Proc. Natl. Acad. Sci. U. S. A.* 98, 171–175. doi:10.1073/pnas.98.1.171

Garagna, S., Zuccotti, M., Capanna, E., and Redi, C. A. (2002). High-resolution organization of mouse telomeric and pericentromeric DNA. *Cytogenet. Genome Res.* 96, 125–129. doi:10.1159/000063028

Garagna, S., Zuccotti, M., Thornhill, A., Fernández-Donoso, R., Berrios, S., Capanna, E., et al. (2001b). Alteration of nuclear architecture in male germ cells of chromosomally derived subfertile mice. *J. Cell Sci.* 114, 4429–4434. doi:10.1242/jcs.114.24.4429

Guenatri, M., Bailly, D., Maison, C., and Almouzni, G. (2004). Mouse centric and pericentric satellite repeats form distinct functional heterochromatin. *J. Cell Biol.* 166, 493–505. doi:10.1083/jcb.200403109

Hauffe, H. C., Gimenez, M. D., and Searle, J. B. (2012). "Chromosomal hybrid zones in the house mouse," in *Evolution of the house mouse*. Editors M. Macholán, S. J. E. Baird, P. Munclinger, and J. Piálek (Cambridge: Cambridge University Press), 407–430.

Iwata-Otsubo, A., Dawicki-McKenna, J. M., Akera, T., Falk, S. J., Chmátal, L., Yang, K., et al. (2017). Expanded satellite repeats amplify a discrete CENP-A nucleosome assembly site on chromosomes that drive in female meiosis. *Curr. Biol.* 7 (2715), 2365–2373. e8. doi:10.1016/j.cub.2017.06.069

Kalitsis, P., Griffiths, B., and Choo, K. H. A. (2006). Mouse telocentric sequences reveal a high rate of homogenization and possible role in Robertsonian translocation. *Proc. Natl. Acad. Sci. U. S. A.* 103, 8786–8791. doi:10.1073/pnas.0600250103

King, M. (1993). *Species evolution: The role of chromosome change*. Cambridge (UK): Cambridge University Press.

Kruger, A. N., and Mueller, J. L. (2021). Mechanisms of meiotic drive in symmetric and asymmetric meiosis. *Cell. Mol. Life Sci.* 78 (7), 3205–3218. doi:10.1007/s00018-020-03735-0

Lamotte, A., Martinez, G., Devillard, F., Hograindleur, J. P., Satre, V., Coutton, C., et al. (2018). Is sperm FISH analysis still useful for robertsonian translocations? Meiotic analysis for 23 patients and review of the literature. *Basic Clin. Androl.* 28 (5), 5–11. doi:10.1186/s12610-018-0069-z

Lindholm, A. K., Dyer, K. A., Firman, R. C., Fishman, L., Forstmeier, W., Holman, L., et al. (2016). The ecology and evolutionary dynamics of meiotic drive. *Trends Ecol. Evol.* 31, 315–326. doi:10.1016/j.tree.2016.02.001

Malinovskaya, L. P., Zadesenets, K. S., Karamysheva, T. V., Akberdina, E. A., Kizilova, E. A., Romanenko, M. V., et al. (2020). Germline-restricted chromosome (GRC) in the sand Martin and the pale Martin (Hirundinidae, Aves): Synapsis, recombination and copy number variation. *Sci. Rep.* 10, 1058–1110. doi:10.1038/s41598-020-58032-4

Manieu, C., González, M., López-Fenner, J., Page, J., Ayarza, E., Fernández-Donoso, R., et al. (2014). Aneuploidy in spermatids of Robertsonian (Rb) chromosome heterozygous mice. *Chromosome Res.* 22, 545–557. doi:10.1007/s10577-014-9443-7

Manterola, M., Page, J., Vasco, C., Berríos, S., Parra, M. T., Viera, A., et al. (2009). A high incidence of meiotic silencing of unsynapsed chromatin is not associated with substantial pachytene loss in heterozygous male mice carrying multiple simple Robertsonian translocations. *PLoS Genet.* 5, e1000625. doi:10.1371/journal.pgen.1000625

Nanda, I., Schneider-Rasp, S., Winking, H., and Schmid, M. (1995). Loss of telomeric sites in the chromosomes of *Mus musculus* domesticus (Rodentia: Muridae) during Robertsonian rearrangements. *Chromosome Res.* 3, 399–409. doi:10.1007/BF00713889

Pajpach, F., Wu, T., Shearwin-Whyatt, L., Jones, K., and Grützner, F. (2021). Flavors of non-random meiotic segregation of autosomes and sex chromosomes. *Genes (Basel)* 12 (9), 1338–1360. doi:10.3390/genes12091338

Pialek, J., Hauffe, H. C., and Searle, J. B. (2005). Chromosomal variation in the house mouse. *Biol. J. Linn. Soc. Lond.* 84, 535–563. doi:10.1111/j.1095-8312.2005.00454.x

Presgraves, D. (2009). "Drive and sperm," in *The evolution and genetics of male meiotic drive*. Editors T. Birkhead, D. Hosken, and S. Pitnick. 1st ed. (Amsterdam, Netherlands: Elsevier). 9780123725684.

Pylyp, L. Y., Zukin, V. D., and Bilko, N. M. (2013). Chromosomal segregation in sperm of Robertsonian translocation carriers. *J. Assist. Reprod. Genet.* 30 (9), 1141–1145. doi:10.1007/s10815-013-0067-1

Rieseberg, L. H. (2001). Chromosomal rearrangements and speciation. *Trends Ecol. Evol.* 16, 351–358. doi:10.1016/s0169-5347(01)02187-5

Sutton, W. S. (1903). The chromosomes in heredity. *Biol. Bull.* 4, 231–250. doi:10.2307/1535741

Wallace, B. M. N., Searle, J. B., and Everett, C. A. (2002). The effect of multiple simple Robertsonian heterozygosity on chromosome pairing and fertility of wild-stock house mice (*Mus musculus* domesticus). *Cytogenet. Genome Res.* 96, 276–286. doi:10.1159/000063054

Wang, B., Nie, B., Tang, D., Li, R., Liu, X., Song, J., et al. (2017). Analysis of meiotic segregation patterns and interchromosomal effects in sperm from 13 robertsonian translocations. *Balk. J. Med. Genet.* 20 (1), 43–50. doi:10.1515/bjmg-2017-0003

White, T. A., Bordewich, M., and Searle, J. B. (2010). A network approach to study karyotypic evolution: The chromosomal races of the common shrew (*Sorex araneus*) and house mouse (*Mus musculus*) as model systems. *Syst. Biol.* 59, 262–276. doi:10.1093/sysbio/syq004

Wu, T., Lane, S. I. R., Morgan, S. L., and Jones, K. T. (2018). Spindle tubulin and MTOC asymmetries may explain meiotic drive in oocytes. *Nat. Commun.* 9, 2952. doi:10.1038/s41467-018-05338-7

Yoshida, K., and Kitano, J. (2012). The contribution of female meiotic drive to the evolution of neo-sex chromosomes. *Evolution* 66 (10), 3198–3208. doi:10.1111/j.1558-5646.2012.01681.x

frontiers | Frontiers in Cell and Developmental Biology

TYPE Review
PUBLISHED 29 November 2022
DOI 10.3389/fcell.2022.1069064

OPEN ACCESS

EDITED BY
Mónica Pradillo,
Complutense University of Madrid,
Spain

REVIEWED BY
Akira Shinohara,
Osaka University, Japan
Judith Yanowitz,
Magee-Womens Research Institute,
United States

*CORRESPONDENCE
Cristina Martín-Castellanos,
cmartin@usal.es

SPECIALTY SECTION
This article was submitted to Nuclear Organization and Dynamics, a section of the journal Frontiers in Cell and Developmental Biology

RECEIVED 13 October 2022
ACCEPTED 14 November 2022
PUBLISHED 29 November 2022

CITATION
Palacios-Blanco I and Martín-Castellanos C (2022), Cyclins and CDKs in the regulation of meiosis-specific events.
Front. Cell Dev. Biol. 10:1069064.
doi: 10.3389/fcell.2022.1069064

Cyclins and CDKs in the regulation of meiosis-specific events

Inés Palacios-Blanco and Cristina Martín-Castellanos*

Instituto de Biología Funcional y Genómica (IBFG), CSIC-USAL, Salamanca, Spain

How eukaryotic cells control their duplication is a fascinating example of how a biological system self-organizes specific activities to temporally order cellular events. During cell cycle progression, the cellular level of CDK (Cyclin-Dependent Kinase) activity temporally orders the different cell cycle phases, ensuring that DNA replication occurs prior to segregation into two daughter cells. CDK activity requires the binding of a regulatory subunit (cyclin) to the core kinase, and both CDKs and cyclins are well conserved throughout evolution from yeast to humans. As key regulators, they coordinate cell cycle progression with metabolism, DNA damage, and cell differentiation. In meiosis, the special cell division that ensures the transmission of genetic information from one generation to the next, cyclins and CDKs have acquired novel functions to coordinate meiosis-specific events such as chromosome architecture, recombination, and synapsis. Interestingly, meiosis-specific cyclins and CDKs are common in evolution, some cyclins seem to have evolved to acquire CDK-independent functions, and even some CDKs associate with a non-cyclin partner. We will review the functions of these key regulators in meiosis where variation has specially flourished.

KEYWORDS

meiosis, prophase, cyclins, CDKs, nuclear architecture, recombination, synapsis, substrates

Introduction

Meiosis is the cell division program that ensures sexual reproduction by the generation of haploid gametes from diploid cells. Different meiosis-specific hallmarks help to the accurate partitioning and shuffling of the genetic information, which is essential for the viability of gametes, and the efficient transmission and variability of genomes from one generation to the next. These characteristics range from a new nuclear architecture, the formation of a highly organized zipper-like structure between homologous chromosomes (synaptonemal complex, SC) and the promotion of homologous recombination, to the mono-orientation of sister-kinetochores and the sequential degradation of sister-chromatid cohesion (Petronczki et al., 2003; Marston and Amon, 2004; Sakuno and Watanabe, 2009; Keeney et al., 2014; Lam and Keeney, 2014; Zickler and Kleckner, 2015). As a result of these new meiotic features, gametes receive the correct number of chromosomes that after fertilization will ensure the

maintenance of species ploidy. Errors during meiosis produce gametes with an abnormal number of chromosomes (aneuploidy), that in some species such as mammals (specially in humans) are very frequent and the leading cause of miscarriages (Hassold et al., 2007; Hunt and Hassold, 2010; Nagaoka et al., 2012). In addition, deregulation of meiotic genes in somatic cells is a common feature of cancer cells, probably contributing to their characteristic genomic instability (Tuna et al., 2009; Folco et al., 2017; Sou et al., 2022).

As in the case of the mitotic cell cycle, meiotic progression is driven by kinase activities provided by cyclin-CDK (Cyclin-Dependent Kinase) complexes, a serine/threonine kinase bound to a regulatory cyclin subunit (Morgan, 1995). In unicellular eukaryotes such as yeasts, a unique CDK binds to different cyclins to temporally order the cell cycle phases, ensuring that DNA replication (S-phase) occurs prior to segregation into two daughter cells (M-phase); and in fission yeast, even a single cyclin-CDK complex is sufficient to drive a "minimal" mitotic and meiotic cycle (Stern and Nurse, 1996; Coudreuse and Nurse, 2010; Uhlmann et al., 2011; Gutierrez-Escribano and Nurse, 2015). Notably, early cell cycle substrates are very efficiently phosphorylated and require lower CDK activity than the late targets, what contributes to the sequential ordering of S and M-phases (Swaffer et al., 2016). From this minimal conception of the cell cycle, cyclins and CDKs have evolved and diversified, especially in organisms with a more complex developmental biology as higher eukaryotes, indicating a corresponding expansion of functions (Harashima et al., 2013; Malumbres, 2014). Functional diversification of CDK activities is clearly observed in meiosis, where CDK complexes already present in vegetative cells have acquired novel meiotic functions, and meiosis-specific variants have also emerged. We will review these aspects of cyclins and CDKs in meiosis, focusing on their meiosis-specific functions. The meiotic-progression properties of CDK complexes have been recently reviewed (Chotiner et al., 2019; Li et al., 2019; Palmer et al., 2019; MacKenzie and Lacefield, 2020). Phosphorylation networks conducted by several kinases during meiotic prophase are also reviewed in (Kar and Hochwagen, 2021).

Meiosis-specific events regulated by cyclins and CDKs

A key difference from mitosis is the establishment in meiosis of an extended gap phase (G2), known as meiotic prophase, prior to chromosome segregation. Prophase is cytologically visualized by the remodeling of the nuclear architecture and the formation of the SC or related structures. During prophase, homologous chromosomes align, tightly pair, and recombine. In organisms with a canonical SC, meiotic prophase is divided in different stages depending on the SC assembly; and in budding yeast, mouse, and plants, SC formation and recombination are functionally linked (Padmore et al., 1991; Cohen and Pollard, 2001; Hunter and Kleckner, 2001; Zickler and Kleckner, 2015). Briefly, recombination is initiated by programmed Double-Strand Breaks (DSBs) in the DNA during leptotene, when axial elements of the SC are forming. Processing of these DSBs generates single-stranded DNA nucleofilaments that invade the homologous chromosome searching for homology, which brings homologs closer and promotes local nucleation of the central element of the SC (zygotene). Full SC assembly along the entire chromosome length is the hallmark of pachytene, which correlates with the production of DNA joint molecules between homologs. Finally, at diplotene SC disassembles and resolution of the joint molecules generates final recombination products (Figure 1A). As discuss below, CDKs, cyclins, and non-cyclin CDK activators play an important role in these aspects of meiotic prophase (Figure 1B and Table 1).

Nuclear architecture

A conserved feature of meiosis is the remodeling of the nuclear architecture to acquire the so-called *bouquet* configuration (Bass, 2003; Harper et al., 2004; Tomita and Cooper, 2006; Scherthan, 2007; Klutstein and Cooper, 2014). Telomeres, that during vegetative cycle are scattered around the nuclear periphery, polarize in tight proximity to the nuclear envelope (NE), in some organisms close by or even bound to the centrosome. This reorganization requires telomere anchoring to the Linker Nucleoskeleton and Cytoskeleton (LINC)-complex, which is composed of SUN (Sad1, UNC-84) and KASH (Klarsicht, ANC-1, Syne homology) family proteins. SUN-domain proteins are inserted in the inner nuclear membrane and KASH-domain proteins are inserted in the outer nuclear membrane, interacting in the transluminal space. The binding of telomeres to this complex is mediated by meiosis-specific proteins that provide the connection of chromosomes with the cytoskeleton, and, in doing so, promote chromosomal movements that facilitate proper chromosome alignment and recombination (Hiraoka and Dernburg, 2009; Koszul and Kleckner, 2009; Shibuya and Watanabe, 2014; Link et al., 2015; Shibuya et al., 2015; Fan et al., 2022). Depending on the organisms, the *bouquet* configuration is a transient feature or it can be maintained during the entire meiotic prophase. This is the case of the fission yeast *Schizosaccharomyces pombe* where, in the absence of a canonical SC, *bouquet*-led chromosome movements have acquired a prominent role in chromosome pairing (Ding et al., 2004). In addition, this nuclear configuration seems to play unanticipated functions in centromere maturation and spindle formation (Tomita and Cooper, 2007; Klutstein et al., 2015).

The striking stable *bouquet* structure and its extremely vigorous motion has made fission yeast an extensively used model to study *bouquet* formation and chromosome movements (Yamamoto and Hiraoka, 2001). In this organism,

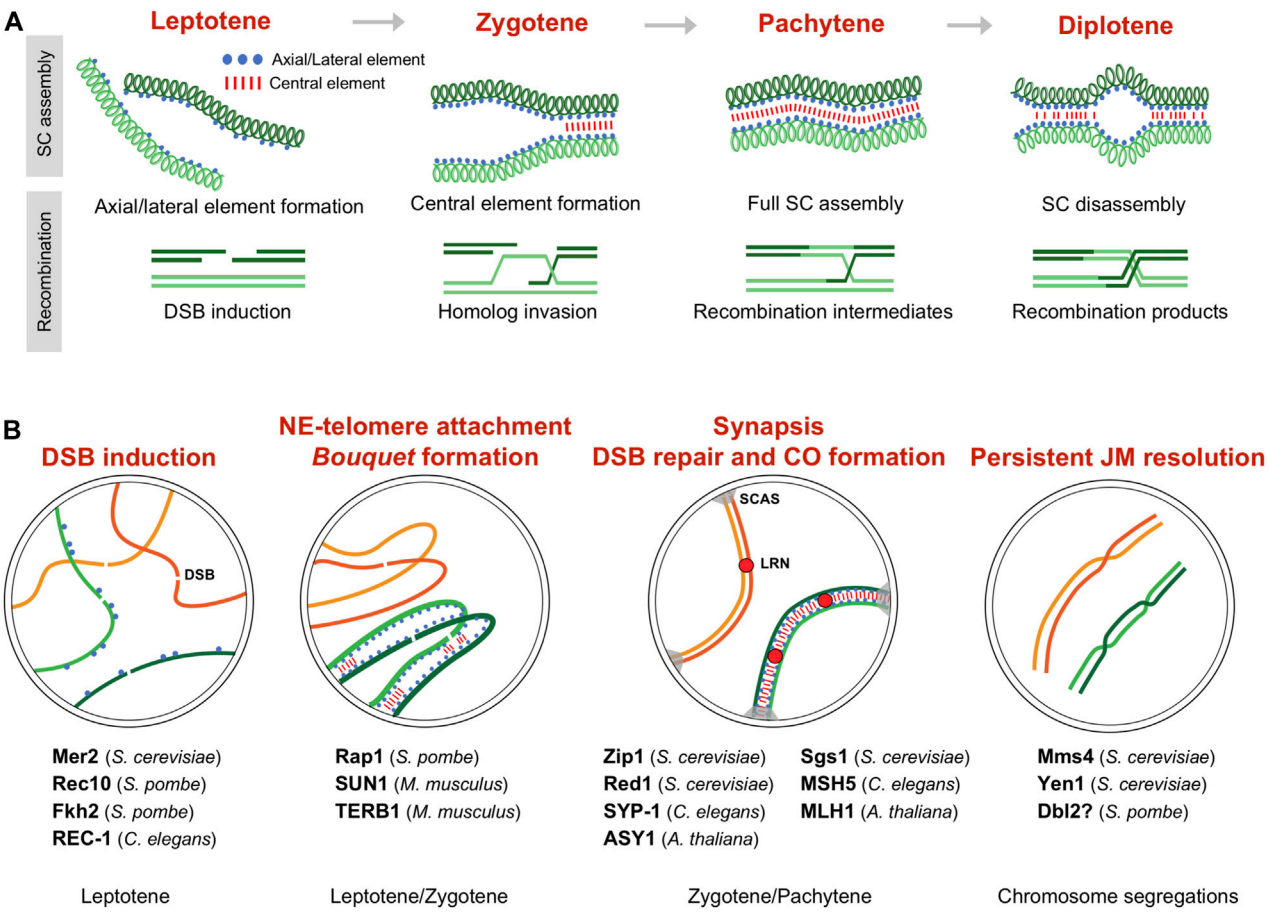

FIGURE 1
Meiotic prophase and CDK activity. **(A)** Synaptonemal complex (SC) formation and recombination during meiotic prophase between a pair of homologous chromosomes. Prophase is divided in different stages depending on the SC assembly (upper scheme). Recombination occurs in the context of the SC (lower scheme), and, in some organisms, it is linked to SC formation; for simplicity only the chromatid pair involved in recombination is depicted. **(B)** Meiotic events regulated by CDK activity and substrates. The regulated processes during the different prophase stages are highlighted. Identified substrates indicating the species are listed. SC assembly is shown only in one pair of homologs (green colored). DSB double-strand break, SCAS synaptonemal complex attachment sites, LRN late recombination nodule.

telomere binding to the Spindle Pole Body (centrosome equivalent) is mediated by pheromone-induced Bqt1 and Bqt2. These proteins connect the conserved telomeric protein Rap1 and the SPB-component Sad1 (SUN-domain protein). This interaction initially delocalizes Sad1 to the scattered telomeres at the NE, and the subsequent travelling of Sad1 back to the SPB promotes the *bouquet* formation (Chikashige et al., 2006; Tomita and Cooper, 2006). Since Sad1 is a NE protein, Bqt1-Bqt2 binding requires previous telomere-NE association, which is mediated by the binding of Rap1 to the NE-anchoring complex Bqt3-Bqt4 during vegetative cell cycle (Chikashige et al., 2009) (Figure 2). Notably, Cdc2 (CDK) and the meiosis-specific Crs1 cyclin localize to the SPB during *bouquet* (Moiseeva et al., 2017; Bustamante-Jaramillo et al., 2021). Crs1 localization is independent of *bouquet* formation, and in the absence of Crs1 the clustering of telomeres is unstable though the integrity of the SPB is preserved (Bustamante-Jaramillo et al., 2021). Although less severe, this phenotype is reminiscent of the defects observed in *bqt1* and *bqt2* mutants. As for *bqt1* and *bqt2*, *crs1* gene expression is induced by pheromone signaling, the protein localizes at the SPB in early prophase, and it remains at SPBs in meiosis I (Chikashige et al., 2006; Tang et al., 2006; Bustamante-Jaramillo et al., 2021). At present, it is not known how Crs1 influences telomere positioning during meiosis and whether it is required for the localization of Bqt1-Bqt2 proteins at the SPB.

Interestingly, Rap1 is highly phosphorylated during meiotic prophase, including at five Cdc2 sites, raising the possibility that CDK phosphorylation could modulate Rap1 interaction with Bqt1-Bqt2 proteins (Amelina et al., 2015) (Figure 2). Three of

TABLE 1 CDK substrates in meiotic prophase.

Substrate	Organism	Residues	Evidences	Function	References
Mer2	*S. cerevisiae*	S30	*In vitro* kinase assay, SDS-PAGE mobility, CDK inhibition (*cdc28-as1*), *mer2*^{S30A} and *mer2*^{S30D} phosphomutants	DSB formation	Henderson et al. (2006); Wan et al. (2008)
Rec10	*S. pombe*	S347, T482, and S529	Mass spectrometry	DSB formation (*rec10*^{8A} no recombination phenotype)	Spirek et al. (2010); Bustamante-Jaramillo et al. (2019)
Fkh2	*S. pombe*	S481	*In vitro* kinase assay, SDS-PAGE mobility, EMSA assays, *fkh2*^{S481A} and *fkh2*^{S481D} phosphomutants	Transcriptional activation of mid-meiotic genes	Alves-Rodrigues et al. (2016)
REC-1	*C. elegans*	T39, T96, T160, **S146**, S205, S218, S281, T305	*In vitro* peptide array, *in vitro* kinase assay, CDK inhibition S146 (Roscovitine)	DSB formation (*rec-1*$^{8S/TA}$ and *rec-1*$^{8S/TD}$ loss-of-function phenotype)	Chung et al. (2015)
Rap1	*S. pombe*	S213, T378, S422, S513, S549	Mass spectrometry, phosphoaffinity SDS-PAGE mobility	*Bouquet* formation (*rap1*^{32A} and *rap1*^{32E} no phenotype)	Amelina et al. (2015)
SUN1	*M. musculus*	S48	*In vitro* kinase assay	NE-telomere attachment/ *Bouquet* formation	Viera et al. (2015); Mikolcevic et al. (2016)
TERB1	*M. musculus*	T647	Mass spectrometry, phospho-specific antibody, CDK inhibition (Roscovitine), *terb1*^{T647A} and *terb1*^{T647D} phosphomutants	NE-telomere attachment/ *Bouquet* formation	Huttlin et al. (2010); Shibuya et al. (2014) and Shibuya et al. (2015)
Zip1	*S. cerevisiae*	-	*In vitro* kinase assay, SDS-PAGE mobility, CDK inhibition (*cdc28-as1*), Clb5 and Clb6 dependency	Synapsis (*zip1*^{4SA} no phenotype)	Ubersax et al. (2003); Zhu et al. (2010)
Red1	*S. cerevisiae*	-	Phosphoaffinity SDS-PAGE mobility, CDK inhibition (*cdc28-as1*), Clb5 and Clb6 dependency	Synapsis (*red1*^{7A} no phenotype)	Zhu et al. (2010); Lai et al. (2011)
SYP-1	*C. elegans*	T452	*In vitro* kinase assay, phospho-specific antibody, *syp1*^{T452A} phosphomutant	Synapsis	Brandt et al. (2020)
ASY1	*A. thaliana*	**T142,** T184	Mass spectrometry, *in vitro* kinase assay, *asy1*^{T142V}, *asy1*^{T142D} and *asy1*$^{T142V;T184V}$ phosphomutants	Synapsis	Yang et al. (2020)
Sgs1	*S. cerevisiae*	S46, T50, T122, S272, S348, S493, S617	Mass spectrometry (mitosis), *in vitro* kinase assay, SDS-PAGE mobility, CDK inhibition (*cdc28-as1*), *sgs1*^{9A} phosphomutant	DSB Repair	Grigaitis et al. (2020)
MSH-5	*C. elegans*	T1009, T1109, S1278	Mass spectrometry (*in vitro* phosphorylated protein), *in vitro* kinase assay, phospho-specific T1009 antibody, *msh5*^{13A} phosphomutant	CO formation	Haversat et al. (2022)
MLH1	*A. thaliana*	-	*In vitro* kinase assay	CO formation	Wijnker et al. (2019)
Mms4	*S. cerevisiae*	S56	Mass spectrometry (mitosis), phosphoaffinity SDS-PAGE mobility, *mms4*^{14A} phosphomutant	DSB Repair (persistent JM resolution)	Matos et al. (2011)
Yen1	*S. cerevisiae*	S71, S245, S500, S583, S655, S679	Mass spectrometry (mitosis), phosphoaffinity SDS-PAGE mobility, Yen$^{ON(9A)}$ phosphomutant	DSB Repair (persistent JM resolution)	Matos et al. (2011); Blanco et al. (2014); Eissler et al. (2014); Alonso-Ramos et al. (2021)

these sites (Thr378, Ser422, and Ser513) are also specifically phosphorylated at early M-phase in vegetative cell cycle, and Ser513 is critical for releasing telomeres from the NE to facilitate chromosome segregation (Fujita et al., 2012). Cdc2-dependent phosphorylation at these residues weakens the interaction with the NE-anchoring complex Bqt3-Bqt4. Indeed, structural studies support that Ser513 phosphorylation could impair the binding to Bqt4, and the Rap1-S513E mutant protein, mimicking this serine phosphorylation, shows a reduced binding affinity (Hu et al., 2019). Similarly, once the scattered telomeres have bound to Bqt1-Bqt2 and Sad1 in meiosis, Cdc2-dependent Rap1 phosphorylation could diminish the interaction with the Bqt3-Bqt4 complex, facilitating the natural travelling of the telomeres along the NE to gather at the SPB. Otherwise, once the telomeres reach the SPB, local Cdc2-dependent inhibition of the interaction with the Bqt3-Bqt4 complex could enhance Bqt1-Bqt2 binding and reinforce telomere attachment to the SPB. However, *rap1-32A* and *rap1-32E* mutants, in which all the meiosis-identified phosphorylated sites were substituted with non-phosphorylatable residues (alanine) or phosphomimetic residues (glutamic acid), show normal *bouquet* dynamic, and telomeres timely cluster and dissociate from the SPB (Amelina

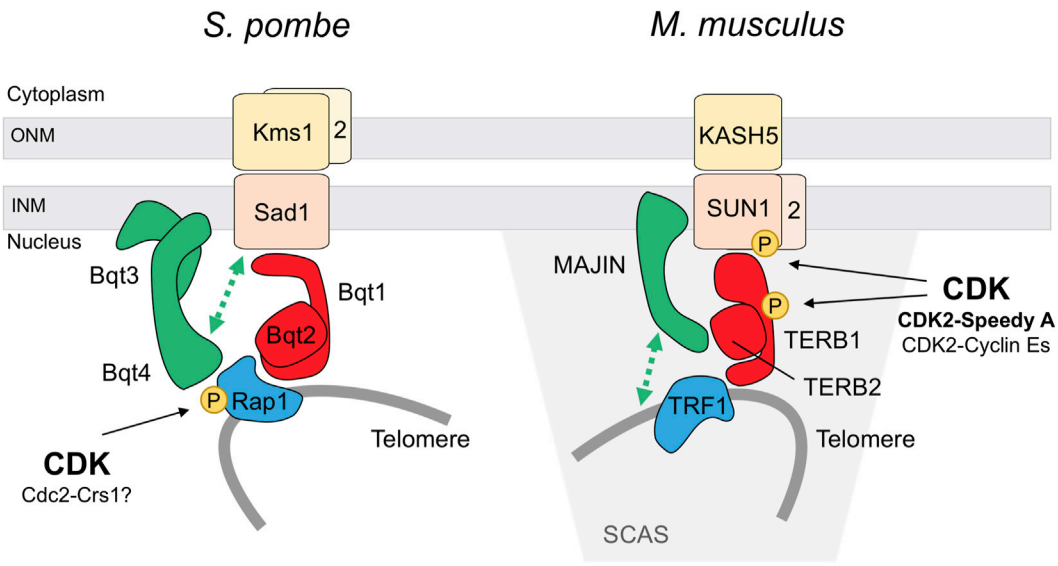

Component		*S. pombe*	*M. musculus*
LINC-complex	**KASH domain module**	Kms1/2	KASH5
	SUN domain module	Sad1	SUN1/2
INM telomere proteins		Bqt3/4	MAJIN (meiosis-specific)
Meiosis-specific telomeric proteins		Bqt1/2	TERB1/2
Telomeric proteins		Rap1	TRF1

FIGURE 2
CDK regulation of the meiotic telomere attachment to the nuclear envelope. *S. pombe* and *M. musculus* models. Functional conservation of the different elements is highlighted by the same color. INM inner nuclear membrane, ONM outer nuclear membrane, SCAS synaptonemal complex attachment sites. Protein interactions are based on Chikashige et al., 2006, Chikashige et al., 2009, and Hu et al., 2019 for fission yeast, and Shibuya et al., 2014, Shibuya et al., 2015, and Wang et al., 2020 for mouse.

et al., 2015). It is worth noting that these mutants harbor additional mutations apart from the Cdc2-phosphomutant sites, which can obscure the contribution of CDK. Interestingly, by yeast two-hybrid (Y2H) assays the Rap1-32E proteins seems to interact more efficiently with Bqt1-Bqt2 than the wild type protein. In addition, structural studies of a minimal Rap1-Bqt4 complex have identified a Bqt4-binding motif in Rap1 which is also present in other known and newly identified Bqt4-interacting proteins, including Sad1, and these proteins bind to Bqt4 in a competitive manner (Hu et al., 2019). It will be worthy to explore the contribution of Thr378, Ser422, and particularly, Ser513 phosphorylation sites to *bouquet* formation, and their possible regulation by the meiosis-specific Crs1 cyclin.

More recently, telomere anchorage to the NE during meiosis has been also studied in mice, where different components of the LINC-complex and the meiosis-specific linker to telomeres have been identified (Shibuya and Watanabe, 2014; Shibuya et al., 2015) (Figure 2). Interestingly, meanwhile CDK2 is not essential for vegetative growth, it plays a crucial role in meiosis, and knock out (KO) mice are sterile due to spermatocyte and oocyte arrest in prophase and death by apoptosis (Berthet et al., 2003; Ortega et al., 2003). CDK2 localizes to telomeres from leptotene to pachytene (Ashley et al., 2001), and in spermatocytes it is observed in the NE-attachment plates by electron microscopy (Viera et al., 2015). In the absence of CDK2 50% of the telomeres are not properly associated to the NE and the *bouquet* conformation is not observed. *Cdk2* KO spermatocytes present aberrant dynamics in chromosome pairing, with frequent unsynapsed regions, non-homologous associations, and formation of chromosome rings (Viera et al., 2009; Viera et al., 2015). These phenotypes are also observed in *Speedy A* and *cyclin E* mutants.

Speedy A, also known as Ringo A, is a non-cyclin CDK interactor that seems to act as the main activator for CDK2 in telomere dynamics. The protein is specifically expressed in the adult testis, being present in spermatocytes from preleptotene to pachytene, and in embryonic ovary when meiotic prophase I occurs (Tu et al., 2017). Speedy A colocalizes with CDK2 in NE-

associated telomeres and is essential for the telomeric recruitment of CDK2; indeed, a CDK2 protein carrying mutations on the key residues for Speedy A binding does not localize to the telomeres (Mikolcevic et al., 2016; Tu et al., 2017). The interaction between these proteins is also supported by co-immunoprecipitation and, moreover, by the fact that CDK2 kinase activity is approx. 70% decreased in *Speedy A* KO testis (Mikolcevic et al., 2016; Tu et al., 2017). Similarly to the *Cdk2* KO, lack of Speedy A also impairs homologous pairing and telomere dynamics, showing NE-unattached telomeres inside the nucleus and telomere fusions (Mikolcevic et al., 2016; Tu et al., 2017). Specifically, the telomeric cap-remodeling observed at late prophase is defective in the mutant, and telomeres do not show the characteristic TRF2 (shelterin core component) redistribution into a ring structure (Shibuya et al., 2015; Tu et al., 2017; Chen et al., 2021). Interestingly, Speedy A reaches the telomeres prior to CDK2 and harbors a telomere localization domain that is sufficient to restore the telomere-NE interactions in *Speedy A* KO spermatocytes, indicating a docking function beyond its known CDK2-activation function (Tu et al., 2017).

The mechanism underlying the CDK2-Speedy A essential role in telomere-NE attachment and *bouquet* formation is not completely elucidated. SUN1 is a component of the LINC complex located at the telomere attachment plates associated with the inner nuclear membrane (Ding et al., 2007; Link et al., 2014). In *Cdk2* and *Speedy A* KO mutants, SUN1 protein is delocalized from these spots and observed as a polarized cap-shaped signal at the NE. Lack of SUN1 interactions at the NE could explain the telomere dynamics defects observed in these mutants (Viera et al., 2015; Mikolcevic et al., 2016; Tu et al., 2017). Indeed, SUN1 and CDK2-Speedy A directly interact, and a SUN1 mutant protein in the Speedy A-binding domain exhibits similar phenotypes to those of *Speedy A* and *SUN1* mutants with approx. 50% of the telomeres unattached to the NE (Wang et al., 2020; Chen et al., 2021). Moreover, *in vitro* experiments showed that SUN1 is phosphorylated by CDK2-Speedy A, at least on Ser48 (Viera et al., 2015; Mikolcevic et al., 2016). SUN1 phosphorylation by CDK2-Speedy A could be an important regulatory step to control telomere-NE interactions, and their proper diffusion along the NE necessary for telomere dynamics and *bouquet* formation (Figure 2). Recent studies support this notion (see below).

Cyclin E1 and cyclin E2 also contribute to maintain the integrity of the telomeres and ensure their attachment to the NE in meiosis (Martinerie et al., 2014; Manterola et al., 2016). Although they are not essential for vegetative growth and both KO mice are viable, *E2* KO males are subfertile. In addition, the meiotic phenotypes of *E2* KO mice are enhanced when cyclin E1 levels are disminished, and $E1^{+/-}$ $E2^{-/-}$ male mice, which reduce cyclin E in *E2 KO* background, are infertile (Martinerie et al., 2014). Deficiency of *E1* and *E2* cyclins in spermatocytes reduces localization of components of the shelterin complex to the chromosome ends. This defect correlates with an increased amount of the DNA-damage γH2AX marker at telomeres, indicating a loss of telomere protection (Manterola et al., 2016). Cyclin E1 and E2 are important for the formation of the synaptonemal complex attachment sites (SCAS, expansions of chromosome ends reflecting the formation of the attachment plates), which are crucial for the stable association of telomeres to NE. Spermatocytes depleted in E1 and E2 cyclins develop narrower SCAS and, in fact, telomere attachment to the NE is compromised since the TRF1 telomere marker (shelterin core component) is detected inside the nuclear space in 47% of the spermatocytes (Martinerie et al., 2014; Manterola et al., 2016). In correlation with these alterations, lack of E2 cyclin causes telomeric and synaptic abnormalities that are enhanced in $E1^{+/-}$ $E2^{-/-}$ spermatocytes. Although E-type cyclins do not show specific telomeric enrichment, they are likely to act in combination with CDK2 given the similar defects in telomere-NE attachment and synapsis observed in the mutants; particularly the presence of residual membranes in the detached telomeres is observed in both mutants (Viera et al., 2015; Manterola et al., 2016). Indeed, E-type cyclins are necessary for the telomeric localization of CDK2. In the absence of E2 approx. 40% of telomeres exhibit a reduced CDK2 loading, raising up to 93% in $E1^{+/-}$ $E2^{-/-}$ mice. Moreover, co-immunoprecipitacion analysis confirm that both cyclins interact with CDK2 in spermatocytes *in vivo* (Martinerie et al., 2014).

Defects in shelterin complex integrity at the telomeres in E-cyclin deficient mutants might affect cap-remodeling. In fact, this process is influenced by CDK activity in mouse spermatocytes. At cap-remodeling the telomere ends are reorganized by the meiosis-specific TERB1/2-MAJIN connecting complex to ensure a stable telomere-NE attachment (Shibuya et al., 2015; Chen et al., 2021). Treatment with the CDK inhibitor Roscovitine was shown to avoid cap-remodeling. Interestingly, TERB1 Thr647 is a CDK susbtrate implicated in the downregulation of the TERB1-TRF1 interaction (Shibuya et al., 2014) (Figure 2). This phosphorylation was detected in NE-attached telomeres and shown to be important for the stabilization of telomere attachments (Shibuya et al., 2015). However, other CDK targets must exist to regulate cap-remodeling, since TERB1 phosphorylation is not essential for this process and the *TERB1-T647A* mutant is able to perform cap-remodeling. CDK2 could potentially exert this regulation given its essential function in telomere dynamics.

How the LINC and TERB1/2-MAJIN complexes interact to anchor telomeres to the NE was not clear, althought an interaction between SUN1 and TERB1 was reported (Shibuya et al., 2014). Recent studies dissecting these interactions, as well as the interaction and structural studies with Speedy A, support a model whereby Speedy A interacts with SUN1 to anchor CDK2-Speedy A to the NE which promotes SUN1 phosphorylation and

the strengthening of the SUN1-MAJIN interaction. In addition, SUN1 also binds to TERB1 reinforcing the interaction between the complexes (Wang et al., 2020; Chen et al., 2021). Intestingly, in contrast to Speedy A, cyclin E1 and E2 do not bind to SUN1, pointing to Speedy A as the key triggering element to promote telomere-NE attachments (Wang et al., 2020). However, which SUN1 residues are phosphorylated and, in particular, the implication of Ser48 phosphorylation in MAJIN binding is unknown. Overall, CDK phosphorylation of SUN proteins seems to play an important role in the LINC-complex regulation; in fact, in worms and humans CDK1 is required for the phosphorylation of SUN proteins in mitosis (Patel et al., 2014; Zuela and Gruenbaum, 2016). Strikingly, in the case of worms, the expression in adults of the phosphomimetic SUN1-S34E protein drastically reduces fertility and abolishes bivalent formation (Zuela and Gruenbaum, 2016). Additionally, SUN1 phosphorylation mediated by other kinases controls meiotic chromosome dynamics in this organism (Penkner et al., 2009; Woglar et al., 2013).

Bouquet formation is regulated by a meiosis-specfic B3-type cyclin, Cyc2p, in *Tetrahymena thermophila*. In the absence of this cyclin micronuclei arrest at early prophase and fail to form the elongate-crecent shape characteristic of the *bouquet*-like organization in this ciliate (Xu et al., 2019). Cyc2p might be required to organize the microtubules that support crecent formation, which could explain the phenotype.

Finally, in addition to the positive effect of CDK phosphorylation in *bouquet* formation and telomeric dynamics, CDK regulation of *bouquet* disassembly has been reported in the budding yeast *Saccharomyces cerevisiae*. In this organism where *bouquet* conformation is very transient, controlled chemical inhibition of Cdc28 (CDK) stabilizes telomere clustering (Prasada Rao et al., 2021). However, the mechanism is currently unknown.

DSB formation

A key feature of meiosis is recombination, the physical exchange of genetic information between each pair of parental chromosomes (homologs) (Hunter, 2015). In addition to produce variability in the offspring, it is essential for generating tension in the spindle-bound homologous pair which ensures proper alignment and chromosome segregation (Petronczki et al., 2003). Recombination is initiated by programmed DSBs in the DNA introduced by Spo11, a conserved meiosis-specific topo-like protein similar to TopVI of archaea (Keeney et al., 1997; Lam and Keeney, 2014; Bouuaert and Keeney, 2016; Robert et al., 2016; Vrielynck et al., 2016). DSBs are one of the most dangerous lesions in the DNA and cells have developed surveillance mechanisms to sense and repair these lesions. However, meiotic cells have integrated their production as part of the cell physiology, and have acquired a network of mechanisms to place and balance them (Keeney et al., 2014). DSB formation is coordinated with meiotic progression and DSBs occur locally after DNA replication during prophase (Borde et al., 2000; Murakami and Keeney, 2014). Indeed, replication-fork stalling blocks DSB formation by the activation of the S-phase checkpoint (Tonami et al., 2005; Ogino and Masai, 2006; Blitzblau and Hochwagen, 2013). In budding yeast, CDK (Cdc28) activity participates in this coordination phosphorylating Mer2, a conserved Spo11-accessory protein of the RMM complex (Henderson et al., 2006; Murakami and Keeney, 2008; Wan et al., 2008; Claeys Bouuaert et al., 2021). S-phase Cdc28 activity (associated to cyclin Clb5 and Clb6) phosphorylates Mer2 at Ser30 which primes adjacent Ser29 (and S28) for subsequent phosphorylation by DDK (Dbf4-Dependent Kinase). Mer2 phosphorylation at these sites is essential to promote the binding to other Spo11-accessory proteins, Spo11 loading at the recombination *hotspots* in the DNA, and DSB formation. However, additional CDK and DDK targets exist since the DSBs observed in cells expressing the phosphomimetic Mer2-DDD protein still depends on each of these kinases (Wan et al., 2008). Mer2 phosphorylation likely occurs upon replication-fork passage since DDK travels with the fork, and fork passage correlates with the loading onto chromatin of the Spo11-accessory protein Rec114, which it is known to depend on Mer2 phosphorylation (Panizza et al., 2011; Murakami and Keeney, 2014).

DSB formation also depends on CDK in fission yeast (Bustamante-Jaramillo et al., 2019). Although several CDK complexes contribute to this function, the meiosis-specific Crs1 cyclin has a prominent role and *crs1* mutants show a 50% reduction in DSB and recombination levels. In addition to its SPB location (see above), Crs1 has a pan-nuclear localization during meiotic prophase compatible with this role in DSB formation (Bustamante-Jaramillo et al., 2021). Interestingly, CDK downregulation impairs the chromatin binding of Rec25, a structural component of the Linear Elements (LinEs). LinEs are chromosome axis structures with similarity to the SC axial/lateral elements of other eukaryotes (Lorenz et al., 2004; Davis et al., 2008; Ding et al., 2021; Chuang and Smith, 2022). They are required for DSB formation and preferentially enriched at recombination *hotspots*; furthermore, when misplaced they induce DSBs (Fowler et al., 2013; Martin-Castellanos et al., 2013; Nambiar and Smith, 2018). Thus, modulation of the loading of LinEs onto chromatin may be a mechanism for CDK to control DSB formation. However, phosphonull *rec10-8A* or *rec27-A* mutants, the only two LinE-components harboring CDK sites, have no impact on meiotic recombination, even though several CDK sites in Rec10 are phosphorylated *in vivo* (Spirek et al., 2010; Bustamante-Jaramillo et al., 2019). Thus, it seems that these alterations alone would not significantly impair LinE chromatin association. In addition, similarly to budding yeast Mer2, the

conserved RMM component Rec7 is a phosphoprotein that harbors a CDK site adjacent to potential DDK sites (Thr243 Ser244 Ser245) and DDK is also required for DSB formation (Ogino et al., 2006; Miyoshi et al., 2012). However, phosphonull *rec7-AAA* mutants show wild type levels of recombination (Bustamante-Jaramillo et al., 2019). Thus, a key target for this function of CDK has not yet been identified in fission yeast. It is possible that in this organism several CDK targets contribute to the regulation of DSB formation, and the reduction in recombination would not be observed until cumulative deregulation of several targets. Alternatively, regulation may be indirect. In this regard, LinE formation depends on the meiotic cohesins Rec8 and Rec11 which are phosphoproteins with several phospho-CDK sites detected *in vivo* (Molnar et al., 2003; Lorenz et al., 2004; Davis et al., 2008; Ishiguro et al., 2010; Rumpf et al., 2010; Fowler et al., 2013; Phadnis et al., 2015). Moreover, different levels of CDK regulation may exists. The cyclin Cig2-CDK complex regulates promoter occupancy of the mid-meiotic genes by phospho-regulation of the forkhead transcription factor Fkh2 (Alves-Rodrigues et al., 2016). Cig2-CDK phosphorylation of Fkh2 Ser481 reduces its promoter binding affinity and facilitates the loading of the transcriptional activator Mei4. One of these genes is *mde2*, which is essential for the organization of the pre-recombination complexes (Miyoshi et al., 2012). Therefore, timely expression of *mde2* by CDK might establish a temporal window for DSB formation.

REC-1 and HIM-5 are paralog related proteins required for normal levels of DSBs in *Caenorhabditis elegans* (Chung et al., 2015). Foci of the recombinase RAD-51 are reduced in each single mutant, particularly in *him-5*, and the reduction is significantly aggravated in the double mutants. This defect correlates well with the percentage of univalents at diakinesis (last prophase stage with highly condensed chromosomes). It was proposed that these proteins may function as Spo11-accessory proteins similarly to the proteins forming the pre-recombination complexes in budding and fission yeast; however, this has not been formally determined, and indeed, in contrast to Spo11-accessory proteins in yeasts, these *C. elegans* proteins are not essential for DSB formation. Interestingly, REC-1 is a CDK target that is phosphorylated *in vitro* by recombinant Cyclin B3-CDK4 complexes; moreover, it is also phosphorylated by cell extracts but not when the extracts are previously treated with Roscovitine (Chung et al., 2015). However, the *in vivo* relevance of this phosphorylation is unclear since both phosphomimetic and phosphonull *rec-1* mutants show a loss-of-function phenotype. It is possible that CDK does not play a crucial role in early meiotic events in this organism, where the meiosis-specific checkpoint kinase CHK-2 has acquired a prominent role in the regulation of chromosome architecture and movements, DSB formation, and homologous pairing and synapsis (MacQueen and Villeneuve, 2001; Penkner et al., 2009; Rosu et al., 2013; Stamper et al., 2013; Kim et al., 2015).

Recombinational repair

After DSB formation Spo11-bound break sites are endonucleolytically resected to generate single-stranded DNA nucleofilaments that, coated with strand-exchange proteins Rad51/Dmc1, invade the homologous chromosome for repair. The efficient and differential resolution of the recombination intermediates is essential for several reasons (Hunter, 2015; San-Segundo and Clemente-Blanco, 2020). First, to produce viable gametes without DNA lesions. Second, to resolve enough DNA joint molecules (JM) as crossovers (CO). COs result in the reciprocal exchange of genetic material and the formation of physical links between the pair of homologs, which ensures their correct reductional segregation at first meiotic division (meiosis I). And finally, to resolve and release the physical connections between chromosomes on time before anaphase; otherwise, persistent JMs can impede chromosome segregations. Regarding this, some structure-selective endonucleases (SSEs) as Mus81-Mms4 and Yen1 in *S. cerevisiae* are tightly temporally controlled by cell cycle-regulated phosphorylation cycles to ensure that JMs are resolved and eliminated (Blanco and Matos, 2015) (Figure 3A). Of note that although CDK regulated targets that operate in DNA damage repair during vegetative growth has been broadly documented (reviewed in (Trovesi et al., 2013; Kciuk et al., 2022)), this is not the case for the meiotic DSB repair. It is expected that some of these targets are common to both mitotic and meiotic repair, while others will be specific to meiotic cells, given the formation of JMs between homologous chromosomes and the biased repair to generate COs.

In *S. cerevisiae* Mus81-Mms4 SSE activity is regulated by phosphorylation in meiotic and mitotic cells (Matos et al., 2011). Mms4 hyperphosphorylation in meiosis I strongly increases the nuclease activity of the complex, promoting the resolution of JMs before anaphase I. *mms4* deletion mutant accumulates aberrant multichromatid JMs. The non-phosphorylatable *mms4-14A* mutant shows a delay in the resolution of JMs and, similarly to *mus81* deletion mutants, fails to segregate homologous chromosomes at anaphase I (Matos et al., 2011). Despite the fact that Polo Kinase Cdc5 seems to play the major role in Mus81-Mms4 phospho-regulation, CDK (Cdc28) is involved as well, although this CDK regulation have mostly been studied in mitosis (Gallo-Fernandez et al., 2012; Matos et al., 2013; Szakal and Branzei, 2013). Indeed, the Mms-14A protein harbors changes to alanines in the 5 CDK sites present in the protein, and at least one of them is phosphorylated *in vivo*. The other ones were not confirmed due to incomplete peptide coverage of the mass spectrometry (MS) analysis (Matos et al., 2011). Cyclin Clb1-CDK activity is induced at the end of prophase (Carlile and

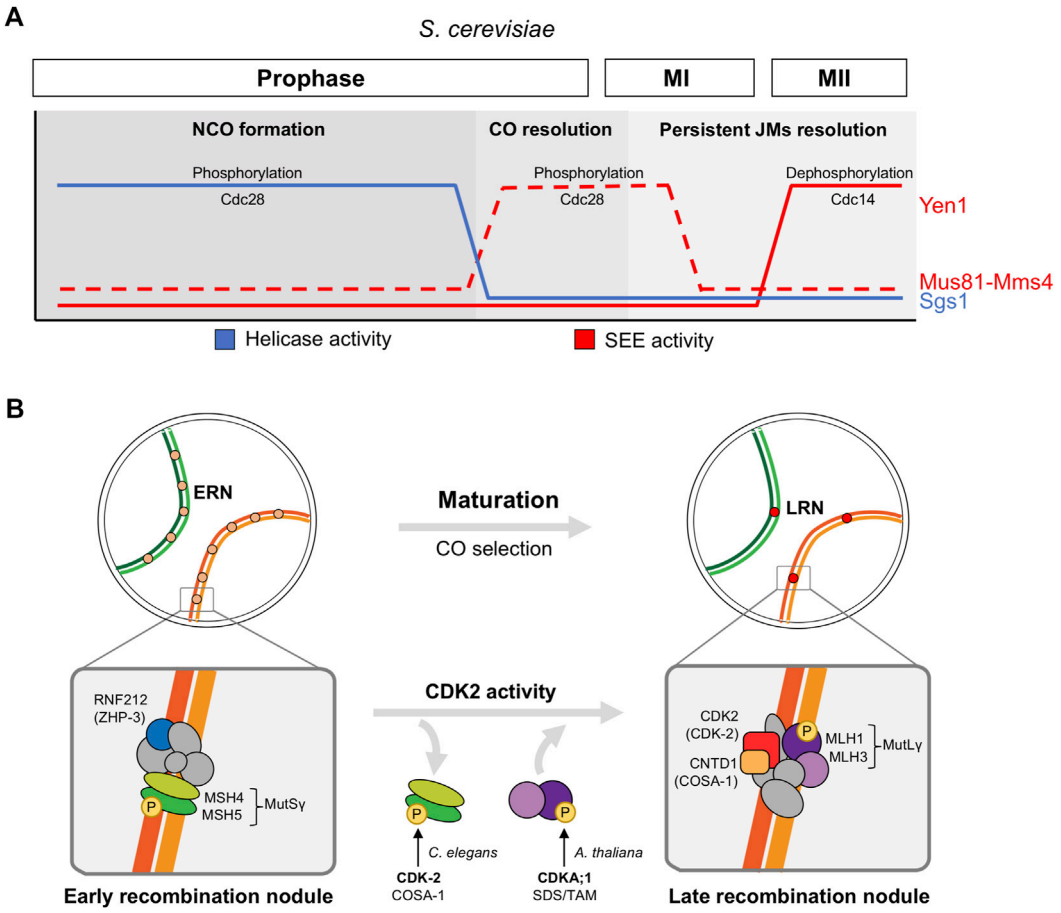

FIGURE 3
CDK regulation of recombinational repair in meiosis. **(A)** Role of CDK (Cdc28) in the sequential regulation of helicase and structure-selective endonuclease (SEE) activities in *S. cerevisiae*. Low Cdc28 activity activates the RecQ-family DNA helicase Sgs1 during early prophase to promote NCO formation, high levels of Cdc28 activity at meiosis I entry activates Mus81-Mms4 SSE to implement CO resolution prior to chromosome segregations, and Yen1 SSE activation by the Cdc14 phosphatase at meiosis II releases its earlier Cdc28-dependent inhibition to process persistent unresolved joint molecules (JMs). **(B)** Role of CDK2 in the maturation of early recombination nodules (ERN) and CO selection (late recombination nodules, LRN) in higher eukaryotes. Protein complexes are only illustrative and they do not represent protein-protein interaction nor stoichiometry. Only key proteins conserved in several organisms are highlighted: MutSγ complex MSH4-MSH5, RNF212 (ZHP-3 in *C. elegans*), MutLγ complex MLH1-MLH3, CDK2 (CDK-2 in *C. elegans*, CDKA;1 in *A. thaliana*), CNTD1 (COSA-1 in *C. elegans*). These proteins are key factors that reduce foci numbers from early pachytene to mid-pachytene (RNF212 and MutSγ) and that load at LRNs from mid pachytene (MutLγ, CDK2, and CNTD1).

Amon, 2008), and therefore, it is a candidate to participate in this regulation.

Mechanisms of CDK regulation have also been identified in fission yeast Mus81-Eme1 and human MUS81-EME1 in vegetative cells. In *S. pombe*, CDK (Cdc2)-dependent phosphorylation of Eme1 is cell-cycle regulated, and it is required to respond to DNA damage and to maintain chromosome stability in the absence of the RecQ-type DNA helicase Rqh1 (Dehe et al., 2013). In contrast to *S. cerevisiae*, fission yeast Eme1 phosphorylation does not depend on Polo kinase. In human cells, CDK stimulates MUS81-EME1 resolvase activity by promoting the interaction with SLX1-SLX4 SSE (Wyatt et al., 2013; Payliss et al., 2022). However, the relevance in meiosis of these phospho-regulations have not been studied.

Yen1 SSE has been widely studied in *S. cerevisiae*. During meiotic cell cycle, in sharp contrast to Mms4, CDK (Cdc28)-mediated phosphorylation of Yen1 restrains its function until anaphase II when it acts as an additional back-up system for late persistent JMs (Matos et al., 2011; Alonso-Ramos et al., 2021). *yen1* deletion mutant does not present obvious defects in chromosome segregations under unchallenged conditions, but additional deletion of other repair pathways as Sgs1 and Mus81-Mms4 results in defective JM resolution and abnormal anaphase I and II segregations, that unveils the safeguard activity of Yen1 (Matos et al., 2011; Alonso-Ramos et al., 2021). The specific

mechanism of Yen1 dual phospho-regulation by Cdc28 and Cdc14 phosphatase was first elucidated in vegetative cells (Blanco et al., 2014; Eissler et al., 2014; Garcia-Luis et al., 2014), but it has also been described in meiosis. Cdc28-mediated phosphorylation not only inhibits Yen1 catalytic activity, but also prevents its precocious nuclear accumulation. At anaphase II, Cdc14 released from the nucleolus dephosphorylates Yen1, promoting its activation and nuclear enrichment (Alonso-Ramos et al., 2021). Regarding this mechanism, a mutant protein where the 9 CDK-consensus serines are mutated to alanines, named Yen1^{ON}, bypasses this phospho-regulation. Therefore, Yen^{ON} is constitutively active and accumulated in the nucleus, even in early stages of meiosis (as S-phase and prophase), in a Cdc14 independent manner (Blanco et al., 2014; Arter et al., 2018; Alonso-Ramos et al., 2021). Early Yen1 activation induces premature CO formation and avoids the transitory accumulation of JMs. As a consequence, some aspects of the CO physiology such as CO interference (nearby CO inhibition) and distribution are defective (Arter et al., 2018). Although Yen1 reaches its maximum activity in meiosis II, some evidence indicates that it might exert a previous function at anaphase I, especially when other repair pathways are compromised (Alonso-Ramos et al., 2021).

Similarly to Yen1, human ortolog GEN1 contains several CDK consensus sites, although they are not conserved in position and context. Indeed, GEN1 is phosphorylated in a CDK-dependent manner in mitosis; however, this modification has no impact on the catalytic activity, and wild type and GEN1-8A proteins resolve JMs with the same efficiency (Chan and West, 2014). Furthermore, the relevance of this modification in meiosis has not been studied.

The same phospho-regulatory network that tightly controls SSE activity during nuclear divisions, also regulates Sgs1 in *S. cerevisiae* meiosis and mitosis (Grigaitis et al., 2020) (Figure 3A). The RecQ-family DNA helicase Sgs1, together with Top3 and Rmi1 (STR complex), contributes to DSB repair by disassembling different recombination intermediates favouring the production of non-crossover (NCO) products over COs. In addition, a meiotic pro-CO function of Sgs1 is uncovered in the absence of SSEs (Zakharyevich et al., 2012). During meiotic S-phase and prophase, CDK (Cdc28) phosphorylation of Sgs1 substantially increases its DNA unwinding activity. This phospho-stimulation is essential for proper JM processing, and the phosphonull *sgs1-9A* mutant accumulates aberrant multichromatid JMs. Indeed, *sgs1-9A* mutant fails to segregate homologous chromosomes at anaphase I, a defect that is enhanced in the absence of Mms4 and alleviated in the presence of the Yen1^{ON} version. Cdc28 phosphorylation also primes Sgs1 for Cdc5 hyperphosphorylation as cells exit prophase, what has been suggested to inhibit its activity, but the meaning of this modification is not completely elucidated (Grigaitis et al., 2020). It is tempting to think that the differential phosphorylation state may modulate Sgs1 functions to promote NCOs in early prophase and JM resolution later on prior to chromosome segregation as SSEs do.

Overall, CDK plays a crucial role in the metabolism of the JMs generated during meiotic DSB repair, at least in budding yeast (Figure 3A). It enhances or inhibits different activities involved in the process and, in doing so, it temporally orders their actions to ensure an efficient JM processing that guarantees a faithful chromosome segregation. In addition, it restrains JM resolution to stablish a correct CO pattern.

It is quite possible that the role of CDK in averting late JMs is a conserved feature. In fission yeast, the UvrD-type DNA helicase Fbh1 is required to remove Rad51 from the DNA. Both, *fbh1* mutants, and mutants in its loading factor *dbl2*, show a retention of Rad51 foci at meiosis I and defects in chromosome segregation (Sun et al., 2011; Polakova et al., 2016); moreover, persistence of JMs is observed in the *dbl2* mutant (Polakova et al., 2016). Interestingly, Dbl2 is potentially a good CDK substrate. It harbours several putative CDK sites, and 3 of them are phosphorylated in vegetative cycle (https://www.pombase.org/gene/SPCC553.01c). It will be worthy to explore any meiotic contribution of CDK to Dbl2 function and JM resolution.

In fission yeast the meiosis-specific Rem1 cyclin is required for normal levels of recombination. Interestingly, in its absence NCOs are reduced but CO levels are not affected, suggesting a regulatory role in DSB repair (Malapeira et al., 2005). However, this function does not depend on CDK (Cdc2). Intron retention produces a short isoform that lacks the cyclin-box motif involved in Cdc2 binding, and this short version restores the recombination defects of the *rem1* mutant (Moldon et al., 2008). It is currently unknown how short Rem1 controls the recombination output. Intron processing depends on Mei4 binding to *rem1* promoter, which recruits the spliceosome, and produces a larger protein that shows a peak of associated kinase activity at meiosis I and promotes meiosis I progression (Malapeira et al., 2005; Moldon et al., 2008). Thus, Rem1 represents an example of gene economy where splicing regulation produces a cyclin and a non-cyclin protein with different meiotic functions. Differential gene expression regulation has been also reported for other meiotic genes. For the unconventional CNTD1 mouse cyclin a short isoform has been recently described as the only detectable species in mouse testis (see below, (Gray et al., 2020)). In this case, the function of the full length CNTD1 protein is unclear. Interestingly, mouse CDK2 also shows a larger isoform *via* alternative splicing that is highly induced in meiotic prophase (Ellenrieder et al., 2001; Liu et al., 2014; Tu et al., 2017). It has been proposed that the larger protein may add new binding domains to accommodate different meiotic functions. Indeed, some interactors preferentially bind to the long CDK2 isoform *in vitro* (Liu et al., 2014; Bondarieva et al., 2020).

In mouse, in addition to its telomeric localization, CDK2 is also observed in 1-2 interstitial sites along the chromosomal axes

in mid-pachytene spermatocytes and oocytes (Ashley et al., 2001) (Figure 3B). At these spots, it colocalizes with late recombination nodule (LRN) pro-CO factors as RNF212, HEI10, PRR19, CNTD1, and MLH1, and this localization is lost in the corresponding mutants (Ashley et al., 2001; Ward et al., 2007; Reynolds et al., 2013; Holloway et al., 2014; Liu et al., 2014; Qiao et al., 2014; Bondarieva et al., 2020). Based on localization studies, CDK2 was proposed to act with the HEI10 E3-sumo-targeting ubiquitin ligase in the dissociation of early recombination factors and final CO selection (Qiao et al., 2014). Interestingly, human HEI10 was shown to interact with cyclin B1 in Y2H assays, and it is specifically phosphorylated *in vitro* by cyclin B-Cdk1 complexes (Toby et al., 2003); however, cyclin B1-Cdk1 has not been implicated in CO selection. Recently, the use of a partial loss-of-function and a gain-of-function *Cdk2* allele has helped to further explore the role in CO regulation of CDK2 activity (Palmer et al., 2020). The hypomorphic $Cdk2^{T160A}$ allele harbors a point mutation in the so-called T-loop of the protein. Upon binding to the cyclin, the loop is displayed out of the catalytic cleft and exposed to phosphorylation by CAK (CDK activating kinase), stabilizing the complex and, therefore, promoting maximal activation (Malumbres, 2014). Telomeric CDK2 localization and function remains mostly unaffected in $Cdk2^{T160A}$ mutants, which allows the study of CDK2 roles in later events (Palmer et al., 2020). CDK2 location in LRNs depends on T-loop phosphorylation since $Cdk2^{T160A}$ spermatocytes lose these interstitial foci and the associated MLH1 loading (component of the conserved MutLγ SSE with bias for CO resolution). Correspondingly, increased kinase activity in the gain-of-function $Cdk2^{Y15S}$ mutant, which precludes inhibition by phosphorylation at Tyr15 in the catalytic pocket (Malumbres, 2014), correlates with elevated numbers of interstitial foci and the associated MLH1 loading. In addition, similarly to other mutants in pro-CO factors, $Cdk2^{T160A}$ spermatocytes show persistence of foci of earlier recombination proteins as RPA2 and MSH4 (component of the conserved MutSγ complex), reflecting aberrant stabilization and repair of intermediates. In particular, the typical reduction in RNF212 foci correlated with "selection" of meiotic CO sites does not occur in $Cdk2^{T160A}$ spermatocytes what indicates a defective CO designation process when CDK2 activity is reduced (Reynolds et al., 2013; Qiao et al., 2014; Palmer et al., 2020). Thus, CDK2 might phosphorylate substrates in the recombination nodules leading the repair process towards CO formation; however, the molecular mechanism is currently unknown. Interestingly, $Cdk2^{T160A}$ mutant primarily affects the activity of CDK2 complexes with conventional cyclin activators, since CDK2-Speedy A complexes do not require Thr160 phosphorylation for activation (Karaiskou et al., 2001). This excludes Speedy A from any role in this LRN associated function of CDK2; and, indeed, Speedy A is not located in interstitial foci along chromosomes axes (Mikolcevic et al., 2016; Tu et al., 2017). Furthermore, CDK2 phosphorylation at Thr160 is observed in LRNs and not in telomeres (Liu et al., 2014).

The role of CDK2 in the maturation of early recombination sites and CO designation is conserved in *C. elegans* (Figure 3B). CDK-2 homolog also localizes at CO-selected sites, and it is eventually detected as six strong foci in pachytene (one per homolog pair). Absence of bivalents in CDK-2 depleted oocytes reflects a failure to properly generate COs. Specifically, the CO selection pathway is disrupted, as seen by the fact that ZHP-3 (RNF212 in mouse) and MSH-5 (component of the conserved MutSγ complex) signals fail to restrict to the six CO sites as normally happens in late pachytene (Haversat et al., 2022). Some studies identified the cyclin-like protein COSA-1 (Crossover Site-Associated-1) as a partner for CDK-2 in *C. elegans* meiosis. COSA-1 and CDK-2 colocalize at CO sites in a mutually-dependent manner and their absence similarly impairs the dynamics of CO designation factors, what support their functional association (Yokoo et al., 2012; Haversat et al., 2022). In the *cosa-1* mutant, bivalents are also absent, and at late pachytene ZHP-3 aberrantly remains at high levels along the SC and MSH5 foci are lost (Yokoo et al., 2012). Moreover, *in vitro* experiments showed that CDK-2 and COSA-1 are able to form a complex (Haversat et al., 2022).

Key meiotic substrates of CDK2 for this crossover-related function are not clearly determined. Recent studies describe MSH-5 as a key target in *C. elegans* (Haversat et al., 2022). MSH-5 contains thirteen CDK consensus motifs in a disordered C-terminal tail, and this domain is essential for its function in CO formation. In a C-terminal truncated mutant ($msh\text{-}5^{\Delta 339aa}$), ZHP-3 signal aberrantly persists and most recombination intermediates fail to mature into COs. Three of these sites are, indeed, *in vitro* phosphorylated by recombinant human CDK1-cyclin A2 complexes. Moreover, phospho-specific antibodies to one of these sites, Thr1009, show that MSH-5 is actually phosphorylated *in vivo* in a CDK-2 and COSA-1 dependent manner. Phosphorylated-MSH5 signal was enriched at CO-designated sites in late pachytene, colocalizing with COSA-1 during meiotic progression. CDK phosphorylation of MSH-5 promotes its pro-CO activity since, in a sensitized condition (*him-14(it44)* mutant, MSH4 in mouse), the $msh5^{13A}$ phospho-null mutant is unable to form bivalents. Moreover, at late prophase colocalization between MSH-5^{13A} and COSA-1 is lost and the MSH-5^{13A} protein persists as multiple foci instead of pairing down to six bright foci, reminiscent of what it is observed in CDK-2 depleted germlines. The disordered C-terminal tail containing CDK sites in MSH-5 is not conserved outside *Caenorhabditis* species, indicating that, although the role of CDK2 in CO selection is conserved, the mechanism may differ from one organism to another (Haversat et al., 2022).

The mammalian COSA-1 homolog, CNTD1, also presents a conserved function in CO selection (Figure 3B). It is highly enriched in mouse and human testis, and in mouse spermatocytes CNTD1 foci are observed at CO sites

colocalizing with CDK2 and MLH1 in mid-pachytene (Bondarieva et al., 2020; Gray et al., 2020). Similarly to other CO machinery mutants (as *Mlh1*, *Mlh3*, *Hei10*, *Rnf212*), when Cntd1 function is depleted early prophase events including homolog pairing and initial DSB processing remain normal, but severe defects in DSB repair and CO formation are observed (Holloway et al., 2014). In *Cntd1* mutant spermatocytes, MutLγ complex (MLH1 and MLH3) and CDK2 do not localize to LRNs, indicating a disruption in the canonical CO pathway. In addition, the earlier recombination factors MSH4 and RNF212 are not properly removed from these sites as seen by persistence (or even increase) of foci and co-foci of these proteins during late pachytene. Thus, CNTD1 seems to act specifically in the final selection of CO sites, coordinating RNF212 and MutSγ dissociation with the recruitment of MutLγ.

The identification of CNTD1 as a member of the cyclin superfamily indicates that it may function in a CDK-CNTD1 kinase complex. CDK2 is a good partner for CNTD1 because its associated kinase activity is also involved in CO designation (see above); in fact, interstitial CDK2 foci are absent in *Cntd1* mutants and, although the interaction has not been detected *in vivo*, CNTD1 has been shown to interact with CDK2 by Y2H assays (Holloway et al., 2014; Bondarieva et al., 2020; Gray et al., 2020). The CNTD1–CDK2 interaction requires the first predicted cyclin box located in CNTD1 N-terminus; hence, mutants that alter this first cyclin box diminish the interaction in Y2H assays and impair CNTD1 function (Bondarieva et al., 2020). Consistent with this mechanism, other studies have identified a short CNTD1 isoform that lacks the first cyclin homology domain and is not able to interact with CDK2 by Y2H assays (Gray et al., 2020). Currently, the function of the long CNTD1 protein is unclear, since apparently the short form is the only detectable species in adult mouse testis (Gray et al., 2020). Further studies are needed to shed light into the function and regulation of the distinct CNTD1 isoforms. Given that long variants have been found in different vertebrates including mouse (Gray et al., 2020), the use of specific antibodies for the detection of the long isoforms will be particularly informative. Nevertheless, given that CDK2 activity is required for CO selection, there must be other cyclin/s or activators/s to provide this activity.

Molecularly, in extracts from adult testis no relevant interactions between short-CNTD1 and the CO machinery (MSH4, MSH5, MLH1, MLH3, RNF212, HEI10, or CDK2) have been identified by MS (Gray et al., 2020). However, MS data shows unexpected interactions with components of the Replication Factor C (RFC) complex, the loader of the Proliferating Cell Nuclear Antigen (PCNA). Indeed, RFC3, RFC4 and PCNA proteins are expressed during meiotic prophase (after DNA replication), and in the case of RFC4 clearly detected forming CNTD1-dependent foci on synapsed chromosomes in pachytene spermatocytes. Given the role of human RFC and PCNA in the activation of the MutLγ endonuclease complex *in vitro*, and the localization of PCNA at a subset of prospective CO sites in budding yeast cells arrested in pachytene (Cannavo et al., 2020; Kulkarni et al., 2020), it has been proposed that CNTD1 association with components of the RFC-PCNA complex would stimulate MutLγ activity and promote CO formation (Gray et al., 2020).

In *Arabidopsis thaliana* CDK activity also regulates CO formation (Figure 3B). CDKA;1, the homolog for mammalian CDK1 and CDK2, regulates CO formation in a dose-dependent manner (Wijnker et al., 2019). Though CDKA;1 is essential, weak loss-of-function alleles are viable and produce flowers containing abnormal meiocytes (Dissmeyer et al., 2007; Wijnker et al., 2019). The hypomorphic *cdka;1*^{DBD} mutant expresses a fusion of *CDKA;1* to an inactive (dead) destruction box of *CYCLINB1;1*, and it exhibits partial kinase activity and reduced fertility (Wijnker et al., 2019). Early stages of prophase are largely unaffected in *cdka;1*^{DBD} mutants; however, at diplotene reduced numbers of bivalents are often observed, and univalents are also frequent at metaphase I. The conventional CO pathway is affected as seen by a significant decrease of approx. 50% in MLH1 foci. Conversely, enhanced CDKA;1 activity increases recombination by approx. 10%. Regarding the molecular mechanism, *in vitro* kinase assays show that CDKA;1 in complex with meiosis-specific cyclins SDS (SOLO DANCERS) or TAM (TARDY ASYNCHRONOUS MEIOSIS) can phosphorylate MLH1, especially the CDKA;1-SDS complex, what can represent a mechanism to control CO formation. Interestingly, the SDS cyclin contains an unusually long N-terminal region. This structure resembles COSA-1/CTND1 unconventional cyclins, whose sequences also comprise an insertion of 26–33 amino acids in the highly conserved N-terminal cyclin box domain (Azumi et al., 2002; Yokoo et al., 2012).

Synapsis

The synapsis of homologous chromosomes is essential for recombination given the close proximity required for recombination to occur. This physical constraint has evolutionarily associated both processes and recombination occurs in the context of the SC; moreover, in many organisms as budding yeast, mouse, and plants, early recombination intermediates promote SC formation and chromosome synapsis (Zickler and Kleckner, 2015). However, CDK plays a role in SC regulation independently of its function in DSB formation, and some SC proteins are known CDK substrates.

In budding yeast, CDK (Cdc28) foci appear early in prophase and depend on S-phase Clb5 and Clb6 cyclins and the axial-element components Red1 and Hop1 (Zhu et al., 2010). Later on, Cdc28 tends to localize on synapsed chromosomes. Chemical inhibition of Cdc28 after DSB formation impairs polymerization of the SC central-element component Zip1. However, although Zip1 is an *in vitro* CDK substrate (Ubersax et al., 2003) and its electrophoretic gel-mobility depends on Cdc28, Clb5, and Clb6, a phospho-null Zip1-4SA protein supports normal SC formation

(Zhu et al., 2010). Additionally, Red1 is also phosphorylated in a Cdc28-depedent manner independently of DSB formation (Lai et al., 2011). Even though the phospho-null Red1-7A protein is hypophosphorylated during meiotic prophase, it does not impair sporulation efficiency or spore viability, suggesting normal SC formation (Lai et al., 2011). Thus, although SC formation requires CDK activity in budding yeast, it is not well understood how this function is accomplished. It is possible that multiple CDK regulated pathways converge to ensure efficient SC formation. Moreover, given the link between recombination and SC formation in this organism, it is possible that a putative CDK role downstream of DSB formation may also contribute to SC development.

Similarly, CDKA;1 is required for ZYP1 (Zip1) assembly in *Arabidopsis* meiotic chromosomes (Yang et al., 2020). The infertile hypomorphic *cdka;1*^{T161D} allele harbors a point mutation in the so-called T-loop of the protein that impairs fully activation (see above) (Dissmeyer et al., 2007). *cdka;1*^{T161D} mutants show pachytene-like meiocytes with ZYP1-depleted unpaired chromosomes and the absence of bivalents. The mutant does not affect Dmc1 recombinase loading, indicating that the synaptic defect is not due to the lack of DSBs. CDKA;1 co-localizes with ASY1 (Hop1 homolog) at chromosomes axis and both proteins disappear from the axis of synapsed chromosomes. ASY1 is a CDKA;1 substrate and, particularly, phosphorylation of Thr142 and Thr184 residues in the HORMA domain of the protein promotes self-interaction and increases the binding affinity to ASY3 (Red1 homolog), which facilitates ASY1 chromosomal loading (Yang et al., 2020).

CDKG is also required for full ZYP1 assembly in *Arabidopsis* (Zheng et al., 2014). In this case, the function is sex and environmental-condition specific, since the null *cdkg1-1* mutant exhibits only male sterility under high temperature. Regarding the mechanism, an indirect role through gene expression regulation was proposed, since CDKG associates with the spliceosome and controls the expression of a gene involved in pollen differentiation (Huang et al., 2013). The conserved role of CDKs in mRNA metabolism is well documented (Malumbres, 2014).

In mouse, the use of the hypomorphic *Cdk2*^{T160A} allele (see above) has also uncovered a role in synapsis maintenance (Palmer et al., 2020). Since CDK2 is required for the telomere attachment to the NE early in prophase (see above), the observed defects in synapsis of the null mutant were difficult to evaluate as a direct consequence. The CDK2^{T160A} mutant protein localizes properly at telomeres, and spermatocytes progress normally to early pachytene with normal synapsed chromosomes. However, later on partially unsynapsed chromosomes are observed, and loading of the transverse element SYCP1 is diminished; by diplotene a complete separation of the homologs is frequently observed. As in budding yeast, mouse SC formation also depends on early recombination intermediates, and, as mentioned above, *Cdk2*^{T160A} mutants accumulate RPA2, RNF212, and MSH4 foci, suggesting a problem in the processing of intermediates that might affect the stability of the SC (Palmer et al., 2020). However, since mutations in pro-CO factors also show an increased number of these foci but normal chromosome synapsis (Ward et al., 2007; Reynolds et al., 2013; Holloway et al., 2014; Bondarieva et al., 2020), CDK2 activity is likely to be directly involved in synapsis maintenance. Finally, given that *Cdk2*^{T160A} primarily affects the activity of CDK2 complexes with conventional cyclin activators (Karaiskou et al., 2001), this role in synapsis stabilization might depend on E cyclins (see above). The importance of CDK2 in different aspects of meiotic prophase, herein reviewed, has pointed it as a target for nonhormonal male contraception (Faber et al., 2020).

SC disassembly at the end of prophase is equally as important as SC formation. In *C. elegans* CDK-1 regulates the chromosomal relocation of the Polo kinase PLK-2 from the pairing centers to the SC at late pachytene (Brandt et al., 2020). SYP-1 (Zip1) is phosphorylated by CDK-1 at Thr452 located in the PBD (Polo Box Domain)-binding motif. This modification primes for PLK-2 binding that sustains SYP-1 phosphorylation and promotes SC disassembly. Meiotic depletion of CDK-1 does not affect PLK-2 recruitment to the pairing centers, and both synapsis and CO formation are normal. However, SYP-1-T452 phosphorylation is completely abolished and PLK-2 is not recruited to SC; as a consequence, chromosome axis remodeling is impaired, and SC disassembly is delayed until diakinesis (Brandt et al., 2020).

Concluding remarks

Since the molecular identification of the MPF (Maturation Promoting Factor) activity of *Xenopus laevis* oocytes in the late 80′s, the study of cyclins and CDKs has generated a vast amount of knowledge on how eukaryotic cells divide and coordinate division with internal and external cues in many species. Indeed, cyclins and CDKs have emerged as broadly conserved key regulators of the eukaryotic cell cycle. However, how these regulators control important aspects of meiosis, particularly during prophase where critical cellular events for the generation of healthy gametes occur, is not well understood. In fact, as summarized in this review, no many direct CDK meiotic-targets have been clearly identified. In addition, meiosis represents a very interesting scenario to study CDK activity diversification with the emergence of meiosis-specific cyclins and new associated functions. The important role of CDK activity in meiosis is pointed by the fact that in a recent phosphoproteomic study of mouse spermatocytes undergoing prophase, 10 of the top 30 enriched kinases were CDKs with CDK2 in the second position (Li et al., 2022). The increased number of proteomic studies in several organisms, the development of improved techniques to enrich cell populations in specific prophase stages, along with the analysis of the corresponding phosphomutants, will help to broad our current knowledge of the fascinating process of

gamete generation and the efficient genome transmission from one generation to the next.

Author contributions

IP-B and CM-C contributed to conceptualization, original draft preparation, writing and editing.

Funding

Work in our laboratory is funded by grants from the MCIN/AEI/10.13039/501100011033/& FEDER "*Una manera de hacer Europa*," Grant Number FEDER-PGC2018-101908-B-I00; and Junta de Castilla y León, Grant Number CSI259P20 which is co-funded by FEDER program. Furthermore, our institute (IBFG) is funded by the Program "Escalera de Excelencia" of the Junta de Castilla y León Ref. CLU-2017-03 co-funded by the P.O. FEDER of Castilla y León 14-20; and the Internationalization Project "CL-EI-2021-08 - IBFG Unit of Excellence" of the CSIC, funded by the Junta de Castilla y León and co-financed by the European Union (ERDF "Europe drives our growth").

Acknowledgments

We acknowledge support of the publication fee by the CSIC Open Access Publication Support Initiative through its Unit of Information Resources for Research (URICI). IP-B. is a Ph.D. student funded by the "Ministerio de Universidades" with an FPU19/03456 grant.

Conflict of interest

The authors declare that the research was conducted in the absence of any commercial or financial relationships that could be construed as a potential conflict of interest.

Publisher's note

References

Alonso-Ramos, P., Alvarez-Melo, D., Strouhalova, K., Pascual-Silva, C., Garside, G. B., Arter, M., et al. (2021). The Cdc14 phosphatase controls resolution of recombination intermediates and crossover formation during meiosis. *Int. J. Mol. Sci.* 22 (18), 9811. doi:10.3390/ijms22189811

Alves-Rodrigues, I., Ferreira, P. G., Moldon, A., Vivancos, A. P., Hidalgo, E., Guigo, R., et al. (2016). Spatiotemporal control of forkhead binding to DNA regulates the meiotic gene expression program. *Cell Rep.* 14 (4), 885–895. doi:10.1016/j.celrep.2015.12.074

Amelina, H., Subramaniam, S., Moiseeva, V., Armstrong, C. A., Pearson, S. R., and Tomita, K. (2015). Telomere protein Rap1 is a charge resistant scaffolding protein in chromosomal bouquet formation. *BMC Biol.* 13, 37. doi:10.1186/s12915-015-0149-x

Arter, M., Hurtado-Nieves, V., Oke, A., Zhuge, T., Wettstein, R., Fung, J. C., et al. (2018). Regulated crossing-over requires inactivation of yen1/GEN1 resolvase during meiotic prophase I. *Dev. Cell* 45 (6), 785–800. e786. doi:10.1016/j.devcel.2018.05.020

Ashley, T., Walpita, D., and de Rooij, D. G. (2001). Localization of two mammalian cyclin dependent kinases during mammalian meiosis. *J. Cell Sci.* 114 (4), 685–693. doi:10.1242/jcs.114.4.685

Azumi, Y., Liu, D., Zhao, D., Li, W., Wang, G., Hu, Y., et al. (2002). Homolog interaction during meiotic prophase I in Arabidopsis requires the SOLO DANCERS gene encoding a novel cyclin-like protein. *EMBO J.* 21 (12), 3081–3095. doi:10.1093/emboj/cdf285

Bass, H. W. (2003). Telomere dynamics unique to meiotic prophase: Formation and significance of the bouquet. *Cell. Mol. Life Sci.* 60 (11), 2319–2324. doi:10.1007/s00018-003-3312-4

Berthet, C., Aleem, E., Coppola, V., Tessarollo, L., and Kaldis, P. (2003). Cdk2 knockout mice are viable. *Curr. Biol.* 13 (20), 1775–1785. doi:10.1016/j.cub.2003.09.024

Blanco, M. G., and Matos, J. (2015). Hold your horSSEs: Controlling structure-selective endonucleases MUS81 and yen1/GEN1. *Front. Genet.* 6, 253. doi:10.3389/fgene.2015.00253

Blanco, M. G., Matos, J., and West, S. C. (2014). Dual control of Yen1 nuclease activity and cellular localization by Cdk and Cdc14 prevents genome instability. *Mol. Cell* 54 (1), 94–106. doi:10.1016/j.molcel.2014.02.011

Blitzblau, H. G., and Hochwagen, A. (2013). ATR/Mec1 prevents lethal meiotic recombination initiation on partially replicated chromosomes in budding yeast. *Elife* 2, e00844. doi:10.7554/eLife.00844

Bondarieva, A., Raveendran, K., Telychko, V., Rao, H., Ravindranathan, R., Zorzompokou, C., et al. (2020). Proline-rich protein PRR19 functions with cyclin-like CNTD1 to promote meiotic crossing over in mouse. *Nat. Commun.* 11 (1), 3101. doi:10.1038/s41467-020-16885-3

Borde, V., Goldman, A. S., and Lichten, M. (2000). Direct coupling between meiotic DNA replication and recombination initiation. *Science* 290 (5492), 806–809. doi:10.1126/science.290.5492.806

Bouuaert, C. C., and Keeney, S. (2016). DNA. Breaking DNA. *Science* 351 (6276), 916–917. doi:10.1126/science.aaf2509

Brandt, J. N., Hussey, K. A., and Kim, Y. (2020). Spatial and temporal control of targeting Polo-like kinase during meiotic prophase. *J. Cell Biol.* 219 (11), e202006094. doi:10.1083/jcb.202006094

Bustamante-Jaramillo, L. F., Ramos, C., Alonso, L., Sesmero, A., Segurado, M., and Martin-Castellanos, C. (2019). CDK contribution to DSB formation and recombination in fission yeast meiosis. *PLoS Genet.* 15 (1), e1007876. doi:10.1371/journal.pgen.1007876

Bustamante-Jaramillo, L. F., Ramos, C., and Martin-Castellanos, C. (2021). The meiosis-specific Crs1 cyclin is required for efficient S-phase progression and stable nuclear architecture. *Int. J. Mol. Sci.* 22 (11), 5483. doi:10.3390/ijms22115483

Cannavo, E., Sanchez, A., Anand, R., Ranjha, L., Hugener, J., Adam, C., et al. (2020). Regulation of the MLH1-MLH3 endonuclease in meiosis. *Nature* 586 (7830), 618–622. doi:10.1038/s41586-020-2592-2

Carlile, T. M., and Amon, A. (2008). Meiosis I is established through division-specific translational control of a cyclin. *Cell* 133 (2), 280–291. doi:10.1016/j.cell.2008.02.032

Chan, Y. W., and West, S. C. (2014). Spatial control of the GEN1 Holliday junction resolvase ensures genome stability. *Nat. Commun.* 5, 4844. doi:10.1038/ncomms5844

Chen, Y., Wang, Y., Chen, J., Zuo, W., Fan, Y., Huang, S., et al. (2021). The SUN1-SPDYA interaction plays an essential role in meiosis prophase I. *Nat. Commun.* 12 (1), 3176. doi:10.1038/s41467-021-23550-w

Chikashige, Y., Tsutsumi, C., Yamane, M., Okamasa, K., Haraguchi, T., and Hiraoka, Y. (2006). Meiotic proteins bqt1 and bqt2 tether telomeres to form the bouquet arrangement of chromosomes. *Cell* 125 (1), 59–69. doi:10.1016/j.cell.2006.01.048

Chikashige, Y., Yamane, M., Okamasa, K., Tsutsumi, C., Kojidani, T., Sato, M., et al. (2009). Membrane proteins Bqt3 and -4 anchor telomeres to the nuclear envelope to ensure chromosomal bouquet formation. *J. Cell Biol.* 187 (3), 413–427. doi:10.1083/jcb.200902122

Chotiner, J. Y., Wolgemuth, D. J., and Wang, P. J. (2019). Functions of cyclins and CDKs in mammalian gametogenesis. *Biol. Reprod.* 101 (3), 591–601. doi:10.1093/biolre/ioz070

Chuang, Y. C., and Smith, G. R. (2022). Dynamic configurations of meiotic DNA-break hotspot determinant proteins. *J. Cell Sci.* 135 (3), jcs259061. doi:10.1242/jcs.259061

Chung, G., Rose, A. M., Petalcorin, M. I., Martin, J. S., Kessler, Z., Sanchez-Pulido, L., et al. (2015). REC-1 and HIM-5 distribute meiotic crossovers and function redundantly in meiotic double-strand break formation in *Caenorhabditis elegans*. *Genes Dev.* 29 (18), 1969–1979. doi:10.1101/gad.266056.115

Claeys Bouuaert, C., Pu, S., Wang, J., Oger, C., Daccache, D., Xie, W., et al. (2021). DNA-driven condensation assembles the meiotic DNA break machinery. *Nature* 592 (7852), 144–149. doi:10.1038/s41586-021-03374-w

Cohen, P. E., and Pollard, J. W. (2001). Regulation of meiotic recombination and prophase I progression in mammals. *Bioessays* 23 (11), 996–1009. doi:10.1002/bies.1145

Coudreuse, D., and Nurse, P. (2010). Driving the cell cycle with a minimal CDK control network. *Nature* 468 (7327), 1074–1079. doi:10.1038/nature09543

Davis, L., Rozalen, A. E., Moreno, S., Smith, G. R., and Martin-Castellanos, C. (2008). Rec25 and Rec27, novel linear-element components, link cohesin to meiotic DNA breakage and recombination. *Curr. Biol.* 18 (11), 849–854. doi:10.1016/j.cub.2008.05.025

Dehe, P. M., Coulon, S., Scaglione, S., Shanahan, P., Takedachi, A., Wohlschlegel, J. A., et al. (2013). Regulation of Mus81-Eme1 Holliday junction resolvase in response to DNA damage. *Nat. Struct. Mol. Biol.* 20 (5), 598–603. doi:10.1038/nsmb.2550

Ding, D. Q., Matsuda, A., Okamasa, K., and Hiraoka, Y. (2021). Linear elements are stable structures along the chromosome axis in fission yeast meiosis. *Chromosoma* 130 (2-3), 149–162. doi:10.1007/s00412-021-00757-w

Ding, D. Q., Yamamoto, A., Haraguchi, T., and Hiraoka, Y. (2004). Dynamics of homologous chromosome pairing during meiotic prophase in fission yeast. *Dev. Cell* 6 (3), 329–341. doi:10.1016/s1534-5807(04)00059-0

Ding, X., Xu, R., Yu, J., Xu, T., Zhuang, Y., and Han, M. (2007). SUN1 is required for telomere attachment to nuclear envelope and gametogenesis in mice. *Dev. Cell* 12 (6), 863–872. doi:10.1016/j.devcel.2007.03.018

Dissmeyer, N., Nowack, M. K., Pusch, S., Stals, H., Inze, D., Grini, P. E., et al. (2007). T-loop phosphorylation of Arabidopsis CDKA;1 is required for its function and can be partially substituted by an aspartate residue. *Plant Cell* 19 (3), 972–985. doi:10.1105/tpc.107.050401

Eissler, C. L., Mazon, G., Powers, B. L., Savinov, S. N., Symington, L. S., and Hall, M. C. (2014). The Cdk/cDc14 module controls activation of the Yen1 holliday junction resolvase to promote genome stability. *Mol. Cell* 54 (1), 80–93. doi:10.1016/j.molcel.2014.02.012

Ellenrieder, C., Bartosch, B., Lee, G. Y., Murphy, M., Sweeney, C., Hergersberg, M., et al. (2001). The long form of CDK2 arises via alternative splicing and forms an active protein kinase with cyclins A and E. *DNA Cell Biol.* 20 (7), 413–423. doi:10.1089/104454901750361479

Faber, E. B., Wang, N., and Georg, G. I. (2020). Review of rationale and progress toward targeting cyclin-dependent kinase 2 (CDK2) for male contraception. *Biol. Reprod.* 103 (2), 357–367. doi:10.1093/biolre/ioaa107

Fan, J., Sun, Z., and Wang, Y. (2022). The assembly of a noncanonical LINC complex in *Saccharomyces cerevisiae*. *Curr. Genet.* 68 (1), 91–96. doi:10.1007/s00294-021-01220-0

Folco, H. D., Chalamcharla, V. R., Sugiyama, T., Thillainadesan, G., Zofall, M., Balachandran, V., et al. (2017). Untimely expression of gametogenic genes in vegetative cells causes uniparental disomy. *Nature* 543 (7643), 126–130. doi:10.1038/nature21372

Fowler, K. R., Gutierrez-Velasco, S., Martin-Castellanos, C., and Smith, G. R. (2013). Protein determinants of meiotic DNA break hot spots. *Mol. Cell* 49 (5), 983–996. doi:10.1016/j.molcel.2013.01.008

Fujita, I., Nishihara, Y., Tanaka, M., Tsujii, H., Chikashige, Y., Watanabe, Y., et al. (2012). Telomere-nuclear envelope dissociation promoted by Rap1 phosphorylation ensures faithful chromosome segregation. *Curr. Biol.* 22 (20), 1932–1937. doi:10.1016/j.cub.2012.08.019

Gallo-Fernandez, M., Saugar, I., Ortiz-Bazan, M. A., Vazquez, M. V., and Tercero, J. A. (2012). Cell cycle-dependent regulation of the nuclease activity of Mus81-Eme1/Mms4. *Nucleic Acids Res.* 40 (17), 8325–8335. doi:10.1093/nar/gks599

Garcia-Luis, J., Clemente-Blanco, A., Aragon, L., and Machin, F. (2014). Cdc14 targets the Holliday junction resolvase Yen1 to the nucleus in early anaphase. *Cell Cycle* 13 (9), 1392–1399. doi:10.4161/cc.28370

Gray, S., Santiago, E. R., Chappie, J. S., and Cohen, P. E. (2020). Cyclin N-terminal domain-containing-1 coordinates meiotic crossover formation with cell-cycle progression in a cyclin-independent manner. *Cell Rep.* 32 (1), 107858. doi:10.1016/j.celrep.2020.107858

Grigaitis, R., Ranjha, L., Wild, P., Kasaciunaite, K., Ceppi, I., Kissling, V., et al. (2020). Phosphorylation of the RecQ helicase Sgs1/BLM controls its DNA unwinding activity during meiosis and mitosis. *Dev. Cell* 53 (6), 706–723. e705. doi:10.1016/j.devcel.2020.05.016

Gutierrez-Escribano, P., and Nurse, P. (2015). A single cyclin-CDK complex is sufficient for both mitotic and meiotic progression in fission yeast. *Nat. Commun.* 6, 6871. doi:10.1038/ncomms7871

Harashima, H., Dissmeyer, N., and Schnittger, A. (2013). Cell cycle control across the eukaryotic kingdom. *Trends Cell Biol.* 23 (7), 345–356. doi:10.1016/j.tcb.2013.03.002

Harper, L., Golubovskaya, I., and Cande, W. Z. (2004). A bouquet of chromosomes. *J. Cell Sci.* 117 (18), 4025–4032. doi:10.1242/jcs.01363

Hassold, T., Hall, H., and Hunt, P. (2007). The origin of human aneuploidy: Where we have been, where we are going. *Hum. Mol. Genet.* 16 (2), R203–R208. doi:10.1093/hmg/ddm243

Haversat, J., Woglar, A., Klatt, K., Akerib, C. C., Roberts, V., Chen, S. Y., et al. (2022). Robust designation of meiotic crossover sites by CDK-2 through phosphorylation of the MutSγ complex. *Proc. Natl. Acad. Sci. U. S. A.* 119 (21), e2117865119. doi:10.1073/pnas.2117865119

Henderson, K. A., Kee, K., Maleki, S., Santini, P. A., and Keeney, S. (2006). Cyclin-dependent kinase directly regulates initiation of meiotic recombination. *Cell* 125 (7), 1321–1332. doi:10.1016/j.cell.2006.04.039

Hiraoka, Y., and Dernburg, A. F. (2009). The SUN rises on meiotic chromosome dynamics. *Dev. Cell* 17 (5), 598–605. doi:10.1016/j.devcel.2009.10.014

Holloway, J. K., Sun, X., Yokoo, R., Villeneuve, A. M., and Cohen, P. E. (2014). Mammalian CNTD1 is critical for meiotic crossover maturation and deselection of excess precrossover sites. *J. Cell Biol.* 205 (5), 633–641. doi:10.1083/jcb.201401122

Hu, C., Inoue, H., Sun, W., Takeshita, Y., Huang, Y., Xu, Y., et al. (2019). Structural insights into chromosome attachment to the nuclear envelope by an inner nuclear membrane protein Bqt4 in fission yeast. *Nucleic Acids Res.* 47 (3), 1573–1584. doi:10.1093/nar/gky1186

Huang, X. Y., Niu, J., Sun, M. X., Zhu, J., Gao, J. F., Yang, J., et al. (2013). CYCLIN-DEPENDENT KINASE G1 is associated with the spliceosome to regulate CALLOSE SYNTHASE5 splicing and pollen wall formation in Arabidopsis. *Plant Cell* 25 (2), 637–648. doi:10.1105/tpc.112.107896

Hunt, P., and Hassold, T. (2010). Female meiosis: Coming unglued with age. *Curr. Biol.* 20 (17), R699–R702. doi:10.1016/j.cub.2010.08.011

Hunter, N., and Kleckner, N. (2001). The single-end invasion: An asymmetric intermediate at the double-strand break to double-holliday junction transition of meiotic recombination. *Cell* 106 (1), 59–70. doi:10.1016/s0092-8674(01)00430-5

Hunter, N. (2015). Meiotic recombination: The essence of heredity. *Cold Spring Harb. Perspect. Biol.* 7 (12), a016618. doi:10.1101/cshperspect.a016618

Huttlin, E. L., Jedrychowski, M. P., Elias, J. E., Goswami, T., Rad, R., Beausoleil, S. A., et al. (2010). A tissue-specific atlas of mouse protein phosphorylation and expression. *Cell* 143 (7), 1174–1189. doi:10.1016/j.cell.2010.12.001

Ishiguro, T., Tanaka, K., Sakuno, T., and Watanabe, Y. (2010). Shugoshin-PP2A counteracts casein-kinase-1-dependent cleavage of Rec8 by separase. *Nat. Cell Biol.* 12 (5), 500–506. doi:10.1038/ncb2052

Kar, F. M., and Hochwagen, A. (2021). Phospho-regulation of meiotic prophase. *Front. Cell Dev. Biol.* 9, 667073. doi:10.3389/fcell.2021.667073

Karaiskou, A., Perez, L. H., Ferby, I., Ozon, R., Jessus, C., and Nebreda, A. R. (2001). Differential regulation of Cdc2 and Cdk2 by RINGO and cyclins. *J. Biol. Chem.* 276 (38), 36028–36034. doi:10.1074/jbc.M104722200

Kciuk, M., Gielecinska, A., Mujwar, S., Mojzych, M., and Kontek, R. (2022). Cyclin-dependent kinases in DNA damage response. *Biochim. Biophys. Acta. Rev. Cancer* 1877 (3), 188716. doi:10.1016/j.bbcan.2022.188716

Keeney, S., Giroux, C. N., and Kleckner, N. (1997). Meiosis-specific DNA double-strand breaks are catalyzed by Spo11, a member of a widely conserved protein family. *Cell* 88 (3), 375–384. doi:10.1016/s0092-8674(00)81876-0

Keeney, S., Lange, J., and Mohibullah, N. (2014). Self-organization of meiotic recombination initiation: General principles and molecular pathways. *Annu. Rev. Genet.* 48, 187–214. doi:10.1146/annurev-genet-120213-092304

Kim, Y., Kostow, N., and Dernburg, A. F. (2015). The chromosome Axis mediates feedback control of CHK-2 to ensure crossover formation in *C. elegans*. *Dev. Cell* 35 (2), 247–261. doi:10.1016/j.devcel.2015.09.021

Klutstein, M., and Cooper, J. P. (2014). The Chromosomal Courtship Dance-homolog pairing in early meiosis. *Curr. Opin. Cell Biol.* 26, 123–131. doi:10.1016/j.ceb.2013.12.004

Klutstein, M., Fennell, A., Fernandez-Alvarez, A., and Cooper, J. P. (2015). The telomere bouquet regulates meiotic centromere assembly. *Nat. Cell Biol.* 17 (4), 458–469. doi:10.1038/ncb3132

Koszul, R., and Kleckner, N. (2009). Dynamic chromosome movements during meiosis: A way to eliminate unwanted connections? *Trends Cell Biol.* 19 (12), 716–724. doi:10.1016/j.tcb.2009.09.007

Kulkarni, D. S., Owens, S. N., Honda, M., Ito, M., Yang, Y., Corrigan, M. W., et al. (2020). PCNA activates the MutLγ endonuclease to promote meiotic crossing over. *Nature* 586 (7830), 623–627. doi:10.1038/s41586-020-2645-6

Lai, Y. J., Lin, F. M., Chuang, M. J., Shen, H. J., and Wang, T. F. (2011). Genetic requirements and meiotic function of phosphorylation of the yeast axial element protein Red1. *Mol. Cell. Biol.* 31 (5), 912–923. doi:10.1128/MCB.00895-10

Lam, I., and Keeney, S. (2014). Mechanism and regulation of meiotic recombination initiation. *Cold Spring Harb. Perspect. Biol.* 7 (1), a016634. doi:10.1101/cshperspect.a016634

Li, H., Chen, H., Zhang, X., Qi, Y., Wang, B., Cui, Y., et al. (2022). Global phosphoproteomic analysis identified key kinases regulating male meiosis in mouse. *Cell. Mol. Life Sci.* 79 (8), 467. doi:10.1007/s00018-022-04507-8

Li, J., Qian, W. P., and Sun, Q. Y. (2019). Cyclins regulating oocyte meiotic cell cycle progression. *Biol. Reprod.* 101 (5), 878–881. doi:10.1093/biolre/ioz143

Link, J., Jahn, D., and Alsheimer, M. (2015). Structural and functional adaptations of the mammalian nuclear envelope to meet the meiotic requirements. *Nucleus* 6 (2), 93–101. doi:10.1080/19491034.2015.1004941

Link, J., Leubner, M., Schmitt, J., Gob, E., Benavente, R., Jeang, K. T., et al. (2014). Analysis of meiosis in SUN1 deficient mice reveals a distinct role of SUN2 in mammalian meiotic LINC complex formation and function. *PLoS Genet.* 10 (2), e1004099. doi:10.1371/journal.pgen.1004099

Liu, W., Wang, L., Zhao, W., Song, G., Xu, R., Wang, G., et al. (2014). Phosphorylation of CDK2 at threonine 160 regulates meiotic pachytene and diplotene progression in mice. *Dev. Biol.* 392 (1), 108–116. doi:10.1016/j.ydbio.2014.04.018

Lorenz, A., Wells, J. L., Pryce, D. W., Novatchkova, M., Eisenhaber, F., McFarlane, R. J., et al. (2004). *S. pombe* meiotic linear elements contain proteins related to synaptonemal complex components. *J. Cell Sci.* 117 (15), 3343–3351. doi:10.1242/jcs.01203

MacKenzie, A. M., and Lacefield, S. (2020). CDK regulation of meiosis: Lessons from *S. cerevisiae* and *S. pombe*. *Genes (Basel)* 11 (7), E723. doi:10.3390/genes11070723

MacQueen, A. J., and Villeneuve, A. M. (2001). Nuclear reorganization and homologous chromosome pairing during meiotic prophase require *C. elegans* chk-2. *Genes Dev.* 15 (13), 1674–1687. doi:10.1101/gad.902601

Malapeira, J., Moldon, A., Hidalgo, E., Smith, G. R., Nurse, P., and Ayte, J. (2005). A meiosis-specific cyclin regulated by splicing is required for proper progression through meiosis. *Mol. Cell. Biol.* 25 (15), 6330–6337. doi:10.1128/MCB.25.15.6330-6337.2005

Malumbres, M. (2014). Cyclin-dependent kinases. *Genome Biol.* 15 (6), 122. doi:10.1186/gb4184

Manterola, M., Sicinski, P., and Wolgemuth, D. J. (2016). E-type cyclins modulate telomere integrity in mammalian male meiosis. *Chromosoma* 125 (2), 253–264. doi:10.1007/s00412-015-0564-3

Marston, A. L., and Amon, A. (2004). Meiosis: Cell-cycle controls shuffle and deal. *Nat. Rev. Mol. Cell Biol.* 5 (12), 983–997. doi:10.1038/nrm1526

Martin-Castellanos, C., Fowler, K. R., and Smith, G. R. (2013). Making chromosomes hot for breakage. *Cell Cycle* 12 (9), 1327–1328. doi:10.4161/cc.24576

Martinerie, L., Manterola, M., Chung, S. S., Panigrahi, S. K., Weisbach, M., Vasileva, A., et al. (2014). Mammalian E-type cyclins control chromosome pairing, telomere stability and CDK2 localization in male meiosis. *PLoS Genet.* 10 (2), e1004165. doi:10.1371/journal.pgen.1004165

Matos, J., Blanco, M. G., Maslen, S., Skehel, J. M., and West, S. C. (2011). Regulatory control of the resolution of DNA recombination intermediates during meiosis and mitosis. *Cell* 147 (1), 158–172. doi:10.1016/j.cell.2011.08.032

Matos, J., Blanco, M. G., and West, S. C. (2013). Cell-cycle kinases coordinate the resolution of recombination intermediates with chromosome segregation. *Cell Rep.* 4 (1), 76–86. doi:10.1016/j.celrep.2013.05.039

Mikolcevic, P., Isoda, M., Shibuya, H., del Barco Barrantes, I., Igea, A., Suja, J. A., et al. (2016). Essential role of the Cdk2 activator RingoA in meiotic telomere tethering to the nuclear envelope. *Nat. Commun.* 7, 11084. doi:10.1038/ncomms11084

Miyoshi, T., Ito, M., Kugou, K., Yamada, S., Furuichi, M., Oda, A., et al. (2012). A central coupler for recombination initiation linking chromosome architecture to S phase checkpoint. *Mol. Cell* 47 (5), 722–733. doi:10.1016/j.molcel.2012.06.023

Moiseeva, V., Amelina, H., Collopy, L. C., Armstrong, C. A., Pearson, S. R., and Tomita, K. (2017). The telomere bouquet facilitates meiotic prophase progression and exit in fission yeast. *Cell Discov.* 3, 17041. doi:10.1038/celldisc.2017.41

Moldon, A., Malapeira, J., Gabrielli, N., Gogol, M., Gomez-Escoda, B., Ivanova, T., et al. (2008). Promoter-driven splicing regulation in fission yeast. *Nature* 455 (7215), 997–1000. doi:10.1038/nature07325

Molnar, M., Doll, E., Yamamoto, A., Hiraoka, Y., and Kohli, J. (2003). Linear element formation and their role in meiotic sister chromatid cohesion and chromosome pairing. *J. Cell Sci.* 116 (9), 1719–1731. doi:10.1242/jcs.00387

Morgan, D. O. (1995). Principles of CDK regulation. *Nature* 374 (6518), 131–134. doi:10.1038/374131a0

Murakami, H., and Keeney, S. (2008). Regulating the formation of DNA double-strand breaks in meiosis. *Genes Dev.* 22 (3), 286–292. doi:10.1101/gad.1642308

Murakami, H., and Keeney, S. (2014). Temporospatial coordination of meiotic DNA replication and recombination via DDK recruitment to replisomes. *Cell* 158 (4), 861–873. doi:10.1016/j.cell.2014.06.028

Nagaoka, S. I., Hassold, T. J., and Hunt, P. A. (2012). Human aneuploidy: Mechanisms and new insights into an age-old problem. *Nat. Rev. Genet.* 13 (7), 493–504. doi:10.1038/nrg3245

Nambiar, M., and Smith, G. R. (2018). Pericentromere-specific cohesin complex prevents meiotic pericentric DNA double-strand breaks and lethal crossovers. *Mol. Cell* 71 (4), 540–553. e544. doi:10.1016/j.molcel.2018.06.035

Ogino, K., Hirota, K., Matsumoto, S., Takeda, T., Ohta, K., Arai, K., et al. (2006). Hsk1 kinase is required for induction of meiotic dsDNA breaks without involving checkpoint kinases in fission yeast. *Proc. Natl. Acad. Sci. U. S. A.* 103 (21), 8131–8136. doi:10.1073/pnas.0602498103

Ogino, K., and Masai, H. (2006). Rad3-Cds1 mediates coupling of initiation of meiotic recombination with DNA replication. Mei4-dependent transcription as a potential target of meiotic checkpoint. *J. Biol. Chem.* 281 (3), 1338–1344. doi:10.1074/jbc.M505767200

Ortega, S., Prieto, I., Odajima, J., Martin, A., Dubus, P., Sotillo, R., et al. (2003). Cyclin-dependent kinase 2 is essential for meiosis but not for mitotic cell division in mice. *Nat. Genet.* 35 (1), 25–31. doi:10.1038/ng1232

Padmore, R., Cao, L., and Kleckner, N. (1991). Temporal comparison of recombination and synaptonemal complex formation during meiosis in *S. cerevisiae*. *Cell* 66 (6), 1239–1256. doi:10.1016/0092-8674(91)90046-2

Palmer, N., Talib, S. Z. A., and Kaldis, P. (2019). Diverse roles for CDK-associated activity during spermatogenesis. *FEBS Lett.* 593 (20), 2925–2949. doi:10.1002/1873-3468.13627

Palmer, N., Talib, S. Z. A., Singh, P., Goh, C. M. F., Liu, K., Schimenti, J. C., et al. (2020). A novel function for CDK2 activity at meiotic crossover sites. *PLoS Biol.* 18 (10), e3000903. doi:10.1371/journal.pbio.3000903

Panizza, S., Mendoza, M. A., Berlinger, M., Huang, L., Nicolas, A., Shirahige, K., et al. (2011). Spo11-accessory proteins link double-strand break sites to the chromosome axis in early meiotic recombination. *Cell* 146 (3), 372–383. doi:10.1016/j.cell.2011.07.003

Patel, J. T., Bottrill, A., Prosser, S. L., Jayaraman, S., Straatman, K., Fry, A. M., et al. (2014). Mitotic phosphorylation of SUN1 loosens its connection with the nuclear lamina while the LINC complex remains intact. *Nucleus* 5 (5), 462–473. doi:10.4161/nucl.36232

Payliss, B. J., Tse, Y. W. E., Reichheld, S. E., Lemak, A., Yun, H. Y., Houliston, S., et al. (2022). Phosphorylation of the DNA repair scaffold SLX4 drives folding of the SAP domain and activation of the MUS81-EME1 endonuclease. *Cell Rep.* 41 (4), 111537. doi:10.1016/j.celrep.2022.111537

Penkner, A. M., Fridkin, A., Gloggnitzer, J., Baudrimont, A., Machacek, T., Woglar, A., et al. (2009). Meiotic chromosome homology search involves modifications of the nuclear envelope protein Matefin/SUN-1. *Cell* 139 (5), 920–933. doi:10.1016/j.cell.2009.10.045

Petronczki, M., Siomos, M. F., and Nasmyth, K. (2003). Un menage a quatre: The molecular biology of chromosome segregation in meiosis. *Cell* 112 (4), 423–440. doi:10.1016/s0092-8674(03)00083-7

Phadnis, N., Cipak, L., Polakova, S., Hyppa, R. W., Cipakova, I., Anrather, D., et al. (2015). Casein kinase 1 and phosphorylation of cohesin subunit Rec11 (SA3) promote meiotic recombination through linear element formation. *PLoS Genet.* 11 (5), e1005225. doi:10.1371/journal.pgen.1005225

Polakova, S., Molnarova, L., Hyppa, R. W., Benko, Z., Misova, I., Schleiffer, A., et al. (2016). Dbl2 regulates Rad51 and DNA joint molecule metabolism to ensure proper meiotic chromosome segregation. *PLoS Genet.* 12 (6), e1006102. doi:10.1371/journal.pgen.1006102

Prasada Rao, H. B., Sato, T., Challa, K., Fujita, Y., Shinohara, M., and Shinohara, A. (2021). Phosphorylation of luminal region of the SUN-domain protein Mps3 promotes nuclear envelope localization during meiosis. *Elife* 10, e63119. doi:10.7554/eLife.63119

Qiao, H., Prasada Rao, H. B., Yang, Y., Fong, J. H., Cloutier, J. M., Deacon, D. C., et al. (2014). Antagonistic roles of ubiquitin ligase HEI10 and SUMO ligase

RNF212 regulate meiotic recombination. *Nat. Genet.* 46 (2), 194–199. doi:10.1038/ng.2858

Reynolds, A., Qiao, H., Yang, Y., Chen, J. K., Jackson, N., Biswas, K., et al. (2013). RNF212 is a dosage-sensitive regulator of crossing-over during mammalian meiosis. *Nat. Genet.* 45 (3), 269–278. doi:10.1038/ng.2541

Robert, T., Nore, A., Brun, C., Maffre, C., Crimi, B., Bourbon, H. M., et al. (2016). The TopoVIB-Like protein family is required for meiotic DNA double-strand break formation. *Science* 351 (6276), 943–949. doi:10.1126/science.aad5309

Rosu, S., Zawadzki, K. A., Stamper, E. L., Libuda, D. E., Reese, A. L., Dernburg, A. F., et al. (2013). The *C. elegans* DSB-2 protein reveals a regulatory network that controls competence for meiotic DSB formation and promotes crossover assurance. *PLoS Genet.* 9 (8), e1003674. doi:10.1371/journal.pgen.1003674

Rumpf, C., Cipak, L., Dudas, A., Benko, Z., Pozgajova, M., Riedel, C. G., et al. (2010). Casein kinase 1 is required for efficient removal of Rec8 during meiosis I. *Cell Cycle* 9 (13), 2657–2662. doi:10.4161/cc.9.13.12146

Sakuno, T., and Watanabe, Y. (2009). Studies of meiosis disclose distinct roles of cohesion in the core centromere and pericentromeric regions. *Chromosome Res.* 17 (2), 239–249. doi:10.1007/s10577-008-9013-y

San-Segundo, P. A., and Clemente-Blanco, A. (2020). Resolvases, dissolvases, and helicases in homologous recombination: Clearing the road for chromosome segregation. *Genes (Basel)* 11 (1), E71. doi:10.3390/genes11010071

Scherthan, H. (2007). Telomere attachment and clustering during meiosis. *Cell. Mol. Life Sci.* 64 (2), 117–124. doi:10.1007/s00018-006-6463-2

Shibuya, H., Hernandez-Hernandez, A., Morimoto, A., Negishi, L., Hoog, C., and Watanabe, Y. (2015). MAJIN links telomeric DNA to the nuclear membrane by exchanging telomere cap. *Cell* 163 (5), 1252–1266. doi:10.1016/j.cell.2015.10.030

Shibuya, H., Ishiguro, K., and Watanabe, Y. (2014). The TRF1-binding protein TERB1 promotes chromosome movement and telomere rigidity in meiosis. *Nat. Cell Biol.* 16 (2), 145–156. doi:10.1038/ncb2896

Shibuya, H., and Watanabe, Y. (2014). The meiosis-specific modification of mammalian telomeres. *Cell Cycle* 13 (13), 2024–2028. doi:10.4161/cc.29350

Sou, I. F., Hamer, G., Tee, W.-W., Vader, G., and McClurg, U. L. (2022). Cancer and meiotic gene expression: Two sides of the same coin? *Curr. Top. Dev. Biol.* E-pub ahead of print. doi:10.1016/bs.ctdb.2022.06.002

Spirek, M., Estreicher, A., Csaszar, E., Wells, J., McFarlane, R. J., Watts, F. Z., et al. (2010). SUMOylation is required for normal development of linear elements and wild-type meiotic recombination in *Schizosaccharomyces pombe*. *Chromosoma* 119 (1), 59–72. doi:10.1007/s00412-009-0241-5

Stamper, E. L., Rodenbusch, S. E., Rosu, S., Ahringer, J., Villeneuve, A. M., and Dernburg, A. F. (2013). Identification of DSB-1, a protein required for initiation of meiotic recombination in *Caenorhabditis elegans*, illuminates a crossover assurance checkpoint. *PLoS Genet.* 9 (8), e1003679. doi:10.1371/journal.pgen.1003679

Stern, B., and Nurse, P. (1996). A quantitative model for the cdc2 control of S phase and mitosis in fission yeast. *Trends Genet.* 12 (9), 345–350. doi:10.1016/s0168-9525(96)80016-3

Sun, W., Lorenz, A., Osman, F., and Whitby, M. C. (2011). A failure of meiotic chromosome segregation in a fbh1Delta mutant correlates with persistent Rad51-DNA associations. *Nucleic Acids Res.* 39 (5), 1718–1731. doi:10.1093/nar/gkq977

Swaffer, M. P., Jones, A. W., Flynn, H. R., Snijders, A. P., and Nurse, P. (2016). CDK substrate phosphorylation and ordering the cell cycle. *Cell* 167 (7), 1750–1761. e1716. doi:10.1016/j.cell.2016.11.034

Szakal, B., and Branzei, D. (2013). Premature Cdk1/Cdc5/Mus81 pathway activation induces aberrant replication and deleterious crossover. *EMBO J.* 32 (8), 1155–1167. doi:10.1038/emboj.2013.67

Tang, X., Jin, Y., and Cande, W. Z. (2006). Bqt2p is essential for initiating telomere clustering upon pheromone sensing in fission yeast. *J. Cell Biol.* 173 (6), 845–851. doi:10.1083/jcb.200602152

Toby, G. G., Gherraby, W., Coleman, T. R., and Golemis, E. A. (2003). A novel RING finger protein, human enhancer of invasion 10, alters mitotic progression through regulation of cyclin B levels. *Mol. Cell. Biol.* 23 (6), 2109–2122. doi:10.1128/MCB.23.6.2109-2122.2003

Tomita, K., and Cooper, J. P. (2006). The meiotic chromosomal bouquet: SUN collects flowers. *Cell* 125 (1), 19–21. doi:10.1016/j.cell.2006.03.020

Tomita, K., and Cooper, J. P. (2007). The telomere bouquet controls the meiotic spindle. *Cell* 130 (1), 113–126. doi:10.1016/j.cell.2007.05.024

Tonami, Y., Murakami, H., Shirahige, K., and Nakanishi, M. (2005). A checkpoint control linking meiotic S phase and recombination initiation in fission yeast. *Proc. Natl. Acad. Sci. U. S. A.* 102 (16), 5797–5801. doi:10.1073/pnas.0407236102

Trovesi, C., Manfrini, N., Falcettoni, M., and Longhese, M. P. (2013). Regulation of the DNA damage response by cyclin-dependent kinases. *J. Mol. Biol.* 425 (23), 4756–4766. doi:10.1016/j.jmb.2013.04.013

Tu, Z., Bayazit, M. B., Liu, H., Zhang, J., Busayavalasa, K., Risal, S., et al. (2017). Speedy A-Cdk2 binding mediates initial telomere-nuclear envelope attachment during meiotic prophase I independent of Cdk2 activation. *Proc. Natl. Acad. Sci. U. S. A.* 114 (3), 592–597. doi:10.1073/pnas.1618465114

Tuna, M., Knuutila, S., and Mills, G. B. (2009). Uniparental disomy in cancer. *Trends Mol. Med.* 15 (3), 120–128. doi:10.1016/j.molmed.2009.01.005

Ubersax, J. A., Woodbury, E. L., Quang, P. N., Paraz, M., Blethrow, J. D., Shah, K., et al. (2003). Targets of the cyclin-dependent kinase Cdk1. *Nature* 425 (6960), 859–864. doi:10.1038/nature02062

Uhlmann, F., Bouchoux, C., and Lopez-Aviles, S. (2011). A quantitative model for cyclin-dependent kinase control of the cell cycle: Revisited. *Philos. Trans. R. Soc. Lond. B Biol. Sci.* 366 (1584), 3572–3583. doi:10.1098/rstb.2011.0082

Viera, A., Alsheimer, M., Gomez, R., Berenguer, I., Ortega, S., Symonds, C. E., et al. (2015). CDK2 regulates nuclear envelope protein dynamics and telomere attachment in mouse meiotic prophase. *J. Cell Sci.* 128 (1), 88–99. doi:10.1242/jcs.154922

Viera, A., Rufas, J. S., Martinez, I., Barbero, J. L., Ortega, S., and Suja, J. A. (2009). CDK2 is required for proper homologous pairing, recombination and sex-body formation during male mouse meiosis. *J. Cell Sci.* 122 (12), 2149–2159. doi:10.1242/jcs.046706

Vrielynck, N., Chambon, A., Vezon, D., Pereira, L., Chelysheva, L., De Muyt, A., et al. (2016). A DNA topoisomerase VI-like complex initiates meiotic recombination. *Science* 351 (6276), 939–943. doi:10.1126/science.aad5196

Wan, L., Niu, H., Futcher, B., Zhang, C., Shokat, K. M., Boulton, S. J., et al. (2008). Cdc28-Clb5 (CDK-S) and Cdc7-Dbf4 (DDK) collaborate to initiate meiotic recombination in yeast. *Genes Dev.* 22 (3), 386–397. doi:10.1101/gad.1626408

Wang, G., Wu, X., Zhou, L., Gao, S., Yun, D., Liang, A., et al. (2020). Tethering of telomeres to the nuclear envelope is mediated by SUN1-MAJIN and possibly promoted by SPDYA-CDK2 during meiosis. *Front. Cell Dev. Biol.* 8, 845. doi:10.3389/fcell.2020.00845

Ward, J. O., Reinholdt, L. G., Motley, W. W., Niswander, L. M., Deacon, D. C., Griffin, L. B., et al. (2007). Mutation in mouse hei10, an e3 ubiquitin ligase, disrupts meiotic crossing over. *PLoS Genet.* 3 (8), e139. doi:10.1371/journal.pgen.0030139

Wijnker, E., Harashima, H., Muller, K., Parra-Nunez, P., de Snoo, C. B., van de Belt, J., et al. (2019). The Cdk1/Cdk2 homolog CDKA;1 controls the recombination landscape in Arabidopsis. *Proc. Natl. Acad. Sci. U. S. A.* 116 (25), 12534–12539. doi:10.1073/pnas.1820753116

Woglar, A., Daryabeigi, A., Adamo, A., Habacher, C., Machacek, T., La Volpe, A., et al. (2013). Matefin/SUN-1 phosphorylation is part of a surveillance mechanism to coordinate chromosome synapsis and recombination with meiotic progression and chromosome movement. *PLoS Genet.* 9 (3), e1003335. doi:10.1371/journal.pgen.1003335

Wyatt, H. D., Sarbajna, S., Matos, J., and West, S. C. (2013). Coordinated actions of SLX1-SLX4 and MUS81-EME1 for Holliday junction resolution in human cells. *Mol. Cell* 52 (2), 234–247. doi:10.1016/j.molcel.2013.08.035

Xu, J., Li, X., Song, W., Wang, W., and Gao, S. (2019). Cyclin Cyc2p is required for micronuclear bouquet formation in Tetrahymena thermophila. *Sci. China. Life Sci.* 62 (5), 668–680. doi:10.1007/s11427-018-9369-3

Yamamoto, A., and Hiraoka, Y. (2001). How do meiotic chromosomes meet their homologous partners?: Lessons from fission yeast. *Bioessays* 23 (6), 526–533. doi:10.1002/bies.1072

Yang, C., Sofroni, K., Wijnker, E., Hamamura, Y., Carstens, L., Harashima, H., et al. (2020). The Arabidopsis Cdk1/Cdk2 homolog CDKA;1 controls chromosome axis assembly during plant meiosis. *EMBO J.* 39 (3), e101625. doi:10.15252/embj.2019101625

Yokoo, R., Zawadzki, K. A., Nabeshima, K., Drake, M., Arur, S., and Villeneuve, A. M. (2012). COSA-1 reveals robust homeostasis and separable licensing and reinforcement steps governing meiotic crossovers. *Cell* 149 (1), 75–87. doi:10.1016/j.cell.2012.01.052

Zakharyevich, K., Tang, S., Ma, Y., and Hunter, N. (2012). Delineation of joint molecule resolution pathways in meiosis identifies a crossover-specific resolvase. *Cell* 149 (2), 334–347. doi:10.1016/j.cell.2012.03.023

Zheng, T., Nibau, C., Phillips, D. W., Jenkins, G., Armstrong, S. J., and Doonan, J. H. (2014). CDKG1 protein kinase is essential for synapsis and male meiosis at high ambient temperature in *Arabidopsis thaliana*. *Proc. Natl. Acad. Sci. U. S. A.* 111 (6), 2182–2187. doi:10.1073/pnas.1318460111

Zhu, Z., Mori, S., Oshiumi, H., Matsuzaki, K., Shinohara, M., and Shinohara, A. (2010). Cyclin-dependent kinase promotes formation of the synaptonemal complex in yeast meiosis. *Genes cells.* 15 (10), 1036–1050. doi:10.1111/j.1365-2443.2010.01440.x

Zickler, D., and Kleckner, N. (2015). Recombination, pairing, and synapsis of homologs during meiosis. *Cold Spring Harb. Perspect. Biol.* 7 (6), a016626. doi:10.1101/cshperspect.a016626

Zuela, N., and Gruenbaum, Y. (2016). Matefin/SUN-1 phosphorylation on serine 43 is mediated by CDK-1 and required for its localization to centrosomes and normal mitosis in *C. elegans* embryos. *Cells* 5 (1), E8. doi:10.3390/cells5010008

frontiers | Frontiers in Cell and Developmental Biology

TYPE Review
PUBLISHED 06 January 2023
DOI 10.3389/fcell.2022.1097446

OPEN ACCESS

EDITED BY
Ricardo Benavente,
Julius Maximilian University of Würzburg, Germany

REVIEWED BY
Kevin Corbett,
University of California, San Diego, United States
Alyssa Rodriguez,
University of California, San Diego, in collaboration with reviewer KC
Rocio Gomez,
Autonomous University of Madrid, Spain

*CORRESPONDENCE
Masaru Ito,
msrito2@protein.osaka-u.ac.jp
Akira Shinohara,
ashino@protein.osaka-u.ac.jp

SPECIALTY SECTION
This article was submitted to Nuclear Organization and Dynamics, a section of the journal Frontiers in Cell and Developmental Biology

RECEIVED 13 November 2022
ACCEPTED 22 December 2022
PUBLISHED 06 January 2023

CITATION
Ito M and Shinohara A (2023), Chromosome architecture and homologous recombination in meiosis. *Front. Cell Dev. Biol.* 10:1097446. doi: 10.3389/fcell.2022.1097446

Chromosome architecture and homologous recombination in meiosis

Masaru Ito* and Akira Shinohara*

Institute for Protein Research, Osaka University, Suita, Osaka, Japan

Meiocytes organize higher-order chromosome structures comprising arrays of chromatin loops organized at their bases by linear axes. As meiotic prophase progresses, the axes of homologous chromosomes align and synapse along their lengths to form ladder-like structures called synaptonemal complexes (SCs). The entire process of meiotic recombination, from initiation *via* programmed DNA double-strand breaks (DSBs) to completion of DSB repair with crossover or non-crossover outcomes, occurs in the context of chromosome axes and SCs. These meiosis-specific chromosome structures provide specialized environments for the regulation of DSB formation and crossing over. In this review, we summarize insights into the importance of chromosome architecture in the regulation of meiotic recombination, focusing on cohesin-mediated axis formation, DSB regulation *via* tethered loop-axis complexes, inter-homolog template bias facilitated by axial proteins, and crossover regulation in the context of the SCs. We also discuss emerging evidence that the SUMO and the ubiquitin-proteasome system function in the organization of chromosome structure and regulation of meiotic recombination.

KEYWORDS

cohesin, axis-loop structure, synaptonemal complex, meiotic recombination, crossover

Introduction

Homologous recombination during meiosis underlies biological diversity and ensures proper chromosome segregation during the first division to create haploid gametes. During meiotic prophase-I, chromosomes develop highly organized three-dimensional structures where loops of chromatin emanate from structural axes that also interconnect sister chromatids. Programmed DNA double-strand breaks (DSBs) at recombination hotspots, which initiate meiotic recombination, are localized to DNA sequences found in chromatin loops while many factors responsible for DSB formation reside on the axes, indicating that tethering of DSB sites in loops to their corresponding chromosome axes–loop-axis tethering–is a crucial step in the initiation of meiotic recombination (Blat et al., 2002; Panizza et al., 2011). Following DSB formation, homolog search of the DSB ends for homologous chromosomes leads to pairing of the structural axes of two homologous chromosomes and synapsis along their lengths to form the synaptonemal complexes (SCs). The SCs are zipper-like structures where the lateral/axial elements localized to each homolog sandwich the central region composed of transverse filaments and a central element (Figure 1). Later steps of recombination such as the formation of double-Holliday junctions and their resolution into crossover products, occur within the context of the SCs. In this review, we present key findings about the regulation of meiotic recombination in relation to chromosome architecture.

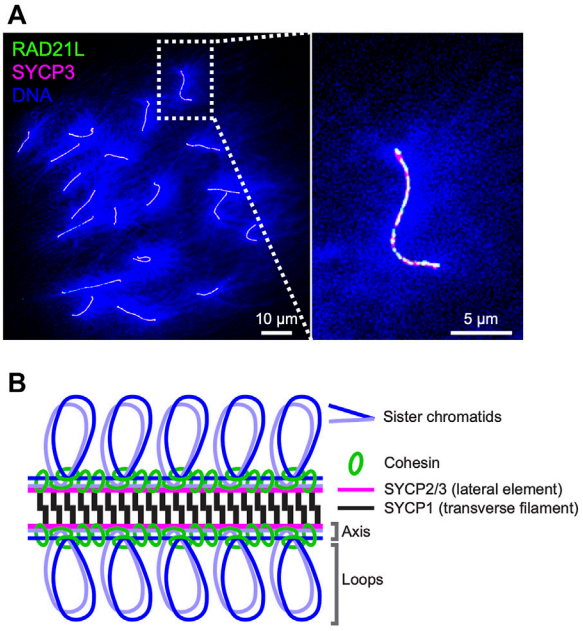

FIGURE 1
Axis-loop chromosome structure and the synaptonemal complex in mice **(A)** Surface spreads of mouse oocyte pachytene chromosomes immunostained for RAD21L (green), SYCP3 (magenta), and DNA (DAPI; blue). DNA is condensed on chromosome axes where cohesin complexes and axis core proteins localize and spread as loops from axes. RAD21L and SYCP3 are shown as a representative of meiotic cohesin and axis core protein, respectively **(B)** Schematic representation of the mouse synaptonemal complex. Cohesin complexes interconnect axes of sister chromatids and lateral elements SYCP2 and SYCP3 and a transverse filament protein SYCP1 form a ladder/zipper-like structure.

Cohesin as a basis of axis-loop higher-order chromosome structure

During the meiotic S-phase, cohesin complexes interconnect sister chromatids and are assumed to establish the core unit of chromosome axis *via* loop extrusion, likely with help of evolutionarily related axis core proteins (budding yeast Red1, mammalian SYCP2/SYCP3, and plant ASY3/ASY4; West et al., 2019; Figures 1A,B). The cohesin complexes consist of two SMCs (structure maintenance of chromosome), SMC1 and SMC3; and two non-SMC kleisin subunits, SCC3/STAG and the α-kleisin RAD21/SCC1 (Nasmyth and Haering, 2005). REC8 is a meiosis-specific α-kleisin subunit that is well-conserved from yeast to mammals and is required for the formation of chromosome axes and the SCs in budding yeast, *C. elegans*, and mice (Klein et al., 1999; Pasierbek et al., 2001; Xu et al., 2005). Recent Hi-C analysis of yeast meiosis revealed Rec8-dependent intra-chromosome interactions between distal chromosomal loci and high-frequency contacts between Rec8 binding sites (Muller et al., 2018; Schalbetter et al., 2019), supporting a model in which interactions between adjacent cohesin-binding sites assemble structural axes. Deletion of the budding yeast *REC8* gene causes various defects in meiotic recombination; the redistribution and reduction of DSBs, impaired choice of recombination template, and persistence of joint molecule DNA intermediates (Kugou et al., 2009; Kim et al., 2010), indicating important roles of cohesin-mediated chromosome structures and/or the cohesin complexes themselves in the regulation of recombination. Recent work in fission yeast identified a *rec8* separation-of-function mutant, *rec8-F204S,* that is proficient for sister chromatid cohesion (SCC) but deficient for axis-loop structure (Sakuno et al., 2022). This *rec8* mutant was defective in meiotic recombination, revealing an essential role for Rec8-cohesin-mediated axis-loop chromosome structure and not cohesion *per se* in meiotic recombination.

In mice, the topologically associating domains (TADs, comprising ~1 Mbp-intra-chromosomal interactions), characteristic of interphase chromosomes, are diminished and intra-chromosomal interactions around 2.5–4.5 Mbp became more evident during meiotic prophase-I, consistent with the formation of axis-loop structures (Alavattam et al., 2019; Wang Y. et al., 2019; Patel et al., 2019; Vara et al., 2019; Luo et al., 2020; Zuo et al., 2021). REC8, SMC1β, STAG3, and RAD21L (a second meiosis-specific α-kleisin; Figure 1A) are known meiosis-specific cohesin subunits that localize to chromosome axes in mice as six distinct complexes; three SMC1β-cohesin complexes (RAD21-SMC1β-SMC3-STAG3, RAD21L-SMC1β-SMC3-STAG3, and REC8-SMC1β-SMC3-STAG3) and three SMC1α-cohesin complexes (RAD21-SMC1α-SMC3-STAG1/2, RAD21-SMC1α-SMC3-STAG3, and RAD21L-SMC1α-SMC3-STAG3) (Revenkova et al., 2004; Ishiguro et al., 2011; Lee and Hirano, 2011; Fukuda et al., 2014). With the exception of *Rad21L*$^{-/-}$ females, all mice that are knockout mutants for the meiosis-specific cohesin components are sterile, and show defects in synapsis and compromised meiotic recombination (Revenkova et al., 2004; Herran et al., 2011; Llano et al., 2012; Fukuda et al., 2014). Axis lengths in meiocytes are shorter in all mutants, and double mutant mice such as *Smc1β*$^{-/-}$ *Rec8*$^{-/-}$ show much shorter axis lengths than the corresponding single mutants (Biswas et al., 2016; Ward et al., 2016). These observations highlight the importance of the multiple cohesin complexes in the organization of meiotic chromosome axis structure in mice.

During meiosis, cohesin plays a dual role in sister chromatid cohesion (SCC) and the formation of axis-loop structure. A recent series of studies established the loop extrusion activity of SMC complexes including the mitotic SCC1/RAD21-based cohesin (RAD21-SMC1A-SMC3-STAG1), which requires the cohesin loader complex SCC2/NIPBL-SCC4/MAU2 (Davidson et al., 2019; Kim et al., 2019; Kaur et al., 2022). This loop extrusion seems to be distinct from cohesin's SCC activity (Davidson and Peters, 2021). It follows that meiotic chromosome structure and cohesion may be mediated by two independent ensembles of cohesin complexes. Importantly, several organisms including vertebrates and nematodes contain two distinct meiotic cohesins (Severson et al., 2009; Ishiguro et al., 2011; Lee and Hirano, 2011; Severson and Meyer, 2014). In mice, the cohesins with REC8 and RAD21L localize to non-overlapping sites along chromosome axes (Ishiguro et al., 2011). Moreover, REC8, and thus REC8-based cohesin, localizes to the chromosomes as early as meiotic S-phase and persists until metaphase-II; whereas RAD21L-cohesin appears on the chromosome later, in leptonema and disappears earlier in late prophase-I (Herran et al., 2011; Lee and Hirano, 2011; Ishiguro et al., 2014; Biswas et al., 2016). One simple idea is that REC8-cohesin functions for SCC and RAD21L-cohesin functions for loop extrusion and thus axis-loop formation. Future studies are essential to evaluate the hypothesis.

WAPL and PDS5 are highly conserved cohesin regulators that contribute to the association and dissociation of cohesin complexes from chromosomes, and thereby modulate chromosome architecture in somatic cells (Kueng et al., 2006; Tedeschi et al., 2013; Haarhuis

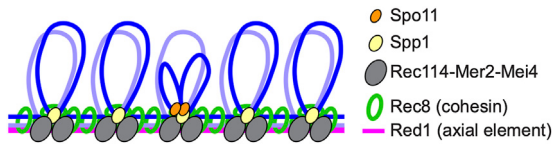

FIGURE 2
Tethered loop-axis complex (TLAC) formation to regulate DSB formation in budding yeast. Schematic representation of the budding yeast TLAC. Spo11 partner Rec114-Mer2-Mei4 complex localizes to chromosome axes where Rec8 cohesin and an axial element Red1 reside, and Spp1, a component of the Set1/COMPASS complex, tethers Spo11-bound DSB hotspots within loops to chromosome axes *via* the interaction with Mer2.

et al., 2017; Wutz et al., 2017). In *C. elegans*, cytological analysis of *wapl-1* null mutants indicated minor defects in the repair of meiotic DSBs (Crawley et al., 2016). Physical analysis of meiotic recombination at a well-characterized DSB hotspot in budding yeast revealed a subtle reduction in the levels of meiotic DSBs and the homolog bias of DSB repair in *rad61/wpl1* deletion mutants (Challa et al., 2016; Hong et al., 2019). More severe defects were seen in *pds5* meiotic null mutants with an interhomolog bias defect similar to that of a *rec8* deletion mutant (Hong et al., 2019). Both *rad61/wpl1* and *pds5* mutants showed shortened chromosome axes in budding yeast (Challa et al., 2016; Yang et al., 2022) and in fission yeast (Ding et al., 2006; Sakuno et al., 2022). Importantly, the budding yeast *pds5* mutant forms SCs between sister chromatids instead of homologs (Jin et al., 2009), which is reminiscent of the phenotypes seen in mouse *Rec8, Rad21L*, *Stag3*, and *Smc1β* knockout mutant spermatocytes (Xu et al., 2005; Ishiguro et al., 2011; Llano et al., 2012; Agostinho et al., 2016). Recent studies also revealed that depletion of PDS5 (both PDS5A and PDS5B) in mice leads to shortened chromosome axes, which form normal SCs between homologs, but are compromised for meiotic recombination (Viera et al., 2020). The prophase-I phenotypes of *Wapl* mutant mice have not been reported yet.

Notably, budding yeast Pds5 interacts with the proteasome and the shortened chromosome axis length of *pds5* mutants is rescued by reducing levels of ubiquitin, suggesting that Pds5 regulates axis length *via* the ubiquitin-proteasome system (Yang et al., 2022). Consistently, the proteasome is indeed localized on chromosome axes in budding yeast, *C. elegans*, and mice (Ahuja et al., 2017; Rao et al., 2017). Although changes in chromosome structures resulting from mutation of *PDS5* might indirectly affect meiotic recombination in mice, physical interaction between PDS5 and two RAD51 mediators, BRCA2 and the SWS1-SWSAP1, has been reported. Moreover, DSB repair is defective in *PDS5* mutant somatic cells from fly and human (Brough et al., 2012; Kusch, 2015; Couturier et al., 2016; Martino et al., 2019). These data support more direct roles for PDS5 in meiotic recombination, either as a component of cohesin or as an independent complex.

DSB formation in tethered loop-axis complexes

Meiotic recombination is initiated by programmed DSBs formed *via* an evolutionarily conserved topoisomerase VI-like protein, Spo11, and its partners (Bergerat et al., 1997; Keeney et al., 1997; de Massy, 2013; Robert et al., 2016). DSB sites are located in chromatin loops while Spo11 partners such as Rec114-Mer2-Mei4 in budding yeast, Rec7-Rec15-Rec24 in fission yeast, and REC114-IHO1-MEI4 in mice localize to chromosome axes where cohesin also localizes, suggesting that tethered loop-axis complexes (TLACs) form during the initiation of meiotic recombination to regulate both DSB formation and the ensuing steps of meiotic recombination (Blat et al., 2002; Kumar et al., 2010; Panizza et al., 2011; Miyoshi et al., 2012; Fowler et al., 2013; Ito et al., 2014; Kumar et al., 2015; Stanzione et al., 2016); (Figure 2).

Molecular mechanisms of TLAC formation have been studied in yeasts. Spp1 in budding yeast and Mde2 in fission yeast are identified as proteins important for the formation of TLACs (Miyoshi et al., 2012; Acquaviva et al., 2013; Sommermeyer et al., 2013; Adam et al., 2018). In budding yeast, DSB hotspots are preferentially located in promoter regions within chromatin loops (Pan et al., 2011; Ito et al., 2014). Spp1, a component of the COMPASS/Set1 complex that catalyzes histone H3K4 trimethylation, is thought to recognize H3K4 trimethylation marks around DSB hotspots *via* its PHD domain, and connect these sites to chromosome axes by interacting with axis-associated Mer2. Spp1 is likely to mediate TLAC formation independently from the role in the COMPASS/Set1 complex (Karanyi et al., 2018). Although Spp1-mediated TLACs contribute to DSB formation, meiotic cells are equipped with another layer of regulation for meiotic DSB formation, since *spp1* mutants still form relatively high levels of DSBs (Acquaviva et al., 2013; Sommermeyer et al., 2013; Zhang et al., 2020). Given that Mer2 itself has an ability to directly bind to nucleosomes and the association of Mer2 to chromosome axes is regulated by its interacting axis-associated protein Hop1, the Hop1-Mer2 may contribute to TLAC formation both *via* and independently of Spp1 (Panizza et al., 2011; Rousova et al., 2021). In fission yeast, where most DSB hotspots are in long intergenic regions (Fowler et al., 2014), DSB hotspots are marked by another epigenetic mark, H3K9 acetylation, and the H3K4 trimethylation mark is dispensable for meiotic DSB formation (Yamada et al., 2013). Mde2 expresses only after the meiotic S-phase and is thought to bridge $Rec12^{Spo11}$-containing subcomplex at DSB hotspots and an axis-located subcomplex containing $Rec15^{Mer2}$ (budding yeast homologs in superscript) (Miyoshi et al., 2012). Importantly, fission yeast Hop1 also physically interacts with $Rec15^{Mer2}$ and promotes chromosomal localization of $Rec15^{Mer2}$, suggesting significant contribution of Hop1 to TLAC formation in both yeasts (Kariyazono et al., 2019).

Whether or not the mechanism of TLAC formation is conserved remains unclear. In mice, PRDM9, a germ cell-specific H3K4 trimethylation transferase with a zinc-finger array domain, recognizes specific DNA sequences, deposits H3K4me3 and H3K36me3 marks, and directs DSB formation at its binding sites (Baudat et al., 2010; Diagouraga et al., 2018). Recent ChIP-seq analysis for meiotic cohesin components REC8 and RAD21L revealed their localization to promoter regions (Vara et al., 2019) and no overlap of meiotic cohesin binding sites with DMC1 (the meiosis-specific RAD51 homolog) and PRDM9 binding sites (Jin et al., 2021). CXXC1 is an ortholog of budding yeast Spp1, and the physical interaction of CXXC1 with PRDM9 and IHO1, an axis-associated protein considered to be the ortholog of budding yeast Mer2, suggested a similar mechanism of TLAC formation between budding yeast and mouse (Imai et al., 2017; Parvanov et al., 2017). However, depletion of CXXC1 in mouse germ cells caused no or small defects in DSB formation and the early steps of DSB repair (Tian et al., 2018; Jiang et al., 2020), suggesting that factor(s) other than

CXXC1 plays a critical role in TLAC formation and meiotic DSB formation in mice. A mammalian ortholog of fission yeast Mde2 has not been identified yet.

Inter-homolog bias controlled by axial proteins

DSB formation is followed by nuclease-mediated 5′-strand resection to form long single-stranded tails. Invasion of the resected DSB end into a template homologous duplex DNA forms a nascent D (displacement)-loop structure. At this stage, D-loop intermediates are thought to differentiate into crossover and non-crossover pathways (Hunter, 2015). The majority are matured as non-crossovers *via* DNA synthesis to extend the invading end, dissociation of the D-loop, and annealing of the displaced strand to seal the DSB (synthesis-dependent strand annealing) (Allers and Lichten, 2001; Hunter and Kleckner, 2001). Along the crossover pathways, D-loops differentiate into metastable D-loops called Single-End Invasions (SEIs) which then form double-Holliday junctions (dHJs) *via* DNA synthesis and capture of the second DSB end. dHJs are specifically resolved into crossover products. These events also occur in the context of meiotic chromosome axes and SCs. A prominent feature of meiotic recombination is that homology search and strand exchange are biased to occur between homologous chromosomes (inter-homolog) rather than between sister chromatids (inter-sister). This biased template choice is regulated by components of the axial/lateral elements of the SC and axis-associated proteins.

In budding yeast deletion mutants of axis-associated proteins Red1, Hop1, and the associated recombination-checkpoint kinase Mek1, DSBs are repaired primarily *via* inter-sister recombination (Kim et al., 2010; Lao and Hunter, 2010). The Hop1-Red1-Mek1 pathway, along with other factors that promote inter-homolog recombination (Zierhut et al., 2004), may mediate inter-homolog bias by inhibiting inter-sister recombination, promoting inter-homolog recombination, and/or by impeding the progression of recombination until homologs have been engaged (Lao and Hunter, 2010). Further mutant analysis suggested that meiotic cohesin Rec8 promotes inter-sister bias, which is counteracted by Red1 and Mek1/Mre4 (Kim et al., 2010). Mek1 is a meiosis-specific, axis-associated kinase that phosphorylates various targets including Rad54 and Hed1. The phosphorylation of both Rad54 and Hed1 suppresses Rad51-mediated inter-sister recombination, which partly explains the involvement of Mek1 in the suppression of inter-sister recombination (Niu et al., 2007; Niu et al., 2009; Callender et al., 2016; Kniewel et al., 2017). Importantly, the meiotic Rad51 homolog, Dmc1, bears an ability to promote inter-homolog bias (Brown and Bishop, 2014). However, the exact mechanism of inter-homolog bias and the relationship between Mek1-mediated phosphorylation and Rec8-cohesin remain to be resolved.

Hop1 is a conserved HORMA domain-containing protein that specifically localizes to unsynapsed axes and is locally depleted from sites of synapsis (Smith and Roeder, 1997), distinct from its binding partner Red1 and the cohesin complexes that appear to be constitutive components of chromosome axes before and after SC formation. Removal of Hop1 from synapsed axes is mediated by an evolutionarily conserved AAA+ ATPase Pch2, and yeast *pch2Δ* mutants show increased inter-sister recombination, suggesting that Pch2 also contributes to inter-homolog bias *via* the Hop1-Red1-Mek1 axis (Borner et al., 2008; Zanders et al., 2011). In mice, the two HORMA domain-containing proteins HORMAD1 and HORMAD2 also preferentially localize to unsynapsed axes (Wojtasz et al., 2009). In the absence of the HORMADs, the repair of radiation-induced exogenous DSBs was accelerated in *Spo11*-and *Dmc1*-deficient meiocytes in which inter-sister recombination is preferred, suggesting that, like budding yeast Hop1, mouse HORMADs may impede inter-sister recombination (Shin et al., 2013; Rinaldi et al., 2017; Carofiglio et al., 2018). The removal of HORMADs from synapsed axes is mediated by the Pch2 homolog TRIP13 (Wojtasz et al., 2009; Roig et al., 2010; Ye et al., 2017). In *Trip13* mutant meiocytes, unrepaired DSBs persist (Li and Schimenti, 2007; Roig et al., 2010; Rinaldi et al., 2017), supporting the idea that HORMADs suppress inter-sister DSB repair.

Synaptonemal complexes and crossing over

Synaptonemal Complexes (SCs) are tripartite protein structures where the two lateral/axial elements of homologous chromosomes are connected along their lengths by a central region comprising tightly-packed transverse filaments and a central element. The dependency of SC formation on DSBs and recombination differs among species, with recombination-dependent synapsis in most analyzed fungi, plants, and mammals where SC formation tends to initiate at sites of recombination (SC also initiates at centromeres in budding yeast). By contrast, DSBs are dispensable for the SC formation in *Drosophila* and *C. elegans* in which synapsis initiates at centromeres and terminal pairing centers, respectively (MacQueen et al., 2005; Takeo et al., 2011). Despite these differences, SCs have a common function in the formation and/or regulation of crossing over in all organisms (with known exceptions being *Schizosaccharomyces pombe* and *Aspergillus nidulans* that have no typical SC structure).

The ZMM proteins are a group of meiosis-specific proteins that facilitate crossing over by promoting/stabilizing the crossover-pathway joint-molecule intermediates, SEIs and dHJs, and promoting the crossover-specific resolution of dHJs *via* MutLγ. Initially identified in budding yeast, the ZMMs comprise eight members that define five structures or activities: Zip1^{SYCP1} is the transverse filament components of SCs but also functions locally at recombination sites; Zip2^{SHOC1}-Spo16 is related to XPF-ERCC1 and thought to bind and stabilize recombination intermediates; Zip4^{TEX11} is a long TPR-repeat protein that appears to bridge chromosome axes and recombination complexes by forming the ZZS complex with Zip2^{SHOC1}-Spo16; Zip3^{RNF212} is inferred to be an E3-ligase for SUMO modification that promotes the localization of other ZMMs to recombination sites; Msh4-Msh5 (MutSγ), homologous to DNA mismatch-repair factor MutS, binds and stabilizes joint molecules; and Mer3^{HFM1} is a DNA helicase that stabilizes joint molecules and regulates the length of recombination-associated DNA synthesis (mammalian homologs in superscript) (Lynn et al., 2007; De Muyt et al., 2018; Arora and Corbett, 2019). In budding yeast, all ZMM proteins are also required for SC formation, with Zip2-Spo16-Zip4 and Zip3 being defined as synapsis initiation complexes (SICs) that assemble at synapsis initiation sites, which mature into crossover sites, indicating a close link between SC initiation and

crossing over at least in budding yeast and similarly in *Sordaria macrospora* (Chua and Roeder, 1998; Agarwal and Roeder, 2000; Borner et al., 2004; Fung et al., 2004; Tsubouchi et al., 2006; Shinohara et al., 2008; Zhang et al., 2014a). In mice, the number of ZMM-associated recombination sites, detected as cytological foci, is in large excess relative to SC-initiation sites and crossovers. Meiocytes from mouse *zmm* knockouts for *Hfm1, Msh4*, *Msh5*, *Shoc1*, *Spo16,* and *Tex11* show defects in synapsis and crossover formation, as seen in budding yeast. The exception is mouse knockout mutant for the *ZIP3* homolog *Rnf212*, in which synapsis occurs efficiently but crossing over fails (de Vries et al., 1999; Kneitz et al., 2000; Yang et al., 2008; Guiraldelli et al., 2013; Reynolds et al., 2013; Zhang Q. et al., 2018; Guiraldelli et al., 2018; Zhang et al., 2019).

Like the budding yeast *zip1Δ* mutant, knockout mutation of components of the SC central region, SYCP1, SYCE1, SYCE2, SYCE3, TEX12, and SIX6OS1, in mice abolishes both synapsis and crossing over (de Vries et al., 2005; Bolcun-Filas et al., 2007; Hamer et al., 2008; Bolcun-Filas et al., 2009; Schramm et al., 2011; Gomez et al., 2016). In *C. elegans*, mutation of components of the SC central region (SYP-1, SYP-2, SYP-3, and SYP-4) also causes a severe reduction or loss of crossovers (MacQueen et al., 2002; Colaiacovo et al., 2003; Smolikov et al., 2007a; Smolikov et al., 2007b; Smolikov et al., 2009), indicating a coupling between SC formation and crossing over in most organisms. A notable exception is *Arabidopsis thaliana,* in which meiocytes lacking the SC central element ZYP1 are defective for synapsis but form elevated numbers of crossovers (Capilla-Perez et al., 2021). Similarly, the absence of the central element proteins Ecm11 and Gmc2 in budding yeast causes defective SC formation but increased crossing over (Voelkel-Meiman et al., 2016; Lee et al., 2021). These observations suggest that full synapsis and the SC central region are not essential for crossing over *per se*, but may function to control a proper number of crossovers.

Despite the close link between SC formation and crossing over in most species, uncoupling of the two events is implicated in a meiosis-specific depletion mutant of a component of SCF (Skp1-Cullin-F box) E3 ubiquitin ligase, Cdc53. The budding yeast *cdc53* mutant is largely proficient in crossover formation, but is severely defective for the elongation of SCs and shows the abnormal accumulation of ZMM proteins (Zhu et al., 2021). Moreover, when Cdc53 depletion is combined with the *pch2* deletion mutation, lacking the AAA+ ATPase that removes $Hop1^{HORMAD1}$ from synapsed axes, the formation of full-length SCs is restored, but now DSB repair and crossing over are stalled. This uncoupling is unexpected since most yeast mutants defective for meiotic DSB repair also impair SC elongation. A possible explanation is that SCF is part of a regulatory surveillance mechanism that couples SC elongation and DSB repair in meiotic cells.

Crossover patterning on synaptonemal complexes

Crossovers, in concert with cohesion between sister chromatids, create connections between homologs called chiasmata that enable stable bipolar orientation of homologs on the meiosis-I spindle and consequently accurate disjunction at the first meiotic division. The number and position of crossovers, and thus chiasmata, are strictly controlled: each pair of homologous chromosomes (a bivalent) obtains at least one crossover (the obligate crossover or crossover assurance) and when multiple crossovers form between a bivalent they are evenly spaced (crossover interference). Crossover homeostasis can maintain crossover numbers at the expense of non-crossovers to buffer against variation in DSB numbers and inter-homolog bias (Martini et al., 2006; Cole et al., 2012; Lao et al., 2013). In addition, the phenomenon of crossover covariation describes the observation that within individual nuclei, crossover frequencies covary across different chromosomes, which may have adaptative advantages by balancing the cost-benefit ratio of crossing over (Wang S. et al., 2019). The precise mechanisms of these crossover control processes remain unresolved.

In budding yeast, crossover interference has been analyzed genetically by analyzing the segregation patterns of linked gene alleles and spore autonomous fluorescent makers in tetrads (Cao et al., 1990; Sym and Roeder, 1994; Shinohara et al., 2003; Thacker et al., 2011; Lao et al., 2013); and in prophase-I nuclei by analyzing the distribution of crossover-specific Zip2 and Zip3 immunostaining foci along SCs (Fung et al., 2004; Zhang et al., 2014b). Zip3 foci are evenly spaced, implying the establishment of interference patterning at or before the time of Zip3 loading, which depends on DSB formation (Zhang et al., 2014b). Mutant analysis revealed that the SUMO-targeted ubiquitin ligase (STUbL), Slx5/8 and SUMOylation of Top2 and axis protein Red1 are required for crossover interference (Zhang et al., 2014c). These and other observations support the proposal of Kleckner and colleagues that crossover interference is mediated by the imposition and relief of mechanical stress along meiotic chromosome axes (the beam-film model; Kleckner et al., 2004; Zhang et al., 2014b).

ZHP-3 is a *C. elegans* RING-domain protein related to Zip3 and is essential for crossover formation (Jantsch et al., 2004). ZHP-3 functions with three paralogs (ZHP-1,2,4) inferred to act as two heterodimeric complexes ZHP-1/2 and ZHP-3/4 (Zhang L. et al., 2018). ZHP-3 localizes along SCs in two phases; first as multiple foci along each SC before becoming restricted to a single crossover-specific focus in late pachynema (Bhalla et al., 2008). In *C. elegans*, robust crossover assurance and absolute interference ensures that each pair of homologous chromosomes obtains exactly one crossover. *In vivo* imaging using Fluorescence Recovery After Photobleaching (FRAP) technology revealed the dynamic properties of the SC central region and a switch from a dynamic to a stable state as pachytene progresses, the timing of which coincides with crossover designation (Pattabiraman et al., 2017). Other *in vivo* imaging studies support the idea that the SC has liquid crystalline properties, suggesting that the diffusion of the ZHP complexes within the SC might govern crossover patterning *via* a diffusion-mediated or coarsening or condensation process (Rog et al., 2017; Stauffer et al., 2019; Zhang et al., 2021).

Diffusion-mediated coarsening as a mechanism for crossover patterning is also suggested from analysis in *Arabidopsis*. Both plants and *Sordaria* encode a sole RING-domain crossover factor called HEI10 (without $Zip3^{RNF212}$ orthologs). The localization pattern of HEI10 is also dynamic: forming multiple discrete foci along the SCs in early pachynema, which then reduce in number until most foci have disappeared while a few sites accumulate HEI10 and mature into crossover sites marked by MutLγ (Chelysheva et al., 2012; Wang et al., 2012; De Muyt et al., 2014). Analysis of HEI10-focus patterning in several different contexts *via* super-resolution structure-illumination microscopy (SIM) imaging of fixed cells combined with modeling by computational simulation is compatible with diffusion-mediated

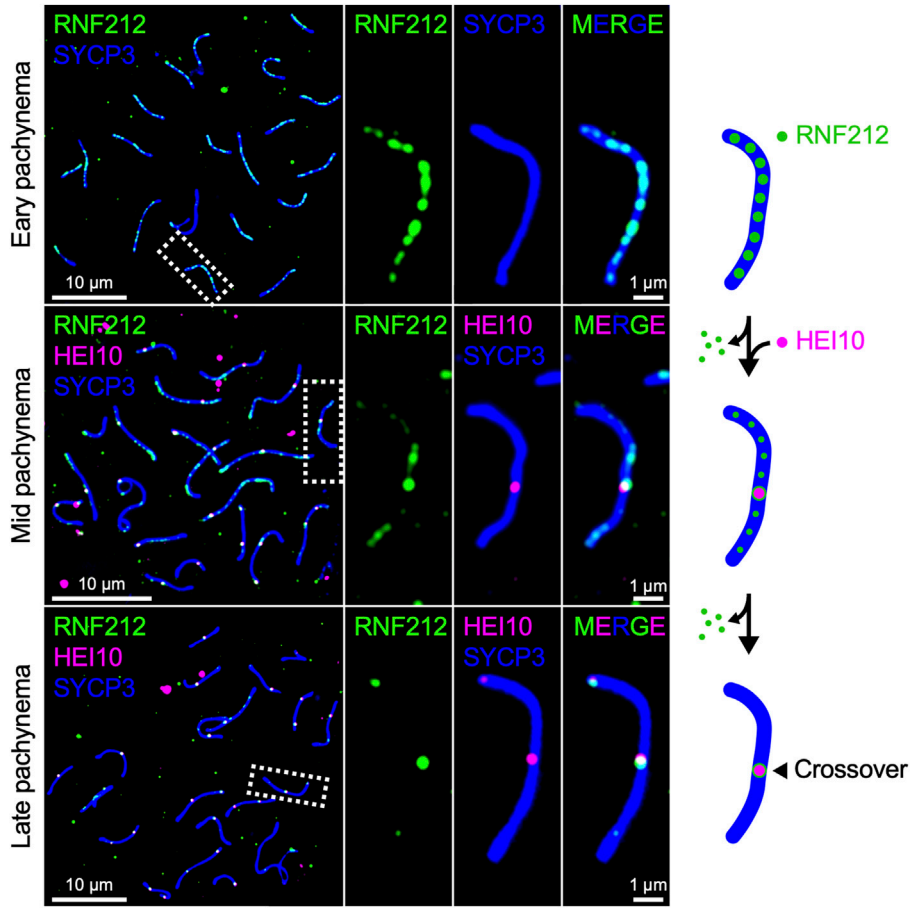

FIGURE 3
Chromosomal localization of RNF212 and HEI10 in mice. Successive stages of mouse pachytene spermatocytes immunostained for RNF212 (green), HEI10 (magenta), and SYCP3 (blue), HEI10 and SYCP3. RNF212 forms numerous discrete foci along the entire SCs (marked by SYCP3) in early pachynema before HEI10 foci emerge (top), loses most of foci but accumulates at HEI10-bound crossover sites in mid pachynema (middle), and eventually is restricted to crossover sites in late pachynema (bottom).

coarsening of HEI10 foci as a mechanism for crossover patterning (Morgan et al., 2021).

Mammals encode both Zip3 homolog RNF212 and HEI10, both of which are essential for crossover regulation in mice (Ward et al., 2007; Strong and Schimenti, 2010; Reynolds et al., 2013; Qiao et al., 2014). RNF212 shows dynamic localization along SCs similar to that of HEI10 in *Arabidopsis* and *Sordaria*, forming numerous discrete foci during early pachynema, which become restricted to crossover sites as pachytene progresses. By contrast, mouse HEI10 localizes only to crossover sites during mid-late pachynema and is not detected along SCs at earlier stages (Figure 3). It is suggested that RNF212-dependent SUMOylation stabilizes ZMM factors to confer crossover-competency to recombination sites, and HEI10-dependent ubiquitination subsequently licenses crossover/non-crossover differentiation by recruiting proteasomes to SCs to degrade as yet unknown factors (Rao et al., 2017). Importantly, the dosage of *Rnf212* and *Hei10* affects crossover rate in humans and mice, as seen for *Arabidopsis Hei10* (Kong et al., 2008; Chowdhury et al., 2009; Fledel-Alon et al., 2011; Kong et al., 2014; Ziolkowski et al., 2017). This similarity in the dosage effect on crossover numbers is consistent with the possibility that crossover patterning in mammals may also involve the diffusion-mediated accumulation of RNF212 and HEI10 at crossover sites.

Discussion (perspective)

Meiotic chromosomes organize into specialized structures that help strictly regulate the number and position of meiotic DSBs, the choice of recombination template, and the differentiation of crossovers and non-crossovers to ultimately ensure the completion of DSB repair and accurate chromosome segregation. A diversity of approaches and model species are providing major insights into this molecular basis of the chromosome structure-recombination interface. However, major questions still remain to be addressed, including: Do cohesins and associated factors have direct functions in the regulation of meiotic recombination? Which factor(s) are responsible for TLAC formation in other organisms than yeasts, and how is TLAC formation coupled to DSB formation? How is inter-homolog bias established? What mechanisms underlie crossover patterning in mammals in which both Zip3/RNF212-family and HEI10-family RING-domain proteins are present? Recently, structural analysis of axis core proteins, Hop1/HORMADs, DSB

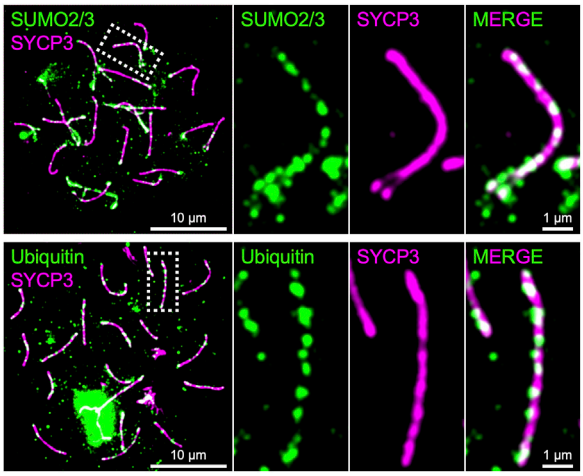

FIGURE 4
Chromosome axes decorated by SUMO and Ubiquitin in mice. Surface spreads of mouse spermatocyte chromosomes immunostained for SYCP3 (green) and SUMO2/3 (green; top) and Ubiquitin (green; bottom), respectively. Both SUMO and ubiquitin are enriched on chromosome axes where SYCP3 localizes.

proteins and associated proteins, and SC components is providing mechanistic insights into their functions (West et al., 2018; Boekhout et al., 2019; West et al., 2019; Sanchez-Saez et al., 2020; Claeys Bouuaert et al., 2021; Dunce et al., 2021; Rousova et al., 2021; Nore et al., 2022). Further mutant analysis based on protein structure will be a key to answer these unaddressed questions.

As presented above, SUMO, ubiquitin, and proteasome are involved in the regulation of chromosome axis length and crossover interference in budding yeast, and presumptive SUMO and ubiquitin ligases, RNF212 and HEI10, are essential for crossover regulation in mice, highlighting central roles for the SUMO and ubiquitin-proteasome systems in meiotic chromosome organization and the regulation of meiotic recombination. Indeed, SUMO is enriched on chromosome axes and SCs in budding yeast, *Sordaria*, mice, and humans, and ubiquitin and proteasome have been localized to chromosome axes in budding yeast, *C. elegans*, and mice (Voelkel-Meiman et al., 2013; Klug et al., 2013; Brown et al., 2008; De Muyt et al., 2014; Ahuja et al., 2017; Rao et al., 2017; Figure 4). Numerous meiotic factors, including cohesin and recombination proteins, undergo SUMOylation in budding yeast (Bhagwat et al., 2021), and the SCF ubiquitin ligase, which regulates SC elongation in conjunction to Pch2^{TRIP13} in budding yeast (Zhu et al., 2021), localizes to synapsed chromosome axes and targets HORMAD1 in mouse (Guan et al., 2020; Guan et al., 2022). Future analysis will further elucidate molecular roles of SUMO and the ubiquitin-proteasome system in the regulation of meiotic recombination in conjunction with chromosome architecture.

Author contributions

Both authors wrote the manuscript and approved it for publication.

Funding

This study was supported by JSPS KAKENHI Grant Number 22125001 and 22125002 to AS and 20K15716 to MI.

Acknowledgments

We thank Neil Hunter for his insightful comments on the manuscript. We apologize for those whose work could not be cited due to the focused aspect of this study.

Conflict of interest

The authors declare that the research was conducted in the absence of any commercial or financial relationships that could be construed as a potential conflict of interest.

Publisher's note

References

Acquaviva, L., Szekvolgyi, L., Dichtl, B., Dichtl, B. S., de La Roche Saint Andre, C., Nicolas, A., et al. (2013). The COMPASS subunit Spp1 links histone methylation to initiation of meiotic recombination. *Science* 339, 215–218. doi:10.1126/science.1225739

Adam, C., Guerois, R., Citarella, A., Verardi, L., Adolphe, F., Beneut, C., et al. (2018). The PHD finger protein Spp1 has distinct functions in the Set1 and the meiotic DSB formation complexes. *PLoS Genet.* 14, e1007223. doi:10.1371/journal.pgen.1007223

Agarwal, S., and Roeder, G. S. (2000). Zip3 provides a link between recombination enzymes and synaptonemal complex proteins. *Cell* 102, 245–255. doi:10.1016/s0092-8674(00)00029-5

Agostinho, A., Manneberg, O., van Schendel, R., Hernandez-Hernandez, A., Kouznetsova, A., Blom, H., et al. (2016). High density of REC8 constrains sister chromatid axes and prevents illegitimate synaptonemal complex formation. *EMBO Rep.* 17, 901–913. doi:10.15252/embr.201642030

Ahuja, J. S., Sandhu, R., Mainpal, R., Lawson, C., Henley, H., Hunt, P. A., et al. (2017). Control of meiotic pairing and recombination by chromosomally tethered 26S proteasome. *Science* 355, 408–411. doi:10.1126/science.aaf4778

Alavattam, K. G., Maezawa, S., Sakashita, A., Khoury, H., Barski, A., Kaplan, N., et al. (2019). Attenuated chromatin compartmentalization in meiosis and its maturation in sperm development. *Nat. Struct. Mol. Biol.* 26, 175–184. doi:10.1038/s41594-019-0189-y

Allers, T., and Lichten, M. (2001). Differential timing and control of noncrossover and crossover recombination during meiosis. *Cell* 106, 47–57. doi:10.1016/s0092-8674(01)00416-0

Arora, K., and Corbett, K. D. (2019). The conserved XPF:ERCC1-like Zip2:Spo16 complex controls meiotic crossover formation through structure-specific DNA binding. *Nucleic Acids Res.* 47, 2365–2376. doi:10.1093/nar/gky1273

Baudat, F., Buard, J., Grey, C., Fledel-Alon, A., Ober, C., Przeworski, M., et al. (2010). PRDM9 is a major determinant of meiotic recombination hotspots in humans and mice. *Science* 327, 836–840. doi:10.1126/science.1183439

Bergerat, A., de Massy, B., Gadelle, D., Varoutas, P. C., Nicolas, A., Forterre, P., et al. (1997). An atypical topoisomerase II from Archaea with implications for meiotic recombination. *Nature* 386, 414–417. doi:10.1038/386414a0

Bhagwat, N. R., Owens, S. N., Ito, M., Boinapalli, J. V., Poa, P., Ditzel, A., et al. (2021). SUMO is a pervasive regulator of meiosis. *Elife* 10, e57720. doi:10.7554/eLife.57720

Bhalla, N., Wynne, D. J., Jantsch, V., and Dernburg, A. F. (2008). ZHP-3 acts at crossovers to couple meiotic recombination with synaptonemal complex disassembly and bivalent formation in *C. elegans*. *PLoS Genet.* 4, e1000235. doi:10.1371/journal.pgen.1000235

Biswas, U., Hempel, K., Llano, E., Pendas, A., and Jessberger, R. (2016). Distinct roles of meiosis-specific cohesin complexes in mammalian spermatogenesis. *PLoS Genet.* 12, e1006389. doi:10.1371/journal.pgen.1006389

Blat, Y., Protacio, R. U., Hunter, N., and Kleckner, N. (2002). Physical and functional interactions among basic chromosome organizational features govern early steps of meiotic chiasma formation. *Cell* 111, 791–802. doi:10.1016/s0092-8674(02)01167-4

Boekhout, M., Karasu, M. E., Wang, J., Acquaviva, L., Pratto, F., Brick, K., et al. (2019). REC114 partner ANKRD31 controls number, timing, and location of meiotic DNA breaks. *Mol. Cell* 74, 1053–1068. doi:10.1016/j.molcel.2019.03.023

Bolcun-Filas, E., Costa, Y., Speed, R., Taggart, M., Benavente, R., De Rooij, D. G., et al. (2007). SYCE2 is required for synaptonemal complex assembly, double strand break repair, and homologous recombination. *J. Cell Biol.* 176, 741–747. doi:10.1083/jcb.200610027

Bolcun-Filas, E., Hall, E., Speed, R., Taggart, M., Grey, C., de Massy, B., et al. (2009). Mutation of the mouse Syce1 gene disrupts synapsis and suggests a link between synaptonemal complex structural components and DNA repair. *PLoS Genet.* 5, e1000393. doi:10.1371/journal.pgen.1000393

Borner, G. V., Barot, A., and Kleckner, N. (2008). Yeast Pch2 promotes domainal axis organization, timely recombination progression, and arrest of defective recombinosomes during meiosis. *Proc. Natl. Acad. Sci. U. S. A.* 105, 3327–3332. doi:10.1073/pnas.0711864105

Borner, G. V., Kleckner, N., and Hunter, N. (2004). Crossover/noncrossover differentiation, synaptonemal complex formation, and regulatory surveillance at the leptotene/zygotene transition of meiosis. *Cell* 117, 29–45. doi:10.1016/s0092-8674(04)00292-2

Brough, R., Bajrami, I., Vatcheva, R., Natrajan, R., Reis-Filho, J. S., Lord, C. J., et al. (2012). APRIN is a cell cycle specific BRCA2-interacting protein required for genome integrity and a predictor of outcome after chemotherapy in breast cancer. *EMBO J.* 31, 1160–1176. doi:10.1038/emboj.2011.490

Brown, M. S., and Bishop, D. K. (2014). DNA strand exchange and RecA homologs in meiosis. *Cold Spring Harb. Perspect. Biol.* 7, a016659. doi:10.1101/cshperspect.a016659

Brown, P. W., Hwang, K., Schlegel, P. N., and Morris, P. L. (2008). Small ubiquitin-related modifier (SUMO)-1, SUMO-2/3 and SUMOylation are involved with centromeric heterochromatin of chromosomes 9 and 1 and proteins of the synaptonemal complex during meiosis in men. *Hum. Reprod.* 23, 2850–2857. doi:10.1093/humrep/den300

Callender, T. L., Laureau, R., Wan, L., Chen, X., Sandhu, R., Laljee, S., et al. (2016). Mek1 down regulates Rad51 activity during yeast meiosis by phosphorylation of Hed1. *PLoS Genet.* 12, e1006226. doi:10.1371/journal.pgen.1006226

Cao, L., Alani, E., and Kleckner, N. (1990). A pathway for generation and processing of double-strand breaks during meiotic recombination in *S. cerevisiae*. *Cell* 61, 1089–1101. doi:10.1016/0092-8674(90)90072-m

Capilla-Perez, L., Durand, S., Hurel, A., Lian, Q., Chambon, A., Taochy, C., et al. (2021). The synaptonemal complex imposes crossover interference and heterochiasmy in Arabidopsis. *Proc. Natl. Acad. Sci. U. S. A.* 118, e2023613118. doi:10.1073/pnas.2023613118

Carofiglio, F., Sleddens-Linkels, E., Wassenaar, E., Inagaki, A., van Cappellen, W. A., Grootegoed, J. A., et al. (2018). Repair of exogenous DNA double-strand breaks promotes chromosome synapsis in SPO11-mutant mouse meiocytes, and is altered in the absence of HORMAD1. *DNA Repair (Amst)* 63, 25–38. doi:10.1016/j.dnarep.2018.01.007

Challa, K., Lee, M. S., Shinohara, M., Kim, K. P., and Shinohara, A. (2016). Rad61/Wpl1 (Wapl), a cohesin regulator, controls chromosome compaction during meiosis. *Nucleic Acids Res.* 44, 3190–3203. doi:10.1093/nar/gkw034

Chelysheva, L., Vezon, D., Chambon, A., Gendrot, G., Pereira, L., Lemhemdi, A., et al. (2012). The Arabidopsis HEI10 is a new ZMM protein related to Zip3. *PLoS Genet.* 8, e1002799. doi:10.1371/journal.pgen.1002799

Chowdhury, R., Bois, P. R., Feingold, E., Sherman, S. L., and Cheung, V. G. (2009). Genetic analysis of variation in human meiotic recombination. *PLoS Genet.* 5, e1000648. doi:10.1371/journal.pgen.1000648

Chua, P. R., and Roeder, G. S. (1998). Zip2, a meiosis-specific protein required for the initiation of chromosome synapsis. *Cell* 93, 349–359. doi:10.1016/s0092-8674(00)81164-2

Claeys Bouuaert, C., Pu, S., Wang, J., Oger, C., Daccache, D., Xie, W., et al. (2021). DNA-driven condensation assembles the meiotic DNA break machinery. *Nature* 592, 144–149. doi:10.1038/s41586-021-03374-w

Colaiacovo, M. P., MacQueen, A. J., Martinez-Perez, E., McDonald, K., Adamo, A., La Volpe, A., et al. (2003). Synaptonemal complex assembly in *C. elegans* is dispensable for loading strand-exchange proteins but critical for proper completion of recombination. *Dev. Cell* 5, 463–474. doi:10.1016/s1534-5807(03)00232-6

Cole, F., Kauppi, L., Lange, J., Roig, I., Wang, R., Keeney, S., et al. (2012). Homeostatic control of recombination is implemented progressively in mouse meiosis. *Nat. Cell Biol.* 14, 424–430. doi:10.1038/ncb2451

Couturier, A. M., Fleury, H., Patenaude, A. M., Bentley, V. L., Rodrigue, A., Coulombe, Y., et al. (2016). Roles for APRIN (PDS5B) in homologous recombination and in ovarian cancer prediction. *Nucleic Acids Res.* 44, 10879–10897. doi:10.1093/nar/gkw921

Crawley, O., Barroso, C., Testori, S., Ferrandiz, N., Silva, N., Castellano-Pozo, M., et al. (2016). Cohesin-interacting protein WAPL-1 regulates meiotic chromosome structure and cohesion by antagonizing specific cohesin complexes. *Elife* 5, e10851. doi:10.7554/eLife.10851

Davidson, I. F., Bauer, B., Goetz, D., Tang, W., Wutz, G., and Peters, J. M. (2019). DNA loop extrusion by human cohesin. *Science* 366, 1338–1345. doi:10.1126/science.aaz3418

Davidson, I. F., and Peters, J. M. (2021). Genome folding through loop extrusion by SMC complexes. *Nat. Rev. Mol. Cell Biol.* 22, 445–464. doi:10.1038/s41580-021-00349-7

de Massy, B. (2013). Initiation of meiotic recombination: How and where? Conservation and specificities among eukaryotes. *Annu. Rev. Genet.* 47, 563–599. doi:10.1146/annurev-genet-110711-155423

De Muyt, A., Pyatnitskaya, A., Andreani, J., Ranjha, L., Ramus, C., Laureau, R., et al. (2018). A meiotic XPF-ERCC1-like complex recognizes joint molecule recombination intermediates to promote crossover formation. *Genes Dev.* 32, 283–296. doi:10.1101/gad.308510.117

De Muyt, A., Zhang, L., Piolot, T., Kleckner, N., Espagne, E., and Zickler, D. (2014). E3 ligase Hei10: A multifaceted structure-based signaling molecule with roles within and beyond meiosis. *Genes Dev.* 28, 1111–1123. doi:10.1101/gad.240408.114

de Vries, F. A., de Boer, E., van den Bosch, M., Baarends, W. M., Ooms, M., Yuan, L., et al. (2005). Mouse Sycp1 functions in synaptonemal complex assembly, meiotic recombination, and XY body formation. *Genes Dev.* 19, 1376–1389. doi:10.1101/gad.329705

de Vries, S. S., Baart, E. B., Dekker, M., Siezen, A., de Rooij, D. G., de Boer, P., et al. (1999). Mouse MutS-like protein Msh5 is required for proper chromosome synapsis in male and female meiosis. *Genes Dev.* 13, 523–531. doi:10.1101/gad.13.5.523

Diagouraga, B., Clement, J. A. J., Duret, L., Kadlec, J., de Massy, B., and Baudat, F. (2018). PRDM9 methyltransferase activity is essential for meiotic DNA double-strand break formation at its binding sites. *Mol. Cell* 69, 853–865. doi:10.1016/j.molcel.2018.01.033

Ding, D. Q., Sakurai, N., Katou, Y., Itoh, T., Shirahige, K., Haraguchi, T., et al. (2006). Meiotic cohesins modulate chromosome compaction during meiotic prophase in fission yeast. *J. Cell Biol.* 174, 499–508. doi:10.1083/jcb.200605074

Dunce, J. M., Salmon, L. J., and Davies, O. R. (2021). Structural basis of meiotic chromosome synaptic elongation through hierarchical fibrous assembly of SYCE2-TEX12. *Nat. Struct. Mol. Biol.* 28, 681–693. doi:10.1038/s41594-021-00636-z

Fledel-Alon, A., Leffler, E. M., Guan, Y., Stephens, M., Coop, G., and Przeworski, M. (2011). Variation in human recombination rates and its genetic determinants. *PLoS One* 6, e20321. doi:10.1371/journal.pone.0020321

Fowler, K. R., Gutierrez-Velasco, S., Martin-Castellanos, C., and Smith, G. R. (2013). Protein determinants of meiotic DNA break hot spots. *Mol. Cell* 49, 983–996. doi:10.1016/j.molcel.2013.01.008

Fowler, K. R., Sasaki, M., Milman, N., Keeney, S., and Smith, G. R. (2014). Evolutionarily diverse determinants of meiotic DNA break and recombination landscapes across the genome. *Genome Res.* 24, 1650–1664. doi:10.1101/gr.172122.114

Fukuda, T., Fukuda, N., Agostinho, A., Hernandez-Hernandez, A., Kouznetsova, A., and Hoog, C. (2014). STAG3-mediated stabilization of REC8 cohesin complexes promotes chromosome synapsis during meiosis. *EMBO J.* 33, 1243–1255. doi:10.1002/embj.201387329

Fung, J. C., Rockmill, B., Odell, M., and Roeder, G. S. (2004). Imposition of crossover interference through the nonrandom distribution of synapsis initiation complexes. *Cell* 116, 795–802. doi:10.1016/s0092-8674(04)00249-1

Gomez, H. L., Felipe-Medina, N., Sanchez-Martin, M., Davies, O. R., Ramos, I., Garcia-Tunon, I., et al. (2016). C14ORF39/SIX6OS1 is a constituent of the synaptonemal complex and is essential for mouse fertility. *Nat. Commun.* 7, 13298. doi:10.1038/ncomms13298

Guan, Y., Leu, N. A., Ma, J., Chmatal, L., Ruthel, G., Bloom, J. C., et al. (2020). SKP1 drives the prophase I to metaphase I transition during male meiosis. *Sci. Adv.* 6, eaaz2129. doi:10.1126/sciadv.aaz2129

Guan, Y., Lin, H., Leu, N. A., Ruthel, G., Fuchs, S. Y., Busino, L., et al. (2022). SCF ubiquitin E3 ligase regulates DNA double-strand breaks in early meiotic recombination. *Nucleic Acids Res.* 50, 5129–5144. doi:10.1093/nar/gkac304

Guiraldelli, M. F., Eyster, C., Wilkerson, J. L., Dresser, M. E., and Pezza, R. J. (2013). Mouse HFM1/Mer3 is required for crossover formation and complete synapsis of homologous chromosomes during meiosis. *PLoS Genet.* 9, e1003383. doi:10.1371/journal.pgen.1003383

Guiraldelli, M. F., Felberg, A., Almeida, L. P., Parikh, A., de Castro, R. O., and Pezza, R. J. (2018). SHOC1 is a ERCC4-(HhH)2-like protein, integral to the formation of crossover recombination intermediates during mammalian meiosis. *PLoS Genet.* 14, e1007381. doi:10.1371/journal.pgen.1007381

Haarhuis, J. H. I., van der Weide, R. H., Blomen, V. A., Yanez-Cuna, J. O., Amendola, M., van Ruiten, M. S., et al. (2017). The cohesin release factor WAPL restricts chromatin loop extension. *Cell* 169, 693–707. doi:10.1016/j.cell.2017.04.013

Hamer, G., Wang, H., Bolcun-Filas, E., Cooke, H. J., Benavente, R., and Hoog, C. (2008). Progression of meiotic recombination requires structural maturation of the central element of the synaptonemal complex. *J. Cell Sci.* 121, 2445–2451. doi:10.1242/jcs.033233

Herran, Y., Gutierrez-Caballero, C., Sanchez-Martin, M., Hernandez, T., Viera, A., Barbero, J. L., et al. (2011). The cohesin subunit RAD21L functions in meiotic synapsis and exhibits sexual dimorphism in fertility. *EMBO J.* 30, 3091–3105. doi:10.1038/emboj.2011.222

Hong, S., Joo, J. H., Yun, H., Kleckner, N., and Kim, K. P. (2019). Recruitment of Rec8, Pds5 and Rad61/Wapl to meiotic homolog pairing, recombination, axis formation and S-phase. *Nucleic Acids Res.* 47, 11691–11708. doi:10.1093/nar/gkz903

Hunter, N., and Kleckner, N. (2001). The single-end invasion: An asymmetric intermediate at the double-strand break to double-holliday junction transition of meiotic recombination. *Cell* 106, 59–70. doi:10.1016/s0092-8674(01)00430-5

Hunter, N. (2015). Meiotic recombination: The essence of heredity. *Cold Spring Harb. Perspect. Biol.* 7, a016618. doi:10.1101/cshperspect.a016618

Imai, Y., Baudat, F., Taillepierre, M., Stanzione, M., Toth, A., and de Massy, B. (2017). The PRDM9 KRAB domain is required for meiosis and involved in protein interactions. *Chromosoma* 126, 681–695. doi:10.1007/s00412-017-0631-z

Ishiguro, K., Kim, J., Fujiyama-Nakamura, S., Kato, S., and Watanabe, Y. (2011). A new meiosis-specific cohesin complex implicated in the cohesin code for homologous pairing. *EMBO Rep.* 12, 267–275. doi:10.1038/embor.2011.2

Ishiguro, K., Kim, J., Shibuya, H., Hernandez-Hernandez, A., Suzuki, A., Fukagawa, T., et al. (2014). Meiosis-specific cohesin mediates homolog recognition in mouse spermatocytes. *Genes Dev.* 28, 594–607. doi:10.1101/gad.237313.113

Ito, M., Kugou, K., Fawcett, J. A., Mura, S., Ikeda, S., Innan, H., et al. (2014). Meiotic recombination cold spots in chromosomal cohesion sites. *Genes cells.* 19, 359–373. doi:10.1111/gtc.12138

Jantsch, V., Pasierbek, P., Mueller, M. M., Schweizer, D., Jantsch, M., and Loidl, J. (2004). Targeted gene knockout reveals a role in meiotic recombination for ZHP-3, a Zip3-related protein in *Caenorhabditis elegans*. *Mol. Cell Biol.* 24, 7998–8006. doi:10.1128/MCB.24.18.7998-8006.2004

Jiang, Y., Zhang, H. Y., Lin, Z., Zhu, Y. Z., Yu, C., Sha, Q. Q., et al. (2020). CXXC finger protein 1-mediated histone H3 lysine-4 trimethylation is essential for proper meiotic crossover formation in mice. *Development* 147, dev183764. doi:10.1242/dev.183764

Jin, H., Guacci, V., and Yu, H. G. (2009). Pds5 is required for homologue pairing and inhibits synapsis of sister chromatids during yeast meiosis. *J. Cell Biol.* 186, 713–725. doi:10.1083/jcb.200810107

Jin, X., Fudenberg, G., and Pollard, K. S. (2021). Genome-wide variability in recombination activity is associated with meiotic chromatin organization. *Genome Res.* 31, 1561–1572. doi:10.1101/gr.275358.121

Karanyi, Z., Halasz, L., Acquaviva, L., Jonas, D., Hetey, S., Boros-Olah, B., et al. (2018). Nuclear dynamics of the Set1C subunit Spp1 prepares meiotic recombination sites for break formation. *J. Cell Biol.* 217, 3398–3415. doi:10.1083/jcb.201712122

Kariyazono, R., Oda, A., Yamada, T., and Ohta, K. (2019). Conserved HORMA domain-containing protein Hop1 stabilizes interaction between proteins of meiotic DNA break hotspots and chromosome axis. *Nucleic Acids Res.* 47, 10166–10180. doi:10.1093/nar/gkz754

Kaur, P., Shi, Z., Lu, X., Zhang, H., Finkelstein, I. J., Tao, Y. J., et al. 2022. DNA capture and loop extrusion dynamics by cohesin-NIPBL. bioRxiv[preprint]. doi:10.1101/2022.08.18.504320

Keeney, S., Giroux, C. N., and Kleckner, N. (1997). Meiosis-specific DNA double-strand breaks are catalyzed by Spo11, a member of a widely conserved protein family. *Cell* 88, 375–384. doi:10.1016/s0092-8674(00)81876-0

Kim, K. P., Weiner, B. M., Zhang, L., Jordan, A., Dekker, J., and Kleckner, N. (2010). Sister cohesion and structural axis components mediate homolog bias of meiotic recombination. *Cell* 143, 924–937. doi:10.1016/j.cell.2010.11.015

Kim, Y., Shi, Z., Zhang, H., Finkelstein, I. J., and Yu, H. (2019). Human cohesin compacts DNA by loop extrusion. *Science* 366, 1345–1349. doi:10.1126/science.aaz4475

Kleckner, N., Zickler, D., Jones, G. H., Dekker, J., Padmore, R., Henle, J., et al. (2004). A mechanical basis for chromosome function. *Proc. Natl. Acad. Sci. U. S. A.* 101, 12592–12597. doi:10.1073/pnas.0402724101

Klein, F., Mahr, P., Galova, M., Buonomo, S. B., Michaelis, C., Nairz, K., et al. (1999). A central role for cohesins in sister chromatid cohesion, formation of axial elements, and recombination during yeast meiosis. *Cell* 98, 91–103. doi:10.1016/S0092-8674(00)80609-1

Klug, H., Xaver, M., Chaugule, V. K., Koidl, S., Mittler, G., Klein, F., et al. (2013). Ubc9 sumoylation controls SUMO chain formation and meiotic synapsis in *Saccharomyces cerevisiae*. *Mol. Cell* 50, 625–636. doi:10.1016/j.molcel.2013.03.027

Kneitz, B., Cohen, P. E., Avdievich, E., Zhu, L., Kane, M. F., Hou, H., Jr., et al. (2000). MutS homolog 4 localization to meiotic chromosomes is required for chromosome pairing during meiosis in male and female mice. *Genes Dev.* 14, 1085–1097. doi:10.1101/gad.14.9.1085

Kniewel, R., Murakami, H., Liu, Y., Ito, M., Ohta, K., Hollingsworth, N. M., et al. (2017). Histone H3 threonine 11 phosphorylation is catalyzed directly by the meiosis-specific kinase Mek1 and provides a molecular readout of Mek1 activity *in vivo*. *Genetics* 207, 1313–1333. doi:10.1534/genetics.117.300359

Kong, A., Thorleifsson, G., Frigge, M. L., Masson, G., Gudbjartsson, D. F., Villemoes, R., et al. (2014). Common and low-frequency variants associated with genome-wide recombination rate. *Nat. Genet.* 46, 11–16. doi:10.1038/ng.2833

Kong, A., Thorleifsson, G., Stefansson, H., Masson, G., Helgason, A., Gudbjartsson, D. F., et al. (2008). Sequence variants in the RNF212 gene associate with genome-wide recombination rate. *Science* 319, 1398–1401. doi:10.1126/science.1152422

Kueng, S., Hegemann, B., Peters, B. H., Lipp, J. J., Schleiffer, A., Mechtler, K., et al. (2006). Wapl controls the dynamic association of cohesin with chromatin. *Cell* 127, 955–967. doi:10.1016/j.cell.2006.09.040

Kugou, K., Fukuda, T., Yamada, S., Ito, M., Sasanuma, H., Mori, S., et al. (2009). Rec8 guides canonical Spo11 distribution along yeast meiotic chromosomes. *Mol. Biol. Cell* 20, 3064–3076. doi:10.1091/mbc.E08-12-1223

Kumar, R., Bourbon, H. M., and de Massy, B. (2010). Functional conservation of Mei4 for meiotic DNA double-strand break formation from yeasts to mice. *Genes Dev.* 24, 1266–1280. doi:10.1101/gad.571710

Kumar, R., Ghyselinck, N., Ishiguro, K., Watanabe, Y., Kouznetsova, A., Hoog, C., et al. (2015). MEI4 - a central player in the regulation of meiotic DNA double-strand break formation in the mouse. *J. Cell Sci.* 128, 1800–1811. doi:10.1242/jcs.165464

Kusch, T. (2015). Brca2-Pds5 complexes mobilize persistent meiotic recombination sites to the nuclear envelope. *J. Cell Sci.* 128, 717–727. doi:10.1242/jcs.159988

Lao, J. P., Cloud, V., Huang, C. C., Grubb, J., Thacker, D., Lee, C. Y., et al. (2013). Meiotic crossover control by concerted action of Rad51-Dmc1 in homolog template bias and robust homeostatic regulation. *PLoS Genet.* 9, e1003978. doi:10.1371/journal.pgen.1003978

Lao, J. P., and Hunter, N. (2010). Trying to avoid your sister. *PLoS Biol.* 8, e1000519. doi:10.1371/journal.pbio.1000519

Lee, J., and Hirano, T. (2011). RAD21L, a novel cohesin subunit implicated in linking homologous chromosomes in mammalian meiosis. *J. Cell Biol.* 192, 263–276. doi:10.1083/jcb.201008005

Lee, M. S., Higashide, M. T., Choi, H., Li, K., Hong, S., Lee, K., et al. (2021). The synaptonemal complex central region modulates crossover pathways and feedback control of meiotic double-strand break formation. *Nucleic Acids Res.* 49, 7537–7553. doi:10.1093/nar/gkab566

Li, X. C., and Schimenti, J. C. (2007). Mouse pachytene checkpoint 2 (trip13) is required for completing meiotic recombination but not synapsis. *PLoS Genet.* 3, e130. doi:10.1371/journal.pgen.0030130

Llano, E., Herran, Y., Garcia-Tunon, I., Gutierrez-Caballero, C., de Alava, E., Barbero, J. L., et al. (2012). Meiotic cohesin complexes are essential for the formation of the axial element in mice. *J. Cell Biol.* 197, 877–885. doi:10.1083/jcb.201201100

Luo, Z., Wang, X., Jiang, H., Wang, R., Chen, J., Chen, Y., et al. (2020). Reorganized 3D genome structures support transcriptional regulation in mouse spermatogenesis. *iScience* 23, 101034. doi:10.1016/j.isci.2020.101034

Lynn, A., Soucek, R., and Borner, G. V. (2007). ZMM proteins during meiosis: Crossover artists at work. *Chromosome Res.* 15, 591–605. doi:10.1007/s10577-007-1150-1

MacQueen, A. J., Colaiacovo, M. P., McDonald, K., and Villeneuve, A. M. (2002). Synapsis-dependent and -independent mechanisms stabilize homolog pairing during meiotic prophase in *C. elegans*. *Genes Dev.* 16, 2428–2442. doi:10.1101/gad.1011602

MacQueen, A. J., Phillips, C. M., Bhalla, N., Weiser, P., Villeneuve, A. M., and Dernburg, A. F. (2005). Chromosome sites play dual roles to establish homologous synapsis during meiosis in *C. elegans*. *Cell* 123, 1037–1050. doi:10.1016/j.cell.2005.09.034

Martini, E., Diaz, R. L., Hunter, N., and Keeney, S. (2006). Crossover homeostasis in yeast meiosis. *Cell* 126, 285–295. doi:10.1016/j.cell.2006.05.044

Martino, J., Brunette, G. J., Barroso-Gonzalez, J., Moiseeva, T. N., Smith, C. M., Bakkenist, C. J., et al. (2019). The human Shu complex functions with PDS5B and SPIDR to promote homologous recombination. *Nucleic Acids Res.* 47, 10151–10165. doi:10.1093/nar/gkz738

Miyoshi, T., Ito, M., Kugou, K., Yamada, S., Furuichi, M., Oda, A., et al. (2012). A central coupler for recombination initiation linking chromosome architecture to S phase checkpoint. *Mol. Cell* 47, 722–733. doi:10.1016/j.molcel.2012.06.023

Morgan, C., Fozard, J. A., Hartley, M., Henderson, I. R., Bomblies, K., and Howard, M. (2021). Diffusion-mediated HEI10 coarsening can explain meiotic crossover positioning in Arabidopsis. *Nat. Commun.* 12, 4674. doi:10.1038/s41467-021-24827-w

Muller, H., Scolari, V. F., Agier, N., Piazza, A., Thierry, A., Mercy, G., et al. (2018). Characterizing meiotic chromosomes' structure and pairing using a designer sequence optimized for Hi-C. *Mol. Syst. Biol.* 14, e8293. doi:10.15252/msb.20188293

Nasmyth, K., and Haering, C. H. (2005). The structure and function of SMC and kleisin complexes. *Annu. Rev. Biochem.* 74, 595–648. doi:10.1146/annurev.biochem.74.082803.133219

Niu, H., Li, X., Job, E., Park, C., Moazed, D., Gygi, S. P., et al. (2007). Mek1 kinase is regulated to suppress double-strand break repair between sister chromatids during budding yeast meiosis. *Mol. Cell Biol.* 27, 5456–5467. doi:10.1128/MCB.00416-07

Niu, H., Wan, L., Busygina, V., Kwon, Y., Allen, J. A., Li, X., et al. (2009). Regulation of meiotic recombination via Mek1-mediated Rad54 phosphorylation. *Mol. Cell* 36, 393–404. doi:10.1016/j.molcel.2009.09.029

Nore, A., Juarez-Martinez, A. B., Clement, J., Brun, C., Diagouraga, B., Laroussi, H., et al. (2022). TOPOVIBL-REC114 interaction regulates meiotic DNA double-strand breaks. *Nat. Commun.* 13, 7048. doi:10.1038/s41467-022-34799-0

Pan, J., Sasaki, M., Kniewel, R., Murakami, H., Blitzblau, H. G., Tischfield, S. E., et al. (2011). A hierarchical combination of factors shapes the genome-wide topography of yeast meiotic recombination initiation. *Cell* 144, 719–731. doi:10.1016/j.cell.2011.02.009

Panizza, S., Mendoza, M. A., Berlinger, M., Huang, L., Nicolas, A., Shirahige, K., et al. (2011). Spo11-accessory proteins link double-strand break sites to the chromosome axis in early meiotic recombination. *Cell* 146, 372–383. doi:10.1016/j.cell.2011.07.003

Parvanov, E. D., Tian, H., Billings, T., Saxl, R. L., Spruce, C., Aithal, R., et al. (2017). PRDM9 interactions with other proteins provide a link between recombination hotspots and the chromosomal axis in meiosis. *Mol. Biol. Cell* 28, 488–499. doi:10.1091/mbc.E16-09-0686

Pasierbek, P., Jantsch, M., Melcher, M., Schleiffer, A., Schweizer, D., and Loidl, J. (2001). A *Caenorhabditis elegans* cohesion protein with functions in meiotic chromosome pairing and disjunction. *Genes Dev.* 15, 1349–1360. doi:10.1101/gad.192701

Patel, L., Kang, R., Rosenberg, S. C., Qiu, Y., Raviram, R., Chee, S., et al. (2019). Dynamic reorganization of the genome shapes the recombination landscape in meiotic prophase. *Nat. Struct. Mol. Biol.* 26, 164–174. doi:10.1038/s41594-019-0187-0

Pattabiraman, D., Roelens, B., Woglar, A., and Villeneuve, A. M. (2017). Meiotic recombination modulates the structure and dynamics of the synaptonemal complex during *C. elegans* meiosis. *PLoS Genet.* 13, e1006670. doi:10.1371/journal.pgen.1006670

Qiao, H., Prasada Rao, H. B., Yang, Y., Fong, J. H., Cloutier, J. M., Deacon, D. C., et al. (2014). Antagonistic roles of ubiquitin ligase HEI10 and SUMO ligase RNF212 regulate meiotic recombination. *Nat. Genet.* 46, 194–199. doi:10.1038/ng.2858

Rao, H. B., Qiao, H., Bhatt, S. K., Bailey, L. R., Tran, H. D., Bourne, S. L., et al. (2017). A SUMO-ubiquitin relay recruits proteasomes to chromosome axes to regulate meiotic recombination. *Science* 355, 403–407. doi:10.1126/science.aaf6407

Revenkova, E., Eijpe, M., Heyting, C., Hodges, C. A., Hunt, P. A., Liebe, B., et al. (2004). Cohesin SMC1 beta is required for meiotic chromosome dynamics, sister chromatid cohesion and DNA recombination. *Nat. Cell Biol.* 6, 555–562. doi:10.1038/ncb1135

Reynolds, A., Qiao, H., Yang, Y., Chen, J. K., Jackson, N., Biswas, K., et al. (2013). RNF212 is a dosage-sensitive regulator of crossing-over during mammalian meiosis. *Nat. Genet.* 45, 269–278. doi:10.1038/ng.2541

Rinaldi, V. D., Bolcun-Filas, E., Kogo, H., Kurahashi, H., and Schimenti, J. C. (2017). The DNA damage checkpoint eliminates mouse oocytes with chromosome synapsis failure. *Mol. Cell* 67, 1026–1036. doi:10.1016/j.molcel.2017.07.027

Robert, T., Vrielynck, N., Mezard, C., de Massy, B., and Grelon, M. (2016). A new light on the meiotic DSB catalytic complex. *Semin. Cell Dev. Biol.* 54, 165–176. doi:10.1016/j.semcdb.2016.02.025

Rog, O., Kohler, S., and Dernburg, A. F. (2017). The synaptonemal complex has liquid crystalline properties and spatially regulates meiotic recombination factors. *Elife* 6, e21455. doi:10.7554/eLife.21455

Roig, I., Dowdle, J. A., Toth, A., de Rooij, D. G., Jasin, M., and Keeney, S. (2010). Mouse TRIP13/PCH2 is required for recombination and normal higher-order chromosome structure during meiosis. *PLoS Genet.* 6, e1001062. doi:10.1371/journal.pgen.1001062

Rousova, D., Nivsarkar, V., Altmannova, V., Raina, V. B., Funk, S. K., Liedtke, D., et al. (2021). Novel mechanistic insights into the role of Mer2 as the keystone of meiotic DNA break formation. *Elife* 10, e72330. doi:10.7554/eLife.72330

Sakuno, T., Tashiro, S., Tanizawa, H., Iwasaki, O., Ding, D. Q., Haraguchi, T., et al. (2022). Rec8 Cohesin-mediated Axis-loop chromatin architecture is required for meiotic recombination. *Nucleic Acids Res.* 50, 3799–3816. doi:10.1093/nar/gkac183

Sanchez-Saez, F., Gomez, H. L., Dunne, O. M., Gallego-Paramo, C., Felipe-Medina, N., Sanchez-Martin, M., et al. (2020). Meiotic chromosome synapsis depends on multivalent SYCE1-SIX6OS1 interactions that are disrupted in cases of human infertility. *Sci. Adv.* 6, eabb1660. doi:10.1126/sciadv.abb1660

Schalbetter, S. A., Fudenberg, G., Baxter, J., Pollard, K. S., and Neale, M. J. (2019). Principles of meiotic chromosome assembly revealed in *S. cerevisiae*. *Nat. Commun.* 10, 4795. doi:10.1038/s41467-019-12629-0

Schramm, S., Fraune, J., Naumann, R., Hernandez-Hernandez, A., Hoog, C., Cooke, H. J., et al. (2011). A novel mouse synaptonemal complex protein is essential for loading of central element proteins, recombination, and fertility. *PLoS Genet.* 7, e1002088. doi:10.1371/journal.pgen.1002088

Severson, A. F., Ling, L., van Zuylen, V., and Meyer, B. J. (2009). The axial element protein HTP-3 promotes cohesin loading and meiotic axis assembly in *C. elegans* to implement the meiotic program of chromosome segregation. *Genes Dev.* 23, 1763–1778. doi:10.1101/gad.1808809

Severson, A. F., and Meyer, B. J. (2014). Divergent kleisin subunits of cohesin specify mechanisms to tether and release meiotic chromosomes. *Elife* 3, e03467. doi:10.7554/eLife.03467

Shin, Y. H., McGuire, M. M., and Rajkovic, A. (2013). Mouse HORMAD1 is a meiosis i checkpoint protein that modulates DNA double-strand break repair during female meiosis. *Biol. Reprod.* 89, 29. doi:10.1095/biolreprod.112.106773

Shinohara, M., Oh, S. D., Hunter, N., and Shinohara, A. (2008). Crossover assurance and crossover interference are distinctly regulated by the ZMM proteins during yeast meiosis. *Nat. Genet.* 40, 299–309. doi:10.1038/ng.83

Shinohara, M., Sakai, K., Shinohara, A., and Bishop, D. K. (2003). Crossover interference in *Saccharomyces cerevisiae* requires a TID1/RDH54- and DMC1-dependent pathway. *Genetics* 163, 1273–1286. doi:10.1093/genetics/163.4.1273

Smith, A. V., and Roeder, G. S. (1997). The yeast Red1 protein localizes to the cores of meiotic chromosomes. *J. Cell Biol.* 136, 957–967. doi:10.1083/jcb.136.5.957

Smolikov, S., Eizinger, A., Hurlburt, A., Rogers, E., Villeneuve, A. M., and Colaiacovo, M. P. (2007a). Synapsis-defective mutants reveal a correlation between chromosome conformation and the mode of double-strand break repair during *Caenorhabditis elegans* meiosis. *Genetics* 176, 2027–2033. doi:10.1534/genetics.107.076968

Smolikov, S., Eizinger, A., Schild-Prufert, K., Hurlburt, A., McDonald, K., Engebrecht, J., et al. (2007b). SYP-3 restricts synaptonemal complex assembly to bridge paired chromosome axes during meiosis in *Caenorhabditis elegans*. *Genetics* 176, 2015–2025. doi:10.1534/genetics.107.072413

Smolikov, S., Schild-Prufert, K., and Colaiacovo, M. P. (2009). A yeast two-hybrid screen for SYP-3 interactors identifies SYP-4, a component required for synaptonemal complex assembly and chiasma formation in *Caenorhabditis elegans* meiosis. *PLoS Genet.* 5, e1000669. doi:10.1371/journal.pgen.1000669

Sommermeyer, V., Beneut, C., Chaplais, E., Serrentino, M. E., and Borde, V. (2013). Spp1, a member of the Set1 Complex, promotes meiotic DSB formation in promoters by tethering histone H3K4 methylation sites to chromosome axes. *Mol. Cell* 49, 43–54. doi:10.1016/j.molcel.2012.11.008

Stanzione, M., Baumann, M., Papanikos, F., Dereli, I., Lange, J., Ramlal, A., et al. (2016). Meiotic DNA break formation requires the unsynapsed chromosome axis-binding protein IHO1 (CCDC36) in mice. *Nat. Cell Biol.* 18, 1208–1220. doi:10.1038/ncb3417

Stauffer, W. T., Zhang, L., and Dernburg, A. (2019). Diffusion through a liquid crystalline compartment regulates meiotic recombination. *SPIE Proc.* 2019. doi:10.1117/12.2513378

Strong, E. R., and Schimenti, J. C. (2010). Evidence implicating CCNB1IP1, a RING domain-containing protein required for meiotic crossing over in mice, as an E3 SUMO ligase. *Genes (Basel)* 1, 440–451. doi:10.3390/genes1030440

Sym, M., and Roeder, G. S. (1994). Crossover interference is abolished in the absence of a synaptonemal complex protein. *Cell* 79, 283–292. doi:10.1016/0092-8674(94)90197-x

Takeo, S., Lake, C. M., Morais-de-Sa, E., Sunkel, C. E., and Hawley, R. S. (2011). Synaptonemal complex-dependent centromeric clustering and the initiation of synapsis in Drosophila oocytes. *Curr. Biol.* 21, 1845–1851. doi:10.1016/j.cub.2011.09.044

Tedeschi, A., Wutz, G., Huet, S., Jaritz, M., Wuensche, A., Schirghuber, E., et al. (2013). Wapl is an essential regulator of chromatin structure and chromosome segregation. *Nature* 501, 564–568. doi:10.1038/nature12471

Thacker, D., Lam, I., Knop, M., and Keeney, S. (2011). Exploiting spore-autonomous fluorescent protein expression to quantify meiotic chromosome behaviors in *Saccharomyces cerevisiae*. *Genetics* 189, 423–439. doi:10.1534/genetics.111.131326

Tian, H., Billings, T., and Petkov, P. M. (2018). CXXC1 is not essential for normal DNA double-strand break formation and meiotic recombination in mouse. *PLoS Genet.* 14, e1007657. doi:10.1371/journal.pgen.1007657

Tsubouchi, T., Zhao, H., and Roeder, G. S. (2006). The meiosis-specific zip4 protein regulates crossover distribution by promoting synaptonemal complex formation together with zip2. *Dev. Cell* 10, 809–819. doi:10.1016/j.devcel.2006.04.003

Vara, C., Paytuvi-Gallart, A., Cuartero, Y., Le Dily, F., Garcia, F., Salva-Castro, J., et al. (2019). Three-dimensional genomic structure and cohesin occupancy correlate with transcriptional activity during spermatogenesis. *Cell Rep.* 28, 352–367. doi:10.1016/j.celrep.2019.06.037

Viera, A., Berenguer, I., Ruiz-Torres, M., Gomez, R., Guajardo, A., Barbero, J. L., et al. (2020). PDS5 proteins regulate the length of axial elements and telomere integrity during male mouse meiosis. *EMBO Rep.* 21, e49273. doi:10.15252/embr.201949273

Voelkel-Meiman, K., Cheng, S. Y., Morehouse, S. J., and MacQueen, A. J. (2016). Synaptonemal complex proteins of budding yeast define reciprocal roles in MutSγ-mediated crossover formation. *Genetics* 203, 1091–1103. doi:10.1534/genetics.115.182923

Voelkel-Meiman, K., Taylor, L. F., Mukherjee, P., Humphryes, N., Tsubouchi, H., and Macqueen, A. J. (2013). SUMO localizes to the central element of synaptonemal complex and is required for the full synapsis of meiotic chromosomes in budding yeast. *PLoS Genet.* 9, e1003837. doi:10.1371/journal.pgen.1003837

Wang, K., Wang, M., Tang, D., Shen, Y., Miao, C., Hu, Q., et al. (2012). The role of rice HEI10 in the formation of meiotic crossovers. *PLoS Genet.* 8, e1002809. doi:10.1371/journal.pgen.1002809

Wang, S., Veller, C., Sun, F., Ruiz-Herrera, A., Shang, Y., Liu, H., et al. (2019a). Per-nucleus crossover covariation and implications for evolution. *Cell* 177, 326–338. doi:10.1016/j.cell.2019.02.021

Wang, Y., Wang, H., Zhang, Y., Du, Z., Si, W., Fan, S., et al. (2019b). Reprogramming of meiotic chromatin architecture during spermatogenesis. *Mol. Cell* 73, 547–561. doi:10.1016/j.molcel.2018.11.019

Ward, A., Hopkins, J., McKay, M., Murray, S., and Jordan, P. W. (2016). Genetic interactions between the meiosis-specific cohesin components, STAG3, REC8, and RAD21L. *G3 (Bethesda)* 6, 1713–1724. doi:10.1534/g3.116.029462

Ward, J. O., Reinholdt, L. G., Motley, W. W., Niswander, L. M., Deacon, D. C., Griffin, L. B., et al. (2007). Mutation in mouse hei10, an e3 ubiquitin ligase, disrupts meiotic crossing over. *PLoS Genet.* 3, e139. doi:10.1371/journal.pgen.0030139

West, A. M., Rosenberg, S. C., Ur, S. N., Lehmer, M. K., Ye, Q., Hagemann, G., et al. (2019). A conserved filamentous assembly underlies the structure of the meiotic chromosome axis. *Elife* 8, e40372. doi:10.7554/eLife.40372

West, A. M. V., Komives, E. A., and Corbett, K. D. (2018). Conformational dynamics of the Hop1 HORMA domain reveal a common mechanism with the spindle checkpoint protein Mad2. *Nucleic Acids Res.* 46, 279–292. doi:10.1093/nar/gkx1196

Wojtasz, L., Daniel, K., Roig, I., Bolcun-Filas, E., Xu, H., Boonsanay, V., et al. (2009). Mouse HORMAD1 and HORMAD2, two conserved meiotic chromosomal proteins, are depleted from synapsed chromosome axes with the help of TRIP13 AAA-ATPase. *PLoS Genet.* 5, e1000702. doi:10.1371/journal.pgen.1000702

Wutz, G., Varnai, C., Nagasaka, K., Cisneros, D. A., Stocsits, R. R., Tang, W., et al. (2017). Topologically associating domains and chromatin loops depend on cohesin and are regulated by CTCF, WAPL, and PDS5 proteins. *EMBO J.* 36, 3573–3599. doi:10.15252/embj.201798004

Xu, H., Beasley, M. D., Warren, W. D., van der Horst, G. T., and McKay, M. J. (2005). Absence of mouse REC8 cohesin promotes synapsis of sister chromatids in meiosis. *Dev. Cell* 8, 949–961. doi:10.1016/j.devcel.2005.03.018

Yamada, S., Ohta, K., and Yamada, T. (2013). Acetylated Histone H3K9 is associated with meiotic recombination hotspots, and plays a role in recombination redundantly with other factors including the H3K4 methylase Set1 in fission yeast. *Nucleic Acids Res.* 41, 3504–3517. doi:10.1093/nar/gkt049

Yang, F., Gell, K., van der Heijden, G. W., Eckardt, S., Leu, N. A., Page, D. C., et al. (2008). Meiotic failure in male mice lacking an X-linked factor. *Genes Dev.* 22, 682–691. doi:10.1101/gad.1613608

Yang, X., Song, M., Wang, Y., Tan, T., Tian, Z., Zhai, B., et al. (2022). The ubiquitin-proteasome system regulates meiotic chromosome organization. *Proc. Natl. Acad. Sci. U. S. A.* 119, e2106902119. doi:10.1073/pnas.2106902119

Ye, Q., Kim, D. H., Dereli, I., Rosenberg, S. C., Hagemann, G., Herzog, F., et al. (2017). The AAA+ ATPase TRIP13 remodels HORMA domains through N-terminal engagement and unfolding. *EMBO J.* 36, 2419–2434. doi:10.15252/embj.201797291

Zanders, S., Sonntag Brown, M., Chen, C., and Alani, E. (2011). Pch2 modulates chromatid partner choice during meiotic double-strand break repair in *Saccharomyces cerevisiae*. *Genetics* 188, 511–521. doi:10.1534/genetics.111.129031

Zhang, L., Espagne, E., de Muyt, A., Zickler, D., and Kleckner, N. E. (2014a). Interference-mediated synaptonemal complex formation with embedded crossover designation. *Proc. Natl. Acad. Sci. U. S. A.* 111, E5059–E5068. doi:10.1073/pnas.1416411111

Zhang, L., Kohler, S., Rillo-Bohn, R., and Dernburg, A. F. (2018a). A compartmentalized signaling network mediates crossover control in meiosis. *Elife* 7, e30789. doi:10.7554/eLife.30789

Zhang, L., Liang, Z., Hutchinson, J., and Kleckner, N. (2014b). Crossover patterning by the beam-film model: Analysis and implications. *PLoS Genet.* 10, e1004042. doi:10.1371/journal.pgen.1004042

Zhang, L., Stauffer, W., Zwicker, D., and Dernburg, A. F. 2021. Crossover patterning through kinase-regulated condensation and coarsening of recombination nodules. bioRxiv [preprint]. doi:10.1101/2021.08.26.457865

Zhang, L., Wang, S., Yin, S., Hong, S., Kim, K. P., and Kleckner, N. (2014c). Topoisomerase II mediates meiotic crossover interference. *Nature* 511, 551–556. doi:10.1038/nature13442

Zhang, Q., Ji, S. Y., Busayavalasa, K., and Yu, C. (2019). SPO16 binds SHOC1 to promote homologous recombination and crossing-over in meiotic prophase I. *Sci. Adv.* 5, eaau9780. doi:10.1126/sciadv.aau9780

Zhang, Q., Shao, J., Fan, H. Y., and Yu, C. (2018b). Evolutionarily-conserved MZIP2 is essential for crossover formation in mammalian meiosis. *Commun. Biol.* 1, 147. doi:10.1038/s42003-018-0154-z

Zhang, Y., Suzuki, T., Li, K., Gothwal, S. K., Shinohara, M., and Shinohara, A. (2020). Genetic interactions of histone modification machinery Set1 and PAF1C with the recombination complex rec114-mer2-mei4 in the formation of meiotic DNA double-strand breaks. *Int. J. Mol. Sci.* 21, 2679. doi:10.3390/ijms21082679

Zhu, Z., Bani Ismail, M., Shinohara, M., and Shinohara, A. (2021). SCF(Cdc4) ubiquitin ligase regulates synaptonemal complex formation during meiosis. *Life Sci. Alliance* 4, e202000933. doi:10.26508/lsa.202000933

Zierhut, C., Berlinger, M., Rupp, C., Shinohara, A., and Klein, F. (2004). Mnd1 is required for meiotic interhomolog repair. *Curr. Biol.* 14, 752–762. doi:10.1016/j.cub.2004.04.030

Ziolkowski, P. A., Underwood, C. J., Lambing, C., Martinez-Garcia, M., Lawrence, E. J., Ziolkowska, L., et al. (2017). Natural variation and dosage of the HEI10 meiotic E3 ligase control Arabidopsis crossover recombination. *Genes Dev.* 31, 306–317. doi:10.1101/gad.295501.116

Zuo, W., Chen, G., Gao, Z., Li, S., Chen, Y., Huang, C., et al. (2021). Stage-resolved Hi-C analyses reveal meiotic chromosome organizational features influencing homolog alignment. *Nat. Commun.* 12, 5827. doi:10.1038/s41467-021-26033-0

frontiers | Frontiers in Cell and Developmental Biology

TYPE Original Research
PUBLISHED 13 January 2023
DOI 10.3389/fcell.2022.1069946

OPEN ACCESS

EDITED BY
Ricardo Benavente,
Julius Maximilian University of Würzburg, Germany

REVIEWED BY
Anna Kouznetsova,
Karolinska Institutet (KI), Sweden
Zickler Denise,
Université Paris-Saclay, France

*CORRESPONDENCE
Rocío Gómez,
rocio.gomez@uam.es
José A. Suja,
jose.suja@uam.es

†PRESENT ADDRESS
Inés Berenguer,
Departamento de Neuropatología Molecular, Centro de Biología Molecular Severo Ochoa, Campus de la Universidad Autónoma de Madrid, Madrid, Spain
Andrea Guajardo-Grence,
Hospital Universitario Santa Cristina, Instituto de Investigación Sanitaria del Hospital Universitario de La Princesa, Universidad Autónoma de Madrid, Madrid, Spain

SPECIALTY SECTION
This article was submitted to Nuclear Organization and Dynamics, a section of the journal Frontiers in Cell and Developmental Biology

RECEIVED 14 October 2022
ACCEPTED 19 December 2022
PUBLISHED 13 January 2023

CITATION
Gómez R, Viera A, Moreno-Mármol T, Berenguer I, Guajardo-Grence A, Tóth A, Parra MT and Suja JA (2023), Kinase PLK1 regulates the disassembly of the lateral elements and the assembly of the inner centromere during the diakinesis/metaphase I transition in male mouse meiosis.
Front. Cell Dev. Biol. 10:1069946.
doi: 10.3389/fcell.2022.1069946

Kinase PLK1 regulates the disassembly of the lateral elements and the assembly of the inner centromere during the diakinesis/metaphase I transition in male mouse meiosis

Rocío Gómez[1]*, Alberto Viera[1], Tania Moreno-Mármol[1], Inés Berenguer[1,2†], Andrea Guajardo-Grence[1,3†], Attila Tóth[4], María Teresa Parra[1] and José A. Suja[1]*

[1]Unidad de Biología Celular, Departamento de Biología, Facultad de Ciencias, Universidad Autónoma de Madrid, Madrid, Spain, [2]Departamento de Neuropatología Molecular, Centro de Biología Molecular Severo Ochoa, Campus de la Universidad Autónoma de Madrid, Madrid, Spain, [3]Hospital Universitario Santa Cristina, Instituto de Investigación Sanitaria del Hospital Universitario de La Princesa, Universidad Autónoma de Madrid, Madrid, Spain, [4]Institute of Physiological Chemistry, Faculty of Medicine, Technische Universität Dresden, Dresden, Germany

PLK1 is a serine/threonine kinase with crucial roles during mitosis. However, its involvement during mammalian male meiosis remains largely unexplored. By inhibiting the kinase activity of PLK1 using BI 2536 on organotypic cultures of seminiferous tubules, we found that the disassembly of SYCP3 and HORMAD1 from the lateral elements of the synaptonemal complex during diakinesis is impeded. We also found that the normal recruitment of SYCP3 and HORMAD1 to the inner centromere in prometaphase I spermatocytes did not occur. Additionally, we analyzed the participation of PLK1 in the assembly of the inner centromere by studying its implication in the Bub1-H2AT120ph-dependent recruitment of shugoshin SGO2, and the Haspin-H3T3ph-dependent recruitment of Aurora B/C and Borealin. Our results indicated that both pathways are regulated by PLK1. Altogether, our results demonstrate that PLK1 is a master regulator of the late prophase I/metaphase I transition in mouse spermatocytes.

KEYWORDS

mouse, meiosis, PLK1, lateral elements, inner centromere, H2AT120ph, H3T3ph

Introduction

Meiosis is a specialized cell division process characterized by a single round of DNA replication followed by two rounds of chromosome segregation, which promotes the generation of haploid gametes. During prophase of the first meiotic division (prophase I), the homologous chromosomes must correctly achieve their pairing, synapsis and recombination to allow a successful chromosome segregation during the first meiotic division (Handel and Schimenti, 2010; Bolcun-Filas and Handel, 2018). These processes lead to the formation of a meiosis-

Abbreviations: AEs, axial elements; CE, central element; LEs, lateral elements; SC, synaptonemal complex.

specific zipper-like proteinaceous structure known as the synaptonemal complex (SC), the hallmark of meiosis (Fraune et al., 2012; Zhang et al., 2021). The SC is formed by two lateral elements (LEs), one per homolog, and a series of transverse filaments connecting them. The transverse filaments interact at the SC central region forming the central element (CE) (Fraune et al., 2012). During the leptotene stage of prophase I the so-called axial elements (AEs) form along each homolog and are then named LEs once the homologs begin to pair during the zygotene stage. Mammalian AEs/LEs are mainly composed of the proteins SYCP2 and SYCP3 (Moens et al., 1987; Dobson et al., 1994; Schalk et al., 1998), different cohesin complexes (Suja and Barbero, 2009; McNicoll et al., 2013), the cohesin regulatory proteins NIPBL and MAU2 (Visnes et al., 2014), condensin complexes (Visnes et al., 2014), and the recruited HORMA-domain proteins HORMAD1 and HORMAD2 (Wojtasz et al., 2009). During pachytene, the homologs are synapsed and SCs are fully formed along the length of the autosomal bivalents. Once recombination is completed, the homologs and their LEs desynapse by diplotene due to the disassembly of CE proteins (Jordan et al., 2012). Studies on mouse spermatocytes indicated a gradual disassembly of the LE protein SYCP3 during late prophase I stages, and its accumulation at metaphase I inner centromeres (Dobson et al., 1994; Prieto et al., 2001; Eijpe et al., 2003; Parra et al., 2004; Gómez et al., 2007). However, the precise sequence of events leading to these processes, and their regulation, are poorly understood in vertebrates (Cahoon and Hawley, 2016; Gao and Colaiácovo, 2018; Láscarez-Lagunas et al., 2022).

Different studies have pointed out to potential kinases that would be responsible for the SC and LE disassembly. In budding yeast meiosis, the kinases Cdc5/PLK1, Ipl1/Aurora B, Ddk and Cdk play important roles (Clyne et al., 2003; Sourirajan and Lichten, 2008; Jordan et al., 2009; Argunhan et al., 2017). In male mouse meiosis, the Polo-like kinase PLK1 also promotes SC disassembly (Ishiguro et al., 2011). PLK1 phosphorylates the CE proteins SYCP1 and TEX12 to allow desynapsis of homolog LEs (Jordan et al., 2012). Interestingly, it has been recently reported that the kinases Aurora B and C, as well as PLK1, regulate the disassembly of LEs during the late prophase I/metaphase I transition (Wellard et al., 2020; Wellard et al., 2022).

PLKs are a family of serine/threonine kinases conserved from yeast to mammals (Korns et al., 2022). There are several PLK paralogs in mammals, PLK1-5, but PLK1 is the most studied one. Many publications have shown that during mammalian mitotic and meiotic divisions PLK1 is localized at the centrosomes, acentriolar microtubule organizing centres (MTOCs), kinetochores, the central spindle and the mid-body. Accordingly, PLK1 is a key regulator of mitosis and female mouse meiosis since it has key roles in mitotic entry and meiotic resumption, formation of acentriolar MTOCs, centrosome maturation and separation, bipolar spindle assembly, kinetochore-microtubule attachment, chromosome condensation, alignment and segregation, regulation of the anaphase-promoting complex/cyclosome (APC/C), and cytokinesis (Tong et al., 2002; Schmucker and Sumara, 2014; Kim et al., 2015; Solc et al., 2015; Combes et al., 2017; Little and Jordan, 2020). In contrast, the role of PLK1 in male meiosis is much less understood in comparison with female meiosis.

By phosphorylating some cohesin subunits PLK1 is also responsible for the partial release of cohesin complexes from chromosome arms during vertebrate mitotic prophase and prometaphase, the so-called "prophase pathway" (Giménez-Abián et al., 2004; Hauf et al., 2005). In addition, it has been proposed that in mammalian somatic cells PLK1 phosphorylates and activates the kinase Haspin (Ghenoiu et al., 2013; Zhou et al., 2014). Haspin then phosphorylates histone H3 at threonine 3 (H3T3ph) (Dai et al., 2005) creating a platform for the recruitment of the kinase Aurora B and other chromosomal passenger complex (CPC) proteins to the inner centromere (Kelly et al., 2010; Wang et al., 2010; Yamagishi et al., 2010; Wang et al., 2011; De Antoni et al., 2012; Wang et al., 2012).

Here, we analyzed the participation of PLK1 in the disassembly of the SC LEs and the REC8 cohesin axes of chromosomes during the diakinesis/metaphase I transition. We first studied the accurate pattern of distribution of the LE proteins SYCP3 and HORMAD1, and of the REC8-containing cohesin axes, during the diakinesis/metaphase I transition in wild-type (WT) spermatocytes. Then, we inhibited the kinase activity of PLK1 by treating organotypic cultures of seminiferous tubules with BI 2536, a small potent molecule that specifically inhibits PLK1 in somatic cells (Lénárt et al., 2007; Steegmaier et al., 2007; Zhou et al., 2014; Su et al., 2022), and mouse spermatocytes (Alfaro et al., 2021) and oocytes (Pomerantz et al., 2012; Du et al., 2015; Kim et al., 2015; Solc et al., 2015). Moreover, we also analyzed the putative participation of PLK1 in the H2AT120ph- and H3T3ph-dependent recruitment of the inner centromere proteins SGO2 and the CPC proteins Aurora B/C and Borealin, respectively. Our results show that PLK1 is needed for the disassembly of LEs during the diakinesis/metaphase I transition, and the loading of SGO2 and CPC proteins to the inner centromeres during the first meiotic division in mouse spermatocytes.

Results

SYCP3 and HORMAD1 disassemble similarly from LEs during the diakinesis/metaphase I transition

Since one of our main goals was to determine the potential role of PLK1 in the disassembly of the LEs during the diakinesis/metaphase I transition, a meiotic window poorly characterized in males, we first analyzed the accurate and "step-by-step" dynamics of SYCP3 and HORMAD1 during this transition in WT spermatocytes. For this purpose, we made a double immunolabeling of these proteins on squashed spermatocytes. We used the squashing technique because it doesn't disturb nuclear volume and integrity, and chromosome condensation and distribution in prophase I nuclei and dividing spermatocytes are preserved (Page et al., 1998; Parra et al., 2002). In fact, we used this technique previously to describe a concise distribution of SYCP3 (Parra et al., 2004; Parra et al., 2006). Our present results showed, as previously described (Wojtasz et al., 2009), that HORMAD1 and SYCP3 colocalized along the asynapsed AEs in zygotene spermatocytes (Figures 1A,B), and that during the pachytene stage HORMAD1 preferentially labeled the asynapsed AEs of the sex chromosomes (Figure 1C). During the diplotene stage, HORMAD1 and SYCP3 colocalized again along the desynapsed LEs except at their ends, that were only

labeled by SYCP3, in both autosomal and sex bivalents (Figures 1D,E; Supplementary Video S1). Interestingly, in early diakinesis spermatocytes both proteins colocalized not only along the desynapsed LEs, with some of their stretches becoming thinner at this stage, but also at elongated bulges that began to appear along them (Figure 1F; Supplementary Video S1). In diakinesis spermatocytes, SYCP3 also appeared as a homogeneous and intense nuclear background, a hallmark of all diakinesis substages, when observed by the squashing technique. Since about 75–85 focal planes were captured for each diakinesis nucleus, and Z-projections in a single plane obscured the SYCP3 labeling along the LEs, we substracted this background with the ImageJ software for improving clarity (Supplementary Figure S1). Shortly afterwards, in mid diakinesis spermatocytes, HORMAD1 and SYCP3 also colocalized along the thin desynapsed LEs and at numerous round thickenings along them (Figure 1G). The colocalization and distribution patterns of these proteins were likewise present in late diakinesis spermatocytes (Figures 1H,I). However, at this stage, in addition to the round thickenings along the LEs, which began to appear discontinuous, both proteins colocalized at some large round agglomerates that didn't localize at LEs or centromeres, and apparently were in the nucleoplasm (Figures 1H,I). In order to precisely determine the staging of diakinesis spermatocytes and avoid a confusion with prometaphases I and metaphases I, we made a double immunolabeling of SYCP3 and lamin B, to indirectly reveal the integrity of the nuclear envelope. Our results showed the presence of a continuous nuclear envelope even in late diakinesis spermatocytes, and its initial disintegration in prometaphase I spermatocytes (Supplementary Figures S2A–E). A double immunolabeling of SYCP3 and the inner nuclear membrane protein SUN1, that associates to the telomeres, showed that even in late diakinesis spermatocytes the ends of desynapsed LEs appeared attached to the nuclear envelope (Supplementary Figures S2F–H).

In metaphase I autosomal bivalents, HORMAD1 and SYCP3 also colocalized at small patches present along the region of contact between sister-chromatid arms, previously named the interchromatid domain (Suja et al., 1999; Prieto et al., 2001; Parra et al., 2004) (Figures 1J,K; Supplementary Figure S3). The labeling of both proteins was more continuous at the interchromatid domain of the sex bivalent (Figure 1L, Supplementary Figure S3). Moreover, both proteins also appeared highly accumulated at the centromeres (Figures 1J,K; Supplementary Figure S3). A double immunolabeling of SYCP3 or HORMAD1 and the kinetochores, revealed by an ACA serum, showed that they were accumulated at the inner centromere domain below the associated sister kinetochores (Supplementary Figures S4, S5). It is worth noting that at this stage both proteins also appeared at large round agglomerates in the cytoplasm like those observed in the nucleoplasm of late diakinesis nuclei (Supplementary Figures S2E, S3, S5E). We also analyzed the distribution of SYCP3 during the diplotene/metaphase I transition with the spreading technique, that is the procedure commonly used in male mouse meiosis studies. Our results showed that diakinesis spermatocytes were scarce and difficult to find, but the dynamics of SYCP3 was like that observed on squashed spermatocytes at autosomal and sex bivalents (Supplementary Figures S6, S7). However, bulges and thickenings along desynapsed LEs, as well as nucleoplasmic agglomerates in spread diakinesis nuclei were difficult to observe, probably due to the spreading procedure. Altogether, our results indicate that SYCP3 and HORMAD1 are released similarly from the LEs during the diakinesis/metaphase I transition, to then accumulate preferentially at the inner centromeres in metaphase I chromosomes.

SYCP3 and REC8-containing cohesin complexes are differentially released during the diakinesis/metaphase I transition

We also aimed to ascertain the potential role of PLK1 in the partial disassembly of the meiotic cohesin axes during the diakinesis/metaphase I transition. To this end, and although the pattern of localization of the meiotic cohesin subunit REC8 has been previously reported in mouse spermatocytes (Eijpe et al., 2003; Lee et al., 2003; Kudo et al., 2006), we first analyzed in detail its dynamics and compared it with that of SYCP3. For this, we codetected REC8, in *myc* tagged version of REC8 mice (REC8-*myc*) (Kudo et al., 2006) and SYCP3 on squashed spermatocytes. REC8 and SYCP3 axes colocalized in their trajectories from leptotene up to diplotene (Supplementary Figure S8; Figure 2A). By contrast, in early and late diakinesis spermatocytes REC8 appeared as discontinuous lines at the cohesin axes (Figures 2B,C). In prometaphase I and metaphase I spermatocytes, REC8 and SYCP3 decorated similarly the interchromatid domain of autosomal and sex bivalents (Figures 2D–F′). Nevertheless, REC8 didn't colocalized with SYCP3 at the cytoplasmic agglomerates and at the inner centromeres (Figures 2F–H). An accurate analysis of the dynamics of REC8 and SYCP3 on autosomal and sex bivalents corroborated that these proteins had different behaviors during the late prophase I/metaphase I transition (Figures 2I–T). The labeling of REC8 at cohesin axes, which underlie the autosomal LEs and the asynapsed sex chromosomes AEs, became discontinuous from late diplotene/early diakinesis on (Figures 2K–P, R–T). These results indicate that a partial release of REC8-containing cohesin complexes along cohesin axes occurs during these stages. By contrast, the labeling of SYCP3 became discontinuous along autosomal LEs from mid diakinesis on, concomitantly with the appearance of thickenings along them (Figures 2N–P). Altogether, our results point that SYCP3 and REC8 are differentially released from the desynapsed autosomal LEs and cohesin axes, respectively, during diakinesis, and that REC8 doesn't accumulate at the whole inner centromeres in prometaphase I and metaphase I chromosomes (Figures 2G,H; Supplementary Figure S9).

In vitro inhibition of PLK1 kinase activity in organotypic cultures of seminiferous tubules

In order to determine the role of PLK1 in the disassembly of the LEs we inhibited its kinase activity *in vitro* with the pharmacological inhibitor BI 2536 on organotypic cultures of seminiferous tubules, as previously reported (Jordan et al., 2012; Alfaro et al., 2021). In a previous study we tested different concentrations of BI 2536 on cultured seminiferous tubules to

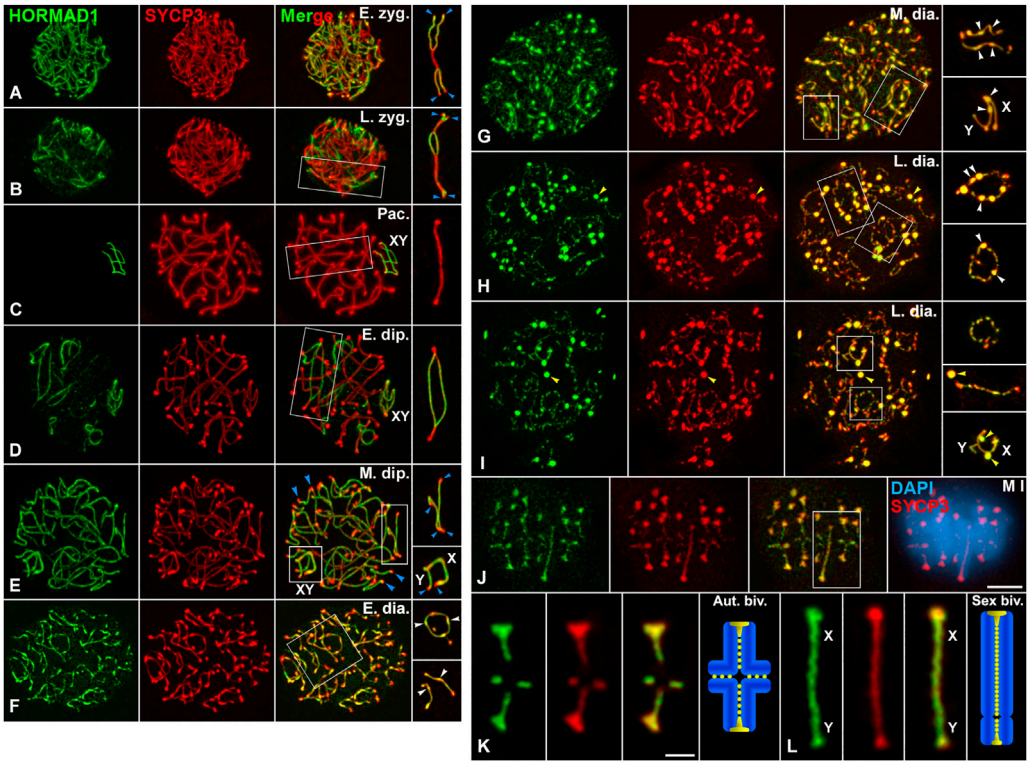

FIGURE 1
HORMAD1 and SYCP3 are similarly released from the LEs during the diakinesis/metaphase I transition. Double immunolabeling of HORMAD1 (green) and SYCP3 (red), and counterstaining of the chromatin with DAPI (blue) on squashed WT spermatocytes. Representative spermatocytes at **(A)** early zygotene (E. zyg.), **(B)** late zygotene (L. zyg.), **(C)** pachytene (Pac.), **(D)** early diplotene (E. dip.), **(E)** mid diplotene (M. dip.), **(F)** early diakinesis (E. dia.), **(G)** mid diakinesis (M. dia.), **(H,I)** late diakinesis (L. dia.), and **(J)** metaphase I (M I) spermatocytes are shown. **(K,L)** Selected metaphase I autosomal (Aut. biv.) **(K)** and sex (Sex biv.) **(L)** bivalents. The sex body (XY) is indicated if recognizable. Selected autosomal and sex (XY) bivalents in squared regions are shown in the right column **(A–J)** and the lower right line **(K,L)**. Blue arrowheads indicate telomere regions with absence of HORMAD1 labeling. White arrowheads indicate elongated bulges and round thickenings of HORMAD1 and SYCP3 along desynapsed autosomal LEs, and asynapsed AEs of the X chromosome. Yellow arrowheads indicate HORMAD1 and SYCP3 agglomerates in the nucleoplasm of late diakinesis spermatocytes **(H,I)**. Scale bars represent 5 μm in **(A–J)**, and 2 μm in **(K,L)**.

inhibit the kinase activity of PLK1 without affecting the viability of cultured spermatocytes (Alfaro et al., 2021). We decided to use a concentration of 100 μM BI 2536 and 8 h of treatment since with these conditions low levels of apoptosis were found as detected with Caspase 3 (Alfaro et al., 2021), and a TUNEL assay on squashed control non-inhibited spermatocytes (3.3% of apoptotic spermatocytes, n = 1,000) and inhibited spermatocytes (5.40% of apoptotic spermatocytes, *n* = 1,000) (Supplementary Figure S10). We confirmed the efficiency of the inhibition in three different individuals by detecting, after double immunolabeling of α-Tubulin and Pericentrin, that 55,36% of metaphases I (*n* = 466) were altered and showed unaligned bivalents, monopolar spindles and unseparated centrosomes, as previously reported (Alfaro et al., 2021; Wellard et al., 2021) (Figures 3A–F). In this regard, this kind of altered metaphases I was never observed in control non-inhibited spermatocytes (*n* = 500). Moreover, we determined that in all altered metaphases I (*n* = 30) the phosphorylation of CENP-U at its threonine 78, a phosphorylation introduced by PLK1 (Kang et al., 2006), wasn't detected at centrosomes or kinetochores (Figures 3G,H).

In all control 8 h cultured diakinesis spermatocytes (*n* = 25), as in WT spermatocytes, thin SYCP3-labelled LEs with thickenings along them were observed (Figure 4A). By contrast, with an 8 h BI 2536 treatment we found that in all diakinesis spermatocytes (*n* = 30) the labeling of SYCP3 was more continuous along desynapsed LEs, no thickenings were detected along them, and nucleoplasmic agglomerates were never observed (Figure 4B; Supplementary Video S2). After an 8 h treatment, altered metaphases I with unaligned bivalents, always (*n* = 235) presented an intense and continuous labeling of SYCP3 at the interchromatid domain of autosomal and sex bivalents (Figures 4C,D; Supplementary Video S3). Concomitantly, we found that in those altered metaphases I SYCP3 wasn't accumulated at the inner centromere of the chromosomes, albeit the close association of sister kinetochores hadn't changed (Figures 4C,D; Supplementary Video S3). Interestingly, no anaphase I or telophase I spermatocytes were detected in 8 h BI 2536-treated seminiferous tubules indicating that altered metaphases I remained arrested and didn't progress in the division process. This contrasted with the situation found in control seminiferous tubules were anaphases I and telophases I were always observed. The characteristic and recognizable SYCP3 labelling displayed by altered monopolar metaphases I, being continuous at the interchromatid domain but absent at the inner centromere (Figures 3B,D, 4C,D), was employed in the rest of our analyses to identify metaphases I altered by the *in vitro* inhibition of PLK1 kinase activity.

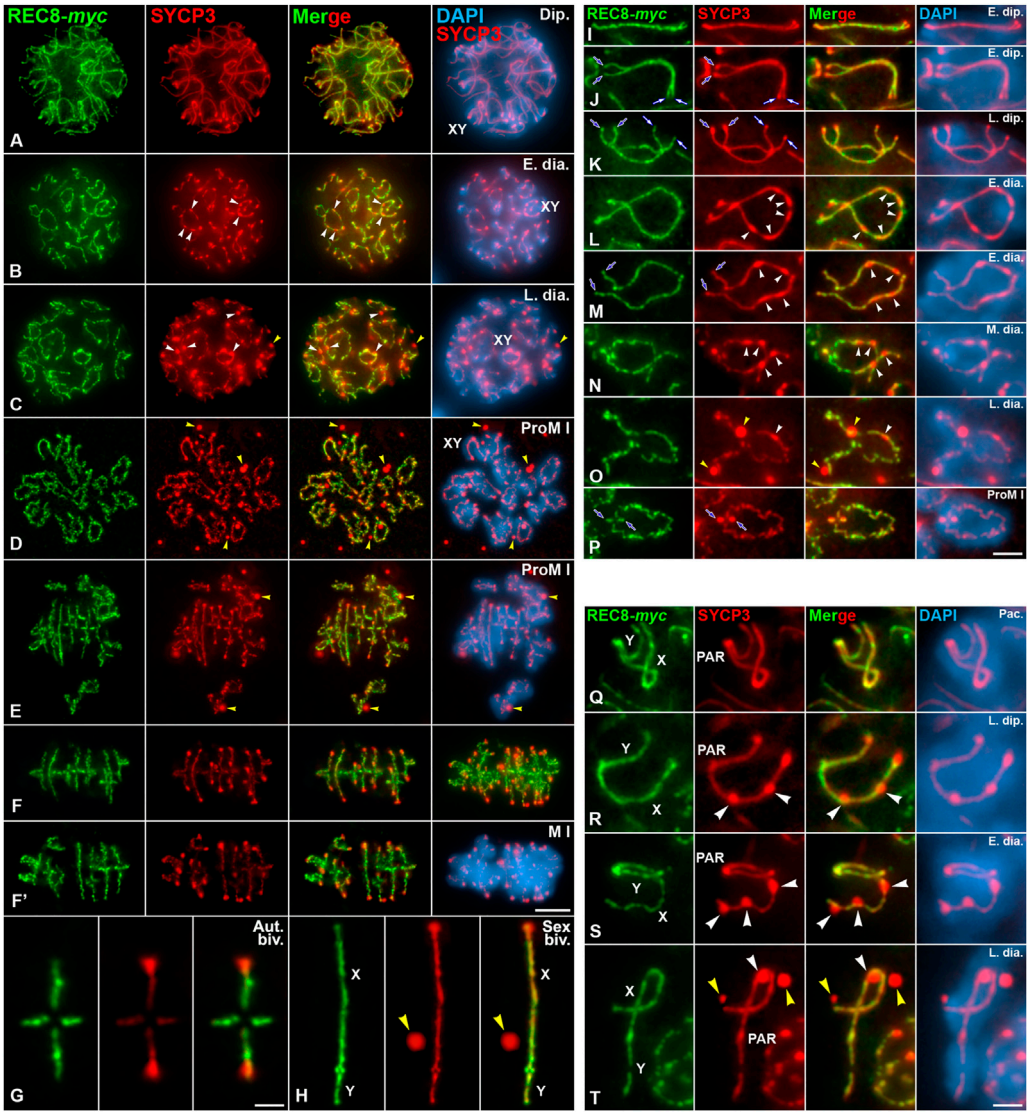

FIGURE 2
Dynamics of REC8 and SYCP3 are distinct during the diakinesis/metaphase I transition. Double immunolabeling of REC8-*myc* (green) and SYCP3 (red), and counterstaining of the chromatin with DAPI (blue) on squashed WT spermatocytes. Representative spermatocytes at **(A)** diplotene (Dip.), **(B)** early diakinesis (E. dia.), **(C)** late diakinesis (L. dia.), **(D,E)** prometaphase I (ProM I), and **(F,F')** metaphase I (M I) are shown. **(G,H)** Selected metaphase I autosomal (Aut. biv.) **(G)** and sex (Sex biv.) **(H)** bivalents. The sex body and the sex bivalents (XY) are indicated in prophase I and prometaphase I spermatocytes. White arrowheads indicate elongated bulges and round SYCP3 thickenings along the desynapsed LEs in early **(B)** and late **(C)** diakinesis. Yellow arrowheads indicate SYCP3 agglomerates in the nucleoplasm of late diakinesis **(C)**, and in the cytoplasm of prometaphase I **(D,E)** and metaphase I **(H)** spermatocytes. Selected autosomal bivalents are shown at **(I,J)** early diplotene (E. dip.), **(K)** late diplotene (L. dip.), **(L,M)** early diakinesis (E. dia.), **(N)** mid diakinesis (M. dia.), **(O)** late diakinesis (L. dia.), and **(P)** prometaphase I (ProM I). Blue and white arrows indicate the proximal centromeric and distal telomere regions, respectively. White arrowheads indicate elongated bulges and round SYCP3 thickenings along the desynapsed LEs in early **(L,M)**, mid **(N)**, and late **(O)** diakinesis. Yellow arrowheads indicate SYCP3 agglomerates in the nucleoplasm of a late diakinesis **(O)** spermatocyte. Selected sex bivalents are shown at **(Q)** pachytene (Pac.), **(R)** late diplotene (L. dip.), **(S)** early diakinesis (E. dia.), and **(T)** late diakinesis (L. dia.). The X and Y chromosomes, and the PAR region, are indicated. White arrowheads indicate round SYCP3 thickenings along the asynapsed AE of the X chromosome in late diplotene **(R)**, and early and late diakinesis **(S,T)**. Yellow arrowheads indicate SYCP3 agglomerates in the nucleoplasm of a late diakinesis spermatocyte **(T)**. Scale bars represent 5 μm in **(A–F')**, 1 μm in **(G,H)**, 2 μm in **(I–P)**, and 1 μm in **(Q–T)**.

PLK1 regulates the dynamics of HORMAD1 and SYCP3 during the diakinesis/metaphase I transition

We analyzed the putative role of PLK1 in the disassembly of desynapsed LEs during the diakinesis/metaphase I transition. First, we double immunolabeled HORMAD1 and SYCP3 on 8 h BI 2536-cultured seminiferous tubules. We found that in all altered diakinesis spermatocytes both proteins colocalized as continuous lines decorating the desynapsed LEs without thickenings along them, a completely different appearance in relation to that found in control spermatocytes (Figures 4E,F; Supplementary Video S4). Similarly, in all altered metaphase I bivalents HORMAD1 and SYCP3 colocalized at their interchromatid domain showing an intense labeling along them (Figures 4G,H; Supplementary Video S5). Interestingly, both proteins were not enriched at the inner

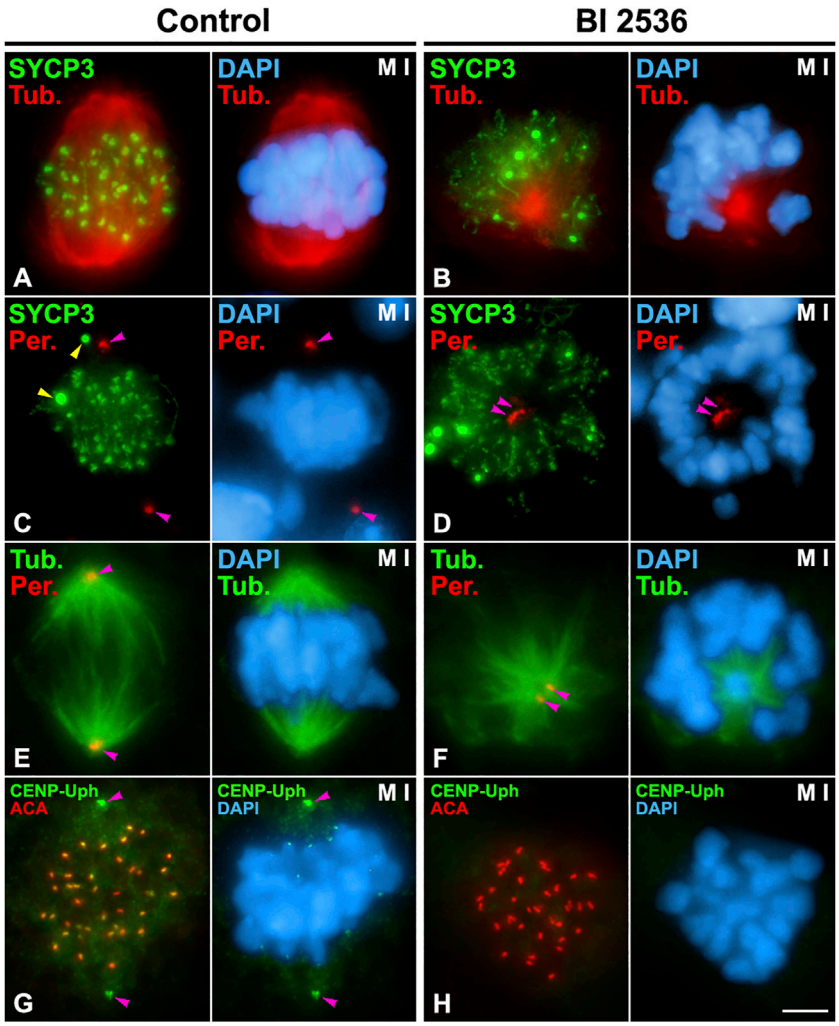

FIGURE 3
Efficiency of BI 2536 on cultured seminiferous tubules. Double immunolabelings of SYCP3 (green) and α-Tubulin (red) **(A,B)**; SYCP3 (green) and Pericentrin (red) **(C,D)**; α-Tubulin (green) and Pericentrin (red) **(E,F)**; or CENP-Uph (phosphorylated at T78) (green) and kinetochores (ACA, red) **(G,H)**, and counterstaining of the chromatin with DAPI (blue) on squashed control **(A,C,E,G)** and 8 h BI 2536-treated **(B,D,F,H)** metaphase I spermatocytes. Yellow arrowheads indicate SYCP3 agglomerates in the cytoplasm of a control metaphase I spermatocyte **(C)**. Pink arrowheads indicate the centrosomes **(C,D,E,F,G)**. Scale bar represents 5 μm.

centromeres, contrasting with the labeling observed in control spermatocytes (Figures 4G,H; Supplementary Video S5). These results indicate that the kinase activity of PLK1 is necessary for the regular disassembly of HORMAD1 and SYCP3 from the desynapsed LEs and their subsequent accumulation at the inner centromeres.

Inhibition of PLK1 has no apparent direct effect on REC8, RAD21, and RAD21L distributions during the diakinesis/metaphase I transition

We next examined the behavior of REC8 on BI 2536-treated altered diakinesis and metaphase I spermatocytes. The double labeling of REC-*myc* and SYCP3 demonstrated that the distribution of REC8 along cohesin axes on altered diakinesis spermatocytes was like that found in control ones (Figures 5A,B; Supplementary Video S6). REC8 appeared as a discontinuous labeling along the cohesin axes (Figures 5A,B). On the other hand, in altered metaphase I bivalents REC8 was found as a series of bright patches along the interchromatid domain of chromosome arms that slightly penetrated the inner centromeres, as in control bivalents (Figures 5C,D; Supplementary Video S7). We also analyzed whether the inhibition of PLK1 could affect the distributions of RAD21-and RAD21L-containing cohesin complexes in metaphase I spermatocytes. It has been reported that RAD21 (Parra et al., 2004; Gómez et al., 2007; Viera et al., 2007) and RAD21L (Herrán et al., 2011; Ishiguro et al., 2011) appear highly accumulated at the inner centromere of WT metaphase I chromosomes, in contrast to REC8 distribution (Suja and Barbero, 2009). Our results showed that RAD21 (Figures 5E,F) and RAD21L (Figures 5G,H) showed the same distribution at the inner centromeres in both control and BI 2536-treated metaphase I chromosomes. Altogether, our results indicate that the kinase activity of PLK1 is needed for the regular disassembly and redistribution of HORMAD1 and SYCP3, but it apparently doesn't affect the distribution of REC8, RAD21 or RAD21L-containing cohesin complexes.

10.3389/fcell.2022.1069946

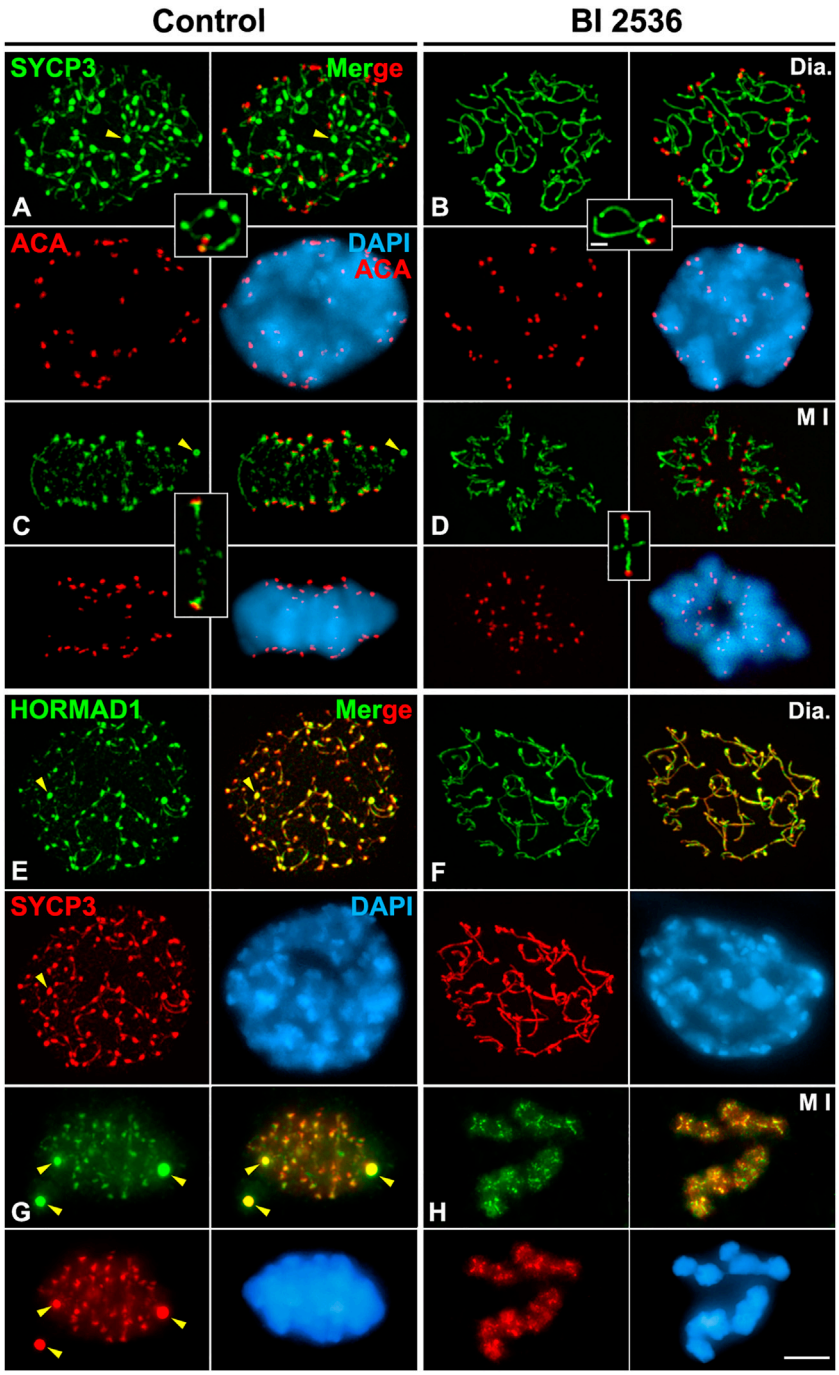

FIGURE 4
PLK1 regulates the release of SYCP3 and HORMAD1 from desynapsed LEs in diakinesis and its accumulation at the inner centromeres in metaphase I spermatocytes. Double immunolabelings of SYCP3 (green) and kinetochores (ACA, red) **(A–D)**, and SYCP3 (red) and HORMAD1 (green) **(E–H)**, and counterstaining of the chromatin with DAPI (blue) on squashed control **(A,C,E,G)** and BI 2536-treated **(B,D,F,H)** spermatocytes. Representative spermatocytes and selected autosomal bivalents at **(A,B,E,F)** diakinesis (Dia.), and **(C,D,G,H)** metaphase I (M I) are shown. Yellow arrowheads indicate SYCP3 agglomerates in the nucleoplasm of diakinesis spermatocytes **(A,E)**, and in the cytoplasm of metaphase I **(C,G)** spermatocytes. Scale bars represent 5 μm in **(A–H)**, and 1 μm in selected diakinesis and metaphase I bivalents in **(A–D)**.

PLK1 regulates H2AT120ph phosphorylation and the loading of shugoshin SGO2 and MCAK to the inner centromere

Since we observed that HORMAD1 and SYCP3 weren't loaded to the inner centromeres in altered metaphase I bivalents, we also tested a potential PLK1 function in the loading of other proteins that normally load to the inner centromere. For this purpose, we studied the two main pathways that regulate the assembly of the inner centromere domain: the pathway Bub1-H2AT120ph-Shugoshin SGO2, and the pathway Haspin-H3T3ph-Aurora B. The phosphorylation of histone H2A at threonine 120 by the

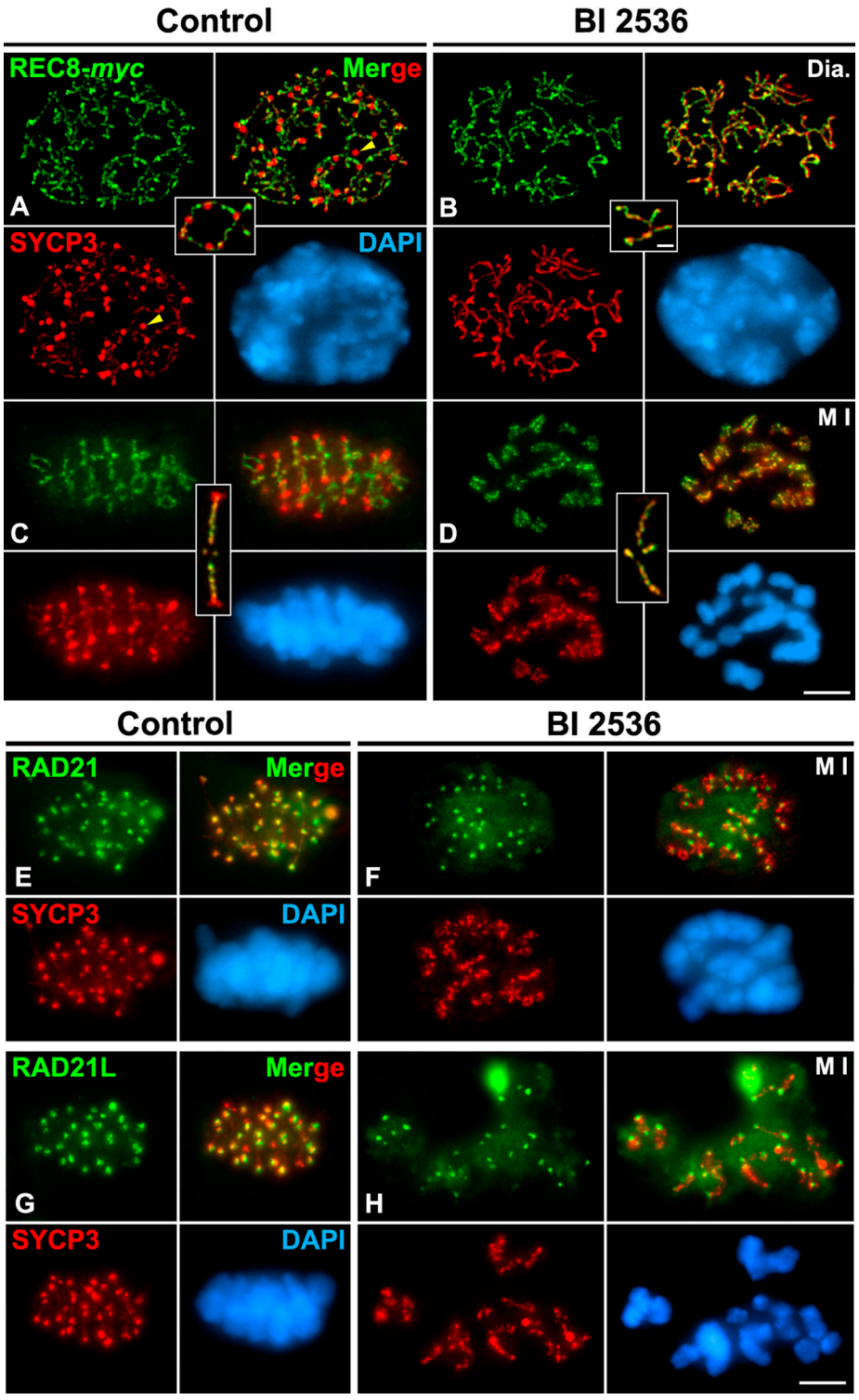

FIGURE 5
Inhibition of PLK1 does not alter the distribution of REC8, RAD21 and RAD21L-contanining cohesin complexes in diakinesis and metaphase I spermatocytes. Double immunolabelings of REC8-*myc* (green in **A–D**), RAD21 (green in **E,F**) or RAD21L (green in **G,H**) and SYCP3 (red), and counterstaining of the chromatin with DAPI (blue) on squashed control **(A,C,E,G)** and BI 2536-treated **(B,D,F,H)** diakinesis (Dia.) **(A,B)** and metaphase I (M I) spermatocytes **(C–G)**. Selected autosomal bivalents in diakinesis **(A,B)** and metaphase I **(C,D)** spermatocytes are shown. Yellow arrowheads indicate agglomerates of SYCP3 in the nucleoplasm of the control diakinesis spermatocyte. Scale bars represent 5 μm in **(A–H)**, and 1 μm in selected diakinesis and metaphase I bivalents in **(A–D)**.

kinase Bub1 is necessary to recruit the cohesin protector protein Shugoshin SGO1 to the centromeres (Jeganathan et al., 2007; Kawashima et al., 2010; Wang and Higgins, 2012; Watanabe, 2012). The histone modification H2AT120ph was not detected at the centromeres in altered diakinesis and metaphase I spermatocytes (Figures 6A–D). Accordingly, we corroborated

10.3389/fcell.2022.1069946

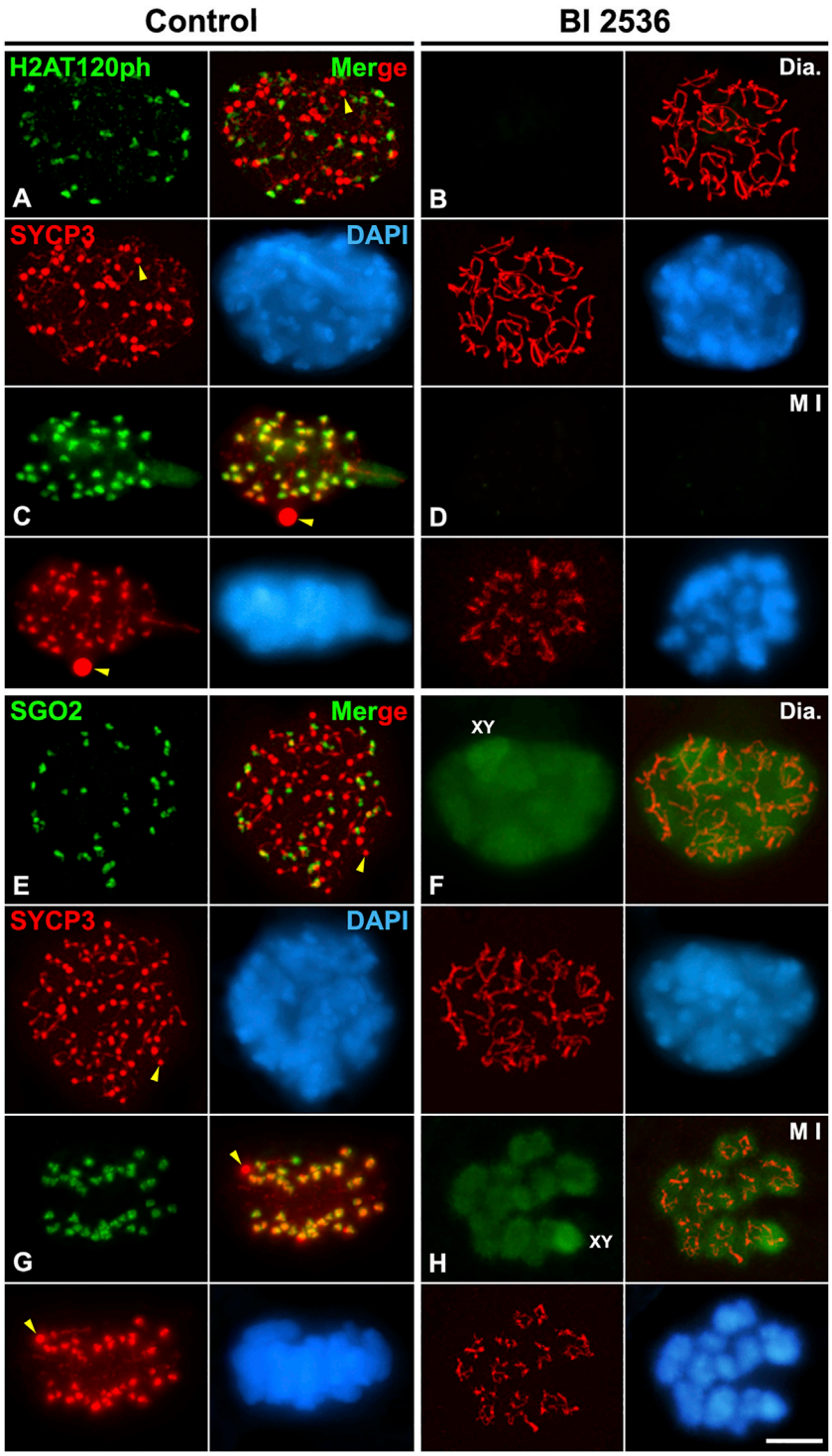

FIGURE 6
PLK1 regulates the H2AT120ph-dependent loading of SGO2 to the inner centromeres. Double immunolabelings of SYCP3 (red) with either H2AT120ph (green in **A–D**), or SGO2 (green in **E–H**), and counterstaining of the chromatin with DAPI (blue) on squashed diakinesis (Dia.) **(A,E)** and metaphase I (M I) **(C,G)** control spermatocytes, and diakinesis **(B,F)** and metaphase I **(D,H)** BI 2536-treated spermatocytes. The sex bivalent (XY) is indicated in **(F,H)**. Yellow arrowheads indicate SYCP3 agglomerates in the nucleoplasm and cytoplasm of control diakinesis and metaphase I spermatocytes, respectively. Scale bar represents 5 µm.

that without the centromere presence of H2AT120ph, SGO2 wasn't detected at the inner centromeres in altered diakinesis and metaphase I spermatocytes. Nevertheless, SGO2 appeared dispersed over the chromatin in diakinesis nuclei and metaphase I bivalents, particularly on the sex bivalent (Figures 6E–H). In addition, since it has been reported that SGO2 recruits the

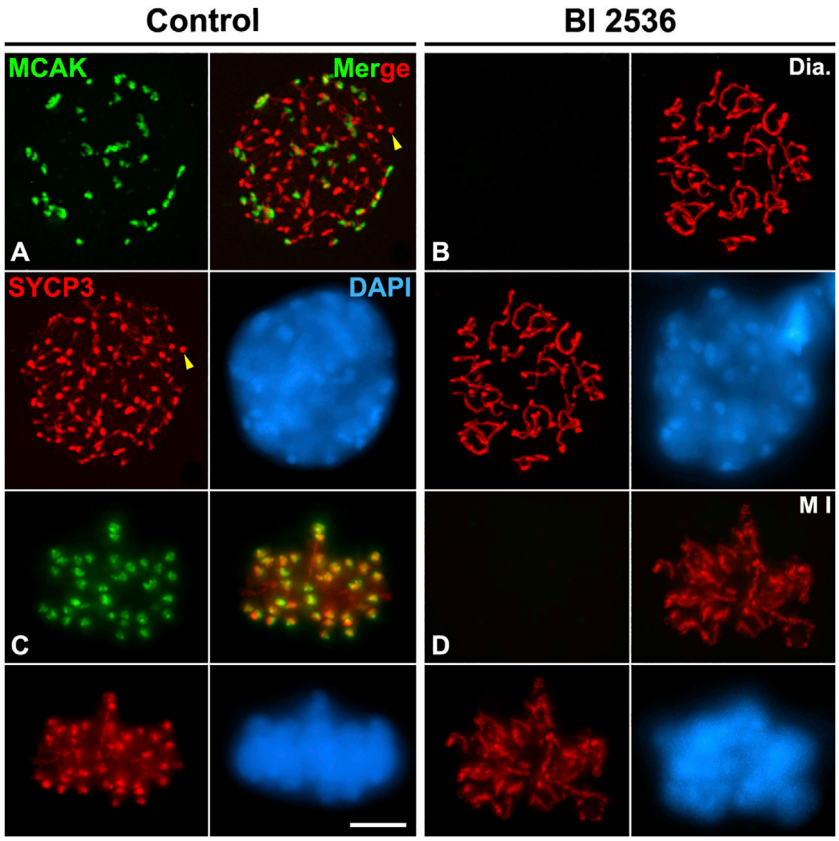

FIGURE 7
PLK1 regulates the SGO2-dependent loading of MCAK to the inner centromeres. Double immunolabeling of MCAK (green) and SYCP3 (red), and counterstaining of the chromatin with DAPI (blue) on squashed diakinesis (Dia.) **(A)** and metaphase I (M I) **(C)** control spermatocytes, and diakinesis **(B)** and metaphase I **(D)** BI 2536-treated spermatocytes. Yellow arrowheads indicate SYCP3 agglomerates in the nucleoplasm of the control diakinesis spermatocyte. Scale bar represents 5 μm.

microtubule depolymerizing kinesin MCAK to the inner centromeres in mouse spermatocytes and oocytes (Llano et al., 2008; Tanno et al., 2010; Rattani et al., 2013), we compared the distribution of MCAK in control and BI 2536-treated diakinesis and metaphase I spermatocytes. We found that MCAK wasn't recruited at the inner centromere in altered diakinesis and metaphase I spermatocytes (Figures 7A–D). Our results thus indicate that PLK1 regulates the phosphorylation of H2AT120ph at the centromeres, and the subsequent loading of SGO2 and MCAK to the inner centromeres in diakinesis and metaphase I bivalents.

PLK1 regulates the phosphorylations of H3T3ph and Aurora B/C, and the loading of Borealin at the inner centromere

We next tested whether PLK1 regulates the Haspin-H3T3ph-dependent loading of Aurora B/C to the inner centromere during the diakinesis/metaphase I transition. We found that H3T3ph was present at chromocenters, which represent clustered centromeres, in control diakinesis spermatocytes, and covering the chromatin in control metaphase I bivalents (Figures 8A,C). However, H3T3ph was undetectable in altered diakinesis or metaphase I spermatocytes (Figures 8B,D). Then, we analyzed the distribution of Aurora B/C at the centromeres by using an antibody that recognizes phosphorylated forms of Aurora A, B, and C, an antibody herein called Aurora Tph. With this antibody we detected a labeling at the centromeres in control diakinesis spermatocytes, as previously reported (Parra et al., 2003; Parra et al., 2009) (Figure 8E). In control metaphase I, we observed a labeling at the centrosomes, which corresponds to the labeling of Aurora A (Willems et al., 2018; Alfaro et al., 2021; Berenguer et al., 2022), and at the inner centromeres, which corresponds to the labeling of the kinases Aurora B/C (Watanabe, 2010; Balboula and Schindler, 2014; Hindriksen et al., 2017; Alfaro et al., 2021; Berenguer et al., 2022) (Figure 8G). In contrast, no labeling was observed in altered diakinesis and metaphase I spermatocytes (Figures 8F,H). We also analyzed whether the loading of the CPC protein Borealin was disturbed after inhibiting PLK1. Our results showed that Borealin appeared at the inner centromeres in diakinesis and metaphase I control spermatocytes (Figures 9A,C), butn't in altered diakinesis and metaphase I spermatocytes (Figures 9B,D). Altogether these results indicate that PLK1 regulates the phosphorylations of H3T3ph and Aurora B/C, and the loading of Borealin at the inner centromeres during male mouse meiosis I.

10.3389/fcell.2022.1069946

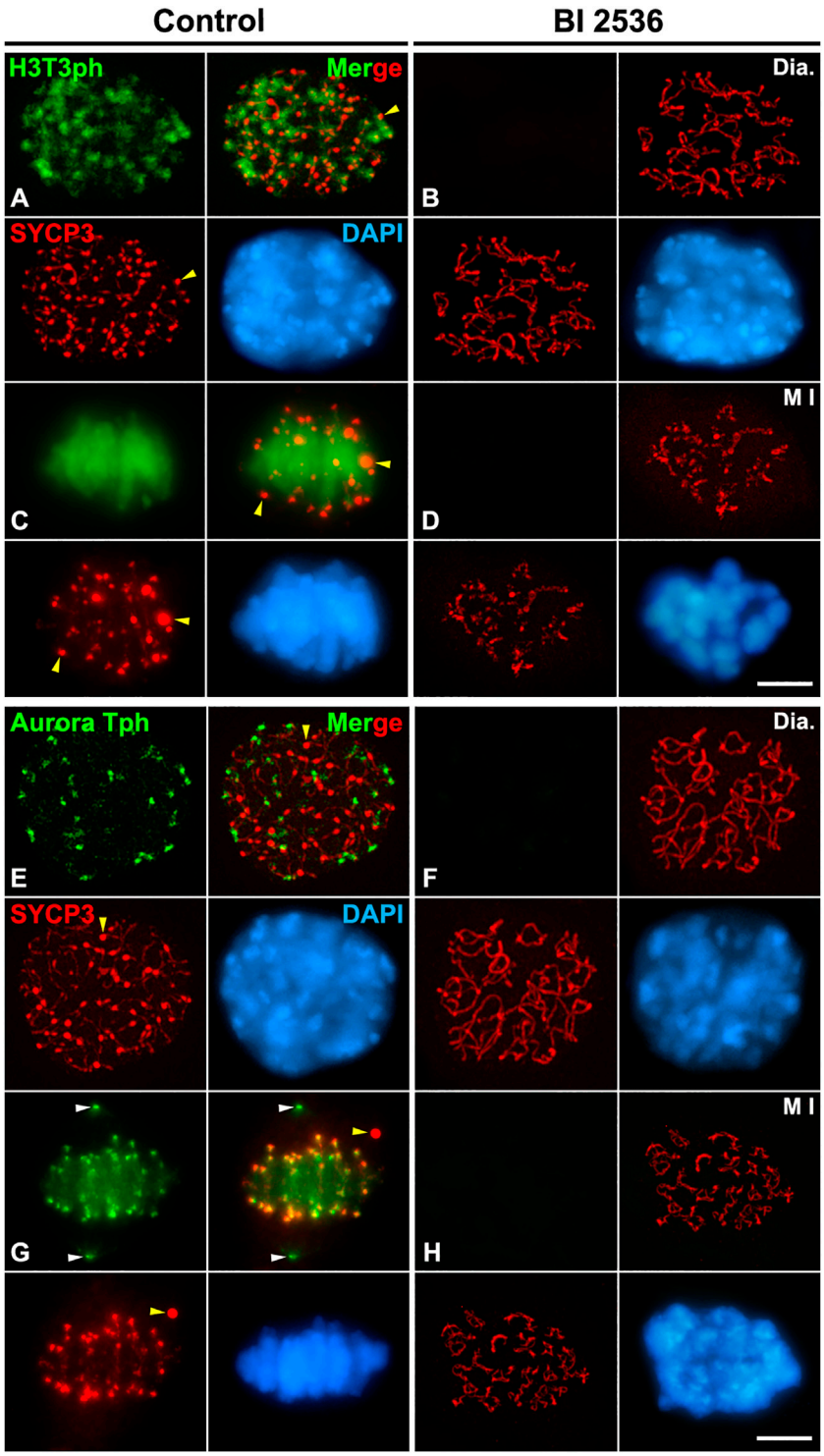

FIGURE 8
PLK1 regulates the H3T3ph-dependent phosphorylation of Aurora B/C at the inner centromeres. Double immunolabelings of SYCP3 (red) with either H3T3ph (green in **A–D**) or AuroraTph (green in **E–H**), and counterstaining of the chromatin with DAPI (blue) on squashed diakinesis (Dia.) **(A,E)** and metaphase I (M I) **(C,G)** control spermatocytes, and diakinesis **(B,F)** and metaphase I **(D,H)** BI 2536-treated spermatocytes. Yellow arrowheads indicate SYCP3 agglomerates in the nucleoplasm and cytoplasm of control diakinesis and metaphase I spermatocytes, respectively. White arrowheads in **(G)** indicate the centrosomes. Scale bar represents 5 μm.

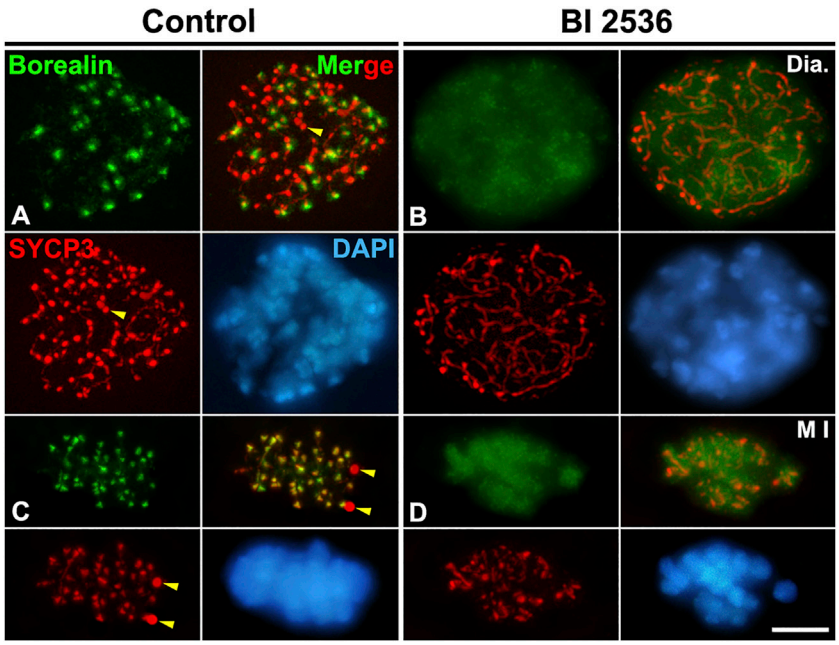

FIGURE 9
PLK1 regulates the loading of Borealin to the inner centromeres. Double immunolabeling of Borealin (green) and SYCP3 (red), and counterstaining of the chromatin with DAPI (blue) on squashed diakinesis (Dia.) **(A)** and metaphase I (M I) **(C)** control spermatocytes, and diakinesis **(B)** and metaphase I **(D)** BI 2536-treated spermatocytes. Yellow arrowheads indicate SYCP3 agglomerates in the nucleoplasm and cytoplasm of the control diakinesis and metaphase I spermatocytes, respectively. Scale bar represents 5 μm.

Phosphorylated forms of PLK1 localize at LEs and inner centromeres

Our results indicated that PLK1 regulated the disassembly of HORMAD1 and SYCP3 from the LEs, the phosphorylations of H2AT120ph, H3T3ph and Aurora B/C, and the loading of SGO2, MCAK, and Borealin at the inner centromeres during the diakinesis/metaphase I transition. In order to study whether PLK1 could be present at SCs and inner centromeres, we studied the distribution of PLK1 phosphorylated at serine 137 (PLK1S137ph) and at threonine 210 (PLK1T210ph) in spread spermatocytes. We found that PLK1S137ph appeared at the centrosomes and on the AEs/LEs from leptotene up to the diakinesis stage (Supplementary Figures S11A–J). Interestingly, PLK1S137ph colocalized with SYCP3 at the bulges and thickenings present along the asynapsed AEs of the sex chromosomes in late diplotene spermatocytes (Supplementary Figures S11G–I), and along the desynapsed LEs in diakinesis spermatocytes (Supplementary Figure S11J). On the other hand, PLK1S137ph appeared accumulated at the inner centromeres of prometaphase I and metaphase I bivalents (Supplementary Figures S11K,L). Differentially, PLK1T210ph didn't appear at the centrosomes, and was only detected at the centromeres from diplotene stage on, and was observed enriched at the inner centromere domain, colocalizing with SYCP3, in diakinesis, prometaphase I, and metaphase I spermatocytes (Supplementary Figure S12). These results indicate that different posttranslational modifications of PLK1 are at the right place to presumably mediate either in the disassembly of LEs and/or the assembly of the inner centromere in mouse spermatocytes.

Discussion

Dynamics of LEs disassembly during the diakinesis/metaphase I transition

In previous reports a concise description of the distribution of SYCP3 and HORMAD1 in diakinesis and metaphase I spermatocytes was presented (Parra et al., 2004; Parra et al., 2006; Wojtasz et al., 2009). In this sense, SYCP3 disassembles from the LEs during late prophase I stages and then accumulate at the centromeres in metaphase I spermatocytes (Cahoon and Hawley, 2016; Gao and Colaiácovo, 2018; Láscarez-Lagunas et al., 2022). However, a precise description of this dynamic hasn't been reported. Here we have analyzed, for the first time, the accurate behavior of SYCP3 and HORMAD1 during the diakinesis/metaphase I transition in WT mouse spermatocytes. Our results show that both proteins have the same pattern of distribution and behavior during this transition. Thus, in early diakinesis spermatocytes the HORMAD1-and SYCP3-labeled desynapsed LEs become thinner, and frequent bulges along them appear concomitantly with an increase of the nuclear background. In mid diakinesis spermatocytes, round thickenings along the LEs are observed, while in late diakinesis spermatocytes LEs become discontinuous and nucleoplasmic agglomerates appear. Remnants of HORMAD1 and SYCP3 are detected at the interchromatid domain, and are preferentially accumulated at the inner centromere domain, of prometaphase I and metaphase I bivalents. This observed sequence of events is summarized in Figure 10. Considering these data, we propose a working model for the disassembly of the LEs during the diakinesis/metaphase I transition. SYCP3 and HORMAD1, which interact between them

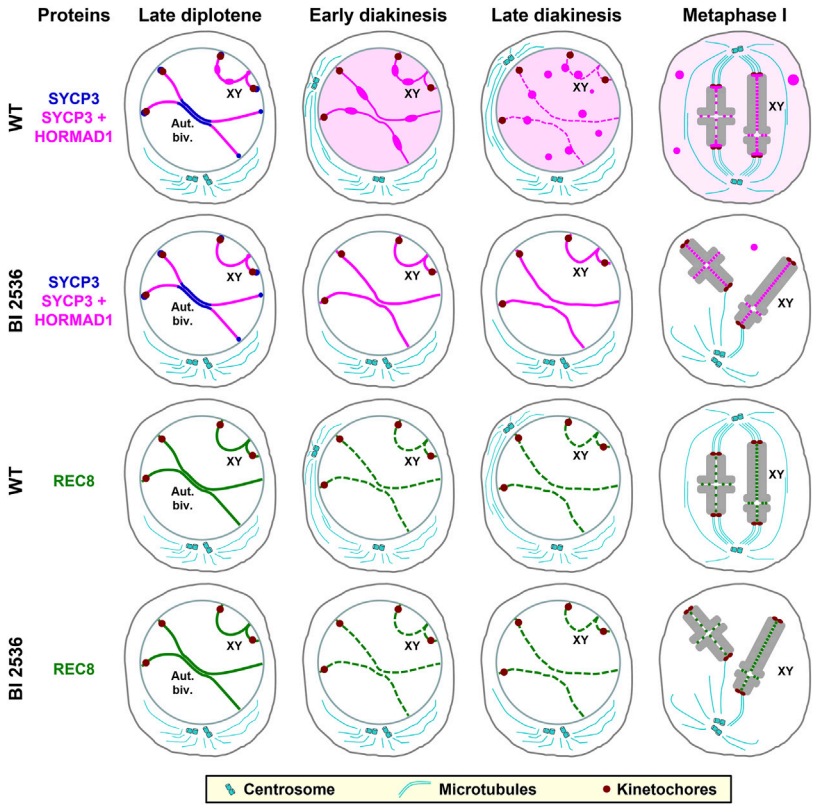

FIGURE 10
Schematic representation of the distribution of SYCP3, HORMAD1 and REC8 in WT and BI 2536-treated late diplotene, early and late diakinesis, and metaphase I spermatocytes. For clarity, a single autosomal bivalent (Aut. Biv.) and the sex bivalent (XY) are represented. SYCP3 is indicated in blue, the merge of SYCP3 and HORMAD1 in pink, and REC8 in green. Bulges and round thickenings along desynapsed LEs, as well as nucleoplasmic or cytoplasmic agglomerates of SYCP3 and HORMAD1, are indicated. A nucleoplasmic and cytoplasmic background of SYCP3 and HORMAD1 are indicated as a pale pink background in WT late diakinesis and metaphase I spermatocytes. Kinetochore regions are shown in brown, and centrioles and microtubules in light blue. The condensed chromatin of the autosomal bivalent, with a single interstitial chiasma, and of the sex bivalent (XY), with a distal chiasma, is shown in light grey in metaphase I spermatocytes.

and form complexes (Fukuda et al., 2010; Fujiwara et al., 2020), could begin to be released from desynapsed autosomal LEs at early diakinesis. During this stage, one population of these complexes could accumulate at bulges along LEs, while another population could diffuse in the nucleoplasm. With the ongoing release of these proteins in mid and late diakinesis, there could be a concentration of these proteins on previous bulges to appear as larger round thickenings along the LEs, that in turn become discontinuous. We hypothesize that some SYCP3/HORMAD1 complexes present at those thickenings could diffuse to aggregate as nucleoplasmic agglomerates. Alternatively, among other possibilities, the thickenings could detach as agglomerates from LEs to directly lie in the nucleoplasm. The formation of agglomerates in the nucleoplasm is supported by the fact that SYCP3 self-assembles in the nucleoplasm and cytoplasm when expressed in cultured somatic cells (Yuan et al., 1998). However, a population of SYCP3 and HORMAD1 still persists as small patches at the interchromatid domain in prometaphase I and metaphase I bivalents. Another interesting question is how those proteins accumulate at the inner centromere in prometaphase I bivalents. In this regard, newly synthesized proteins or non-degraded proteins that previously diffused from the LEs to the nucleoplasm or were present at nucleoplasmic agglomerates could be recruited to the inner centromeres. Obviously, more reserch is needed to evaluate these or other possibilities. We consider that high-resolution observations on living spermatocytes expressing SYCP3 and/or HORMAD1 tagged with GFP during the diakinesis/metaphase I transition would allow a better definition of the observed steps of LEs disassembly. In addition, FRAP experiments would offer outstanding information on the rate of synthesis and behavior of these proteins during this transition.

Concerning the dynamics of REC8-containing cohesin axes during the diakinesis/metaphase I transition, our results point that these cohesin complexes would initiate their release from desynapsed LEs earlier that SYCP3 and HORMAD1 do. In this sense, the partial release of those cohesin complexes could lead to the discontinuity of cohesin axes from early diakinesis on. Interestingly, released cohesin complexes weren't cytologically detected in the nuclear background. Thus, we suggest that the released cohesin complexes, probably not cleaved by Separase, could be degraded as it seems to occur during the mitotic "prophase pathway" (Giménez-Abián et al., 2004; Hauf et al., 2005). Other REC8-containing cohesin complexes would be protected against their release from chromosome arms during diakinesis to persist at the interchromatid domain of metaphase I bivalents to ensure sister-chromatid arm and centromere cohesion until anaphase I segregation. In summary, REC8-containing cohesin complexes, and

SYCP3 and HORMAD1 are differentially released from cohesin axes and desynapsed LEs during the diakinesis/metaphase I transition, probably by still non-characterized and different molecular mechanisms.

PLK1 regulates the disassembly of LEs during the diakinesis/metaphase I transition

Previous experiments on *in vitro* cultures of mouse spermatocytes with the PLK1 inhibitor GW843682X, and posterior induction to undergo metaphase I with the addition of okadaic acid, promoted the retention of SYCP3 along the arms of metaphase I bivalents (Ishiguro et al., 2011). Accordingly, these authors proposed that PLK1 might promote the release of SYCP3 during late prophase I stages. In addition, it has been recently observed that in *Plk1* cKO male mice the disassembly of the LEs is aberrant (Wellard et al., 2022). In this sense, the LE proteins SYCP3 and SYCP2 were retained at the interchromatid domain of metaphase I bivalents, and these proteins were absent at the centromeres. These results led the authors to propose that PLK1 is required for LEs disassembly (Wellard et al., 2022). We have found that after the *in vitro* inhibition of the kinase activity of PLK1 with BI 2536 altered diakinesis spermatocytes show a continuous labeling of SYCP3 and HORMAD1 along the desynapsed LEs. Remarkably, in these spermatocytes neither thickenings along them nor nucleoplasmic agglomerates are found. Moreover, altered metaphases I, that probably enter the first meiotic division as altered diakinesis during the duration of the BI 2536 treatment, show a continuous labeling of these proteins at the interchromatid domain of bivalents, and don't accumulate at their inner centromeres. These data suggest that the SYCP3 and HORMAD1 proteins that normally accumulate at the inner centromeres in prometaphase I bivalents derive from the population of proteins that are previously released from the LEs throughout the diakinesis stage. Altogether, our results strongly support previous results (Ishiguro et al., 2011; Wellard et al., 2022) indicating that PLK1 regulates the disassembly of the LEs during the diakinesis/metaphase I transition by enabling the release not only of SYCP3, but also of HORMAD1. Since during budding yeast meiosis Cdc5/PLK1 also controls this disassembly (Sourirajan and Lichten, 2008; Argunhan et al., 2017), we suggest that PLK1 could be considered as a master kinase that controls this meiotic process.

It is worth noting that we have found that PLK1 phosphorylated at serine S137 (PLK1S137ph) is present along the AEs/LEs during all prophase I stages, and at bulges and thickenings along desynapsed LEs in late diplotene and diakinesis spermatocytes. The phosphorylation of PLK1S137ph is necessary to activate PLK1 to phosphorylate some targets in the S interphase stage (Jang et al., 2002), and has been detected in mouse oocytes (Du et al., 2015; Feitosa et al., 2018) and spermatocytes (Wellard et al., 2022). Our results suggest that this active phosphorylated form of PLK1 is at the right place to mediate the phosphorylation of the LE proteins leading to their release.

Our results show that the distribution of REC8 at desynapsed cohesin axes during diakinesis, and at the interchromatid domain of metaphase I bivalents, are similar in altered, control and WT spermatocytes. These results apparently suggest that PLK1 would not be required for the partial release of REC8-complexes during the diakinesis/metaphase I transition. However, it must be considered that desynapsed REC8 axes appeared discontinuous at early diakinesis. Thus, with our experimental conditions, i.e., an 8 h BI 2536 treatment, we cannot disregard the possibility that PLK1, by promoting the phosphorylation of REC8 or other subunits of those complexes during late diplotene, could promote the partial release of REC8 from cohesin axes. This early release of REC8 cohesin complexes during late diplotene/early diakinesis could allow the posterior PLK1-dependent release of SYCP3 and HORMAD1 from LEs, as previously suggested (Ishiguro et al., 2011). It has been proposed that the cohesin regulator WAPL could allow the dissociation of cohesin complexes from the cohesin axes in prophase I mouse spermatocytes and oocytes (Brieño-Enríquez et al., 2016; Silva et al., 2020). On the other hand, it has been reported that during the so-called "prophase I-like pathway" in budding yeast meiosis there is a cleavage-independent release of Rec8 cohesin complexes from the SC during late prophase I promoted by Cdc5/PLK1, Rad61/Wpl1/WAPL, and the Dbf4-dependent Cdc7 kinase (DDK) in a collaborative way (Challa et al., 2019a; Challa et al., 2019b).

On the other hand, our results on the distribution of the cohesin subunits RAD21 and RAD21L in control and BI 2536-altered metaphases I showed that their distributions at the centromeres weren't affected. These results suggest that their accumulation at the inner centromeres in metaphase I spermatocytes, as previously reported (Parra et al., 2004; Gómez et al., 2007; Viera et al., 2007; Herrán et al., 2011; Ishiguro et al., 2011), aren't dependent of PLK1.

PLK1 regulates the loading of inner centromere proteins

There are two main pathways that regulate the assembly of the inner centromere domain: the pathway Bub1-H2AT120ph-Shugoshin SGO2, and the pathway Haspin-H3T3ph-Aurora B (Watanabe, 2010; Yamagishi et al., 2010; Hadders et al., 2020; Schmitz et al., 2020). In the first pathway, the kinase Bub1 phosphorylates histone H2A at threonine 120, which then recruits the centromere cohesin protector protein Shugoshin SGO1/2 in somatic cells, and mouse oocytes and spermatocytes (Jeganathan et al., 2007; Kawashima et al., 2010; Ricke et al., 2012; Wang and Higgins, 2012; Watanabe, 2012; El Yakoubi et al., 2017). In the second pathway, the kinase Haspin phosphorylates histone H3 at threonine 3 (H3T3ph) (Dai et al., 2005), which then recruits the kinase Aurora B to the inner centromere (Kelly et al., 2010; Wang et al., 2010; Yamagishi et al., 2010; Wang et al., 2011; De Antoni et al., 2012; Wang et al., 2012). Our results indicate that in the absence of PLK1 kinase activity H2AT120ph isn't phosphorylated, and SGO2 isn't loaded to the centromeres in altered diakinesis and metaphase I spermatocytes. Similarly, MCAK, that is recruited to WT meiotic centromeres in a SGO2-dependent manner (Gómez et al., 2007; Llano et al., 2008; Parra et al., 2009), isn't loaded to the centromeres. The presence of a monopolar spindle together with the absence of the microtubule depolymerizing kinesin MCAK at the inner centromeres explains why bivalents aren't able to align properly at the equatorial plate in altered metaphases I. Our data suggest that PLK1 is a key upstream regulator of the Bub1-H2AT120ph-SGO2 pathway during male mouse meiosis. This agrees with the fact that PLK1 associates with (Singh et al., 2021) and phosphorylates Bub1 (Qi et al., 2006; Grosstessner-Hain et al., 2011). All these findings support our suggestion that PLK1 could be directly phosphorylating and activating the kinase activity of Bub1, that in turn regulates the H2AT120ph phosphorylation and H2AT120ph-dependent loading of SGO2 and MCAK.

On the other hand, we have found that the inhibition of PLK1 doesn't allow the phosphorylations of H3T3ph and Aurora B/C, and the loading of the CPC protein Borealin, at the inner centromere of altered diakinesis and metaphase I spermatocytes. It has been proposed that in mammalian somatic cells PLK1 phosphorylates and activates the kinase Haspin (Ghenoiu et al., 2013; Zhou et al., 2014). Thus, it is expected that by inhibiting PLK1, the kinase Haspin isn't activated, and consequently, H3T3ph isn't phosphorylated at the centromeres as we have found in spermatocytes. Our present results complement those we have recently reported after the chemical inhibition of the kinase Haspin on cultured seminiferous tubules, as well as in Haspin$^{-/-}$ KO spermatocytes, indicating that in these situations H3T3ph isn't phosphorylated at the inner centromere of metaphase I chromosomes (Berenguer et al., 2022). It is interesting to mention that we have found that PLK1 phosphorylated at serine S137 and T210 (PLK1S137ph and PLK1T210ph), both activated forms of PLK1 (Jang et al., 2002), are present at the inner centromere of WT metaphase I bivalents (Alfaro et al., 2021). Therefore, both PLK1 modifications are at the right place to regulate the phosphorylations of H2AT120ph, H3T3ph, and Aurora B/C, and the loading of SGO2, MCAK, and Borealin to the inner centromere of metaphase I bivalents.

In summary, this work presents data that support that PLK1 is a master regulator of male mouse meiosis progression *via* its involvement in the disassembly of LEs, and the assembly of the inner centromere domain.

Materials and methods

Mice

Seminiferous tubules from adult C57BL/6 wild-type (WT) male mice and REC8-*myc* transgenic male mice (Kudo et al., 2006) were used for this study.

Organotypic culture of seminiferous tubules and inhibition of PLK1

The culture of seminiferous tubules from WT and REC8-*myc* mice was performed as previously described (Sato et al., 2011). Testes were removed, detunicated and fragments of seminiferous tubules were cultured for 2 h in agarose gel half-soaked in Minimum Essential Medium α culture medium (MEM α) (Gibco, A10490-01) supplemented with Knock Out Serum Replacement (KSR) (Gibco, 10828-010) and antibiotics (Penicillin/Streptomycin; Biochrom AG, A2213) at 34°C in an atmosphere with 5% CO_2. The fragments of seminiferous tubules weren't immersed in the medium, but rather deposited over the agarose gel absorbing the media from below, therefore requiring high concentrations when developing drug treatments (Alfaro et al., 2021). To inhibit PLK1, 100 μM BI 2536 (Selleck Chemicals, S1109) diluted in 10% DMSO was added to the culture medium, and seminiferous tubules were recovered after 8 h of treatment as we previously published (Alfaro et al., 2021). Controls were done with seminiferous tubules cultured with culture medium with added 10% DMSO.

Indirect immunofluorescence

Seminiferous tubules were processed for squashing or chromatin spreading techniques as follows. For the squashing technique, portions of seminiferous tubules were collected from the culture and processed for indirect immunofluorescence as previously described (Page et al., 1998; Parra et al., 2002). Briefly, seminiferous tubules were fixed in freshly prepared 2% formaldehyde in PBS (137 mM NaCl, 2.7 mM KCl, 10.1 mM Na_2HPO_4, 1.7 mM KH_2PO_4, pH 7.4) containing .05% Triton X-100 (Sigma). After 10 min, several seminiferous tubules fragments were placed on a slide coated with 1 mg/ml poly-L-lysine (Sigma) with a small drop of fixative, and gently minced with tweezers. The tubules were then squashed, and the coverslip removed after freezing in liquid nitrogen. For the spreading technique, portions of seminiferous tubules were processed by the drying-down technique as previously described (Peters et al., 1997). For indirect immunofluorescence, slides of squashed or spreaded spermatocytes were rinsed three times for 5 min in PBS and incubated overnight at 4°C with primary antibodies diluted in PBS. Then, the slides were rinsed three times for 5 min in PBS and incubated for 1 h at room temperature with secondary antibodies. After other three rinsing steps, the slides were counterstained with 10 μg/ml 4′,6-diamidino-2-phenylindole (DAPI) for 3 min, rinsed in PBS for 1 min, mounted with Vectashield (Vector Laboratories) and sealed with nail polish.

Antibodies

For indirect immunofluorescence the following primary antibodies were used at the indicated dilution in PBS: rabbit polyclonal anti-hSYCP3 (Abcam, ab-15092) at 1:100; mouse monoclonal anti-mSYCP3 (Santa Cruz, sc-74569) at 1:50; purified human anti-centromere autoantibody (ACA serum) revealing kinetochores (Antibodies Incorporated, 435-2RG-7) at 1:20; guinea-pig polyclonal anti-mHORMAD1 AB146, a gift of Attila Tóth (Wojtasz et al., 2009), at 1:50; rat monoclonal anti-α-Tubulin (Abcam, ab-6160) at 1:100; rabbit polyclonal anti-Pericentrin (Abcam, ab-4448) at 1:10; rabbit polyclonal anti-CENP-U phosphorylated at T78ph (Abcam, ab-34911) at 1:10; mouse monoclonal antibody against *myc* tag (GeneTex, GTX628259) at 1: 20; rabbit polyclonal anti-H2AT120ph (Active Motif, 39,391) at 1:30; rabbit polyclonal anti-mSGO2 K1059, a gift of José Luis Barbero (Gómez et al., 2007) at 1:20; rabbit polyclonal anti-H3T3ph (Abcam, ab-17352) at 1:800; mouse monoclonal anti-hAurora A (T288ph)/ Aurora B (T232ph)/Aurora C (T198ph), that we called Aurora Tph (Cell Signaling, 2914S) at 1:10; goat polyclonal against Lamin B (Santa Cruz, sc-6216) at 1:50; guinea-pig polyclonal anti-mSUN1, a gift of Manfred Alsheimer and Ricardo Benavente (Adelfalk et al., 2009) at 1: 30, rabbit polyclonal anti-mREC8, a gift of Jibak Lee (Lee et al., 2003) at 1:10; rabbit polyclonal anti-RAD21L, a gift of Alberto Pendas (Herrán et al., 2011) at 1:10; rabbit polyclonal anti-RAD21, a gift of José Luis Barbero (Parra et al., 2004) at 1:10; sheep polyclonal anti-hMCAK, a gift of Linda Wordeman (Andrews et al., 2004) at 1:40; rabbit polyclonal anti-Borealin serum 1,647, a gift of William Earnshaw at 1:50; rabbit polyclonal anti-PLK1S137ph (Merk, 07-1348) at 1:10 (Du et al., 2015); and mouse monoclonal anti-PLK1T210ph (Abcam, ab-39068) at 1:10 (Du et al., 2015).

The secondary antibodies used were as follows: donkey anti-mouse conjugated with Alexa 488 (Molecular Probes, A-21202) or Alexa 594 (Molecular Probes, A-21203), donkey anti-rabbit conjugated with Alexa 488 (Molecular Probes, A-21206), goat anti-rabbit conjugated with Alexa 594 (Molecular Probes, A-11012), goat anti-human conjugated with Alexa 594 (Molecular Probes, A-11014), goat anti-guinea pig conjugated with Alexa 488 (Molecular Probes, A-11073), and donkey anti-sheep conjugated with FITC (Jackson ImmunoResearch, 713-095-147). All of them were employed at a 1:100 dilution in PBS.

TUNEL assay

The DNA fragmentation-associated apoptosis of control and BI 2536-treated spermatocytes was detected by the TdT-mediated dUTP-fluorescein nick end labeling (TUNEL) assay by using a kit (Roche, 11684795910) according to manufacturer's protocol. Nuclei were counterstained for 3 min with 10 µg/ml DAPI. Tests were developed on squashed 8 h control and 8 h BI 2536-treated seminiferous tubules. The percentage of apoptotic cells was calculated counting one thousand spermatocytes per condition.

Image capture and processing

Immunofluorescence images were collected using an Olympus BX61 microscope equipped with epifluorescence optics, a motorized Z-drive and an Olympus digital camera (DP70 or DP71) controlled by analySIS software (Soft Imaging System). Figures presenting data obtained in squashed spermatocytes were obtained as image stacks and were processed to obtain complete Z-projections from 60–80 focal planes throughout the complete spermatocyte volume. Stacks were analyzed and processed, and in some cases three dimensional (3D) recontructions were made using the public domain software ImageJ (National Institutes of Health, United States; http://rsb.info.nih.gov/ij) for the generation of the supplementary videos. Final images were processed with Adobe Photoshop CS5 software.

Data availability statement

The raw data supporting the conclusion of this article will be made available by the authors, without undue reservation.

Ethics statement

The animal study was reviewed and approved by the UAM Animal Experimentation Ethics Committee (CEI 115-2277).

Author contributions

RG and JS conceived, supervised and designed the project. JS, AV, MP, AT, and RG obtained funding. TM-M, RG, IB, MP, AV, AG-G, and JS performed the experiments and analyzed the data. JS and RG wrote the manuscript. All authors reviewed and approved the final version of the manuscript.

Funding

This work was supported by funding from Ministerio de Ciencia e Innovación (Spain) grant PID2020-117491GB-I00 (to JS). TM-M was supported by grant "Ayuda para Inicio de Estudios en Programas de Posgrado" from Universidad Autónoma de Madrid (Spain). IB was supported by an FPI predoctoral fellowship from Ministerio de Economía y Competitividad (Spain). AG-G was supported by grant "Ayuda para el Fomento de la Investigación en Estudios de Máster," and "Ayudas PostMáster from the Department of Biology at Universidad Autónoma de Madrid.

Acknowledgments

We express our sincere thanks to Kim Nasmyth for providing REC8-*myc* transgenic male mice, and to Jibak Lee, José Luis Barbero, Alberto Pendás, William Earnshaw, Manfred Alsheimer, Ricardo Benavente, and Linda Wordeman for providing antibodies. We also thank Lorena Barreras for her technical assistance.

Conflict of interest

The authors declare that the research was conducted in the absence of any commercial or financial relationships that could be construed as a potential conflict of interest.

Publisher's note

All claims expressed in this article are solely those of the authors and do not necessarily represent those of their affiliated organizations, or those of the publisher, the editors and the reviewers. Any product that may be evaluated in this article, or claim that may be made by its manufacturer, is not guaranteed or endorsed by the publisher.

Supplementary material

The Supplementary Material for this article can be found online at: https://www.frontiersin.org/articles/10.3389/fcell.2022.1069946/full#supplementary-material

SUPPLEMENTARY FIGURE S1
Distribution of SYCP3 (green) and kinetochores (ACA, red) in diplotene (Dip.) , early diakinesis (E. dia.) **(C,D)**, and late diakinesis **(E,F)** WT squashed spermatocytes. Spermatocytes with unsubstracted **(A,C,E)** and substracted **(B,D,F)** SYCP3 nuclear background are shown. Numbers in each panel indicate the Z-projection of the indicated focal planes. White arrowheads indicate bulges and round SYCP3 thickenings along the desynapsed LEs, and yellow arrowheads indicate agglomerates at the nucleoplasm. Scale bar represents 2 µm.

SUPPLEMENTARY FIGURE S2
The breakdown of the nuclear envelope occurs in prometaphase I spermatocytes, and telomeres maintain their attachment to the nuclear envelope in diakinesis spermatocytes. Double immunolabelings of SYCP3 (red) with either Lamin B (green) or SUN1 (green), and counterstaining of the chromatin with DAPI (blue) on diplotene (Dip.) , early diakinesis (E. dia.) **(G)**, mid diakinesis (M. dia.) **(B)**, late diakinesis (L. dia.) **(C,H)**, prometaphase I (ProM I) **(D)** and metaphase I (M I) **(E)** WT squashed spermatocytes. Numbers in panels **(F–H)** indicate the Z-projection of different focal planes at top, equator and bottom regions of the spermatocytes and

the complete projection. White arrowheads indicate bulges of SYCP3 along desynapsed LEs, whereas yellow arrowheads indicate SYCP3 agglomerates in the nucleoplasm or cytoplasm of diakinesis and metaphase I spermatocytes, respectively. Scale bar represents 5 μm.

SUPPLEMENTARY FIGURE S3
Distribution of SYCP3 in a representative metaphase I (M I) WT squashed spermatocyte. Immunolabeling of SYCP3 (green in the top row and pseudocolored in red in the bottom row), and counterstaining of the chromatin with DAPI. Numbers in each panel indicate the Z-projection of the indicated focal planes. Yellow arrowheads indicate SYCP3 agglomerates in the cytoplasm. Scale bar represents 2 μm.

SUPPLEMENTARY FIGURE S4
Distribution of SYCP3 and kinetochores during the diplotene/metaphase I transition. Double immunolabeling of SYCP3 (green) and kinetochores (ACA, red), and counterstaining of the chromatin with DAPI on WT squashed spermatocytes. Representative spermatocytes at mid diplotene (M. dip.), **(B)** early diakinesis (E. dia.), **(C)** mid diakinesis (M. dia.), **(D)** late diakinesis (L. dia.), **(E)** prometaphase I (ProM I), and **(F)** metaphase I (M I) spermatocytes are shown. **(A'–E')** Enlarged autosomal bivalents at the corresponding prophase I stages. Enlarged autosomal **(G)** and sex **(H)** metaphase I bivalents. White arrowheads indicate elongated bulges and round thickenings of SYCP3 along desynapsed autosomal LEs. Yellow arrowheads indicate SYCP3 agglomerates in the nucleoplasm and cytoplasm of late diakinesis **(D)** and prometaphase I **(E)** spermatocytes. The sex chromosomes are indicated in **(H)**. Scale bars represent 5 μm in **(A–F)**, 2 μm in **(A'–E',G)**, and 1 μm in **(H)**.

SUPPLEMENTARY FIGURE S5
Distribution of HORMAD1 and kinetochores during the late diplotene/metaphase I transition. Double immunolabeling of HORMAD1 (green) and kinetochores (ACA, red), and counterstaining of the chromatin with DAPI on WT squashed spermatocytes. Representative spermatocytes at late diplotene (L. dip.), **(B)** early diakinesis (E. dia.), **(C)** late diakinesis (L. dia.), **(D)** prometaphase I (ProM I), and **(E)** metaphase I (M I) spermatocytes are shown. **(F)** Enlarged autosomal metaphase I bivalent. White arrowheads indicate elongated bulges and round thickenings of HORMAD1 along asynapsed AEs of the sex chromosomes and desynapsed autosomal LEs. Yellow arrowheads indicate HORMAD1 agglomerates in the nucleoplasm and cytoplasm of late diakinesis **(C)**, prometaphase I **(D)** and metaphase I **(E)** spermatocytes. The sex bivalent is indicated in **(A)**. Scale bars represent 5 μm in **(A–E)**, and 2 μm in **(F)**.

SUPPLEMENTARY FIGURE S6
Distribution of SYCP3 in WT spread spermatocytes. Representative spermatocytes at early diplotene (E. dip.), **(C,D)** mid diplotene (M. dip.), **(E)** late diplotene (L. dip.), **(F)** early diakinesis (E. dia.), **(G)** mid diakinesis (M. dia.), **(H)** late diakinesis (L. dia.), **(I–K)** prometaphase I (ProM I), and **(L)** metaphase I (M I) WT spermatocytes are shown. The sex bivalent (XY) is indicated. Blue arrows denote the PAR region in the sex bivalent. White arrowheads indicate elongated bulges and thickenings along the asynapsed AE of the X chromosome and the desynapsed autosomal LEs. Yellow arrowheads denote agglomerates in the nucleoplasm of the late diakinesis nucleus **(H)** and cytoplasms of prometaphase I and metaphase I spermatocytes **(I–L)**. Scale bar represents 5 μm.

SUPPLEMENTARY FIGURE S7
Distribution of SYCP3 (green) in selected autosomal and sex bivalents from WT spread spermatocytes. Representative examples showing the morphological changes of the AEs/LEs in autosomal and **(B)** sex bivalents from diplotene up to metaphase I. Two autosomal bivalents, one of them with one interstitial and one distal chiasma **(A–F)**, and another one with a single interstitial chiasma **(G–L)**, are shown. White arrowheads indicate bulges and thickenings along the desynapsed autosomal LEs and asynapsed AEs of the X chromosome. Blue arrows denote the PAR region in the sex bivalent. Asterisks indicate the centromere region of the X chromosome. Yellow arrowheads denote agglomerates in the nucleoplasm and cytoplasms. Scale bar represents 1 μm.

SUPPLEMENTARY FIGURE S8
Distribution of REC8 and SYCP3 in early WT prophase I spermatocytes. Double immunolabeling of REC8-*myc* (green) and SYCP3 (red), and counterstaining of the chromatin with DAPI (blue) on squashed WT spermatocytes. Representative spermatocytes at leptotene (Lep.), **(B)** zygotene (Zyg.), and **(C)** pachytene (Pac.) stages are shown. White arrowheads indicate accumulations of SYCP3 at putative nucleoli. Scale bar represents 5 μm.

SUPPLEMENTARY FIGURE S9
Distribution of REC8 and SYCP3 in WT meiosis I spermatocytes. Double immunolabeling of REC8 (green) and kinetochores (ACA, red), and counterstaining of the chromatin with DAPI (blue) on squashed spermatocytes. Representative spermatocytes at diakinesis (Dia.) and **(B)** metaphase I (M I) are shown. The squared region in **(B)** appears enlarged. Scale bar represents 5 μm.

SUPPLEMENTARY FIGURE S10
TUNEL assay in 8 h control and BI 2536-treated **(B)** seminiferous tubules. TUNEL assay (red) and counterstaining of the chromatin with DAPI (blue). Unaltered and altered metaphases I denoted by white arrowheads are enlarged.

SUPPLEMENTARY FIGURE S11
Distribution of PLK1S137ph in WT spread spermatocytes. Double immunolabeling of PLK1S137ph (green) and SYCP3 (red), and counterstaining of the chromatin with DAPI (blue). Representative spermatocytes at leptotene (Lep.), **(B)** late zygotene (L. zyg.), **(C)** pachytene (Pac.), **(D)** early diplotene (E. dip.), **(E)** mid diplotene (M. dip), **(F)** late diplotene (L. dip.), **(J)** early diakinesis (E. dia.), **(K)** prometaphase I (ProM I), and **(L)** metaphase I are shown. **(G–I)** Selected late diplotene sex bivalents. Sex chromosomes (X, Y) and bivalents (XY) are indicated. White arrows point to centrosomes. Red arrowheads denote nuclear dense bodies. White arrowheads indicate elongated bulges and thickenings along the asynapsed AE of the X chromosome, and the desynapsed autosomal LEs. Scale bar represent 5 μm.

SUPPLEMENTARY FIGURE S12
Distribution of PLK1T210ph during the diplotene/metaphase I transition. Double immunolabeling of PLK1T210ph (green) and SYCP3 (red), and counterstaining of the chromatin with DAPI (blue). Representative spermatocytes at mid diplotene (M. dip), **(B)** late diplotene (L. dip.), **(C)** early diakinesis (E. dia.), **(D)** prometaphase I (ProM I), and **(E)** metaphase I are shown. Sex bivalents (XY) are indicated. White arrowheads indicate SYCP3 elongated bulges and thickenings along the asynapsed AE of the X chromosome, and the desynapsed autosomal LEs. Yellow arrowheads indicate SYCP3 agglomerates in the cytoplasm of prometaphase I and metaphase I **(D,E)** spermatocytes. Scale bar represent 5 μm.

SUPPLEMENTARY VIDEO S1
3D reconstruction of WT spermatocytes in diplotene, early diakinesis (Early dia.) and late diakinesis (Late dia.) after the immunolabeling of SYCP3 (green) and kinetochores (ACA, red) and chromatin counterstaining with DAPI (blue).

SUPPLEMENTARY VIDEO S2
3D reconstruction of control and BI 2536-treated diakinesis spermatocytes after the immunolabeling of SYCP3 (green) and kinetochores (ACA, red).

SUPPLEMENTARY VIDEO S3
3D reconstruction of control and BI 2536-treated metaphase I spermatocytes after the immunolabeling of SYCP3 (red) and kinetochores (ACA, red) and chromatin counterstaining with DAPI (blue).

SUPPLEMENTARY VIDEO S4
3D reconstruction of control and BI 2536-treated diakinesis spermatocytes after the immunolabeling of SYCP3 (red) and HORMAD1 (green) and chromatin counterstaining with DAPI (blue). The Z-projections of these spermatocytes are shown in Figures 5A,B.

SUPPLEMENTARY VIDEO S5
3D reconstruction of control and BI 2536-treated metaphase I spermatocytes after the immunolabeling of SYCP3 (red) and HORMAD1 (green) and chromatin counterstaining with DAPI (blue).

SUPPLEMENTARY VIDEO S6
3D reconstruction of control and BI 2536-treated diakinesis spermatocytes after the immunolabeling of SYCP3 (red) and REC8-*myc* (green) and chromatin counterstaining with DAPI (blue).

SUPPLEMENTARY VIDEO S7
3D reconstruction of control and BI 2536-treated metaphase I spermatocytes after the immunolabeling of SYCP3 (red) and REC8-*myc* (green) and chromatin counterstaining with DAPI (blue).

References

Adelfalk, C., Janschek, J., Revenkova, E., Blei, C., Liebe, B., Göb, E., et al. (2009). Cohesin SMC1beta protects telomeres in meiocytes. *J. Cell Biol.* 187, 185–199. doi:10.1083/jcb.200808016

Alfaro, E., López-Jiménez, P., González-Martínez, J., Malumbres, M., Suja, J. A., and Gómez, R. (2021). PLK1 regulates centrosome migration and spindle dynamics in male mouse meiosis. *EMBO Rep.* 22, e51030. doi:10.15252/embr.202051030

Andrews, P. D., Ovechkina, Y., Morrice, N., Wagenbach, M., Duncan, K., Wordeman, L., et al. (2004). Aurora B regulates MCAK at the mitotic centromere. *Dev. Cell* 6, 253–268. doi:10.1016/s1534-5807(04)00025-5

Argunhan, B., Leung, W. K., Afshar, N., Terentyev, Y., Subramanian, V. V., Murayama, Y., et al. (2017). Fundamental cell cycle kinases collaborate to ensure timely destruction of the synaptonemal complex during meiosis. *EMBO J.* 36, 2488–2509. doi:10.15252/embj.201695895

Balboula, A. Z., and Schindler, K. (2014). Selective disruption of aurora C kinase reveals distinct functions from aurora B kinase during meiosis in mouse oocytes. *PLoS Genet.* 10, e1004194. doi:10.1371/journal.pgen.1004194

Berenguer, I., López-Jiménez, P., Mena, I., Viera, A., Page, J., González-Martínez, J., et al. (2022). Haspin participates in AURKB recruitment to centromeres and contributes to chromosome congression in male mouse meiosis. *J. Cell Sci.* 135, jcs259546. doi:10.1242/jcs.259546

Bolcun-Filas, E., and Handel, M. A. (2018). Meiosis: The chromosomal foundation of reproduction. *Biol. Reprod.* 99, 112–126. doi:10.1093/biolre/ioy021

Brieño-Enríquez, M. A., Moak, S. L., Toledo, M., Filter, J. J., Gray, S., Barbero, J. L., et al. (2016). Cohesin removal along the chromosome arms during the first meiotic division depends on a NEK1-PP1γ-WAPL axis in the mouse. *Cell Rep.* 17, 977–986. doi:10.1016/j.celrep.2016.09.059

Cahoon, C. K., and Hawley, R. S. (2016). Regulating the construction and demolition of the synaptonemal complex. *Nat. Struct. Mol. Biol.* 23, 369–377. doi:10.1038/nsmb.3208

Challa, K., Fajish, V. G., Shinohara, M., Klein, F., Gasser, S. M., and Shinohara, A. (2019a). Meiosis-specific prophase-like pathway controls cleavage-independent release of cohesin by Wapl phosphorylation. *PLoS Genet.* 15, e1007851. doi:10.1371/journal.pgen.1007851

Challa, K., Shinohara, M., and Shinohara, A. (2019b). Meiotic prophase-like pathway for cleavage-independent removal of cohesin for chromosome morphogenesis. *Curr. Genet.* 65, 817–827. doi:10.1007/s00294-019-00959-x

Clyne, R. K., Katis, V. L., Jessop, L., Benjamin, K. R., Herskowitz, I., Lichten, M., et al. (2003). Polo-like kinase Cdc5 promotes chiasmata formation and cosegregation of sister centromeres at meiosis I. *Nat. Cell Biol.* 5, 480–485. doi:10.1038/ncb977

Combes, G., Alharbi, I., Braga, L. G., and Elowe, S. (2017). Playing polo during mitosis: PLK1 takes the lead. *Oncogene* 36, 4819–4827. doi:10.1038/onc.2017.113

Dai, J., Sultan, S., Taylor, S. S., and Higgins, J. M. (2005). The kinase haspin is required for mitotic histone H3 Thr 3 phosphorylation and normal metaphase chromosome alignment. *Genes Dev.* 19, 472–488. doi:10.1101/gad.1267105

De Antoni, A., Maffini, S., Knapp, S., Musacchio, A., and Santaguida, S. (2012). A small-molecule inhibitor of Haspin alters the kinetochore functions of Aurora B. *J. Cell Biol.* 199, 269–284. doi:10.1083/jcb.201205119

Dobson, M. J., Pearlman, R. E., Karaiskakis, A., Spyropoulos, B., and Moens, P. B. (1994). Synaptonemal complex proteins: Occurrence, epitope mapping and chromosome disjunction. *J. Cell Sci.* 107, 2749–2760. doi:10.1242/jcs.107.10.2749

Du, J., Cao, Y., Wang, Q., Zhang, N., Liu, X., Chen, D., et al. (2015). Unique subcellular distribution of phosphorylated Plk1 (Ser137 and Thr210) in mouse oocytes during meiotic division and pPlk1(Ser137) involvement in spindle formation and REC8 cleavage. *Cell Cycle* 14, 3566–3579. doi:10.1080/15384101.2015.1100770

Eijpe, M., Offenberg, H., Jessberger, R., Revenkova, E., and Heyting, C. (2003). Meiotic cohesin REC8 marks the axial elements of rat synaptonemal complexes before cohesins SMC1beta and SMC3. *J. Cell Biol.* 160, 657–670. doi:10.1083/jcb.200212080

El Yakoubi, W., Buffin, E., Cladière, D., Gryaznova, Y., Berenguer, I., Touati, S. A., et al. (2017). Mps1 kinase-dependent Sgo2 centromere localisation mediates cohesin protection in mouse oocyte meiosis I. *Nat. Commun.* 8, 694. doi:10.1038/s41467-017-00774-3

Feitosa, W. B., Hwang, K., and Morris, P. L. (2018). Temporal and SUMO-specific SUMOylation contribute to the dynamics of Polo-like kinase 1 (PLK1) and spindle integrity during mouse oocyte meiosis. *Dev. Biol.* 434, 278–291. doi:10.1016/j.ydbio.2017.12.011

Fraune, J., Schramm, S., Alsheimer, M., and Benavente, R. (2012). The mammalian synaptonemal complex: Protein components, assembly and role in meiotic recombination. *Exp. Cell Res.* 318, 1340–1346. doi:10.1016/j.yexcr.2012.02.018

Fujiwara, Y., Horisawa-Takada, Y., Inoue, E., Tani, N., Shibuya, H., Fujimura, S., et al. (2020). Meiotic cohesins mediate initial loading of HORMAD1 to the chromosomes and coordinate SC formation during meiotic prophase. *PLoS Genet.* 16, e1009048. doi:10.1371/journal.pgen.1009048

Fukuda, T., Daniel, K., Wojtasz, L., Toth, A., and Höög, C. (2010). A novel mammalian HORMA domain-containing protein, HORMAD1, preferentially associates with unsynapsed meiotic chromosomes. *Exp. Cell Res.* 316, 158–171. doi:10.1016/j.yexcr.2009.08.007

Gao, J., and Colaiácovo, M. P. (2018). Zipping and unzipping: Protein modifications regulating synaptonemal complex dynamics. *Trends Genet.* 34, 232–245. doi:10.1016/j.tig.2017.12.001

Ghenoiu, C., Wheelock, M. S., and Funabiki, H. (2013). Autoinhibition and Polo-dependent multisite phosphorylation restrict activity of the histone H3 kinase Haspin to mitosis. *Mol. Cell* 52, 734–745. doi:10.1016/j.molcel.2013.10.002

Giménez-Abián, J. F., Sumara, I., Hirota, T., Hauf, S., Gerlich, D., de la Torre, C., et al. (2004). Regulation of sister chromatid cohesion between chromosome arms. *Curr. Biol.* 14, 1187–1193. doi:10.1016/j.cub.2004.06.052

Gómez, R., Valdeolmillos, A., Parra, M. T., Viera, A., Carreiro, C., Roncal, F., et al. (2007). Mammalian SGO2 appears at the inner centromere domain and redistributes depending on tension across centromeres during meiosis II and mitosis. *EMBO Rep.* 8, 173–180. doi:10.1038/sj.embor.7400877

Grosstessner-Hain, K., Hegemann, B., Novatchkova, M., Rameseder, J., Joughin, B. A., Hudecz, O., et al. (2011). Quantitative phospho-proteomics to investigate the polo-like kinase 1-dependent phospho-proteome. *Mol. Cell. Proteomics* 10, M111.008540. doi:10.1074/mcp.m111.008540

Hadders, M. A., Hindriksen, S., Truong, M. A., Mhaskar, A., Wopken, J. P., Vromans, M. J. M., et al. (2020). Untangling the contribution of haspin and Bub1 to aurora B function during mitosis. *J. Cell Biol.* 219, e201907087. doi:10.1083/jcb.201907087

Handel, M. A., and Schimenti, J. C. (2010). Genetics of mammalian meiosis: Regulation, dynamics and impact on fertility. *Nat. Rev. Genet.* 11, 124–136. doi:10.1038/nrg2723

Hauf, S., Roitinger, E., Koch, B., Dittrich, C. M., Mechtler, K., and Peters, J. M. (2005). Dissociation of cohesin from chromosome arms and loss of arm cohesion during early mitosis depends on phosphorylation of SA2. *PLoS Biol.* 3, e69. doi:10.1371/journal.pbio.0030069

Herrán, Y., Gutiérrez-Caballero, C., Sánchez-Martín, M., Hernández, T., Viera, A., Barbero, J. L., et al. (2011). The cohesin subunit RAD21L functions in meiotic synapsis and exhibits sexual dimorphism in fertility. *EMBO J.* 30, 3091–3105. doi:10.1038/emboj.2011.222

Hindriksen, S., Lens, S. M. A., and Hadders, M. A. (2017). The Ins and Outs of Aurora B inner centromere localization. *Front. Cell Dev. Biol.* 5, 112. doi:10.3389/fcell.2017.00112

Ishiguro, K., Kim, J., Fujiyama-Nakamura, S., Kato, S., and Watanabe, Y. (2011). A new meiosis-specific cohesin complex implicated in the cohesin code for homologous pairing. *EMBO Rep.* 12, 267–275. doi:10.1038/embor.2011.2

Jang, Y. J., Ma, S., Terada, Y., and Erikson, R. L. (2002). Phosphorylation of threonine 210 and the role of serine 137 in the regulation of mammalian polo-like kinase. *J. Biol. Chem.* 277, 44115–44120. doi:10.1074/jbc.m202172200

Jeganathan, K., Malureanu, L., Baker, D. J., Abraham, S. C., and van Deursen, J. M. (2007). Bub1 mediates cell death in response to chromosome missegregation and acts to suppress spontaneous tumorigenesis. *J. Cell Biol.* 179, 255–267. doi:10.1083/jcb.200706015

Jordan, P., Copsey, A., Newnham, L., Kolar, E., Lichten, M., and Hoffmann, E. (2009). Ipl1/Aurora B kinase coordinates synaptonemal complex disassembly with cell cycle progression and crossover formation in budding yeast meiosis. *Genes Dev.* 23, 2237–2251. doi:10.1101/gad.536109

Jordan, P. W., Karppinen, J., and Handel, M. A. (2012). Polo-like kinase is required for synaptonemal complex disassembly and phosphorylation in mouse spermatocytes. *J. Cell Sci.* 125, 5061–5072. doi:10.1242/jcs.105015

Kang, Y. H., Park, J. E., Yu, L. R., Soung, N. K., Yun, S. M., Bang, J. K., et al. (2006). Self-regulated Plk1 recruitment to kinetochores by the Plk1–PBIP1 interaction is critical for proper chromosome segregation. *Mol. Cell* 24, 409–422. doi:10.1016/j.molcel.2006.10.016

Kawashima, S. A., Yamagishi, Y., Honda, T., Ishiguro, K., and Watanabe, Y. (2010). Phosphorylation of H2A by Bub1 prevents chromosomal instability through localizing shugoshin. *Science* 327, 172–177. doi:10.1126/science.1180189

Kelly, A. E., Ghenoiu, C., Xue, J. Z., Zierhut, C., Kimura, H., and Funabiki, H. (2010). Survivin reads phosphorylated histone H3 threonine 3 to activate the mitotic kinase Aurora B. *Science* 330, 235–239. doi:10.1126/science.1189505

Kim, J., Ishiguro, K., Nambu, A., Akiyoshi, B., Yokobayashi, S., Kagami, A., et al. (2015). Meikin is a conserved regulator of meiosis-I-specific kinetochore function. *Nature* 517, 466–471. doi:10.1038/nature14097

Korns, J., Liu, X., and Takiar, V. (2022). A review of Plks: Thinking outside the (polo) box. *Mol. Carcinog.* 61, 254–263. doi:10.1002/mc.23388

Kudo, N. R., Wassmann, K., Anger, M., Schuh, M., Wirth, K. G., Xu, H., et al. (2006). Resolution of chiasmata in oocytes requires separase-mediated proteolysis. *Cell* 126, 135–146. doi:10.1016/j.cell.2006.05.033

Láscarez-Lagunas, L. I., Martinez-Garcia, M., and Colaiácovo, M. P. (2022). Loss, gain, and retention: Mechanisms driving late prophase I chromosome remodeling for accurate meiotic chromosome segregation. *Genes* 13, 546. doi:10.3390/genes13030546

Lee, J., Iwai, T., Yokota, T., and Yamashita, M. (2003). Temporally and spatially selective loss of Rec8 protein from meiotic chromosomes during mammalian meiosis. *J. Cell Sci.* 116, 2781–2790. doi:10.1242/jcs.00495

Lénárt, P., Petronczki, M., Steegmaier, M., Di Fiore, B., Lipp, J. J., Hoffmann, M., et al. (2007). The small-molecule inhibitor BI 2536 reveals novel insights into mitotic roles of polo-like kinase 1. *Curr. Biol.* 17, 304–315. doi:10.1016/j.cub.2006.12.046

Little, T. M., and Jordan, P. W. (2020). PLK1 is required for chromosome compaction and microtubule organization in mouse oocytes. *Mol. Biol. Cell* 31, 1206–1217. doi:10.1091/mbc.e19-12-0701

Llano, E., Gómez, R., Gutiérrez-Caballero, C., Herrán, Y., Sánchez-Martín, M., Vázquez-Quinones, L., et al. (2008). Shugoshin-2 is essential for the completion of meiosis but not for mitotic cell division in mice. *Genes Dev.* 22, 2400–2413. doi:10.1101/gad.475308

McNicoll, F., Stevense, M., and Jessberger, R. (2013). Cohesin in gametogenesis. *Curr. Top. Dev. Biol.* 102, 1–34. doi:10.1016/b978-0-12-416024-8.00001-5

Moens, P. B., Heyting, C., Dietrich, A. J., van Raamsdonk, W., and Chen, Q. (1987). Synaptonemal complex antigen location and conservation. *J. Cell Biol.* 105, 93–103. doi:10.1083/jcb.105.1.93

Page, J., Suja, J. A., Santos, J. L., and Rufas, J. S. (1998). Squash procedure for protein immunolocalization in meiotic cells. *Chromosome Res.* 6, 639–642. doi:10.1023/a:1009209628300

Parra, M. T., Gómez, R., Viera, A., Llano, E., Pendás, A. M., Rufas, J. S., et al. (2009). Sequential assembly of centromeric proteins in male mouse meiosis. *PLoS Genet.* 5, e1000417. doi:10.1371/journal.pgen.1000417

Parra, M. T., Gómez, R., Viera, A., Page, J., Calvente, A., Wordeman, L., et al. (2006). A perikinetochoric ring defined by MCAK and Aurora-B as a novel centromere domain. *PLoS Genet.* 2, e84. doi:10.1371/journal.pgen.0020084

Parra, M. T., Page, J., Yen, T. J., He, D., Valdeolmillos, A., Rufas, J. S., et al. (2002). Expression and behaviour of CENP-E at kinetochores during mouse spermatogenesis. *Chromosoma* 111, 53–61. doi:10.1007/s00412-002-0185-5

Parra, M. T., Viera, A., Gómez, R., Page, J., Benavente, R., Santos, J. L., et al. (2004). Involvement of the cohesin Rad21 and SCP3 in monopolar attachment of sister kinetochores during mouse meiosis I. *J. Cell Sci.* 117, 1221–1234. doi:10.1242/jcs.00947

Parra, M. T., Viera, A., Gómez, R., Page, J., Carmena, M., Earnshaw, W. C., et al. (2003). Dynamic relocalization of the chromosomal passenger complex proteins inner centromere protein (INCENP) and aurora-B kinase during male mouse meiosis. *J. Cell Sci.* 116, 961–974. doi:10.1242/jcs.00330

Peters, A. H., Plug, A. W., van Vugt, M. J., and de Boer, P. (1997). A drying-down technique for the spreading of mammalian meiocytes from the male and female germline. *Chromosome Res.* 5, 66–68. doi:10.1023/a:1018445520117

Pomerantz, Y., Elbaz, J., Ben-Eliezer, I., Reizel, Y., David, Y., Galiani, D., et al. (2012). From ubiquitin-proteasomal degradation to CDK1 inactivation: Requirements for the first polar body extrusion in mouse oocytes. *FASEB J.* 26, 4495–4505. doi:10.1096/fj.12-209866

Prieto, I., Suja, J. A., Pezzi, N., Kremer, L., Martínez, A. C., Rufas, J. S., et al. (2001). Mammalian STAG3 is a cohesin specific to sister chromatid arms in meiosis I. *Nat. Cell Biol.* 3, 761–766. doi:10.1038/35087082

Qi, W., Tang, Z., and Yu, H. (2006). Phosphorylation- and polo-box-dependent binding of Plk1 to Bub1 is required for the kinetochore localization of Plk1. *Mol. Biol. Cell* 17, 3705–3716. doi:10.1091/mbc.e06-03-0240

Rattani, A., Wolna, M., Ploquin, M., Helmhart, W., Morrone, S., Mayer, B., et al. (2013). Sgol2 provides a regulatory platform that coordinates essential cell cycle processes during meiosis I in oocytes. *Elife* 2, e01133. doi:10.7554/elife.01133

Ricke, R. M., Jeganathan, K. B., Malureanu, L., Harrison, A. M., and van Deursen, J. M. (2012). Bub1 kinase activity drives error correction and mitotic checkpoint control but not tumor suppression. *J. Cell Biol.* 199, 931–949. doi:10.1083/jcb.201205115

Sato, T., Katagiri, K., Yokonishi, T., Kubota, Y., Inoue, K., Ogonuki, N., et al. (2011). *In vitro* production of fertile sperm from murine spermatogonial stem cell lines. *Nat. Commun.* 2, 472. doi:10.1038/ncomms1478

Schalk, J. A., Dietrich, A. J., Vink, A. C., Offenberg, H. H., van Aalderen, M., and Heyting, C. (1998). Localization of SCP2 and SCP3 protein molecules within synaptonemal complexes of the rat. *Chromosoma* 107, 540–548. doi:10.1007/s004120050340

Schmitz, M. L., Higgins, J. M. G., and Seibert, M. (2020). Priming chromatin for segregation: Functional roles of mitotic histone modifications. *Cell Cycle* 19, 625–641. doi:10.1080/15384101.2020.1719585

Schmucker, S., and Sumara, I. (2014). Molecular dynamics of PLK1 during mitosis. *Mol. Cell. Oncol.* 1, e954507. doi:10.1080/23723548.2014.954507

Silva, M. C. C., Powell, S., Ladstätter, S., Gassler, J., Stocsits, R., Tedeschi, A., et al. (2020). Wapl releases Scc1-cohesin and regulates chromosome structure and segregation in mouse oocytes. *J. Cell Biol.* 219, e201906100. doi:10.1083/jcb.201906100

Singh, P., Pesenti, M. E., Maffini, S., Carmignani, S., Hedtfeld, M., Petrovic, A., et al. (2021). Bub1 and CENP-U, primed by CDK1, are the main PLK1 kinetochore receptors in mitosis. *Mol. Cell* 81, 67–87. e9. doi:10.1016/j.molcel.2020.10.040

Solc, P., Kitajima, T. S., Yoshida, S., Brzakova, A., Kaido, M., Baran, V., et al. (2015). Multiple requirements of PLK1 during mouse oocyte maturation. *PLoS One* 10, e0116783. doi:10.1371/journal.pone.0116783

Sourirajan, A., and Lichten, M. (2008). Polo-like kinase Cdc5 drives exit from pachytene during budding yeast meiosis. *Genes Dev.* 22, 2627–2632. doi:10.1101/gad.1711408

Steegmaier, M., Hoffmann, M., Baum, A., Lénárt, P., Petronczki, M., Krssak, M., et al. (2007). BI 2536, a potent and selective inhibitor of polo-like kinase 1, inhibits tumor growth *in vivo*. *Curr. Biol.* 17, 316–322. doi:10.1016/j.cub.2006.12.037

Su, S., Chhabra, G., Singh, C. K., Ndiaye, M. A., and Ahmad, N. (2022). PLK1 inhibition-based combination therapies for cancer management. *Transl. Oncol.* 16, 101332. doi:10.1016/j.tranon.2021.101332

Suja, J. A., Antonio, C., Debec, A., and Rufas, J. S. (1999). Phosphorylated proteins are involved in sister-chromatid arm cohesion during meiosis I. *J. Cell Sci.* 112, 2957–2969. doi:10.1242/jcs.112.17.2957

Suja, J. A., and Barbero, J. L. (2009). Cohesin complexes and sister chromatid cohesion in mammalian meiosis. *Genome Dyn.* 5, 94–116. doi:10.1159/000166622

Tanno, Y., Kitajima, T. S., Honda, T., Ando, Y., Ishiguro, K., and Watanabe, Y. (2010). Phosphorylation of mammalian Sgo2 by Aurora B recruits PP2A and MCAK to centromeres. *Genes Dev.* 24, 2169–2179. doi:10.1101/gad.1945310

Tong, C., Fan, H. Y., Lian, L., Li, S. W., Chen, D. Y., Schatten, H., et al. (2002). Polo-like kinase-1 is a pivotal regulator of microtubule assembly during mouse oocyte meiotic maturation, fertilization, and early embryonic mitosis. *Biol. Reprod.* 67, 546–554. doi:10.1095/biolreprod67.2.546

Viera, A., Gómez, R., Parra, M. T., Schmiesing, J. A., Yokomori, K., Rufas, J. S., et al. (2007). Condensin I reveals new insights on mouse meiotic chromosome structure and dynamics. *PLoS One* 2, e783. doi:10.1371/journal.pone.0000783

Visnes, T., Giordano, F., Kuznetsova, A., Suja, J. A., Lander, A. D., Calof, A. L., et al. (2014). Localisation of the SMC loading complex Nipbl/Mau2 during mammalian meiotic prophase I. *Chromosoma* 123, 239–252. doi:10.1007/s00412-013-0444-7

Wang, F., Dai, J., Daum, J. R., Niedzialkowska, E., Banerjee, B., Stukenberg, P. T., et al. (2010). Histone H3 Thr-3 phosphorylation by Haspin positions Aurora B at centromeres in mitosis. *Science* 330, 231–235. doi:10.1126/science.1189435

Wang, F., and Higgins, J. M. (2012). Histone modifications and mitosis: Countermarks, landmarks, and bookmarks. *Trends Cell Biol.* 23, 175–184. doi:10.1016/j.tcb.2012.11.005

Wang, F., Ulyanova, N. P., Daum, J. R., Patnaik, D., Kateneva, A. V., Gorbsky, G. J., et al. (2012). Haspin inhibitors reveal centromeric functions of Aurora B in chromosome segregation. *J. Cell Biol.* 199, 251–268. doi:10.1083/jcb.201205106

Wang, F., Ulyanova, N. P., van der Waal, M. S., Patnaik, D., Lens, S. M., and Higgins, J. M. (2011). A positive feedback loop involving Haspin and Aurora B promotes CPC accumulation at centromeres in mitosis. *Curr. Biol.* 21, 1061–1069. doi:10.1016/j.cub.2011.05.016

Watanabe, Y. (2012). Geometry and force behind kinetochore orientation: Lessons from meiosis. *Nat. Rev. Mol. Cell. Biol.* 13, 370–382. doi:10.1038/nrm3349

Watanabe, Y. (2010). Temporal and spatial regulation of targeting aurora B to the inner centromere. *Cold Spring Harb. Symp. Quant. Biol.* 75, 419–423. doi:10.1101/sqb.2010.75.035

Wellard, S. R., Schindler, K., and Jordan, P. W. (2020). Aurora B and C kinases regulate chromosome desynapsis and segregation during mouse and human spermatogenesis. *J. Cell Sci.* 133, jcs248831. doi:10.1242/jcs.248831

Wellard, S. R., Skinner, M. W., Zhao, X., Shults, C., and Jordan, P. W. (2022). PLK1 depletion alters homologous recombination and synaptonemal complex disassembly events during mammalian spermatogenesis. *Mol. Biol. Cell* 33, ar37. doi:10.1091/mbc.e21-03-0115

Wellard, S. R., Zhang, Y., Shults, C., Zhao, X., McKay, M., Murray, S. A., et al. (2021). Overlapping roles for PLK1 and Aurora A during meiotic centrosome biogenesis in mouse spermatocytes. *EMBO Rep.* 22, e54106. doi:10.15252/embr.202154106

Willems, E., Dedobbeleer, M., Digregorio, M., Lombard, A., Lumapat, P. N., and Rogister, B. (2018). The functional diversity of aurora kinases: A comprehensive review. *Cell Div.* 13, 7. doi:10.1186/s13008-018-0040-6

Wojtasz, L., Daniel, K., Roig, I., Bolcun-Filas, E., Xu, H., Boonsanay, V., et al. (2009). Mouse HORMAD1 and HORMAD2, two conserved meiotic chromosomal proteins, are depleted from synapsed chromosome axes with the help of TRIP13 AAA-ATPase. *PLoS Genet.* 5, e1000702. doi:10.1371/journal.pgen.1000702

Yamagishi, Y., Honda, T., Tanno, Y., and Watanabe, Y. (2010). Two histone marks establish the inner centromere and chromosome bi-orientation. *Science* 330, 239–243. doi:10.1126/science.1194498

Yuan, L., Pelttari, J., Brundell, E., Bjorkroth, B., Zhao, J., Liu, J. G., et al. (1998). The synaptonemal complex protein SCP3 can form multistranded, cross-striated fibers *in vivo*. *J. Cell Biol.* 142, 331–339. doi:10.1083/jcb.142.2.331

Zhang, F. G., Zahng, R. R., and Gao, J. M. (2021). The organization, regulation, and biological functions of the synaptonemal complex. *Asian J. Androl.* 23, 580–589. doi:10.4103/aja202153

Zhou, L., Tian, X., Zhu, C., Wang, F., and Higgins, J. M. (2014). Polo-like kinase-1 triggers histone phosphorylation by Haspin in mitosis. *EMBO Rep.* 15, 273–281. doi:10.1002/embr.201338080

frontiers | Frontiers in Cell and Developmental Biology

TYPE Brief Research Report
PUBLISHED 19 January 2023
DOI 10.3389/fcell.2023.1005145

OPEN ACCESS

EDITED BY
Pedro A. San-Segundo,
CSIC-University of Salamanca, Spain

REVIEWED BY
Marina Martinez-Garcia,
Universidad Politécnica de Madrid, Spain
Jiri Forejt,
Institute of Molecular Genetics (ASCR), Czechia

*CORRESPONDENCE
Elena de la Casa-Esperon,
elena.casaesperon@uclm.es

SPECIALTY SECTION
This article was submitted to Nuclear Organization and Dynamics, a section of the journal Frontiers in Cell and Developmental Biology

RECEIVED 28 July 2022
ACCEPTED 09 January 2023
PUBLISHED 19 January 2023

CITATION
Soriano J, Belmonte-Tebar A and de la Casa-Esperon E (2023), Synaptonemal & CO analyzer: A tool for synaptonemal complex and crossover analysis in immunofluorescence images. *Front. Cell Dev. Biol.* 11:1005145. doi: 10.3389/fcell.2023.1005145

Synaptonemal & CO analyzer: A tool for synaptonemal complex and crossover analysis in immunofluorescence images

Joaquim Soriano[1], Angela Belmonte-Tebar[1] and Elena de la Casa-Esperon[1,2]*

[1]Centro Regional de Investigaciones Biomédicas (CRIB), Universidad de Castilla-La Mancha, Albacete, Spain, [2]Biology of Cell Growth, Differentiation and Activation Group, Department of Inorganic and Organic Chemistry and Biochemistry, School of Pharmacy, Universidad de Castilla-La Mancha, Albacete, Spain

During the formation of ova and sperm, homologous chromosomes get physically attached through the synaptonemal complex and exchange DNA at crossover sites by a process known as meiotic recombination. Chromosomes that do not recombine or have anomalous crossover distributions often separate poorly during the subsequent cell division and end up in abnormal numbers in ova or sperm, which can lead to miscarriage or developmental defects. Crossover numbers and distribution along the synaptonemal complex can be visualized by immunofluorescent microscopy. However, manual analysis of large numbers of cells is very time-consuming and a major bottleneck for recombination studies. Some image analysis tools have been created to overcome this situation, but they are not readily available, do not provide synaptonemal complex data, or do not tackle common experimental difficulties, such as overlapping chromosomes. To overcome these limitations, we have created and validated an open-source ImageJ macro routine that facilitates and speeds up the crossover and synaptonemal complex analyses in mouse chromosome spreads, as well as in other vertebrate species. It is free, easy to use and fulfills the recommendations for enhancing rigor and reproducibility in biomedical studies.

KEYWORDS

meiotic recombination, crossover, synaptonemal complex, image analysis, ImageJ, Fiji, open-source software

Introduction

Ova and sperm are formed through a special type of cell division known as meiosis, in which homologous chromosomes exchange genetic information. This process, known as meiotic recombination, requires programmed, developmentally regulated double strand breaks (DSBs) initiating pairing of homologous chromosomes and assembly of a zipper-like multiprotein structure between them (the synaptonemal complex, SC); then, crossovers (COs) between paired chromosomes result in the mutual exchange of genetic material at the pachytene meiosis stage (Figure 1). COs are important for subsequent chromosome segregation during the first meiotic division: those that do not recombine often appear in abnormal numbers in ova, sperm and the resulting embryos, leading to infertility, miscarriage and birth defects (Hassold and Hunt, 2001). Therefore, crossovers not only generate genetic diversity, but are also required for proper chromosome segregation in many sexually reproducing organisms. Hence, meiotic recombination studies are of paramount interest in farming, stockbreeding and human fertility

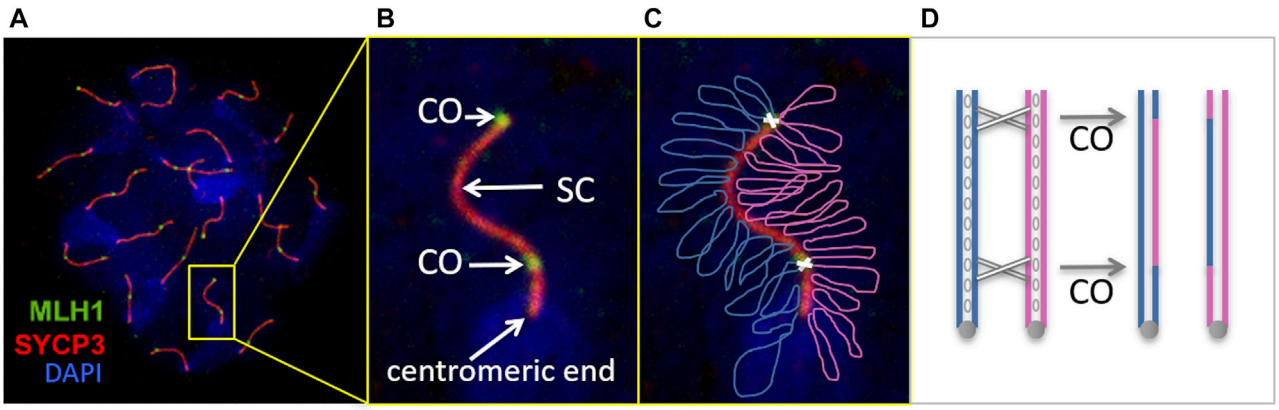

FIGURE 1
Male meiosis recombination visualized by immunofluorescence of a mouse pachytene-stage nucleus spread. **(A, B)** The spermatocyte was immunostained with antibodies against MLH1 in order to identify the crossover sites (CO) between paired homologous chromosomes. These are joined together through the synaptonemal complex (SC), visualized with antibodies against the protein SYCP3, one of SC components. Chromosomes are not fully condensed at this stage, but DNA staining with DAPI allows to identify each nucleus spread. Consequently, centromeres are not visible yet as a chromosomes constrictions, but can be located with specific probes or by brighter DAPI staining (as indicated in B; notice that mouse centromeres are not central, but distal). **(C)** Simplified representation over the previous image of the two homologous chromosomes (blue and magenta) with two COs (white crosses). These result in the mutual exchange of genetic material between homologous chromosomes, as schematized in **(D)** (each chromosome represented by two identical DNA copies (sister chromatids, resulting from previous DNA replication) joined by the centromere (grey circles) as well as other proteins (cohesins, blank ovals)).

and health (Notter, 1999; Hassold and Hunt, 2001; Handel and Schimenti, 2010; Henderson and Bomblies, 2021).

Immunofluorescence of chromosome spreads of pachytene-stage oocytes or spermatocytes (ova and sperm precursors) has become the most common approach to study meiotic recombination in animals (Baker et al., 1996; Anderson et al., 1999; de Boer et al., 2009; Cole et al., 2012; Imai et al., 2021). For instance, a typical protocol for mouse and other vertebrates' recombination studies uses antibodies against the mismatch repair protein MLH1 to identify CO sites, antibodies against SYCP3 to label SCs, and DAPI to stain DNA and delimit the nuclei, since chromosomes are not fully condensed and discernible at pachytene stage (Figure 1). Since MLH1 signal is usually weak, in order to tell apart false positives, only MLH1 foci over SYCP3 labeling are considered true COs. If necessary, the centromeric regions of the chromosomes can be recognized with specific labels (CREST serum) or by a more intense DAPI staining (Anderson et al., 1999; Froenicke et al., 2002; Segura et al., 2013) (Figure 1).

The frequency and distribution of COs along SCs are characteristic of each species, though differences may occur between the sexes. Usually, there is at least one CO per SC [the "obligate" crossover required for proper chromosome segregation (Mather, 1937)]. The maximum number depends on the length of the chromosome and the degree of interference between COs, a phenomenon by which the occurrence of one CO interferes with the appearance of a second one nearby (Sturtevant, 1915; Muller, 1916; Sym and Roeder, 1994; Kleckner, 2006). Consequently, high CO frequencies have been associated with either long SCs or weak interference (Anderson et al., 1999; de Boer et al., 2009). Other factor that affects the CO distribution in many species is the CO suppression around the centromeres -chromosome constrictions that play important roles during cell division. For instance, in mouse spermatocytes centromeres are located at one extreme of the chromosomes and, consequently, crossovers accumulate towards the opposite end (Anderson et al., 1999) (Figure 1). This distribution is biologically relevant, because COs too close to the centromeres lead to abnormal chromosome disjunction during cell division (Koehler et al., 1996; Lamb et al., 1996; Hassold and Hunt, 2001).

The relevant data for recombination studies that can be extracted from immunostained pachytene-stage cells are: 1) number of COs per cell and per individual SC; 2) number of SCs per cell and length of each one; 3) distribution of COs on each individual SC relative to, for instance, the centromere. This requires unambiguous identification of the SCs (as they often overlap) and COs on them, as well as the location of the centromeres. In mouse and other eutherian mammals, X and Y chromosomes behave differently than the rest (autosomes) because they only pair and recombine through a small (pseudoautosomal) region; for this reason, they are excluded from many recombination studies in males (Baier et al., 2014; Dumont, 2017).

While MLH1 immunodetection has become a common procedure for many recombination studies, manual COs and SCs image analysis can be very time-consuming and, hence, constitute a major bottleneck. The analysis is also prone to a certain degree of subjectivity, a problem that has been circumvented in some studies by duplicating the image scoring by two independent observers (Baier et al., 2014; Vrooman et al., 2015). Image analysis automation could solve these problems by fastening the procedure and applying objective detection algorithms. A common approach is to develop custom-made software solutions. Regrettably, they usually do not find widespread usage outside the originating lab (Swedlow and Eliceiri, 2009; Prevedello and Khorasani, 2012; Karopka et al., 2014) due to what some authors call a lack of usability (Carpenter et al., 2012), rigor and reproducibility (Brito et al., 2020). In order to facilitate recombination analyses to a broad research community, software should be easy to access and use, well documented and supported (Carpenter et al., 2012; Brito et al., 2020).

Indeed, a few tools have been developed for SC analysis (de Boer et al., 2009; Milano et al., 2019; Peterson et al., 2019; Wang et al., 2019), but none of them are able to extract all the aforementioned meaningful data from recombination studies while fulfilling the requirements for software usability and reproducibility (Carpenter et al., 2012; Brito et al., 2020). The software quoted in de Boer et al. (2009) (Object Image and MicroMeasure) are no longer available in the cited websites. They are intended for SC measurement only and, even though the authors cite the possibility of using a specific macro to measure CO sites and SC length, regrettably it has not been published and is only available upon demand. The macros published in Milano et al. (2019); Wang et al. (2019) do not consider CO nor centromere analysis, and while no information on how to implement the former is available, the latter relies on a specific Python 3 package that is not accessible to users without programming skills. CO detection software based on MLH1 foci detection have also been developed (Martin et al., 2014; Enguita-Marruedo et al., 2019) however, they do not analyze SCs and, therefore, are unable to discriminate true COs from artifacts. Finally, the application developed by Peterson et al. (2019) undertakes a different approach by analyzing large numbers of images in an unsupervised manner while relying in post-processing analyses to remove undesired outcomes. This results in relevant data losses, because overlapping SCs are manually eliminated and sex chromosomes are excluded by size filtering along with other long chromosomes, restricting the analysis to short chromosomes. Overall, this approach is only useful in very large experimental datasets, but implies manual curation of thousands of images (Peterson et al., 2019). Moreover, this solution relies on a software, CyVerse, that is not very common among image analyzers and is only available upon demand.

We decided to develop our own application to study meiotic recombination and to share our efforts by meeting the requirements stated for free software distribution in Carpenter et al. (2012) and the recommendations of Brito et al. (2020) to enhance rigor and reproducibility in biomedical research. Hence, we chose to develop an open-source application as an extension of ImageJ/FIJI (Schindelin et al., 2012; Schneider et al., 2012) because it is the most popular, open-source software for bioimage analysis with a large and interactive user's community (ImageJ, n.d.; FIJI, n.d.; ImageJ Information and Documentation Portal, n.d.; FIJI Software, n.d.; ImageJ Conferences, n.d.). Therefore, our software has the potential of being easily improved or adapted by other ImageJ/FIJI users to the particular needs of their recombination studies.

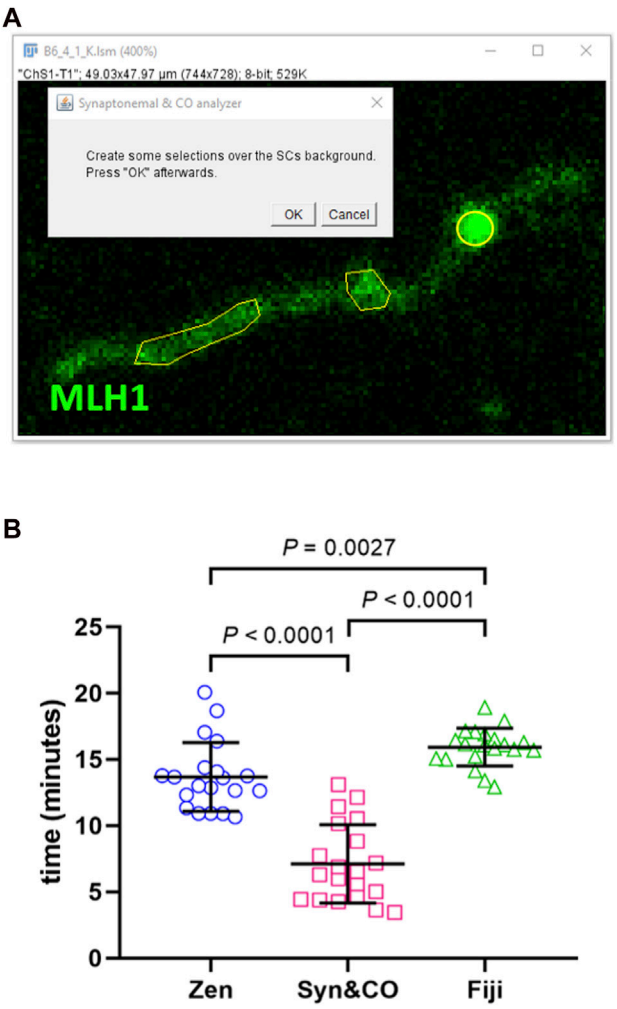

FIGURE 2
Synaptonemal & CO Analyzer facilitates recombination analysis. **(A)** The macro reduces a complex analysis to easy steps. For instance, the user is asked to draw a few selections (yellow polyhedrons) to launch an automated algorithm to detect COs (yellow circle). **(B)** Synaptonemal & CO Analyzer is, on average, two times faster than manual methods. Synaptonemal & CO Analyzer (Syn&CO) performance compared to FIJI and Zen Lite manual analysis. The same blinded images (n = 20) were analyzed by each method. The results were analyzed by generalized linear models and Bonferroni *post hoc* test. Bars and whiskers represent means and SDs.

Materials and methods

Hardware and software characteristics

The software was written in ImageJ's script language on FIJI, using ImageJ 1.53c. On a PC with Windows 10 operative system working on an Intel Core i5-4200 CPU @ 1.60 GHz 2.30 GHz and 4.00 GB RAM. Gabriel Landini's Morphology package (Landini, 2008) and the Bio-Formats importer plugin (Linkert et al., 2010) are required for the software to work.

Validation data sets

Software's efficiency and accuracy were validated on images from mouse pachytene spermatocytes immunostained with antibodies against MLH1 and SYCP3, counterstained with DAPI and captured under a confocal microscope as previously described (Anderson et al., 1999; de Boer et al., 2009; Milano et al., 2019; Belmonte-Tebar et al., 2022).

Software's flexibility and applicability were validated on pachytene-stage nuclei images from other species, antibodies and capturing methods (Supplementary Figure S1). Images labeled with MLH1 and SYCP3 antibodies were obtained with protocols similar to ours; some lacked DAPI staining or used human calcinosis, Raynaud's phenomenon, oesophageal dysfunction, sclerodactyly and telangiectasia (CREST) serum for centromere detection (Segura et al., 2013). They were generously donated as follows: wild-captured house mice *Mus musculus domesticus* with standard karyotype and with Robertsonian translocations (courtesy of Cristina Marin and Aurora Ruiz-Herrera (Vara et al., 2021));

Matthey's mouse (*Mus matheyi*, courtesy of Jesus Page (Universidad Autonoma de Madrid (UMA), Spain) and Frederic Veyrunes (Universite Montpellier, France); mongolian gerbil (*Meriones unguiculatus,* also of Jesus Page); zebrafish (*Danio rerio*, courtesy of Yukiko Imai, National Institute of Genetics, Japan); chicken (*Gallus gallus* (del Priore and Pigozzi, 2020)) and duck (*Anas platyrhynchos*; both bird images were obtained with antibodies against SMC3 instead of SYCP3 for SC labeling and donated by Maria Ines Pigozzi, Instituto de Investigaciones Biomedicas, Universidad de Buenos Aires-CONICET, Argentina). Generous donations were also *Mus musculus* images stained with antibodies against RAD51 (Jesus Page, UMA) and RPA2 (Parijat Chakraborty and Francesca Cole, The University of Texas MD Anderson Cancer Center, United States).

Software development and validation processes

Image analysis using Synaptonemal & CO Analyzer is a semi-automated process. Semi-automated SC identification relies on automatically subtracting background using a gaussian filter and a rolling ball algorithm (Sternberg, 1983). The user setting an intensity threshold is the only manual step needed. Afterwards, some binary operations are automatically performed: a reconstruction to get rid of small objects, a closing and an opening to smooth surfaces, and finally getting a SCs' skeleton. Semi-automatic CO and centromere detection is based on an intensity and size algorithm: whatever is brighter than the background and bigger than pixels is selected. The user needs to determine the background by creating a selection over it (Figure 2).

Exact details on SCs, COs, and centromeres' detection algorithms can be found in the macro source code by looking for "function SC_analysis," "function CO_analysis" and "function centromere_analysis," respectively. Although they work well with most of the tested images, isolating detection algorithms into functions eases adapting detection to new image characteristics. In order to do so, users only need to change the function's code by a new one. This task has been eased to users with no image analysis background by providing two extra macros (skeletonize_SC_macro_recorder.ijm,foci_detection_macro_recorder.ijm) that generate detection code, (Supplementary Video tutorial 2 and User Manual). Modifying objects detection algorithms avoids manual steps (such as setting an intensity level on each analyzed image) making the macro more automated. Macro source codes are available at https://github.com/joaquim-soriano/Synaptonemal-and-CO-analyzer.

The macro was developed following a two-step procedure. First, we developed an initial version on mice pachytene spreads (as mentioned above), that was validated for efficiency and accuracy. Second, we adapted the macro to ease work on other species and labels. In the first phase, the software development team consisted of an image analyst, a project manager and a beta tester. The project manager, a meiosis expert, determined the software requirements for recombination studies. The image analyst devised the algorithm and wrote the code, and the beta tester checked the resulting script on a set of standard images. Errors detected and new requirements were reported to the image analyst that fixed the former and implemented the latter. Software's first version was released after no further requirements were found and results were consistent with those obtained from manual analyses of a set of standard images. These consisted of a representative sample of 20 images of 20 immunostained mouse spermatocytes of an ongoing research project. Each image was manually analyzed with FIJI and with the software previously employed in our laboratory, Zen lite (Zeiss, Oberkochen, Germany), as well as with our semi-automated software. Images were randomized and the identities were blinded and coded differently for each of the three analyses until all were completed in order to avoid bias. The beta tester was previously trained on the use of each analysis method with an independent set of images. Data were obtained on a PC running Windows 10 operative system on an Intel Core i7-7500U @ 2.70 GHz 2.90 GHz and 8.00 GB RAM. Total SC length, number of COs per cell (excluding X and Y chromosomes) and duration of the analysis were compared between the three methods in order to determine the script's accuracy and efficiency. Results were analyzed by generalized linear models (GLM repeated measures) and Bonferroni *post hoc* test with SPSS software (NIH, Bethesda, MA, United States).

In a second phase, software's first released version was checked against a diversity of images (Supplementary Figure S1) resulting on a second macro version that opens different image formats, works on centromere-specific labeling (e.g., with CREST serum) and provides means to easily adapting the macro to detect objects under different image conditions.

Results and discussion

Software analysis process and outcomes

Image analysis using Synaptonemal & CO Analyzer is a semi-automated process. Once launched, a set of windows ask the user to perform easy tasks (Figure 2 and Supplementary Material: Video tutorial 1 and User Manual) until the software gathers all needed data to automatically perform the analysis. Once done, SCs, COs and centromeres are analyzed sequentially (Supplementary Figure S2) following a similar process (Supplementary Figure S3). Basically, the user decides whether to detect COs or centromeres manually (if the image quality is too low) or introduce parameters for an automated analysis (SC automated detection is always done by default), some checking steps are then performed that might need further user interaction (for example, replacing a CO that does not lay over a SC or isolating overlapping SCs) before the analysis is complete.

Synaptonemal & CO Analyzer obtains the following data from pachytene-stage nuclei images: 1) SC length of each chromosome, 2) sum of the length of all the SC per cell, 3) number of COs per SC (i.e., number of COs between each pair of homologous chromosomes), 4) total number of COs per cell and 5) CO location along each SC (Figure 3). CO distances are measured starting from one end, with the option of automatically selecting the centromeric end when discernible. If centromeres' detection is based upon centromere labels, the position of each centromere will be also delivered, as well as lengths between SCs ends and COs relative to centromere position and the number of COs per chromosome arm. The application also allows for excluding sex chromosomes, thus restricting the analysis to autosomal chromosomes (Baier et al., 2014; Dumont, 2017). Moreover, the macro solves frequent practical issues by providing tools, for instance, to analyze overlapping SCs.

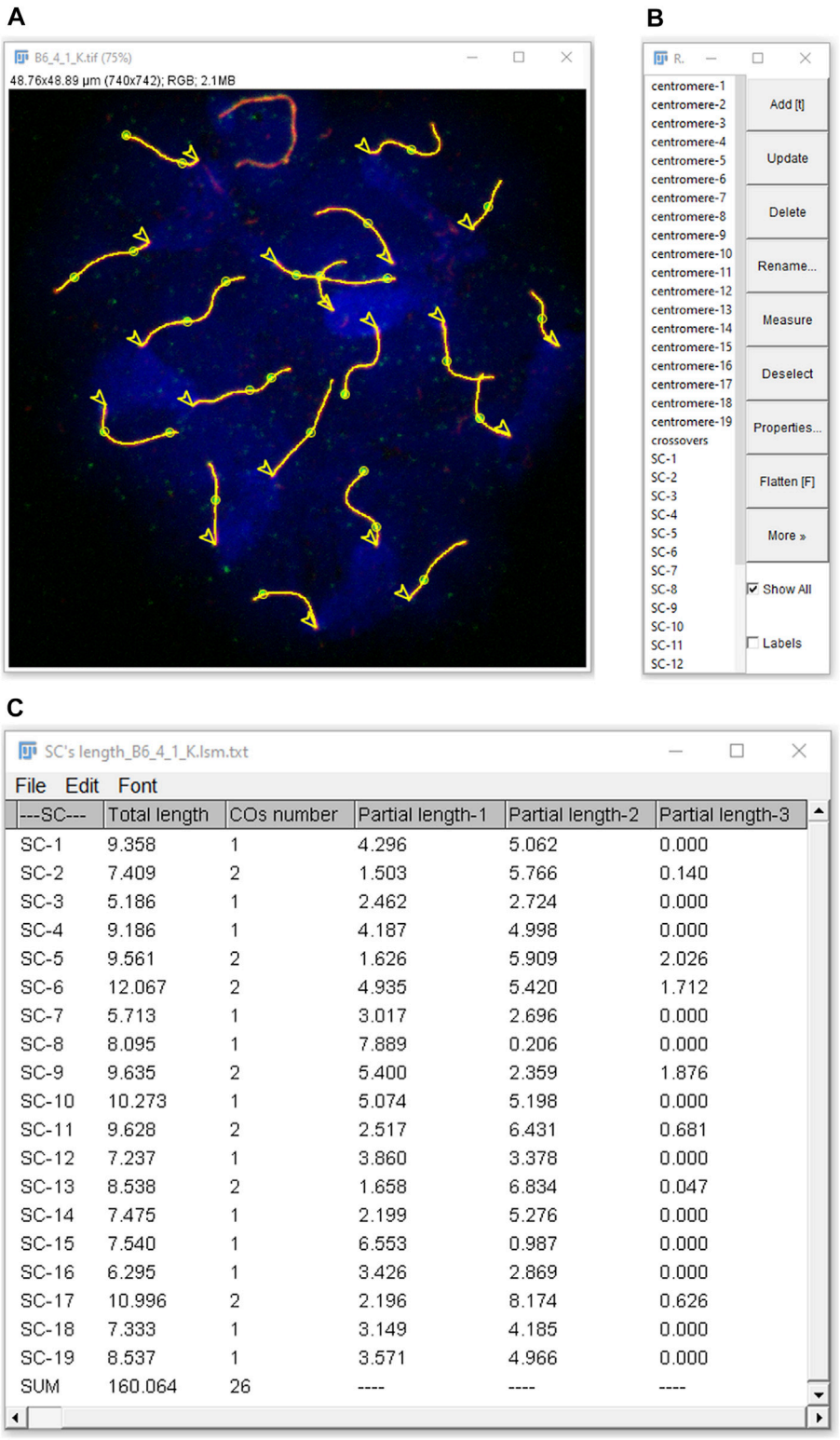

---SC---	Total length	COs number	Partial length-1	Partial length-2	Partial length-3
SC-1	9.358	1	4.296	5.062	0.000
SC-2	7.409	2	1.503	5.766	0.140
SC-3	5.186	1	2.462	2.724	0.000
SC-4	9.186	1	4.187	4.998	0.000
SC-5	9.561	2	1.626	5.909	2.026
SC-6	12.067	2	4.935	5.420	1.712
SC-7	5.713	1	3.017	2.696	0.000
SC-8	8.095	1	7.889	0.206	0.000
SC-9	9.635	2	5.400	2.359	1.876
SC-10	10.273	1	5.074	5.198	0.000
SC-11	9.628	2	2.517	6.431	0.681
SC-12	7.237	1	3.860	3.378	0.000
SC-13	8.538	2	1.658	6.834	0.047
SC-14	7.475	1	2.199	5.276	0.000
SC-15	7.540	1	6.553	0.987	0.000
SC-16	6.295	1	3.426	2.869	0.000
SC-17	10.996	2	2.196	8.174	0.626
SC-18	7.333	1	3.149	4.185	0.000
SC-19	8.537	1	3.571	4.966	0.000
SUM	160.064	26	----	----	----

FIGURE 3
Analysis results as displayed in FIJI. Detected elements (SCs, COs, centromeres and nucleus) can be selected in the ROI Manager **(B)** to be highlighted in the RGB image **(A)**. In this example, selecting "show all" displays everything (lines: SCs; circles: COs; arrow heads: centromeres, from which SC measurements start), except on the XY chromosomes (on the top), which were excluded from the analysis during the nucleus selection step. **(C)** Results are either global (sum of COs number and of total length of the SCs per nucleus) or SC-related: COs number per SC, total length of each SC and partial lengths from one SC end (centromeric, if selected as in the figure) to closest CO (partial length-1), between consecutive COs (if more than one) and between opposite SC end to closest CO (partial length-2, *etc.*).

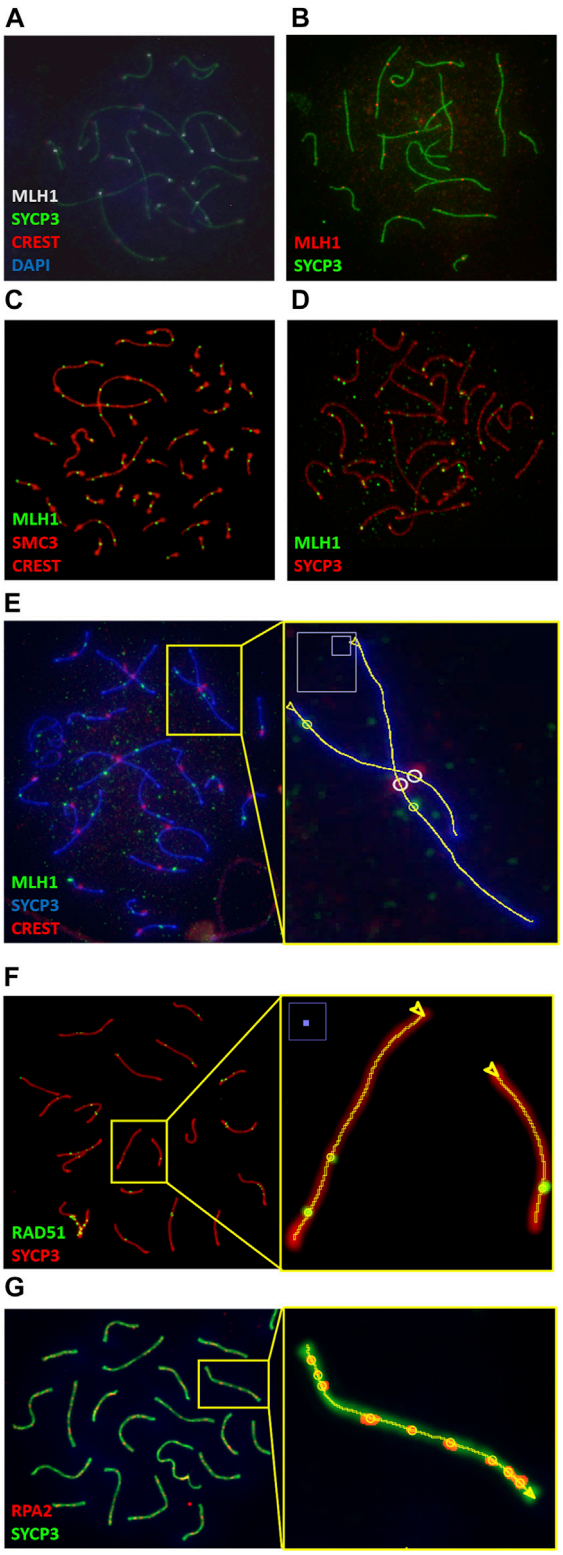

FIGURE 4
Synaptonemal & CO Analyzer is a versatile tool for the analysis of immunostained pachytene cells. Examples of image analyses from diverse vertebrates: **(A)** wild-captured house mice (*Mus musculus domesticus*) with Robertsonian translocations [courtesy of Cristina Marín and Aurora Ruiz-Herrera (Vara et al., 2021)]. **(B)** Matthey's mouse (*Mus matheyi*, courtesy of Jesus Page and Frederic Veyrunes); **(C)** chicken (*Gallus gallus*, courtesy of María Inés Pigozzi (del Priore and Pigozzi, 2020)); **(D)** Zebrafish (*Danio rerio*, courtesy of Yukiko Imai); **(E)** mongolian gerbil (*Meriones unguiculatus*, courtesy of Jesus Page), **(F, G)** nuclei from mouse inbred
(*Continued*)

Software requirements and limitations

The macro assumes that SCs are linear, COs and centromeres lay over SCs, and that the number of centromeres per SC is either one or none. These criteria allow to discriminate true from background foci and are optimal for the analysis of pachytene-stage cells, but not for other stages when SCs are not fully formed. The macro does not impose limits to image quality; however, poor stained materials and ill captured images limit results' quality and increase analysis' time. According to our experience, confocal microscopes deliver better results than conventional fluorescence ones, plan apochromatic objectives and close-emitting fluorochromes avoid signal mismatch due to lack of color aberration correction and meeting the Nyquist theorem assures optimal image resolution (Sanderson, 2020).

The macro relies on the Bio-Formats importer plugin to open many dozens of proprietary life science image formats (Linkert et al., 2010) besides the standard ones (tiff, jpeg, *etc.*). Up to seven channel images are supported; however, the macro is designed to analyze 2D images only. Users willing to analyze images with different planes need to collapse them on a single one. This might introduce changes on SCs' length and shape or cause too many SC overlaps as for the application to efficiently discriminate them. Therefore, the tool is not suitable for immunostained intact nuclei such as those employed in *C. elegans* recombination studies (Garcia-Muse, 2021). In other cases, the user should inspect the images to tell whether these changes occur and are relevant for the desired analysis. In contrast, 2D images with good chromosome spreads minimize the amount of SC overlapping and the macro analysis time and are, therefore, recommended.

Synaptonemal & CO analyzer provides reliable and fast CO and SC data

When comparing our new application with manual analyses using FIJI or Zen lite, similar results both in number of COs and in total autosomal SC length per cell (the sum of the length of all the SC, excluding the X and Y chromosomes) were obtained (p = 0.308 and p = 0.147, respectively, GLM). This indicates that the method of choice has no significant effect in the results, thus validating our application. However, when the duration of the complete analysis of COs and SCs was compared, a significant effect of the software of choice was observed ($p < 0.0001$, GLM). Bonferroni *post hoc* analyses revealed that Synaptonemal & CO Analyzer (7.1 ± 3.0 min, mean ± SD) is significantly faster (about two times quicker) than the rest (Zen lite: 13.7 ± 2.6 min, and FIJI: 15.9 ± 1.4 min) (Figure 2). The analysis time is variable depending on the quality of the image and the manual CO and SC corrections required; nevertheless, differences are clearly significant (Figure 2).

FIGURE 4 (Continued)
strains (*Mus musculus*) labeled with antibodies against RPA2 and RAD51 (courtesy of Parijat Chakraborty and Francesca Cole, and Jesus Page, respectively). **(E, F)** show magnified views of the elements detected by the macro in sections on the right. The software identifies SCs (lines), COs (yellow circles) and, when applicable, centromeres (white circles); arrow heads indicate the SC end from which SC measurements start. It performs well with diverse fluorochromes, central or distal centromeres stained with DAPI or CREST, and diverse antibodies for CO and SC identification.

Given the accuracy and speed of Synaptonemal & CO Analyzer, we have already successfully used it in a study performed by our group (Belmonte-Tebar et al., 2022)

Applicability: Synaptonemal & CO analyzer for the analysis of images immunostained with various antibodies and from diverse vertebrate species

Immunostaining of pachytene-stage chromosome spreads with MLH1 and SYCP3 antibodies and DAPI is a common technique for the study of recombination in diverse species. Our application is capable of successfully analyze such images in many vertebrates, including mammals with diverse karyotypes, birds and fish (Figure 4 and Supplementary Figure S1).

Recombination studies are also performed with other immunostaining methods. COs are one of the results of the repair of the hundreds of DSBs that occur at the beginning of meiosis. The progression of recombination intermediates can be examined by labeling proteins other than MLH1 (Hunter, 2015; Zickler and Kleckner, 2015; Gray and Cohen, 2016). The analysis of pachytene-stage nuclei images obtained with antibodies against some of these proteins, such as RAD51 and RPA2 (Cole et al., 2012; Gil-Fernandez et al., 2021), can benefit from the use of our macro as shown in Figure 4 and Supplementary Figure S1; these foci appear at earlier stages and significant presence at pachytene stage reflects a problem in DSB repair. In addition, the application also successfully analyzes images obtained with specific centromere markers (e.g., CREST serum), which are often employed in meiosis studies (Segura et al., 2013) (Figure 4 and Supplementary Figure S1). Centromere identification is not a requirement to obtain SC and CO data, but whether they are identified by DAPI or by CREST serum, centromeres can be used as SC measurement reference points.

In summary, Synaptonemal & CO analyzer is a versatile tool for recombination studies in vertebrate nuclei immunostained with diverse antibodies: it can be used in experiments analyzing SCs only, or SCs plus COs, and it will work with various stainings and antibodies. Unlike other applications (Peterson et al., 2019), it provides means to discriminate overlapping SCs and to exclude sex chromosomes from the analysis without further data loss. In addition, results can be easily verified: the software creates a results folder with an image, a table and a set of files. The results image contains the analyzed structures and merges all analyzed channels. The results table provides all relevant recombination meiotic studies' data. Finally, there is a file for all detected structures that allows for overlaying them to the results image, enabling visual inspection and verification (Figure 3).

Other advantages of the application

The macro has several additional advantages: 1) it is free, has been released under an open-source license (GNU General Public License), is accessible through stable public repositories (https://github.com/joaquim-soriano/Synaptonemal-and-CO-analyzer, https://zenodo.org) and has been assigned a DOI (https://zenodo.org/badge/latestdoi/410606632). 2) It is very intuitive and the learning process is facilitated by a user manual and video tutorials provided as Supplementary Material and at https://github.com/joaquim-soriano/Synaptonemal-and-CO-analyzer. Further support about ImageJ/FIJI can be received by using the wikis (ImageJ Information and Documentation Portal, n.d.; FIJI Software, n.d.) and mailing lists (ImageJ, n.d.; FIJI, n.d.) indicated in the bibliography. 3) It has been developed under ImageJ/FIJI (running on Java), which is free, open-source, well documented and ensures operative system compatibility (Windows and MacOS). It is also the most popular image analysis and processing software in biological science (Cardona and Tomancak, 2012; Eliceiri et al., 2012; Schindelin et al., 2012; Schneider et al., 2012). By using ImageJ scripting language, Synaptonemal & CO Analyzer can reach a large number of users that might get involved in further software's development.

Conclusion

Our application will facilitate studies about the genetic, epigenetic and environmental factors that affect the recombination rate and, hence, that can increase the frequency of chromosomal abnormalities and fertility problems. Among the environmental effects that affect recombination in mice, bisphenol A (an endocrine disruptor found in plastics used in a wide variety of consumer products) has been an object of study for a long time (Hunt et al., 2003; Susiarjo et al., 2007; Vrooman et al., 2015). These findings motivated us to search and identify a new effector, diet, in a study that was substantially accelerated by our application (Belmonte-Tebar et al., 2022). We continue successfully using it in our current research about recombination in male mice (Belmonte-Tebar et al., in preparation), proving that Synaptonemal & CO Analyzer performs very well, not only in a theoretical, controlled environment, but also with real complex data.

Synaptonemal & CO Analyzer meets an important need in the recombination field by providing an efficient and consistent tool for the analysis of SC length and COs number and distribution. Unlike other applications, it is free, hosted on an archivally stable platform, well documented and intuitive, runs in most computers and does not require computational skills or extensive training, thus facilitating usability (Carpenter et al., 2012), rigor and reproducibility of the analyses (Brito et al., 2020).

More importantly, the application facilitates the analysis of pachytene nuclei from diverse vertebrate species immunostained with different antibodies and centromere identification methods. In summary, Synaptonemal & CO Analyzer is a novel and versatile application tool for the study of recombination that is accessible for future improvements.

Data availability statement

The raw data supporting the conclusion of this article will be made available by the authors, without undue reservation.

Ethics statement

The animal study was reviewed and approved by the Committee of Ethics in Animal Care of the University of Castilla-La Mancha.

The animal study was performed previously, but some of the images have been used in the present article to test and validate the software.

Author contributions

EC-E and JS designed the study. JS developed the application under the instructions of EC-E and the requests of AB-T. Efficiency validation with a set of images was performed by AB-T, flexibility validation was performed by JS and the results were analyzed and checked by EC-E. EC-E and JS wrote the manuscript. AB-T reviewed it and EC-E edited it. AB-T and JS generated the instructions manual and video tutorial and EC-E reviewed them. All authors read and approved the final manuscript.

Acknowledgments

We thank Izchel Loyo Navarrete for testing the initial versions of this software. We are also very thankful to all the researchers who generously donated images, as indicated in Materials and Methods.

Conflict of interest

The authors declare that the research was conducted in the absence of any commercial or financial relationships that could be construed as a potential conflict of interest.

Publisher's note

Supplementary material

The Supplementary Material for this article can be found online at: https://www.frontiersin.org/articles/10.3389/fcell.2023.1005145/full#supplementary-material

References

Anderson, L. K., Reeves, A., Webb, L. M., and Ashley, T. (1999). Distribution of crossing over on mouse synaptonemal complexes using immunofluorescent localization of MLH1 protein. *Genetics* 151 (4), 1569–1579. doi:10.1093/genetics/151.4.1569

Baier, B., Hunt, P., Broman, K. W., and Hassold, T. (2014). Variation in genome-wide levels of meiotic recombination is established at the onset of prophase in mammalian males. *PLoS Genet.* 10 (1), e1004125. doi:10.1371/journal.pgen.1004125¥

Baker, S. M., Plug, A. W., Prolla, T. A., Bronner, C. E., Harris, A. C., Yao, X., et al. (1996). Involvement of mouse Mlh1 in DNA mismatch repair and meiotic crossing over. *Nat. Genet.* 13 (3), 336–342. doi:10.1038/ng0796-336

Belmonte-Tebar, A., San Martin Perez, E., Nam Cha, S., Soler Valls, A. J., Singh, N. D., and de la Casa-Esperon, E. (2022). Diet effects on mouse meiotic recombination: A warning for recombination studies. *Genetics* 220 (1), iyab190. doi:10.1093/genetics/iyab190

Brito, J. J., Li, J., Moore, J. H., Greene, C. S., Nogoy, N. A., Garmire, L. X., et al. (2020). Recommendations to enhance rigor and reproducibility in biomedical research. *Gigascience* 9 (6), giaa056–6. doi:10.1093/gigascience/giaa056

Cardona, A., and Tomancak, P. (2012). Current challenges in open-source bioimage informatics. *Nat. Methods* 9 (7), 661–665. doi:10.1038/nmeth.2082

Carpenter, A. E., Kamentsky, L., and Eliceiri, K. W. (2012). A call for bioimaging software usability. *Nat. Methods* 9 (7), 666–670. doi:10.1038/nmeth.2073

Cole, F., Kauppi, L., Lange, J., Roig, I., Wang, R., Keeney, S., et al. (2012). Homeostatic control of recombination is implemented progressively in mouse meiosis. *Nat. Cell Biol.* 14 (4), 424–430. doi:10.1038/ncb2451

de Boer, E., Lhuissier, F. G., and Heyting, C. (2009). Cytological analysis of interference in mouse meiosis. *Methods Mol. Biol.* 558, 355–382. doi:10.1007/978-1-60761-103-5_21

del Priore, L., and Pigozzi, M. I. (2020). MLH1 focus mapping in the Guinea fowl (*Numida meleagris*) give insights into the crossover landscapes in birds. *PLoS ONE* 15 (10), e0240245. doi:10.1371/journal.pone.0240245

Dumont, B. L. (2017). Variation and evolution of the meiotic requirement for crossing over in mammals. *Genetics* 205 (1), 155–168. doi:10.1534/genetics.116.192690

Eliceiri, K. W., Berthold, M. R., Goldberg, I. G., Ibañez, L., Manjunath, B. S., Martone, M. E., et al. (2012). Biological imaging software tools. *Nat. Methods* 9 (7), 697–710. doi:10.1038/nmeth.2084

Enguita-Marruedo, A., Sleddens-Linkels, E., Ooms, M., de Geus, V., Wilke, M., Blom, E., et al. (2019). Meiotic arrest occurs most frequently at metaphase and is often incomplete in azoospermic men. *Fertil. Steril.* 112 (6), 1059–1070. doi:10.1016/j.fertnstert.2019.08.004

FIJI (2022a). Fiji is just imageJ. Available at: https://fiji.sc/(Accessed June 22, 2022).

FIJI (2022b). Software. Available at: https://imagej.net/software/fiji/(Accessed June 22, 2022).

Froenicke, L., Anderson, L. K., Wienberg, J., and Ashley, T. (2002). Male mouse recombination maps for each autosome identified by chromosome painting. *Am. J. Hum. Genet.* 71 (6), 1353–1368. doi:10.1086/344714

Garcia-Muse, T. (2021). Detection of DSBs in *C. elegans* meiosis. *Methods Mol. Biol.* 2153, 287–293. doi:10.1007/978-1-0716-0644-5_20

Gil-Fernandez, A., Ribagorda, M., Martín-Ruiz, M., López-Jiménez, P., Laguna, T., Gómez, R., et al. (2021). Meiotic behavior of achiasmate sex chromosomes in the african pygmy mouse *Mus mattheyi* offers new insights into the evolution of sex chromosome pairing and segregation in mammals. *Genes* 12, 1434. doi:10.3390/genes12091434

Gray, S., and Cohen, P. E. (2016). Control of meiotic crossovers: From doublestrand break formation to designation. *Annu. Rev. Genet.* 50, 175–210. doi:10.1146/annurev-genet-120215-035111

Handel, M. A., and Schimenti, J. C. (2010). Genetics of mammalian meiosis: Regulation, dynamics and impact on fertility. *Nat. Rev. Genet.* 11 (2), 124–136. doi:10.1038/nrg2723

Hassold, T., and Hunt, P. (2001). To err (meiotically) is human: The Genesis of human aneuploidy. *Nat. Rev. Genet.* 2 (4), 280–291. doi:10.1038/35066065

Henderson, I. R., and Bomblies, K. (2021). Evolution and plasticity of genome-wide meiotic recombination rates. *Annu. Rev. Genet.* 55, 23–43. doi:10.1146/annurev-genet-021721-033821

Hunt, P. A., Koehler, K. E., Susiarjo, M., Hodges, C. A., Ilagan, A., Voigt, R. C., et al. (2003). Bisphenol a exposure causes meiotic aneuploidy in the female mouse. *Curr. Biol.* 13 (7), 546–553. doi:10.1016/s0960-9822(03)00189-1

Hunter, N. (2015). Meiotic recombination: The essence of heredity. *Cold Spring Harb. Perspect. Biol.* 7, a016618. doi:10.1101/cshperspect.a016618

ImageJ Docs (2022). Conferences. Available at: https://imagej.net/events/conferences (Accessed June 22, 2022).

ImageJ (2022). Image processing and analysis in java. Available at: https://imagej.nih.gov/ij/(Accessed June 22, 2022).

ImageJ Information and Documentation Portal (2022). Welcome to the ImageJ information and documentation portal. Available at: https://imagejdocu.list.lu/ (Accessed June 22, 2022).

Imai, Y., Olaya, I., Sakai, N., and Burgess, S. M. (2021). Meiotic chromosome dynamics in zebrafish. *Front. Cell Dev. Biol.* 9, 757445. doi:10.3389/fcell.2021.757445

Karopka, T., Schmuhl, H., and Demski, H. (2014). Free/libre open source software in health care: A review. *Healthc. Inf. Res.* 20 (1), 11–22. doi:10.4258/hir.2014.20.1.11

Kleckner, N. (2006). Chiasma formation: chromatin/axis interplay and the role(s) of the synaptonemal complex. *Chromosoma* 115 (3), 175–194. doi:10.1007/s00412-006-0055-7

Koehler, K. E., Boulton, C. L., Collins, H. E., French, R. L., Herman, K. C., Lacefield, S. M., et al. (1996). Spontaneous X chromosome MI and MII nondisjunction events in *Drosophila melanogaster* oocytes have different recombinational histories. *Nat. Genet.* 14 (4), 406–414. doi:10.1038/ng1296-406

Lamb, N. E., Freeman, S. B., Savage-Austin, A., Pettay, D., Taft, L., Hersey, J., et al. (1996). Susceptible chiasmate configurations of chromosome 21 predispose to non-disjunction in both maternal meiosis I and meiosis II. *Nat. Genet.* 14 (4), 400–405. doi:10.1038/ng1296-400

Landini, G. (2008). "Advanced shape analysis with ImageJ," in Proceedings of the Second ImageJ User and Developer Conference, Luxembourg, 6-7 Nov 2008, 116–121.

Linkert, M., Rueden, C. T., Allan, C., Burel, J. M., Moore, W., Patterson, A., et al. (2010). Metadata matters: Access to image data in the real world. *J. Cell Biol.* 189 (5), 777–782. doi:10.1083/jcb.201004104

Martin, A. C., Shaw, P., Phillips, D., Reader, S., and Moore, G. (2014). Licensing MLH1 sites for crossover during meiosis. *Nat. Commun.* 5, 4580. doi:10.1038/ncomms5580

Mather, K. (1937). The determination of position in crossing-over. II. The chromosome length-chiasma frequency relation. *Cytologia* 1, 514–526. doi:10.1508/cytologia.fujiijubilaei.514

Milano, C. R., Holloway, J. K., Zhang, Y., Jin, B., Smith, C., Bergman, A., et al. (2019). Mutation of the ATPase domain of MutS homolog-5 (MSH5) reveals a requirement for a functional MutSγ complex for all crossovers in mammalian meiosis. *G3 (Bethesda)* 9 (6), 1839–1850. doi:10.1534/g3.119.400074

Muller, H. J. (1916). The mechanism of crossing-over. IV. *Am. Nat.* 50, 421–434. 193–221, 284–305, 350–366. doi:10.1086/279553

Notter, D. R. (1999). The importance of genetic diversity in livestock populations of the future. *J. Anim. Sci.* 77 (1), 61–69. doi:10.2527/1999.77161x

OME (2022). The open microscopy environment-OME. Available at: http://www.openmicroscopy.org/(Accessed June 22, 2022).

Peterson, A. L., Miller, N. D., and Payseur, B. A. (2019). Conservation of the genome-wide recombination rate in white-footed mice. *Hered. (Edinb)* 123 (4), 442–457. doi:10.1038/s41437-019-0252-9

Prevedello, L., and Khorasani, R. (2012). Should you use open-source software applications in your practice? *J. Am. Coll. Radiol.* 9 (10), 751–752. doi:10.1016/j.jacr.2012.06.033

Sanderson, J. (2020). Fundamentals of microscopy. *Curr. Protoc. Mouse Biol.* 10 (2), e76. doi:10.1002/cpmo.76

Schindelin, J., Arganda-Carreras, I., Frise, E., Kaynig, V., Longair, M., Pietzsch, T., et al. (2012). Fiji: An open-source platform for biological-image analysis. *Nat. Methods* 9 (7), 676–682. doi:10.1038/nmeth.2019

Schneider, C. A., Rasband, W. S., and Eliceiri, K. W. (2012). NIH image to ImageJ: 25 years of image analysis. *Nat. Methods* 9 (7), 671–675. doi:10.1038/nmeth.2089

Segura, J., Ferretti, L., Ramos-Onsins, S., Capilla, L., Farre, M., Reis, F., et al. (2013). Evolution of recombination in eutherian mammals: Insights into mechanisms that affect recombination rates and crossover interference. *Proc. Biol. Sci.* 280 (1771), 20131945. doi:10.1098/rspb.2013.1945

Sternberg, S. R. (1983). Biomedical image processing. *IEEE Comput.* 16 (1), 22–34. doi:10.1109/MC.1983.1654163

Sturtevant, A. H. (1915). The behavior of the chromosomes as studied through linkage. *Z Indukt. Abstammungs- Vererbungslehre* 13, 234–287. doi:10.1007/bf01792906

Susiarjo, M., Hassold, T. J., Freeman, E., and Hunt, P. A. (2007). Bisphenol A exposure *in utero* disrupts early oogenesis in the mouse. *PLoS Genet.* 3 (1), e5. doi:10.1371/journal.pgen.0030005

Swedlow, J. R., and Eliceiri, K. W. (2009). Open source bioimage informatics for cell biology. *Trends Cell Biol.* 19 (11), 656–660. doi:10.1016/j.tcb.2009.08.007

Sym, M., and Roeder, G. S. (1994). Crossover interference is abolished in the absence of a synaptonemal complex protein. *Cell* 79 (2), 283–292. doi:10.1016/0092-8674(94)90197-x

Vara, C., Paytuvi-Gallart, A., Cuartero, Y., Alvarez-Gonzalez, L., Marin-Gual, L., Garcia, F., et al. (2021). The impact of chromosomal fusions on 3D genome folding and recombination in the germ line. *Nat. Comm.* 12 (1), 2981. doi:10.1038/s41467-021-23270-1

Vrooman, L. A., Oatley, J. M., Griswold, J. E., Hassold, T. J., and Hunt, P. A. (2015). Estrogenic exposure alters the spermatogonial stem cells in the developing testis, permanently reducing crossover levels in the adult. *PLoS Genet.* 11 (1), e1004949. doi:10.1371/journal.pgen.1004949

Wang, R. J., Dumont, B. L., Jing, P., and Payseur, B. A. (2019). A first genetic portrait of synaptonemal complex variation. *PLoS Genet.* 15 (8), e1008337. doi:10.1371/journal.pgen.1008337

Zickler, D., and Kleckner, N. (2015). Recombination, pairing, and synapsis of homologs during meiosis. *Cold Spring Harb. Perspect. Biol.* 7 (6), a016626. doi:10.1101/cshperspect.a016626

frontiers | Frontiers in Cell and Developmental Biology

TYPE Original Research
PUBLISHED 06 February 2023
DOI 10.3389/fcell.2023.1098468

OPEN ACCESS

EDITED BY
Pedro A. San-Segundo,
CSIC-University of Salamanca, Spain

REVIEWED BY
Ofer Rog,
The University of Utah, United States
Amy MacQueen,
Wesleyan University, United States

*CORRESPONDENCE
Jennifer C. Fung,
jennifer.fung@ucsf.edu

SPECIALTY SECTION
This article was submitted to Nuclear Organization and Dynamics, a section of the journal Frontiers in Cell and Developmental Biology

RECEIVED 15 November 2022
ACCEPTED 19 January 2023
PUBLISHED 06 February 2023

CITATION
Pollard MG, Rockmill B, Oke A, Anderson CM and Fung JC (2023), Kinetic analysis of synaptonemal complex dynamics during meiosis of yeast *Saccharomyces cerevisiae* reveals biphasic growth and abortive disassembly. *Front. Cell Dev. Biol.* 11:1098468. doi: 10.3389/fcell.2023.1098468

Kinetic analysis of synaptonemal complex dynamics during meiosis of yeast *Saccharomyces cerevisiae* reveals biphasic growth and abortive disassembly

Michael G. Pollard, Beth Rockmill, Ashwini Oke, Carol M. Anderson and Jennifer C. Fung*

Department of Obstetrics, Gynecology and Reproductive Sciences, Center of Reproductive Sciences, University of California, San Francisco, San Francisco, CA, United States

The synaptonemal complex (SC) is a dynamic structure formed between chromosomes during meiosis which stabilizes and supports many essential meiotic processes such as pairing and recombination. In budding yeast, Zip1 is a functionally conserved element of the SC that is important for synapsis. Here, we directly measure the kinetics of Zip1-GFP assembly and disassembly in live cells of the yeast *S. cerevisiae*. The imaging of SC assembly in yeast is challenging due to the large number of chromosomes packed into a small nucleus. We employ a *zip3Δ* mutant in which only a few chromosomes undergo synapsis at any given time, initiating from a single site on each chromosome, thus allowing the assembly and disassembly kinetics of single SCs to be accurately monitored in living cells. SC assembly occurs with both monophasic and biphasic kinetics, in contrast to the strictly monophasic assembly seen in *C. elegans*. In wild-type cells, once maximal synapsis is achieved, programmed final disassembly rapidly follows, as Zip1 protein is actively degraded. In *zip3Δ*, this period is extended and final disassembly is prolonged. Besides final disassembly, we found novel disassembly events involving mostly short SCs that disappeared in advance of programmed final disassembly, which we termed "abortive disassembly." Abortive disassembly is distinct from final disassembly in that it occurs when Zip1 protein levels are still high, and exhibits a much slower rate of disassembly, suggesting a different mechanism for removal in the two types of disassembly. We speculate that abortive disassembly events represent defective or stalled SCs, possibly representing SC formation between non-homologs, that is then targeted for dissolution. These results reveal novel aspects of SC assembly and disassembly, potentially providing evidence of additional regulatory pathways controlling not just the assembly, but also the disassembly, of this complex cellular structure.

KEYWORDS

synaptonemal complex, meiosis, Zip1, Zip3, yeast, synapsis, *in vivo* microscopy, polymer dynamics

Introduction

Meiosis is a crucial part of gametogenesis in sexually reproducing organisms. The meiotic program is unique in that replicated chromosomes find and align lengthwise along their homologous partners, exchange genetic material, and then segregate twice, resulting in haploid gametes. The pairwise alignment of homologous chromosomes ensures that genetic exchange will occur between homologs. Crossovers, or reciprocal genetic exchanges, result in physical connections between the chromosome pairs that serve to align them for proper segregation. The synaptonemal complex (SC) is the protein matrix that forms along the lengths of homologs and is thought to stabilize the paired homologs and regulate the number of recombination events that occur along the length of chromosomes (Lake and Hawley, 2021). The SC is composed of lateral elements, formed along each replicated homolog, and a central region of ordered proteins that unite these axes. The central region of the SC, but not the axes, appears to have fluid-like properties in both yeast and worms (Rog et al., 2017), where the weakly-bonded proteins can move around within the structure. The assembly of the SC is a dynamic process that appears to be aided by the pulling of chromosome ends from outside the nucleus using a connection of the chromosome to the nuclear envelope *via* the LINC complex and either microtubules or actin fibers to pull them (Alleva and Smolikove, 2017). Disassembly of the SC is coordinated with the resolution of connections between the chromosomes, and its timing is subject to cell cycle regulation (Hochwagen and Amon, 2006; Jordan et al., 2009). Since failures in meiosis can lead to infertility, miscarriages and potentially developmental problems in offspring, it is important to gain a better understanding of SC assembly and disassembly. Moreover, formation of the SC is a massive feat of molecular self-assembly, whose mechanism may hold lessons for other large-scale assembly processes in the cell.

There are three identified central region proteins in yeast. Zip1, a major component of the SC central region, is a structurally-conserved protein that was first identified in yeast (Sym et al., 1993). Zip1 and functionally analogous proteins in mice, worms, plants and mammals consist of a long coiled-coil filament with unstructured domains at either end (Page and Hawley, 2004). These transverse filaments, through the interactions of their central coiled-coil region are thought to form N-terminal tetrameric building blocks that self-assemble into the SC with the C-terminal regions interacting with the lateral elements (Dong and Roeder, 2000; Dunce et al., 2018). This configuration and the length of the coiled coil are responsible for the conserved 100 nm width of the SC (Sym and Roeder, 1995). GFP-tags inserted in the middle of Zip1 and its homologs (White et al., 2004) have been widely used to visualize chromosome dynamics during meiosis, including rapid telomere-led movements (Koszul et al., 2008) and SC fluidity (Rog et al., 2017). The other two identified central region proteins are Ecm11 and Gmc2 which facilitate the assembly of Zip1 (Humphryes et al., 2013). Gcm2 promotes the sumoylation of Ecm11 by the E3 SUMO ligases, Siz1 and Siz2 (Leung et al., 2015). The Zip1, at the N-terminus, activates the further sumoylation of Ecm11 and this positive feedback loop forms the SC (Leung et al., 2015). Voelkel-Meiman et al. (2012) using additional copies of *ZIP1* demonstrated a positive correlation between the concentration of Zip1 and speed of synapsis onset.

The initiation of SC formation appears to occur at either of two locations: 1) presumptive crossover sites and/or 2) specific chromosome domains. In budding yeast, sites of genetic exchange accumulate proteins that attract components important for SC initiation (Chua and Roeder, 1998; Agarwal and Roeder, 2000; Tsubouchi et al., 2006; Pyatnitskaya et al., 2022). A subset of these sites is likely to be responsible for most SC initiations. Yeast centromeres are also sites of SC initiation in which centromeres appear to be among the first regions to accumulate SC proteins and to initiate SC formation (Tsubouchi et al., 2008). SC initiation at centromeres is licensed only after recombination has initiated (Macqueen and Roeder, 2009). In organisms that do not rely on recombination to engage homologous chromosomes, special chromosomal sites are used to pair and initiate synapsis. In the nematode *C. elegans*, the pairing centers are present on one end of each chromosome and are responsible for assembling SC along the homologs. In this case, SC formation is independent of recombination (Dernburg et al., 1998). In the fly, *D. melanogaster*, SC initiation occurs at centromeres and is also independent of recombination (Takeo et al., 2011; Tanneti et al., 2011).

In nematode oocytes, chromosomes initiate SC formation at the end of the chromosome where the pairing center resides, and rapidly and irreversibly complete the SC (Rog and Dernburg, 2015). The rate of SC assembly is 150 nm/min. The nematode's six chromosomes initiate synapsis independently and stochastically, completing synapsis within 5 hours as nuclei pass through the transition zone. Movements of the chromosomes by dynein aid the extension of the SC, since Sun mutants that reduce dynein-directed chromosome motion cause a severe reduction in the rate of assembly (34 nm/min). Since *C. elegans* is the only organism so far in which SC kinetics have been measured, the question remains whether SC kinetics show similar behavior in organisms such as yeast and humans, which rely on recombination for synapsis to occur.

In budding yeast, it is difficult to visualize SC kinetics due to the large number of chromosomes in a small nucleus; there are 16 pairs of chromosomes in a ~2.0 µm diameter nucleus. Fission yeast has only three chromosomes, but fission yeast does not form SC (Bähler et al., 1993). However, the reduced number of synapsed chromosomes in the *zip3Δ* mutant in budding yeast could allow the tracking of SC kinetics. Zip3 is an E3 ubiquitin ligase for which orthologs have been found in many diverse organisms (Agarwal and Roeder, 2000; Jantsch et al., 2004; Chelysheva et al., 2012). Whereas mutants in the *ZIP3* gene in most organisms appear to affect crossover formation, yeast mutants additionally exhibit a reduction in synapsis initiation (Agarwal and Roeder, 2000). When *ZIP3* is deleted, SC initiation occurs predominantly at the centromere and fewer chromosomes form SC (Macqueen and Roeder, 2009).

Here, we take advantage of the reduced number of synapsing chromosomes and initiation sites in the *zip3Δ* mutant to permit the measurement of the real-time kinetics of both assembly and disassembly of the SC on individual chromosomes in yeast. We find that SC assembly in budding yeast occurs by a monotonic increase in length, similar to that observed in *C. elegans*, but that the rate of assembly in yeast is on average about half the rate observed in the nematode. We show that both monophasic and biphasic growth rates are observed, unlike the dynamics in the nematode. The biphasic growth consists of an initial fast rate followed by a slower rate to complete assembly. Final disassembly exhibits a monophasic rate of disassembly. Finally, we uncover a process that we term "abortive SC disassembly" which is distinct from final SC disassembly, in which SCs depolymerize before the cell completes the SC assembly phase. We

propose that abortive SC disassembly may represent the dissolution of defective/non-productive or non-homologous SCs. We suggest that this is a mechanism that the cell might employ to correct synapsis or to resolve interlocks before interactions between chromosomes are cemented in place.

Materials and methods

Meiotic time course and detection of SCs

For all strains, meiosis was induced by first growing the cells in 2 mL of YPD supplemented with 1.0 mM adenine, and incubating in a roller drum at 30°C for exactly 24 h, then isolating cells by centrifugation and transferring to 10 mL of 2% potassium acetate in 125 mL flasks at 30°C on a platform shaker at 230 rpm. Cells were then harvested at defined time points, and prepared for live microscopy by concentrating harvested cells in sporulation media and then centrifuging them onto a Concanavalin A-treated dish environmental chamber (Bioptechs Inc. # 04200415C, Butler, PA) in the well of a silicone gasket (Grace Bio-Labs #CWCS 50R-1.0, Bend, OR). Cells in the Bioptechs dish were then mounted on an OMX microscope (Dobbie et al., 2011) at 30°C and viewed using a heated objective (×100 Olympus 1.45 NA oil immersion at 30°). Details for live cell imaging can be found in Pollard and Fung (2017).

Zip1-GFP and synapsed chromosomes were detected in a 50 nm window centered at 525 nm using an excitation frequency of 488. The excitation laser was attenuated to 3.5% or 0.86% and individual exposures were 5 ms. Images were acquired in 4 or 10 μm z-stacks with 0.2 μm intervals between sections. The post-acquisition processing of imaged nuclei involved concatenation of all time points, denoising (Boulanger et al., 2010), and deconvolution. Image screening and manipulation, as well as the quantitation of Zip1-GFP signal and the measurement of synaptonemal complex lengths, were performed using PRIISM software (Chen et al., 1992). Automated SC tracing and kinetic measurements were performed using scripts written with MATLAB (Mathworks, Natick MA), although manual tracing of SCs was also performed in PRIISM. 2D projections are either overlaid maximum and summation (max-sum) projections in Z (axial dimension of microscopy) or triple overlays, in which an additional overlay was made with an inverted background and scaled differentially in order to display the nuclear boundary defining the diffuse Zip1-GFP in blue.

Chromosome spreads, FISH and immunostaining

Chromosome spreads were performed as described previously (Fung et al., 2004). Fluorescent *in situ* hybridization (FISH) was carried out using two adjacent interval-specific DNA probes. For the *LEU2-MAT* interval, the plasmid 12B (Newlon et al., 1991) containing a 20-kb region of chromosome III extending ~5 kb centromere-distal and ~15 kb centromere-proximal of the *RPS14A* gene was used to make probe. For the *HIS4-LEU2* interval, a 15-kb region starting at *HIS4* and ending in the middle of *KCC4* was PCR-amplified from genomic DNA in 2-kb segments. Probes were labeled with biotin-14-dATP (Invitrogen # 19524016, Waltham, MA) or digoxygenin-11-dUTP (Roche #11093088910, Basel, CH) and hybridization was performed as described in Dernburg and Sedat (Dernburg and Sedat, 1998). Slides were stained with anti-rabbit Zip1 antibody and then with secondary antibodies: rhodamine anti-DIG and FITC-streptavidin and Cy5 anti-rabbit antibody. To stain DNA, 1 μg/mL DAPI was added to the mount made from 0.1% p-phenylenediamine (Sigma Aldrich #P6001, Burlington, MA) in glycerol. Zip1 polyclonal antibodies were generously provided by G.S. Roeder (Yale University).

Sporulation frequency

Log-phase cultures in YPAD were transferred to 10 mL of 2% potassium acetate and then shaken in a flask at 30° for 5 days. Cell samples were then prepared on slides and visualized with 3D bright-field microscopy on the OMX microscope. The number of spores present in each cell within the bright field image volume was tabulated.

Spore viability

Diploids were patched to 2% potassium acetate plates and grown at 30°C for 3 days. Tetrads were dissected onto YPD plates. The frequency of viable spores was determined after 3 days of growth at 30°C.

Model fitting, adjusted R-square and PRESS statistics

Segmented regression and press statistic calculations for assembly, final disassembly and abortive disassembly rates were performed using R. Code was adapted from https://gist.github.com/tomhopper/8c204d978c4a0cbcb8c0 and https://cran.r-project.org/web/packages/segmented/segmented.pdf.

Calculation of expected frequency of multiple initiation

Based on the Poisson distribution, we can calculate the probability of seeing k number of initiations with an average number of events, λ.

$$f(k,\lambda) = P(k) = \frac{\lambda^k e^{-\lambda}}{k!}$$

The frequency of seeing ≥ 2 initiations is $f\ (\geq 2) = 1 - f(0) - f(1)$. Using a binomial test calculator, the probability of not seeing ≥ 2 initiations after n number of observations can be calculated using n; $f\ (\geq 2)$.

Results

In vivo visualization of single chromosome synapsis in *zip3Δ* during meiosis

To visualize synapsis of chromosomes in yeast, we performed three-dimensional (3D) time-lapse studies of the synapsis protein

10.3389/fcell.2023.1098468

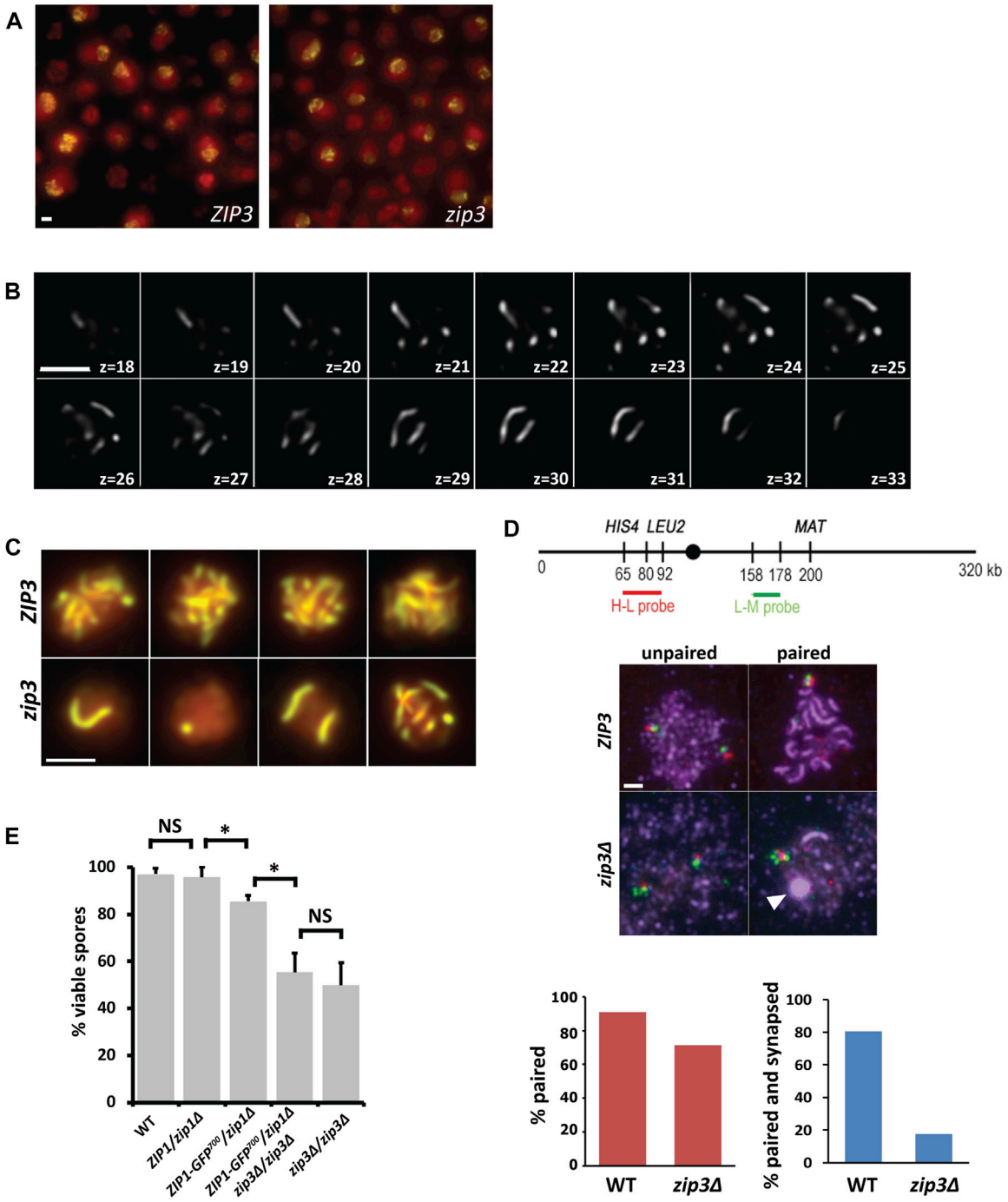

FIGURE 1
zip3Δ improves visualization of synapsis. **(A)** Example of a typical acquisition field of WT (left panel) and *zip3Δ* (right panel) *in vivo* yeast cells expressing Zip1-GFP undergoing meiosis (14 h after meiotic induction) shown as a 2D max-sum projection. Zip1-GFP on synapsed chromosomes is shown in yellow. Nuclei are defined by overall nuclear Zip1-GFP signal shown in red. These images are not for quantitative intensity comparisons. **(B)** z-slices every 0.2 µm from 3D image stack of a nucleus containing 9 Zip1-GFP SCs in a zip3. mutant after denoising and deconvolution. **(C)** 2D max-sum projections of pachytene nuclei expressing Zip1-GFP in ZIP3 (top panel) compared to the equivalent stage in zip3. (bottom panel). Scale bar—2 µm. **(D)** Top panel. Map of FISH probes made to the *HIS4-LEU2* region (H-L probe) and to the *LEU2-MAT* region (L-M probe) on chromosome III. Middle panel. WT and *zip3Δ* pachytene chromosome spreads hybridized with H-L probes (red) and L-M probes (green) and stained with anti-Zip1 antibodies (purple) for WT and *zip3Δ* (middle panel). The white arrowhead indicates a polycomplex. Scale bar 2 µm. Bottom Panel. Red graph shows the percent of HL and LM FISH probes colocalizing for WT (n = 33) and *zip3Δ* (n = 40). The blue graph shows percent of colocalized probes that are within synapsed regions for WT and *zip3Δ*. **(E)** Histogram of the percent of viable spores for each genotype. For each genotype, between 120–170 tetrads were dissected. A z-test for proportions was used to test for significance (*). Z = 5.64, $p < 0.00001$ between *ZIP1/zip1Δ* and *ZIP1-GFP/zip1Δ*. Z = 5.62 $p < 0.00001$ between *ZIP1-GFP/zip1Δ* and *ZIP1-GFP/zip1Δ zip3Δ/zip3Δ*. NS—not significant. Error bars—STD.

Zip1 fused to GFP (Zip1-GFP^{700}) in a meiosis-proficient diploid yeast strain (BR 1919-8B) (see Materials and Methods). We constructed a *zip3Δ* mutation in this background to assess SC assembly and disassembly kinetics for individual chromosomes more easily (Figure 1). In *zip3Δ*, the maximal number of synapsed chromosomes attained varies from 0 to 16 chromosomes (Agarwal and Roeder, 2000; MacQueen and Roeder, 2009) (Figures 1A,B). This aspect of the *zip3Δ* mutant strain allows us to monitor synapsis kinetics in nuclei containing only one or two synapsing chromosomes (Figure 1C). Additionally, the use of the *zip3Δ* mutant reduces the complication of interpreting synapsis that normally would start at multiple sites along the chromosome, since ~85% of synapsis initiates exclusively from centromeres (Macqueen and Roeder, 2009). Despite the reduced extent of synapsis in *zip3Δ*, a high level of pairing is achieved, as measured using a pair of adjacent FISH loci on chromosome III in pachytene chromosome spreads (Figure 1D). These results agree with a prior study of centromere-associated lacO pairing in *zip3Δ* (Voelkel-Meiman et al., 2019). By simultaneously measuring pairing (association of both FISH loci) and synapsis (Zip1 immunofluorescence along chromosomes), we found that the paired loci were only associated with synapsis 17.5% of the time in *zip3Δ* compared to WT (80%) (Figure 1D). Together, these results suggest that a high level of pairing does not ensure high levels of synapsis, and conversely that synapsis is not necessary for high levels of pairing. This ability to align without subsequent synapsis likely contributes to the relatively high spore viability of the *zip3Δ* mutant (50%–58%, ((Macqueen and Roeder, 2009), Figure 1E).

As seen in Figure 1, the *zip3Δ* mutant often forms a polycomplex during pachytene (Figure 1D, last panel, white arrowhead). In the BR background, polycomplexes are aggregates of synapsis-associated proteins that form when the stoichiometry of SC proteins is disrupted, as in the case of various meiotic mutants or with altered expression of meiotic proteins (Sym and Roeder, 1995; Chua and Roeder, 1998). Other organisms and other yeast strains such as SK1 may form polycomplexes in the context of wild-type meiosis, either as a prelude to SC formation or as SCs dissolve (Hughes and Hawley, 2020). The formation of SC is difficult to visualize quantitatively when two copies of the *ZIP1-GFP^{700}* allele reside in a *zip3Δ* background, since the polycomplex is about five times brighter than the synapsing chromosomes. By incorporating a single copy of *ZIP1-GFP^{700}* into a *zip3Δ* diploid whose endogenous copies of *ZIP1* are deleted, the frequency of polycomplex formation was reduced to only 2.2% of nuclei compared to 100% when both copies of *ZIP1-GFP^{700}* are present. In the BR background, only a small difference in spore viability is seen when using hemizygous *ZIP1-GFP^{700}* (85%) in place of hemizygous *ZIP1* (96%). No difference in spore viability is observed between *zip3Δ* strains containing either *ZIP1* allele (Figure 1E), suggesting that replacing *ZIP1* with *ZIP1-GFP* and reducing the copy number of *ZIP1-GFP* has only a minor impact on meiosis. With these strain modifications in place, kinetic measurements of individual SCs are feasible.

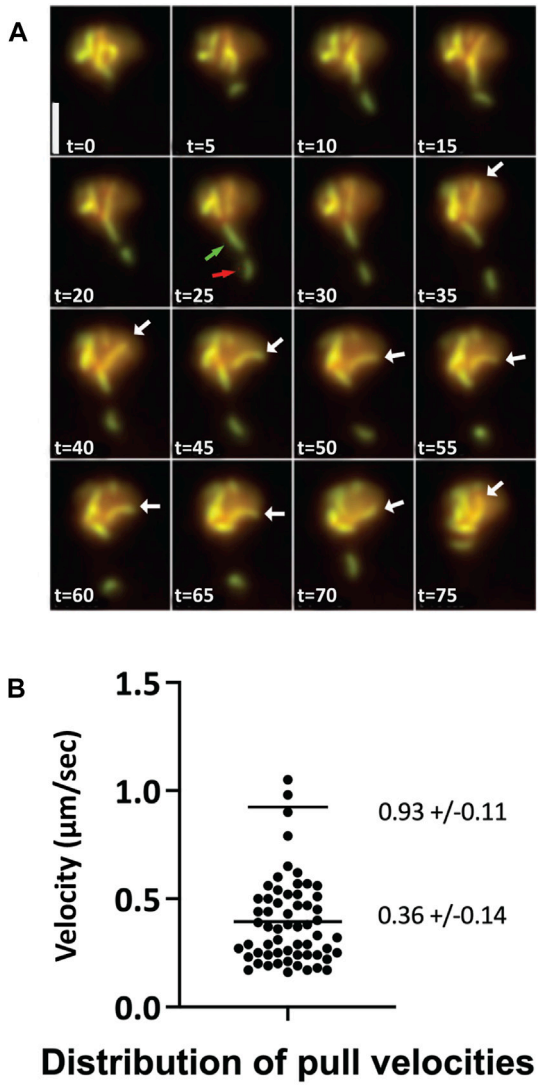

FIGURE 2
Chromosome dynamics and sporulation observed in *zip3Δ* **(A)** Max-sum projections from a 3-D time series at 5 s intervals of a *zip3Δ* cell expressing Zip1-GFP during pachytene. An example of telomere-led chromosome motion is illustrated by a single long chromosome moving between t = 35 s to t = 75 s (white arrow). Maverick chromosomes (green and red arrows). Scale bar—2 µm. **(B)** Distribution of velocity measurements for telomere-led motions of pachytene chromosomes from nuclei expressing Zip1-GFP in *zip3Δ*. Averages and STDs are given for the low and high velocity clusters. N = 60.

Normal chromosome motion during pachytene exhibited in a *zip3Δ* mutant

Meiotic chromosomes undergo rapid, large-scale motions whose function is important in attaining proper and timely homologous alignment (Conrad et al., 2008; Koszul et al., 2008; Navarro et al., 2022). In *C. elegans*, the disruption of this motion in a Sun mutant leads to perturbed pairing and synapsis elongation (Sato et al., 2009; Rog and Dernburg, 2015). Therefore, it is important to establish whether the behavior of chromosomes in *zip3Δ* yeast cells resembles the motion of chromosomes observed in wild type. Koszul et al. (2008) characterized the motion of fully synapsed chromosomes marked with Zip1-GFP in permeabilized cells and *in vivo* pachytene nuclei. They observed dramatic movements of chromosomes during the pachytene stage of meiosis mediated by attachment of the chromosomes to actin cables proximal to the nuclear envelope. These telomere-led movements exhibit velocities

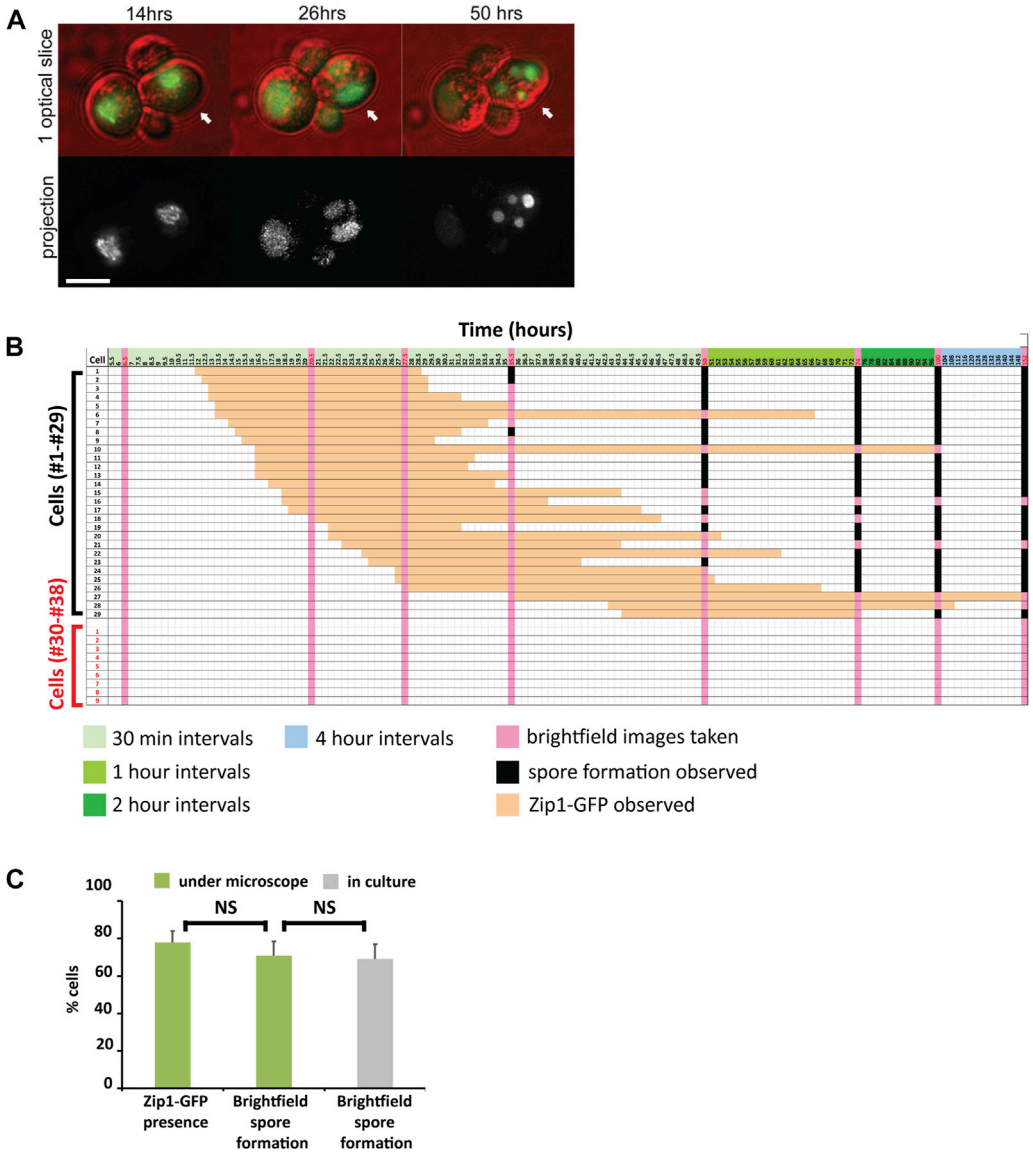

FIGURE 3
Imaging conditions do not perturb meiotic progression **(A)** Examples of Zip1-GFP and spore formation examples are shown at three timepoints as meiosis progresses in live cells. Zip1-GFP signal (green) is overlayed by brightfield to detect cell and spores (red). Both single optical slice and 2D projections are shown. Although 3 cells show Zip1-GFP expression during the time course, only one progresses to spore formation. Scale bar 5 μm. **(B)** Cells were tracked for meiotic progression for 152 h to determine the frequency of cells that enter meiosis as well as the frequency of cells that eventually form spores, to determine if the imaging conditions perturbed sporulation. A representative experiment in which 38 cells were tracked, of which 29 entered meiosis (cells with black numbers, first column) as determined by Zip1-GFP detection (orange squares) and 9 (cells with red numbers) did not. Cells were imaged for Zip-GFP initially at 30-minute intervals until 50 h (pale green, top column headers), then 1-hour intervals until 74 h (olive green), then 2-hour intervals until 100 h (dark green), followed by 4-hour intervals until 152 h (blue). At 6.5, 20.5, 27.5, 35.5, 50, 74, 100, and 152 h, brightfield images were acquired to assess for spore formation (pink columns). Black boxes indicate when spores were detected. **(C)** The number of cells entering meiosis and the number of cells forming spores are compared. Cells were counted if any spores (1–4) were observed. The average percentages were determined from five experiments performed as described in **(B)** above. A total of 179 cells were tracked. Experiments performed under the microscope using our optimized imaging conditions are shown in green. The frequency of sporulation was also calculated by counting spore formation in brightfield for comparison (gray) after 5 days of normal culturing in flasks.

of 0.3–0.5 μm/s (up to 0.8 μm/s) and are characterized by abrupt transitions of increased velocity. We observe comparable motion in *zip3Δ* (Figure 2A, movies Supplementary Figures S1–S3) with average motion in the 0.2–0.6 μm/s range and higher transitions up to 1.0 μm/s (Figure 2B). Our measurements in *zip3Δ* also agree with the results reported in wild-type cells by (Conrad et al., 2008), who examined the rapid prophase motion by imaging *lacO*-marked regions of the chromosome. Another characteristic of wild-type chromosome behavior in pachytene nuclei, also observed in *zip3Δ* cells, is the presence of "maverick" chromosomes (White et al., 2004). Occasionally, maverick chromosomes are observed to protrude out at a great distance from the bulk of the chromosomes, often with end-

10.3389/fcell.2023.1098468

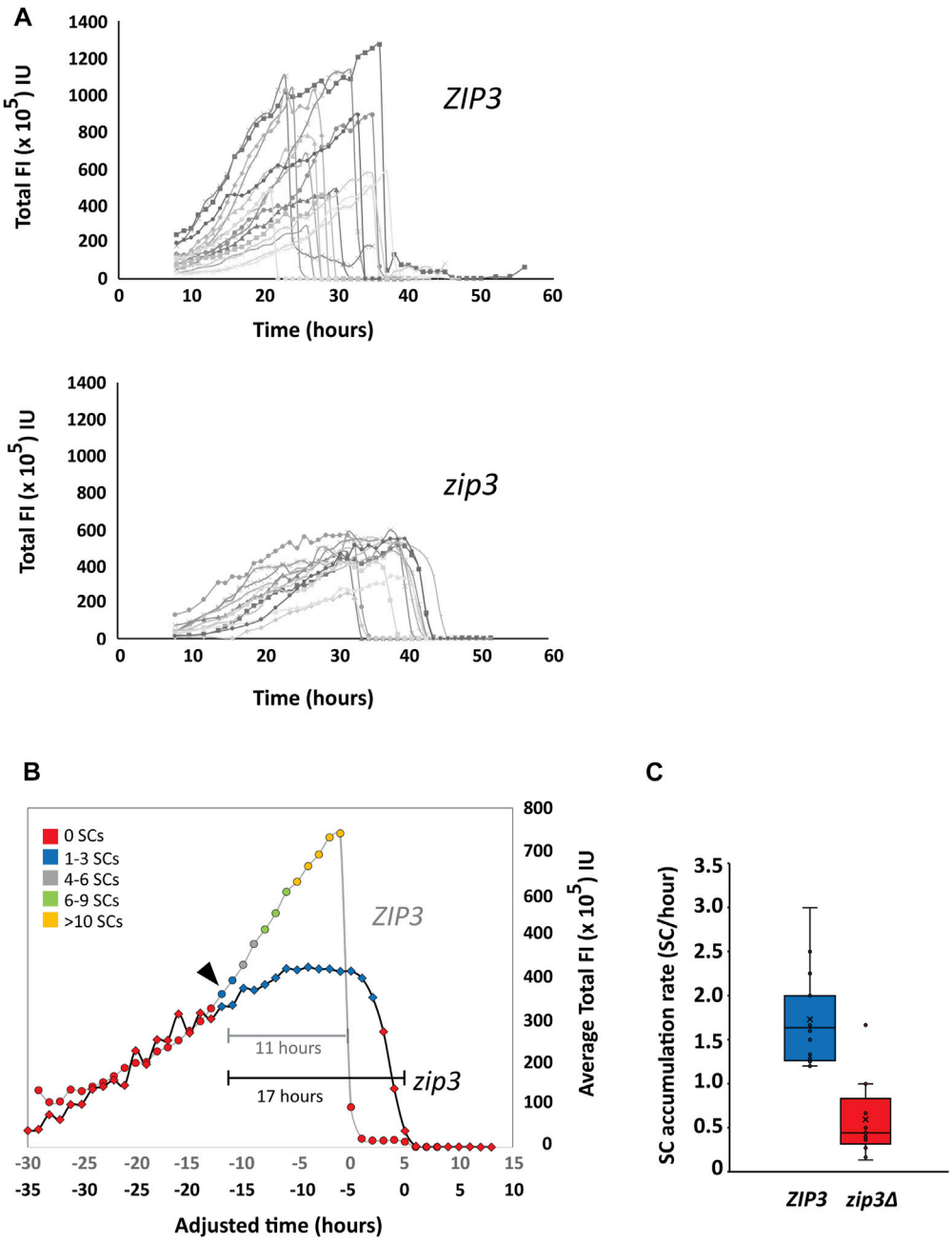

FIGURE 4
Quantitation of Zip1 levels. **(A)** Top Panel. Profiles of Zip1 levels from individual time courses of *ZIP3* cells expressing Zip1-GFP. *n* = 16.3D optical sections of Zip1-GFP in sporulating strains were acquired for 50 h at 1-h intervals starting at 8 h after induction of sporulation. Fluorescence intensity (FI) was measured as a proxy for Zip1 levels at each time point in arbitrary intensity units (IU). Bottom Panel. Profiles of Zip1 levels from individual time courses of *zip3Δ* cells expressing Zip1-GFP. *n* = 13. **(B)** A comparison of average total Zip1 FI levels during prophase in *ZIP3* (circles) vs. *zip3Δ* (diamonds) strains. Given the asynchrony of synapsis initiation times, individual time courses for *ZIP3* (*n* = 16) and *zip3Δ* (*n* = 13) were aligned such that time zero represented the time at which Zip1-GFP was depleted. The time points were adjusted relative to time zero and average Zip1 levels were calculated for each time point for both strains. These profiles were then aligned to each other based on the time synapsis is first detected. Two adjusted time axes are presented for *ZIP3* (grey) and *zip3Δ* (black). The general number of SCs is distinguished with colored markers: Red—0, Blue—1–3, Gray—4–6, Green—7–9, and Orange—>10 synapsed regions. The black arrow indicates the Zip1 threshold at which synapsis is first observed. Brackets shows length of time for synapsis for *ZIP3* (gray) and *zip3Δ* (black). **(C)** The rate of SC accumulation for *ZIP3* (blue) and *zip3Δ* (red). The rate was calculated by calculating the time it took to first reach the maximum number of distinguishable SCs.

to-end chromosome connections in which chromosomes resemble sausages on a string. Figure 2A highlights an example of a time course projection showing both types of behavior, telomere-led motion and maverick chromosomes, in the *zip3Δ* mutant within a single nucleus. Overall, prophase chromosome movement in *zip3Δ* appears to be comparable to that previously observed in wild type.

Optimization of conditions for *in vivo* microscopy

It is essential for *in vivo* microscopy studies to demonstrate that the imaging conditions do not perturb the event of interest and subsequent cellular progression (Carlton et al., 2010). Our protocol ensures that cells can complete meiosis without exhibiting phototoxic effects (Supplementary Figure S4). To document whether our imaging conditions permit completion of meiosis, cells were continuously imaged to determine whether they formed spores (Figure 3A). We used fluorescence microscopy to collect 3D optical sections (Figure 1B) of wild-type Zip1-GFP strains starting at 8 h after meiotic induction through early zygotene (~12–16 h) when synapsis is initiating, through pachytene (~16–21 h), when synapsis is complete and then at greater time intervals up to 152 h to determine further meiotic progression (Figure 3B). Spore formation was monitored by brightfield microscopy at various times throughout the time course (Figure 3B, pink vertical columns). For the *ZIP3* strain, on average 77.8% ±0.6 SD (n = 179, 5 experiments) of the cells enter meiosis, based on number of cells expressing Zip1-GFP. The overall sporulation frequency (69%) observed under our imaging conditions was equivalent to the sporulation frequency measured under normal sporulation conditions in culture (69%) (Figure 3C). Thus, the ability to sporulate is not affected by the imaging conditions, suggesting that photodamage is minimal.

Reduced Zip1 expression and delayed synapsis kinetics in the *zip3Δ* mutant

Zip1 expression was monitored over the course of prophase to determine the relationship between Zip1 expression and SC assembly. To measure Zip1 expression *via* fluorescence intensity (FI), 3-D optical sections of Zip1-GFP in sporulating strains were acquired for 50 h at 1-h intervals (Materials and Methods). We measured the total nuclear FI of Zip1-GFP and the volume for each nucleus to assess the amount of Zip1-GFP at each time point. Profiles of total nuclear Zip1 Fl for several individual cells over the course of prophase I are shown for *ZIP3* and *zip3Δ* (Figure 4A). We observe a large variation in the duration of Zip1 presence for both *ZIP3* and *zip3Δ* in individual cells.

In order to compare Zip1 profiles in wild type and *zip3Δ* cells that start accumulating Zip1-GFP at different times (Figure 4A), we aligned each profile by setting time to zero when Zip1-GFP is first depleted for both *ZIP3* and *zip3Δ*. The average total Zip1-GFP FI and number of SCs for the time courses were then calculated and these two averaged profiles were aligned to each other at the point at which synapsis initiates (Figure 4B, arrowhead). We find that Zip1 expression initially increases before the first SC appears and continues to rise both for *ZIP3* and *zip3Δ*. Before Zip1 levels decline at the end of pachytene, Zip1 expression plateaus in *ZIP3* for 1.5 h on average, while this period lasts ~4 times longer (6.3 h) for *zip3Δ* (Figure 4B). We also observe a difference in the maximum Zip1 intensity achieved for *ZIP3* (740 FU ± 66 SE) as compared to *zip3Δ* (424 FU ± 29 SE) which only attains 57% of wild-type levels. The abrupt degradation of Zip1 at the end of pachytene occurs within 1 hour in *ZIP3* wild-type cells, which is much faster than that observed for *zip3Δ* mutants, which on average occurs over ~3 h. Overall, this leads to an average 6-h greater duration of synapsis for *zip3Δ* (17 h) than for *ZIP3* (11 h) (Figure 4B).

SC formation occurs after equivalent Zip1 levels are reached

We observe that SCs first appear when the average total Zip1 FI reaches about 380×10^5 FI for wild type and similarly to 310×10^5 FI for *zip3Δ* (Figure 4B, black arrowhead). This suggests that synapsis initiation may require a threshold level of Zip1 concentration. However, we cannot distinguish at this point whether it is a threshold concentration of Zip1 or the stage of meiotic progression that is permissive for SC initiation. Like Zip1 production, the rate of accumulation of SCs is faster for wild type (1.7 ± 0.5 SD synapsed chromosomes/hour) than for *zip3Δ* (0.6 ± 0.4 SD synapsed chromosomes/hour) synapsed chromosomes/hr) during this period (Figure 4C). For wild type, the maximal number of SCs could not be accurately counted but was determined to be greater than ten. A previous study using fixed nuclear spreads showed an average of five synapsed chromosomes in *zip3Δ* compared to the 16 expected in wild type (MacQueen and Roeder, 2009). From Figure 4B, it appears the number of SCs peaks at 1–3 SCs in *zip3Δ*. This discrepancy is likely due to the inability to accurately count nuclei with 10–16 SCs in intact cells as compared to chromosome spreads as well as the lower number of nuclei used to determine the average in Figure 4A.

SC assembles continuously with either monophasic or biphasic kinetics in *zip3Δ*

In *zip3Δ*, it is possible to observe and measure individual SCs assembling from initiation, through elongation, to completion of synapsis (Figure 5). Quantitation of synapsis elongation rates is greatly facilitated by the tracking of cells when no other synapsed chromosomes are present. In live yeast, chromosomes range from less than 0.5 μm to over 3 μm in length. To obtain enough measurements during elongation, our analysis focused on nuclei in which only a single long chromosome synapsed (~0.14% of observed nuclei). Cells were imaged at intervals ranging from 3 to 10 min between each 3-D stack (shown as 2-D projections in Figure 5A) with most examples at 3-minute intervals. To determine whether the observed SC elongation represents continuous, discontinuous and/or step-wise assembly, we plotted the length of the synapsed region over time (Figure 5B). Segmented regression was used to determine whether SC assembly occurred at single or at multiple rates (Figure 5C). A predicted R-squared was calculated and cross-validated with the predicted residual error sum of squares (PRESS) statistic to distinguish the best model to minimize overfitting (Alcantara et al., 2022). Logarithmic fits were also performed, but the average R^2 compared to R^2 obtained from the segmented regression was worse (0.84 vs. 0.98).

In 34 SC assembly events measured, 65% of the assembly was monophasic and the rest (35%) showed biphasic assembly. In all cases, SC assembly monotonically increased, as no long pauses between steps were observed. The average assembly rate was 67 nm/min (range from 12 to 165 nm/min, Figure 5D), which is about half the rate seen for SC assembly in *C. elegans*. The average monophasic growth (56 ± 23 SD nm/min) is significantly slower than that observed for the first and faster part of biphasic growth (88 ± 42 SD nm/min). For all biphasic SC growth, the second phase of SC assembly (Figure 5D, blue lines) is slower (19 ± 12 nm/min $P_{t.\ test} = 0.002$) than the first phase. For biphasic growth, the first rate of growth contributes on average to

10.3389/fcell.2023.1098468

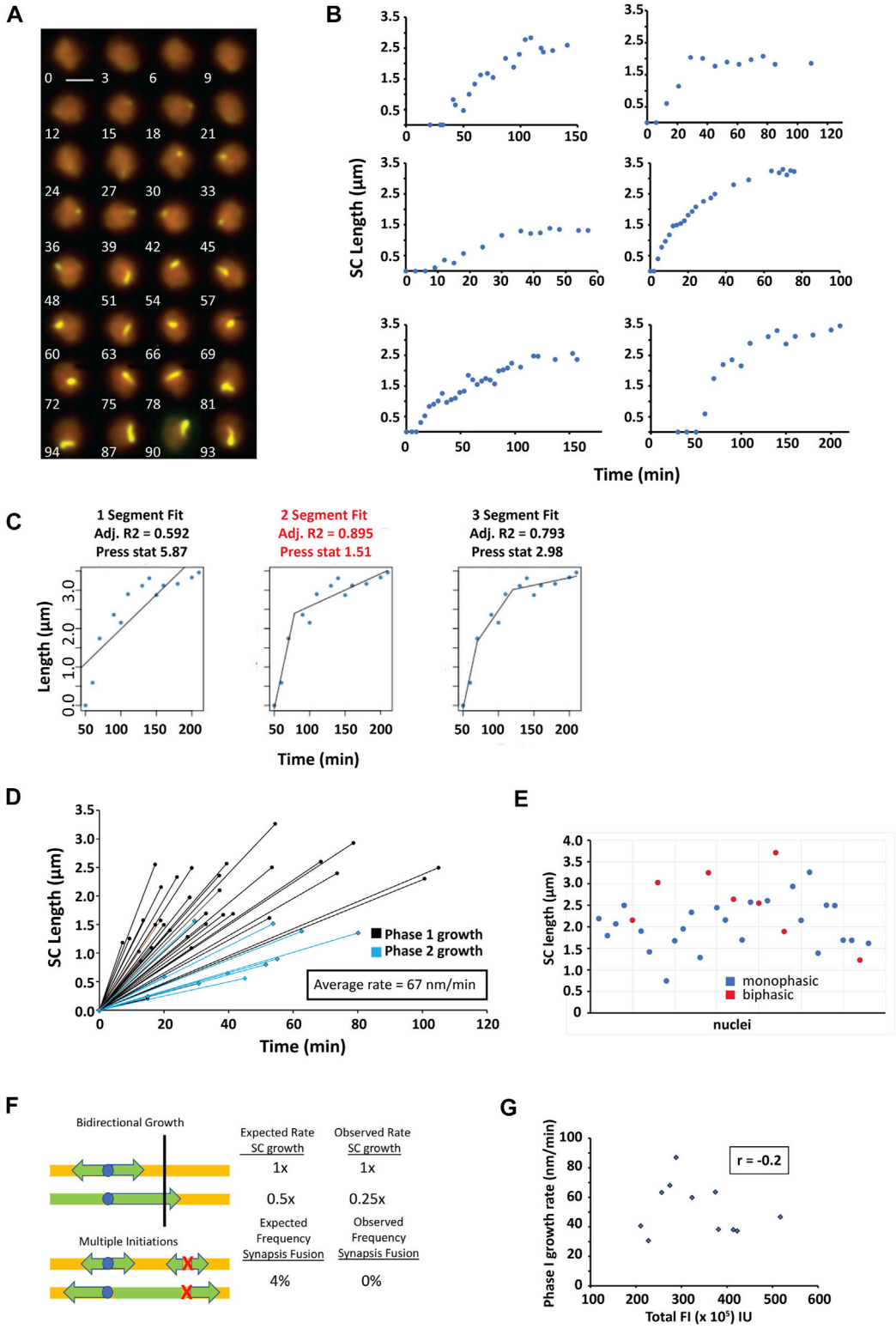

FIGURE 5
Synapsis assembly. **(A)** A time series of 2D max-sum projections at 3-min intervals from 3D image stacks of a single nucleus undergoing synapsis assembly visualized by Zip1-GFP. Scale bar—2 µm. **(B)** Six representative nuclei containing a single chromosome for which SC length was measured as a function of time during SC assembly. **(C)** Segmented regression was applied to the assembly data using 1–3 segments. The best fit model was determined using the adjusted R2 (adj. R2) and cross-validated with the PRESS statistic. Best fit models have the highest adjusted R2 and lowest PRESS statistic. In this example, the 2-segment fit (text highlighted in red) represents the best model. **(D)** Both monophasic and biphasic models were found for SC assembly. The initial rate of SC growth for both monophasic and biphasic models are shown illustrated as black lines with round markers. For the biphasic models, the second SC growth rate is shown as blue lines with diamond markers. **(E)** Total SC length for all nuclei with monophasic and biphasic growth indicated (blue circles–monophasic, red circles–biphasic) **(F)** A model in which SC growth initiates bidirectionally from an acrocentric centromere. A faster bidirectional (initial) SC assembly rate is predicted to slow to 50% of the initial rate once the shorter end is reached (top panel). Predicted and observed rates are shown. Expected and observed detection of individual synapsis initiation sites fusing into one synapsed chromosome are shown (bottom panel). **(G)** Plot of the phase 1 rate vs. total Zip1-GFP FI when the appearance the first SC is observed. r is calculated correlation coefficient. A subset of the data was used due to only a few data sets had intensities associated with the growth under the exact same conditions.

59% ± 16% (SD) of the final SC length. SC lengths for each assembly event can be found in Supplementary Table S2 and Figure 5E.

zip3Δ chromosomes synapse from a single initiation

In *zip3* mutants, there are fewer initiation events, of which 85% of the SC initiations come from centromeres (Macqueen and Roeder, 2009). In wild type, synapsis initiation occur at centromeres but more frequently at recombination-associated sites, and multiple initiations are observed on each chromosome (Tsubouchi et al., 2008). Because we did not observe multiple initiations in the 230 SC assembly events monitored, we wanted to assess whether this could be attributed to an insufficient number of observations. Based on Poisson statistics and the average number of SCs in a *zip3Δ*, we can calculate the likelihood of seeing multiple initiations on the same chromosome (see Materials and Methods). Given that there are five SCs on average in *zip3Δ*, we would expect to see two or more initiation sites occurring on the same chromosome ~4% of the time. In the 230 SC assembly events that we observed, we see no instances of multiple nucleation events which would be detected by the fusion of elongating SC stretches (Figure 5F, bottom panel). Since the binomial equation predicts that there is a 0.01 percent chance of missing such an event in the 230 SC assemblies observed, this suggests that Zip1 initiates only from one nucleation site in *zip3Δ*.

Potential models for biphasic growth

The longest SCs we measured were ~3 μm long and likely correspond to full length chromosome IV SCs since the next longest chromosome, chromosome XV is estimated to be ~2.3 μm and thus would not be mistaken for chromosome IV. The fact that only one initiation site is used for synapsis in *zip3*Δ implies that the same initiation site is used twice: in opposite directions to complete synapsis on that chromosome. Thus, we consider that the synapsis is bidirectional, although the two initiations may not be simultaneous. One model to explain biphasic growth could be the result of off-center centromeres (i.e., neither acrocentric nor metacentric) as in chromosome IV that initiates synapsis from the same site bidirectionally without much delay between initiations (Figure 5F, top panel). In this scenario we expect that for biphasic SC assembly, the second phase of growth would occur when one end of the SC reaches the end of the chromosome, such that only the other end continues to grow with a second phase growth rate 50% of the initial rate (Figure 5F, top panel). Instead, the second phase growth rate was 25% of the initial rate, significantly lower than expected ($P_{t.test}$ = 0.002). Another possibility is that nuclear Zip1 concentration influences SC elongation rates given the results that cells with extra copies of *ZIP1* synapse earlier (Voelkel-Meiman et al., 2012). To test whether changing Zip1 levels influences the elongation rate, we asked whether Zip-GFP total FI correlates with SC elongation rates at the time of appearance of the first SC (Figure 5G). A correlation coefficient $r = -0.2$ was observed indicating no correlation between the starting concentration of Zip1 and SC elongation rate. This suggests that different nuclear concentrations of Zip1 may not be dictating the observed biphasic rates.

Final disassembly of SCs is accompanied by degradation of Zip1

Final SC disassembly is accompanied by a rapid decrease in Zip1 levels, such that the majority of Zip1 is removed within 1 hour for *ZIP3* (Figure 4B) and ~3 h for *zip3*Δ. At exit from pachytene, Zip1 is removed from chromosomes with a minor amount of Zip1 protein remaining at the centromeres (Jordan et al., 2009; Newnham et al., 2010). The disassembly of single long chromosomes in *zip3*Δ was assessed as in our previous SC assembly measurements. Final SC disassembly occurs *via* shortening of the SC from the ends (Figure 6A). We also explored the possibility that SCs were also dismantled at specific foci, similar to foci used for initiation. However, we saw no appearance of gaps within the shortening SCs that would have been indicative that SC were being dismantled at specific internal sites.

To assess the rates of disassembly, we plotted the SC length as a function of time and performed segmented regression to determine whether disassembly was monophasic or occurred at multiple stages (Figure 6B). In all cases, final disassembly was monophasic with an average rate of −66 ± 30 (SD) nm/min, which is similar in magnitude to the initial rate observed for SC elongation. It is possible that the disassembly rate is actually slower than appears since if disassembly occurred simultaneously at the ends, each end would disassemble at half the rate at which the overall length was shortening. In many instances, there was an initial phase that occurred at a very low rate at which SCs were degraded (5 nm/min ± 5 SD). Since this rate was so low, we did not include this period as a separate phase given the error of measurements. This programmed loss of Zip1 is distinguishable from bleaching artifacts (Figure 6C). Figure 6D shows the distribution of SC lengths as a function of time from which the rates were calculated.

Abortive disassembly occurs during the SC accumulation phase

While obtaining examples of SC disassembly, numerous cells were found in which the disappearance of an SC is not immediately followed by Zip1 degradation. Indeed, in many of these cases, other SCs persist, and additional SCs continue to form as shown in Figure 7A. Whereas the great majority of examples were obtained from *zip3*Δ strains, rare examples were uncovered from *ZIP3* (Figure 7B). These cells have not progressed to the end of prophase, since Zip1 levels remained high and nascent SCs were often still accumulating. We have termed this type of SC disassembly "abortive SC disassembly." Unlike final disassembly in which Zip1 levels decrease by 50% within an hour and a half (Figure 4B), during abortive disassembly, Zip1 levels remain high well after no SCs are seen (Figure 7C). In a 5-h period, about 30% of nuclei show an instance of abortive disassembly (n = 191).

Another difference between final and abortive disassembly is in the size distribution of SCs that are involved in the two processes (Figure 7C). Yeast chromosomes range widely in size from ~0.5 μm to ~3 μm with about 25% small (<0.5 microns, as determined from live cells, Figure 7). Whereas the distribution of SC sizes observed for assembly and final disassembly are similar, there is a much stronger bias for small SCs (88%) to be disassembled abortively than during final disassembly (51%) (Figure 7D). Though rare, 15 medium and

10.3389/fcell.2023.1098468

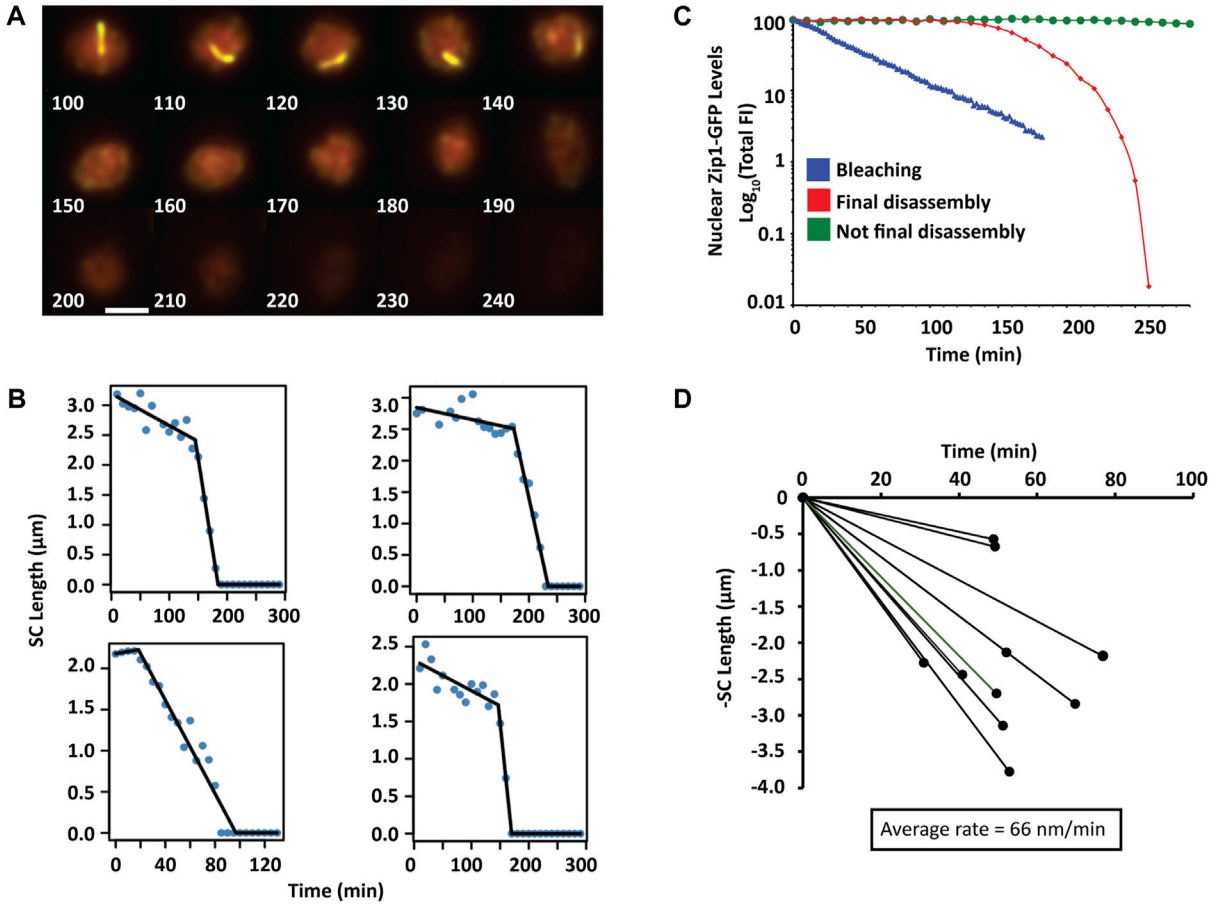

FIGURE 6
Final SC disassembly **(A)** A time series of 2D max-sum projections at 10-minute intervals from 3D image stacks of a single *zip3Δ* nucleus with a single chromosome undergoing final synapsis disassembly visualized by Zip1-GFP. Scale bar—2 µm. **(B)** Four representative nuclei containing one chromosome for which SC length was measured as a function of time during the final disassembly of the SC. **(C)** Comparison of nuclear Zip1-GFP fluorescence levels when SCs are all disassembling (red diamonds), not at final disassembly (green circles), not disassembling but subjected to heavy bleaching conditions (blue triangles). Log plots are normalized to the respective maximum intensity. **(D)** Disassembly of SC is monophasic. The rate and length of each SC disassembly is plotted (n = 10).

long SCs experiencing abortive disassembly were characterized for the kinetics of abortive disassembly. Like final disassembly, abortive disassembly is monophasic. However, the average rate for abortive disassembly was much lower 25 ± 1 (SD) nm/min vs. 66 ± 30 (SD) nm/min for final disassembly. Together these results suggest that abortive SC disassembly and final disassembly are distinct.

Discussion

Models of biphasic growth

Before this study, the real-time kinetics of synapsis had only been visualized in *C. elegans* (Rog and Dernburg, 2015), an organism that does not rely on recombination to pair or synapse its homologous chromosomes. We set out in this study to examine the kinetics of synapsis in yeast, which is more like humans in that it depends on recombination for its pairing and synapsis. Using a *zip3Δ* mutant in yeast, we were able to unambiguously follow SC assembly and disassembly from a single initiation site on a single chromosome. We saw that SC kinetics in both organisms had distinct differences. In contrast to what has been reported in C. *elegans,* in which the kinetics of SC formation exclusively fit a single rate of elongation, in yeast, we found biphasic elongation 35% of the time. Analysis of synaptic initiation in yeast suggested that synapsis from most centromere-initiated SCs was unidirectional (Tsubouchi et al., 2008). However, a single SC initiation site in *zip3Δ* is responsible for synapsis of both arms, implying that SC initiation must be bidirectional (i.e., proceed in both directions from a single point). Bidirectional synapsis from a non-centric centromere might account for the two rates of elongation as the short arm completes synapsis earlier, leaving the long arm synapsis to finish alone. However, the magnitude of the rate reduction (greater than the expected two-fold reduction if the elongation rates are equal) suggests that other factors could be contributing as well, such as unequal elongation rates for each side of the initiation site.

Another alternative is a model in which the slower second phase of SC elongation may to be due physical constraints that increase as SC lengths become long. In this case, we would have expected that biphasic growth would be seen more frequently on the longer SCs. Consistent with this, the average SC length is longer for cells exhibiting biphasic growth (Figure 5E).

10.3389/fcell.2023.1098468

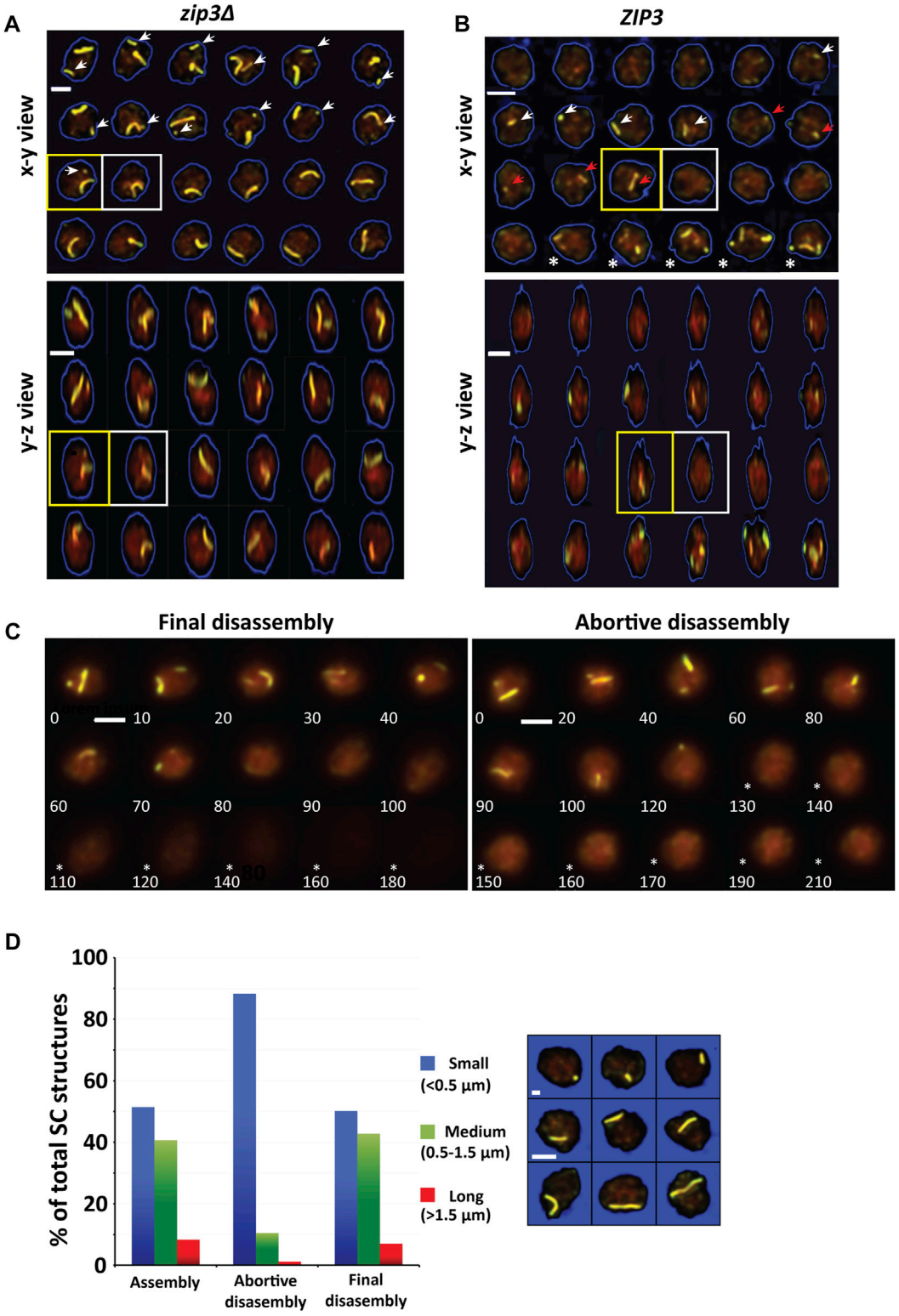

FIGURE 7
Abortive synapsis disassembly. **(A)** A time-series of 2D triple-overlay projections from 3D image stacks of a single *zip3Δ* nucleus at 5-minute intervals showing abortive disassembly for the smaller (white arrow) of the two chromosomes. The yellow square outlines the last time frame in which the smaller chromosome is last observed. The white square shows time frame in which smaller chromosome is no longer observed. Below is the same time-series in a y-z view. Scale bar—2 μm. **(B)** A time-series of 2D triple-overlay projections from 3D image stacks of a single *ZIP3* nucleus at 20-minute intervals showing abortive disassembly chromosomes. The white arrow indicates a SC that formed and then disassembled. The red arrow represents either the same SC as indicated by the white arrow that did not fully disassemble or an SC that newly formed. The yellow square outlines when the chromosome is last observed. The white square outlines time when chromosome has disassembled. Several timepoints later after a period in which there is no SCs, new SCs form in the timeframes indicated by (*). Below is the same time-series in a y-z view. Scale bar—2 μm. **(C)** Abortive synapsis disassembly is distinguishable from final disassembly by the high levels of Zip1 that remains (right panel, timepoints 130–210 indicated by *) as compared to final disassembly of the SC when Zip1 levels decrease (left panel, timepoints 110–180 indicated by *). Left panel–final disassembly. Right panel–abortive disassembly **(D)** Distribution of SC sizes divided into small (<0.5 μm), medium (0.5–1.5 μm) and large (>1.5 μm) for SC assembly (n = 230), abortive disassembly (n = 171) and final disassembly (n = 530). Images show example SCs belonging to each size class.

An intriguing possibility for the observed biphasic growth rate is that the slower rate may be due to chromosome interlocks. Since in yeast, all chromosome ends are embedded in the nuclear membrane, as chromosomes pair, other chromosomes may become trapped and obstruct pairing or alignment in advance of SC formation (Navarro et al., 2022). This would in turn impede synapsis and thereby attenuate the rate of SC assembly in the region of the interlock. It was proposed that entanglements can be resolved by motion of the entrapped chromosome to the telomeric end where the chromosome can escape (Navarro et al., 2022). The delay caused by clearing the entanglement might account for the slower rate of Zip1 assembly. Such a delay might not be seen in *C. elegans*, which is unusual in that only one end of the chromosome is associated with the nuclear envelope, presumably making it easier for interlocks to resolve.

Yeast SC elongation rate is likely not affected by *zip3Δ* mutation

Overall, the rate of SC formation based on Zip1-GFP images in yeast on average was 67 nm/min which is approximately two-fold slower than the average rate obtained from nematodes (150 nm/m) (Rog and Dernburg, 2015). This raises the possibilities that either synapsis is slower in yeast, or that the *zip3Δ* mutant impairs synapsis elongation rates. While the numbers of SCs are reduced in *zip3Δ* mutants, a full complement of SCs is restored by a mutation in *FPR3* (Macqueen and Roeder, 2009). In the *fpr3 zip3* double-mutant, the inhibition of synapsis initiation at the centromeres is removed, which allows the cells to form SC on all chromosomes. They found that in *fpr3 zip3* the cumulative lengths of SCs per nucleus scored at similar time points were not significantly different from wild type. If elongation rates were slower in the *zip3Δ* mutant than wild type, we would not have expected the *fpr3 zip3* mutants to attain wild-type SC lengths at wild-type rates. However, we cannot fully eliminate the possibility that Fpr3 has some effect on elongation rate. To fully address whether the *zip3Δ* SC elongation rate is representative of the wild-type SC elongation rate, future developments to allow observations of single chromosomes in wild type are needed.

Factors that might affect overall synapsis period

Factors other than Zip1 assembly rates influence the time it takes to complete synapsis of the entire complement of chromosomes. In some organisms like *Drosophila*, the centromeres are the synapsis initiation sites and they are already paired at the start of meiosis (Takeo et al., 2011; Tanneti et al., 2011). In nematodes, pairing centers present on a chromosome end initiate synapsis independently of recombination (Dernburg et al., 1998). In contrast to nematodes, SC formation in yeast and mammals is dependent on the early steps of recombination (Giroux et al., 1989; Dernburg et al., 1998; Romanienko and Camerini-Otero, 2000), perhaps prolonging the phase of synapsis and/or delaying its onset. The extent of pairing at the time of synapsis may influence the timing of synapsis completion and could be very different among organisms. Organisms that are dependent on recombination for synapsis tend to use a subset of those recombination sites to initiate synapsis (Joyce and McKim, 2007; Tsubouchi et al., 2008; Pyatnitskaya et al., 2022). Therefore, completed chromosome synapsis depends on both the rate of elongation and the number of initiation sites used as well as the lengths of the chromosomes. Certain yeast strains backgrounds, including SK1, can reach full synapsis in less than 4 h (Padmore et al., 1991), whereas the BR strains spend approximately 11 h undergoing SC formation. Unless the rate of SC formation is significantly different in these two laboratory yeast strains, the shorter time spent synapsis suggests that other regulatory controls such as the number and timing of synapsis initiations, may be responsible.

Threshold vs. meiotic progression models for synapsis initiation

We quantified Zip1-GFP accumulation in the nucleus to monitor cells during the active phase of SC assembly and disassembly. We found that chromosome synapsis initiated when Zip1-GFP levels reached comparable levels in both wild-type and *zip3Δ* cells, suggesting that a threshold of SC components accumulates before SC formation begins. It is also possible that rather than a threshold, reaching a particular stage of meiotic progression licenses SC formation and Zip1 levels are just coincidentally the same in wild type and mutant. Voelkel-Meiman et al. (2012) monitored synapsis in BR strains with 1–6 copies of Zip1 and found that as the copy number increased, synapsis started earlier. In a threshold model, higher levels of Zip1 in SK1 vs. BR strains might explain, in part, how SK1 starts synapsis earlier. It is also consistent with the fact that SK1 normally synapses in the presence of polycomplexes.

Lower abundance of Zip1 in *zip3Δ* mutants

As seen in Figure 4B, in *zip3Δ* less overall Zip1 is seen compared to wild-type as time progresses. One possibility is that SC structures themselves stabilize/maintain abundance of Zip1—i.e., Zip1 that is incorporated into SC may be less likely to degrade than Zip1 floating in the nucleoplasm. Perhaps it is the SC structure that stabilizes Zip1 thereby promoting its accumulation. Another possibility is that a feedback loop exists such that more Zip1 is produced as more is incorporated into chromosomes.

Final disassembly involves removal of SC from the ends

In contrast to the stochastic assembly of Zip1-GFP on individual chromosomes throughout the synapsis phase, the final SC disassembly happens all at once to all synapsed chromosomes. The concentration of Zip1 remains high until programmed SC disassembly, which is abrupt in wild type, and attenuated in *zip3Δ*. In both strains the SCs began rapid disassembly when Zip1 levels begin to decline (within 1.5 h for *zip3Δ*), suggesting that *zip3Δ* diploids retain programmed disassembly signals, but they may be compromised. Disassembly of the SC is monophasic with a similar rate to assembly. The loss of Zip1 occurs at the ends, the reverse of assembly. However, the possibility exists that in wild-type cells, disassembly may also occur interstitially, potentially at the sites of synapsis initiation. This is difficult to measure due to the apparent intensity changes that accompany a change in orientation of the SC.

Abortive disassembly may be a way to correct synapsis

Unexpectedly, we encountered many SCs in *zip3Δ* nuclei that disassembled in advance of final disassembly when Zip1 protein is actively degraded. We refer to the disassembly of these SCs as "abortive disassembly" since these SCs fail to persist to the end of the synapsis phase. The abortive disassembly process represents SCs that are disassembling at the same time that others can be assembling, making it reminiscent of the "dynamic instability" phenomenon in microtubules (Kirschner and Mitchison, 1986). Most of these SCs were very short, but a few larger SCs were observed. Aborted SCs were also observed in wild-type meiosis, but examples were technically harder to identify because so many SCs are assembling at the same time, and it is likely a much rarer event. Abortive disassembly was not observed in the nematode (Rog and Dernburg, 2015). Our data reveal that ~30% of the 5-h time courses (representing about a third of the synaptic period) had one or more abortive SCs, suggesting that in *zip3*Δ mutants, abortive SCs are fairly common. Consistent with our data, examination of fixed nuclei indicated that *zip3* meiotic nuclei did not gain as many SCs as wild type (Voelkel-Meiman et al., 2019). However, the dynamics of assembly and disassembly of SCs can only be revealed from live imaging, illuminating the wealth of data that can be uncovered from real-time imaging. One prediction for future *in vivo* studies is that abortive disassembly should be more frequent in hybrid strains for which there are a lot of polymorphisms.

We hypothesize that the aborted SCs are identified as defective or stalled SCs by a yet uncharacterized surveillance mechanism, and then targeted for disassembly. We speculate that many of the aborted SCs identified in *zip3*Δ mutants represent nascent SCs that were formed between non-homologous chromosomes. Zip3, with Fpr3, has been proposed to have a role in licensing SC formation at centromeres after recombination has initiated (Macqueen and Roeder, 2009). Consequently, when this license is defective as in *zip3 fpr3*, promiscuous SC formation occurs in *spo11* mutants, which are recombination-negative, and in haploids, which do not have homologs. *zip3 fpr3* double mutants attain wild-type levels of SCs but have low spore viability, implying that apparent full synapsis cannot rescue *zip3*. It seems likely that centromere-initiated synapsis, in the absence of regulation, is error-prone. This could explain why most of the aborted SCs were very short, since a lack of homology may slow down elongation or may be a signal for SC abortion or have some physical characteristic that lacks stability. Perhaps these short SCs, doomed to disappear, may not have established a robust central element. We can envision a scenario in which these short non-homologous SCs are tugged apart by the telomere-led movements during prophase. Perhaps by virtue of being non-homologous and relatively short, they are more vulnerable to telomeric pulls. Rather than invoking a sensing mechanism to seek out non-homology, perhaps the physical jerking of the chromosomes is enough to disrupt non-productive SCs. For those SCs that had attained significant length before they are aborted, they may be the result of entanglements with other chromosomes. Perhaps the pachytene checkpoint acts to prolong the synapsis phase in *zip3Δ* to allow time for entanglement resolution. In the future, potentially more elaborate FISH experiments like shown in Figure 1D will be able to test the hypothesis that the abortive disassembly events predominantly stem from non-homologous interactions.

During the past several decades, numerous genes involved in chromosome pairing and synapsis have been identified, and the protein architecture of the SC determined, yet many basic questions remain concerning the links between homology recognition, SC assembly, interlock resolution, recombination, and crossover distribution. The complex dynamics of meiosis are one reason that these questions have been difficult to answer. Genetic methods typically apply a constant-in-time perturbation and then probe the end-point result. The analysis of the dynamics of SC assembly and disassembly in real time provides a different view of the same events that have long been probed by genetic means, and has revealed unexpected features such as biphasic growth and abortive disassembly that had not been predicted on the basis of genetic analysis. Our work thus represents a step towards mechanistic understanding of meiosis as a dynamic process.

Data availability statement

The raw data supporting the conclusion of this article will be made available by the authors, without undue reservation.

Author contributions

MP performed the bulk of the experiments and contributed to the analysis and writing. BR contributed to the writing. AO contributed to the segmented regression and PRESS statistic analysis. CA made the original strains. JF performed some of the experiments, contributed to the analysis and writing and obtained the funding support.

Funding

This work was supported by NIH grants 5 R01GM137126 and 1S10OD010673-01 (JF).

Acknowledgments

We would like to thank Laurel Geraci for dissections of wild-type and *zip3* mutants. We would like to thank Dr. Tim Nelson and Dr. Wallace Marshall for critical reading of the manuscript.

Conflict of interest

The authors declare that the research was conducted in the absence of any commercial or financial relationships that could be construed as a potential conflict of interest.

The reviewer AM declared a past co-authorship with the authors AO and JF to the handling editor.

Publisher's note

claim that may be made by its manufacturer, is not guaranteed or endorsed by the publisher.

Supplementary material

The Supplementary Material for this article can be found online at: https://www.frontiersin.org/articles/10.3389/fcell.2023.1098468/full#supplementary-material

SUPPLEMENTARY FIGURE S1–S3
SC movies in zip3Δ strains. 2D projection movies of the dynamic motion of *zip3Δ* SCs. 200 ms interval time series. S1-movie associated with Figure 2A. S2-movie with 9 SCs. S3-movie with 1 SC.

SUPPLEMENTARY FIGURE S4
Effects of nonoptimal imaging conditions. Preliminary experiments revealed that excessive exposure of the yeast cells to the 488 nm laser at a power greater than 30 μW results in phototoxic effects such that formation of a Zip1 aggregate occurs or that chromosomes adopt a fixed configuration and no longer appear subject to telomere-led pulls (top and middle panel). At our imaging conditions at 11 μW, bleaching rates were reduced and no aberrant chromosome behavior was observed (bottom panel). Frame numbers are indicated. Data was taken at 200 ms time intervals.

SUPPLEMENTARY TABLE S1
Yeast Strains.

SUPPLEMENTARY TABLE S2
SC lengths from monophasic and biphasic assembly.

References

Agarwal, S., and Roeder, G. S. (2000). Zip3 provides a link between recombination enzymes and synaptonemal complex proteins. *Cell* 102, 245–255. doi:10.1016/s0092-8674(00)00029-5

Alcantara, I. M., Naranjo, J., and Lang, Y. (2022). Model selection using PRESS statistic. *Comput. Stat.* doi:10.1007/s00180-022-01228-1

Alleva, B., and Smolikove, S. (2017). Moving and stopping: Regulation of chromosome movement to promote meiotic chromosome pairing and synapsis. *Nucl. Austin Tex* 8, 613–624. doi:10.1080/19491034.2017.1358329

Bähler, J., Wyler, T., Loidl, J., and Kohli, J. (1993). Unusual nuclear structures in meiotic prophase of fission yeast: A cytological analysis. *J. Cell Biol.* 121, 241–256. doi:10.1083/jcb.121.2.241

Boulanger, J., Kervrann, C., Bouthemy, P., Elbau, P., Sibarita, J.-B., and Salamero, J. (2010). Patch-based nonlocal functional for denoising fluorescence microscopy image sequences. *IEEE Trans. Med. Imaging* 29, 442–454. doi:10.1109/TMI.2009.2033991

Carlton, P. M., Boulanger, J., Kervrann, C., Sibarita, J.-B., Salamero, J., Gordon-Messer, S., et al. (2010). Fast live simultaneous multiwavelength four-dimensional optical microscopy. *Proc. Natl. Acad. Sci. U. S. A.* 107, 16016–16022. doi:10.1073/pnas.1004037107

Chelysheva, L., Vezon, D., Chambon, A., Gendrot, G., Pereira, L., Lemhemdi, A., et al. (2012). The Arabidopsis HEI10 is a new ZMM protein related to Zip3. *PLoS Genet.* 8, e1002799. doi:10.1371/journal.pgen.1002799

Chen, H., Clyborne, W. K., Sedat, J. W., and Agard, D. A. (1992). "Priism: An integrated system for display and analysis of 3-D microscope images," in *Presented at the SPIE/IS&T 1992 symposium on electronic imaging: Science and technology*. Editors R. S. Acharya, C. J. Cogswell, and D. B. Goldgof (San Jose, CA, 784–790. doi:10.1117/12.59604

Chua, P. R., and Roeder, G. S. (1998). Zip2, a meiosis-specific protein required for the initiation of chromosome synapsis. *Cell* 93, 349–359. doi:10.1016/S0092-8674(00)81164-2

Conrad, M. N., Lee, C.-Y., Chao, G., Shinohara, M., Kosaka, H., Shinohara, A., et al. (2008). Rapid telomere movement in meiotic prophase is promoted by NDJ1, MPS3, and CSM4 and is modulated by recombination. *Cell* 133, 1175–1187. doi:10.1016/j.cell.2008.04.047

Dernburg, A. F., McDonald, K., Moulder, G., Barstead, R., Dresser, M., and Villeneuve, A. M. (1998). Meiotic recombination in *C. elegans* initiates by a conserved mechanism and is dispensable for homologous chromosome synapsis. *Cell* 94, 387–398. doi:10.1016/s0092-8674(00)81481-6

Dernburg, A. F., and Sedat, J. W. (1998). Mapping three-dimensional chromosome architecture *in situ*. *Methods Cell Biol.* 53, 187–233. doi:10.1016/s0091-679x(08)60880-8

Dobbie, I. M., King, E., Parton, R. M., Carlton, P. M., Sedat, J. W., Swedlow, J. R., et al. (2011). Omx: A new platform for multimodal, multichannel wide-field imaging. *Cold Spring Harb. Protoc.* 2011, 899–909. doi:10.1101/pdb.top121

Dong, H., and Roeder, G. S. (2000). Organization of the yeast Zip1 protein within the central region of the synaptonemal complex. *J. Cell Biol.* 148, 417–426. doi:10.1083/jcb.148.3.417

Dunce, J. M., Milburn, A. E., Gurusaran, M., da Cruz, I., Sen, L. T., Benavente, R., et al. (2018). Structural basis of meiotic telomere attachment to the nuclear envelope by MAJIN-TERB2-TERB1. *Nat. Commun.* 9, 5355–5418. doi:10.1038/s41467-018-07794-7

Fung, J. C., Rockmill, B., Odell, M., and Roeder, G. S. (2004). Imposition of crossover interference through the nonrandom distribution of synapsis initiation complexes. *Cell* 116, 795–802. doi:10.1016/s0092-8674(04)00249-1

Giroux, C. N., Dresser, M. E., and Tiano, H. F. (1989). Genetic control of chromosome synapsis in yeast meiosis. *Genome* 31, 88–94. doi:10.1139/g89-017

Hochwagen, A., and Amon, A. (2006). Checking your breaks: Surveillance mechanisms of meiotic recombination. *Curr. Biol. CB* 16, R217–R228. doi:10.1016/j.cub.2006.03.009

Hughes, S. E., and Hawley, R. S. (2020). Alternative synaptonemal complex structures: Too much of a good thing? *Trends Genet.* 36, 833–844. doi:10.1016/j.tig.2020.07.007

Humphryes, N., Leung, W.-K., Argunhan, B., Terentyev, Y., Dvorackova, M., and Tsubouchi, H. (2013). The Ecm11-Gmc2 complex promotes synaptonemal complex formation through assembly of transverse filaments in budding yeast. *PLoS Genet.* 9, e1003194. doi:10.1371/journal.pgen.1003194

Jantsch, V., Pasierbek, P., Mueller, M. M., Schweizer, D., Jantsch, M., and Loidl, J. (2004). Targeted gene knockout reveals a role in meiotic recombination for ZHP-3, a Zip3-related protein in *Caenorhabditis elegans*. *Mol. Cell. Biol.* 24, 7998–8006. doi:10.1128/MCB.24.18.7998-8006.2004

Jordan, P., Copsey, A., Newnham, L., Kolar, E., Lichten, M., and Hoffmann, E. (2009). Ipl1/Aurora B kinase coordinates synaptonemal complex disassembly with cell cycle progression and crossover formation in budding yeast meiosis. *Genes Dev.* 23, 2237–2251. doi:10.1101/gad.536109

Joyce, E. F., and McKim, K. S. (2007). When specialized sites are important for synapsis and the distribution of crossovers. *BioEssays* 29, 217–226. doi:10.1002/bies.20531

Kirschner, M., and Mitchison, T. (1986). Beyond self-assembly: From microtubules to morphogenesis. *Cell* 45, 329–342. doi:10.1016/0092-8674(86)90318-1

Koszul, R., Kim, K. P., Prentiss, M., Kleckner, N., and Kameoka, S. (2008). Meiotic chromosomes move by linkage to dynamic actin cables with transduction of force through the nuclear envelope. *Cell* 133, 1188–1201. doi:10.1016/j.cell.2008.04.050

Lake, C. M., and Hawley, R. S. (2021). Synaptonemal complex. *Curr. Biol. CB* 31, R225–R227. doi:10.1016/j.cub.2021.01.015

Leung, W.-K., Humphryes, N., Afshar, N., Argunhan, B., Terentyev, Y., Tsubouchi, T., et al. (2015). The synaptonemal complex is assembled by a polySUMOylation-driven feedback mechanism in yeast. *J. Cell Biol.* 211, 785–793. doi:10.1083/jcb.201506103

Macqueen, A. J., and Roeder, G. S. (2009). Fpr3 and Zip3 ensure that initiation of meiotic recombination precedes chromosome synapsis in budding yeast. *Curr. Biol. CB* 19, 1519–1526. doi:10.1016/j.cub.2009.08.048

Navarro, E. J., Marshall, W. F., and Fung, J. C. (2022). Modeling cell biological features of meiotic chromosome pairing to study interlock resolution. *PLoS Comput. Biol.* 18, e1010252. doi:10.1371/journal.pcbi.1010252

Newlon, C. S., Lipchitz, L. R., Collins, I., Deshpande, A., Devenish, R. J., Green, R. P., et al. (1991). Analysis of a circular derivative of Saccharomyces cerevisiae chromosome III: A physical map and identification and location of ARS elements. *Genetics* 129, 343–357. doi:10.1093/genetics/129.2.343

Newnham, L., Jordan, P., Rockmill, B., Roeder, G. S., and Hoffmann, E. (2010). The synaptonemal complex protein, Zip1, promotes the segregation of nonexchange chromosomes at meiosis I. *Proc. Natl. Acad. Sci. U. S. A.* 107, 781–785. doi:10.1073/pnas.0913435107

Padmore, R., Cao, L., and Kleckner, N. (1991). Temporal comparison of recombination and synaptonemal complex formation during meiosis in *S. cerevisiae*. *Cell* 66, 1239–1256. doi:10.1016/0092-8674(91)90046-2

Page, S. L., and Hawley, R. S. (2004). The genetics and molecular biology of the synaptonemal complex. *Annu. Rev. Cell Dev. Biol.* 20, 525–558. doi:10.1146/annurev.cellbio.19.111301.155141

Pollard, M. G., and Fung, J. C. (2017). *In vivo* imaging of budding yeast meiosis. *Methods Mol. Biol.* 1471, 175–186. doi:10.1007/978-1-4939-6340-9_9

Pyatnitskaya, A., Andreani, J., Guérois, R., De Muyt, A., and Borde, V. (2022). The Zip4 protein directly couples meiotic crossover formation to synaptonemal complex assembly. *Genes Dev.* 36, 53–69. doi:10.1101/gad.348973.121

Rog, O., and Dernburg, A. F. (2015). Direct visualization reveals kinetics of meiotic chromosome synapsis. *Cell Rep.* 10, 1639–1645. doi:10.1016/j.celrep.2015.02.032

Rog, O., Köhler, S., and Dernburg, A. F. (2017). The synaptonemal complex has liquid crystalline properties and spatially regulates meiotic recombination factors. *eLife* 6, e21455. doi:10.7554/eLife.21455

Romanienko, P. J., and Camerini-Otero, R. D. (2000). The mouse Spo11 gene is required for meiotic chromosome synapsis. *Mol. Cell* 6, 975–987. doi:10.1016/s1097-2765(00)00097-6

Sato, A., Isaac, B., Phillips, C. M., Rillo, R., Carlton, P. M., Wynne, D. J., et al. (2009). Cytoskeletal forces span the nuclear envelope to coordinate meiotic chromosome pairing and synapsis. *Cell* 139, 907–919. doi:10.1016/j.cell.2009.10.039

Sym, M., Engebrecht, J. A., and Roeder, G. S. (1993). ZIP1 is a synaptonemal complex protein required for meiotic chromosome synapsis. *Cell* 72, 365–378. doi:10.1016/0092-8674(93)90114-6

Sym, M., and Roeder, G. S. (1995). Zip1-induced changes in synaptonemal complex structure and polycomplex assembly. *J. Cell Biol.* 128, 455–466. doi:10.1083/jcb.128.4.455

Takeo, S., Lake, C. M., Morais-de-Sá, E., Sunkel, C. E., and Hawley, R. S. (2011). Synaptonemal complex-dependent centromeric clustering and the initiation of synapsis in Drosophila oocytes. *Curr. Biol. CB* 21, 1845–1851. doi:10.1016/j.cub.2011.09.044

Tanneti, N. S., Landy, K., Joyce, E. F., and McKim, K. S. (2011). A pathway for synapsis initiation during zygotene in Drosophila oocytes. *Curr. Biol. CB* 21, 1852–1857. doi:10.1016/j.cub.2011.10.005

Tsubouchi, T., Macqueen, A. J., and Roeder, G. S. (2008). Initiation of meiotic chromosome synapsis at centromeres in budding yeast. *Genes Dev.* 22, 3217–3226. doi:10.1101/gad.1709408

Tsubouchi, T., Zhao, H., and Roeder, G. S. (2006). The meiosis-specific zip4 protein regulates crossover distribution by promoting synaptonemal complex formation together with zip2. *Dev. Cell* 10, 809–819. doi:10.1016/j.devcel.2006.04.003

Voelkel-Meiman, K., Cheng, S.-Y., Parziale, M., Morehouse, S. J., Feil, A., Davies, O. R., et al. (2019). Crossover recombination and synapsis are linked by adjacent regions within the N terminus of the Zip1 synaptonemal complex protein. *PLoS Genet.* 15, e1008201. doi:10.1371/journal.pgen.1008201

Voelkel-Meiman, K., Moustafa, S. S., Lefrançois, P., Villeneuve, A. M., and MacQueen, A. J. (2012). Full-length synaptonemal complex grows continuously during meiotic prophase in budding yeast. *PLoS Genet.* 8, e1002993. doi:10.1371/journal.pgen.1002993

White, E. J., Cowan, C., Cande, W. Z., and Kaback, D. B. (2004). *In vivo* analysis of synaptonemal complex formation during yeast meiosis. *Genetics* 167, 51–63. doi:10.1534/genetics.167.1.51

frontiers | Frontiers in Cell and Developmental Biology

TYPE Review
PUBLISHED 23 February 2023
DOI 10.3389/fcell.2023.1127440

OPEN ACCESS

EDITED BY
Mónica Pradillo,
Complutense University of Madrid, Spain

REVIEWED BY
Bernard De Massy,
Université de Montpellier, France
John Schimenti,
Cornell University, United States
Karen Schindler,
Rutgers, The State University of New Jersey, United States

*CORRESPONDENCE
Ignasi Roig,
Ignasi.Roig@uab.cat

SPECIALTY SECTION
This article was submitted to Nuclear Organization and Dynamics, a section of the journal Frontiers in Cell and Developmental Biology

RECEIVED 19 December 2022
ACCEPTED 10 February 2023
PUBLISHED 23 February 2023

CITATION
Huang Y and Roig I (2023), Genetic control of meiosis surveillance mechanisms in mammals.
Front. Cell Dev. Biol. 11:1127440.
doi: 10.3389/fcell.2023.1127440

Genetic control of meiosis surveillance mechanisms in mammals

Yan Huang[1,2] and Ignasi Roig[1,2]*

[1]Genome Integrity and Instability Group, Institut de Biotecnologia i Biomedicina, Universitat Autònoma de Barcelona, Cerdanyola del Vallès, Spain, [2]Histology Unit, Department of Cell Biology, Physiology, and Immunology, Cytology, Universitat Autònoma de Barcelona, Cerdanyola del Vallès, Spain

Meiosis is a specialized cell division that generates haploid gametes and is critical for successful sexual reproduction. During the extended meiotic prophase I, homologous chromosomes progressively pair, synapse and desynapse. These chromosomal dynamics are tightly integrated with meiotic recombination (MR), during which programmed DNA double-strand breaks (DSBs) are formed and subsequently repaired. Consequently, parental chromosome arms reciprocally exchange, ultimately ensuring accurate homolog segregation and genetic diversity in the offspring. Surveillance mechanisms carefully monitor the MR and homologous chromosome synapsis during meiotic prophase I to avoid producing aberrant chromosomes and defective gametes. Errors in these critical processes would lead to aneuploidy and/or genetic instability. Studies of mutation in mouse models, coupled with advances in genomic technologies, lead us to more clearly understand how meiosis is controlled and how meiotic errors are linked to mammalian infertility. Here, we review the genetic regulations of these major meiotic events in mice and highlight our current understanding of their surveillance mechanisms. Furthermore, we summarize meiotic prophase genes, the mutations that activate the surveillance system leading to meiotic prophase arrest in mouse models, and their corresponding genetic variants identified in human infertile patients. Finally, we discuss their value for the diagnosis of causes of meiosis-based infertility in humans.

KEYWORDS

meiosis, checkpoint, infertility, human infertility, mammalian

1 General aspects of mammalian gametogenesis

The perpetuation of most living beings and their genetic information across generations relies on a critical biological process-gametogenesis. In mammals, this process includes oogenesis and spermatogenesis, through which unipotent diploid precursor cells develop into mature haploid gametes, eggs in females, or sperm in males. After fertilization, the united egg and sperm form the embryo that develops into a new diploid organism carrying maternal and paternal genomic material.

During early mouse embryonic development, primordial germ cells (PGCs) are singled out at the epiblast (at ~ embryonic day (E) 7.25) (Chiquoine, 1954; Ginsburg et al., 1990), migrate along the developing gut and eventually colonize the future gonads (at ~ E10.5) (Molyneaux et al., 2001). Soon, PGCs switch from multipotential to bipotential and obtain the competence to initiate sexual differentiation and meiosis (Lesch and Page, 2012). At ~ E12.5, the expression of the Y chromosome-encoded gene, Sry, determine the gonads to become the testes (Koopman et al., 1991). Consequently, PGCs commit to divergent

development based on the cues from the somatic environment: female and male PGCs differentiate to their specialized gamete precursors: oogonia and spermatogonia, which initiate meiosis to form eggs through oogenesis or sperm through spermatogenesis (Edson et al., 2009).

In mammals, meiosis exhibits substantial sexual dimorphism (Handel and Eppig, 1997; Morelli and Cohen, 2005). Female meiosis is initiated roughly simultaneously in all oogonia during fetal development and subsequently arrests at the end of meiotic prophase I (dictyotene stage) around birth. It resumes producing eggs periodically after puberty over a defined reproductive lifetime. Female meiosis I does not complete until ovulation, and meiosis II only occurs under the trigger of fertilization, eventually generating only one haploid oocyte from one oogonium. In contrast, male meiosis is initiated in separate cohorts of spermatogonia after the onset of puberty and provides continuous sperm production throughout most of adult life. The two meiotic cell divisions in males are consecutive and result in four haploid sperm from each spermatogonium that initiates meiosis.

Both spermatogonia and oogonia enter meiosis during preleptotenema but before S phase. The sexually dimorphic timing of meiosis entry depends on the Stimulated by Retinoic Acid gene 8 gene (Stra8) (Handel and Schimenti, 2010). In females, retinoic acid (RA) synthesized in the mesonephric ducts (Bowles et al., 2006) induces Stra8 expression, resulting in meiosis initiation (Koubova et al., 2006; Baltus et al., 2006); however, in males, RA is degraded by CYP26B1 (gene cytochrome P450, family 26, subfamily b, polypeptide 1) from Sertoli cells, preventing the induction of Stra8 and thus blocking the meiotic entry (Bowles et al., 2006). The ability to enter meiosis is gained in males postnatally when the expression of CYP26B1 is repressed in male gonads (Koubova et al., 2006; Bowles et al., 2006; Anderson et al., 2008; Lesch and Page, 2012). The exact RA-Stra8 meiotic initiation pathway remains elusive. This is mainly due to the role of RA as a meiosis-inducing substance is unclear and has been challenged (Kumar et al., 2011; Vernet et al., 2020), particularly by a recent study showing that meiosis can normally occur in the absence of all RA receptors in female mice (Vernet et al., 2020). The role of STRA8 in meiotic initiation is more clear and STRA8 is suggested recently to trigger meiosis initiation in mice together with MEIOSIN in a broad transcriptional network, probably by activating genes responsible for suppressing the mitotic program and establishing a meiosis-specific chromosome structure under the presence of RA (Kojima et al., 2019; Ishiguro et al., 2020). Notably, other pathways are also suggested to mediate meiosis initiation in mice, such as the BMP-ZGLP1 pathway that works in parallel with RA-STRA8 signaling (Nagaoka et al., 2020), STRA8-independent RA-REC8 pathway (Koubova et al., 2014; Soh et al., 2015) and epigenetic regulated negative controls (Yamaguchi et al., 2012; Yokobayashi et al., 2013; Endoh et al., 2017).

1.1 Spermatogenesis

Mammalian male fertility requires millions of sperm produced daily by continuous spermatogenesis throughout reproductive life. The continual spermatogenesis is founded on a stem cell pool supplied by spermatogonial stem cells (SSCs) (de Rooij and Russell, 2000; Oatley and Brinster, 2008). Spermatogenesis continues with the mitotic expansion of spermatogonia, the meiotic divisions of spermatocytes, and the morphological transformations of spermatids.

SSCs are testis-specific stem cells derived from PGCs. In mice, male PGCs arrested at the G0/G1 phase migrate and differentiate into SSCs around 3 days *postpartum* (dpp) (Bellve et al., 1977; McLean et al., 2003). One subpopulation of these cells (Neurogenin 3 (NGN3)-negative) initiates the first round of spermatogenesis during the second week after birth; the other subpopulation develops into morphologically distinct, NGN3-positiveSSCs and supplies SSCs for spermatogenesis during adulthood (Yoshida et al., 2006). SSCs (As (A-single) spermatogonia) undergo symmetric division to produce SSCs for self-renewal or progenitor spermatogonia (Apr (A-paired) spermatogonia) for differentiation, which marks the beginning of spermatogenesis. SSC self-renewal predominates during the neonatal period to establish a stem cell pool (Shinohara et al., 2001) but only occurs periodically under steady-state conditions during adulthood to maintain the SCC pool (Oatley and Brinster, 2012). Apr spermatogonia undergo seven rounds of mitotic cell divisions to form undifferentiated Aal spermatogonia (Aal (A-aligned) spermatogonia)and differentiated A1, A2, A3, A4, In (Intermediate), and B spermatogonia. B spermatogonia differentiate into preleptotene spermatocytes *via* a final round of mitosis and initiate meiosis (Russell et al., 1993; de Rooij and Russell, 2000; Rato et al., 2012).

Diploid spermatocytes proceed through meiosis, resulting in haploid round spermatids. Subsequently, these round spermatids undergo structural and functional changes, including nuclear remodeling by chromatin condensation, removing the excess cytoplasm, and forming an acrosome and a sperm tail (spermiogenesis) (Hermo et al., 2010; Lehti and Sironen, 2016). As a result, spermatids become motile spermatozoa and are released to the central seminiferous lumen (spermiation). Spermatozoa will complete the final maturation to become fertilizable sperm in the epididymis.

Spermatogenesis occurs within the seminiferous tubules of the testis, in which germ cells in different stages of development are organized into a series of cell associations known as stages. In mouse testis, 12 stages have been defined (Hasegawa and Saga, 2012). RA pulses progressively stagger along the tubule and stimulate the spermatogonia to enter the rigidly timed pathway committed to meiosis. This determines the seminiferous epithelial cycle initiation and eventually enables the continuous release of spermatozoa (de Rooij and Russell, 2000).

In the seminiferous epithelium, Sertoli cells form specialized tight junctions (so-called “blood-testis barrier” (BTB)) at their base to separate the seminiferous epithelium into basal (where the spermatogonial population resides) and the adluminal compartments (where the meiotic and haploid germ cells reside). The BTB blocks the elements from the interstitial space to maintain homeostasis for meiotic and haploid germ cell development in the adluminal compartment (O’Donnell et al., 2000; Oatley and Brinster, 2008). The BTB remodels periodically (controlled by RA) to ensure preleptotene spermatocytes enter the adluminal compartment to initiate meiosis (Hasegawa and Saga, 2012). The steroidogenic Leydig cells reside in interstitial tissue between the

seminiferous tubules and secrete testosterone under the influence of LH.

1.2 Oogenesis

Mammalian oogenesis begins during embryonic development and generates primary oocytes assembled in primordial follicles perinatally. The establishment of the pool of primordial follicles determines mammalian female fertility. Post-pubertally, primordial follicles are recruited irreversibly and develop into mature follicles during the estrous/menstrual cycle, eventually releasing mature and fertilizable oocytes. As a result, the ovarian reserve is gradually reduced, defining a finite female reproductive life span (Kerr et al., 2013; Li and Albertini, 2013; Wear et al., 2016; Hunter, 2017; Ruth et al., 2021).

In mice, after differentiation of PGCs, oogonia undergo mitotic divisions with incomplete cytokinesis, forming germ cell cysts in which daughter cells are connected by intercellular bridges (McLaren and Monk, 1981; Pepling and Spradling, 1998). On E13.5, oogonia in the cysts initiate meiosis and eventually differentiate into primary oocytes, which will complete the first meiotic prophase and arrest at dictyotene perinatally (Borum, 1961). After cyst breakdown, primary oocytes are enclosed in a layer of somatic pre-granulosa cells, forming primordial follicles by 4dpp (Pepling and Spradling, 2001). The formation of primordial follicles is a complex process. It requires the presence of germ cells (McLaren, 1984) and involves communication between oocytes and pre-granulosa cells (Pepling, 2012).

In mammals, massive oocyte culling accompanies oogenesis. Mouse oocyte numbers begin to decline since E14.5, remain about half at birth, and continue reducing postnatally. At 4dpp, eventually, only 20% of fetal oocytes remain in the ovaries (Malki et al., 2014; Hunter, 2017; Martínez-Marchal et al., 2020). This massive oocyte death might result from oocyte quality control (Hunter, 2017). Oocytes with potential defects due to the activation of LINE1 transposon are eliminated during embryonic development (E15.5-18.5) in mice, leaving only oocytes with limited LINE1 activity (Malki et al., 2014). Postnatally, oocyte culling occurs in response to errors in meiotic prophase I to remove oocytes that might have chromosomal defects (Di Giacomo et al., 2005). Additionally, the loss of oocytes is also suggested to be the self-sacrifice of the so-called nursing oocytes, similarly to a well-characterized process that occurs during oogenesis in *Drosophila* (Lei and Spradling, 2016). In *Drosophila,* during oogenesis, nurse cells surrounding the growing oocyte provide nutrients and other factors required for development. The nurse cells form a syncytium with the egg, where the cytoplasm and organelles are shared among the cells, allowing for efficient transport of substances to the growing egg. Additionally, the nurse cells also help to regulate the developmental program of the egg by providing signals and controlling the expression of specific genes. In this way, the nursing cells play a crucial role in ensuring the proper development and survival of the egg. Thus, the oocyte quality control processes select the most suitable oocytes for the next-generation.

Newly formed primordial follicles remain quiescent until recruited. A cohort of primordial follicles located at the anterior-dorsal region of the mouse ovary is activated to grow during the first week of postnatal development, the first wave of folliculogenesis (Cordeiro et al., 2015). After puberty, quiescent primordial follicles are continually recruited through primordial activation to initiate follicular development, forming primary follicles with a single layer of cuboidal granulosa cells (Lintern-Moore and Moore, 1979).

Primary follicles continue developing through two phases: pre-antral and antral phases. Through the pre-antral phase, primary follicles become secondary/pre-antral follicles with two or more layers of granulosa cells. This development is independent of gonadotropins and is mainly regulated by autocrine and paracrine signaling, specifically, the TGF-β family members such as oocyte-secreted GDF-9 and BMP-15 (Yan et al., 2001; Günesdogan and Surani, 2016; Namwanje and Brown, 2016). Through the antral phase, antral follicles are formed. The presence of an antrum-a granulosa cell-secreted fluid-filled cavity characterizes antral follicles. The follicle development during this phase depends on gonadotropins FSH and LH (Williams and Erickson, 2000). FSH stimulates granulosa cells to proliferate and secrete estrogens. LH stimulates the theca cells to produce progesterone and testosterone. More importantly, the rise of the FSH level during the menstrual cycle allows the selection of dominant follicles, enabling only some of the growing antral follicles to develop into ovulatory follicles (Zeleznik, 2004).

Since the initiation of follicular development, oocytes start to grow in size and are transcriptionally and translationally active (Lintern-Moore and Moore, 1979). However, they remain arrested at the end of the meiotic prophase, marked by a large nucleus-the germinal vesicle-with a prominent nucleolus. This arrest is maintained by the combined effects of the cyclic adenosine monophosphate (cAMP) and cyclic guanosine monophosphate (cGMP) (Norris et al., 2009; Jaffe and Egbert, 2017). When the follicles reach the preovulatory stage, in response to LH surge, oocytes will resume meiosis and complete maturation, as seen by the germinal vesicle breakdown. Subsequently, oocytes complete the first meiotic division but arrest at metaphase II upon ovulation and will resume meiosis if fertilized, eventually generating a mature oocyte with two or three polar bodies that will undergo apoptosis. Besides the nuclear maturation, which involves the haploidization of the genome, the oocyte cytoplasm must also mature through major translational, post-translational, and organellar modifications, which are essential for the completion of meiosis, fertilization, and early embryonic development (reviewed in Li and Albertini, 2013).

2 Meiosis

Meiosis is a specialized cell division critical for gametogenesis in all sexually reproducing organisms. Through meiosis, a diploid parental cell gives rise to haploid daughter cells, and this is achieved by a single round of DNA replication followed by two rounds of cell divisions (Kleckner, 1996). Homologous chromosomes separate during the first division (meiosis I), and sister chromatids separate during the second division (meiosis II) analogously to mitosis, resulting in the generation of haploid cells. A canonical meiotic program present in most organisms (e.g., mammals, budding yeast, plants, *etc.*) will be briefly described in

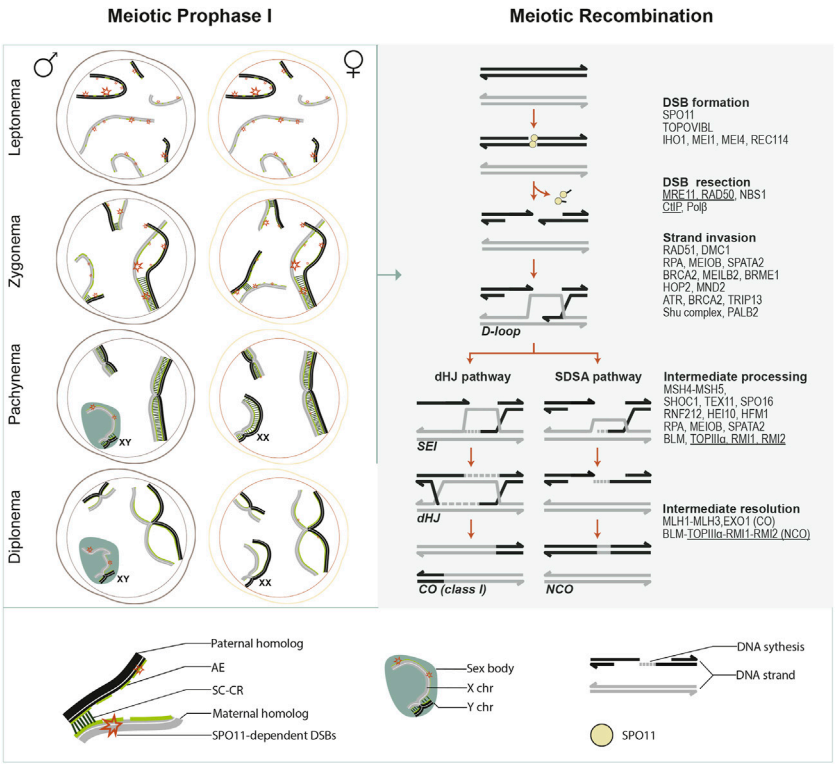

FIGURE 1
Meiotic prophase I overview. This schematic illustrates chromosome dynamics during meiotic prophase I in spermatocytes and oocytes (left panel) and the meiotic recombination pathway (right panel). Left panel, in meiotic prophase I, each paternal (black) or maternal (grey) homologous chromosome is organized around a chromosomal axis. During leptonema, axial elements (AEs) develop for each chromosome, and programmed SPO11-induced DSBs are generated as recombination initiates. During zygonema, synapsis initiates between paired homologs. Then it spreads along with the entire AEs as the SC central region (CR) proteins (consisting of the transverse filaments (TFs) and the central element (CE)) are installed between the AE. AEs are then designated as lateral elements (LEs) of the SC. In the meantime, DSBs are gradually repaired as recombination progresses. By pachynema, homologous chromosomes are fully synapsed, except for the heteromorphic X and Y chromosomes in the spermatocytes, which synapse only in a short pseudoautosomal region and form a transcriptionally silent chromatin compartment known as the sex body. By the end of pachynema in spermatocytes or during late pachynema/early diplonema in oocytes, meiotic recombination completes as DSBs on autosomes are all repaired, and crossovers (COs) are generated. During diplonema, the CR is disassembled, and homologous chromosomes are only held together at the CO sites (chiasmata). From diplonema, spermatocytes progress to metaphase I, completing meiotic divisions without interruption. In contrast, oocytes arrest at the dictyate stage until meiotic resumption after puberty. Right panel, several major events and critical transitions occur during meiotic recombination. Mammalian proteins that are, or are predicted (underlined) to be, involved in each event are listed. SPO11 catalyzes DSB formation in association with its accessory proteins. DSB ends are further resected through a series of nucleolytic activities mediated by the MRN complex (MRE11- RAD50-NBS1) and others. As a result, a short oligonucleotide covalently attached to SPO11 (SPO11 oligo) is released, and 3′ ssDNA tails are generated, which are immediately coated by ssDNA binding proteins (such as RPA, MEIOB, SPATA22, *etc.*). Recombinases DMC1 and RAD51 assemble at resected 3′ ssDNA tails, promoted by recombination proteins such as MEILB2, BRCA2, BRME1, *etc.* RAD51 and DMC1 coated ssDNA are stabilized by HOP2-MND1 and engage in homology search and strand exchange, resulting in D-loop formation. The repair can proceed by either a double Holliday junction (dHJ) pathway or synthesis-dependent strand annealing (SDSA). ZMM proteins and other factors control this by processing and stabilizing the recombination intermediates. In the dHJ pathway, D-loops are further stabilized by MutSγ homologs (MSH4 and MSH5), and the second end of the DSB is captured to form a dHJ, requiring RPA-MEIOB-SPTATA22 complex. ZMM proteins such as HEI10 and RNF212 facilitate the recruitment of mismatch repair factors MutLβ homologs (MLH1, MLH3). MutLβ and EXO1 mediate the resolution of dHJ, primarily giving rise to crossover (CO) products. In SDSA, the invading strand is displaced after DNA synthesis and reanneals to the other end of the DSB, followed by further DNA synthesis and nick ligation, ultimately giving rise to non-crossover (NCO) products.

this section and expanded in detail, focusing on the two major meiotic events, synapsis and meiotic recombination (MR), in the following sections. Findings in mice will be prioritized to discuss in line with the scope of this review. However, data from other species, particularly yeast, will be addressed whenever necessary or of interest.

Meiosis is characterized by an extended prophase I, during which MR occurs (Figure 1). MR initiates in early prophase I with the formation of numerous DNA double-strand breaks (DSBs) catalyzed by the conserved SPO11 protein (Keeney, 2001). DSB ends undergo resection and generate 3′ssDNA ends, subsequently bound by the RecA family of strand exchange proteins (DMC1, RAD51) (San Filippo et al., 2008). This protein nucleofilament searches and invades homologous repair templates, initiating the repair pathways to form crossovers (COs), with reciprocal exchange of chromosome arms flanking the DSB site, or non-crossovers (NCOs), with no exchange of flanking parental sequences (Keeney and Neale, 2006; Hunter, 2015). NCOs promote homolog pairing while COs establish the connections between homologous chromosomes to ensure accurate segregation at meiosis I and reshuffle parental alleles to increase genetic diversity in offspring (Hunter, 2015; Lam and Keeney, 2015).

MR is tightly integrated with a highly-organized and dynamic chromosome structure throughout the five substages of meiotic prophase I (leptonema, zygonema, pachynema, diplonema, and diakinesis) (Zickler and Kleckner, 1999). During leptonema, the chromatin condenses at the developing chromosomal axes, and recombination initiates. The axes provide a rod-like center for the loops of every pair of chromatids to anchor, defining a loop-axis structure essential for DSB formation and repair template choice (Subramanian and Hochwagen, 2014). During zygonema, maternal and paternal homologs progressively pair. The loop-axis organization makes this close alignment of homolog axes possible. However, understanding how base-pair resolution pairing is achieved in the context of the complex meiotic chromosome architecture is limited. Several regulation layers, including meiotic recombination and dynamic chromosome movement, are suggested to promote homolog pairing (Bolcun-Filas and Handel, 2018). Synapsis initiates as a tripartite proteinaceous scaffold–the synaptonemal complex (SC)- which starts to form between the paired homologous chromosome axes to create an intimate association between them. While in some organisms (e.g., *Neurospora*, and *Coprinus*), synapsis initiates only after all homologs complete pairing, in budding yeast and mammals, synapsis begins concomitantly with homolog pairing at zygonema. The telomeres and several interstitial sites of DSB-mediated inter-homolog associations are often where synapsis initiates (Fung et al., 2004), while in mice and several organisms with metacentric chromosomes, including humans, centromeres are often the last to synapse (Roig et al., 2010; Bisig et al., 2012; Qiao et al., 2012). Once it initiates, synapsis quickly spreads along the chromosomes in both directions in a zipper-like manner. At pachynema, the SC is fully installed along the entire length of all homologous chromosomes (Fraune et al., 2012). The last recombination steps after strand invasion occur in the SC context, which further helps keep the homologs in association, generating COs at the end of pachynema. Subsequently, the SC disassembles asymmetrically between homologs throughout diplonema and diakinesis, accompanied by changes in chromosome compaction (Gao and Colaiácovo, 2018). By late diakinesis, the highly condensed bivalents only remain connected by chiasmata, the cytological manifestation of COs. These inter-homologous connections ensure correct segregation under tension by allowing homolog pairs to stably bi-orient at the metaphase I spindle (Handel and Schimenti, 2010). As Meiosis I completes, maternal and paternal chromosomes are separated into daughter cells. Then in Meiosis II, sister chromatids separate, ensured by their centromeric cohesion, resulting in the generation of haploid cells (Ishiguro, 2019).

Meiosis must be carefully monitored to preserve the order of meiotic events and avoid producing aberrant chromosomes and defective gametes (Subramanian and Hochwagen, 2014). In mice, surveillance mechanisms monitor recombination and synapsis at the pachytene stage (meiotic checkpoint) (Roeder, 2000) and control bipolar attachment to the spindle at metaphase I (the spindle assembly checkpoint, SAC) (Touati and Wassmann, 2016). Recent mice findings have revealed new mechanistic insights on how meiotic checkpoints monitor these meiotic prophase events in mammals, which will be mainly discussed below. The roles of the meiotic checkpoint machinery in preserving the order of chromosomal events during the meiotic prophase I will also be presented in the following sections whenever necessary.

2.1 The synaptonemal complex and synapsis

The SC is a highly conserved meiosis-specific feature. This is likely attributed to a conserved SC organization, e.g., the coiled-coil domains (Gao and Colaiácovo, 2018), whereas its component proteins share little similarity at the amino acid sequence level (Grishaeva and Bogdanov, 2014; Fraune et al., 2016). The SC serves as the scaffold for the close juxtaposition of homologous chromosomes and is intimately associated with chromosome pairing, synapsis, and recombination (Fraune et al., 2012; Cahoon and Hawley, 2016; Geisinger and Benavente, 2017; Gao and Colaiácovo, 2018). Fully formed SC is revealed as a tripartite structure by electron microscopy, consisting of two LEs that run along the electron-dense chromatin and flank a CR (Moses, 1969), composed of a central element (CE) and numerous transverse filaments (TFs). In mammals, eight meiotic-specific SC proteins have been identified and characterized so far (Schücker et al., 2018): SYCP2 and SYCP3 as the LE proteins (Lammers et al., 1994; Offenberg et al., 1998); SYCP1 as the TF protein (Meuwissen et al., 1992), and SYCE1, SYCE2, SYCE3, TEX12, and SIX6OS1 as the CE proteins (Costa et al., 2005; Hamer et al., 2006; Schramm et al., 2011; Gómez-H et al., 2016).

The SC plays a universal role, as providing order within the nucleus during prophase, in all species. But it may also have diverse roles in many organisms. Notably, it is essential for multiple steps during MR (Zickler and Kleckner, 2015). The SC regulates programmed DSB formation as synapsis shuts off the SPO11 activity (Kauppi et al., 2013). The AE proteins are closely associated with the development of recombination protein complexes. The CR plays a significant structural role in these complexes' assembly, maintenance, and turnover, thereby enabling the maturation of the DSBs into COs subject to interference. In mice, recombination can not be completed without the CR proteins (Bolcun-Filas et al., 2007; Schramm et al., 2011; Fraune et al., 2012; Gómez-H et al., 2016). Moreover, the SC is responsible for holding homologs after the repair of NCO-fated DSBs and maintaining interhomolog interactions until COs are formed (Zickler and Kleckner, 1999; Qiao et al., 2012). Finally, the SC might be centrally important in the surveillance of meiotic recombination and HORMAD-regulated monitoring of synapsis.

The SC undergoes a dynamic cycle through its assembly, a highly dynamic steady-state, and disassembly (Gao and Colaiácovo, 2018). Its assembly is through integrating the CR proteins to connect two LEs, a poorly understood process that might differ in various organisms due to the divergent SC component proteins (Cahoon and Hawley, 2016).

In mice, a picture of how the SC proteins are assembled in order has been inferred from mouse knockout studies (Fraune et al., 2012; Geisinger and Benavente, 2017). After DNA replication in the pre-meiotic S-phase, each pair of sister chromatids are tightly held together by cohesin complexes. The chromatin of sister chromatids is organized in a linear array of loops emanating from the chromosome axis, forming the meiotic axis-loop organization, which allows the close juxtaposition of homolog axes during

meiotic prophase (Zickler and Kleckner, 2015). During preleptotene stage, the AE/LE proteins: SYCP2 and SYCP3 load onto the cohesin complex together with the HORMA domain-containing proteins (HORMAD1 and HORMAD2) (Wojtasz et al., 2009), forming the chromosome axis during meiotic prophase I (Zickler and Kleckner, 1999; Yuan et al., 2000; Yang et al., 2006; Fujiwara et al., 2020). Recent studies suggest that SYCP2 mediates the anchoring of chromatin loops to the axis by associating with the cohesin complex (Feng et al., 2017; Xu et al., 2019). Moreover, SYCP2 possesses putative 'closure motifs' that might be responsible for HORMADs recruitment (West et al., 2019). Then, the CR proteins: SYCP1, SYCE3, and SYCE1, which are essential for synapsis initiation, are assembled between the AEs in sequence: the TF protein SYCP1 first associates with the AEs, likely through interacting with SYCP2 (Winkel et al., 2009; Schücker et al., 2015); and then recruits SYCE3 through direct interaction (Schramm et al., 2011; Hernández-Hernández et al., 2016). Subsequently, SYCE1 is loaded likely through interacting with SYCE3 (Lu et al., 2014). SYCE1 also interacts with and stabilizes SYCP1 (Costa et al., 2005). Recently, a novel CE protein, SIX6OS1, has been shown to be required downstream of SYCP1 at a similar hierarchy level to SYCE3 (Gómez -H et al., 2016b). Finally, synapsis spread along the entire length of homolog axes with the required loading of SYCE2 and TEX12 (Hamer et al., 2006). These proteins interact with the SC through SYCE2 binding to SYCP1, SYCE3, and SYCE1 (Costa et al., 2005; Bolcun-Filas et al., 2007; Schramm et al., 2011) and interact interdependently to promote the assembly and stabilization of the SC (Cahoon and Hawley, 2016; Geisinger and Benavente, 2017). All these CR proteins are required for fertility in female and male mice, unlike LE proteins, whereas knockout SYCP2 or SYCP3 leads to sterility in males but subfertility in females (Yang et al., 2006; Bolcun-Filas et al., 2007; Gómez-H et al., 2016).

The SC is completely assembled between all the lengthwise-aligned homologs at the pachytene stage. Interestingly, this SC structure is highly dynamic during early pachytene in yeast and C. elegans as the SC subunit composition are constantly changing (Voelkel-Meiman et al., 2012; Pattabiraman et al., 2017) and shifts to a more stable state in late pachytene as recombination progresses.

After CO formation, the SC disassembles as SYCP1 is lost from chromosome arms in diplotene. However, SC fragments remain at centromeres and CO sites, presumably to coordinate local chromosome organization and separate the homologous axes, until diakinesis (Bisig et al., 2012; Qiao et al., 2012). After removing SYCP1 from the centromeres, SYCP3 accumulates and persists in these regions until late diplotene, before the nuclear-envelope breakdown, likely to promote proper homologous centromere bi-orientation, ensuring appropriate homolog segregation (Bisig et al., 2012; Qiao et al., 2012).

Multiple layers of regulation are imposed on the formation and disassembly of the SC to coordinate these mechanisms with the MR in various organisms (Zickler and Kleckner, 2015; Gao and Colaiácovo, 2018). These include the regulation from structural axial protein (cohesin and HORMADs), the transcriptional regulation of the SC genes, translational control of SC proteins mRNAs, the association of non-structural regulators with SC components, protein modifications, *etc.* (Zickler and Kleckner, 2015; Gao and Colaiácovo, 2018).

In mice, AE formation depends on meiotic cohesion with different contributions from different cohesin (reviewed in (Ishiguro, 2019). HORMAD1 is essential for both homolog pairing and synapsis (Shin et al., 2010; Kogo et al., 2012a; Paigen and Petkov, 2018) as HORMAD1 promotes efficient DSB formation and enables DSB-mediated homology search (Shin et al., 2010; Kogo et al., 2012a; Paigen and Petkov, 2018). Moreover, HORMAD1 might also have a direct role in SC formation (Paigen and Petkov, 2018). Additionally, both HORMAD1 and HORMAD2 are required to surveil homolog synapsis (Wojtasz et al., 2009; Kogo et al., 2012b; Paigen and Petkov, 2018). Their absence rescues the loss of asynaptic oocytes in the SPO11-deficient background (details below).

In yeast, synapsis initiation is controlled by the 'ZMM' proteins. Also, the SUMOylation of several SC components is required for SC assembly (Humphryes et al., 2013; Leung et al., 2015). In mice, SC initiation depends on the total number of interhomolog engagements. Reduced DSBs levels lead to fewer interhomolog engagements, causing delayed synapsis (Kauppi et al., 2013). Whether SUMOylation is involved in SC assembly in mice is unclear, although similar to yeast Red1, mouse SYCP3 can also be SUMOylated (Xiao et al., 2016). A positive feedback system in yeast controls SC polymerization. The initial assembly of the transverse filament recruits central-element proteins, which recruit more transverse filaments. The mechanism controlling SC polymerization in mice remains unknown (Cahoon and Hawley, 2016). The control of the timing between the formation of a CO and SC disassembly is vital for proper chromosome segregation. In mice, this relies on cell-cycle kinases (PLK1, Aurora B, CDK1-Cyclin B1), which are regulated through transcriptional and translational mechanisms (Gao and Colaiácovo, 2018).

2.2 Meiotic recombination

Meiotic recombination is homologous recombination (HR)-where the homologous chromosomes are used as the template for DSB repair, generating NCO and CO products and impacting several other meiotic events during meiosis (Keeney, 2008; Lam and Keeney, 2015). In many organisms, including mammals, MR promotes the close juxtaposition of each pair of homologous chromosomes, thus facilitating chromosome synapsis. DSB-mediated interhomolog interactions generate CO products in the context of synapsed chromosomes, resulting in the exchange of alleles between homologs. Besides, COs facilitate the proper orientation of homologous pairs at metaphase and thus ensure they segregate accurately at the first meiotic division, eventually supporting functional gametes formation (Hunter, 2015; Lam and Keeney, 2015; Marsolier-Kergoat et al., 2018) (Figure 1).

MR initiates when numerous programmed DSBs are induced by the conserved SPO11 protein, the ortholog of subunit A of TopoVI DNA topoisomerase (TopoVIA) (Bergerat et al., 1997; Keeney et al., 1997). It catalyzes DNA cleavage *via* a transesterification reaction, generating meiotic DSBs covalently bound by SPO11 at the 5′end (De Massy et al., 1995; Liu et al., 1995) (Figures 1–5).

In many organisms, accessory DSB proteins are also required for SPO11-mediated DSB formation (Lam and Keeney, 2015). Notably, a TopoVIB-like subunit (TOPOVIBL), structurally similar to the

TopoVIB subunit of Topo VI topoisomerase, is also essential for meiotic DSB formation in mice and most likely in most eukaryotic species (Robert et al., 2016; Vrielynck et al., 2016).

In budding yeast, nine other accessory proteins form different subcomplexes, directly or indirectly interacting with SPO11, and are all required for DSB formation, including Ski8, Rec102-Rec104 complex, Rec114-Mei4-Mer2 complex, Mre11–Rad50–Xrs2 (MRX) complex (Lam and Keeney, 2015; Yadav and Claeys Bouuaert, 2021). In mice, three evolutionarily conserved proteins have also been identified to be required for SPO11-mediated DSB formation, including IHO1, MEI4, and REC114, the mouse orthologs of yeast Mer2, Mei4, and Rec114, respectively. These three proteins colocalize on the axes of the meiotic chromosome independently of SPO11 activity (Kumar et al., 2010; Stanzione et al., 2016; Kumar et al., 2018).

IHO1 is a direct interactor of the axial component protein HORMAD1 in mice (Stanzione et al., 2016). It is required for the axis-localization of REC114 and MEI4 *in vivo*. However, its axial localization is independent of MEI4 or REC114. Thus, IHO1 might act as a platform to recruit REC114 and MEI4 to the axes (Stanzione et al., 2016; Kumar et al., 2018). REC114 directly interacts with TOPOVIBL in mice, regulating the SPO11/TOPOVIBL catalytic activity (Nore et al., 2022). It is also inferred to perform this function *via* ATM-dependent inhibition of DSBs (Subramanian and Hochwagen, 2014; Boekhout et al., 2019). ATM might target REC114 directly by phosphorylating it, as in *S. cerevisiae* (Carballo et al., 2013), or indirectly by phosphorylating ANKRD31, a novel interactor of REC114 (Boekhout et al., 2019; Papanikos et al., 2019).

DSBs are non-randomly distributed along the chromosomes. They tend to accumulate preferentially at regions called recombination hot spots (Székvölgyi et al., 2015), which are determined by PRDM9 in most mammals (Paigen and Petkov, 2018). PRDM9 binds to specific DNA sequences in the genome through its zinc finger array. It then methylates histone H3 lysines 4 and 36 (H3K4me3 and H3K36me3) of nearby nucleosomes using its PR/SET domain, activating hot spots (Grey et al., 2018). Activated hot spots are believed to mainly locate at the DNA loops. It is not fully understood how they are further associated with the chromosomal axis where SPO11 and the accessory proteins are located. Studies have speculated that EWSR1, CDYL, EHMT2, and CXXC1 proteins might mediate this association through binding the KRAB domain of PRDM9 and interacting with the DSB proteins (Imai et al., 2017; Parvanov et al., 2017). As a result, PRDM9 targets SPO11 to specific genome regions, generating DSBs. Nevertheless, some DSB sites are targeted independently of PRDM9 in meiosis, e.g., the pseudoautosomal region (PAR) in male meiosis (Brick et al., 2012).

DSB formation is tightly controlled to occur in a narrow time window within prophase I, and in yeast, ATM plays an essential role in this by regulating further DSB formation *via* a negative feedback loop both in trans and cis (Barchi et al., 2008; Lange et al., 2011; Zhang et al., 2011; Garcia et al., 2015; Pacheco et al., 2015). Depleting ATM leads to significantly increased DSBs in multiple organisms, including mice (Joyce et al., 2011; Lange et al., 2011; Kurzbauer et al., 2012; Pacheco et al., 2015). ATM might prevent repeated DSB formation at the same chromosomal locus in mice as in yeast (La Salle and Trasler, 2006; Barchi et al., 2008; Lange et al., 2011; Garcia et al., 2015; Lukaszewicz et al., 2021). Besides, ATM might be involved in other feedback circuits to ensure enough DSBs are formed to support homolog interactions and recombination (Cooper et al., 2014).

After DSB formation, DSB ends are resected to generate ssDNA tails (Baudat et al., 2013; Lam and Keeney, 2015) (Figure 1).

The DSB resection is well elucidated in budding yeast. The MRX complex recognizes DNA-bound Spo11 and generates nicks nearby with Sae2, leading to the release of Spo11 bound to short oligonucleotides (*Spo11 oligos*) (Neale et al., 2005; Cannavo and Cejka, 2014). The nicks serve as entry points for short-range 3′→5′resection, mediated by Mre11 exonuclease activity, and long-range 5′→3′resection, mediated by Exo1 exonuclease activity and Dna2 nuclease (Manfrini et al., 2010; Zakharyevich et al., 2010; Garcia et al., 2011). The consequence is the generation of 3′ssDNA tails on both sides of the DSB. The full-length resection requires the DSB-responsive kinase Tel1, which promotes resection initiation, likely through Sae2 phosphorylation (Cartagena-Lirola et al., 2008), and regulates resection length (Mimitou et al., 2017).

In mammals, EXO1 is dispensable for DSB resection (Wei et al., 2003), and the nucleotide-excision repair factor, DNA polymerase-β, is implicated in SPO11 removal (Kidane et al., 2010). However, the role of the mammalian MRX complex and Sae2 homologs, the MRN complex (MRE11-RAD50-NBS1) and CtIP, respectively, in meiotic DSB repair is poorly understood due to the embryonic lethality of knocked-out mice of any MRN component (Pacheco et al., 2015; Zhang et al., 2020a). A recent study has demonstrated that conditional disruption of NBS1 in mouse testis causes a dramatic reduction of DNA end resection and severe defect in chromosome synapsis, eventually leading to meiotic arrest and infertility (Zhang et al., 2020a). Thus, like MRX in yeast, the MRN complex is likely essential for mammalian DSB resection.

Resected 3′ssDNA tails are immediately bound by replication protein A (RPA) and RPA1-related protein MEIOB and its associated factor, SPATA22. The recombinases DMC1 and RAD51 further replace these. Then, one of the RAD51/DMC1-coated ssDNA commences engaging in homology search and interhomolog interactions. Consequently, unstable nascent D-loop intermediates are likely generated *in vivo*. These are either destabilized in the NCO pathway or stabilized in the CO pathway (Brown and Bishop, 2015; Hunter, 2015) (Figure 1).

DMC1 and RAD51 are strand-exchange proteins. RAD51 functions in somatic and meiotic cell cycles, whereas DMC1 is meiosis-specific (Brown and Bishop, 2015). DMC1 is the essential DNA strand–exchange factor in meiosis, while RAD51 could be dispensable but performs a critical regulatory role in yeast and mammals (Cloud et al., 2012; Hinch et al., 2020).

The assembly of both recombinases is ATP-dependent and promoted by several recombination factors in mammals such as ATR, breast cancer 2 protein (BRCA2), TRIP13, the Shu complex SWS1-SWSAP1, and PALB2, *etc.* (Zelensky, Kanaar, and Wyman, 2014; Abreu et al., 2018; Roig et al., 2010; Pacheco et al., 2018; Felipe-Medina et al., 2020; Zhang et al., 2020b; Zhang et al., 2019a; Widger et al., 2018). Several recent studies identified BRCA2 localizer (MEILB2) and MEILB2's stabilizer (BRME1), both of which form a complex with BRCA2 and function as the recruiter of RAD51 and DMC1 onto ssDNA (Zhang et al., 2019a; 2020b; Felipe-Medina et al., 2020). The activity of the DMC1-RAD51 complex to promote

homology search and strand exchange is driven by the stability of the formed nucleoprotein filament (Brown and Bishop, 2015), which is enhanced by the HOP2-MND1 complex (Petukhova et al., 2003; Petukhova et al., 2005; Chi et al., 2007; Pezza et al., 2007).

In stark contrast to the exclusive inter-sister (IS) recombination interactions occurring in the somatic cell cycle, MR interactions are biased towards homologous chromosomes, thereby promoting pairing, synapsis, and formation of chiasmata between homologous chromosomes. The precise mechanism of this meiotic inter-homolog (IH) bias is unclear but is likely achieved both by inhibiting IS bias and promoting IH bias. The so-far best-understood mechanism was uncovered in yeast, involving Tel1/Mec1 (ATM/ATR), Hop1 (homolog of HORMAD1/2), effector kinase Mek1 (homolog of CHK2), and RAD54, an SWI/SNF-family ATPase (Subramanian and Hochwagen, 2014).

In the contemporary meiotic recombination models that are largely built on yeast studies, single-strand invasions result in less stable nascent joint molecules, presumably D-loops. The differentiation of D-loops leads to either NCOs *via* synthesis-dependent strand annealing (SDSA) or class I COs subject to interference (details of CO interference will be discussed below) *via* forming CO-specific intermediates single-end invasions (SEIs) and double Holliday junctions (dHJs) (Figure 1). D-loops are stabilized along the CO pathway to form SEIs, which are the earliest detectable CO-specific joint molecules. Subsequently, SEIs become more stable dHJs joint molecules through a second-end capture coupled with DNA synthesis. Eventually, dHJs are resolved exclusively into class I COs. By contrast, unstable D-loops are not stabilized in the NCO pathway after the invading strand extends. The nascent DNA is annealed to the other end of the broken DNA molecule resulting in NCOs. Additionally, a minority of D-loops escape from these two pathways and generate NCOs and non-interfering class II COs (Baudat et al., 2013; Hunter, 2015; Ranjha et al., 2018).

The differentiation of the CO and NCO pathways is controlled by a panel of factors through processing and stabilizing the recombination intermediates, including ZMM proteins and a helicase complex, STR/BTR (yeast Sgs1–Top3–Rmi1, metazoan BLM-TOPIIIα-RMI1-RMI2) (Hunter, 2015). ZMMs stabilize recombinational joint molecules and promote the formation of SC, ultimately required for class I CO formation. In budding yeast, ZMMs are CO-specific. However, in mice and several other species, ZMMs' stabilization of recombinational interactions may be a prerequisite for CO designation, and D-loops bound by ZMMs could also form NCOs products (De Vries et al., 1999; Edelmann et al., 1999; Kneitz et al., 2000; Higgins et al., 2008; Yokoo et al., 2012; De Muyt et al., 2014; Zhang et al. Liang, 2014).

ZMM is a group of functionally diverse proteins, and several mammalian ZMM proteins have been identified to have a role in the CO/NCO decision: MSH4, MSH5, TEX11, RNF212, HEI10, HFM1, SHOC1, and SPO16. All of these proteins partially colocalize with recombination foci (defined by RAD51 and DMC1) on synapsed axes (De Vries et al., 1999; Edelmann et al., 1999; Kneitz et al., 2000; Adelman and Petrini, 2008; Guiraldelli et al., 2013; Guiraldelli et al., 2018; Qiao et al., 2014; Prasada Rao et al., 2017; Zhang et al., 2019b).

MSH4 and MSH5 are homologs of the bacterial MutS family of mismatch repair proteins with no known function in mismatch repair and form the MutSγ heterodimer (Pochart et al., 1997), which is essential for chromosome synapsis, CO formation, and thus fertility in mice (De Vries et al., 1999; Edelmann et al., 1999; Kneitz et al., 2000). HFM1 is essential for mammalian fertility as mutated HFM1 was found in human patients with azoospermia or POI syndromes (Baudat et al., 2013; Wang et al., 2014; Zhang et al., 2017) and removing HFM1 causes a drastic reduction of COs and partially affects synapsis in mice (Guiraldelli et al., 2013). The deficiency of SHOC1, TEX11, and SPO16 causes reduced COs with a relatively minor synapsis defect in mice, suggesting a conserved role in CO formation as in yeast (Adelman and Petrini, 2008; De Muyt et al., 2018; Guiraldelli et al., 2018; Zhang et al., 2019b). Mouse RNF212 and HEI10, a ubiquitin-ligase, regulate CO by modifying recombination factors (MutSγ) at CO-designated sites in an antagonistic manner. Subsequently, stabilized recombination factors enable the recruitment of CO-specific factors (MLH1-MLH3, MutLγ) for CO maturation (Reynolds et al., 2013; Qiao et al., 2014; Hunter, 2015; Gray and Cohen, 2016; Prasada Rao et al., 2017).

During early recombination steps, STR/BTR is required for channeling early joint molecules into CO and non-CO pathways. Later, STR/BTR promotes the resolution of the final recombination intermediates into NCOs by its dissolution activity *via* SDSA (Hunter, 2015). Distinguishingly, in the CO pathway, the resolution of joint molecules is mediated by the endonuclease activity of mismatch repair factors MLH1, MLH3, and EXO1 to generate class I COs. MLH1 and MLH3 are invaluable markers of crossovers in the cytological analysis as they localize precisely to future CO sites in many organisms (Kolas and Cohen, 2004). Additional factors are found to be required for class I CO formation in mice, including HEI10 (discussed above), CNTD1, PRR19 and CDK2 (Holloway et al., 2014; Qiao et al., 2014; Bondarieva et al., 2020).

For non-interfering class II COs, the resolution of joint molecules is mediated by structure-specific endonucleases, Mus81, Yen1, and Slx1/4 in yeast and MUS81 in mice (Holloway et al., 2008; De Muyt et al., 2012; Zakharyevich et al., 2012). In mice, interfering COs are estimated to account for ~90% of COs (Holloway et al., 2008; Serrentino and Borde, 2012), and consistently, the deletion of MLH1, MLH3, or EXO1 causes significant loss of chiasmata and, consequently, mice sterility (Baker et al., 1996; Edelmann et al., 1996; Lipkin et al., 2002; Wei et al., 2003).

Finally, another layer of control tightly regulates the outcome of DSB repair. CO numbers per meiosis show a low variation despite a much more considerable variation in the numbers of recombinational interactions. This phenomenon is called CO homeostasis, which is underpinned by the lower and upper limits for the CO numbers regulated by CO assurance and interference (Martini et al., 2006; Rosu et al., 2011; Cole et al., 2012; Yokoo et al., 2012; Hunter, 2015). CO assurance guarantees that each homolog pair obtains at least one CO to segregate properly at meiosis I. Meanwhile, interference is defined by an inhibitory zone around CO-designated sites where other DSBs are prevented from becoming COs. Interference results in COs being widely and evenly spaced along the genome (Hillers, 2004; Berchowitz and Copenhaver, 2010; Zhang and Liang, 2014).

The molecular mechanisms responsible for CO assurance and interference have been long elusive. Studies in various species have described different mechanisms regulating CO interference (Zhang and Liang, 2014; Zhang and Wang, 2014; Fowler et al., 2018; Capilla-Pérez et al., 2021; France et al., 2021; Morgan et al., 2021). A study of fission yeast *S. pombe* suggests a clustering model, emphasizing DSB interference as the basis for CO interference (Fowler et al., 2018). In this model, in each cluster containing several DSB hotspots, only one single DSB is formed. Given that DSBs are the precursors to COs, consequently, at most, a single CO is made in the chromosomal interval corresponding to the DSB hotspot-clustered interval (Fowler et al., 2018). Studies in budding yeast described a stress-and-stress relief mechanism for CO interference (the 'beam-film' model), which is SC independent and requires topoisomerase II (Zhang and Liang, 2014; Zhang and Wang, 2014). Distinctly, recent work in *Arabidopsis* demonstrated that the SC is essential for CO interference (Capilla-Pérez et al., 2021; France et al., 2021). Finally, a new model (the diffusion-mediated coarsening model) is proposed to explain CO interference (Morgan et al., 2021). These models may apply to some but likely not all species since the mechanism and control of meiotic recombination varies among species.

How the outcome of DSB repair is regulated in mice is poorly understood, and ATM may have a role in forming the obligate CO in the small pseudoautosomal region of homology between sex chromosomes and controlling the numbers and distributions of COs on autosomes (Barchi et al., 2008). However, this molecular mechanism elucidated in *S. pombe* is likely conserved in diverse organisms, including flies and mice, based on the features of meiotic recombination and pericentric regions in these species (Prieto et al., 2001; Manheim and McKim, 2003; Fukuda et al., 2012; Bhattacharyya et al., 2019; Hartmann et al., 2019; Smith and Nambiar, 2020).

2.3 Meiotic prophase surveillance mechanisms

DSB repair and synapsis are carefully monitored during the meiotic prophase to choreograph nuclear dynamics and cell division programs. An intricate meiotic checkpoint network has emerged to create dependencies between independent processes when homologous chromosomes pair, synapse, and recombine. The machinery of this meiotic checkpoint involves many canonical DNA damage response (DDR) signaling proteins, among which the two evolutionarily conserved sensor kinases, ATM and ATR, play a central role (MacQueen and Hochwagen, 2011). They detect and respond to DSBs with the help of checkpoint cofactors in many organisms. Once activated, ATM and ATR phosphorylate a large set of substrates, preferentially containing serine/threonine-glutamine (S/TQ) cluster domains (Traven and Heierhorst, 2005). Many of these target proteins act directly to implement the checkpoint response, while others work as transmitters to relay the checkpoint signals to downstream effectors, such as CHK1 and CHK2 kinases (Subramanian and Hochwagen, 2014). This section will discuss how the surveillance mechanisms of the meiotic prophase checkpoint monitor these meiotic events, particularly in mammals.

In response to DSB repair or synapsis defects, the cells trigger a cell cycle arrest at the pachytene stage to provide sufficient time to fix the errors. If errors persist, this mechanism can eventually activate apoptosis to cull meiocytes in various organisms (Roeder, 2000; Bhalla and Dernburg, 2005; Di Giacomo et al., 2005; Lu et al., 2010). In mammals, observations in mutant mice deficient in meiotic recombination suggest that two genetically distinct surveillance mechanisms contribute to the activation of the arrest in both males and females: the recombination (DNA damage) checkpoint monitoring the DSB repair process and the synapsis checkpoint monitoring SC formation (Roeder, 2000; MacQueen and Hochwagen, 2011; Subramanian and Hochwagen, 2014; Joshi et al., 2015).

In males defective in DSB repair, like *Trip13*$^{mod/mod}$ and *Dmc1*$^{-/-}$ mice, most spermatocytes arrest before incorporating the testis-specific histone 1t (H1t) at pachynema (Barchi et al., 2005; Marcet-Ortega et al., 2017; Testa et al., 2018). In contrast, *Spo11*$^{-/-}$ spermatocytes, which do not have programmed DSBs, incorporate H1t and progress further, reaching mid/late pachytene. These cells arrest before completing the meiotic prophase and ultimately apoptose (Barchi et al., 2005; Pacheco et al., 2015). Therefore, irrespective of the common apoptosis consequence, spermatocytes respond differently to these two meiotic defects. Furthermore, the removal of DSBs confers a *Spo11*-like phenotype to those DSB repair-deficient mutants (*Dmc1*$^{-/-}$ and *Trip13*$^{mod/mod}$) (Barchi et al., 2005; Li and Schimenti, 2007), indicating that separate checkpoints act sequentially to mediate the apoptosis of these defective spermatocytes.

Likewise, in females, the elimination of oocytes defective for DSB repair (*Trip13*$^{mod/mod}$) or both DSB repair and synapsis (*Dmc1*$^{-/-}$, *Msh5*$^{-/-}$) occurs earlier (around birth) than those defective for synapsis alone (*Spo11*$^{-/-}$, up to 2 months *postpartum*) (Di Giacomo et al., 2005; Li and Schimenti, 2007). Also, mutations disrupting DSB formation (*Spo11* and *Mei1*) are epistatic to those affecting DSB repair (*Dmc1*, *Atm*, *Trip13*, and *Mcmdc2*) (Di Giacomo et al., 2005; Reinholdt and Schimenti, 2005; Li and Schimenti, 2007; Finsterbusch et al., 2016; Martínez-Marchal et al., 2020). These lines of evidence further support the existence of two distinct checkpoint mechanisms in mammals, sensing DNA damage or synapsis errors and resulting in meiotic prophase arrest. However, there are also arguments against a specific "synapsis checkpoint", at least in females, favoring that a canonical DNA damage checkpoint primarily accounts for the oocyte loss in response to both recombination and synapsis defects (discussed below) (Rinaldi et al., 2017; Rinaldi et al., 2020).

2.3.1 The recombination checkpoint

The recombination checkpoint is likely activated when recombination intermediates persist at pachynema in mammals (Di Giacomo et al., 2005; Burgoyne et al., 2009; MacQueen and Hochwagen, 2011). So far, the study of the recombination checkpoint in mammals has been challenged because most mutations that compromise recombination also affect synapsis. However, a gene-trap-disrupted allele of *Trip13*, *Trip13*$^{mod/mod}$ (also known as *Trip13*^{RRB047RRB047}, X. Li and Schimenti, 2007; Roig et al., 2010), which cannot repair DSBs but completes synapsis, has proven to help study the recombination-dependent arrest and meiocyte elimination. Analyses of mice doubly or triply deficient for TRIP13 and other DDR genes uncovered several signaling

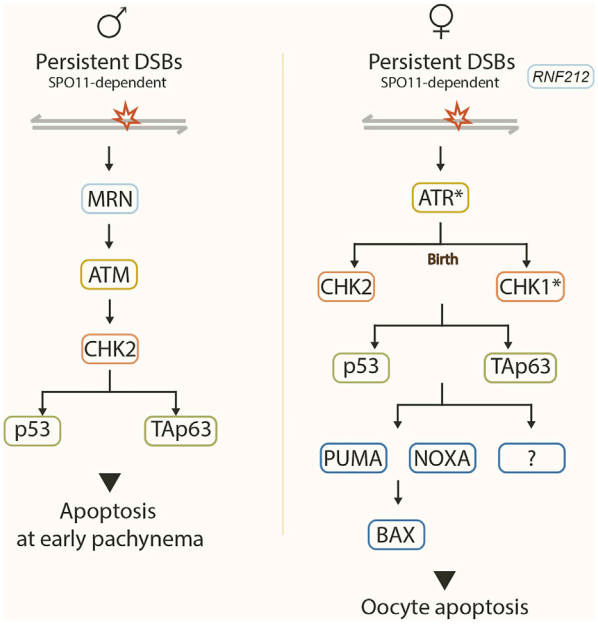

FIGURE 2
Recombination checkpoint pathway. Model showing the proposed signaling pathway in response to unrepaired SPO11-dependent DSBs in male (left) and female (right) mice. Asterisks represent predicted checkpoint factors. In males, DSBs are sensed by the MRN complex, leading to the activation of ATM, which in turn activates effector CHK2. CHK2 acts on target proteins p53 and TAp63, which implement the recombination-dependent arrest that blocks progression to mid/late pachynema. In females, RNF212 prevents the repair of residual DSBs in the late prophase. Unrepaired DSBs likely activate ATR, which may activate CHK2 before birth and CHK1 after birth. CHK1 and CHK2 signal to p53 and TAp3. Pro-apoptotic BCL-2 pathway components PUMA, NOXA, BAX, and other unknown factors act downstream to trigger oocyte apoptosis.

pathways involved in the recombination checkpoint-mediated arrest and/or apoptosis in both males and females (Bolcun-Filas et al., 2014; Pacheco et al., 2015; Marcet-Ortega et al., 2017; Rinaldi et al., 2017; Rinaldi et al., 2020).

In males, the MRN complex, ATM, CHK2, and the p53 family members, p53 and TAp63, are required to arrest spermatocytes with unrepaired DSBs at early pachynema before incorporating H1t into the chromatin (Pacheco et al., 2015; Marcet-Ortega et al., 2017; Marcet-Ortega et al., 2022) (Figure 2).

In *Trip13*$^{mod/mod}$ mice, spermatocytes enter pachynema with homologous chromosomes completely synapsed but with persisting recombination intermediates. Thus, most spermatocytes arrest and undergo apoptosis at epithelial stage IV before incorporating the mid-pachytene histone marker H1t (Li and Schimenti, 2007; Roig et al., 2010; Pacheco et al., 2015). In comparison, in *Trip13*$^{mod/mod}$ *Spo11*$^{+/-}$*Atm*$^{-/-}$ triple mutant mice, where the activity of ATM is removed, a significant proportion of spermatocytes accumulate H1t despite containing high levels of unrepaired DSBs. Thus, eliminating ATM activity allows spermatocytes to progress further, from an H1t-negative to an H1t-positive stage, despite having significant amounts of unrepaired DSBs. These findings suggest that ATM may be required for the recombination-dependent arrest at early pachynema (Barchi et al., 2005; Pacheco et al., 2015).

The MRN complex is responsible for DSBs sensing and activating ATM in somatic cells (Stracker and Petrini, 2011). It is also required for meiotic recombination in many organisms, including mammals (Keeney and Neale, 2006; Cherry et al., 2007). CHK2 is an effector kinase of the ATM signaling pathway activated in response to ionizing radiation (Matsuoka et al., 1998). Interestingly, disruption of the MRN complex or the CHK2 kinase in *Trip13*$^{mod/mod}$ mutants confers a meiotic progression phenotype similar to *Trip13*$^{mod/mod}$ *Spo11*$^{+/-}$*Atm*$^{-/-}$ mutants (Pacheco et al., 2015). Thus, the MRN-ATM-CHK2 signaling cascade is likely to respond to persistent unrepaired DSBs, mediating the recombination-dependent pachytene arrest in male mice (Pacheco et al., 2015). Similarly, p53 and TAp63, two canonical CHK2's downstream targets (Lu et al., 2010; Bolcun-Filas et al., 2014), have been inferred to act in the recombination-dependent arrest mechanism. This is based on the observations that *Trip13*$^{mod/mod}$ *p53*$^{-/-}$ and *Trip13*$^{mod/mod}$ *TAp63*$^{-/-}$ spermatocytes can progress to an H1t-positive stage (Marcet-Ortega et al., 2017).

In *Trip13*$^{mod/mod}$ mutants lacking ATM or with defective MRN complex, spermatocytes cannot correctly repair abundant DSBs caused by the disability of ATM's negative feedback in DSBs formation (Lange et al., 2011; Pacheco et al., 2015). Thus these spermatocytes fail to complete synapsis, which impedes the sex body formation (Barchi et al., 2008; Burgoyne et al., 2009; Roig et al., 2010; Pacheco et al., 2015). On the contrary, in *Trip13*$^{mod/mod}$ *Chk2*$^{-/-}$, *Trip13*$^{mod/mod}$ *p53*$^{-/-}$, and *Trip13*$^{mod/mod}$ *TAp63*$^{-/-}$ spermatocytes, although the sex body is formed, sex chromosomes are not correctly silenced, which explains why these spermatocytes eventually undergo arrest and apoptosis at late pachynema (Pacheco et al., 2015; Marcet-Ortega et al., 2017). These lines of evidence further support an alternative arrest mechanism mediating sex body defects in male mice (Barchi et al., 2005) (discussed below).

In females, an ATR-CHK1/CHK2-p53/TAp63-PUMA/NOXA-BAX signaling pathway is proposed to mediate the DNA damage checkpoint response in the oocytes (Bolcun-Filas et al., 2014; Rinaldi et al., 2017; ElInati et al., 2020; Martínez-Marchal et al., 2020; Rinaldi et al., 2020) (Figure 2).

Deletion of CHK2 rescues developing oocytes in 3-week-postnatal *Dmc1*$^{-/-}$ mice, although the absence of primordial follicles eventually results in a nearly complete oocyte depletion by 2 months *postpartum*. This pattern of oocyte loss is highly similar to that in *Spo11*$^{-/-}$ or *Spo11*$^{-/-}$*Dmc1*$^{-/-}$ mice, suggesting that the loss of CHK2 allows the deficient oocytes to surpass the DSB repair but not the synapsis arrest. Moreover, the deletion of CHK2 can reach a more successful rescue in *Trip13*$^{mod/mod}$ mice, which complete synapsis. *Trip13*$^{mod/mod}$ *Chk2*$^{-/-}$ mice have a significant pool of oocytes at 3 weeks *postpartum*, many follicles at 2 months of age, and sustained fertility for many months. Abundant γH2AX staining was detected in all dictyate *Trip13*$^{mod/mod}$ *Chk2*$^{-/-}$ oocytes indicating the persistence of unrepaired DSBs like in *Trip13*$^{mod/mod}$. Thus, CHK2 is required for the DNA-damage checkpoint-mediated oocyte elimination (Bolcun-Filas et al., 2014).

The lack of p53 and TAp63 enables nearly a complete rescue of *Trip13*$^{mod/mod}$ oocytes. Compared to wild-type mice, indistinguishable numbers of primordial and growing follicles are found in the triple mutant *Trip13*$^{mod/mod}$ *p53*$^{-/-}$ *TAp63*$^{-/-}$ mice (Rinaldi et al., 2020). Therefore, like in males, p53 and TAp63 might also act downstream of CHK2 in the DNA-damage checkpoint pathway in females. However, CHK2 deficiency only rescues *Trip13*$^{mod/mod}$ oocytes to around one-third of wild-type levels (Bolcun-Filas et al., 2014), implying other factors might signal these two effectors p53 and

TAp63 in parallel with CHK2. Indeed, CHK1 is likely to perform this function (Martínez-Marchal et al., 2020; Rinaldi et al., 2020). Studies have shown that when CHK2 is absent in ovaries, CHK1 is activated by persistent DSBs and is responsible for eliminating *Chk2*$^{-/-}$ oocytes (Martínez-Marchal et al., 2020; Rinaldi et al., 2020) (Figure 2).

Interestingly, the pro-apoptotic BCL-2-dependent pathway acts downstream of CHK2/p53/TAp63 and eliminates recombination-defective oocytes (ElInati et al., 2020). The BCL-2-dependent pathway consists of the known targets of p53 and TAp63 PUMA, NOXA, and BAX (Su et al., 2013). PUMA and NOXA or BAX deletion rescue oocyte numbers in DSB-repair mutants (*Dmc1*$^{-/-}$ and *Msh5*$^{-/-}$). However, like CHK2 deletion, this rescue does not reach wild-type levels, indicating that other components of this pathway also control the oocyte population (Bolcun-Filas et al., 2014; Rinaldi et al., 2017; ElInati et al., 2020) (Figure 2). Indeed, other p53 targets (e.g., BAK, PERP, or CDKN1A) have been proposed to play a role in this mechanism (ElInati et al., 2020).

Non-etheless, the factors acting upstream of CHK2 in the recombination checkpoint pathway are not clearly understood in females. The loss of ATM triggers oocyte elimination by DNA damage checkpoint in mice, which can be rescued by the deficiency of CHK2 to a degree similar to the rescue by CHK2 in *Dmc1*$^{-/-}$ ovaries (Bolcun-Filas et al., 2014; Rinaldi et al., 2020). Thus, it has been proposed that ATR, the other canonical DDR kinase, activates CHK2 in the recombination checkpoint pathway in females.

Furthermore, RNF212, a SUMO ligase required for crossover formation, is also suggested to promote the apoptosis of DSB repair-defective oocytes since *Rnf212* deletion significantly restores the oocyte pool at 18 days *postpartum* in DSB-repair mutant females (*Msh4*$^{-/-}$) (Qiao et al., 2018). RNF212 is proposed to impede DSB repair *via* inter-sister recombination (IS-HR) by stabilizing the association of HORMAD1 along desynapsed chromosome axes during the late prophase. Thus, residual DSBs, the repair of which *via* IS-HR are prevented by RNF212, trigger CHK2-mediated DNA damage checkpoint, resulting in oocyte elimination (Qiao et al., 2018; ElInati et al., 2020).

Notably, in both spermatocytes and oocytes, a certain level of unrepaired DSBs is required to activate the recombination-dependent arrest pathways during the meiotic prophase (Marcet-Ortega et al., 2017; Rinaldi et al., 2017). This is particularly important in spermatocytes, where DSBs on the X chromosome arms lacking homologous partners are repaired using the sister chromatids at mid-late pachytene, later than on autosomes (Page et al., 2012; Baudat et al., 2013). Thus, the DSB threshold level for arrest activation must be high enough, or all wild-type spermatocytes would be arrested. Only spermatocytes reaching the threshold could activate both p53 and p63, which work independently but additively to trigger apoptosis response (Marcet-Ortega et al., 2017). In females, the primordial follicle pool is wholely abolished in wild-type ovaries when the newborn ovaries are exposed to more than 0.3 Gy of irradiation. This dosage induces 10.3 RAD51 foci per oocyte (Rinaldi et al., 2017). Therefore, like in males, a threshold level of DSBs also triggers cell arrest in females.

2.3.2 The syapsis checkpoint

Defects in chromosome axis formation or SC assembly can activate a cell response to asynapsis independently of DSB formation in many organisms, leading to cell cycle arrest and even apoptosis (MacQueen and Hochwagen, 2011). In mammals, this synapsis checkpoint is debated: whether a specific surveillance mechanism monitoring asynapsis exists and how it senses it is unclear. Even if the synapsis checkpoint exists, it might not be like a formal checkpoint response (Cloutier et al., 2015; Turner, 2015; Rinaldi et al., 2017). In any case, the meiotic silencing of the unsynapsed chromatin (MSUC) plays a vital surveillance role in this so-called "synapsis checkpoint" in both males and females (Burgoyne et al., 2009; Cloutier et al., 2015; Turner, 2015).

The MSUC is a chromatin remodeling process by which unsynapsed regions are transcriptionally inactivated during meiotic prophase I (Turner, 2015) (Figure 3). It is achieved through the crosstalk between the axially located sensors signaling asynapsis, such as the axial component proteins HORMAD1/2 proteins (Wojtasz et al., 2009; Fukuda et al., 2010), and the loop-located effectors mediating gene silencing such as the histone variant H2AX

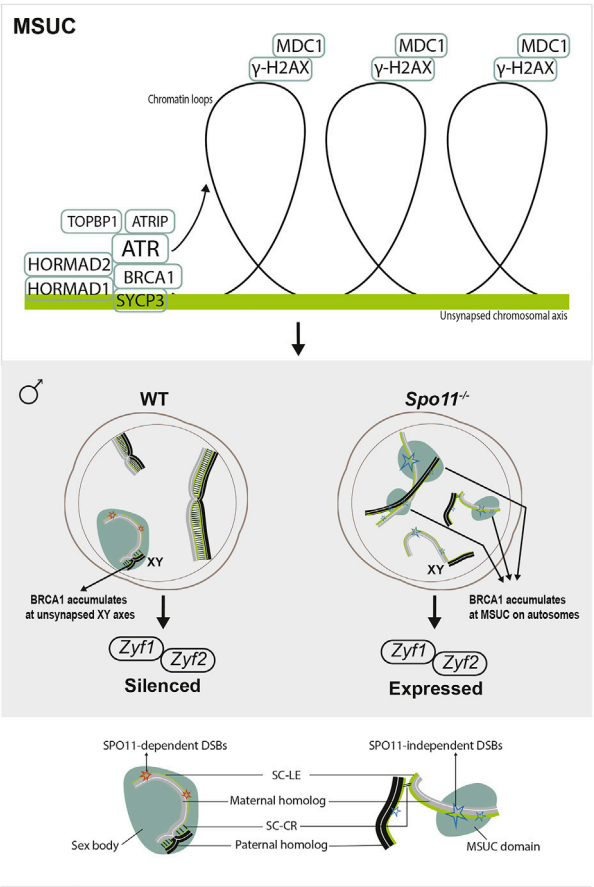

FIGURE 3
Meiotic response to asynapsis in male. Upper panel, meiotic silencing of the unsynapsed chromatin (MSUC). Axially located proteins signal asynapsis and recruit ATR with cofactors, such as BRCA1. If asynapsis persists, ATR translocates to chromatin loops, phosphorylating H2AX (γH2AX). This signaling spreads all over the chromatin with the help of MDC1, leading to the recruitment of silencing factors for the irreversible silencing of this region. Lower panel, in wild-type spermatocytes, the physiological MSUC occurs at XY chromosomes (MSCI), resulting in the silencing of sex chromosome-linked lethal genes (*Zfy1* and *Zfy2*). However, in *Spo11*$^{-/-}$ spermatocytes, despite extensive asynapsis, localized MSUC are triggered by SPO11-independent DSBs on unsynapsed autosomes. As BRCA1 accumulates at these DSB sites, MSCI fails to form, and lethal genes are expressed.

(Fernandez-Capetillo et al., 2003). HORMAD1 and HORMAD2 load onto chromosome axes at leptonema and are depleted from the axes by TRIP13 as the homologs synapse (Wojtasz et al., 2009; Fukuda et al., 2010; Roig et al., 2010; Koubova et al., 2014). By the late zygotene stage, HORMAD1/2 acts together with SYCP3 to recruit the breast cancer 1 (BRCA1) protein to the unsynapsed axes (Turner et al., 2004; Kouznetsova et al., 2009; Royo et al., 2013). Then, in a HORMAD1/2- and BRCA1-dependent manner, ATR is recruited to unsynapsed axes (Turner et al., 2004; Wojtasz et al., 2012; Paigen and Petkov, 2018), which further promotes the enrichment of BRCA1 and ATR-activating cofactors: TOPBP1, ATRIP (Perera et al., 2004; Refolio et al., 2011; Royo et al., 2013) as well as regulate phosphorylation of HORMAD1/2 (Fukuda et al., 2012). If asynapsis persists until pachytene, ATR translocates into the chromatin loops and phosphorylates H2AX (γH2AX) with the help of the γ-H2AX-binding factor MDC1, resulting in the irreversible silencing of this region (Ichijima et al., 2011).

In males, spermatocyte loss mediated by the DSB-independent response to asynapsis involves the failure of Meiotic Sex Chromosome Inactivation (MSCI) (Burgoyne et al., 2009) (Figure 3). MSCI is a physiological MSUC process that responds to the unavoidable partial asynapsis of the sex chromosomes (Turner et al., 2006). MSCI is reflected by the formation of the sex body, a specialized subnuclear domain encompassing the asynapsed portions of the X and Y chromosomes in pachytene spermatocytes. The sex body is characterized by the lack of gene expression and sequestration of an array of proteins, which are primarily heterochromatin-related (e.g., H2A, H3meK9, CBX1/3) and recombination-related (e.g., MRE11, γH2AX, and RAD51) (Handel, 2004). In mutant mice with extensive asynapsis (e.g., *Spo11*$^{-/-}$, *Dmc1*$^{-/-}$), MSCI cannot occur, and the sex body fails to form, likely due to the limited association of silencing factors with the XY axes (Mahadevaiah et al., 2008; Kouznetsova et al., 2009). At the zygotene/pachytene transition in wild-type spermatocytes, as DSBs get repaired, BRCA1 is released from the DSB sites and accumulates at the HORMAD1-coated asynapsed XY axes, initiating MSCI response (Mahadevaiah et al., 2008; Burgoyne et al., 2009). However, in mutants with extensive asynapsis, BRCA1 is widely sequestered at unrepaired SPO11-dependent DSB sites (e.g., *Dnmt3l*$^{-/-}$), thus failing to form MSCI (Mahadevaiah et al., 2008) or accumulates at SPO11-independent DSB sites, randomly triggering localized MSUC response at autosomal axes (Carofiglio et al., 2013). As a result, lethal sex chromosome-linked genes (e.g., Zfy1 and Zfy2) are expressed, leading to spermatocyte progression arrest and apoptosis (Royo et al., 2010). Thus, physiological MSCI is required to allow the exit of the pachytene stage.

On the other hand, females possess two X chromosomes; thus, MSCI does not occur in the oocytes. So, the roles of the MSUC in response to asynapsis are different from that in males (Cloutier et al., 2015; Turner, 2015) (Figure 4).

In asynapsis models without associated recombination defects, such as *Spo11*$^{-/-}$ mice and mice harboring chromosome abnormalities, such as Turner syndrome (XO) with only one X chromosome, unsynapsed chromosomes undergo MSUC, and oocytes with these unsynapsed chromosomes are eliminated (Daniel et al., 2011; Wojtasz et al., 2012; Cloutier et al., 2015). Deletion of the MSUC factors HORMAD1 or HORMAD2 in *Spo11*$^{-/-}$ mice (Daniel et al., 2011; Wojtasz et al., 2012) or H2AX in XO mice (Cloutier et al., 2015) restores the oocyte numbers to wild-type levels. Thus, the MSUC is suggested to transduce asynapsis into germ cell arrest. The MSUC factors, HORMAD1 and HORMAD2 would be the putative synapsis checkpoint components in females (Turner, 2015).

However, it seems that the response to asynapsis in females ca not be simply explained only by this checkpoint signaling model. Other mechanisms are also proposed to account for the loss of oocytes harboring asynapsis: the MUSC might render oocytes deficient in multiple gene products required for oocyte survival and development (Cloutier et al., 2015; Cloutier et al., 2016).

In mouse models carrying extra/supernumerary chromosomes, oocytes with asynapsed chromosomes are not eliminated as in XO females, despite the presence of HORMAD1 and other meiotic silencing factors on the asynaptic supernumerary chromosomes (Cloutier et al., 2015). Silencing these asynaptic supernumerary chromosomes does not affect the normal gene expression from the entire genome. In contrast, asynapsis of chromosomes in XO or other chromosomally unbalanced females would likely lead to the silencing of multiple housekeeping genes, oogenesis-essential genes, or critical genes. Therefore, the fate of oocytes with asynapsis probably depends on the gene content of the silenced asynapsed chromosomes (Cloutier et al., 2015; Turner, 2015). In *Spo11*$^{-/-}$ oocytes, chromosomes are extensively unsynapsed, and the MSUC takes place on only a part of them (Carofiglio et al., 2013). This MSUC might silence some essential genes (e.g., oogenesis-essential genes), leading to oocyte arrest and ultimately triggering oocyte death. The rescue of oocyte loss by the deletion of silencing components HORMADS and H2AX in *Spo11*$^{-/-}$ mice and other asynapsis models (Daniel et al., 2011; Wojtasz et al., 2012; Cloutier et al., 2015) could be explained by the restoration of standard gene expression patterns, rather than the disruption of checkpoint signaling *per se* (Turner, 2015).

Recent findings show that the CHK2-dependent DNA damage checkpoint also culls SPO11-deficient oocytes (Rinaldi et al., 2017; Rinaldi et al., 2020). These data argue against the existence of a specific synapsis-checkpoint mechanism. Most *Spo11*$^{-/-}$ oocytes have some DSBs (Carofiglio et al., 2013; Malki et al., 2014). Thus, authors speculate that it could be enough to reach the threshold to trigger the CHK2-dependent recombination checkpoint (Rinaldi et al., 2017). So, a model in which two major mechanisms are responsible for the elimination of oocytes with synapsis defect is proposed: the meiotic silencing mechanism, as discussed above, which primarily works in oocytes with a small number of asynapsed chromosomes that carry meiotic-essential genes but the amount of unrepaired DSBs does not reach the threshold (Cloutier et al., 2015). The recombination checkpoint could function in oocytes with multiple asynapsed chromosomes (e.g., *Spo11*$^{-/-}$ oocytes) that accumulate a sufficient number of DSBs to trigger the checkpoint (Rinaldi et al., 2017; Rinaldi et al., 2020).

Interestingly, the CHK2 deficiency can only restore a limited number of *Spo11*$^{-/-}$ oocytes (Rinaldi et al., 2017; Martínez-Marchal et al., 2020). Also, HORMAD2 and CHK2 are not functioning in a single linear checkpoint pathway (Rinaldi et al., 2017; Martínez-Marchal et al., 2020). Therefore, other mechanisms eliminating most of the *Spo11*$^{-/-}$ oocytes cannot be excluded, for instance, through the MSUC mechanism and/or the CHK1-dependent DNA damage checkpoint (Rinaldi et al., 2017; Martínez-Marchal et al., 2020). Moreover, the lack of both p53 and TAp63 can protect nearly all *Spo11*$^{-/-}$ oocytes from elimination. However, the deletion of the

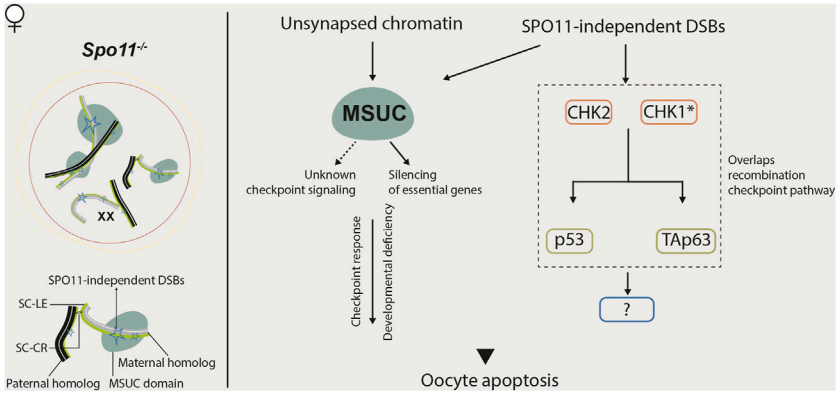

FIGURE 4
Meiotic response to asynapsis in female. Several mechanisms are proposed to be responsible for eliminating *Spo11*$^{-/-}$ oocytes. MSUC might trigger an unknown checkpoint signaling pathway in these oocytes or silence essential genes for development, leading to oocyte apoptosis. In parallel, in response to SPO11-independent DSBs, CHK2-mediated DNA damage signaling, which partially overlaps the recombination checkpoint pathway, also contributes to the elimination of *Spo11*$^{-/-}$ oocytes.

BCL-2 components (PUMA, NOXA, and BAX) does not rescue the oocyte loss in *Spo11*$^{-/-}$ females (ElInati et al., 2020). These data suggest that at least two distinct and partially overlapping genetic signaling pathways likely respond to recombination and synapsis errors in females. Noticeably, a more recent study showed that RAD51 might not be a reliable DSB marker in oocytes, and although DNA damage signaling from asynaptic axes participates in removing *Spo11*$^{-/-}$ oocytes, it does not require high numbers of SPO11-independent DSBs as suggested in the study from Carofiglio et al (Carofiglio et al., 2013; Ravindranathan et al., 2022).

Collectively, compared to the recombination checkpoint, the genetic pathways responsible for the "synapsis checkpoint" control remain much less understood in both males and females. Rather than being a typical checkpoint, the surveillance mechanisms that respond to asynapsis in mammals might be more complex. At least in females, the DNA damage signaling pathway, the MSUC-mediated checkpoint signal-transducing, and the depletion of essential genes for oocyte development and survival might conspire to drive the elimination of oocytes with asynapsed chromosomes.

3 Genetic cause of infertility

Successful reproduction requires the precise regulation of complex processes essential for developing reproductive organs, performing gametogenesis, acquiring neuroendocrine competency, and the ability to carry a pregnancy (Yatsenko and Rajkovic, 2019). Infertility, a common, multifactorial pathological condition defined as the inability to establish a clinical pregnancy after at least 1 year of regular unprotected sexual intercourse, affects approximately 50 million couples worldwide (Mascarenhas et al., 2012). Among the infertility cases with identified causes, one-third is due to a female factor, another third is due to a male factor, and the remaining third is due to combined female and male factors (Mallepaly et al., 2017). Furthermore, genetic defects contribute to nearly 50% of these infertility cases. More unknown genetic causes are suggested in infertility and need to be uncovered (Zorrilla and Yatsenko, 2013).

Male infertility derives etiologically from quantitative spermatogenic defects, ductal obstruction or dysfunction, hypothalamic-pituitary axis dysfunction, and qualitative spermatogenic defects (from most to least common) (Tournaye et al., 2017). Genetic factors account for at least 15% of male infertility and involve all these etiological categories (Krausz and Riera-Escamilla, 2018). Diagnosing male infertility relies on semen (and hormone) analysis, which results in two major phenotypes: oligozoospermia (reduced sperm count) and azoospermia (no spermatozoa in the ejaculate) (Tüttelmann et al., 2018). Qualitative spermatogenic defects or ductal obstruction usually manifest as azoospermia, and multiple genetic factors are validated as the causes, including numerical and structural chromosomal anomalies (e.g., Klinefelter's syndrome, 46, XX male syndrome), Y-chromosome micro-deletions (e.g., azoospermia factor (AZF) deletions), gene mutations (e.g., TEX11 deletions), and cystic fibrosis transmembrane conductance regulator (CFTR) mutations (Krausz and Riera-Escamilla, 2018). AZF deletions are the most frequent genetic cause of azoospermia (Krausz et al., 2014). Most numerical and structural chromosomal anomalies and TEX11 deletions are thought to cause spermatogenic defects due to errors during meiosis that activate the surveillance mechanisms (Sun et al., 2007; Yang et al., 2015; Yatsenko et al., 2015). Currently, some of these genetic infertility causes can be clinically diagnosed by widely applied analyses, such as karyotyping, AZF deletion screening, and CFTR mutation analysis (Tournaye et al., 2017).

Female infertility can result from a wide range of factors affecting ovarian development, oocyte maturation, fertilization competence, and the potential of a fertilized egg for implantation and development (Yatsenko and Rajkovic, 2019). Ovulation disorders are the leading cause of female infertility, which often occur as a result of conditions classified into three categories: hypothalamic failure, dysfunction of hypothalamic-pituitary-ovarian axis-mostly polycystic ovary syndrome (PCOS), and

primary ovarian insufficiency (POI) (National Institute for Health and Care Excellence, 2013). Genetic factors are suggested to play a role in all these disorders. For example, mutations of the GNRHR gene encoding the gonadotropin-releasing hormone (GnRH) receptor and genes causing Kallmann syndrome have been identified in women affected by hypothalamic amenorrhea. Alternations in multiple genes such as CYP17, CYP19, LHCGR, DENND1A are linked to PCOS, suggesting its polygenicity (reviewed in Beke, 2019).

POI has become a significant cause of female infertility due to premature exhaustion of the primordial follicular pool in most cases (Rossetti et al., 2017). The most common contributors to POI are the X chromosome-linked defects, in which Turner syndrome (TS) is the primary cause of syndromic POI. In contrast, premutation of the FMR1 (fragile X mental retardation 1) gene is the most common gene mutation associated with non-syndromic POI. In most cases of POI, the activation of the surveillance mechanisms leading to a reduced ovarian reserve are responsible for infertility. For instance, the absence of one X chromosome in TS causes oocyte loss during early meiotic prophase and ovarian development, leading to ovarian dysgenesis and primary amenorrhea since infancy (Fechner et al., 2006). In other cases, how particular mutations (e.g., FMR1 premutation) lead to POI is not clear yet. The FMR1 premutation may cause a deficiency of proteins required for oocyte or follicle development and survival (Rossetti et al., 2017). Even though nowadays POI cannot be reverted, the identification of the causative genetic alterations in POI patients is beneficial for her female relatives, who can undertake precautionary measures (e.g., egg freezing, embryo cryopreservation, anticipated pregnancy planning, *etc.*) in case of being positive in the genetic screening (Rossetti et al., 2017). This perspective is becoming increasingly important due to the modern tendency to delay childbirth in societies.

Despite the revealed genetic factors contributing to female and male infertility, many genetic causes remain unexplained for the majority of infertility cases, including idiopathic infertility cases, which are identified in 25%–30% of infertility couples and likely have a genetic etiology (Smith et al., 2003; Mallepaly et al., 2017). Furthermore, with the increasing use of assisted reproductive technology (ART), which removes the natural barrier to egg fertilization, concerns about its safety and possible adverse outcomes are rising (Davies et al., 2012). Diagnosing the genetic causes of infertility becomes more clinically significant for infertility treatment and the health of patients and their children. Thus, identifying unknown genes involved in mammalian gametogenesis, which could contribute to human infertility, is demanding and essential for clinical infertility diagnosis in the near future.

3.1 Mutations of meiotic prophase genes in mice

In recent years, advances in genomic approaches, particularly next-generation sequencing (NGS) technologies, allowed unbiased genomic studies of human infertility and uncovered many infertility-associated genes or gene variants in males and females (Yatsenko and Rajkovic, 2019; Precone et al., 2021; Heddar et al., 2022). Advanced filtering techniques are required for selecting the *bona fide* causes of human infertility from the discovered genes or gene variants, and mouse studies are the gold standard for defining the genotype-phenotype connection in fertility, at least in males (Houston et al., 2021). Moreover, functional studies in mouse models are usually prerequisites to attributing a disease-causing role to a newly discovered gene (Riera-Escamilla et al., 2019), thus offering a panel of strong candidate genes for screening human infertility factors.

Here, we summarized genes that are functionally involved in meiotic prophase I, and mutating any of them could trigger recombination/synapsis checkpoint, leading to spermatocyte arrest in males and/or oocyte depletion in females (Supplementary Table S1).

Of these 77 genes, many of them have essential roles in chromosome pairing, synapsis, and meiotic recombination (detailed roles are discussed above), including components of the chromosome axis or the SC, recombination factors required for DSB formation and repair, or proteins participating in telomere-mediated chromosome movements. The rest are mainly functionally related to silencing retrotransposons, chromatin modification, and transcriptional and translational regulation of essential proteins required for SC formation and DSB repair.

Intriguingly, more than half of these meiosis-deficient mutants display sexually dimorphic phenotypes. Less stringent checkpoint controls in females could explain these phenotypic differences. Consequently, oocytes could tolerate more meiotic prophase I error, which would explain why oogenesis is more error-prone than spermatogenesis (Hunt and Hassold, 2002). In male mice deficient for *Brca2*, *Mei1*, *Hormad1*, *Smc1b*, or *Sycp3* genes, spermatocytes are arrested at the pachytene stage due to the defective meiotic prophase events, resulting in male sterility (Supplementary Table S1). However, these mutant oocytes are only partially arrested at meiotic prophase I in females, and some progress beyond prophase I despite carrying asynaptic homologs, unrepaired DSBs, or other chromosomal abnormalities. Other mechanisms during oogenesis can eliminate these defective oocytes later, but some even complete meiosis and form unbalanced oocytes. As a result, some of these meiosis-deficient mutant females are even subfertile (Reinholdt and Schimenti, 2005; Daniel et al., 2011; Felipe-Medina et al., 2020).

Another explanation could be that some of these genes have sexually dimorphic roles. For example, *Hells* and *Rad21l* genes have distinct roles in males and females. While the deficient males are infertile due to meiotic prophase I arrest, the mutant females exhibit lethality (*Hells*), or subfertility (*Rad21l*), due to other defects rather than failed synapsis or incomplete meiotic recombination. On the other hand, *Asz1*, *Dnmt3l*, *Mybl1*, *Mov10l1*, *Piwil2*, *Piwil4*, *Pld6*, and *Tdrd9* are specifically required for the silencing of retrotransposons in males, while *Dmrt7* has significant roles in meiotic silencing of the XY chromosomes which only exist in spermatocytes. Thus, the disruption of these genes causes male infertility due to a complete arrest in spermatocytes, but female fertility is grossly unaffected (Supplementary Table S1).

Furthermore, some recombination factors, such as BRCA1, BRME1, MEILB2, and TEX15, recruit recombinases RAD51/DMC1 to DSB sites in spermatocytes. The mutations of these genes result in male infertility but only have mild or no effects

on female fertility (Supplementary Table S1). While if they have similar roles in females is unclear or cannot be excluded, the milder phenotypes in female mutant mice might be a consequence of combined effects from the weak checkpoint control and less-required roles during meiotic recombination in oocytes.

In humans, meiotic defects typically result in non-obstructive azoospermia (NOA), whereas in females, they are usually associated with POI (Krausz et al., 2020). We searched these 77 meiotic prophase genes, the mutation of which could trigger meiotic prophase arrest in mice, in ClinVar and Pubmed, and found monogenetic mutations of 28 genes (145 variants) have been reported to be associated with human infertility conditions such as spermatogenetic failure, NOA, POI, spermatogenesis maturation arrest, pregnancy loss, *etc.* (Supplementary Table S2).

Based on the interpretations for clinical significance in ClinVar, 55 of these variants are considered as "likely pathogenic" or "uncertain significance" (Supplementary Table S2). This is mainly due to the lack of evidence or inconsistent interpretations. Of the 145 variants, 67 variants from 21 genes are classified as 'pathogenic', 52 variants from 16 genes have only 1 or 2 publications reporting independent probands, and single submitters provide the remainder without publications. Moreover, only five variants from five genes (*Six6os1*, *Meilb2*, *Msh5*, *Stag3*, and *Syce1*) have supporting biological evidence from knockout mouse models in which human phenotypes are recapitulated (Supplementary Table S2). Thus, in the future, more independent validation studies and functional evidence are required, including introducing gene variants using CRISPR/Cas9 genome editing technology in mice to validate the infertility-causing roles of human gene variants (Houston et al., 2021), not only for distinguishing between variants that cause disease from variants that are rare but benign (Araujo et al., 2020), but also for providing robustness to the clinical validity of these possible disease-causing genes linked to human infertility (Oud et al., 2019).

Additionally, multiple levels of evidence should also be considered to confidently link variation in individual genes to human infertility (Oud et al., 2019). Indeed, an unstructured assessment has reported three genes, including *Tex11*, that fulfill this requirement for a link to male infertility (Tüttelmann et al., 2018). Recently, in another study of an extensive literature review and standardized clinical validity assessment of a large number of genes, some of these meiotic prophase genes were shown to be associated with male infertility with 'strong' evidence (*Tex11* and *Tex15*), with 'moderate' evidence (*Sycp3*), or with 'limited' evidence (*Dmc1*, *Mei1*, *Meiob*, *Spo11*, *Syce1*, and *Tdrd9*) (Oud et al., 2019).

Importantly, the associated conditions of all these 28 genes in humans are well matched with the phenotypes of their mutant mice (Supplementary Table S2). For example, the mutation of SYCP3 causes male infertility with complete meiotic prophase arrest. Still, it exhibits subfertility in female mice with a sharp reduction in litter size due to the presence of aneuploid oocytes. Correspondingly, its linked conditions in humans are infertility/spermatogenetic failure in men and pregnancy loss in women. This further support the values of mouse models for attributing a disease-causing role to a new gene. Thus, the remaining meiotic prophase genes with no monogenic mutation identified in this list are worthy of screening in human patients.

However, it is essential to point out that we must be cautious when using the findings from mouse studies to interpret the causative factors and mechanisms underlying human infertility regarding considerable differences still exist between humans and mice (Azhar et al., 2021). A recent study has shown that the metaphase checkpoint is more frequently activated than the pachytene checkpoint in human males with severe spermatogenic impairment (Enguita-Marruedo et al., 2019), which is in contrast to observations in the mouse, where knockout of the meiotic prophase genes (as we summarized above) most frequently results in pachytene checkpoint arrest. The underlying reasons are not clear. It could be that the observed arrest in this study is caused mainly by mutations in proteins required for the metaphase-anaphase transition or functioning in cell cycle regulation rather than involved in meiotic prophase major events (Enguita-Marruedo et al., 2019). Alternatively, mutation of meiotic prophase genes may trigger a later metaphase arrest in humans rather than prophase arrest in mice. Differences in the pachytene surveillance mechanisms between humans and mice could cause this. Most studies (58 out of 78 publications in Supplementary Table S1) reporting mutations of meiotic prophase genes in infertile males lack detailed analysis of meiotic or testicular phenotypes. Thus, to clarify this possibility, it will be worthwhile to assess the exact spermatocyte arrest phase in infertile patients carrying meiotic prophase gene mutations in the future.

Author contributions

YH and IR conceived and wrote the manuscript.

Funding

YH is a recipient of a fellowship from the China Scholarship Council (201607040048). This work was supported by Spanish Ministerio de Economía y Competividad grants to IR(PID 2019-107082RB-I00) and a grant from La Funació Marató de TV3 (677/U/2021).

Conflict of interest

The authors declare that the research was conducted in the absence of any commercial or financial relationships that could be construed as a potential conflict of interest.

Publisher's note

Supplementary material

The Supplementary Material for this article can be found online at: https://www.frontiersin.org/articles/10.3389/fcell.2023.1127440/full#supplementary-material

References

Abreu, C. M., Prakash, R., Romanienko, P. J., Roig, I., Keeney, S., and Jasin, M. (2018). Shu complex SWS1-SWSAP1 promotes early steps in mouse meiotic recombination. *Nat. Commun.* 9 (1), 3961. doi:10.1038/s41467-018-06384-x

Adelman, C. A., and Petrini, J. H. J. (2008). ZIP4H (TEX11) deficiency in the mouse impairs meiotic double strand break repair and the regulation of crossing over. *PLoS Genet.* 4 (3), e1000042. doi:10.1371/journal.pgen.1000042

Anderson, E. L., Baltus, A. E., Roepers-Gajadien, H. L., Hassold, T. J., de Rooij, D. G., van Pelt, A. M. M., et al. (2008). Stra8 and its inducer, retinoic acid, regulate meiotic initiation in both spermatogenesis and oogenesis in mice. *Proc. Natl. Acad. Sci. U. S. A.* 105 (39), 14976–14980. doi:10.1073/pnas.0807297105

Araujo, T. F., Friedrich, C., Grangeiro, C. H. P., Martelli, L. R., Grzesiuk, J. D., Emich, J., et al. (2020). Sequence analysis of 37 candidate genes for male infertility: Challenges in variant assessment and validating genes. *Andrology* 8 (2), 434–441. doi:10.1111/ANDR.12704

Azhar, M., Altaf, S., Uddin, I., Cheng, J., Wu, L., Tong, X., et al. (2021). Towards post-meiotic sperm production: Genetic insight into human infertility from mouse models. *Int. J. Biol. Sci.* 17 (10), 2487–2503. doi:10.7150/ijbs.60384

Baker, S. M., Plug, A. W., Prolla, T. A., Bronner, C. E., Harris, A. C., Yao, X., et al. (1996). Involvement of mouse Mlh1 in DNA mismatch repair and meiotic crossing over. *Nat. Genet.* 13 (3), 336–342. doi:10.1038/ng0796-336

Baltus, A. E., Menke, D. B., Hu, Y. C., Goodheart, M. L., Carpenter, A. E., de Rooij, D. G., et al. (2006). In germ cells of mouse embryonic ovaries, the decision to enter meiosis precedes premeiotic DNA replication. *Nat. Genet.* 38 (12), 1430–1434. doi:10.1038/ng1919

Barchi, M., Mahadevaiah, S., Di Giacomo, M., Baudat, F., de Rooij, D. G., Burgoyne, P. S., et al. (2005). Surveillance of different recombination defects in mouse spermatocytes yields distinct responses despite elimination at an identical developmental stage. *Mol. Cell. Biol.* 25 (16), 7203–7215. doi:10.1128/mcb.25.16.7203-7215.2005

Barchi, M., Roig, I., Di Giacomo, M., de Rooij, D. G., Keeney, S., and Jasin, M. (2008). ATM promotes the obligate XY crossover and both crossover control and chromosome axis integrity on autosomes. *PLoS Genet.* 4 (5), e1000076. doi:10.1371/journal.pgen.1000076

Baudat, F., Imai, Y., and De Massy, B. (2013). Meiotic recombination in mammals: Localization and regulation. *Nat. Rev. Genet.* 14, 794–806. doi:10.1038/nrg3573

Beke, A. (2019). Genetic causes of female infertility. *Exp. Suppl.* 111, 367–383. doi:10.1007/978-3-030-25905-1_17

Bellve, A. R., Cavicchia, J. C., Millette, C. F., O'Brien, D. A., Bhatnagar, Y. M., and Dym, M. (1977). Spermatogenic cells of the prepuberal mouse. Isolation and morphological characterization. *J. Cell. Biol.* 74 (1), 68–85. doi:10.1083/jcb.74.1.68

Berchowitz, L., and Copenhaver, G. (2010). Genetic interference: Dont stand so close to me. *Curr. Genomics* 11 (2), 91–102. doi:10.2174/138920210790886835

Bergerat, A., de Massy, B., Gadelle, D., Varoutas, P. C., Nicolas, A., and Forterre, P. (1997). An atypical topoisomerase II from archaea with implications for meiotic recombination. *Nature* 386 (6623), 414–417. doi:10.1038/386414a0

Bhalla, N., and Dernburg, A. F. (2005). Cell biology: A conserved checkpoint monitors meiotic chromosome synapsis in *Caenorhabditis elegans*. *Science* 310 (5754), 1683–1686. doi:10.1126/science.1117468

Bhattacharyya, T., Walker, M., Powers, N. R., Brunton, C., Fine, A. D., Petkov, P. M., et al. (2019). Prdm9 and meiotic cohesin proteins cooperatively promote DNA double-strand break formation in mammalian spermatocytes. *Curr. Biol.* 29 (6), 1002–1018.e7. doi:10.1016/j.cub.2019.02.007

Bisig, C. G., Guiraldelli, M. F., Kouznetsova, A., Scherthan, H., Hoog, C., Dawson, D. S., et al. (2012). Synaptonemal complex components persist at centromeres and are required for homologous centromere pairing in mouse spermatocytes. *PLoS Genet.* 8 (6), e1002701. doi:10.1371/journal.pgen.1002701

Boekhout, M., Karasu, M. E., Wang, J., Acquaviva, L., Pratto, F., Brick, K., et al. (2019). REC114 partner ANKRD31 controls number, timing, and location of meiotic DNA breaks. *Mol. Cell.* 74 (5), 1053–1068.e8. doi:10.1016/j.molcel.2019.03.023

Bolcun-Filas, E., Costa, Y., Speed, R., Taggart, M., Benavente, R., De Rooij, D. G., et al. (2007). SYCE2 is required for synaptonemal complex assembly, double strand break repair, and homologous recombination. *J. Cell. Biol.* 176 (6), 741–747. doi:10.1083/jcb.200610027

Bolcun-Filas, E., and Handel, M. A. (2018). Meiosis: The chromosomal foundation of reproduction. *Biol. Reproduction* 99, 112–126. doi:10.1093/biolre/ioy021

Bolcun-Filas, E., Rinaldi, V. D., White, M. E., and Schimenti, J. C. (2014). Reversal of female infertility by Chk2 ablation reveals the oocyte DNA damage checkpoint pathway. *Science* 343 (6170), 533–536. doi:10.1126/science.1247671

Bondarieva, A., Raveendran, K., Telychko, V., Rao, H. B. D. P., Ravindranathan, R., Zorzompokou, C., et al. (2020). Proline-rich protein PRR19 functions with cyclin-like CNTD1 to promote meiotic crossing over in mouse. *Nat. Commun.* 11 (1), 3101. doi:10.1038/S41467-020-16885-3

Borum, K. (1961). Oogenesis in the mouse: A study of the meiotic prophase. *Exp. Cell. Res.* 24 (3), 495–507. doi:10.1016/0014-4827(61)90449-9

Bowles, J., Knight, D., Smith, C., Wilhelm, D., Richman, J., Mamiya, S., et al. (2006). Retinoid signaling determines germ cell fate in mice. *Science* 312 (5773), 596–600. doi:10.1126/science.1125691

Brick, K., Smagulova, F., Khil, P., Camerini-Otero, R. D., and Petukhova, G. V. (2012). Genetic recombination is directed away from functional genomic elements in mice. *Nature* 485 (7400), 642–645. doi:10.1038/nature11089

Brown, M. S., and Bishop, D. K. (2015). DNA strand exchange and RecA homologs in meiosis. *Cold Spring Harb. Perspect. Biol.* 7 (1), a016659. doi:10.1101/cshperspect.a016659

Burgoyne, P. S., Mahadevaiah, S. K., and Turner, J. M. A. (2009). The consequences of asynapsis for mammalian meiosis. *Nat. Rev. Genet.* 10, 207–216. doi:10.1038/nrg2505

Cahoon, C. K., and Hawley, R. S. (2016). Regulating the construction and demolition of the synaptonemal complex. *Nat. Struct. Mol. Biol.* 23, 369–377. doi:10.1038/nsmb.3208

Cannavo, E., and Cejka, P. (2014). Sae2 promotes dsDNA endonuclease activity within Mre11-Rad50-Xrs2 to resect DNA breaks. *Nature* 514 (7520), 122–125. doi:10.1038/nature13771

Capilla-Pérez, L., Durand, S., Hurel, A., Lian, Q., Chambon, A., Taochy, C., et al. (2021). The synaptonemal complex imposes crossover interference and heterochiasmy in Arabidopsis. *Proc. Natl. Acad. Sci. U. S. A.* 118 (12), e2023613118. doi:10.1073/pnas.2023613118

Carballo, J. A., Panizza, S., Serrentino, M. E., Johnson, A. L., Geymonat, M., Borde, V., et al. (2013). Budding yeast ATM/ATR control meiotic double-strand break (DSB) levels by down-regulating Rec114, an essential component of the DSB-machinery. *PLoS Genet.* 9 (6), e1003545. doi:10.1371/journal.pgen.1003545

Carofiglio, F., Inagaki, A., de Vries, S., Wassenaar, E., Schoenmakers, S., Vermeulen, C., et al. (2013). SPO11-Independent DNA repair foci and their role in meiotic silencing. *PLoS Genet.* 9 (6), e1003538. doi:10.1371/journal.pgen.1003538

Cartagena-Lirola, H., Guerini, I., Manfrini, N., Lucchini, G., and Longhese, M. P. (2008). Role of the *Saccharomyces cerevisiae* Rad53 checkpoint kinase in signaling double-strand breaks during the meiotic cell cycle. *Mol. Cell. Biol.* 28 (14), 4480–4493. doi:10.1128/mcb.00375-08

Cherry, S. M., Adelman, C. A., Theunissen, J. W., Hassold, T. J., Hunt, P. A., and Petrini, J. H. J. (2007). The Mre11 complex influences DNA repair, synapsis, and crossing over in murine meiosis. *Curr. Biol.* 17 (4), 373–378. doi:10.1016/j.cub.2006.12.048

Chi, P., San Filippo, J., Sehorn, M. G., Petukhova, G. V., and Sung, P. (2007). Bipartite stimulatory action of the Hop2-Mnd1 complex on the Rad51 recombinase. *Genes. Dev.* 21 (14), 1747–1757. doi:10.1101/gad.1563007

Chiquoine, A. D. (1954). The identification, origin, and migration of the primordial germ cells in the mouse embryo. *Anatomical Rec.* 118 (2), 135–146. doi:10.1002/ar.1091180202

Cloud, V., Chan, Y. L., Grubb, J., Budke, B., and Bishop, D. K. (2012). Rad51 is an accessory factor for Dmc1-mediated joint molecule formation during meiosis. *Science* 337 (6099), 1222–1225. doi:10.1126/science.1219379

Cloutier, J. M., Mahadevaiah, S. K., ElInati, E., Nussenzweig, A., Toth, A., and Turner, J. M. A. (2015). Histone H2AFX links meiotic chromosome asynapsis to prophase I oocyte loss in mammals. *PLOS Genet.* 11 (10), e1005462. doi:10.1371/journal.pgen.1005462

Cloutier, J. M., Mahadevaiah, S. K., ElInati, E., Toth, A., and Turner, J. (2016). Mammalian meiotic silencing exhibits sexually dimorphic features. *Chromosoma* 125 (2), 215–226. doi:10.1007/s00412-015-0568-z

Cole, F., Kauppi, L., Lange, J., Roig, I., Wang, R., Keeney, S., et al. (2012). Homeostatic control of recombination is implemented progressively in mouse meiosis. *Nat. Cell. Biol.* 14 (4), 424–430. doi:10.1038/ncb2451

Cooper, T. J., Wardell, K., Garcia, V., and Neale, M. J. (2014). Homeostatic regulation of meiotic DSB formation by ATM/ATR. *Exp. Cell. Res.* 15, 124–131. doi:10.1016/j.yexcr.2014.07.016

Cordeiro, M. H., Kim, S. Y., Ebbert, K., Duncan, F. E., Ramalho-Santos, J., and Woodruff, T. K. (2015). Geography of follicle formation in the embryonic mouse ovary impacts activation pattern during the first wave of folliculogenesis. *Biol. Reproduction* 93 (4), 88–10. doi:10.1095/biolreprod.115.131227

Costa, Y., Speed, R., Ollinger, R., Alsheimer, M., Semple, C. A., Gautier, P., et al. (2005). Two novel proteins recruited by synaptonemal complex protein 1 (SYCP1) are at the centre of meiosis. *J. Cell. Sci.* 118 (12), 2755–2762. doi:10.1242/jcs.02402

Daniel, K., Lange, J., Hached, K., Fu, J., Anastassiadis, K., Roig, I., et al. (2011). Meiotic homologue alignment and its quality surveillance are controlled by mouse HORMAD1. *Nat. Cell. Biol.* 13 (5), 599–610. doi:10.1038/ncb2213

Davies, M. J., Moore, V. M., Willson, K. J., Van Essen, P., Priest, K., Scott, H., et al. (2012). Reproductive technologies and the risk of birth defects. *N. Engl. J. Med.* 366 (19), 1803–1813. doi:10.1056/NEJMoa1008095

De Massy, B., Rocco, V., and Nicolas, A. (1995). The nucleotide mapping of DNA double-strand breaks at the CYS3 initiation site of meiotic recombination in *Saccharomyces cerevisiae*. *EMBO J.* 14 (18), 4589–4598. doi:10.1002/J.1460-2075.1995.TB00138.X

De Muyt, A., Jessop, L., Kolar, E., Sourirajan, A., Chen, J., Dayani, Y., et al. (2012). BLM helicase ortholog Sgs1 is a central regulator of meiotic recombination intermediate metabolism. *Mol. Cell.* 46 (1), 43–53. doi:10.1016/j.molcel.2012.02.020

De Muyt, A., Pyatnitskaya, A., Andreani, J., Ranjha, L., Ramus, C., Laureau, R., et al. (2018). A meiotic XPF–ERCC1-like complex recognizes joint molecule recombination intermediates to promote crossover formation. *Genes. Dev.* 32 (3–4), 283–296. doi:10.1101/gad.308510.117

De Muyt, A., Zhang, L., Piolot, T., Kleckner, N., Espagne, E., and Zickler, D. (2014). E3 ligase Hei10: A multifaceted structure-based signaling molecule with roles within and beyond meiosis. *Genes. Dev.* 28 (10), 1111–1123. doi:10.1101/gad.240408.114

de Rooij, D. G., and Russell, L. D. (2000). All you wanted to know about spermatogonia but were afraid to ask. *J. Androl.* 21 (6), 776–798.

De Vries, S. S., Baart, E. B., Dekker, M., Siezen, A., de Rooij, D. G., de Boer, P., et al. (1999). Mouse MutS-like protein Msh5 is required for proper chromosome synapsis in male and female meiosis. *Genes. Dev.* 13 (5), 523–531. doi:10.1101/gad.13.5.523

Di Giacomo, M., Barchi, M., Baudat, F., Edelmann, W., Keeney, S., and Jasin, M. (2005). Distinct DNA-damage-dependent and -independent responses drive the loss of oocytes in recombination-defective mouse mutants. *Proc. Natl. Acad. Sci. U. S. A.* 102 (3), 737–742. doi:10.1073/pnas.0406212102

Edelmann, W., Cohen, P. E., Kane, M., Lau, K., Morrow, B., Bennett, S., et al. (1996). Meiotic pachytene arrest in MLH1-deficient mice. *Cell.* 85 (7), 1125–1134. doi:10.1016/S0092-8674(00)81312-4

Edelmann, W., Cohen, P. E., Kneitz, B., Winand, N., Lia, M., Heyer, J., et al. (1999). Mammalian MutS homologue 5 is required for chromosome pairing in meiosis. *Nat. Genet.* 21 (1), 123–127. doi:10.1038/5075

Edson, M. A., Nagaraja, A. K., and Matzuk, M. M. (2009). The mammalian ovary from Genesis to revelation. *Endocr. Rev.* 30 (6), 624–712. doi:10.1210/er.2009-0012

ElInati, E., Zielinska, A. P., McCarthy, A., Kubikova, N., Maciulyte, V., Mahadevaiah, S., et al. (2020). The BCL-2 pathway preserves mammalian genome integrity by eliminating recombination-defective oocytes. *Nat. Commun.* 11 (1), 2598. doi:10.1038/s41467-020-16441-z

Endoh, M., Endo, T. A., Shinga, J., Hayashi, K., Farcas, A., Ma, K. W., et al. (2017). PCGF6-PRC1 suppresses premature differentiation of mouse embryonic stem cells by regulating germ cell-related genes. *eLife* 6, e21064. doi:10.7554/eLife.21064

Enguita-Marruedo, A., Sleddens-Linkels, E., Oomsde, M., de Geus, V., Wilke, M., Blom, E., et al. (2019). Meiotic arrest occurs most frequently at metaphase and is often incomplete in azoospermic men. *Fertil. Steril.* 112 (6), 1059–1070.e3. doi:10.1016/J.FERTNSTERT.2019.08.004

Fechner, P. Y., Davenport, M. L., Qualy, R. L., Ross, J. L., Gunther, D. F., Eugster, E. A., et al. (2006). Differences in follicle-stimulating hormone secretion between 45,X monosomy Turner syndrome and 45,X/46,XX mosaicism are evident at an early age. *J. Clin. Endocrinol. metabolism* 91 (12), 4896–4902. doi:10.1210/jc.2006-1157

Felipe-Medina, N., Caburet, S., Sanchez-Saez, F., Condezo, Y. B., de Rooij, D. G., Gomez-H, L., et al. (2020). A missense in HSF2BP causing primary ovarian insufficiency affects meiotic recombination by its novel interactor c19orf57/brme1. *eLife* 9, e56996. doi:10.7554/ELIFE.56996

Feng, J., Fu, S., Cao, X., Wu, H., Lu, J., Zeng, M., et al. (2017). Synaptonemal complex protein 2 (SYCP2) mediates the association of the centromere with the synaptonemal complex. *Protein & Cell.* 8 (7), 538–543. doi:10.1007/s13238-016-0354-6

Fernandez-Capetillo, O., Mahadevaiah, S. K., Celeste, A., Romanienko, P. J., Camerini-Otero, R. D., Bonner, W. M., et al. (2003). H2AX is required for chromatin remodeling and inactivation of sex chromosomes in male mouse meiosis. *Dev. Cell.* 4 (4), 497–508. doi:10.1016/S1534-5807(03)00093-5

Finsterbusch, F., Ravindranathan, R., Dereli, I., Stanzione, M., Trankner, D., and Toth, A. (2016). Alignment of homologous chromosomes and effective repair of programmed DNA double-strand breaks during mouse meiosis require the minichromosome maintenance domain containing 2 (MCMDC2) protein. *PLoS Genet.* 12 (10), e1006393. doi:10.1371/journal.pgen.1006393

Fowler, K. R., Hyppa, R. W., Cromie, G. A., and Smith, G. R. (2018). Physical basis for long-distance communication along meiotic chromosomes. *Proc. Natl. Acad. Sci. U. S. A.* 115 (40), E9333–E9342. doi:10.1073/pnas.1801920115

France, M. G., Enderle, J., Rohrig, S., Puchta, H., Franklin, F. C. H., and Higgins, J. D. (2021). ZYP1 is required for obligate cross-over formation and cross-over interference in Arabidopsis. *Proc. Natl. Acad. Sci. U. S. A.* 118 (14), e2021671118. doi:10.1073/PNAS.2021671118

Fraune, J., Brochier-Armanet, C., Alsheimer, M., Volff, J. N., Schücker, K., and Benavente, R. (2016). Evolutionary history of the mammalian synaptonemal complex. *Chromosoma* 125, 355–360. doi:10.1007/s00412-016-0583-8

Fraune, J., Schramm, S., Alsheimer, M., and Benavente, R. (2012). The mammalian synaptonemal complex: Protein components, assembly and role in meiotic recombination. *Exp. Cell. Res.* 318 (12), 1340–1346. doi:10.1016/j.yexcr.2012.02.018

Fujiwara, Y., Horisawa-Takada, Y., Inoue, E., Tani, N., Shibuya, H., Fujimura, S., et al. (2020). Meiotic cohesins mediate initial loading of HORMAD1 to the chromosomes and coordinate SC formation during meiotic prophase. *PLoS Genet.* 16 (9), e1009048. doi:10.1371/journal.pgen.1009048

Fukuda, T., Daniel, K., Wojtasz, L., Toth, A., and Hoog, C. (2010). A novel mammalian HORMA domain-containing protein, HORMAD1, preferentially associates with unsynapsed meiotic chromosomes. *Exp. Cell. Res.* 316 (2), 158–171. doi:10.1016/j.yexcr.2009.08.007

Fukuda, T., Pratto, F., Schimenti, J. C., Turner, J. M. A., Camerini-Otero, R. D., and Hoog, C. (2012). Phosphorylation of chromosome core components may serve as axis marks for the status of chromosomal events during mammalian meiosis. *PLoS Genet.* 8 (2), e1002485. doi:10.1371/journal.pgen.1002485

Fung, J. C., Rockmill, B., Odell, M., and Roeder, G. S. (2004). Imposition of crossover interference through the nonrandom distribution of synapsis initiation complexes. *Cell.* 116 (6), 795–802. doi:10.1016/S0092-8674(04)00249-1

Gao, J., and Colaiácovo, M. P. (2018). Zipping and unzipping: Protein modifications regulating synaptonemal complex dynamics. *Trends Genet.* 34, 232–245. doi:10.1016/j.tig.2017.12.001

Garcia, V., Gray, S., Allison, R. M., Cooper, T. J., and Neale, M. J. (2015). Tel1ATM-mediated interference suppresses clustered meiotic double-strand-break formation. *Nature* 520 (7545), 114–118. doi:10.1038/nature13993

Garcia, V., Phelps, S. E. L., Gray, S., and Neale, M. J. (2011). Bidirectional resection of DNA double-strand breaks by Mre11 and Exo1. *Nature* 479 (7372), 241–244. doi:10.1038/nature10515

Geisinger, A., and Benavente, R. (2017). Mutations in genes coding for synaptonemal complex proteins and their impact on human fertility. *Cytogenet. Genome Res.* 150, 77–85. doi:10.1159/000453344

Ginsburg, M., Snow, M. H. L., and McLaren, A. (1990). Primordial germ cells in the mouse embryo during gastrulation. *Development* 110 (2), 521–528. doi:10.1242/dev.110.2.521

Gómez-H, L., Felipe-Medina, N., Sanchez-Martin, M., Davies, O. R., Ramos, I., Garcia-Tunon, I., et al. (2016). C14ORF39/SIX6OS1 is a constituent of the synaptonemal complex and is essential for mouse fertility. *Nat. Commun.* 7 (1), 13298. doi:10.1038/ncomms13298

Gray, S., and Cohen, P. E. (2016). Control of meiotic crossovers: From double-strand break formation to designation. *Annu. Rev. Genet.* 50 (1), 175–210. doi:10.1146/annurev-genet-120215-035111

Grey, C., Baudat, F., and de Massy, B. (2018). Prdm9, a driver of the genetic map. *PLoS Genet. NLM (Medline)* 14, e1007479. doi:10.1371/JOURNAL.PGEN.1007479

Grishaeva, T. M., and Bogdanov, Y. F. (2014). *Conservation and variability of synaptonemal complex proteins in phylogenesis of eukaryotes*. doi:10.1155/2014/856230

Guiraldelli, M. F., Eyster, C., Wilkerson, J. L., Dresser, M. E., and Pezza, R. J. (2013). Mouse HFM1/mer3 is required for crossover formation and complete synapsis of homologous chromosomes during meiosis. *PLoS Genet.* 9 (3), e1003383. doi:10.1371/journal.pgen.1003383

Guiraldelli, M. F., Felberg, A., Almeida, L. P., Parikh, A., de Castro, R. O., and Pezza, R. J. (2018). SHOC1 is a ERCC4-(HhH)2-like protein, integral to the formation of crossover recombination intermediates during mammalian meiosis. *PLoS Genet.* 14 (5), e1007381. doi:10.1371/journal.pgen.1007381

Günesdogan, U., and Surani, M. A. (2016). Developmental competence for primordial germ cell fate. *Curr. Top. Dev. Biol.* 117, 471–496. doi:10.1016/bs.ctdb.2015.11.007

Hamer, G., Gell, K., Kouznetsova, A., Novak, I., Benavente, R., and Hoog, C. (2006). Characterization of a novel meiosis-specific protein within the central element of the synaptonemal complex. *J. Cell. Sci.* 119 (19), 4025–4032. doi:10.1242/jcs.03182

Handel, M. A., and Eppig, J. J. (1997). Sexual dimorphism in the regulation of mammalian meiosis. *Curr. Top. Dev. Biol.* 37 (C), 333–358. doi:10.1016/S0070-2153(08)60179-9

Handel, M. A., and Schimenti, J. C. (2010). *'Genetics of mammalian meiosis: Regulation, dynamics and impact on fertility'*, Nature Reviews Genetics. London: Nature Publishing Group, 124–136. doi:10.1038/nrg2723

Handel, M. A. (2004). *'The XY body: A specialized meiotic chromatin domain'*, experimental cell research. Academic Press, 57–63. doi:10.1016/j.yexcr.2004.03.008

Hartmann, M., Umbanhowar, J., and Sekelsky, J. (2019) Centromere-proximal meiotic crossovers in *Drosophila melanogaster* are suppressed by both highly-repetitive heterochromatin and proximity to the centromere. doi:10.1534/genetics.119.302509

Hasegawa, K., and Saga, Y. (2012). Retinoic acid signaling in Sertoli cells regulates organization of the blood-testis barrier through cyclical changes in gene expression. *Dev. Camb. Engl.* 139 (23), 4347–4355. doi:10.1242/dev.080119

Heddar, A., Ogur, C., Da Costa, S., Braham, I., Billaud-Rist, L., Findikli, N., et al. (2022). Genetic landscape of a large cohort of Primary Ovarian Insufficiency: New genes

and pathways and implications for personalized medicine. *EBioMedicine* 84, 104246. doi:10.1016/J.EBIOM.2022.104246

Hermo, L., Pelletier, R. M., Cyr, D. G., and Smith, C. E. (2010). Surfing the wave, cycle, life history, and genes/proteins expressed by testicular germ cells. Part 2: Changes in spermatid organelles associated with development of spermatozoa. *Part 2 Changes spermatid organelles Assoc. Dev. spermatozoa' Microsc. Res. Tech.* 73 (4), 279–319. doi:10.1002/jemt.20787

Hernández-Hernández, A., Masich, S., Fukuda, T., Kouznetsova, A., Sandin, S., Daneholt, B., et al. (2016). The central element of the synaptonemal complex in mice is organized as a bilayered junction structure. *J. Cell. Sci.* 129 (11), 2239–2249. doi:10.1242/jcs.182477

Higgins, J. D., Vignard, J., Mercier, R., Pugh, A. G., Franklin, F. C. H., and Jones, G. H. (2008). AtMSH5 partners AtMSH4 in the class I meiotic crossover pathway in *Arabidopsis thaliana*, but is not required for synapsis. *Plant J.* 55 (1), 28–39. doi:10.1111/j.1365-313X.2008.03470.x

Hillers, K. J. (2004). Crossover interference.', *Current biology: CB. Curr. Biol.* 14, R1036–R1037. doi:10.1016/j.cub.2004.11.038

Hinch, A. G., Becker, P. W., Li, T., Moralli, D., Zhang, G., Bycroft, C., et al. (2020). The configuration of RPA, RAD51, and DMC1 binding in meiosis reveals the nature of critical recombination intermediates. *Mol. Cell.* 79 (4), 689–701.e10. doi:10.1016/J.MOLCEL.2020.06.015

Holloway, J. K., Booth, J., Edelmann, W., McGowan, C. H., and Cohen, P. E. (2008). MUS81 generates a subset of MLH1-MLH3-independent crossovers in mammalian meiosis. *PLoS Genet.* 4 (9), e1000186. doi:10.1371/journal.pgen.1000186

Holloway, J. K., Sun, X., Yokoo, R., Villeneuve, A. M., and Cohen, P. E. (2014). Mammalian CNTD1 is critical for meiotic crossover maturation and deselection of excess precrossover sites. *J. Cell. Biol.* 205 (5), 633–641. doi:10.1083/jcb.201401122

Houston, B. J., Conrad, D. F., and O'Bryan, M. K. (2021). A framework for high-resolution phenotyping of candidate male infertility mutants: From human to mouse. *Hum. Genet.* 140 (1), 155–182. doi:10.1007/s00439-020-02159-x

Humphryes, N., Leung, W. K., Argunhan, B., Terentyev, Y., Dvorackova, M., and Tsubouchi, H. (2013). The ecm11-gmc2 complex promotes synaptonemal complex formation through assembly of transverse filaments in budding yeast. *PLOS Genet.* 9 (1), e1003194. doi:10.1371/JOURNAL.PGEN.1003194

Hunt, P. A., and Hassold, T. J. (2002). Sex matters in meiosis. *Sci. (New York, N.Y.)* 296 (5576), 2181–2183. doi:10.1126/SCIENCE.1071907

Hunter, N. (2015). Meiotic recombination: The essence of heredity. *Cold Spring Harb. Perspect. Biol.* 7 (12), a016618. doi:10.1101/cshperspect.a016618

Hunter, N. (2017). Oocyte quality control: Causes, mechanisms, and consequences. *Cold Spring Harb. symposia quantitative Biol.* 82, 235–247. doi:10.1101/sqb.2017.82.035394

Ichijima, Y., Ichijima, M., Lou, Z., Nussenzweig, A., Camerini-Otero, R. D., Chen, J., et al. (2011). MDC1 directs chromosome-wide silencing of the sex chromosomes in male germ cells. *Genes. Dev.* 25 (9), 959–971. doi:10.1101/gad.2030811

Imai, Y., Baudat, F., Taillepierre, M., Stanzione, M., Toth, A., and de Massy, B. (2017). The PRDM9 KRAB domain is required for meiosis and involved in protein interactions. *Chromosoma* 126 (6), 681–695. doi:10.1007/s00412-017-0631-z

Ishiguro, K. I., Matsuura, K., Tani, N., Takeda, N., Usuki, S., Yamane, M., et al. (2020). MEIOSIN directs the switch from mitosis to meiosis in mammalian germ cells. *Dev. Cell.* 52 (4), 429–445.e10. doi:10.1016/j.devcel.2020.01.010

Ishiguro, K. I. (2019). *'The cohesin complex in mammalian meiosis'*, Genes to Cells. Hoboken: Blackwell Publishing Ltd, 6–30. doi:10.1111/gtc.12652

Jaffe, L. A., and Egbert, J. R. (2017). *Annual review of physiology*. Bethesda: NIH Public Access, 237–260. doi:10.1146/annurev-physiol-022516-034102Regulation of mammalian oocyte meiosis by intercellular communication within the ovarian follicle

Joshi, N., Brown, M. S., Bishop, D. K., and Borner, G. V. (2015). Gradual implementation of the meiotic recombination program via checkpoint pathways controlled by global DSB levels. *Mol. Cell.* 57 (5), 797–811. doi:10.1016/j.molcel.2014.12.027

Joyce, E. F., Pedersen, M., Tiong, S., White-Brown, S. K., Paul, A., Campbell, S. D., et al. (2011). Drosophila ATM and ATR have distinct activities in the regulation of meiotic DNA damage and repair. *J. Cell. Biol.* 195 (3), 359–367. doi:10.1083/jcb.201104121

Kauppi, L., Barchi, M., Lange, J., Baudat, F., Jasin, M., and Keeney, S. (2013). Numerical constraints and feedback control of double-strand breaks in mouse meiosis. *Genes. Dev.* 27 (8), 873–886. doi:10.1101/gad.213652.113

Keeney, S., Giroux, C. N., and Kleckner, N. (1997). Meiosis-specific DNA double-strand breaks are catalyzed by Spo11, a member of a widely conserved protein family. *Cell.* 88 (3), 375–384. doi:10.1016/S0092-8674(00)81876-0

Keeney, S. (2001). *Current topics in developmental Biology*. Academic Press, 1–53. doi:10.1016/s0070-2153(01)52008-6Mechanism and control of meiotic recombination initiation

Keeney, S., and Neale, M. J. (2006).Initiation of meiotic recombination by formation of DNA double-strand breaks: Mechanism and regulation. *Biochem. Soc. Trans.*, 523–525. doi:10.1042/BST0340523

Keeney, S. (2008). *'Spo11 and the formation of DNA double-strand breaks in meiosis'*, Genome Dynamics and Stability. Berlin, Heidelberg: Springer, 81–123. doi:10.1007/7050_2007_026

Kerr, J. B., Myers, M., and Anderson, R. A. (2013)., 146. BioScientifica, R205–R215. –R215. doi:10.1530/REP-13-0181The dynamics of the primordial follicle reserve*Reproduction*

Kidane, D., Jonason, A. S., Gorton, T. S., Mihaylov, I., Pan, J., Keeney, S., et al. (2010). DNA polymerase B is critical for mouse meiotic synapsis. *EMBO J.* 29 (2), 410–423. doi:10.1038/emboj.2009.357

Kleckner, N. (1996). *'Meiosis: How could it work?'*, Proceedings of the national Academy of Sciences of the united States of America. Washington: Proc Natl Acad Sci U S A, 8167. –8174. doi:10.1073/pnas.93.16.8167

Kneitz, B., Cohen, P. E., Avdievich, E., Zhu, L., Kane, M. F., Hou, H., Jr, et al. (2000). MutS homolog 4 localization to meiotic chromosomes is required for chromosome pairing during meiosis in male and female mice. *Genes. Dev.* 14 (9), 1085–1097. doi:10.1101/gad.14.9.1085

Kogo, H., Tsutsumi, M., Ohye, T., Inagaki, H., Abe, T., and Kurahashi, H. (2012a). HORMAD1-dependent checkpoint/surveillance mechanism eliminates asynaptic oocytes. *Genes. Cells* 17 (6), 439–454. doi:10.1111/j.1365-2443.2012.01600.x

Kogo, H., Tsutsumi, M., Inagaki, H., Ohye, T., Kiyonari, H., and Kurahashi, H. (2012b). HORMAD2 is essential for synapsis surveillance during meiotic prophase via the recruitment of ATR activity. *Genes. Cells* 17 (11), 897–912. doi:10.1111/gtc.12005

Kojima, M. L., De Rooij, D. G., and Page, D. C. (2019). Amplification of a broad transcriptional program by a common factor triggers the meiotic cell cycle in mice. *eLife* 8, e43738. doi:10.7554/eLife.43738

Kolas, N. K., and Cohen, P. E. (2004). *'Novel and diverse functions of the DNA mismatch repair family in mammalian meiosis and recombination'*,. Basel: Cytogenet Genome. Res., 216–231. doi:10.1159/000080600

Koopman, P., Gubbay, J., Vivian, N., Goodfellow, P., and Lovell-Badge, R. (1991). Male development of chromosomally female mice transgenic for Sry. *Nature* 351 (6322), 117–121. doi:10.1038/351117A0

Koubova, J., Hu, Y. C., Bhattacharyya, T., Soh, Y. Q. S., Gill, M. E., Goodheart, M. L., et al. (2014). Retinoic acid activates two pathways required for meiosis in mice. *PLoS Genet.* 10 (8), e1004541. doi:10.1371/journal.pgen.1004541

Koubova, J., Menke, D. B., Zhou, Q., Capel, B., Griswold, M. D., and Page, D. C. (2006). Retinoic acid regulates sex-specific timing of meiotic initiation in mice. *Proc. Natl. Acad. Sci. U. S. A.* 103 (8), 2474–2479. doi:10.1073/pnas.0510813103

Kouznetsova, A., Wang, H., Bellani, M., Camerini-Otero, R. D., Jessberger, R., and Hoog, C. (2009). BRCA1-mediated chromatin silencing is limited to oocytes with a small number of asynapsed chromosomes. *J. Cell. Sci.* 122 (14), 2446–2452. doi:10.1242/jcs.049353

Krausz, C., Hoefsloot, L., Simoni, M., and Tüttelmann, F. (2014). EAA/EMQN best practice guidelines for molecular diagnosis of Y-chromosomal microdeletions: State-of-the-art 2013. *Andrology*, 5–19. doi:10.1111/j.2047-2927.2013.00173.x

Krausz, C., and Riera-Escamilla, A. (2018). Genetics of male infertility. *Nat. Rev. Urol.* 15 (6), 369–384. doi:10.1038/s41585-018-0003-3

Krausz, C., Riera-Escamilla, A., Moreno-Mendoza, D., Holleman, K., Cioppi, F., Algaba, F., et al. (2020). Genetic dissection of spermatogenic arrest through exome analysis: Clinical implications for the management of azoospermic men. *Genet. Med. official J. Am. Coll. Med. Genet.* 22 (12), 1956–1966. doi:10.1038/S41436-020-0907-1

Kumar, R., Bourbon, H. M., and De Massy, B. (2010). Functional conservation of Mei4 for meiotic DNA double-strand break formation from yeasts to mice. *Genes. Dev.* 24 (12), 1266–1280. doi:10.1101/gad.571710

Kumar, R., Oliver, C., Brun, C., Juarez-Martinez, A. B., Tarabay, Y., Kadlec, J., et al. (2018). Mouse REC114 is essential for meiotic DNA double-strand break formation and forms a complex with MEI4. *Life Sci. Alliance* 1 (6), e201800259. doi:10.26508/lsa.201800259

Kumar, S., Chatzi, C., Brade, T., Cunningham, T. J., Zhao, X., and Duester, G. (2011). Sex-specific timing of meiotic initiation is regulated by Cyp26b1 independent of retinoic acid signalling. *Nat. Commun.* 2 (1), 151. doi:10.1038/NCOMMS1136

Kurzbauer, M. T., Uanschou, C., Chen, D., and Schlogelhofer, P. (2012). The recombinases DMC1 and RAD51 are functionally and spatially separated during meiosis in Arabidopsis. *Plant Cell.* 24 (5), 2058–2070. doi:10.1105/tpc.112.098459

La Salle, S., and Trasler, J. M. (2006). Dynamic expression of DNMT3a and DNMT3b isoforms during male germ cell development in the mouse. *Dev. Biol.* 296 (1), 71–82. doi:10.1016/J.YDBIO.2006.04.436

Lam, I., and Keeney, S. (2015). Mechanism and regulation of meiotic recombination initiation. *Cold Spring Harb. Perspect. Biol.* 7 (1), a016634. doi:10.1101/cshperspect.a016634

Lammers, J. H., Offenberg, H. H., van Aalderen, M., Vink, A. C., Dietrich, A. J., and Heyting, C. (1994). The gene encoding a major component of the lateral elements of synaptonemal complexes of the rat is related to X-linked lymphocyte-regulated genes. *Mol. Cell. Biol.* 14 (2), 1137–1146. doi:10.1128/mcb.14.2.1137-1146.1994

Lange, J., Pan, J., Cole, F., Thelen, M. P., Jasin, M., and Keeney, S. (2011). ATM controls meiotic double-strand-break formation. *Nature* 479 (7372), 237–240. doi:10.1038/nature10508

Lehti, M. S., and Sironen, A. (2016). Formation and function of the manchette and flagellum during spermatogenesis. *Reproduction* 151 (4), R43–R54. doi:10.1530/REP-15-0310

Lei, L., and Spradling, A. C. (2016). Mouse oocytes differentiate through organelle enrichment from sister cyst germ cells. *Science* 352 (6281), 95–99. doi:10.1126/science.aad2156

Lesch, B. J., and Page, D. C. (2012). Genetics of germ cell development. *Nat. Rev. Genet.*, 781–794. doi:10.1038/nrg3294

Leung, W.-K., Humphryes, N., Afshar, N., Argunhan, B., Terentyev, Y., Tsubouchi, T., et al. (2015). The synaptonemal complex is assembled by a polySUMOylation-driven feedback mechanism in yeast. *J. Cell. Biol.* 211 (4), 785–793. doi:10.1083/JCB.201506103

Li, R., and Albertini, D. F. (2013). The road to maturation: Somatic cell interaction and self-organization of the mammalian oocyte. *Nat. Rev. Mol. Cell. Biol.*, 141–152. doi:10.1038/nrm3531

Li, X., and Schimenti, J. C. (2007). Mouse pachytene checkpoint 2 (Trip13) is required for completing meiotic recombination but not synapsis. *PLoS Genet.* 3 (8), e130–e1376. doi:10.1371/journal.pgen.0030130

Lintern-Moore, S., and Moore, G. P. (1979). The initiation of follicle and oocyte growth in the mouse ovary. *Biol. reproduction* 20 (4), 773–778. doi:10.1095/biolreprod20.4.773

Lipkin, S. M., Moens, P. B., Wang, V., Lenzi, M., Shanmugarajah, D., Gilgeous, A., et al. (2002). Meiotic arrest and aneuploidy in MLH3-deficient mice. *Nat. Genet.* 31 (4), 385–390. doi:10.1038/ng931

Liu, J., Wu, T. C., and Lichten, M. (1995). The location and structure of double-strand DNA breaks induced during yeast meiosis: Evidence for a covalently linked DNA-protein intermediate. *EMBO J.* 14 (18), 4599–4608. doi:10.1002/j.1460-2075.1995.tb00139.x

Lu, J., Gu, Y., Feng, J., Zhou, W., Yang, X., and Shen, Y. (2014). Structural insight into the central element assembly of the synaptonemal complex. *Sci. Rep.* 4 (1), 7059. doi:10.1038/srep07059

Lu, W. J., Chapo, J., Roig, I., and Abrams, J. M. (2010). Meiotic recombination provokes functional activation of the p53 regulatory network. *Science* 328 (5983), 1278–1281. doi:10.1126/science.1185640

Lukaszewicz, A., Lange, J., Keeney, S., and Jasin, M. (2021). De novo deletions and duplications at recombination hotspots in mouse germlines. *Cell.* 184 (24), 5970–5984.e18. doi:10.1016/J.CELL.2021.10.025

MacQueen, A. J., and Hochwagen, A. (2011). Checkpoint mechanisms: The puppet masters of meiotic prophase. *Trends Cell. Biol.* 21 (7), 393–400. doi:10.1016/j.tcb.2011.03.004

Mahadevaiah, S. K., Bourc'his, D., de Rooij, D. G., Bestor, T. H., Turner, J. M. A., and Burgoyne, P. S. (2008). Extensive meiotic asynapsis in mice antagonises meiotic silencing of unsynapsed chromatin and consequently disrupts meiotic sex chromosome inactivation. *J. Cell. Biol.* 182 (2), 263–276. doi:10.1083/jcb.200710195

Malki, S., van der Heijden, G. W., O'Donnell, K. A., Martin, S. L., and Bortvin, A. (2014). A Role for retrotransposon LINE-1 in fetal oocyte attrition in mice. *Dev. Cell.* 29 (5), 521–533. doi:10.1016/j.devcel.2014.04.027

Mallepaly, R., Butler, P. R., Herati, A. S., and Lamb, D. J. (2017). Genetic basis of male and female infertility. *Monogr. Hum. Genet.* 21, 1–16. doi:10.1159/000477275

Manfrini, N., Guerini, I., Citterio, A., Lucchini, G., and Longhese, M. P. (2010). Processing of meiotic DNA double strand breaks requires cyclin-dependent kinase and multiple nucleases. *J. Biol. Chem.* 285 (15), 11628–11637. doi:10.1074/JBC.M110.104083

Manheim, E. A., and McKim, K. S. (2003). The synaptonemal complex component C(2)M regulates meiotic crossing over in Drosophila. *Curr. Biol.* 13 (4), 276–285. doi:10.1016/S0960-9822(03)00050-2

Marcet-Ortega, M., Maldonado-Linares, A., Lopez-Panades, M., and Roig, I. (2022). p53 controls meiotic prophase progression and crossover formation. *Int. J. Mol. Sci.* 23 (17), 9818. doi:10.3390/ijms23179818

Marcet-Ortega, M., Pacheco, S., Martinez-Marchal, A., Castillo, H., Flores, E., Jasin, M., et al. (2017). p53 and TAp63 participate in the recombination-dependent pachytene arrest in mouse spermatocytes. *PLoS Genet.* 13 (6), e1009067. doi:10.1371/journal.pgen.1006845

Marsolier-Kergoat, M. C., Khan, M. M., Schott, J., Zhu, X., and Llorente, B. (2018). Mechanistic view and genetic control of DNA recombination during meiosis. *Mol. Cell.* 70 (1), 9–20.e6. doi:10.1016/j.molcel.2018.02.032

Martínez-Marchal, A., Huang, Y., Guillot-Ferriols, M. T., Ferrer-Roda, M., Guixe, A., Garcia-Caldes, M., et al. (2020). The DNA damage response is required for oocyte cyst breakdown and follicle formation in mice. *PLOS Genet.* 16 (11), e1009067. doi:10.1371/journal.pgen.1009067

Martini, E., Diaz, R. L., Hunter, N., and Keeney, S. (2006). Crossover homeostasis in yeast meiosis. *Cell.* 126 (2), 285–295. doi:10.1016/j.cell.2006.05.044

Mascarenhas, M. N., Flaxman, S. R., Boerma, T., Vanderpoel, S., and Stevens, G. A. (2012). National, regional, and global trends in infertility prevalence since 1990: A systematic analysis of 277 health surveys. *PLoS Med.* 9 (12), e1001356. doi:10.1371/journal.pmed.1001356

Matsuoka, S., Huang, M., and Elledge, S. J. (1998). Linkage of ATM to cell cycle regulation by the Chk2 protein kinase. *Science* 282 (5395), 1893–1897. doi:10.1126/science.282.5395.1893

McLaren, A. (1984). Meiosis and differentiation of mouse germ cells. *Symposia Soc. Exp. Biol.* 38, 7–23.

McLaren, A., and Monk, M. (1981). X-chromosome activity in the germ cells of Sex-reversed mouse embryos. *J. Reproduction Fertil.* 63 (2), 533–537. doi:10.1530/jrf.0.0630533

McLean, D. J., Friel, P. J., Johnston, D. S., and Griswold, M. D. (2003). Characterization of spermatogonial stem cell maturation and differentiation in neonatal mice. *Biol. reproduction* 69 (6), 2085–2091. doi:10.1095/biolreprod.103.017020

Meuwissen, R. L. J., Offenberg, H. H., Dietrich, A. J., Riesewijk, A., van Iersel, M., and Heyting, C. (1992). A coiled-coil related protein specific for synapsed regions of meiotic prophase chromosomes. *EMBO J.* 11 (13), 5091–5100. doi:10.1002/j.1460-2075.1992.tb05616.x

Mimitou, E. P., Yamada, S., and Keeney, S. (2017). A global view of meiotic double-strand break end resection. *Science* 355 (6320), 40–45. doi:10.1126/science.aak9704

Molyneaux, K. A., Stallock, J., Schaible, K., and Wylie, C. (2001). Time-lapse analysis of living mouse germ cell migration. *Dev. Biol.* 240 (2), 488–498. doi:10.1006/dbio.2001.0436

Morelli, M. A., and Cohen, P. E. (2005). Not all germ cells are created equal: Aspects of sexual dimorphism in mammalian meiosis. *Reproduction*, 761–781. doi:10.1530/rep.1.00865

Morgan, C., Fozard, J. A., Hartley, M., Henderson, I. R., Bomblies, K., and Howard, M. (2021). Diffusion-mediated HEI10 coarsening can explain meiotic crossover positioning in Arabidopsis. *Nat. Commun.* 12 (1), 4674. doi:10.1038/S41467-021-24827-W

Moses, M. J. (1969). Structure and function of the synaptonemal complex. *Genetics* 61 (1), 41–51.

Nagaoka, S. I., Nakaki, F., Miyauchi, H., Nosaka, Y., Ohta, H., and Yabuta, Y. (2020). ZGLP1 is a determinant for the oogenic fate in mice. *Science* 4115, 1–15. doi:10.1126/science.aaw4115

Namwanje, M., and Brown, C. W. (2016). Activins and inhibins: Roles in development, physiology, and disease. *Cold Spring Harb. Perspect. Biol.* 8 (7), a021881. doi:10.1101/cshperspect.a021881

National Institute for Health and Care Excellence (2013). *'National Institute for health and Care excellence.',* fertility: Assessment and Treatment for People with fertility problems. [NICE Guideline CG156]. Available at: https://www.nice.org.uk/guidance/cg156 (Accessed December 22, 2021).

Neale, M. J., Pan, J., and Keeney, S. (2005). Endonucleolytic processing of covalent protein-linked DNA double-strand breaks. *Nature* 436 (7053), 1053–1057. doi:10.1038/nature03872

Nore, A., Juarez-Martinez, A. B., Clement, J., Brun, C., Diagouraga, B., Laroussi, H., et al. (2022). TOPOVIBL-REC114 interaction regulates meiotic DNA double-strand breaks. *Nat. Commun.* 13 (1), 7048. doi:10.1038/S41467-022-34799-0

Norris, R. P., Ratzan, W. J., Freudzon, M., Mehlmann, L. M., Krall, J., Movsesian, M. A., et al. (2009). Cyclic GMP from the surrounding somatic cells regulates cyclic AMP and meiosis in the mouse oocyte. *Dev. Camb. Engl.* 136 (11), 1869–1878. doi:10.1242/DEV.035238

Oatley, J. M., and Brinster, R. L. (2008). Regulation of spermatogonial stem cell self-renewal in mammals. *Annu. Rev. Cell. Dev. Biol.* 24, 263–286. doi:10.1146/annurev.cellbio.24.110707.175355

Oatley, J. M., and Brinster, R. L. (2012). The germline stem cell niche unit in mammalian testes. *Physiol. Rev.*, 577–595. doi:10.1152/physrev.00025.2011

O'Donnell, L., Stanton, P., and de Kretser, D. M. (2000). Endocrinology of the male reproductive system and spermatogenesis, endotext. Available at: http://www.ncbi.nlm.nih.gov/pubmed/25905260.

Offenberg, H. H., Schalk, J. A. C., Meuwissen, R. L. J., van Aalderen, M., Kester, H. A., Dietrich, A. J. J., et al. (1998). SCP2: A major protein component of the axial elements of synaptonemal complexes of the rat. *Nucleic Acids Research*. 26 (11), 2572–2579. doi:10.1093/nar/26.11.2572

Oud, M. S., Volozonoka, L., Smits, R. M., Vissers, L. E. L. M., Ramos, L., and Veltman, J. A. (2019). A systematic review and standardized clinical validity assessment of male infertility genes. *male Infertil. Genes.'* 34 (5), 932–941. doi:10.1093/humrep/dez022

Pacheco, S., Maldonado-Linares, A., Marcet-Ortega, M., Rojas, C., Martinez-Marchal, A., Fuentes-Lazaro, J., et al. (2018). ATR is required to complete meiotic recombination in mice. *Nat. Commun.* 9 (1), 2622. doi:10.1038/s41467-018-04851-z

Pacheco, S., Marcet-Ortega, M., Lange, J., Jasin, M., Keeney, S., and Roig, I. (2015). The ATM signaling cascade promotes recombination-dependent pachytene arrest in mouse spermatocytes. *PLoS Genet.* 11 (3), e1005017–e1005027. doi:10.1371/journal.pgen.1005017

Page, J., Fuente, R. De, and Manterola, M. (2012). *Inactivation or non-reactivation: What accounts better for the silence of sex chromosomes during mammalian male meiosis ?* 307–326. doi:10.1007/s00412-012-0364-y

Paigen, K., and Petkov, P. M. (2018). *'PRDM9 and its role in genetic recombination'*, Trends in genetics. Elsevier, 291–300. doi:10.1016/j.tig.2017.12.017

Papanikos, F., Clement, J. A. J., Testa, E., Ravindranathan, R., Grey, C., Dereli, I., et al. (2019). Mouse ANKRD31 regulates spatiotemporal patterning of meiotic recombination initiation and ensures recombination between X and Y sex chromosomes. *Mol. Cell.* 74 (5), 1069–1085.e11. doi:10.1016/j.molcel.2019.03.022

Parvanov, E. D., Tian, H., Billings, T., Saxl, R. L., Spruce, C., Aithal, R., et al. (2017). PRDM9 interactions with other proteins provide a link between recombination hotspots and the chromosomal axis in meiosis. *Mol. Biol. Cell.* 28 (3), 488–499. doi:10.1091/mbc.E16-09-0686

Pattabiraman, D., Roelens, B., Woglar, A., and Villeneuve, A. M. (2017). Meiotic recombination modulates the structure and dynamics of the synaptonemal complex during *C. elegans* meiosis. *PLoS Genet.* 13 (3), e1006670. doi:10.1371/journal.pgen.1006670

Pepling, M. E. (2012)., 143. BioScientifica, 139–149. doi:10.1530/REP-11-0299Follicular assembly: Mechanisms of action*Reproduction*

Pepling, M. E., and Spradling, A. C. (1998). Female mouse germ cells form synchronously dividing cysts. *Dev. Camb. Engl.* 125 (17), 3323–3328. doi:10.1242/dev.125.17.3323

Pepling, M. E., and Spradling, A. C. (2001). Mouse ovarian germ cell cysts undergo programmed breakdown to form primordial follicles. *Dev. Biol.* 234 (2), 339–351. doi:10.1006/dbio.2001.0269

Perera, D., Perez-Hidalgo, L., Moens, P. B., Reini, K., Lakin, N., Syvaoja, J. E., et al. (2004). ToPBP1 and ATR colocalization at meiotic chromosomes: Role of TopBP1/cut5 in the meiotic recombination checkpoint. *Mol. Biol. Cell.* 15 (4), 1568–1579. doi:10.1091/mbc.E03-06-0444

Petukhova, G. V., Pezza, R. J., Vanevski, F., Ploquin, M., Masson, J. Y., and Camerini-Otero, R. D. (2005). The Hop2 and Mnd1 proteins act in concert with Rad51 and Dmc1 in meiotic recombination. *Nat. Struct. Mol. Biol.* 12 (5), 449–453. doi:10.1038/nsmb923

Petukhova, G. V., Romanienko, P. J., and Camerini-Otero, R. D. (2003). The Hop2 protein has a direct role in promoting interhomolog interactions during mouse meiosis. *Dev. Cell.* 5 (6), 927–936. doi:10.1016/S1534-5807(03)00369-1

Pezza, R. J., Voloshin, O. N., Vanevski, F., and Camerini-Otero, R. D. (2007). Hop2/Mnd1 acts on two critical steps in Dmc1-promoted homologous pairing. *Genes. Dev.* 21 (14), 1758–1766. doi:10.1101/gad.1562907

Pochart, P., Woltering, D., and Hollingsworth, N. M. (1997). Conserved properties between functionally distinct MutS homologs in yeast. *J. Biol. Chem.* 272 (48), 30345–30349. doi:10.1074/jbc.272.48.30345

Prasada Rao, H. B. D., Qiao, H., Bhatt, S. K., Bailey, L. R. J., Tran, H. D., Bourne, S. L., et al. (2017). A SUMO-ubiquitin relay recruits proteasomes to chromosome axes to regulate meiotic recombination. *Science* 355 (6323), 403–407. doi:10.1126/science.aaf6407

Precone, V., Cannarella, R., Paolacci, S., Busetto, G. M., Beccari, T., Stuppia, L., et al. (2021). Male infertility diagnosis: Improvement of genetic analysis performance by the introduction of pre-diagnostic genes in a next-generation sequencing custom-made panel. *Front. Endocrinol.* 11, 605237. doi:10.3389/fendo.2020.605237

Prieto, I., Suja, J. A., Pezzi, N., Kremer, L., Martinez-A, C., Rufas, J. S., et al. (2001). Mammalian STAG3 is a cohesin specific to sister chromatid arms in meiosis I. *Nat. Cell. Biol.* 3 (8), 761–766. doi:10.1038/35087082

Qiao, H., Chen, J. K., Reynolds, A., Hoog, C., Paddy, M., and Hunter, N. (2012). Interplay between synaptonemal complex, homologous recombination, and centromeres during mammalian meiosis. *PLoS Genet.* 8 (6), e1002790. doi:10.1371/journal.pgen.1002790

Qiao, H., Prasada Rao, H. B. D., Yang, Y., Fong, J. H., Cloutier, J. M., Deacon, D. C., et al. (2014). Antagonistic roles of ubiquitin ligase HEI10 and SUMO ligase RNF212 regulate meiotic recombination. *Nat. Genet.* 46 (2), 194–199. doi:10.1038/ng.2858

Qiao, H., Rao, H. B. D. P., Yun, Y., Sandhu, S., Fong, J. H., Sapre, M., et al. (2018). Impeding DNA break repair enables oocyte quality control. *Mol. Cell.* 72 (2), 211–221.e3. doi:10.1016/j.molcel.2018.08.031

Ranjha, L., Howard, S. M., and Cejka, P. (2018). Main steps in DNA double-strand break repair: An introduction to homologous recombination and related processes. *Chromosoma* 127, 187–214. doi:10.1007/s00412-017-0658-1

Rato, L., Alves, M. G., Socorro, S., Duarte, A. I., Cavaco, J. E., and Oliveira, P. F. (2012). Metabolic regulation is important for spermatogenesis. *Nat. Rev. Urol.* 9 (6), 330–338. doi:10.1038/nrurol.2012.77

Ravindranathan, R., Raveendran, K., Papanikos, F., San-Segundo, P. A., and Toth, A. (2022). Chromosomal synapsis defects can trigger oocyte apoptosis without elevating numbers of persistent DNA breaks above wild-type levels. *Nucleic acids Res.* 50 (10), 5617–5634. doi:10.1093/NAR/GKAC355

Refolio, E., Cavero, S., Marcon, E., Freire, R., and San-Segundo, P. A. (2011). The Ddc2/ATRIP checkpoint protein monitors meiotic recombination intermediates. *J. Cell. Sci.* 124 (14), 2488–2500. doi:10.1242/jcs.081711

Reinholdt, L. G., and Schimenti, J. C. (2005). Mei1 is epistatic to Dmc1 during mouse meiosis. *Chromosoma* 114 (2), 127–134. doi:10.1007/s00412-005-0346-4

Reynolds, A., Qiao, H., Yang, Y., Chen, J. K., Jackson, N., Biswas, K., et al. (2013). RNF212 is a dosage-sensitive regulator of crossing-over during mammalian meiosis. *Nat. Genet.* 45 (3), 269–278. doi:10.1038/ng.2541

Riera-Escamilla, A., Enguita-Marruedo, A., Moreno-Mendoza, D., Chianese, C., Sleddens-Linkels, E., Contini, E., et al. (2019). Sequencing of a "mouse azoospermia" gene panel in azoospermic men: Identification of RNF212 and STAG3 mutations as novel genetic causes of meiotic arrest. *Hum. Reprod.* 34 (6), 978–988. doi:10.1093/humrep/dez042

Rinaldi, V. D., Bloom, J. C., and Schimenti, J. C. (2020). Oocyte elimination through DNA damage signaling from CHK1/CHK2 to p53 and p63. *Genetics* 215 (2), 373–378. doi:10.1534/genetics.120.303182

Rinaldi, V. D., Bolcun-Filas, E., Kogo, H., Kurahashi, H., and Schimenti, J. C. (2017). The DNA damage checkpoint eliminates mouse oocytes with chromosome synapsis failure. *Mol. Cell.* 67 (6), 1026–1036.e2. doi:10.1016/j.molcel.2017.07.027

Robert, T., Nore, A., Brun, C., Maffre, C., Crimi, B., Bourbon, H. M., et al. (2016). The Topo VIB-Like protein family is required for meiotic DNA double-strand break formation. *Science* 351 (6276), 943–949. doi:10.1126/science.aad5309

Roeder, G., and Bailis, J. M. (2000). The pachytene checkpoint. *Trends Genet.* 16 (9), 395–403. doi:10.1016/S0168-9525(00)02080-1

Roig, I., Dowdle, J. A., Toth, A., de Rooij, D. G., Jasin, M., and Keeney, S. (2010). Mouse TRIP13/PCH2 is required for recombination and normal higher-order chromosome structure during meiosis. *PLoS Genet.* 6 (8), e1001062. doi:10.1371/journal.pgen.1001062

Rossetti, R., Ferrari, I., Bonomi, M., and Persani, L. (2017). Genetics of primary ovarian insufficiency. *Clin. Genet.* 91, 183–198. doi:10.1111/cge.12921

Rosu, S., Libuda, D. E., and Villeneuve, A. M. (2011). Robust crossover assurance and regulated interhomolog access maintain meiotic crossover number. *Science* 334 (6060), 1286–1289. doi:10.1126/science.1212424

Royo, H., Polikiewicz, G., Mahadevaiah, S. K., Prosser, H., Mitchell, M., Bradley, A., et al. (2010). Evidence that meiotic sex chromosome inactivation is essential for male fertility. *Curr. Biol.* 20 (23), 2117–2123. doi:10.1016/j.cub.2010.11.010

Royo, H., Prosser, H., Ruzankina, Y., Mahadevaiah, S. K., Cloutier, J. M., Baumann, M., et al. (2013). ATR acts stage specifically to regulate multiple aspects of mammalian meiotic silencing. *Genes. Dev.* 27 (13), 1484–1494. doi:10.1101/gad.219477.113

Russell, L. D., Ettlin, R. A., Hikim, A. P. S., and Clegg, E. D. (1993) Histological and histopathological evaluation of the testis, *Int. J. Androl.*, 16(1), 83. doi:10.1111/j.1365-2605.1993.tb01156.x

Ruth, K. S., Day, F. R., Hussain, J., Martinez-Marchal, A., Aiken, C. E., Azad, A., et al. (2021). Genetic insights into biological mechanisms governing human ovarian ageing. *Nature* 596 (7872), 7872596393–7872596397. doi:10.1038/s41586-021-03779-7

San Filippo, J., Sung, P., and Klein, H. (2008). Mechanism of eukaryotic homologous recombination. *Annu. Rev. Biochem.* 77 (1), 229–257. doi:10.1146/annurev.biochem.77.061306.125255

Schramm, S., Fraune, J., Naumann, R., Hernandez-Hernandez, A., Hoog, C., Cooke, H. J., et al. (2011). A novel mouse synaptonemal complex protein is essential for loading of central element proteins, recombination, and fertility. *PLoS Genet.* 7 (5), e1002088. doi:10.1371/journal.pgen.1002088

Schücker, K., Holm, T., Franke, C., Sauer, M., and Benavente, R. (2015). Elucidation of synaptonemal complex organization by super-resolution imaging with isotropic resolution. *Proc. Natl. Acad. Sci. U. S. A.* 112 (7), 2029–2033. doi:10.1073/pnas.1414814112

Schücker, K., Sauer, M., and Benavente, R. (2018). "Superresolution imaging of the synaptonemal complex," in *Methods in cell Biology*, 335–346. doi:10.1016/bs.mcb.2018.03.033

Serrentino, M. E., and Borde, V. (2012). The spatial regulation of meiotic recombination hotspots: Are all DSB hotspots crossover hotspots? *Exp. Cell. Res.*, 1347–1352. doi:10.1016/j.yexcr.2012.03.025

Shin, Y. H., Choi, Y., Erdin, S. U., Yatsenko, S. A., Kloc, M., Yang, F., et al. (2010). Hormad1 mutation disrupts synaptonemal complex formation, recombination, and chromosome segregation in mammalian meiosis. *PLoS Genet.* 6 (11), e1001190. doi:10.1371/journal.pgen.1001190

Shinohara, T., Orwig, K. E., Avarbock, M. R., and Brinster, R. L. (2001). Remodeling of the postnatal mouse testis is accompanied by dramatic changes in stem cell number and niche accessibility. *Proc. Natl. Acad. Sci. U. S. A.* 98 (11), 6186–6191. doi:10.1073/pnas.111158198

Smith, G. R., and Nambiar, M. (2020). New solutions to old problems: Molecular mechanisms of meiotic crossover control. *Trends Genet.*, 337–346. doi:10.1016/j.tig.2020.02.002

Smith, S., Pfeifer, S. M., and Collins, J. A. (2003). Diagnosis and management of female infertility. *JAMA* 290 (13), 1767–1770. doi:10.1001/jama.290.13.1767

Soh, Y. Q. S., Junker, J. P., Gill, M. E., Mueller, J. L., van Oudenaarden, A., and Page, D. C. (2015). A gene regulatory program for meiotic prophase in the fetal ovary. *PLoS Genet.* 11 (9), e1005531. doi:10.1371/journal.pgen.1005531

Stanzione, M., Baumann, M., Papanikos, F., Dereli, I., Lange, J., Ramlal, A., et al. (2016). Meiotic DNA break formation requires the unsynapsed chromosome axis-binding protein IHO1 (CCDC36) in mice. *Nat. Cell. Biol.* 18 (11), 1208–1220. doi:10.1038/ncb3417

Stracker, T. H., and Petrini, J. H. J. (2011). The MRE11 complex: Starting from the ends. *Nat. Rev. Mol. Cell. Biol.*, 90–103. doi:10.1038/nrm3047

Su, X., Chakravarti, D., and Flores, E. R. (2013). P63 steps into the limelight: Crucial roles in the suppression of tumorigenesis and metastasis. *Nat. Rev. Cancer* 13 (2), 136–143. doi:10.1038/nrc3446

Subramanian, V. V., and Hochwagen, A. (2014). The meiotic checkpoint network: Step-by-step through meiotic prophase. *Cold Spring Harb. Perspect. Biol.* 6 (10), a016675. doi:10.1101/cshperspect.a016675

Sun, F., Turek, P., Greene, C., Ko, E., Rademaker, A., and Martin, R. H. (2007). Abnormal progression through meiosis in men with nonobstructive azoospermia. *Fertil. Steril.* 87 (3), 565–571. doi:10.1016/j.fertnstert.2006.07.1531

Székvölgyi, L., Ohta, K., and Nicolas, A. (2015). Initiation of meiotic homologous recombination: Flexibility, impact of histone modifications, and chromatin remodeling. *Cold Spring Harb. Perspect. Biol.* 7 (5), a016527. doi:10.1101/cshperspect.a016527

Testa, E., Nardozi, D., Antinozzi, C., Faieta, M., Di Cecca, S., Caggiano, C., et al. (2018). H2AFX and MDC1 promote maintenance of genomic integrity in male germ cells. *J. Cell. sciencejcs214411* 131 (6). doi:10.1242/JCS.214411

Touati, S. A., and Wassmann, K. (2016). How oocytes try to get it right: Spindle checkpoint control in meiosis. *Chromosoma*, 321–335. doi:10.1007/s00412-015-0536-7

Tournaye, H., Krausz, C., and Oates, R. D. (2017). Novel concepts in the aetiology of male reproductive impairment. *lancet. Diabetes & Endocrinol.* 5 (7), 544–553. doi:10.1016/S2213-8587(16)30040-7

Traven, A., and Heierhorst, J. (2005). SQ/TQ cluster domains: Concentrated ATM/ATR kinase phosphorylation site regions in DNA-damage-response proteins. *BioEssays* 27 (4), 397–407. doi:10.1002/bies.20204

Turner, J. M. A., Aprelikova, O., Xu, X., Wang, R., Kim, S., Chandramouli, G. V. R., et al. (2004). BRCA1, histone H2AX phosphorylation, and male meiotic sex chromosome inactivation. *Curr. Biol.* 14 (23), 2135–2142. doi:10.1016/j.cub.2004.11.032

Turner, J. M. A., Mahadevaiah, S. K., Ellis, P. J. I., Mitchell, M. J., and Burgoyne, P. S. (2006). Pachytene asynapsis drives meiotic sex chromosome inactivation and leads to substantial postmeiotic repression in spermatids. *Dev. Cell.* 10 (4), 521–529. doi:10.1016/j.devcel.2006.02.009

Turner, J. M. A. (2015). Meiotic silencing in mammals. *Annu. Rev. Genet.* 49 (1), 395–412. doi:10.1146/annurev-genet-112414-055145

Tüttelmann, F., Ruckert, C., and Röpke, A. (2018). Disorders of spermatogenesis. Perspectives for novel genetic diagnostics after 20 years of unchanged routine. *Med. Genet.* 30 (1), 12–20. doi:10.1007/s11825-018-0181-7

Vernet, N., Condrea, D., Mayere, C., Feret, B., Klopfenstein, M., Magnant, W., et al. (2020). Meiosis occurs normally in the fetal ovary of mice lacking all retinoic acid receptors. *Sci. Adv.* 6 (21), eaaz1139. doi:10.1126/SCIADV.AAZ1139

Voelkel-Meiman, K., Moustafa, S. S., Lefrancois, P., Villeneuve, A. M., and MacQueen, A. J. (2012). Full-length synaptonemal complex grows continuously during meiotic prophase in budding yeast. *PLOS Genet.* 8 (10), e1002993. doi:10.1371/JOURNAL.PGEN.1002993

Vrielynck, N., Chambon, A., Vezon, D., Pereira, L., Chelysheva, L., De Muyt, A., et al. (2016). A DNA topoisomerase VI-like complex initiates meiotic recombination. *Science* 351 (6276), 939–943. doi:10.1126/science.aad5196

Wang, J., Zhang, W., Jiang, H., and Wu, B. L.Primary Ovarian Insufficiency Collaboration (2014). Mutations in HFM1 in recessive primary ovarian insufficiency. *N. Engl. J. Med.* 370 (10), 972–974. doi:10.1056/nejmc1310150

Wear, H. M., McPike, M. J., and Watanabe, K. H. (2016). From primordial germ cells to primordial follicles: A review and visual representation of early ovarian development in mice. *J. Ovarian Res.* 9 (1), 36–11. doi:10.1186/s13048-016-0246-7

Wei, K., Clark, A. B., Wong, E., Kane, M. F., Mazur, D. J., Parris, T., et al. (2003). Inactivation of Exonuclease 1 in mice results in DNA mismatch repair defects, increased cancer susceptibility, and male and female sterility. *Genes. Dev.* 17 (5), 603–614. doi:10.1101/gad.1060603

West, A. M. V., Rosenberg, S. C., Ur, S. N., Lehmer, M. K., Ye, Q., Hagemann, G., et al. (2019). A conserved filamentous assembly underlies the structure of the meiotic chromosome axis. *eLife* 8, e40372. doi:10.7554/eLife.40372

Widger, A., Mahadevaiah, S. K., Lange, J., ElInati, E., Zohren, J., Hirota, T., et al. (2018). ATR is a multifunctional regulator of male mouse meiosis. *Nat. Commun.* 9 (1), 2621. doi:10.1038/s41467-018-04850-0

Williams, C. J., and Erickson, G. F. (2000). *Morphology and physiology of the ovary*. South Dartmouth (MA).

Winkel, K., Alsheimer, M., Ollinger, R., and Benavente, R. (2009). Protein SYCP2 provides a link between transverse filaments and lateral elements of mammalian synaptonemal complexes. *Chromosoma* 118 (2), 259–267. doi:10.1007/s00412-008-0194-0

Wojtasz, L., Cloutier, J. M., Baumann, M., Daniel, K., Varga, J., Fu, J., et al. (2012). Meiotic DNA double-strand breaks and chromosome asynapsis in mice are monitored by distinct HORMAD2-independent and -dependent mechanisms. *Genes. & Dev.* 26 (9), 958–973. doi:10.1101/gad.187559.112

Wojtasz, L., Daniel, K., Roig, I., Bolcun-Filas, E., Xu, H., Boonsanay, V., et al. (2009). Mouse HORMAD1 and HORMAD2, two conserved meiotic chromosomal proteins, are depleted from synapsed chromosome axes with the help of TRIP13 AAA-ATPase. *PLoS Genet.* 5 (10), e1000702. doi:10.1371/journal.pgen.1000702

Xiao, Y., Pollack, D., Andrusier, M., Levy, A., Callaway, M., Nieves, E., et al. (2016). Identification of cell-specific targets of sumoylation during mouse spermatogenesis. *Reproduction* 151 (2), 149–166. doi:10.1530/REP-15-0239

Xu, H., Tong, Z., Ye, Q., Sun, T., Hong, Z., Zhang, L., et al. (2019). Molecular organization of mammalian meiotic chromosome axis revealed by expansion STORM microscopy. *Proc. Natl. Acad. Sci. U. S. A.* 116 (37), 18423–18428. doi:10.1073/pnas.1902440116

Yadav, V. K., and Claeys Bouuaert, C. (2021). Mechanism and control of meiotic DNA double-strand break formation in *S. cerevisiae*. *Front. Cell. Dev. Biol.* 9, 642737. doi:10.3389/FCELL.2021.642737

Yamaguchi, S., Hong, K., Liu, R., Shen, L., Inoue, A., Diep, D., et al. (2012). Tet1 controls meiosis by regulating meiotic gene expression. *Nature* 492 (7429), 443–447. doi:10.1038/nature11709

Yan, C., Wang, P., DeMayo, J., DeMayo, F. J., Elvin, J. A., Carino, C., et al. (2001). Synergistic roles of bone morphogenetic protein 15 and growth differentiation factor 9 in ovarian function. *Mol. Endocrinol. Baltim. Md* 15 (6), 854–866. doi:10.1210/mend.15.6.0662

Yang, F., De La Fuente, R., Leu, N. A., Baumann, C., McLaughlin, K. J., and Wang, P. J. (2006). Mouse SYCP2 is required for synaptonemal complex assembly and chromosomal synapsis during male meiosis. *J. Cell. Biol.* 173 (4), 497–507. doi:10.1083/jcb.200603063

Yang, F., Silber, S., Leu, N. A., Oates, R. D., Marszalek, J. D., Skaletsky, H., et al. (2015). TEX11 is mutated in infertile men with azoospermia and regulates genome-wide recombination rates in mouse. *EMBO Mol. Med.* 7 (9), 1198–1210. doi:10.15252/emmm.201404967

Yatsenko, A. N., Georgiadis, A. P., Ropke, A., Berman, A. J., Jaffe, T., Olszewska, M., et al. (2015). X-linked TEX11 mutations, meiotic arrest, and azoospermia in infertile men. *N. Engl. J. Med.* 372 (22), 2097–2107. doi:10.1056/NEJMoa1406192

Yatsenko, S. A., and Rajkovic, A. (2019). Genetics of human female infertility. *Biol. Reproduction* 101 (3), 549–566. doi:10.1093/biolre/ioz084

Yokobayashi, S., Liang, C. Y., Kohler, H., Nestorov, P., Liu, Z., Vidal, M., et al. (2013). PRC1 coordinates timing of sexual differentiation of female primordial germ cells. *Nature* 495 (7440), 236–240. doi:10.1038/nature11918

Yokoo, R., Zawadzki, K. A., Nabeshima, K., Drake, M., Arur, S., and Villeneuve, A. M. (2012). COSA-1 reveals robust homeostasis and separable licensing and reinforcement steps governing meiotic crossovers. *Cell.* 149 (1), 75–87. doi:10.1016/j.cell.2012.01.052

Yoshida, S., Sukeno, M., Nakagawa, T., Ohbo, K., Nagamatsu, G., Suda, T., et al. (2006). *The first round of mouse spermatogenesis is a distinctive program that lacks the self-renewing spermatogonia stage*, 1505, 1495–1505. doi:10.1242/dev.02316

Yuan, L., Liu, J. G., Zhao, J., Brundell, E., Daneholt, B., and Hoog, C. (2000). The murine SCP3 gene is required for synaptonemal complex assembly, chromosome synapsis, and male fertility. *Mol. Cell.* 5 (1), 73–83. doi:10.1016/S1097-2765(00)80404-9

Zakharyevich, K., Ma, Y., Tang, S., Hwang, P. Y. H., Boiteux, S., and Hunter, N. (2010). Temporally and biochemically distinct activities of Exo1 during meiosis: Double-strand break resection and resolution of double Holliday junctions. *Mol. Cell.* 40 (6), 1001–1015. doi:10.1016/j.molcel.2010.11.032

Zakharyevich, K., Tang, S., Ma, Y., and Hunter, N. (2012). Delineation of joint molecule resolution pathways in meiosis identifies a crossover-specific resolvase. *Cell.* 149 (2), 334–347. doi:10.1016/j.cell.2012.03.023

Zelensky, A., Kanaar, R., and Wyman, C. (2014). Mediators of homologous DNA pairing. *Cold Spring Harb. Perspect. Biol.* 6 (12), a016451. doi:10.1101/cshperspect.a016451

Zeleznik, A. J. (2004). *The physiology of follicle selection*. Reproductive Biology and EndocrinologyBioMed Central, 31. doi:10.1186/1477-7827-2-31

Zhang, B., Tang, Z., Li, L., and Lu, L. Y. (2020a). NBS1 is required for SPO11-linked DNA double-strand break repair in male meiosis. *Cell. Death Differ.* 27 (7), 2176–2190. doi:10.1038/s41418-020-0493-4

Zhang, J., Fujiwara, Y., Yamamoto, S., and Shibuya, H. (2019a). A meiosis-specific BRCA2 binding protein recruits recombinases to DNA double-strand breaks to ensure homologous recombination. *Nat. Commun.* 10 (11), 722. doi:10.1038/s41467-019-08676-2

Zhang, J., Gurusaran, M., Fujiwara, Y., Zhang, K., Echbarthi, M., Vorontsov, E., et al. (2020b). The BRCA2-MEILB2-BRME1 complex governs meiotic recombination and impairs the mitotic BRCA2-RAD51 function in cancer cells. *Nat. Commun.* 11 (11), 2055. doi:10.1038/s41467-020-15954-x

Zhang, L., Kim, K. P., Kleckner, N. E., and Storlazzi, A. (2011). Meiotic double-strand breaks occur once per pair of (sister) chromatids and, via Mec1/ATR and Tel1/ATM, once per quartet of chromatids. *Proc. Natl. Acad. Sci. U. S. A.* 108 (50), 20036–20041. doi:10.1073/pnas.1117937108

Zhang, L., Liang, Z., Hutchinson, J., and Kleckner, N. (2014). Crossover patterning by the beam-film model: Analysis and implications. *PLoS Genet.* 10 (1), e1004042. doi:10.1371/journal.pgen.1004042

Zhang, L., Wang, S., Yin, S., Hong, S., Kim, K. P., and Kleckner, N. (2014). Topoisomerase II mediates meiotic crossover interference. *Nature* 511 (7511), 551–556. doi:10.1038/nature13442

Zhang, Q., Ji, S. Y., Busayavalasa, K., and Yu, C. (2019b). SPO16 binds SHOC1 to promote homologous recombination and crossing-over in meiotic prophase I. *Sci. Adv.* 5 (1), eaau9780. doi:10.1126/sciadv.aau9780

Zhang, W., Song, X., Ni, F., Cheng, J., Wu, B. L., and Jiang, H. (2017). Association analysis between HFM1 variations and idiopathic azoospermia or severe oligozoospermia in Chinese Men. *Sci. China Life Sci.*, 315–318. doi:10.1007/s11427-016-0274-9

Zickler, D., and Kleckner, N. (1999). Meiotic chromosomes: Integrating structure and function. *Annu. Rev. Genet.*, 603–754. doi:10.1146/annurev.genet.33.1.603

Zickler, D., and Kleckner, N. (2015). Recombination, pairing, and synapsis of homologs during meiosis. *Cold Spring Harb. Lab. Press* 1, 2. doi:10.1101/cshperspect.a016626

Zorrilla, M., and Yatsenko, A. N. (2013). The genetics of infertility: Current status of the field. *Curr. Genet. Med. Rep.* 1 (4), 247–260. doi:10.1007/s40142-013-0027-1

frontiers | Frontiers in Cell and Developmental Biology

TYPE Original Research
PUBLISHED 25 April 2023
DOI 10.3389/fcell.2023.1147610

OPEN ACCESS

EDITED BY
Ricardo Benavente,
Julius Maximilian University of Würzburg, Germany

REVIEWED BY
Roberta B. Sciurano,
National Scientific and Technical Research Council (CONICET), Argentina
Frédéric Baudat,
Université de Montpellier, France

*CORRESPONDENCE
Jesús Page,
jesus.page@uam.es

†These authors have contributed equally to this work

RECEIVED 18 January 2023
ACCEPTED 06 April 2023
PUBLISHED 25 April 2023

CITATION
Valero-Regalón FJ, Solé M, López-Jiménez P, Valerio-de Arana M, Martín-Ruiz M, de la Fuente R, Marín-Gual L, Renfree MB, Shaw G, Berríos S, Fernández-Donoso R, Waters PD, Ruiz-Herrera A, Gómez R and Page J (2023), Divergent patterns of meiotic double strand breaks and synapsis initiation dynamics suggest an evolutionary shift in the meiosis program between American and Australian marsupials.
Front. Cell Dev. Biol. 11:1147610.
doi: 10.3389/fcell.2023.1147610

Divergent patterns of meiotic double strand breaks and synapsis initiation dynamics suggest an evolutionary shift in the meiosis program between American and Australian marsupials

F. Javier Valero-Regalón[1†], Mireia Solé[1,2†], Pablo López-Jiménez[1], María Valerio-de Arana[1], Marta Martín-Ruiz[1], Roberto de la Fuente[3], Laia Marín-Gual[4,5], Marilyn B. Renfree[6], Geoff Shaw[6], Soledad Berríos[7], Raúl Fernández-Donoso[7], Paul D. Waters[8], Aurora Ruiz-Herrera[4,5], Rocío Gómez[1] and Jesús Page[1*]

[1]Departamento de Biología, Facultad de Ciencias, Universidad Autónoma de Madrid, Madrid, Spain, [2]Genetics of Male Fertility Group, Unitat de Biologia Cel·lular, Universitat Autònoma de Barcelona, Spain, [3]Department of Experimental Embryology, Institute of Genetics and Animal Biotechnology of The Polish Academy of Sciences, Jastrzębiec, Poland, [4]Departament de Biologia Cel·lular, Universitat Autònoma de Barcelona, Barcelona, Spain, [5]Genome Integrity and Instability Group, Institut de Biotecnologia i Biomedicina, Barcelona, Spain, [6]School of BioSciences, The University of Melbourne, Melbourne, VIC, Australia, [7]Programa de Genética Humana, Facultad de Medicina, Instituto de Ciencias Biomédicas, Universidad de Chile, Santiago, Chile, [8]School of Biotechnology and Biomolecular Science, Faculty of Science, University of New South Wales, Sydney, NSW, Australia

In eutherian mammals, hundreds of programmed DNA double-strand breaks (DSBs) are generated at the onset of meiosis. The DNA damage response is then triggered. Although the dynamics of this response is well studied in eutherian mammals, recent findings have revealed different patterns of DNA damage signaling and repair in marsupial mammals. To better characterize these differences, here we analyzed synapsis and the chromosomal distribution of meiotic DSBs markers in three different marsupial species (*Thylamys elegans*, *Dromiciops gliorides,* and *Macropus eugenii*) that represent South American and Australian Orders. Our results revealed inter-specific differences in the chromosomal distribution of DNA damage and repair proteins, which were associated with differing synapsis patterns. In the American species *T. elegans* and *D. gliroides,* chromosomal ends were conspicuously polarized in a *bouquet* configuration and synapsis progressed exclusively from the telomeres towards interstitial regions. This was accompanied by sparse H2AX phosphorylation, mainly accumulating at chromosomal ends. Accordingly, RAD51 and RPA were mainly localized at chromosomal ends throughout prophase I in both American marsupials, likely resulting in reduced recombination rates at interstitial positions. In sharp contrast, synapsis initiated at both interstitial and distal chromosomal regions in the Australian representative *M. eugenii*, the *bouquet* polarization was incomplete and ephemeral, γH2AX had a broad nuclear distribution, and RAD51 and RPA foci displayed an even chromosomal distribution. Given the basal evolutionary position of *T. elegans*, it is likely that

the meiotic features reported in this species represent an ancestral pattern in marsupials and that a shift in the meiotic program occurred after the split of *D. gliroides* and the Australian marsupial clade. Our results open intriguing questions about the regulation and homeostasis of meiotic DSBs in marsupials. The low recombination rates observed at the interstitial chromosomal regions in American marsupials can result in the formation of large linkage groups, thus having an impact in the evolution of their genomes.

KEYWORDS

marsupial, meiosis, evolution, synapsis, recombination, *Thylamys*, *Dromiciops*, *Macropus*

Introduction

Meiosis is a complex and highly regulated process, by which homologous chromosomes synapse, recombine and segregate. Synapsis refers to the tight association of homologs during meiotic prophase I by a structure called the synaptonemal complex (SC). The SC is formed by two axial/lateral elements (AE/LEs), one per homologue, held together by transverse filaments (TFs), which emanate from each of the LEs and overlap in a central region to form the central element (CE) (von Wettstein et al., 1984; Page and Hawley, 2004). Recognition of homologues in mammals (and many other organisms) is mediated by the formation of hundreds of programmed DNA double-strand breaks (DSBs) by the SPO11 protein at the beginning of prophase I (leptotene stage) (Keeney et al., 2014). The formation of DSBs triggers a DNA damage response that follows the homologous recombination pathway, leading to the molecular interaction of chromosomes. The broken DNA molecule uses the intact DNA sequence of the homologue as a template for DNA repair during zygotene. These molecular interactions, in turn, stimulate and facilitate the synapsis of homologous chromosomes. In mammals, most DSBs produced during meiosis are repaired through a process that leads to gene conversion (non-reciprocal recombination events), whereas some of them result in reciprocal exchange events that lead to the formation of crossovers (COs) at the end of pachytene (at least one CO per bivalent) (Cole et al., 2012). These COs are visualized cytologically as chiasmata, which hold recombined homologous chromosomes together until they segregate during anaphase of the first meiotic division (Roeder, 1997).

Besides a role in ensuring faithful chromosome segregation, it is commonly accepted that recombination increases genetic variability in natural populations through the generation of new haplotypes, which are later subjected to evolutionary drift and selection (Barton and Charlesworth, 1998; Otto and Lenormand, 2002). In contrast, suppression of recombination at specific chromosomal regions leads to the genetic isolation of these chromosome segments and the formation of large linkage groups. If allele combinations cannot be reshuffled by recombination, beneficial alleles are likely to be lost by either background selection or random drift (Graves, 1995; Charlesworth et al., 2005; Bachtrog, 2013). Finally, both gene conversion and CO formation can alter the GC content of genomic regions where these events accumulate (called hotspots) by a process known as GC-biased gene conversion (gBGC) (Duret and Galtier, 2009). Therefore, the frequency and distribution of meiotic recombination have a significant impact on genome evolution (Lenormand et al., 2016; Bergero et al., 2021).

In mammals, meiotic studies have been traditionally focused in model species, mainly the house mouse and humans. However, comparative studies are important to understand if the features described in these models are present in other species. For instance, the organization and composition of the SC seem to be particularly well conserved (Fraune et al., 2012). Other features, like the frequency of recombination, have also received great attention, though they are more variable between species (Dumont and Payseur, 2008; Segura et al., 2013). Additional aspects, like the regulation of chromosome segregation, remain unexplored in most mammals, especially in non-eutherians. This is the case in marsupials, the sister group of eutherian mammals, which diverged from each other around 165 million years ago. There are currently about 270 marsupial species, distributed in America and Australia. They are grouped into two main clades: Ameridelphia, which comprises the Orders Didelphimorphia and Paucituberculata; and Australidelphia, which includes the Australian Orders Dasyuromorphia, Peramelemorphia, Notoryctemorphia and Diprodontia (Figure 1A) (Duchêne et al., 2017). Intriguingly, Australidelphia also includes an American sister clade, the Order Microbiotheria, only represented by two species of monito del monte (*Dromiciops gliroides* and *D. bozinovici*) (D'Elía et al., 2016; Feng et al., 2022; Fontúrbel et al., 2022).

Marsupials are characterized by their unique reproductive strategy, in which pregnancy is uniformly short and the altricial young are born at an early developmental stage. Development is usually completed within an abdominal pouch, with the pouch young dependent on a highly specialized milk (Tyndale-Biscoe and Renfree, 1987). Marsupials also present a number of genetic and chromosomal differences compared to eutherians (Graves and Renfree, 2013). Two of the most relevant are: 1) Their reduced number of chromosomes (Hayman, 1990; Deakin, 2018). Although chromosome numbers range from 2n = 10 to 2n = 34, they present a bimodal distribution and most species have either 2n = 14 or 2n = 24 (Deakin and Potter, 2019; Deakin and O'Neill, 2020). Since the genome size is comparable to that of eutherians, marsupial chromosomes are usually much larger. 2) The Y chromosome is generally tiny and does not share a pseudoautosomal region (PAR) with the X due to extreme degeneration of the former over evolutionary time (Graves et al., 1998). In fact, the Y chromosome can be lost in some somatic tissues, as reported in males of the family Peramelidae (Watson et al., 1998).

The special features of marsupial chromosomes also have an impact on their behavior during meiosis. The most noticeable

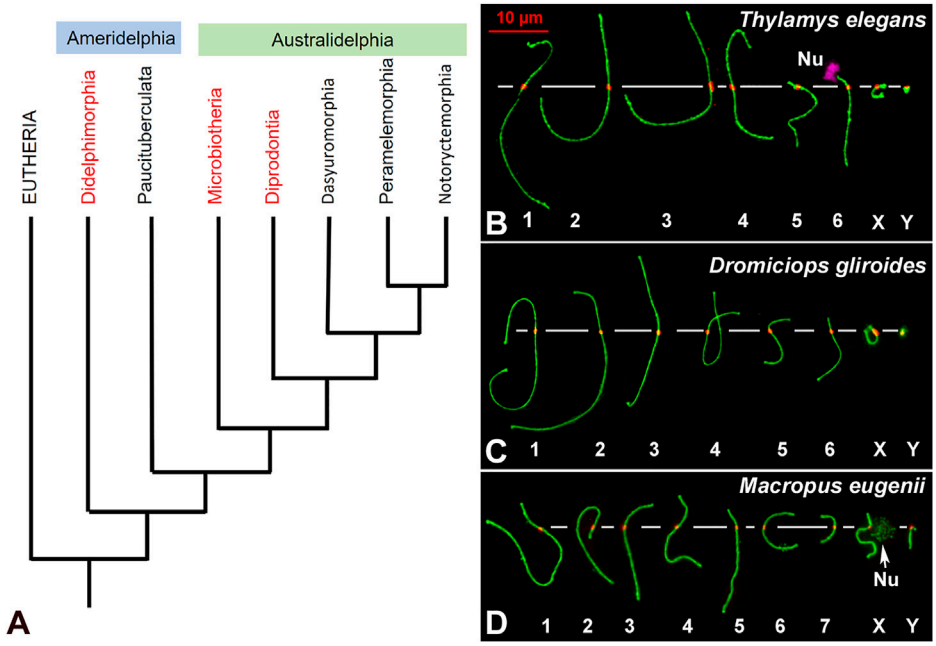

FIGURE 1
(A). Phylogenetic relationships of extant marsupial orders. The arrangement presented is based on the phylogeny published by Duchêne and coworkers (Duchêne et al., 2017). Although the topology of the tree is still controversial, Microbiotheria is grouped to Australidelphia in all the trees consulted. The Orders included in this study are highlighted in red. **(B–D)**. Meiotic karyotypes of the three studied species: SYCP3 in green and centromeres in red. Bivalents are ordered by size, according to previous reports. In *Thylamys elegans* **(B)** the position of the NOR (Nu) on the short arm of bivalent 6 was detected using anti-fibrillarin antibody (pink). The position of the NOR on the X chromosome of *Macropus eugenii* was detected by an accumulation of SYCP3. Scale bar in red: 10 µm.

feature is the behavior of sex chromosomes. The absence of a PAR on the XY pair precludes their reciprocal synapsis and recombination in male meiosis, thus challenging the usual way by which homologous chromosomes ensure their segregation during first meiotic division. Instead, sex chromosomes in marsupials present an alternative mode of association, which relies on the formation of a specific structure called the dense plate (DP) that maintains the sex chromosome association from prophase I (Solari and Bianchi, 1975; Sharp, 1982; Seluja et al., 1987; Page et al., 2003) until they segregate at anaphase-I (Page et al., 2006). Although small differences between species have been found regarding the timing of DP formation (Marín-Gual et al., 2022b), the development and dynamics of the DP are well conserved (Sharp, 1982; Page et al., 2005; Fernández-Donoso et al., 2010), indicating that the DP represents a feature that originated before the radiation of marsupials (Page et al., 2005). The emergence of this alternative mechanism of segregation allowed for the proper transmission of sex chromosomes after their complete differentiation. Interestingly, analogous mechanisms of sex chromosome segregation have independently appeared in eutherian species with completely differentiated sex chromosomes (de la Fuente et al., 2007; de la Fuente et al., 2012; Gil-Fernández et al., 2020; Gil-Fernández et al., 2021).

The striking behavior of sex chromosomes may have obscured other meiotic differences in marsupials. This includes recombination rates, i.e., the number of COs per cell, which are lower in marsupials compared to eutherians (Zenger et al., 2002; Samollow et al., 2004; Samollow et al., 2007; Dumont and Payseur, 2008; Wang et al., 2011). Moreover, marsupial males seem to be more recombinogenic than females, as opposed to the higher recombination rates in most female eutherian mammals (Bennett et al., 1986; Samollow et al., 2004; Samollow et al., 2007). Many factors seem to regulate the genome-wide rate of recombination in eukaryotes. These include chromosome number, length of the SC and of chromatin loops (Segura et al., 2013; Mercier et al., 2015; Ruiz-Herrera et al., 2017; Wang et al., 2019). Other factors like genetic background and sex are also relevant (Gruhn et al., 2013; Baier et al., 2014). In particular, we have recently proposed that the low recombination rates observed in marsupial males might result from the induction of fewer DSBs during prophase I, potentially leading to the formation of fewer COs (Marín-Gual et al., 2022b). Our previous study revealed that in three species of phylogenetically distant marsupials, the overall number of DSBs was significantly lower than in eutherian mammals (i.e., mice and humans), concomitant with low γH2AX levels on autosomes.

In addition to overall recombination rates, the distribution of recombination events along chromosome is a field of intense research. Among eutherians, DSBs have been reported to appear fairly evenly distributed in mice, whereas COs tend to accumulate towards the distal regions of chromosomes in this species (Froenicke et al., 2002; de Boer et al., 2006; Grey et al., 2009; Brick et al., 2018; Li et al., 2019). In contrast, both DSBs and COs clearly accumulate at distal regions in humans (Oliver-Bonet et al., 2007; Pratto et al., 2014). However, studies in non-model mammals are scarce. In this regard, in our previous study on marsupials we detected inter-specific differences in the pattern of DSBs distribution along

chromosomes (Marín-Gual et al., 2022b). Here we test whether DSB occurrence is evenly distributed along chromosomes in marsupials. To achieve this, we analyzed the localization of proteins related to DNA damage response and repair (γH2AX, RAD51, and RPA), along with SC components (SYCP1 and SYCP3) and telomeric DNA sequences, during meiosis in species that capture the deepest divergences within marsupials: the American species *Thylamys elegans* and *D. gliroides*, and the Australian species *Macropus eugenii*. Our results uncover remarkable differences in the initiation and progression of synapsis between homologous chromosomes, as well as in the distribution pattern of DNA repair markers, with American species showing an extreme polarization towards chromosomal ends. This behavior may have important consequences for recombination rates and distribution, which in turn could impact genome evolution.

Materials and methods

Animals

Two *T. elegans* (Didelphidae) and two *D. gliroides* (Microbiotheriidae) males were collected in central and Southern Chile, respectively, from natural populations under permission of Corporación Nacional Forestal (Conaf). Handling of animals was performed according to the ethical rules stablished by the University of Chile. Two *M. eugenii* (Macropodidae) males were collected from wild populations originating on Kangaroo Island (South Australia) that were later held in a breeding colony in Melbourne (Victoria, Australia). Sampling was conducted under ethics approval from the University of Melbourne Animal Experimentation Ethics Committees and followed the Australian National Health and Medical Research (2013) guidelines. The karyotypes of these species are as follows: *T. elegans* 2n = 14; *D. gliroides* 2n = 14; *M. eugenii* 2n = 16. The meiotic karyotypes of the three species were arranged according to length and centromere position of each bivalent (Figures 1B–D), in agreement with previous reports (Page et al., 2003; Fernández-Donoso et al., 2010; Marín-Gual et al., 2022b).

Spermatocyte spreads and squashes

Testicular samples were obtained and subsequently processed. For spreads, we used the protocol previously described by Peters and coworkers (Peters et al., 1997), with slight modifications for marsupial samples (Page et al., 2005). Briefly, a cell suspension was incubated in 10 mM sucrose solution in distilled water for 15 min. The suspension was spread onto a slide dipped in 1% formaldehyde in distilled water (pH 9.5), containing 100 mM sodium tetraborate and 0.15% Triton-X100. Cells were left to settle for 1.5 h in a humid chamber and subsequently washed with 0.4% Photoflo (Kodak) in distilled water. Slides were air dried at room temperature and then rehydrated in phosphate saline buffered (PBS: NaCl 137 mM, KCl 2.7 mM, Na_2HPO_4 10,1 mM, KH_2PO_4 1.7 mM, pH 7.4) before immunostaining. For squashes, we used a previously described method (Page et al., 1998; Page et al., 2003). Seminiferous tubules were fixed in 2% formaldehyde in PBS for 10 min and then squashed on a slide. Coverslip was removed after freezing in liquid nitrogen and slides were rehydrated in PBS until use.

Immunofluorescence

Slides were incubated overnight at 4°C with the following antibodies diluted in PBS: rabbit anti-SYCP3 (ab15093, Abcam, 1:200 dilution), rabbit anti-SYCP1 (ab15087, Abcam, 1:200 dilution), mouse anti-γH2AX (05-636, Upstate, 1:1000 dilution), rabbit anti-RAD51 (PC130, Calbiochem, 1:50 dilution), rabbit anti-RPA2 (ab10359, Abcam, 1:50 dilution), mouse anti-fibrillarin (ab4566, Abcam; 1:50 dilution), human anti-centromere (441-10BK-50, Antibodies Incorporated, 1:50 dilution). In addition, many antibodies were used against DMC1, MLH1, MLH3, and other proteins associated with COs (PRR19, CNTD1, CDK2) that yielded no positive labeling. After incubation, slides were washed three times in PBS and subsequently incubated for 1 hour at room temperature with secondary antibodies conjugated with Alexafluor 350, Alexafluor 488, Cy3 or Cy5 (Jackson ImmunoResearch Laboratories) all of them diluted 1:100 in PBS. After three washes in PBS slides were stained with 10 μg/ml DAPI, washed in PBS and mounted with Vectashield.

Fluorescence *In Situ* hybridization for telomeric DNA repeats

FISH was conducted as previously described (de la Fuente et al., 2014). After immunofluorescence, slides were rinsed in PBS, fixed in 4% formaldehyde in PBS for 10 min, dehydrated in an ethanol series (70%, 90%, and 100%) for 5 min each and air dried. Hybridization mixture containing 70% deionized formamide (Sigma), 10 μM FITC-labelled $(C_3TA_2)_3$ peptide-nucleic acid (PNA) probe (Applied Biosystems), and 2.1 mM $MgCl_2$ buffer (pH 7.0) in 8 mM Tris (pH 7.2) was added to each slide. DNA was denatured for 3 min at 80°C. Hybridization was performed for 2 h at room temperature. Slides were then washed twice for 15 min each with 70% formamide in distilled water containing 10 mM Tris (pH 7.2) and 10% BSA, and then three times with TBS (1 M Tris, 1.5 M NaCl (pH 7.5) containing 0.005% Tween-20) for 5 min each. Slides were then dehydrated in an ethanol series, air-dried, stained with 10 μg/ml DAPI and mounted with Vectashield.

Microscopy and image processing

Observations were made on an Olympus BX61 microscope equipped with appropriate fluorescence filters and an Olympus DP72 digital camera. The images were processed using the public domain software ImageJ (National Institutes of Health, United States; http://rsb.info.nih.gov/ij) and Adobe Photoshop 7.0 (Adobe). Spread images were taken as single-plane pictures, whereas squashed spermatocytes were photographed at 0.2 μm intervals and the resulting stack images processed in ImageJ.

Quantitative analysis of RPA distribution

For the analysis of RPA foci chromosomal distribution, only early pachytene spermatocytes in which bivalents could be clearly discerned from each other were chosen from the overall cell population study. Bivalents were identified according to their length and centromere position. In the case of *T. elegans*, the location of fibrillarin signal associated to the short arm allowed the identification of bivalent 6. Each bivalent was measured using the *Free Hand* tool in ImageJ. The distance of centromeres and RPA foci from the tip of the short arm of the bivalents was assessed as follows: each focus was manually drawn as an intersection line with the outline of the SC, yielding the longitudinal position of the focus. Then, each bivalent was divided into 10 different segments, being segment 1 the distal portion of the shortest arm. Finally, the position of each RPA focus was ascribed to a specific segment (from 1 to 10). A minimum of 15 spermatocytes were recorded for each individual (2 *T. elegans* and 2 *M. eugenii* males).

Statistical analyses

Quantitative data were analyzed using Prism GraphPad 7.0. The distribution of RPA foci along chromosomes was compared to a random distribution by a χ^2 goodness of fit test with 9 degrees of freedom. Statistical significance was considered for $p < 0.05$. The relationship between RPA foci number and SC length was evaluated by Spearman correlation coefficient (r).

Results

Chromosome synapsis dynamics

We first studied the synaptic behavior of chromosomes during meiosis in the selected species via the immunolocalization of the proteins SYCP3 and SYCP1, the main components of the axial/lateral elements (AE/LEs) and transverse filaments of the SC, respectively. The localization patterns of these proteins were used to classify spermatocytes into the different prophase I stages, following previous observations in marsupials (Page et al., 2003; Page et al., 2005; Marín-Gual et al., 2022b).

In *T. elegans*, during early prophase I SYCP3 was usually accompanied by the appearance of a SYCP1 signal (Figure 2A), making it difficult to discriminate between leptotene and zygotene. This suggests that the formation of the AEs was concurrent with the initiation of synapsis early in prophase I in this species. Thus, at early stages of prophase I the AEs were just partially formed, appearing with dotted signal along most of the chromosome, but forming short lines at the regions where two AEs associate (Figure 2A). These synapsed segments were mostly grouped in a small region (i.e., a *bouquet* configuration). In addition, SYCP3 revealed a thickening at the ends of the AEs. Therefore, we refer to this stage as the leptotene-zygotene transition. At a subsequent stage, early zygotene (Figure 2B), the AEs were almost completely formed. Synapsis began at chromosomal ends, which was evidenced by the presence of SYCP1 in the region where the AEs (now called LEs) of homologous chromosomes were associated. Moreover, the ends of chromosomes were still polarized in a *bouquet* conformation at this stage. SYCP1 was observed as continuous lines that regularly expanded from the ends towards the centers of the chromosomes, and there was no interstitial initiation of synapsis. This feature was still observable at late zygotene (Figure 2C). The only exception to synapsis beginning from telomeres was for the chromosome pair bearing the nucleolar organizing region (NOR) (see Figure 4C). The NOR is located near the telomere of the short arm (Figure 1) and it had delayed synapsis. Even though synapsis in the autosomes was completed by pachytene, the sex chromosomes remained unsynapsed at this stage (Figure 2D). In the other American species, *D. gliroides*, the pattern of AE formation and synapsis progression was almost identical, including the conspicuous *bouquet* configuration, the thickening of the distal regions of the LEs at early zygotene, the distal initiation of synapsis, and its subsequent progression to interstitial regions (Figures 2E–H).

Remarkably, AE formation and SC assembly in *M. eugenii* contrasted the pattern in American species. Overall, we observed three main differences. First, at the leptotene-zygotene transition, the AEs appeared as short fragments or dots evenly distributed, instead of accumulated in the region where fragments of SYCP1 signal were observed (Figure 2I). Second, SYCP1 fragments did not adopt a markedly polarized distribution, indicating that the *bouquet* is not as evident as in the American species. Third, at early zygotene synapsis initiated both at the distal and interstitial regions of each chromosome (Figure 2J), a feature that was still detectable at late zygotene (Figure 2K). At pachytene, synapsis of the autosomes was complete, whereas sex chromosomes remained unsynapsed (Figure 2L).

In order to better characterize the differences in the formation and dynamics of the *bouquet* polarization, we combined the immunolabeling of SYCP3 protein with the localization of telomeric DNA sequences by FISH (Figure 3). In *T. elegans*, telomeres appeared clearly polarized in all spermatocytes at the transition between leptotene and zygotene (Figure 3A) and also at early zygotene (Figure 3B). This polarization was subsequently lost with zygotene progression, but some telomeres occasionally remained associated with each other at late zygotene (Figure 3C) and even at early pachytene (Figure 3D). In contrast, chromosomal ends were more dispersed in *M. eugenii*. We observed that in 50% of spermatocytes at the leptotene-zygotene transition (n = 84) telomeres did not form clusters, although many times they were observed preferentially distributed in one-half of the nucleus (Figure 3E). The remaining spermatocytes showed one or two (sometimes more) telomere clusters, but these groups usually did not incorporate all chromosome ends (Figure 3F). At early zygotene, clusters were usually dissolved, and telomeres were dispersed (Figure 3G). These results suggest that in *M. eugenii* the *bouquet* polarization is incomplete and more ephemeral than in the American species.

FISH against telomeric DNA repeats also revealed the presence of interstitial telomeric sequences in the largest bivalent of *T. elegans* (Figure 3D), as previously described (Page et al., 2006). Intriguingly, the interstitial telomeric signals of the two homologous chromosomes often appeared displaced along that bivalent, which is concurrent with a displacement of the centromeric signals (see detail in Figure 3D). This displacement suggests the presence of a

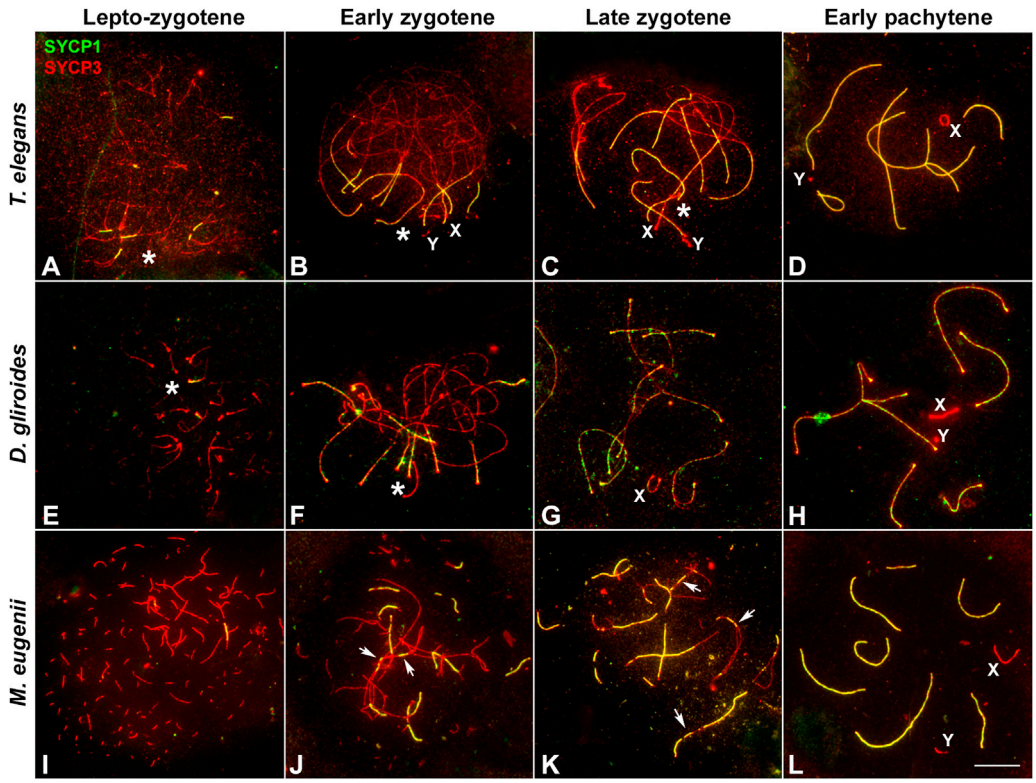

FIGURE 2
Synapsis progression during prophase **(I)**. Spread spermatocytes labeled with antibodies against SYCP3 (red) and SYCP1 (green). **(A–D)**. *Thylamys elegans*. Short filaments of SYCP1 are seen between AEs at the leptotene-zygotene transition **(A)**. These filaments appear mostly polarized to a specific nuclear region, the *bouquet* area (asterisk). Synapsis progresses during early **(B)** and late zygotene **(C)**. Polarization of chromosomal ends is still observed (asterisks). Sex chromosomes (X, Y) lie in the *bouquet* region. Synapsis is complete at pachytene **(D)** except for the sex chromosomes. **(E–H)**. *D. gliroides*. Chromosomal ends are polarized to the *bouquet* area (asterisks) at leptotene-zygotene transition **(E)** and early zygotene **(F)**. Synapsis progresses during late zygotene **(G)** and is complete at pachytene **(H)**. Sex chromosomes remain separated. (**I–L**) *Macropus eugenii*. AEs appear as short fragments in the whole nucleus during the leptotene-zygotene transition **(I)**. At early zygotene **(J)** synapsis is initiated both at the chromosomes ends and at interstitial regions (arrows). This is also observed at late zygotene **(K)**. Synapsis is complete at pachytene (**L**), with sex chromosomes lying separately. Bar: 10 μm.

synaptic mismatch in the central region of the bivalent. We also revealed the presence of interstitial telomeric repeats in *M. eugenii* bivalents (Figure 3H), as previously described (Bender et al., 2012; Marín-Gual et al., 2022b). No displacement of centromeres or telomeric repeats was detected in this species (detail in Figure 3H).

Distribution of DSBs during prophase I

In mammals, synapsis initiation is dependent on the occurrence of DNA DSBs at the beginning of meiosis (Baudat et al., 2000; Romanienko and Camerini-Otero, 2000). To assess if the differences detected in the progression of synapsis could be linked to a differential distribution of DSBs, we studied the localization of the phosphorylated form of histone H2AX (γH2AX), a widely used marker of DNA damage during meiosis (Mahadevaiah et al., 2001; Turner et al., 2004). Mirroring previous observation (Marín-Gual et al., 2022b) we found that in *T. elegans* only a few small foci of γH2AX became detectable at leptotene-zygotene on the chromatin around the AEs formation (Figure 4A). This location followed the pattern of chromosome synapsis described above, corresponding with chromosomal ends polarized in the *bouquet* configuration. At early zygotene, γH2AX labeling was mostly associated with the chromosomal regions where synapsis was initiated, whereas the rest of the nucleus remained devoid of γH2AX (Figure 4B). At this stage, the *bouquet* polarization was still observed. At late zygotene, an increase of γH2AX signal was observed, localized mainly over the regions of autosomes that had not completed synapsis, as well as over the chromatin around the AEs of the sex chromosomes (Figure 4C). At pachytene, once autosomes had completed full synapsis, γH2AX signal was only detectable over the sex chromosomes (Figure 4D). The distribution of γH2AX during meiosis in *D. gliroides* was similar, albeit not completely identical, to that of *T. elegans*. γH2AX was mostly detected at the chromosomal ends at leptotene and early zygotene (Figures 4E,F) and accumulated at unsynapsed chromosomes in late zygotene, where the signal seemed to be more intense than in *T. elegans*. (Figure 4G). During pachytene γH2AX labeling remained only on sex chromosomes (Figure 4H).

Crucially, in *M. eugenii* the γH2AX signal was different. At the leptotene-zygotene transition (Figure 4I) the signal was distributed over all chromosomes, with no specific

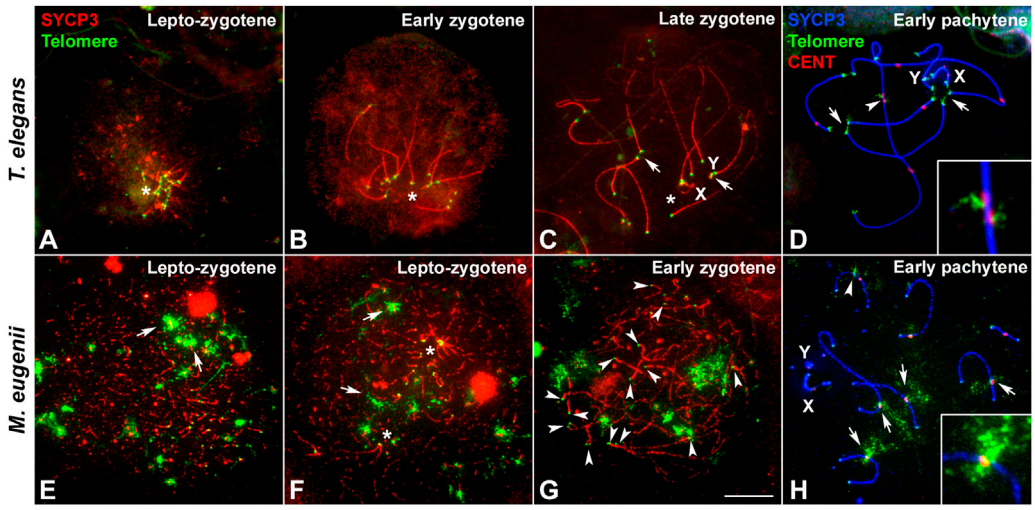

FIGURE 3
Localization of telomeric sequences in *Thylamys elegans* and *Macropus eugenii*. Spread spermatocytes were labeled with antibodies against SYCP3 (red) and telomeric sequences revealed by FISH (green) in **(A–C)** and **(E–G)**, and SYCP3 (blue), centromeric proteins (red) and telomeric sequences (green) in **(D)** and **(H)** **(A–D)**. *Thylamys elegans*. Telomeres are clustered (asterisks) at the lepto-zygotene transition **(A)** and early zygotene **(B)**. At late zygotene **(C)** a slight polarization is still evident (asterisk), and some telomeres appear associated (arrows). At pachytene **(D)**, some telomeric associations (arrows) are occasionally observed. Displacement of interstitial telomeric and centromere signals is evident in the largest bivalent (arrowhead), enlarged in the squared image. **(E–H)**. *Macropus eugenii*. At the leptotene-zygotene transition **(E,F)** telomeric signals (small dots) may appear greatly dispersed **(E)** or forming several clusters (asterisks in **F**). Some large FISH signals are also observed (arrows). Chromosomal ends do not show any specific clustering at early zygotene **(G)** or at pachytene **(H)**. Immunolabeling of centromeric proteins **(H)** reveal that the large FISH signals correspond to interstitial telomeric sequences located at centromeres (arrows) or near centromeres (arrowhead). No displacement of the centromeres or telomeric signal was observed (enlarged imaged in **H**). Bar: 10 μm.

accumulations at chromosomal ends or any other region. This broad distribution was also observed at early zygotene (Figure 4J). At late zygotene, γH2AX tends to disappear from synapsed chromosomes but an intense signal was detected over the still unsynapsed autosomal regions and over the sex chromosomes (Figure 4K). At pachytene, γH2AX signal remained only over the sex chromosomes (Figure 4L).

The striking differences in the intensity and distribution of γH2AX between marsupial species lead us to test whether the faint signal observed in *T. elegans* could be due to an artifact of the spreading technique. Thus, we evaluated in this species the distribution of γH2AX in spermatocyte squashes, which maintained the three-dimensional organization of the nucleus and provided better preservation of the chromatin (Figure 5). This confirmed the patterns detected in spermatocyte spreads; that is, the almost complete absence of γH2AX at leptotene and early zygotene was a *bona fide* feature of *T. elegans* (Figures 5A–C). The accumulation of γH2AX at the unsynapsed regions started when synapsis had greatly progressed on the autosomes (Figures 5D,E). During pachytene, γH2AX was only present on the sex chromosomes, either before they paired (Figures 5F,G) or after they completed their pairing and the formation of the dense plate (DP) (Figure 5H).

Nuclear distribution of DNA repair proteins

The induction of DSBs triggers the activation of the homologous recombination repair pathway and the incorporation of proteins involved in this process, such as RAD51 and DMC1, the recombinases that mediate the invasion of an intact DNA template to repair the DSBs, and RPA, which protects single stranded DNA molecules generated during homologous recombination (Brown and Bishop, 2015). Here we report the chromosomal distribution of RAD51 and RPA in the species studied. Unfortunately, DMC1 did not yield a positive result.

We first analyzed the distribution of RAD51 in squashed spermatocytes. At the leptotene-zygotene transition, a few RAD51 foci were observed in *T. elegans,* mainly located at chromosomal ends and grouped in the *bouquet* configuration (Figure 6A). Some additional foci were observed scattered over the nucleus. At early zygotene (Figure 6B), foci remained localized mostly close to the chromosomal ends. At late zygotene (Figure 6C), the *bouquet* configuration was lost, and some RAD51 foci were localized interstitially along bivalents. The X chromosome accumulated numerous RAD51 foci at late zygotene and also at early pachytene (Figure 6D). The number of RAD51 foci decreased with pachytene progression and the protein was completely absent by late pachytene (not shown). A similar trend was observed for *D. gliroides* in spermatocyte spreads (Figures 6E–H). Most foci were associated with the short SYCP3 filaments at leptotene (Figure 6E). However, in this species, some RAD51 foci appeared on interstitial regions of chromosomes along with synapsis progression (Figures 6F,G). This suggested progressive incorporation of RAD51 along chromosomes during zygotene. Some foci were still detectable at early pachytene (Figure 6H). Similar to *T. elegans*, the X chromosome presented abundant RAD51 foci (Figure 6H).

In sharp contrast, RAD51 foci appeared evenly distributed over the nucleus in *M. eugenii* spermatocyte spreads. At the leptotene-

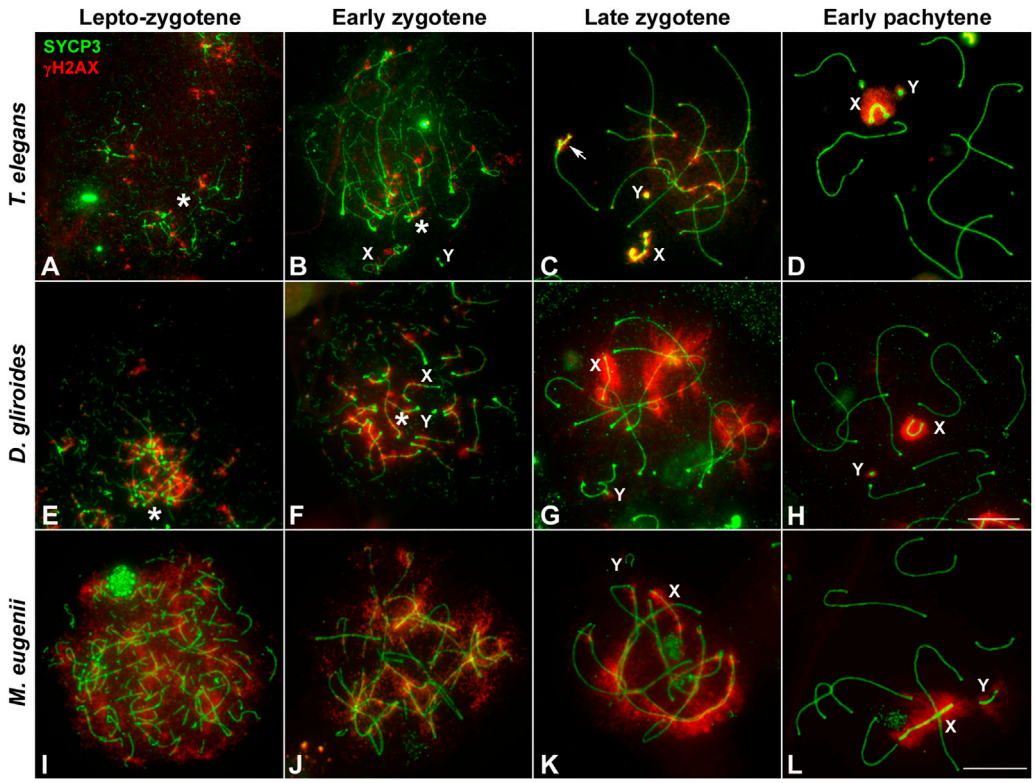

FIGURE 4
Localization of DNA damage-related proteins. Spread spermatocytes labeled with antibodies against SYCP3 (green) and γH2AX (red). **(A–D)**. *Thylamys elegans*. γH2AX is observed as small foci at the leptotene-zygotene transition **(A)** and early zygotene **(B)**, associated to the synapsing chromosomal ends polarized to the *bouquet* (asterisks). A more intense γH2AX labeling is observed at late zygotene **(C)** associated to the AEs of unsynapsed autosomal regions and sex chromosomes (X, Y). The proximal end of chromosome 6 also remains unsynapsed (arrow). At pachytene **(D)** γH2AX is only observed on the chromatin of sex chromosomes. **(E–H)**. *D. gliroides*. The pattern of γH2AX is almost identical to the one described for *Thylamys elegans*, except for a more intense labeling of γH2AX in the unsynapsed regions of chromosomes at zygotene. (**I–L**) *Macropus eugenii*. At the leptotene to zygotene transition **(I)** γH2AX is spread in the whole nucleus. As zygotene proceeds **(J,K)** γH2AX labeling is reduced in the nucleus and concentrates around the AEs of unsynapsed autosomes and the X chromosome, but not on the Y chromosome. Both sex chromosomes exhibit signal of the antibody at pachytene (**L**). Bars in A-H and I–L: 10 μm.

zygotene transition, foci were associated with the short fragments of the forming AEs (Figure 6I). Similarly, from early to late zygotene, RAD51 foci were distributed all along the synapsing bivalents (Figures 6J,K). Even at early pachytene (Figure 6L), RAD51 foci did not concentrate at any particular chromosomal region, even though the number of such foci was prominently reduced.

As for RPA, we only obtained a reliable signal of the antibody in *T. elegans* and *M. eugenii*. The dynamics of RPA foci were similar to that of RAD51. In *T. elegans*, most foci were localized to the chromosomal ends at the leptotene-zygotene transition and early zygotene (Figures 7A,B). Then, foci also appeared at interstitial regions during late zygotene and early pachytene (Figures 7C,D) but remained visibly concentrated at chromosomal ends. In contrast, RPA foci in *M. eugenii* were evenly distributed along chromosomes throughout prophase I (Figures 7E–H).

Chromosomal distribution of RPA

A remarkable feature observed regarding RPA dynamics was that the number of foci remained high even during early pachytene. Because autosomes have completed synapsis at this stage, every bivalent could be identified thanks to the differences in length, centromere position and location of the NOR (Figures 1B,D and Supplementary Figure S1). This permitted a quantitative study of the distribution of RPA along each chromosome in both *T. elegans* and *M. eugenii*. We analyzed at least 15 pachytene spermatocytes in two individuals from each species. Each bivalent was measured, divided into 10 segments and the position of each RPA focus was then scored along the bivalent and assigned to a segment. The same methodology was applied to the X chromosome for both species.

We detected that in *T. elegans* RPA foci accumulated towards the chromosomal ends in all bivalents, particularly in the four largest, in which the two distal segments concentrated near or above 50% of all RPA foci (Figure 8; Table 1). The distribution of RPA foci increased symmetrically in both chromosomal arms, with just a reduction around centromeres. This was especially relevant for bivalent 6, which bears the NOR on the short arm. This region accumulated fewer RPA foci (11.41%) compared to the opposite chromosomal end (20.16%) (Table 1). The X chromosome, which remained as univalent, also showed a non-random distribution of RPA. The X centromere seemed

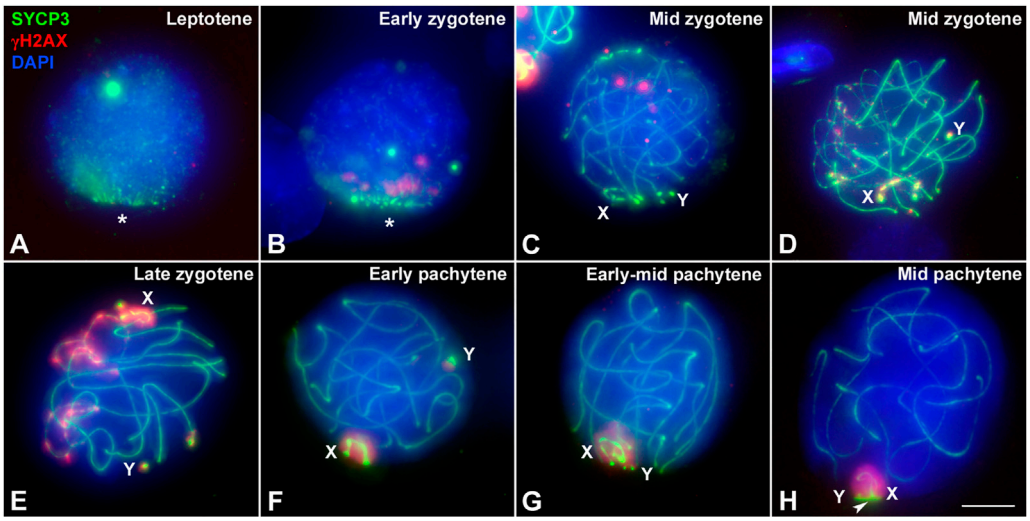

FIGURE 5
Localization of DNA damage in *Thylamys elegans* spermatocytes preserving the 3-dimensional topology of chromosomes. Squashed spermatocytes labeled with antibodies against SYCP3 (green) and γH2AX (red) and DAPI (blue). **(A)**. Leptotene. No γH2AX labeling is observed. AEs appear polarized in a *bouquet* configuration (asterisk). **(B)**. Early zygotene. A few small γH2AX signals are observed at the region where synapsis is initiating. The *bouquet* polarization is still evident. **(C)**. Mid zygotene. Synapsis has progressed. A few γH2AX foci are scattered within the nucleus. **(D)**. Mid zygotene. γH2AX labeling starts to be observed at the unsynapsed regions of autosomes and sex chromosomes (X, Y). **(E)**. Late zygotene. γH2AX signal increases on unsynapsed chromosomes. Sex chromosomes are detected at opposite nuclear spaces and the γH2AX labeling extends from their AEs to the surrounding chromatin. **(F)**. Early pachytene. γH2AX is only detected on the chromatin of sex chromosomes, clearly separated in the nucleus. **(G)**. Early-mid pachytene. Sex chromosomes approach and associate to each other. **(H)**. Mid pachytene. Sex chromosomes pair and form the dense plate (arrowhead). γH2AX labels the whole sex body. Bar: 5 μm.

to have an effect, with a reduced number of RPA in the flanking segments. The Y chromosome could not be analyzed due to its small size.

In contrast, the distribution of RPA foci in *M. eugenii* was quite homogeneous along bivalents. A χ^2 test showed that on most chromosomes RPA location did not significantly depart from a random distribution (Table 1). The only exceptions were chromosomes 1, 7 and X, on which RPA foci were reduced around the centromere. The NOR, which is located in the short arm of the X chromosome (Figure 1D) did not have and apparent effect on accumulation of RPA foci. In fact, RPA distribution was quite similar on the X chromosome in both species.

The quantitative analysis of RPA also allowed us to assess a potential correlation between the number of foci accumulated on every chromosome and their respective length. Because the X chromosome was a univalent and the Y chromosome was too small, we only considered autosomes. We found that in *T. elegans,* RPA foci were underrepresented in bivalents 1 to 3, and conversely overrepresented in bivalents 4 to 6 (Table 2). Accordingly, a Spearman correlation analysis of RPA foci number and SC length showed low correlation ($r = 0.41$, $p < 0.0001$) (Figure 9). In contrast, all *M. eugenii* bivalents presented an increased correlation between chromosome length and RPA proportion (Spearman correlation analysis $r = 0.88$, $p < 0.0001$) (Table 2; Figure 9). This reinforces the hypothesis that RPA distribution in *M. eugenii* is not dependent on specific features of chromosomes. Their location was equiprobable on any chromosome and at any chromosomal region.

Discussion

Meiotic studies in non-eutherian mammalian species are scarce. Only a few reports were devoted to monotremes (Daish et al., 2015; Casey et al., 2017). In marsupials, most studies have focused on the unique behavior of sex chromosomes (Solari and Bianchi, 1975; Sharp, 1982; Roche et al., 1986; Seluja et al., 1987; Page et al., 2003; Page et al., 2005; Fernández-Donoso et al., 2010; Marín-Gual et al., 2022b). Our recent work on marsupials revealed divergent strategies for meiotic DNA repair, recombination and transcription (Marín-Gual et al., 2022b). Here we extend these observations and report previously uncharacterized features of marsupial meiosis: *bouquet* formation, synapsis initiation and chromosomal distribution of DSBs. Remarkably, our observations suggest an evolutionary shift in the meiosis program between American and Australian marsupials. In the context of recently published reports on fish and reptile meiosis (Blokhina et al., 2019; Marín-Gual et al., 2022a), our results reveal the persistence of ancestral vertebrate meiotic features in marsupials. This highlights the relevance of comparative studies to fully understand the causes and consequences of meiosis evolution.

The conspicuous *bouquet* conformation could be an ancient feature of vertebrate meiosis

The polarization of telomeres at the beginning of meiosis has been described in a wide range of species, from fungi to plants and

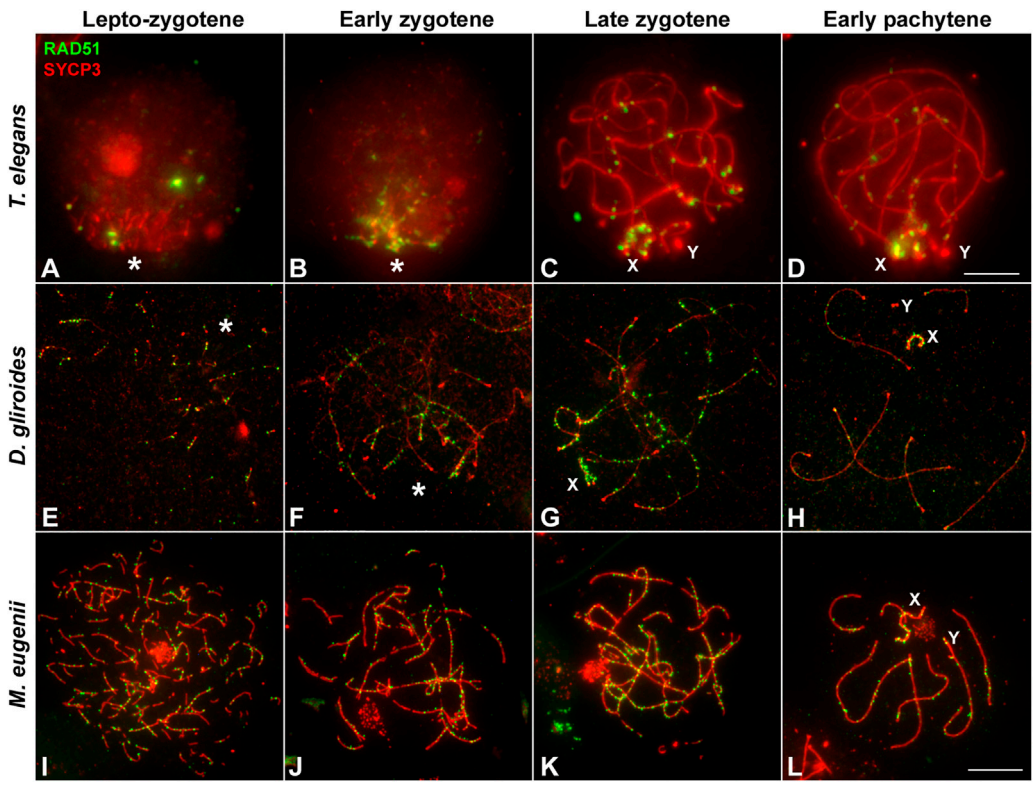

FIGURE 6
Localization of homologous recombination repair. Spermatocytes labeled with antibodies against SYCP3 (red) and RAD51 (green). **(A–D)**. *Thylamys elegans*. Squashed spermatocytes. RAD51 foci are scarce and localized in the *bouquet* (asterisk) during the leptotene-zygotene transition **(A)** and also at early zygotene **(B)**. At late zygotene **(C)** some RAD51 foci are seen at interstitial regions and coat abundantly the X and Y chromosomes (X, Y). At early pachytene **(D)** most RAD51 foci concentrate in the sex chromosomes. **(E–H)**. *D. gliroides*. RAD51 foci associate to the short stretches of SYCP3 at the leptotene-zygotene transition **(E)**. At early zygotene **(F)**, most foci are localized in the already synapsed distal regions. At late zygotene **(G)** discrete foci are also detected over the interstitial regions of autosomes and mostly over the X chromosome. At early pachytene **(H)**, a few foci are still associated to autosomes. (**I–L**) *Macropus eugenii*. Spread spermatocytes. At the leptotene-zygotene transition **(I)** RAD51 foci appear in the whole nucleus. As zygotene proceeds **(J,K)** RAD51 is clearly observed all along the bivalents. At early pachytene (**L**), RAD51 foci number has decreased but they are observed all along autosomal bivalents and the sex chromosomes. Bars: 5 μm in **(A–D)** and 10 μm in **(E–L)**.

animals (Zickler and Kleckner, 1998). However, the presence and the extent of this polarization changes from taxa to taxa, and even between sexes. Formation of the *bouquet* has been considered a crucial factor in chromosome pairing and synapsis initiation (Liebe et al., 2006; Reig-Viader et al., 2016). However, the study of different mutants has provided evidence that such a feature is not an absolute requirement, and some model systems like *Drosophila melanogaster* and *Caenorhabditis elegans* are known to lack a chromosomal *bouquet* during meiosis (Harper et al., 2004).

Our results show the presence of a marked and long-lasting *bouquet* polarization in two of the three marsupial species analyzed. This was correlated with the initiation of synapsis, which was clearly terminal in *T. elegans* and *D. gliroides*. Synapsis in these two species extended from the telomeres to the interstitial regions in a zipper-like manner. Similar observations were reported in the South American marsupial *Rhyncholestes raphanurus*, belonging to the Paucituberculata Order (Page et al., 2005). Thus, this feature seems to be an old character among marsupials. Moreover, according to recent reports in zebrafish (Blokhina et al., 2019) and several species of reptiles (Marín-Gual et al., 2022a), these seem to be ancient features of the vertebrate meiotic program, which have been subsequently maintained in a wide range of groups. However, this chromosomal polarization has suffered regulatory modifications in different linages. In eutherian mammals, the house mouse displays a visible polarization at the beginning of meiosis (Berrios et al., 2010; Berrios et al., 2014), but this is brief and often incomplete (Scherthan et al., 1996; Lopez-Jimenez et al., 2022). Moreover, while synapsis can start at the chromosomal ends in this species, different reports indicated that synapsis initiation is mostly interstitial (Boateng et al., 2013; Gruhn et al., 2016). In humans, a striking sexual dimorphism is observed, with males displaying a brief *bouquet* but initiating synapsis almost exclusively at chromosomal ends and females showing a more persistent *bouquet* but initiating synapsis at interstitial regions (Roig et al., 2004; Gruhn et al., 2016). Thus, the relevance of the *bouquet* to drive synapsis initiation seems to have been attenuated in eutherian mammals. In the present study, we found that the Australian marsupial species analyzed, *M. eugenii*, mimics the pattern described in mouse,

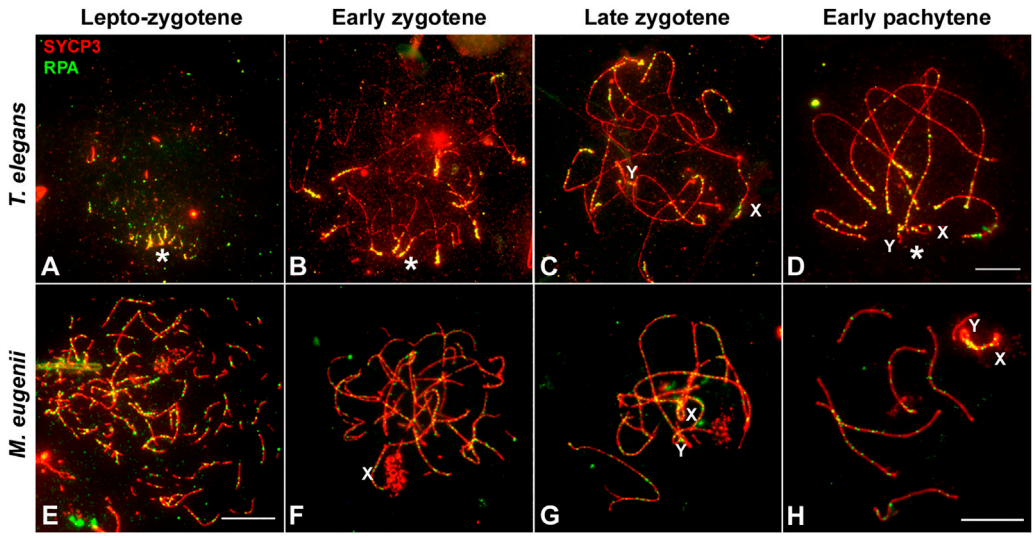

FIGURE 7
Localization of RPA. Spread spermatocytes labeled with antibodies against SYCP3 (red) and RPA (green). **(A–D)**. *Thylamys elegans*. Most RPA foci concentrate in the distal regions of autosomes from leptotene to pachytene. From late zygotene to pachytene, RPA foci also accumulate on the sex chromosomes (X, Y). Asterisk indicates the polarization of chromosomal ends. Sex chromosomes. **(E–H)**. *Macropus eugenii*. RPA foci associate to forming AEs at the leptotene to zygotene transition. From early zygotene onwards, foci are observed along the entire length of the bivalents. Bars in **(A–D)** and **(E–H)**: 10 μm.

FIGURE 8
Chromosomal distribution of RPA foci distribution along bivalents and the X chromosome in *Thylamys elegans* and *Macropus eugenii*. Chromosomes have been divided into 10 segments of equal size between telomeres (proximal to distal). *Y*-axes in the graphs indicate the percentage of RPA foci in each segment. Each bivalent (BV) has been depicted below the corresponding graph. Pink bars indicate the centromere position, yellow bars indicate the NOR. We found a prominent polarization of RPA foci towards the chromosome ends in *Thylamys elegans*. In contrast, in *Macropus eugenii* detection of RPA foci uncovered a relatively homogeneous distribution along the entire length of the chromosomes.

with a loose short-lived *bouquet* and synapsis initiating both near telomeres and interstitially.

Considering the phylogenetic relationships between the marsupials studied here (Figure 1) (Duchêne et al., 2017), and previous reports in other vertebrates (Blokhina et al., 2019; Marín-Gual et al., 2022a), the most parsimonious explanation is that *bouquet* polarization and distal synapsis initiation are ancestral characters in marsupials, and most probably in all vertebrates. Then, the loosening of telomere polarization at the beginning of meiosis (becoming more ephemeral and/or less conspicuous), as well as loss of correlation between *bouquet* and distal synapsis initiation seems to have occurred independently several times in the evolution of mammals (i.e., Australian marsupial species and mouse). What could cause this change in chromosome behavior? The determinants of *bouquet* polarization include the binding of telomeres to the nuclear envelope and their interaction with cytoskeleton components via transmembrane proteins of the nuclear envelope (Scherthan, 2007). It is unlikely that these dynamics have been lost in eutherian mammals or in Australian marsupials, but they could be regulated differently. Interestingly, a recent report revealed that the formation of a primary cilium in spermatocytes is a crucial factor in

TABLE 1 Percentage of RPA foci per chromosomal segment in the different bivalents (BV) and the X chromosome (X) of *Thylamys elegans* and *Macropus eugenii*. A $\chi 2$ of goodness of fit test (9 degrees of freedom) was performed to assess the deviation from a random distribution along chromosomes. Significance was considered when $p \leq 0.05$. n: number of bivalents analyzed; f = number of foci.

Thylamys elegans (% RPA)							
Segment	BV1 (n = 31) (f = 596)	BV2 (n = 35) (f = 540)	BV3 (n = 33) (f = 457)	BV4 (n = 35) (f = 550)	BV5 (n = 33) (f = 498)	BV6 (n = 35) (f = 377)	X (n = 28) (f = 302)
1	26.51	21.85	29.10	27.64	16.87	11.41	14.57
2	9.90	9.07	7.88	10.00	10.24	8.49	9.60
3	5.03	6.30	6.13	5.45	7.43	7.16	9.93
4	2.52	3.15	3.72	6.00	9.44	7.69	2.98
5	5.54	4.81	4.81	3.09	6.22	5.31	3.64
6	4.87	7.22	2.19	3.82	6.02	3.98	8.28
7	3.36	5.56	3.06	4.18	6.83	8.49	10.26
8	6.21	8.15	4.81	6.91	5.62	10.34	10.60
9	11.74	9.26	13.13	8.55	13.45	16.98	12.91
10	24.33	24.63	25.16	24.36	17.87	20.16	17.22
$\chi 2$	397.19	256.15	377.73	377.02	93.28	88.79	52.76
p value	<0.0001	<0.0001	<0.0001	<0.0001	<0.0001	<0.0001	0.0004

Macropus eugenii (% RPA)								
Segment	BV1 (n = 43) (f = 1525)	BV2 (n = 44) (f = 1051)	BV3 (n = 44) (f = 1001)	BV4 (n = 44) (f = 910)	BV5 (n = 43) (f = 808)	BV6 (n = 43) (f = 600)	BV7 (n = 42) (f = 305)	X (n = 31) (f = 408)
1	9.18	9.80	9.59	10.11	10.02	10.17	7.87	10.29
2	7.54	8.56	10.49	9.67	10.02	11.50	12.79	8.82
3	11.54	9.13	9.99	9.56	10.27	10.17	10.49	3.19
4	11.08	10.37	9.99	7.69	8.42	8.83	10.16	6.13
5	9.97	10.75	10.49	10.66	10.27	7.33	4.59	9.56
6	11.02	11.04	9.79	11.43	11.01	10.50	6.23	10.54
7	10.30	11.04	10.99	10.11	10.52	9.83	13.11	11.76
8	11.28	10.75	9.79	10.88	11.51	11.17	11.80	10.78
9	9.38	10.56	10.59	11.32	10.27	11.33	15.08	14.95
10	8.72	7.99	8.29	8.57	7.67	9.17	7.87	13.97
$\chi 2$	22.94	11.16	4.98	11.54	9.47	8.93	30.31	43.81
p value	0.006	0.2649	0.8357	0.2406	0.3946	0.4435	0.0004	<0.0001

the formation of the *bouquet* in zebrafish (Mytlis et al., 2022). This structure is formed in spermatocytes at leptotene-zygotene, and its removal disrupts *bouquet* formation, as well as synapsis and recombination (Mytlis et al., 2022; Xie et al., 2022). Intriguingly, the formation of the primary cilium in mouse seems to be differently regulated, because this structure is formed in a reduced fraction of spermatocytes at the leptotene-zygote transition (Lopez-Jimenez et al., 2022). This seems to correlate with the absence of a conspicuous *bouquet* in the mouse, although a causative relationship has not yet been demonstrated. Further exploration of mammalian species could provide new insight into the role that cilia play in *bouquet* formation.

Induction of DSBs and synapsis initiation and progression

A characteristic hallmark of meiotic DNA damage is the localization of phosphorylated H2AX (γH2AX) (Mahadevaiah et al., 2001; Turner et al., 2004), which appears as scattered foci at early leptotene and then extends to occupy the whole nucleus during late leptotene (Enguita-Marruedo et al., 2019). In eutherian mammals (i.e., mouse) the presence of γH2AX is then reduced as prophase I progresses, and DNA is repaired but remains during late stages of prophase I in regions that do not achieve synapsis. This has been found to occur on both autosomes, as a feature related to the meiotic silencing of unsynapsed chromatin (MSUC) (Baarends et al., 2005; Turner et al., 2005; Manterola et al., 2009), and on the sex chromosomes where it contributes to meiotic sex chromosome inactivation (MSCI) (Turner et al., 2004; Page et al., 2012). Early reports on the localization of γH2AX in marsupials indicated that MSCI also operates in this group (Franco et al., 2007; Hornecker et al., 2007; Namekawa et al., 2007). However, other aspects of the localization of γH2AX in relation to DNA damage in marsupials have remained unexplored until recently.

We have previously shown in marsupials that there are two waves of γH2AX accumulation during prophase I, along with lower

TABLE 2 Proportion of RPA foci and SC length of each bivalent at early pachytene, calculated over the number of foci and SC length of autosomes. Only cells in which all bivalents could be recorded have been included. Values are presented as mean ± standard deviation. n: number of cells analyzed; f = number of foci.

Thylamys elegans (n = 34; f = 2958)							
	BV1	BV2	BV3	BV4	BV5	BV6	
% RPA foci	19.57 ± 4.7	17.91 ± 6.7	15.98 ± 4.9	18.52 ± 7.0	15.20 ± 4.3	12.81 ± 4.9	
% SC length	23.89 ± 1.7	21.89 ± 1.7	19.70 ± 1.9	15.12 ± 2.1	9.82 ± 1.3	8.80 ± 1.0	
Macropus eugenii (n=41; f= 6968)							
	BV1	BV2	BV3	BV4	BV5	BV6	BV7
% RPA foci	23.84 ± 3.9	16.81 ± 3.6	15.75 ± 3.1	14.50 ± 2.8	13.68 ± 3.1	10.49 ± 2.5	4.93 ± 2.0
% SC length	22.91± 1.9	16.96 ± 2.0	15.37 ± 1.5	14.47 ± 2.6	13.89 ± 1.4	10.93 ± 1.8	5.47 ± 0.9

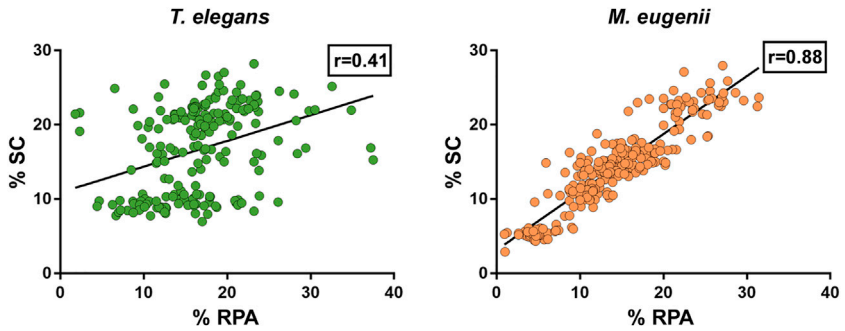

FIGURE 9
Compared proportion of RPA foci number and SC length chromosome in *Thylamys elegans* and *Macropus eugenii*. Each spot represents a bivalent in a cell. Black lines represent the calculated regression line. r = Spearman correlation coefficient.

levels of γH2AX on autosomes when compared to eutherians (Marín-Gual et al., 2022b). Here we extend these initial observations and report previously uncharacterized differences between marsupial species. In *T. elegans* and *D. gliroides* γH2AX signal is scarce and mostly restricted to the regions where homologous chromosomes initiate their synapsis, whereas in *M. eugenii* γH2AX is distributed across the whole nucleus. We suggest that there is a relationship between this finding and the observed patterns of synapsis initiation and progression. Thus, in the two American species a low induction of DSBs would occur in the chromosomal regions polarized to the *bouquet* area, triggering the initiation of synapsis. In the absence of further (or abundant) DSBs along interstitial regions of chromosomes, synapsis would progress from chromosomal ends towards the center of chromosomes, probably owing to the self-assembly capabilities of the SC components. Therefore, the few DSBs scattered along interstitial regions do not seem to promote SC assembly. Interestingly, these interstitial DSBs do not trigger a conspicuous H2AX phosphorylation either. Only later, during late zygotene, was γH2AX observed at interstitial regions of the unsynapsed autosomes, as well as on the sex chromosomes. This could be interpreted as an indication of late DNA damage events produced exclusively in those regions. Alternatively, it might be linked to the silencing of unsynapsed regions, i.e., the MSUC/MSCI processes. In contrast, the widespread generation of DSBs in *M. eugenii* is correlated to synapsis initiation at different regions along the chromosomes, not only chromosomal ends. Thus, the synapsis pattern of homologous chromosomes seems to be conditioned by the way DNA damage is produced during prophase I. The pattern observed in *T. elegans* and *D. gliroides* seems to be ancestral, and even shared by other non-mammalian vertebrates (Blokhina et al., 2019; Marín-Gual et al., 2022a).

Finally, we highlight the possibility that a part of the DNA damage occurring in *T. elegans* and *D. gliroides* was not accompanied by H2AX phosphorylation. Although the restricted localization of γH2AX at the *bouquet* area correlates with accumulation of RPA and RAD51 in these two species, some RPA and RAD51 foci appeared outside the areas of γH2AX accumulation. Previous reports in monotreme mammals (Daish et al., 2015) and some insects (Viera et al., 2017) have indicated that γH2AX is not necessarily a marker of all DNA damage during prophase I. Our own observations indicate that γH2AX is not detected during prophase I in some reptiles (Marín-Gual et al., 2022a) (Page, unpublished). Therefore, it seems that some aspects of DNA damage signaling during meiosis in mammals and other vertebrates are yet to be properly characterized.

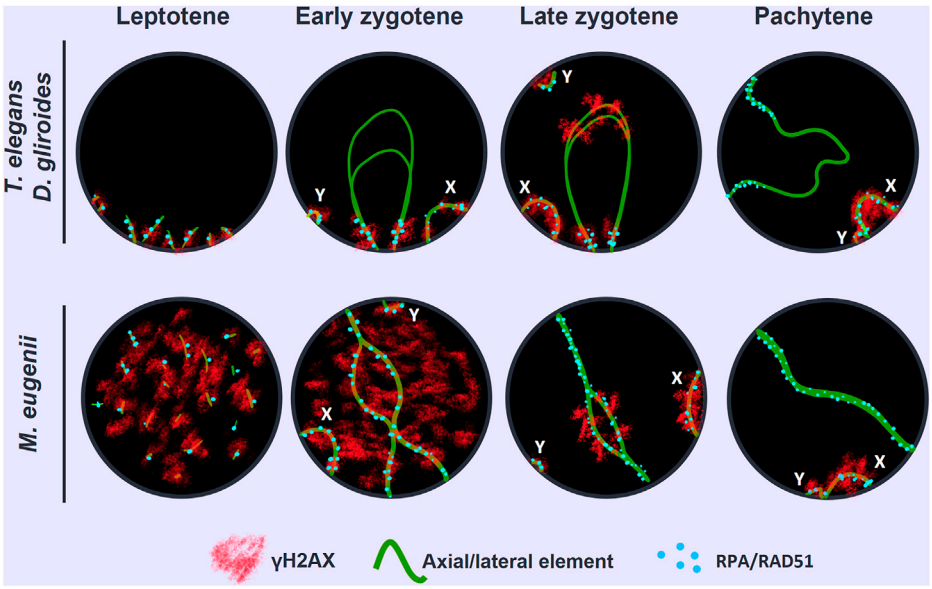

FIGURE 10
Schematic representation of the two different patterns of SC assembly, synapsis progression and DNA repair observed in the marsupial species. Green lines represent AE/LEs, red clouds represent γH2AX and blue spots represent DNA repair proteins (RAD51/RPA). In each nucleus a bivalent and both sex chromosomes (X, Y) are represented. In the top row, the putative ancestral pattern involves: conspicuous *bouquet* polarization, AE assembly and synapsis progression from chromosomal ends and preferential localization of DNA damage and repair towards chromosomal distal regions. In the bottom row, the emergent pattern observed in Australian marsupials: loosened *bouquet*, AEs assembly and synapsis progression at any chromosomal position, and an even distribution of DNA damage and repair events along chromosomes.

Differential chromosomal distribution of meiotic DSBs in marsupials

Perhaps the most striking finding of this study is the extreme difference in the distribution of DNA damage along chromosomes in the species analyzed. Several studies have focused on the overall frequency of recombination across mammals or even eukaryotes (Dumont and Payseur, 2008; Segura et al., 2013; Stapley et al., 2017). In eutherian mammals, previous reports have found that early diverging linages had lower recombination rates (Segura et al., 2013). Furthermore, marsupials show an even lower rate of recombination when compared to eutherians (Zenger et al., 2002; Samollow et al., 2004; Samollow et al., 2007; Dumont and Payseur, 2008; Wang et al., 2011), which has been attributed to the induction of fewer DSBs during early stages of meiotic prophase I (Marín-Gual et al., 2022b).

While many studies have stressed the evolutionary relevance of the recombination rate on chromosomal evolution and populations dynamics (Farré et al., 2012; Capilla et al., 2014; Ullastres et al., 2014; Dapper and Payseur, 2017; Ritz et al., 2017), the genomic implications of the uneven distribution of recombination along chromosomes have received less attention. Initial reports in mouse and human showed that COs tend to locate towards the telomeres (Barlow and Hultén, 1998; Froenicke et al., 2002). Likewise, studies on the localization of DSBs by means of DNA repair markers like RPA and DMC1 reported an accumulation of breaks towards chromosome ends in humans (Oliver-Bonet et al., 2007; Pratto et al., 2014), which is not so evident in mouse (de Boer et al., 2006). Here we reveal striking inter-specific differences in the pattern of RPA distribution (CO distribution could not be analyzed due to the lack of reactivity of many different antibodies against MLH1 and other CO markers) in marsupials. In *T. elegans* RPA foci accumulated towards the chromosomal ends. This pattern resembles the one characterized in humans, although it is much more prominent in the marsupial. In contrast, *M. eugenii* shows a remarkably even distribution of DSBs along the chromosomes, resembling the pattern reported in mouse. Moreover, the number of DSBs per chromosome has a high correlation with SC (Table 2). On the contrary, large chromosomes appear to accumulate less DSB than expected in *T.* elegans, a feature that has been described in other species, from budding yeast to humans (Kaback, 1996; Subramanian et al., 2019). It remains to be determined whether *D. gliroides* adheres to one of these patterns, or a different one.

We can only speculate on the mechanisms and consequences of the differential chromosomal distribution of DSBs detected in marsupials. In mammals, and many other organisms, DSBs are produced preferentially at recurrent sites referred to as hotspots (Paigen and Petkov, 2010; Baudat et al., 2013). Two main types of hotspots are usually recognized. The first are placed in promoter regions of genes, which supposedly present an open chromatin configuration that makes them accessible to the DSBs producing complexes. The second type is determined by the action of the histone methyl transferase PRDM9, which tri-methylates histone H3 at lysine 4 (H3K4me), thus transforming these sites into preferential spots for breakage by the protein SPO11 (Baudat et al., 2010; Parvanov et al., 2010; Brick et al., 2012). Whereas the first kind of hotspots are conserved within and between species, the ones depending on PRDM9 are more variable, owing to the fast-evolving features of this enzyme (Grey et al., 2018). Most mammals,

including marsupials have a copy of the *Prdm9* gene, but it has been partially or completely lost in the platypus and canids (Cavassim et al., 2022). Therefore, it seems unlikely that the different patterns of DSB distribution we observe could be attributable to the absence of PRDM9. Instead, it is possible that a differential distribution, usage, or regulation of the different types of hotspots could be responsible for such differences. One possibility is that *T. elegans* relies more in the use of promoter-related hotspots, with genes concentrated near chromosomal ends.

M. eugenii could be using more PRDM9-dependent hotspots, which would be expected to result in a more uniform distribution of DSBs along chromosomes. This even distribution in *M. eugenii* could be also related to the extensive genomic reorganizations experienced in the family Macropodidae (Deakin, 2018; Deakin and O'Neill, 2020; Álvarez-González et al., 2022). In fact, recent reports have shown that lineage-specific evolutionary genomic reshuffling can influence patterns of higher-order chromatin organization (Farré et al., 2015; Álvarez-González et al., 2022), and that chromosomal reorganizations can have an impact on the three-dimensional genome folding and recombination in the germ line (Vara et al., 2021; Álvarez-González et al., 2022). Thus, genome reshuffling in macropodids could have led to a more even distribution of recombination hotspots genome-wide. Interestingly, we found that the X chromosome behaves similarly in the species compared here. It is possible that the X chromosome escaped this hotspot reorganization. Further analyses in the study of marsupial genomes and the use of ChIP-Seq approaches to map recombination hotspots could yield insightful information about this possibility.

Genomic and evolutionary consequences of divergent recombinogenic patterns

The dissimilar pattern of DSBs chromosomal distribution may have consequences at the genomic level in marsupials. Although not all the DSBs produced during prophase I result into COs, it seems reasonable to assume that COs could be evenly distributed along chromosomes in *M. eugenii*. This would facilitate the recurrent recombination of allele combinations, thus breaking haplotypes. In the case of *T. elegans*, however, the accumulation of DSBs towards chromosomal ends would reduce the possibilities of recombination at the interstitial regions of chromosomes. Supporting this view, a previous study reported that chiasmata are conspicuously terminal in *T. elegans* (Page et al., 2006). Since *T. elegans* has a very low chromosome number, this would mean the formation of few and large regions of linkage disequilibrium. Such a strategy could be beneficial in a very stable environment, as long as allelic combinations at different loci had achieved an optimum (Stapley et al., 2017; Wang et al., 2019). In contrast, with recombination spread all over chromosomes, the resulting generation of new genome-wide allele combinations could have provided some marsupial groups with a higher capacity to adapt to new environments. It is tempting to speculate that this factor could have had an influence in the diversification of marsupials in Australasia after they diverged from Microbiotheria.

Moreover, the fact that most DSBs are repaired as gene conversion events (Cole et al., 2012; Baudat et al., 2013) does not preclude these breaks from being innocuous for the evolution of some genome features, like GC content. Both reciprocal recombination and gene conversion induce a shift to the accumulation of GC in the repaired strand, a phenomenon known as GC-biased gene conversion (gBGC) (Duret and Galtier, 2009). This mechanism has been detected from yeast to mammals and has been proposed to impact the evolution of genomes (Mugal et al., 2015). For instance, it was suggested that the enrichment of GC-rich isochores in mammalian genomes could be in part a consequence of gBGC (Duret and Galtier, 2009). The accumulation of GC content due to gBGC requires the recurrent use of recombination hotspots. Given the differential use of these hotspots across species, different rates of GC accumulation are expected. This could partially explain why in humans, with a rapid turnover of PRDM9-dependent hotspot, GC accumulation is spread in the whole genome, whereas in birds, with more conserved recombination hotspots, the increase of GC content is much more localized to specific genomic regions (Mugal et al., 2015). Thus, given the distribution of DSBs in the marsupial species studied, we foresee an accumulation of GC content due to gBGC at the distal regions of chromosomes in *T. elegans*, compared to *M. eugenii*.

Concluding remarks

Our results suggest that marsupials experienced a major shift in some of the key processes of meiosis, such as SC assembly, synapsis progression and DSB distribution (Figure 10). Many of these changes seems to have occurred after the split of Microbiotheria and the Australian marsupials, about 60 million years ago (Feng et al., 2022), although it remains to be characterized if some features could have already been present in the common ancestor of these two groups. Likewise, further research is required to determine to what extent the features observed in *M. eugenii* are shared by other Australian marsupials. Moreover, the features observed in *T. elegans*, clearly basal to the rest of the marsupial groups, could have been shared with the ancestor of the eutherian mammals before they split apart about 165 million years ago. In view of recent reports, these features could be even dated back to the appearance of early vertebrates (Blokhina et al., 2019; Marín-Gual et al., 2022a). Expansion of meiosis studies to uncharacterized mammals, including eutherians, marsupials and monotremes, as well as to other vertebrates (i.e., reptiles, amphibians or fishes), will shed light on the evolution of meiosis across taxa. Moreover, these studies will undoubtedly have a deep impact in our understanding of genome evolution.

Data availability statement

The original contributions presented in the study are included in the article/Supplementary Material, further inquiries can be directed to the corresponding author.

Ethics statement

The animal study was reviewed and approved by the UAM Ethics Committee for Research and Animal Welfare.

Author contributions

JP, RG, and PL-J conceived the study. JP, RG, AR-H, FV-R, MS, and PL-J designed experiments. FV-R, MS, PL-J, MA, MM-R, RF, RG, and JP processed samples and performed the experiments. MR, GS, SB, and RF-D contributed materials and samples. FV-R, MS, PL-J, MA, MM-R, RF, LM-G, PW, AR-H, RG, and JP and analyzed the data. JP wrote the manuscript and integrated inputs from all authors. All authors read and approved the final version of the manuscript.

Funding

This work was supported by grants CGL 2014-53106-P to JP (Ministerio de Ecomonía y Competitividad, Spain), BIOUAM02-2020 to JP and RG (Departamento de Biología, Universidad Autónoma de Madrid), PID 2020-112557 GB-I00 to AR-H. (Ministerio de Ciencia e Innovación, Spain) and from the Australian Research Council to MBR, GS, and PDW. (DP21103512 and DP220101429). PW is also supported by the NHMRC (APP1182667 and APP2021172). LM-G was supported by a FPU predoctoral fellowship from the Ministry of Science, Innovation and University (FPU18/03867).

Acknowledgments

We are indebted to Dr. Paula Cohen, Dr. Alberto Pendás, Dr. Mónica Pradillo, Dr. José A. Suja and Dr. Attila Toth for sharing antibodies against crossover markers. We thank Corinne van Den Hoek and members of the wallaby research group (Walgroup) for assistance with the wallabies. We also thank the two reviewers for their positive and constructive comments. We dedicate this work to the loving memory of Prof. Francisco Bozinovic, for his enthusiasm and motivation in the study of Chilean fauna.

Conflict of interest

The authors declare that the research was conducted in the absence of any commercial or financial relationships that could be construed as a potential conflict of interest.

Publisher's note

Supplementary material

The Supplementary Material for this article can be found online at: https://www.frontiersin.org/articles/10.3389/fcell.2023.1147610/full#supplementary-material

SUPPLEMENTARY FIGURE S1
Identification of bivalents. Spread spermatocytes at pachytene labeled with antibodies against SYCP3 (red), RPA (green), centromere proteins (blue) and fibrillarin (pink). **(A)**. *T. elegans*. **(B)**. *M. eugenii*. The length and centromere position allowed for the identification of each bivalent. Additionally, bivalent 6 in *T. elegans* was recognized by the position of the nucleolus (Nu), revealed by fibrillarin labeling. Sex chromosomes (X, Y). Bars: 10 µm.

References

Álvarez-González, L., Arias-Sardá, C., Montes-Espuña, L., Marín-Gual, L., Vara, C., Lister, N. C., et al. (2022). Principles of 3D chromosome folding and evolutionary genome reshuffling in mammals. *Cell Rep.* 41 (12), 111839. doi:10.1016/j.celrep.2022.111839

Baarends, W. M., Wassenaar, E., van der Laan, R., Hoogerbrugge, J., Sleddens-Linkels, E., Hoeijmakers, J. H., et al. (2005). Silencing of unpaired chromatin and histone H2A ubiquitination in mammalian meiosis. *Mol. Cell Biol.* 25 (3), 1041–1053. doi:10.1128/MCB.25.3.1041-1053.2005

Bachtrog, D. (2013). Y-Chromosome evolution: Emerging insights into processes of Y-chromosome degeneration. *Nat. Rev. Genet.* 14 (2), 113–124. doi:10.1038/nrg3366

Baier, B., Hunt, P., Broman, K. W., and Hassold, T. (2014). Variation in genome-wide levels of meiotic recombination is established at the onset of prophase in mammalian males. *PLOS Genet.* 10 (1), e1004125. doi:10.1371/journal.pgen.1004125

Barlow, A. L., and Hultén, M. A. (1998). Crossing over analysis at pachytene in man. *Eur. J. Hum. Genet.* 6 (4), 350–358. doi:10.1038/sj.ejhg.5200200

Barton, N. H., and Charlesworth, B. (1998). Why sex and recombination? *Science* 281(5385), 1986–1990. doi:10.1126/science.281.5385.1986

Baudat, F., Buard, J., Grey, C., Fledel-Alon, A., Ober, C., Przeworski, M., et al. (2010). PRDM9 is a major determinant of meiotic recombination hotspots in humans and mice. *Science* 327 (5967), 836–840. doi:10.1126/science.1183439

Baudat, F., Imai, Y., and de Massy, B. (2013). Meiotic recombination in mammals: Localization and regulation. *Nat. Rev. Genet.* 14 (11), 794–806. doi:10.1038/nrg3573

Baudat, F., Manova, K., Yuen, J. P., Jasin, M., and Keeney, S. (2000). Chromosome synapsis defects and sexually dimorphic meiotic progression in mice lacking Spo11. *Mol. Cell* 6 (5), 989–998. doi:10.1016/s1097-2765(00)00098-8

Bender, H. S., Murchison, E. P., Pickett, H. A., Deakin, J. E., Strong, M. A., Conlan, C., et al. (2012). Extreme telomere length dimorphism in the tasmanian devil and related marsupials suggests parental control of telomere length. *PLOS ONE* 7 (9), e46195. doi:10.1371/journal.pone.0046195

Bennett, J. H., Hayman, D. L., and Hope, R. M. (1986). Novel sex differences in linkage values and meiotic chromosome behaviour in a marsupial. *Nature* 323 (6083), 59–60. doi:10.1038/323059a0

Bergero, R., Ellis, P., Haerty, W., Larcombe, L., Macaulay, I., Mehta, T., et al. (2021). Meiosis and beyond – understanding the mechanistic and evolutionary processes shaping the germline genome. *Biol. Rev.* 96 (3), 822–841. doi:10.1111/brv.12680

Berrios, S., Manieu, C., Lopez-Fenner, J., Ayarza, E., Page, J., Gonzalez, M., et al. (2014). Robertsonian chromosomes and the nuclear architecture of mouse meiotic prophase spermatocytes. *Biol. Res.* 47, 16. doi:10.1186/0717-6287-47-16

Berrios, S., Manterola, M., Prieto, Z., Lopez-Fenner, J., Page, J., and Fernandez-Donoso, R. (2010). Model of chromosome associations in Mus domesticus spermatocytes. *Biol. Res.* 43 (3), 275–285. doi:10.4067/S0716-97602010000300003

Blokhina, Y. P., Nguyen, A. D., Draper, B. W., and Burgess, S. M. (2019). The telomere bouquet is a hub where meiotic double-strand breaks, synapsis, and stable homolog juxtaposition are coordinated in the zebrafish, *Danio rerio*. *PLOS Genet.* 15 (1), e1007730. doi:10.1371/journal.pgen.1007730

Boateng, K. A., Bellani, M. A., Gregoretti, I. V., Pratto, F., and Camerini-Otero, R. D. (2013). Homologous pairing preceding SPO11-mediated double-strand breaks in mice. *Dev. Cell* 24 (2), 196–205. doi:10.1016/j.devcel.2012.12.002

Brick, K., Smagulova, F., Khil, P., Camerini-Otero, R. D., and Petukhova, G. V. (2012). Genetic recombination is directed away from functional genomic elements in mice. *Nature* 485 (7400), 642–645. doi:10.1038/nature11089

Brick, K., Thibault-Sennett, S., Smagulova, F., Lam, K.-W. G., Pu, Y., Pratto, F., et al. (2018). Extensive sex differences at the initiation of genetic recombination. *Nature* 561 (7723), 338–342. doi:10.1038/s41586-018-0492-5

Brown, M. S., and Bishop, D. K. (2015). DNA strand exchange and RecA homologs in meiosis. *Cold Spring Harb. Perspect. Biol.* 7 (1), a016659. doi:10.1101/cshperspect.a016659

Capilla, L., Medarde, N., Alemany-Schmidt, A., Oliver-Bonet, M., Ventura, J., and Ruiz-Herrera, A. (2014). Genetic recombination variation in wild robertsonian mice: On the role of chromosomal fusions and Prdm9 allelic background. *Proc. Biol. Sci.* 281 (1786), 20140297. doi:10.1098/rspb.2014.0297

Casey, A. E., Daish, T. J., Barbero, J. L., and Grützner, F. (2017). Differential cohesin loading marks paired and unpaired regions of platypus sex chromosomes at prophase I. *Sci. Rep.* 7 (1), 4217. doi:10.1038/s41598-017-04560-5

Cavassim, M. I. A., Baker, Z., Hoge, C., Schierup, M. H., Schumer, M., and Przeworski, M. (2022). PRDM9 losses in vertebrates are coupled to those of paralogs ZCWPW1 and ZCWPW2. *Proc. Natl. Acad. Sci. U. S. A.* 119 (9), e2114401119. doi:10.1073/pnas.2114401119

Charlesworth, D., Charlesworth, B., and Marais, G. (2005). Steps in the evolution of heteromorphic sex chromosomes. *Hered. (Edinb)* 95 (2), 118–128. doi:10.1038/sj.hdy.6800697

Cole, F., Keeney, S., and Jasin, M. (2012). Preaching about the converted: How meiotic gene conversion influences genomic diversity. *Ann. N. Y. Acad. Sci.* 1267 (1), 95–102. doi:10.1111/j.1749-6632.2012.06595.x

Daish, T. J., Casey, A. E., and Grutzner, F. (2015). Lack of sex chromosome specific meiotic silencing in platypus reveals origin of MSCI in therian mammals. *BMC Biol.* 13 (1), 106. doi:10.1186/s12915-015-0215-4

Dapper, A. L., and Payseur, B. A. (2017). Connecting theory and data to understand recombination rate evolution. *Philosophical Trans. R. Soc. B Biol. Sci.* 372 (1736), 20160469. doi:10.1098/rstb.2016.0469

de Boer, E., Stam, P., Dietrich, A. J. J., Pastink, A., and Heyting, C. (2006). Two levels of interference in mouse meiotic recombination. *Proc. Natl. Acad. Sci.* 103 (25), 9607–9612. doi:10.1073/pnas.0600418103

de la Fuente, R., Manterola, M., Viera, A., Parra, M. T., Alsheimer, M., Rufas, J. S., et al. (2014). Chromatin organization and remodeling of interstitial telomeric sites during meiosis in the Mongolian gerbil (*Meriones unguiculatus*). *Genetics* 197 (4), 1137–1151. doi:10.1534/genetics.114.166421

de la Fuente, R., Parra, M. T., Viera, A., Calvente, A., Gomez, R., Suja, J. A., et al. (2007). Meiotic pairing and segregation of achiasmate sex chromosomes in eutherian mammals: The role of SYCP3 protein. *PLoS Genet.* 3 (11), e198. doi:10.1371/journal.pgen.0030198

de la Fuente, R., Sanchez, A., Marchal, J. A., Viera, A., Parra, M. T., Rufas, J. S., et al. (2012). A synaptonemal complex-derived mechanism for meiotic segregation precedes the evolutionary loss of homology between sex chromosomes in arvicolid mammals. *Chromosoma* 121 (5), 433–446. doi:10.1007/s00412-012-0374-9

Deakin, J. E. (2018). Chromosome evolution in marsupials. *Genes (Basel)* 9 (2), 72. doi:10.3390/genes9020072

Deakin, J. E., and O'Neill, R. J. (2020). Evolution of marsupial genomes. *Annu. Rev. Animal Biosci.* 8 (1), 25–45. doi:10.1146/annurev-animal-021419-083555

Deakin, J. E., and Potter, S. (2019). Marsupial chromosomics: Bridging the gap between genomes and chromosomes. *Reproduction, Fertil. Dev.* 31 (7), 1189–1202. doi:10.1071/RD18201

D'Elía, G., Hurtado, N., and D'Anatro, A. (2016). Alpha taxonomy of Dromiciops (Microbiotheriidae) with the description of 2 new species of monito del monte. *J. Mammal.* 97 (4), 1136–1152. doi:10.1093/jmammal/gyw068

Duchêne, D. A., Bragg, J. G., Duchêne, S., Neaves, L. E., Potter, S., Moritz, C., et al. (2017). Analysis of phylogenomic tree space resolves relationships among marsupial families. *Syst. Biol.* 67 (3), 400–412. doi:10.1093/sysbio/syx076

Dumont, B. L., and Payseur, B. A. (2008). Evolution of the genomic rate of recombination in mammals. *Evolution* 62 (2), 276–294. doi:10.1111/j.1558-5646.2007.00278.x

Duret, L., and Galtier, N. (2009). Biased gene conversion and the evolution of mammalian genomic landscapes. *Annu. Rev. Genomics Hum. Genet.* 10 (1), 285–311. doi:10.1146/annurev-genom-082908-150001

Enguita-Marruedo, A., Martin-Ruiz, M., Garcia, E., Gil-Fernandez, A., Parra, M. T., Viera, A., et al. (2019). Transition from a meiotic to a somatic-like DNA damage response during the pachytene stage in mouse meiosis. *PLoS Genet.* 15 (1), e1007439. doi:10.1371/journal.pgen.1007439

Farré, M., Micheletti, D., and Ruiz-Herrera, A. (2012). Recombination rates and genomic shuffling in human and chimpanzee—a new twist in the chromosomal speciation theory. *Mol. Biol. Evol.* 30 (4), 853–864. doi:10.1093/molbev/mss272

Farré, M., Robinson, T. J., and Ruiz-Herrera, A. (2015). An Integrative Breakage Model of genome architecture, reshuffling and evolution: The Integrative Breakage Model of genome evolution, a novel multidisciplinary hypothesis for the study of genome plasticity. *BioEssays* 37 (5), 479–488. doi:10.1002/bies.201400174

Feng, S., Bai, M., Rivas-González, I., Li, C., Liu, S., Tong, Y., et al. (2022). Incomplete lineage sorting and phenotypic evolution in marsupials. *Cell* 185 (10), 1646–1660.e18. doi:10.1016/j.cell.2022.03.034

Fernández-Donoso, R., Berríos, S., Rufas, J. S., and Page, J. (2010). "Marsupial sex chromosome behaviour during male meiosis," in *Marsupial genetics and genomics* J. A. Deakin, P. D. Waters, and J. A. Marshall Graves (Dordrecht: Springer), 187–206.

Fontúrbel, F. E., Franco, L. M., Bozinovic, F., Quintero-Galvis, J. F., Mejías, C., Amico, G. C., et al. (2022). The ecology and evolution of the monito del monte, a relict species from the southern South America temperate forests. *Ecol. Evol.* 12 (3), e8645. doi:10.1002/ece3.8645

Franco, M. J., Sciurano, R. B., and Solari, A. J. (2007). Protein immunolocalization supports the presence of identical mechanisms of XY body formation in eutherians and marsupials. *Chromosome Res.* 15 (6), 815–824. doi:10.1007/s10577-007-1165-7

Fraune, J., Schramm, S., Alsheimer, M., and Benavente, R. (2012). The mammalian synaptonemal complex: Protein components, assembly and role in meiotic recombination. *Exp. Cell Res.* 318 (12), 1340–1346. doi:10.1016/j.yexcr.2012.02.018

Froenicke, L., Anderson, L. K., Wienberg, J., and Ashley, T. (2002). Male mouse recombination maps for each autosome identified by chromosome painting. *Am. J. Hum. Genet.* 71 (6), 1353–1368. doi:10.1086/344714

Gil-Fernández, A., Ribagorda, M., Martín-Ruiz, M., López-Jiménez, P., Laguna, T., Gómez, R., et al. (2021). Meiotic behavior of achiasmate sex chromosomes in the african pygmy mouse Mus mattheyi offers new insights into the evolution of sex chromosome pairing and segregation in mammals. *Genes* 12 (9), 1434. doi:10.3390/genes12091434

Gil-Fernández, A., Saunders, P. A., Martín-Ruiz, M., Ribagorda, M., López-Jiménez, P., Jeffries, D. L., et al. (2020). Meiosis reveals the early steps in the evolution of a neo-XY sex chromosome pair in the African pygmy mouse Mus minutoides. *PLOS Genet.* 16 (11), e1008959. doi:10.1371/journal.pgen.1008959

Graves, J. A. M., and Renfree, M. B. (2013). Marsupials in the age of genomics. *Annu. Rev. Genomics Hum. Genet.* 14 (1), 393–420. doi:10.1146/annurev-genom-091212-153452

Graves, J. A. (1995). The origin and function of the mammalian Y chromosome and Y-borne genes--an evolving understanding. *Bioessays* 17 (4), 311–320. doi:10.1002/bies.950170407

Graves, J. A., Wakefield, M. J., and Toder, R. (1998). The origin and evolution of the pseudoautosomal regions of human sex chromosomes. *Hum. Mol. Genet.* 7 (13), 1991–1996. doi:10.1093/hmg/7.13.1991

Grey, C., Baudat, F., and de Massy, B. (2009). Genome-wide control of the distribution of meiotic recombination. *PLOS Biol.* 7 (2), e1000035. doi:10.1371/journal.pbio.1000035

Grey, C., Baudat, F., and de Massy, B. (2018). PRDM9, a driver of the genetic map. *PLOS Genet.* 14 (8), e1007479. doi:10.1371/journal.pgen.1007479

Gruhn, Jennifer R., Al-Asmar, N., Fasnacht, R., Maylor-Hagen, H., Peinado, V., Rubio, C., et al. (2016). Correlations between synaptic initiation and meiotic recombination: A study of humans and mice. *Am. J. Hum. Genet.* 98 (1), 102–115. doi:10.1016/j.ajhg.2015.11.019

Gruhn, J. R., Rubio, C., Broman, K. W., Hunt, P. A., and Hassold, T. (2013). Cytological studies of human meiosis: Sex-specific differences in recombination originate at, or prior to, establishment of double-strand breaks. *PLOS ONE* 8 (12), e85075. doi:10.1371/journal.pone.0085075

Harper, L., Golubovskaya, I., and Cande, W. Z. (2004). A bouquet of chromosomes. *J. Cell Sci.* 117 (18), 4025–4032. doi:10.1242/jcs.01363

Hayman, D. L. (1990). Marsupial cytogenetics. *Aust. J. Zool.* 37, 331–349. doi:10.1071/ZO9890331

Hornecker, J. L., Samollow, P. B., Robinson, E. S., Vandeberg, J. L., and McCarrey, J. R. (2007). Meiotic sex chromosome inactivation in the marsupial Monodelphis domestica. *Genesis* 45 (11), 696–708. doi:10.1002/dvg.20345

Kaback, D. B. (1996). Chromosome–size dependent control of meiotic recombination in humans. *Nat. Genet.* 13 (1), 20–21. doi:10.1038/ng0596-20

Keeney, S., Lange, J., and Mohibullah, N. (2014). Self-organization of meiotic recombination initiation: General principles and molecular pathways. *Annu. Rev. Genet.* 48 (1), 187–214. doi:10.1146/annurev-genet-120213-092304

Lenormand, T., Engelstädter, J., Johnston, S. E., Wijnker, E., and Haag, C. R. (2016). Evolutionary mysteries in meiosis. *Philosophical Trans. R. Soc. B Biol. Sci.* 371 (1706), 20160001. doi:10.1098/rstb.2016.0001

Li, R., Bitoun, E., Altemose, N., Davies, R. W., Davies, B., and Myers, S. R. (2019). A high-resolution map of non-crossover events reveals impacts of genetic diversity on mammalian meiotic recombination. *Nat. Commun.* 10 (1), 3900. doi:10.1038/s41467-019-11675-y

Liebe, B., Petukhova, G., Barchi, M., Bellani, M., Braselmann, H., Nakano, T., et al. (2006). Mutations that affect meiosis in male mice influence the dynamics of the mid-preleptotene and bouquet stages. *Exp. Cell Res.* 312 (19), 3768–3781. doi:10.1016/j.yexcr.2006.07.019

Lopez-Jimenez, P., Perez-Martin, S., Hidalgo, I., Garcia-Gonzalo, F. R., Page, J., and Gomez, R. (2022). The male mouse meiotic cilium emanates from the mother centriole at zygotene prior to centrosome duplication. *Cells* 12 (1), 142. doi:10.3390/cells12010142

Mahadevaiah, S. K., Turner, J. M., Baudat, F., Rogakou, E. P., de Boer, P., Blanco-Rodriguez, J., et al. (2001). Recombinational DNA double-strand breaks in mice precede synapsis. *Nat. Genet.* 27 (3), 271–276. doi:10.1038/85830

Manterola, M., Page, J., Vasco, C., Berrios, S., Parra, M. T., Viera, A., et al. (2009). A high incidence of meiotic silencing of unsynapsed chromatin is not associated with substantial pachytene loss in heterozygous male mice carrying multiple simple robertsonian translocations. *PLoS Genet.* 5 (8), e1000625. doi:10.1371/journal.pgen.1000625

Marín-Gual, L., González-Rodelas, L., Garcias, M. M., Kratochvíl, L., Valenzuela, N., Georges, A., et al. (2022a). Meiotic chromosome dynamics and double strand break formation in reptiles. *Front. Cell Dev. Biol.* 10, 1009776. doi:10.3389/fcell.2022.1009776

Marín-Gual, L., González-Rodelas, L., Pujol, G., Vara, C., Martín-Ruiz, M., Berríos, S., et al. (2022b). Strategies for meiotic sex chromosome dynamics and telomeric elongation in Marsupials. *PLOS Genet.* 18 (2), e1010040. doi:10.1371/journal.pgen.1010040

Mercier, R., Mézard, C., Jenczewski, E., Macaisne, N., and Grelon, M. (2015). The molecular biology of meiosis in plants. *Annu. Rev. Plant Biol.* 66 (1), 297–327. doi:10.1146/annurev-arplant-050213-035923

Mugal, C. F., Weber, C. C., and Ellegren, H. (2015). GC-Biased gene conversion links the recombination landscape and demography to genomic base composition: GC-biased gene conversion drives genomic base composition across a wide range of species. *BioEssays* 37 (12), 1317–1326. doi:10.1002/bies.201500058

Mytlis, A., Kumar, V., Qiu, T., Deis, R., Hart, N., Levy, K., et al. (2022). Control of meiotic chromosomal bouquet and germ cell morphogenesis by the zygotene cilium. *Science* 376(6599), eabh3104. doi:10.1126/science.abh3104

Namekawa, S. H., VandeBerg, J. L., McCarrey, J. R., and Lee, J. T. (2007). Sex chromosome silencing in the marsupial male germ line. *Proc. Natl. Acad. Sci.* 104(23), 9730–9735. doi:10.1073/pnas.0700323104

Oliver-Bonet, M., Campillo, M., Turek, P. J., Ko, E., and Martin, R. H. (2007). Analysis of replication protein A (RPA) in human spermatogenesis. *Mol. Hum. Reprod.* 13 (12), 837–844. doi:10.1093/molehr/gam076

Otto, S. P., and Lenormand, T. (2002). Resolving the paradox of sex and recombination. *Nat. Rev. Genet.* 3 (4), 252–261. doi:10.1038/nrg761

Page, J., Berrios, S., Parra, M. T., Viera, A., Suja, J. A., Prieto, I., et al. (2005). The program of sex chromosome pairing in meiosis is highly conserved across marsupial species: Implications for sex chromosome evolution. *Genetics* 170 (2), 793–799. doi:10.1534/genetics.104.039073

Page, J., Berrios, S., Rufas, J. S., Parra, M. T., Suja, J. A., Heyting, C., et al. (2003). The pairing of X and Y chromosomes during meiotic prophase in the marsupial species *Thylamys elegans* is maintained by a dense plate developed from their axial elements. *J. Cell Sci.* 116 (3), 551–560. doi:10.1242/jcs.00252

Page, J., de la Fuente, R., Manterola, M., Parra, M. T., Viera, A., Berrios, S., et al. (2012). Inactivation or non-reactivation: What accounts better for the silence of sex chromosomes during mammalian male meiosis? *Chromosoma* 121 (3), 307–326. doi:10.1007/s00412-012-0364-y

Page, J., Suja, J. A., Santos, J. L., and Rufas, J. S. (1998). Squash procedure for protein immunolocalization in meiotic cells. *Chromosome Res.* 6 (8), 639–642. doi:10.1023/a:1009209628300

Page, J., Viera, A., Parra, M. T., de la Fuente, R., Suja, J. A., Prieto, I., et al. (2006). Involvement of synaptonemal complex proteins in sex chromosome segregation during marsupial male meiosis. *PLoS Genet.* 2 (8), e136. doi:10.1371/journal.pgen.0020136

Page, S. L., and Hawley, R. S. (2004). The genetics and molecular biology of the synaptonemal complex. *Annu. Rev. Cell Dev. Biol.* 20(1), 525–558. doi:10.1146/annurev.cellbio.19.111301.155141

Paigen, K., and Petkov, P. (2010). Mammalian recombination hot spots: Properties, control and evolution. *Nat. Rev. Genet.* 11 (3), 221–233. doi:10.1038/nrg2712

Parvanov, E. D., Petkov, P. M., and Paigen, K. (2010). Prdm9 controls activation of mammalian recombination hotspots. *Science* 327 (5967), 835. doi:10.1126/science.1181495

Peters, A. H., Plug, A. W., van Vugt, M. J., and de Boer, P. (1997). A drying-down technique for the spreading of mammalian meiocytes from the male and female germline. *Chromosome Res.* 5 (1), 66–68. doi:10.1023/a:1018445520117

Pratto, F., Brick, K., Khil, P., Smagulova, F., Petukhova, G. V., and Camerini-Otero, R. D. (2014). DNA recombination. Recombination initiation maps of individual human genomes. *Science* 346 (6211), 1256442. doi:10.1126/science.1256442

Reig-Viader, R., Garcia-Caldés, M., and Ruiz-Herrera, A. (2016). Telomere homeostasis in mammalian germ cells: A review. *Chromosoma* 125 (2), 337–351. doi:10.1007/s00412-015-0555-4

Ritz, K. R., Noor, M. A. F., and Singh, N. D. (2017). Variation in recombination rate: Adaptive or not? *Trends Genet.* 33 (5), 364–374. doi:10.1016/j.tig.2017.03.003

Roche, L., Seluja, G., and Wettstein, R. (1986). The meiotic behaviour of the XY pair in *Lutreolina crassicaudata* (Marsupialia: Didelphoidea). *Genetica* 71, 213–224. doi:10.1007/bf00057694

Roeder, G. S. (1997). Meiotic chromosomes: It takes two to tango. *Genes Dev.* 11 (20), 2600–2621. doi:10.1101/gad.11.20.2600

Roig, I., Liebe, B., Egozcue, J., Cabero, L., Garcia, M., and Scherthan, H. (2004). Female-specific features of recombinational double-stranded DNA repair in relation to synapsis and telomere dynamics in human oocytes. *Chromosoma* 113 (1), 22–33. doi:10.1007/s00412-004-0290-8

Romanienko, P. J., and Camerini-Otero, R. D. (2000). The mouse Spo11 gene is required for meiotic chromosome synapsis. *Mol. Cell* 6 (5), 975–987. doi:10.1016/s1097-2765(00)00097-6

Ruiz-Herrera, A., Vozdova, M., Fernández, J., Sebestova, H., Capilla, L., Frohlich, J., et al. (2017). Recombination correlates with synaptonemal complex length and chromatin loop size in bovids—Insights into mammalian meiotic chromosomal organization. *Chromosoma* 126 (5), 615–631. doi:10.1007/s00412-016-0624-3

Samollow, P. B., Gouin, N., Miethke, P., Mahaney, S. M., Kenney, M., VandeBerg, J. L., et al. (2007). A microsatellite-based, physically anchored linkage map for the gray, short-tailed Opossum (Monodelphis domestica). *Chromosome Res.* 15 (3), 269–281. doi:10.1007/s10577-007-1123-4

Samollow, P. B., Kammerer, C. M., Mahaney, S. M., Schneider, J. L., Westenberger, S. J., VandeBerg, J. L., et al. (2004). First-generation linkage map of the gray, short-tailed opossum, Monodelphis domestica, reveals genome-wide reduction in female recombination rates. *Genetics* 166 (1), 307–329. doi:10.1534/genetics.166.1.307

Scherthan, H. (2007). Telomere attachment and clustering during meiosis. *Cell. Mol. Life Sci.* 64 (2), 117–124. doi:10.1007/s00018-006-6463-2

Scherthan, H., Weich, S., Schwegler, H., Heyting, C., Harle, M., and Cremer, T. (1996). Centromere and telomere movements during early meiotic prophase of mouse and man are associated with the onset of chromosome pairing. *J. Cell Biol.* 134 (5), 1109–1125. doi:10.1083/jcb.134.5.1109

Segura, J., Ferretti, L., Ramos-Onsins, S., Capilla, L., Farré, M., Reis, F., et al. (2013). Evolution of recombination in eutherian mammals: Insights into mechanisms that affect recombination rates and crossover interference. *Proc. R. Soc. B Biol. Sci.* 280 (1771), 20131945. doi:10.1098/rspb.2013.1945

Seluja, G., Roche, L., and Solari, A. J. (1987). Male meiotic prophase in *Didelphis albiventris*. *J. Hered.* 78, 218–222. doi:10.1093/oxfordjournals.jhered.a110369

Sharp, P. (1982). Sex chromosome pairing during male meiosis in marsupials. *Chromosoma* 86 (1), 27–47. doi:10.1007/BF00330728

Solari, A. J., and Bianchi, N. O. (1975). The synaptic behaviour of the X and Y chromosomes in the marsupial *Monodelphis dimidiata*. *Chromosoma* 52 (1), 11–25. doi:10.1007/BF00285785

Stapley, J., Feulner, P. G. D., Johnston, S. E., Santure, A. W., and Smadja, C. M. (2017). Variation in recombination frequency and distribution across eukaryotes: Patterns and processes. *Philosophical Trans. R. Soc. B Biol. Sci.* 372 (1736), 20160455. doi:10.1098/rstb.2016.0455

Subramanian, V. V., Zhu, X., Markowitz, T. E., Vale-Silva, L. A., San-Segundo, P. A., Hollingsworth, N. M., et al. (2019). Persistent DNA-break potential near telomeres increases initiation of meiotic recombination on short chromosomes. *Nat. Commun.* 10 (1), 970. doi:10.1038/s41467-019-08875-x

Turner, J. M., Aprelikova, O., Xu, X., Wang, R., Kim, S., Chandramouli, G. V., et al. (2004). BRCA1, histone H2AX phosphorylation, and male meiotic sex chromosome inactivation. *Curr. Biol.* 14 (23), 2135–2142. doi:10.1016/j.cub.2004.11.032

Turner, J. M., Mahadevaiah, S. K., Fernandez-Capetillo, O., Nussenzweig, A., Xu, X., Deng, C. X., et al. (2005). Silencing of unsynapsed meiotic chromosomes in the mouse. *Nat. Genet.* 37 (1), 41–47. doi:10.1038/ng1484

Tyndale-Biscoe, H., and Renfree, M. (1987). *Reproductive physiology of marsupials*. Cambridge: Cambridge University Press.

Ullastres, A., Farré, M., Capilla, L., and Ruiz-Herrera, A. (2014). Unraveling the effect of genomic structural changes in the rhesus macaque - implications for the adaptive role of inversions. *BMC Genomics* 15 (1), 530. doi:10.1186/1471-2164-15-530

Vara, C., Paytuví-Gallart, A., Cuartero, Y., Álvarez-González, L., Marín-Gual, L., Garcia, F., et al. (2021). The impact of chromosomal fusions on 3D genome folding and recombination in the germ line. *Nat. Commun.* 12 (1), 2981. doi:10.1038/s41467-021-23270-1

Viera, A., Parra, M. T., Rufas, J. S., and Page, J. (2017). Transcription reactivation during the first meiotic prophase in bugs is not dependent on synapsis. *Chromosoma* 126 (1), 179–194. doi:10.1007/s00412-016-0577-6

von Wettstein, D., Rasmussen, S. W., and Holm, P. B. (1984). The synaptonemal complex in genetic segregation. *Annu. Rev. Genet.* 18, 331–413. doi:10.1146/annurev.ge.18.120184.001555

Wang, C., Webley, L., Wei, K.-j., Wakefield, M. J., Patel, H. R., Deakin, J. E., et al. (2011). A second-generation anchored genetic linkage map of the tammar wallaby (*Macropus eugenii*). *BMC Genet.* 12 (1), 72. doi:10.1186/1471-2156-12-72

Wang, S., Veller, C., Sun, F., Ruiz-Herrera, A., Shang, Y., Liu, H., et al. (2019). Per-nucleus crossover covariation and implications for evolution. *Cell* 177 (2), 326–338.e16. doi:10.1016/j.cell.2019.02.021

Watson, C. M., Margan, S. H., and Johnston, P. G. (1998). Sex-chromosome elimination in the bandicoot *Isoodon macrourus* using Y-linked markers. *Cytogenet. Genome Res.* 81 (1), 54–59. doi:10.1159/000015008

Xie, H., Wang, X., Jin, M., Li, L., Zhu, J., Kang, Y., et al. (2022). Cilia regulate meiotic recombination in zebrafish. *J. Mol. Cell Biol.* 14 (7), mjac049. doi:10.1093/jmcb/mjac049

Zenger, K. R., McKenzie, L. M., and Cooper, D. W. (2002). The first comprehensive genetic linkage map of a marsupial: The tammar wallaby (*Macropus eugenii*). *Genetics* 162 (1), 321–330. doi:10.1093/genetics/162.1.321

Zickler, D., and Kleckner, N. (1998). The leptotene-zygotene transition of meiosis. *Annu. Rev. Genet.* 32, 619–697. doi:10.1146/annurev.genet.32.1.619

frontiers | Frontiers in Cell and Developmental Biology

TYPE Original Research
PUBLISHED 18 May 2023
DOI 10.3389/fcell.2023.1170689

OPEN ACCESS

EDITED BY
Mónica Pradillo,
Complutense University of Madrid, Spain

REVIEWED BY
Andreas Hochwagen,
New York University, United States
Joao Matos,
Max F. Perutz Laboratories GmbH, Austria

*CORRESPONDENCE
Miki Shinohara,
mikis@nara.kindai.ac.jp

RECEIVED 21 February 2023
ACCEPTED 09 May 2023
PUBLISHED 18 May 2023

CITATION
Shinohara M and Shinohara A (2023), The Msh5 complex shows homeostatic localization in response to DNA double-strand breaks in yeast meiosis.
Front. Cell Dev. Biol. 11:1170689.
doi: 10.3389/fcell.2023.1170689

The Msh5 complex shows homeostatic localization in response to DNA double-strand breaks in yeast meiosis

Miki Shinohara[1,2,3]* and Akira Shinohara[3]

[1]Department of Advanced Bioscience, Graduate School of Agriculture, Kindai University, Nara, Japan, [2]Agricultural Technology and Innovation Research Institute, Kindai University, Nara, Japan, [3]Institute for Protein Research, Osaka University, Osaka, Japan

Meiotic crossing over is essential for the segregation of homologous chromosomes. The formation and distribution of meiotic crossovers (COs), which are initiated by the formation of double-strand break (DSB), are tightly regulated to ensure at least one CO per bivalent. One type of CO control, CO homeostasis, maintains a consistent level of COs despite fluctuations in DSB numbers. Here, we analyzed the localization of proteins involved in meiotic recombination in budding yeast *xrs2* hypomorphic mutants which show different levels of DSBs. The number of cytological foci with recombinases, Rad51 and Dmc1, which mark single-stranded DNAs at DSB sites is proportional to the DSB numbers. Among the pro-CO factor, ZMM/SIC proteins, the focus number of Zip3, Mer3, or Spo22/Zip4, was linearly proportional to reduced DSBs in the *xrs2* mutant. In contrast, foci of Msh5, a component of the MutSγ complex, showed a non-linear response to reduced DSBs. We also confirmed the homeostatic response of COs by genetic analysis of meiotic recombination in the *xrs2* mutants and found a chromosome-specific homeostatic response of COs. Our study suggests that the homeostatic response of the Msh5 assembly to reduced DSBs was genetically distinct from that of the Zip3 assembly for CO control.

KEYWORDS

crossover control, meiotic recombination, crossover homeostasis, DSB formation, synaptonemal complex, Msh4-Msh5

Introduction

Meiotic recombination generates both crossovers (COs) and non-crossovers (NCOs). Crossing over during meiosis is essential to establish a chiasma as a physical connection between homologous chromosomes to ensure proper segregation of these chromosomes during the first meiotic division, meiosis I. Spo11 generates DNA double-strand breaks (DSBs) to initiate the recombination (Bergerat et al., 1997; Keeney et al., 1997). Spo11 forms a topoisomerase VI-like complex with Rec102, Rec104, and Ski8 (Robert et al., 2016; Claeys Bouuaert et al., 2021) and associates with two complexes, the Rec114-Mei4-Mer2 (RMM) and Mre11-Rad50-Xrs2 (MRX) complexes (Kee et al., 2004; Maleki et al., 2007). The number of DSBs exceeds the number of COs in budding yeast and other organisms; e.g., ~90 COs from ~170 DSBs in the budding yeast (Moens et al., 2002; Pan et al., 2011).

Meiotic CO formation is strictly regulated by several distinct mechanisms, which together are known as crossover control. Crossover interference negatively regulates CO formation to ensure even spacing and to limit the number of COs on each chromosome (Muller, 1916). Crossover assurance (or obligate CO) is a positive regulatory mechanism that ensures at least one CO on

each homolog pair (Jones, 1984). It is thought that a balance between CO interference and assurance is the key feature of CO formation (Kleckner, 2006; Shinohara et al., 2015; Wang et al., 2019a). A third control mechanism, called CO homeostasis, was proposed based on studies of *spo11* hypomorphic mutants with differential DSB activities (Martini et al., 2006). CO homeostasis maintains a consistent number of CO events despite fluctuations in the number of meiotic DSBs (Martini et al., 2006). CO homeostasis may be a reflection of CO assurance mechanisms. However, the molecular mechanisms underlying CO homeostasis remain unknown. Moreover, the additional layer of CO control per nucleus basis, called CO covariation, is proposed (Wang et al., 2019b).

Meiosis-specific ZMM (Zip, Mer, Msh) or SIC (Synaptic Initiation Complex) proteins are components of recombination nodules on the synaptonemal complex (SC) and are required for CO formation and CO control; both CO interference and assurance (Sym et al., 1993; Hollingsworth et al., 1995; Nakagawa and Ogawa, 1999; Agarwal and Roeder, 2000; Novak et al., 2001; Tsubouchi et al., 2006; Shinohara et al., 2008). ZMMs include Zip1, Zip2, Zip3, Spo22 (also called Zip4), Mer3, Msh4, Msh5, and Spo16. Mer3 encodes a 5′-3′ DNA helicase and binds recombination intermediates (Nakagawa et al., 2001). Msh4 and Msh5 are homologs of *Escherichia coli* MutS, forming the Msh4-Msh5 complex (MutSγ), which binds to a recombination intermediate (Hollingsworth et al., 1995; Snowden et al., 2004). Msh4-Msh5 complex activates a nuclease activity of the Mlh1-Mlh3 complex (MutLγ) (Cannavo et al., 2020; Kulkarni et al., 2020; Dai et al., 2021). Zip2, Spo22/Zip4, and Spo16 form a complex (ZZS) required for SC elongation, which also binds to a recombination intermediate (Shinohara et al., 2008; De Muyt et al., 2018; Arora and Corbett, 2019). Msh4-Msh5 and ZZS complexes display differential roles in CO formation and control (Shinohara et al., 2008).

Coordinated activities of two recombinases, Rad51 and Dmc1, are required for proper strand invasion to form a displacement D-loop with a single-stranded DNA of the DSBs with homologous duplex DNA (Bishop et al., 1992; Shinohara et al., 1992; Shinohara et al., 2000; Shinohara et al., 2003). Stabilization of the D-loop to form a single-end invasion (SEI) or ejection of the invading strand is a critical regulatory step in the CO/NCO decision (Allers and Lichten, 2001; Hunter and Kleckner, 2001; Borner et al., 2004). The SEI is a specific intermediate for crossing over, which is converted into double Holliday junctions (dHJ) intermediate (Schwacha and Kleckner, 1994; 1995). Msh4-Msh5 complex stabilizes nascent joint molecules and activate a nuclease activity of the Mlh1-Mlh3 complex (MutLγ) for the resolution of dHJs into COs (Snowden et al., 2004; Cannavo et al., 2020; Kulkarni et al., 2020). Crossover interference is proposed to implement around the SEI formation (Kleckner, 2006; Shinohara et al., 2008). Moreover, recruitment of the Msh4-Msh5 complex to meiotic chromosomes depends on Zip3, but not other ZMM such as Zip2, Spo22/Zip4, or Mer3 (Shinohara et al., 2008). Zip3 has a conserved RING-finger motif and is predicted to function as Ubiquitin-E3 ligase or small ubiquitin-like modifier (SUMO)-E3 ligase (Perry et al., 2005; Cheng et al., 2006; Shinohara et al., 2008).

Xrs2 is a regulatory subunit of the MRX complex, which is required for DSB end resection, the DNA damage response, and nonhomologous end-joining during the vegetative cell growth (Johzuka and Ogawa, 1995; Tsubouchi and Ogawa, 1998; Usui et al., 1998; Palmbos et al., 2005; Matsuzaki et al., 2008; Mimitou and Symington, 2009; Ho and Burgess, 2011). In meiotic prophase I, Xrs2 is necessary for not only DSB end resection but also DSB formation, which could be mediated by the interaction with Mer2 (Arora et al., 2004). In addition, Xrs2 interacts with a meiosis-specific protein Pch2 and the interaction is involved in checkpoint signaling for meiotic recombination (Ho and Burgess, 2011). We previously isolated several *xrs2* mutations, and some showed defects in nonhomologous end-joining through interaction with DNA ligase IV in budding yeast (Shima et al., 2005). The mutants also had differential effects on the frequencies of meiotic DSBs, as seen with *spo11* hypomorphic mutants (Henderson and Keeney, 2004). The effects of various *xrs2* mutations on meiotic DSB frequencies could be explained by varied instability of mutant Xrs2 mutant proteins associated with these alleles (Shima et al., 2005).

Here, we used *xrs2* hypomorphic mutants to examine the relationship of global meiotic DSB frequencies with ZMM/SIC assembly on meiotic chromosomes as well as CO formation and control. Immuno-staining revealed that number of foci containing not only Rad51 and Dmc1 but also most ZMM proteins including Zip3 is proportional to DSB frequencies in the *xrs2* mutants. On the other hand, Msh5 ensembles on chromosomes showed a non-linear response to reduced DSB numbers. Our genetics analysis also confirmed CO homeostasis in response to reduced DSBs and showed a chromosome-specific effect of CO homeostasis. These suggest an important role of yeast MutSγ complex in the implementation of CO homeostasis, thus CO control.

Materials and methods

Strains and media

All yeast strains and their genotypes are shown in Supplementary Table S1. We used the isogenic *Saccharomyces cerevisiae* SK1 strain. The *spo11* mutant strains were derived from crossing a wild-type strain (MSY831) with SKY330 (*spo11-HA*) or SKY531 (*spo11-YF*), gifts from Dr. Scott Keeney. Synthetic complete media with 7.25 μM $CuSO_4$ was used for *cup2* selection.

Antibodies

Antibodies specific for Zip1 (generated in rabbit and rat), Zip3 (rabbit and rat), Mer3 (rabbit), Spo22 (chicken), Msh5 (rabbit), Dmc1 (rabbit), and Rad51 (rabbit and guinea pig) were described previously (Shinohara et al., 2008; Zhu et al., 2010; Matsuzaki et al., 2012; Sasanuma et al., 2013). We used two different rabbit anti-Msh5 antisera (Shinohara et al., 2008) and were able to observe two kinds of Msh5 foci dependent on a lot of Msh5 antibodies. In this study, we used an antibody that recognizes brighter ones specifically, which were used in our previous Chromatin-Immunoprecipitation of Msh5 (Nandanan et al., 2021). This might be a reason why we observed fewer Msh5 foci than in our previous report (Nishant et al., 2010).

Cytology

Immunostaining of yeast meiotic chromosome spreads was performed as described (Shinohara et al., 2000). Stained samples

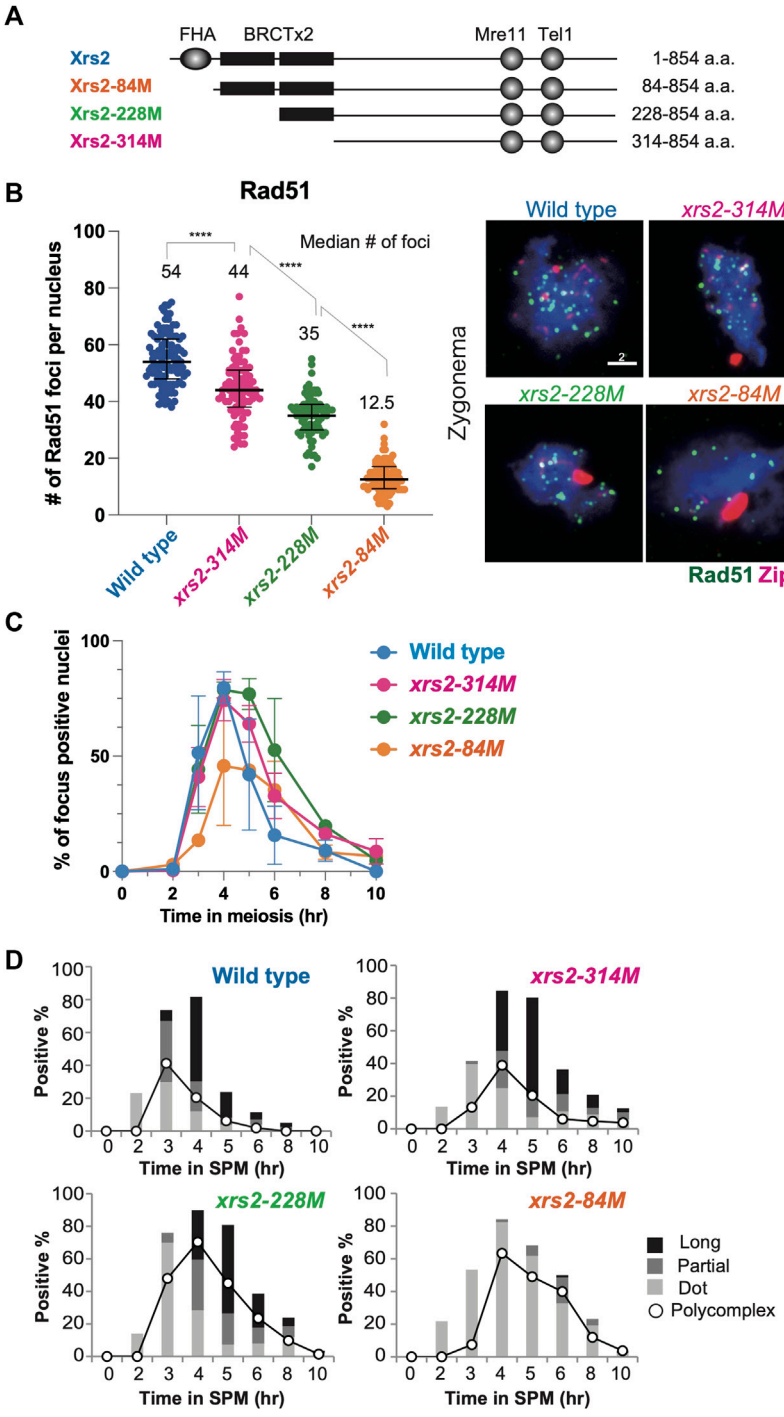

FIGURE 1
Rad51 focus formation and SC elongation in *xrs2* hypomorphic alleles. **(A)** Schematic representation of protein domain structure for yeast Xrs2 and truncated proteins encoded by *xrs2* hypomorphic alleles. The FHA domain and BRCA1 C-terminus (BRCT) domains, Mre11-binding and Tel1-binding domains are shown. **(B)** The number of Rad51 foci in each nucleus of wild-type, *xrs2–314M*, *xrs2–228M*, and *xrs2–84M* strains; wild-type (NKY1551), *xrs2–314M* (MSY 1992), *xrs2–228M* (MSY1524), *xrs2–84M* (MSY1494) was counted at the time point when the presence of focus positive nuclei in each strain peaked (4 h in wild type, *xrs2–314M*, and *xrs2–228M*, and 6 h in *xrs2–84M*). Median numbers of Rad51 were indicated. Error bar shows median and interquartile. Statistical significance was determined using Mann-Whitney *U*-test (****$p < 0.0001$). The right panel shows images of nuclear spreads in the zygotene stage that were labeled for Rad51 (green) and Zip1 (red). Scale bar = 2 μm. **(C)** Kinetics of Rad51-focus assembly and disassembly on meiotic nuclear spreads. A spread with more than 5 Rad51 foci was classified as a focus-positive nucleus. At each time point, more than 100 nuclei were counted. **(D)** Zip1-positive nuclei were classified into three categories: punctate foci (Dot, light gray), partial linear (Partial, gray), and full SC (Long, black). The kinetics of Zip1 poly-complex formation is represented by opened circles.

TABLE 1 Spore viability of the *xrs2* mutants.

Strain	Viable spores per ascus					Viability ±S.D.[a]
	4	3	2	1	0	
Wild type	1,200	69	27	4	8	96.8% ± 2.3%
xrs2–314M	1,200	61	25	2	6	97.3% ± 2.1%
xrs2–228M	1,367	282	100	11	34	90.9% ± 4.2%
xrs2–84M	1,275	590	759	215	1,269	52.4% ± 8.7%

[a]Standard deviation of spore viability among independent crosses.

were observed using an epifluorescence microscope (Zeiss Axioskop 2) and a ×100 objective (Zeiss AxioPlan, NA1.4). Images were captured with a CCD camera (Retiga; Qimaging) and processed using IP lab (Silicon) and Photoshop (Adobe). To count protein foci, >100 nuclei were counted for each sample. Pairs of foci were considered to colocalize if >50% of one side overlapped as described (Shinohara et al., 2000). The fluorescent intensity of Zip3 single-focus was measured by using the auto-thresholding signal intensity in Imaris software (Oxford Instrument). Strains used for this analysis were wild-type (NKY1551), *xrs2–314M* (MSY1992), *xrs2–228M* (MSY1524), and *xrs2–84M* (MSY1494).

Genetic analysis of meiotic recombination

Genetics distances between markers and CO interference were analyzed using the MacTetrad 6.9.1 program (merlot.wekj.jhu.edu) as described (Shinohara et al., 2003; Shinohara et al., 2008; Shinohara et al., 2019). Parental haploid strains were mated for 3 h on YPAD (1% bacto-yeast extract, 2% bacto-peptone, 2% glucose, 0.004% adenine sulfate) plates at 30°C and then transferred onto SPM (0.3% potassium acetate, 0.02% raffinose) plates. After incubation at 30°C for 48 h, tetrads were dissected onto YPAD plates and incubated for 2 days. Genotyping was performed as described (Shinohara et al., 2003). To avoid aberrant clones (e.g., those containing mitotic COs), at least four independent crosses were carried out and pooled for further analysis. When analyzing interference or calculating genetic distances, we excluded tetrads with non-Mendelian segregation of a diagnostic marker from the analysis. Map distances were determined using Perkins equation: [distance in (cM)] = 100/2 (TT + 6NPD)/(PD + TT + NPD) (Perkins, 1949), where tetra types (TT), non-parental ditypes (NPD), parental ditypes (PD) observed. Standard errors were calculated using the Stahl Lab online tool (https://elizabethhousworth.com/StahlLabOnlineTools/). Interference values are expressed as the NPD ratio. The fraction of tetrads expected to be NPDs was determined from the Papazian equation: NPDexp = 1/2 [1 − TT − (1 − 3TT/2)$^{2/3}$] (Papazian, 1952). To measure coincident double COs in adjacent intervals, the frequencies of tetrads with recombination in each of the two intervals were determined by summing TT and NPD tetrads for those intervals and dividing by the total number of tetrads (Shinohara et al., 2003). The expected frequency of coincident recombination is given by the product of two single-interval frequencies. Coefficient of coincidence (CoC) CO is calculated as follows: CoC = [CO(A∩B)]/[CO(A) × CO(B)], where A and B are CO frequencies in an adjacent single interval. Strains used for this analysis are wild-type (MSY4304/4245), *xrs2–314M* (MSY4314/4316), *xrs2–228M* (MSY4310/4312), and *xrs2–84M* (MSY4306/4308).

Results

The *xrs2* hypomorphic mutants showed differential DSB frequencies

We previously reported that N-terminal truncations of Xrs2 significantly reduce meiotic DSB formation at the *HIS4–LEU2* hotspot (Shima et al., 2005). The *xrs2–84M*, *xrs2–228M*, and *xrs2–314M* mutants lack N-terminal 83, 227, and 313 amino acids, respectively (Figure 1A). On the other hand, even in the largest deletion, the *xrs2–314M* mutation does not cause any reduction of meiotic DSBs at the locus (Shima et al., 2005) with normal spore viability (Table 1). Despite the DSB reduction, *xrs2–228M* exhibits normal levels of spore viability. In contrast, the *xrs2–84M* allele, even though it encodes the smallest truncation (Figure 1A), shows significant reductions in spore viability of 52.4% (Table 1), as shown previously (Shima et al., 2005). The reduced spore viability in *xrs2–84M* cells is not caused by the deletion of the Forkhead-associated (FHA) domain of Xrs2 *per se* but rather by reduced levels of Xrs2 protein, as overexpression of Xrs2–84M protein rescues spore viability of the *xrs2-84M* mutant in a dose-dependent manner (Shima et al., 2005).

We further characterized meiotic defects for the three *xrs2* hypomorph mutants in more detail. We estimated the total number of meiotic DSBs in *xrs2* mutants by analyzing the number of immuno-stained Rad51 foci on meiotic chromosome spreads, which correspond to DSB sites (Bishop et al., 1992; Shinohara et al., 2000). We first counted the number of Rad51 foci in *spo11* hypomorphic mutants; *spo11-HA/spo11-HA*, *spo11-HA/spo11-Y135F* and *spo11-Y135F/spo11-Y135F*, which decreases DSB levels on chromosomes III, VII and VIII to ~80%, ~30% and 0%, respectively (Martini et al., 2006). The average Rad51-focus number in the wild type was 54.2 ± 0.7 (± Standard deviation [SD] at 4 h). The number at 4 h in the *spo11-HA/spo11-HA* and *spo11-HA/spo11-Y135F* was 39.4 ± 5.9 and 19.0 ± 0.1, respectively, while the *spo11-Y135F/spo11-Y135F* mutant formed little Rad51 foci as described previously (Bishop, 1994). The number of Rad51 foci is roughly proportional to DSB frequency on the three chromosomes in the various *spo11* hypomorphic mutants (Martini et al., 2006) (Supplementary Figure S1A). Rad51-focus number per spread could be used as a proxy for a total DSB number in a single nucleus.

We then studied the Rad51-focus number in the *xrs2* mutants and found that the average number of Rad51 foci within meiotic nuclei of wild type, *xrs2–314M*, *xrs2–228M*, and *xrs2–84M* was 54.2 ± 0.7, 42.8 ± 7.9, 35.7 ± 1.7 and 14.3 ± 4.8, respectively (Figure 1B). To avoid the kinetic effect, we analyzed the Rad51-focus number at 4, 5, or, 6 h, and then we decided to analyze 4-h samples which are when the peak of focus formation in each *xrs2* mutant (Figure 1C). Thus, from a relative decrease of Rad51 foci, we estimated that DSBs in *xrs2–314M*, *xrs2–228M*, and *xrs2–84M* mutants were reduced by 21%, 35%, and 74% compared with

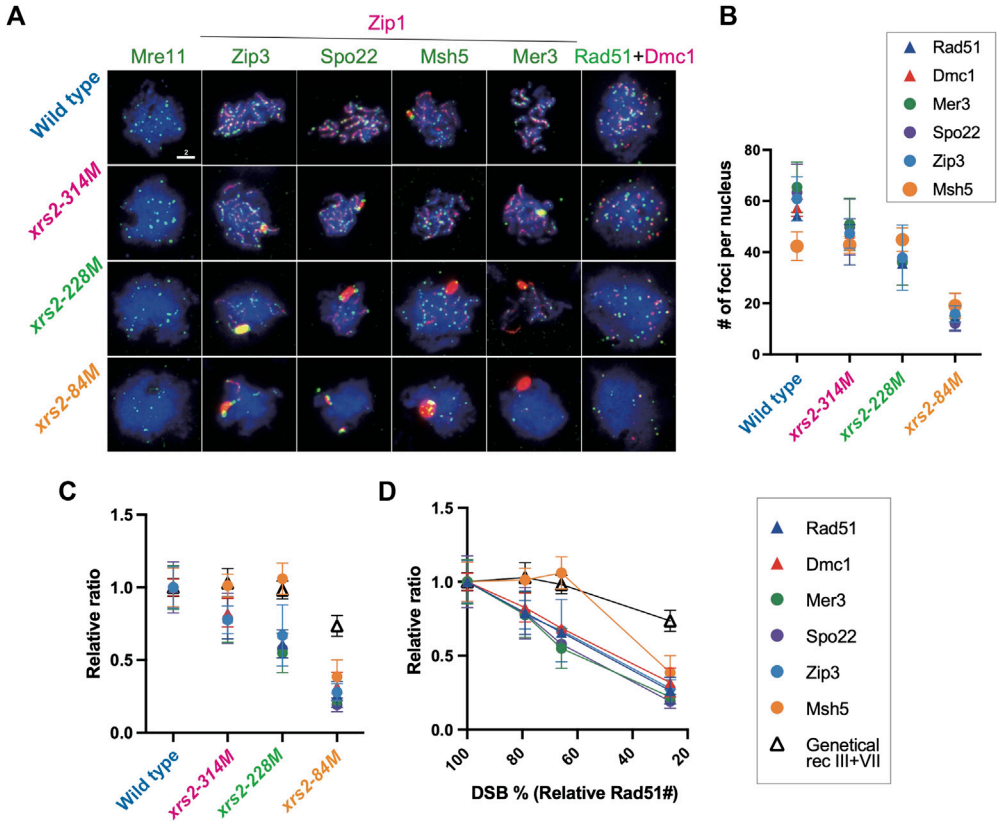

FIGURE 2
Assembly of recombination and ZMM/SIC components when DSB levels are reduced. **(A)** Colocalization of Zip1 (red; rat) and Zip3 (green; rabbit), Spo22/Zip4 (green; chicken), Msh5 (green; rabbit), or Mer3 (green; rabbit). Colocalization of Rad51 (green; guinea pig) and Dmc1 (red; rabbit). Genotypes are indicated. Wild-type (NKY1551), *xrs2–314M* (MSY1992), *xrs2–228M* (MSY1524), *xrs2–84M* (MSY1494) were used. Scale bar = 2 μm. **(B)** The number of foci of indicated proteins per nucleus in wild-type and *xrs2* mutants. The focus number in wild type, *xrs2–314M*, *xrs2–228M*, and *xrs2–84M* was counted at the time point when the presence of focus positive nuclei in each strain peaked (4, 5, or 6 h) as shown 1B. Error bars show the average and SD. **(C)** The number of foci of indicated proteins plotted against each average number of Rad51 foci (i.e., DSBs) associated with each strain (Figure 1B). Values are presented as a ratio relative to the wild type. Open triangles indicate relative CO frequencies as shown in **(B)**. Error bars show the average and SD. **(D)** The number of foci of indicated proteins in wild-type and *xrs2* mutants (non-normalized values). Error bars indicate the mean values and standard deviations from at least three independent experiments. Error bars show the average and SD. A black line with open triangles indicates relative CO frequencies of sums of analyzed intervals in chromosomes III and VII shown in Figure 4B. Values are presented as a ratio relative to the wild type.

wild type, respectively. A similar reduction was observed for Dmc1 foci; an average number at 4 h of wild type, *xrs2–314M*, *xrs2–228M*, and *xrs2–84M* was 57.4 ± 3.3, 47.4 ± 5.6, 39.3 ± 1.9 and 18.3 ± 5.6, respectively. The *xrs2* mutant cells also showed slight delays in the disappearance of Rad51-focus positive spreads during meiosis (Figure 1C). The delayed disassembly of Rad51 foci suggests the role of the Xrs2 in meiotic DSB repair.

Substantial DSB levels are required for Zip1 elongation

A meiosis-specific chromosome structure, the synaptonemal complex (SC), is formed between homologous chromosome axes. SC formation depends on meiotic recombination, thus DSB formation (Alani et al., 1990; Padmore et al., 1991). We also checked the effect of differential DSB levels in the *xrs2* mutants on SC formation by immune-staining analysis of Zip1 protein, which is a component of the central region of the SC (Sym et al., 1993). The Zip1-staining was classified into long, short lines, and dots (Figure 1D) as described previously (Shinohara et al., 2003). Like the wild type, fully-elongated Zip1 lines were observed in both the *xrs2–314M* and *xrs2–228M* mutants although the mutants showed only a 1-h delay in the appearance of long Zip1 lines as compared to the wild type, which is associated with a higher frequency of nuclei containing Zip1 poly-complex structures, an indicator for a defect in Zip1 elongation (Sym and Roeder, 1995). And the mutants delayed disassembly of Zip1 structure, consistent with delayed DSB repair in the mutants. The *xrs2–84M* mutant, which had the lowest level of DSBs (~25%), showed a clear defect in Zip1 elongation with very few Zip1 long lines (Figure 1D). This indicated that substantial levels of DSBs were required for proper Zip1 elongation, thus chromosome synapsis. Similar results are seen with *spo11* mutants (Henderson and Keeney, 2004) and other mutants which reduced DSB levels (Bani Ismail et al., 2014).

The two BRCT-like domains of Xrs2 (amino acids 124-313; Figure 1A) have functions related to Pch2 (Ho and Burgess, 2011), which is required for normal SC formation and timely meiotic

recombination progression (San-Segundo and Roeder, 1999; Borner et al., 2008). The *pch2* mutant cells show unusual localization of Hop1 protein on pachytene chromosomes with a delay in meiotic recombination (Borner et al., 2008). However, like in the wild type, we found dotty staining of Hop1 along long Zip1 lines in the *xrs2-314M* cells, which is different from long Hop1 lines on Zip1 lines seen in *pch2* cells (Supplementary Figure S2). The BRCT domains of Xrs2 do not appear to play a role in the Pch2 function in the Hop1 loading and/or unloading.

Reduced DSBs decrease the association of ZMM/SIC and recombination proteins on meiotic chromosomes in *xrs2* mutants

Previously, it is shown that Zip3-GFP foci show a homeostatic response when DSBs are reduced in *spo11* hypomorphic mutants (Henderson and Keeney, 2004). First, we confirmed that Zip3 foci show the non-linear response in the *spo11* hypomorphic mutants by using our anti-Zip3 antibody without any tag-conjugation to Zip3 protein like previously reported (Supplementary Figures S1B, C). A steady-state number of Zip3 population was 61.5 (median), 58, 22, and 13 in wild-type, *spo11-HA/spo11-HA*, *spo11-HA/spo11-Y135F,* and *spo11-Y135F/spo11-Y135F*, respectively. The *spo11-HA/spo11-HA* mutant with ~78% DSB level maintains a similar Zip3 focus number to the wild type (94%), indicating a non-linear relationship as shown previously (Martini et al., 2006). The *spo11-HA/spo11-Y135F* mutant with ~29% DSB levels shows a higher Zip3 focus number (~36% of the wild-type) that expected.

We also analyzed the number of Zip3 foci as well as other ZMM foci including Spo22/Zip4, Msh5 and Mer3 when DSB frequencies are decreased by the *xrs2* hypomorphs (Figure 2A). Immunostaining was carried out and the focus number was counted at 4 h after meiosis entry for wild-type. To avoid the kinetic effect, we counted the focus number at 4 h (*xrs2–314M* and *–228M*) or 6 h (*xrs2–84M*) which is when the peak of focus formation in each *xrs2* mutant (Supplementary Figure S3A-representative kinetic analysis and Supplementary Figure S3D). The average number of foci per nucleus from four independent time courses (more than 100 focus-positive nuclei were analyzed for each counting) for Rad51, Dmc1, Zip3, and Msh5, and from two independent time courses for Spo22/Zip4 and Mer3 are shown in Figure 2B. As shown above (Figure 1), the average numbers of Rad51 and Dmc1 foci at 4 h in wild-type nuclei were 54.2 ± 0.7 (SD) and 57.4 ± 3.3, respectively (Figure 2B), which is consistent with a previous study (Shinohara et al., 2000). The ZMM/SIC proteins Zip3, Spo22/Zip4, and Mer3 exhibited similar numbers of foci in wild-type nuclei: 60.9 ± 8.6, 63.4 ± 11, and 65.5 ± 9.8, respectively (Figure 2B). There were few significant differences in a steady-state number of foci between ZMM foci with either Zip3, Mer3, or Spo22/Zip4, and the RecA-like recombinases (Figures 2A,B). Of note, the steady state number of Zip3 foci in the wild type detected by anti-Zip3 was almost the same as the numbers reported to Zip3-myc (~60 foci) by two independent groups (Yoon et al., 2016; Hong et al., 2019; Tan et al., 2022) but about twice than that reported to Zip3-GFP (Henderson and Keeney, 2004).

When *xrs2* mutants were examined, the focus number of Rad51, Dmc1, and ZMM/SIC proteins such as Zip3, Spo22/Zip4, and Mer3 reduce linearly along with meiotic DSB frequencies in the mutants (Figures 2B–D). Like Rad51/Dmc1 foci, focus numbers of Zip3, Spo22/Zip4, and Mer3 are decreased when DSB frequencies are reduced. When compared with the number, Zip3, Spo22/Zip4 and Mer3 shows linear correlation with Rad51 (R = 0.999, 0.999, 0.994, and 0.982 for Dmc1, Zip3, Spo22/Zip4 and Mer3, respectively). These suggest that, like Rad51/Dmc1 recombinases, Zip3-, Spo22/Zip4-, and Mer3-focus number is linearly correlated with DSB number. Moreover, these are consistent with the result that the focus formation of these proteins depends on meiotic DSB formation (Agarwal and Roeder, 2000; Nakagawa et al., 2001; Shinohara et al., 2008).

While the Zip3-focus number shows a linear relationship with DSB frequency in the *xrs2* mutants (Figure 2B; see below), the number of Zip3-GFP foci (Henderson and Keeney, 2004) and Zip3 foci detected by anti-Zip3 (Supplementary Figure S1B) exhibit a non-linear relationship in *spo11* hypomorph mutants. This suggests a role of N-terminal regions such as the FHA domain and/or BRCT repeat in the homeostatic response of ZMM foci of Zip3 as well as Mer3 and Spo22/Zip4 to reduced DSBs.

Msh5-focus numbers are maintained even with reduced meiotic DSBs are reduced

We found that Msh5 foci showed a unique behavior on the chromosomes among ZMM proteins. In the wild type, the average (steady-state) number of Msh5 foci is 42.4 ± 5.6, which is significantly lower than those of Rad51, Dmc1, Zip3, Mer3, and Spo22/Zip4 (Figures 2A, B), suggesting the presence of a regulatory mechanism for Msh5-focus formation.

Different from Zip3, Spo22/Zip4, and Mer3 as well as Rad51/Dmc1, Msh5 foci showed a non-linear relationship in its number to reduced DSBs in the *xrs2* mutants. The number of Msh5 foci in the *xrs2–314M* and *xrs2–228M* strains was 42.9 ± 3.4 and 44.9 ± 4.6, respectively, which is similar to that in the wild type of 42.4 (Figure 2B; Supplementary Figure S3B). Thus, Msh5 foci exhibited homeostasis as DSBs were reduced by ~40% (in *xrs2–228M*). This non-linear response of ZMM foci was reported to the foci containing Zip3-GFP (Henderson and Keeney, 2004) and Zip3 foci detected by anti-Zip3 (Supplementary Figure S1B) in *spo11* hypomorph mutants. On the other hand, more dramatic reductions in meiotic DSBs did affect the Msh5-focus number, as the number of Msh5 foci in *xrs2–84M* mutant cells decreased substantially to 19.1 ± 4.9, which represented 38.6% of wild type. However, this reduction of Msh5-focus number in the *xrs2–84M* mutant is much milder than those of Rad51, Zip3, Spo22/Zip4, and Mer3 (26.4, 27.9, 19.2, 22.1%, respectively, in Figures 2C, D). This suggests that the homeostatic response of Msh5 foci substantially operates even in the *xrs2–84M* mutant.

Notably, the similar non-linear relationship was seen for Msh5 foci in *spo11* hypomorphic mutants (Supplementary Figure S1C). Importantly, the number of Msh5 foci (41 [median] and 39 foci in wild-type and *spo11-HA/spo11-HA* strains, respectively) was lower than that of Zip3 foci (61.5 and 58 in wild-type and *spo11-HA/spo11-HA* strains, respectively, in Supplementary Figure S1C), supporting a distinct response between Msh5 and Zip3 foci.

Msh5-focus formation depends on Zip3 (and Zip1), but not on Spo22/Zip4 or Spo16 (Shinohara et al., 2008). We analyzed the relationship between the Zip3 and Msh5 localization by double

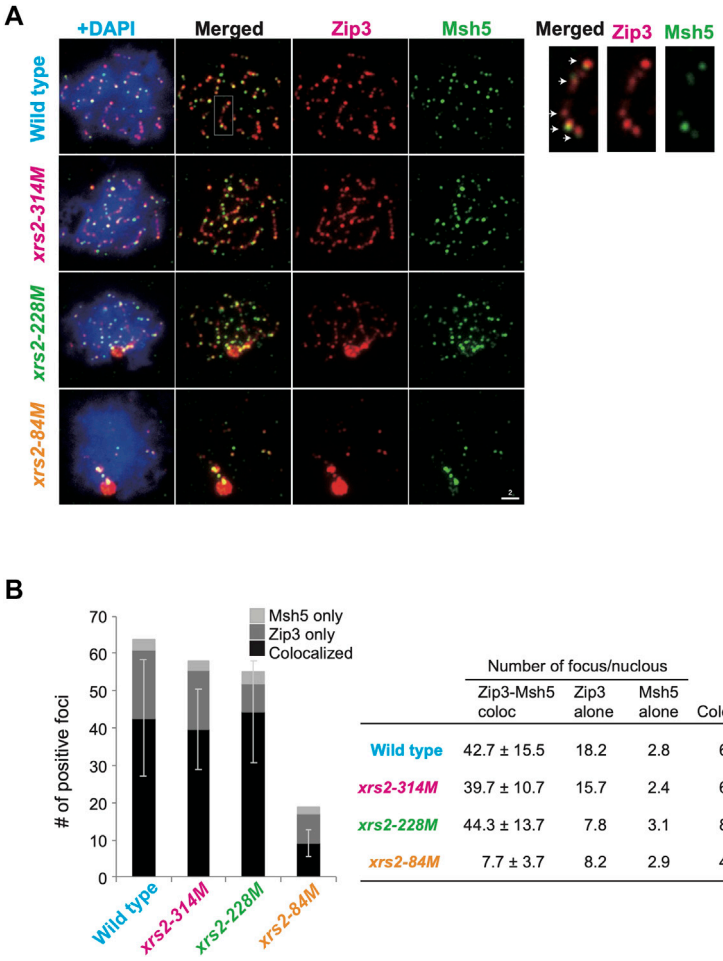

	Number of focus/nucleus				
	Zip3-Msh5 coloc	Zip3 alone	Msh5 alone	Coloc/All	Coloc/Msh5
Wild type	42.7 ± 15.5	18.2	2.8	67%	94%
xrs2-314M	39.7 ± 10.7	15.7	2.4	69%	94%
xrs2-228M	44.3 ± 13.7	7.8	3.1	80%	94%
xrs2-84M	7.7 ± 3.7	8.2	2.9	41%	73%

FIGURE 3
Colocalization of Zip3 and Msh5 on meiotic chromosomes **(A)** Meiotic nuclear spreads were stained for Zip3 (red) and Msh5 (green) by using anti-Zip3 (red; rat) and anti-Msh5 (green; rabbit). Anti-Zip3 used here was different from that in Figure 2. Genotypes are indicated. A magnified image of a wild-type sample is shown on the right. Arrows show colocalization of Zip3 and Msh5. Scale bar = 2 μm. **(B)** Colocalization frequencies for Zip3 and Msh5. Foci were classified into three categories: Zip3 and Msh5 (colocalized, dark gray), Zip3-only (pale gray), and Msh5-only (gray). The average numbers with standard deviations of foci in three categories in wild-type and *xrs2* mutants are shown. The number of nuclei analyzed in wild type (4 h), *xrs2-314M* (4 h), *xrs2-228M* (4 h), and *xrs2-84M* (5 h) is 102, 105, 105, and 59, respectively.

staining of "pachytene" cells (at 4 h in wild-type and 5 h in *xrs2* mutants) (Figure 3A). Medians of Zip3 foci number distribution in wild type, *xrs2–314M*, *xrs2–228M,* and *xrs2–84M* cells were 63, 56, 54, and 16, respectively (Supplementary Figure S3C). Although the number of Zip3 foci co-stained with Msh5 in the *xrs2–84M* is similar to that co-stained with Zip1 shown in Figure 2B (16 versus 14), the focus number of Zip3 co-stained with Msh5 in the *xrs2–314M* and *xrs2–228M* mutants were significantly higher than that co-stained with Zip1 (56 versus 45 and 54 versus 35 in the *xrs2–314M*, and *xrs2–228M* mutants). The focus-number distribution indicates variations of the focus number are smaller in the double-staining of Msh5 and Zip3 than in the co-staining with Zip1 (Supplementary Figures S3B, C). This suggests that Zip3 co-stained with Msh5 showed a homeostatic response as shown previously (Henderson and Keeney, 2004) and in this study (Supplementary Figure S1C). On the other hand, in this double staining of Zip3 and Msh5, the medians of Zip3 focus number distribution were 47, 43, 49, and 10 in wild-type, *xrs2–314M*, *xrs2–228M,* and *xrs2–84M* mutant cells, respectively (Supplementary Figure S3C), which are not different from those co-staining with Zip1. A simple interpretation is a kinetic effect such that the focus numbers of ZMM proteins in the pachytene stage are more than those in earlier stages. Supporting this idea, the focus numbers were increased in later time points of prophase I, especially of Zip3 foci in the *xrs2-228M* mutant (Supplementary Figure S3A).

Importantly, even in the double-staining of Msh5 and Zip3, the Zip3-focus number is higher than the Msh5-focus number in any strains (Figure 3B). In the wild type, 67% of Zip3 foci colocalized with Msh5, and 94% of Msh5 foci colocalized with Zip3. In *xrs2* mutants, Zip3-Msh5 colocalization frequencies in Zip3 foci were 69%, 80%, and 41% for the *xrs2–314M*, *xrs2–228M,* and *xrs2–84M* mutants, respectively. In addition, 94%, 94%, and 73% of Msh5 foci colocalized with Zip3 in *xrs2–314M*, *xrs2–228M,* and *xrs2–84M* mutants, respectively (Figure 3B). This is consistent with the idea that some Zip3 foci become a site for Msh5 assembly, which is regulated by DSB levels. In addition, Zip3 foci colocalized with Msh5 seemed brighter than

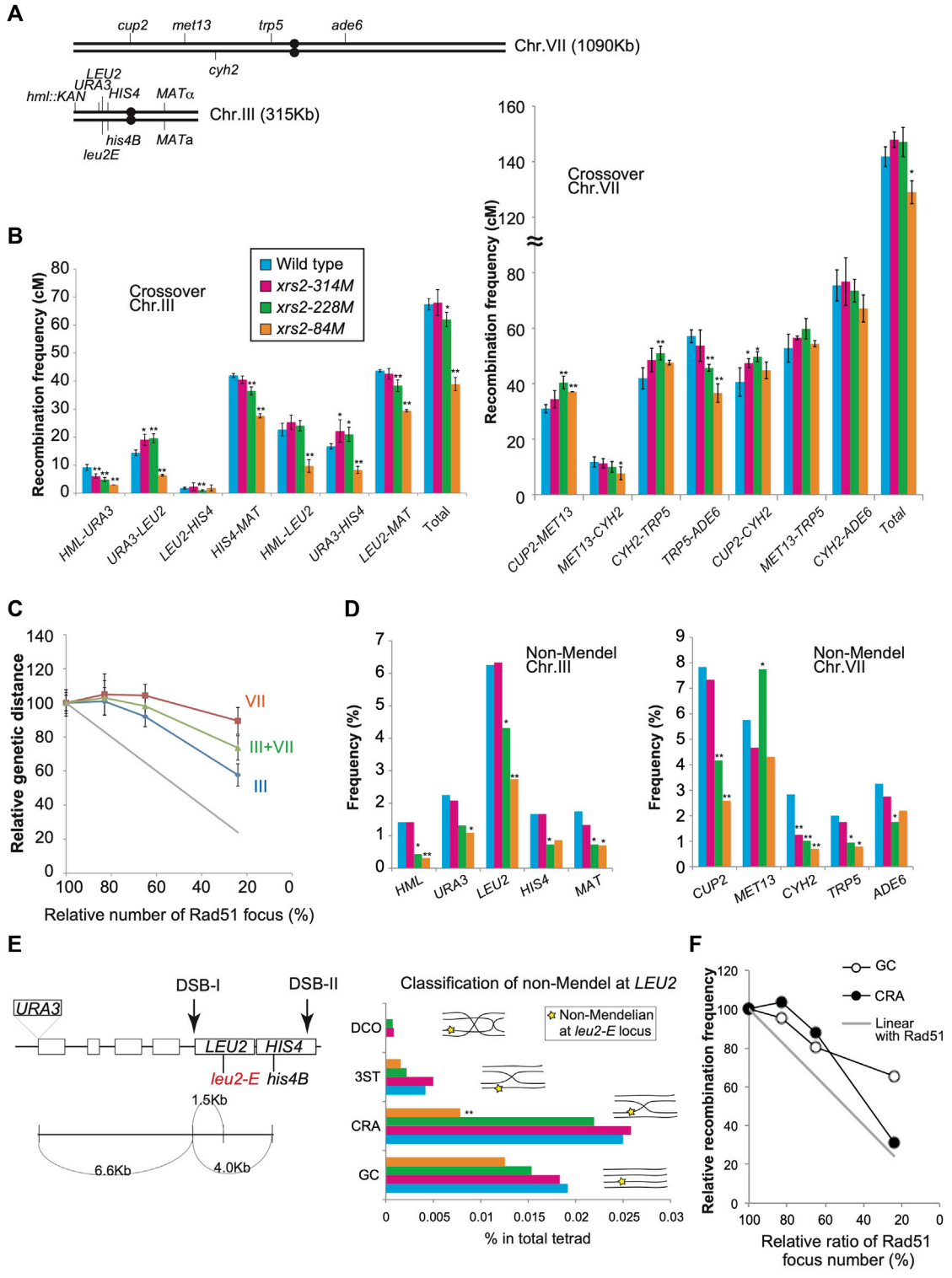

FIGURE 4
Genetic analysis of *xrs2* hypomorphic alleles. **(A)** Schematic representation of genetic markers on chromosomes VII and III. **(B)** CO frequencies within indicated genetic intervals on chromosomes III and VII. Genotypes are color-coded. Error bars indicate the standard deviation from four independent crosses. Wild-type (MSY4304/4245), *xrs2–314M* (MSY4314/4316), *xrs2–228M* (MSY4310/4312), and *xrs2–84M* (MSY4306/4308) were used. Statistical significances were calculated by using Student's t-test. **(C)** Relationships between the CO frequencies and DSB levels. The *x*-axis values indicate the mean number of Rad51 foci for each *xrs2* mutant relative to that in the wild type. The *y*-axis values indicate the mean genetic distance sums for each *xrs2* mutant relative to the wild type (for chromosomes III or VII). The gray line shows a linear relationship. **(D)** Non-Mendelian segregation frequencies at the indicated genetic loci are shown. Statistical differences were analyzed using Fisher's exact test with Yates correction. **(E)** Schematic representation of the *HIS4–LEU2* hotspot on chromosome III. Locations of the *leu2-E* and *his4B* mutations are shown. Rectangles represent genes. The non-Mendelian fraction at the *LEU2* locus was classified by analyzing the linkage of the *URA3*, *LEU2*, and *HIS4* loci. GC; gene conversion at the *LEU2* locus
(*Continued*)

FIGURE 4 (Continued)
without CO between *URA3* and *HIS4*; CRA; CO-associated gene conversion on the same strand as the CO, 3ST; CO-associated gene conversion on the strand lacking CO, DCO; gene conversion associated with a double CO. **(F)** Non-linear relationship of COs or NCOs derived from the non-Mendelian fraction at the *leu2-E*/*LEU2* heteroalleles. The *x*-axis values indicate the relative (the mean) numbers of Rad51 foci for each *xrs2* mutant relative to the wild type. The *y*-axis values indicate the relative frequencies of COs or NCOs for each *xrs2* mutant. The gray line shows a linear relationship. Asterisks indicate statistically significant differences between the *xrs2* mutant and wild type (**$p < 0.01$, *$p < 0.05$) (Supplementary Table S4).

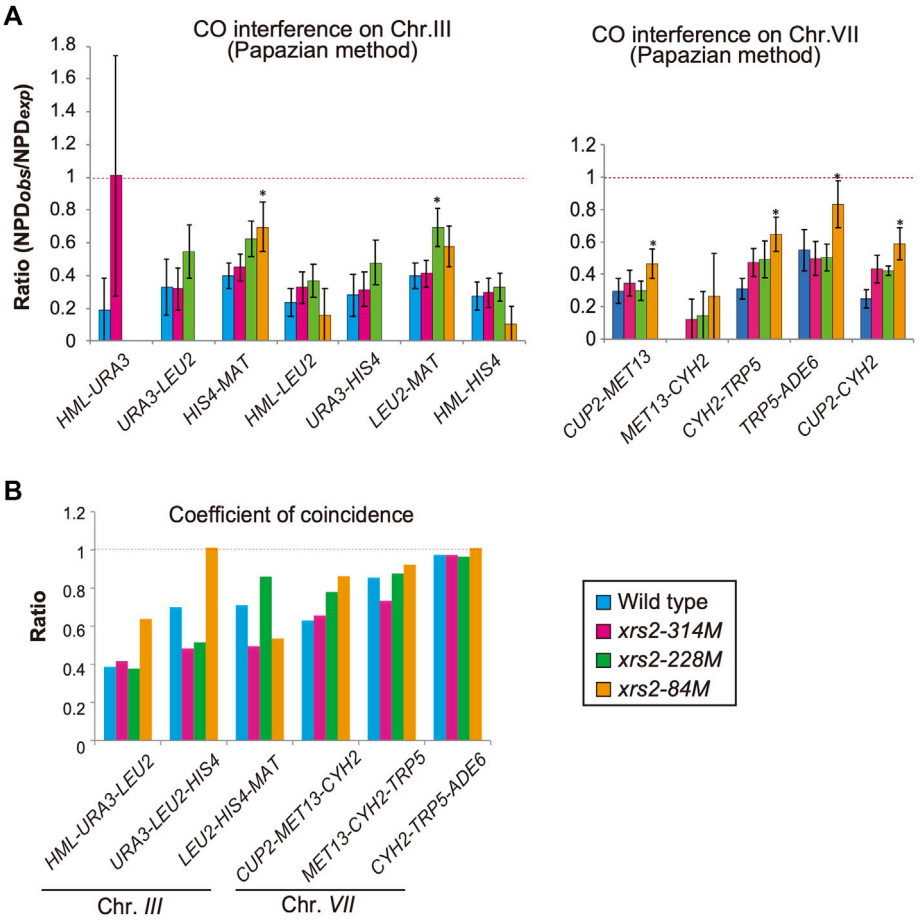

FIGURE 5
CO interference in *xrs2* mutants. **(A)** CO interference for indicated genetic intervals on chromosomes III and VII. Genotypes are color coded. The NPD_{obs}/NPD_{exp} ratio for three intervals was calculated from TT and PD (Supplementary Tables S2, S3). A ratio of 1 indicates no interference. A Ratio <1 indicates positive interference. Error bars indicate the standard error of NPD ratios and the statistical significance of the difference in NPD ratio between the wild type and each *xrs2* mutant was confirmed by an overlap of the SE value around the map distance or NPD ratio. (Supplementary Tables S2, S3). **(B)** The Coefficient of coincidence (CoC) of COs between adjacent intervals on chromosomes III and VII in wild-type and *xrs2* mutants are shown. A ratio of 1 indicates no interference. A ratio of <1 indicates positive interference.

Zip3 without Msh5 (Figure 3A; Supplementary Figure S1E). We speculate the presence of stepwise homeostatic response of ZMM-focus assembly in response to meiotic DSBs in a context-dependent manner (See Discussion).

CO homeostasis functions more effectively on chromosome VII

Using *spo11* alleles with ~80%, ~70%, and ~20% of wild-type DSB levels, Martini et al. (2006) showed CO homeostasis which maintains CO levels despite reduced meiotic DSBs. We, therefore, asked whether *xrs2* alleles with ~80%, ~65%, and ~25% of wild-type DSB levels also exhibited CO homeostasis since Zip3 foci showed non-linear response to reduced DSBs in the *spo11*-mutants, but not in the *xrs2* mutants. We measured CO and NCO frequencies by the dissection of tetrads for SK1 yeast strains with different genetic markers on chromosomes III and VII; a short chromosome (chromosome III with a synthetic recombination hotspot at the *HIS4* locus [*HIS4–LEU2*]) and a long chromosome (chromosome VII) (Higashide and Shinohara, 2016) (Figure 4A). We analyzed the segregation of genetic markers associated with these chromosomes

in >1,200 tetrads with four viable spores to calculate CO frequencies (in centimorgans; cM) for each strain (Supplementary Tables S2, S3); the number of tetrads analyzed was larger than that in the previous study (>750 four-viable tetrads; Martini et al., 2006). Tetrad analysis revealed that wild type of SK1 strain, *xrs2–314M*, *xrs2–228M*, and *xrs2–84M* strains had spore viabilities of 96.8%, 97.3%, 90.9%, and 52.4%, respectively (Table 1). The results of genetic analysis in wild-type controls (Figures 4, 5) are generally consistent with our previous report (Shima et al., 2005; Higashide and Shinohara, 2016; Shinohara et al., 2019). We assumed that DSB distribution in various *xrs2* strains is not altered and DSB levels are uniformly reduced along the genome, which is a simple but cautious assumption given that DSB formation was controlled in various ways (Yadav and Claeys Bouuaert, 2021) and DSBs are proceeded differentially in the mutant (see above).

Chromosome VII: The *xrs2–314M* (~80% DSBs) and *xrs2–228M* (~65%) mutants showed wild-type levels of total CO frequency between the *CUP2* and *ADE6* loci, 127.9 ± 14.6 (105%) and 127.1 ± 7.9 (104%) cM, respectively, compared with 121.8 ± 9.4 cM for wild type (Figure 4B; Supplementary Table S2). The *xrs2–84M* mutant (~25% DSBs) slightly, but significantly reduced CO frequency with 109 ± 9.6 cM (89%) relative to the wild type. These showed that CO levels responded non-linearly to a reduction of DSB frequencies (Figure 4C). This supports the CO homeostasis in response to DSB reduction (Martini et al., 2006). Among different intervals inspected, we see the interval-specific response to reduced DSB levels. The *xrs2–314M* mutant (~80% DSBs) showed similar CO frequencies in all intervals to the wild type. The *xrs2–228M* mutant (~65%) showed a slight reduction in the *TRP5-ADE6* interval and similar CO levels in the *MET13-CYH2* interval compared to the wild type. Interestingly, the mutant showed significantly increased CO frequencies in two intervals (*CUP2-MET13* and *CYH2-TRP5*) relative to the wild type. This increased response of CO frequencies in response to DSB was not reported in the previous study (Martini et al., 2006). For *xrs2–84M*, two of the four single intervals showed wild-type levels of CO, despite a 76% reduction in meiotic DSBs. While the *CUP2-MET13* interval increased the frequency compared to the wild type, the *TRP5-ADE6* interval in the mutant significantly reduced CO frequency.

Chromosome III: The *xrs2–314M* mutant (~80% DSB) showed wild-type levels of the total CO frequency between the *HML* and *MAT* loci, 68.0 ± 5.5 cM compared with 67.4 ± 3.1 cM for wild-type (Figure 4B; Supplementary Table S3). The *xrs2–228M* mutant (~65%) slightly decreased CO frequency of 62.0 ± 4.0 cM (92%). On the other hand, the *xrs2–84M* mutant (~25% DSBs) reduced 57.7% of the wild-type level (38.9 ± 4.4 cM), which is much higher than the expected frequency without the homeostasis (~16.9 cM). For each interval, the *xrs2–314M* mutant slightly decreased CO in one interval (*HML-URA3*) among four intervals on the chromosome. The *xrs2–228M* mutant (~65%) and the *xrs2–84M* mutant (~25% DSBs) showed decreased CO frequencies in two and three intervals, respectively. In the *LEU2-HIS4,* the *xrs2–314M* and *xrs2–228M* mutants maintained wild-type CO levels while the *xrs2–84M* mutant decreased COs relative to the control (see below). Taken together, these suggested that chromosome III is less robust for CO homeostasis than chromosome VII (Figure 4C). Similar results were obtained in the previous study although it was not emphasized (Martini et al., 2006). However, we do need more caution on the interpretation of recombination on chromosome III, since our strains, but not a previous strain, contains an unusual recombination hot spot, *HIS4–LEU2* on the chromosome.

When the combined CO frequencies on chromosomes III and VII are compared with the total DSBs level in the *xrs2* mutants, the CO frequencies are maintained even in the *xrs2–228M* mutant with ~65% DSBs (Figures 4B, C). This CO homeostasis is roughly correlated with that seen for Msh5 foci (Figure 2D).

NCO formation is sensitive to reduced levels of meiotic DSBs

Next, we analyzed frequencies non-Mendelian segregation at 10 genetic loci on chromosome III and VII in different *xrs2* alleles (Figure 4A). For *xrs2–228M* (~65% DSBs) mutant, four of five loci on chromosome III and four of five loci on chromosome VII showed significant decreases in non-Mendelian segregation frequencies (Figure 4D; Supplementary Table S4). The *xrs2–314M* mutant (~80% DSBs) reduced the frequency only at the *CYH2* locus. The *xrs2–228M* mutant, which maintains CO frequencies with 65% DSB reduction, seems to show reduced NCO. Strangely, the *xrs2–228M* mutant increased the frequency at the *MET13* locus. For the *xrs2-84M* (~25% DSBs), four of five loci on chromosome III and three of five loci on chromosome VII showed significant decreases in non-Mendelian segregation frequencies. The other three loci (*HIS4*, *MET13*, and *ADE6*) showed reduced frequencies relative to the wild type, but the difference is not significant. At the *LEU2*, *CUP2,* and *MET13* loci, frequencies in the *xrs2-84M* mutant are significantly lower than those in the *xrs2–228M* mutant. In most cases, however, except for the *HML* locus, reductions in non-Mendelian segregation were not proportional to reductions in meiotic DSBs, as reported (Martini et al., 2006) (Figure 4D; Supplementary Table S4).

HIS4-LEU2: Non-Mendelian segregation is thought to result from a simple gene conversion or mismatch repair of heteroduplexes formed during CO formation (Nicolas and Rossignol, 1983; White et al., 1985). The *URA3–LEU2–HIS4* interval on chromosome III has an artificial meiotic DSB hotspot (DSB-I) with *leu2E* mutation (an insertion allele of the *Eco*RI site) and *URA3* insertion (Figure 4E). As *leu2E* and the *URA3* insertion are very close to the DSB-I site (~1.5 and ~6.6 kb way, respectively), we assumed that *LEU2*/*leu2* gene conversion with or without flanking crossover would come from DSB-I. Non-Mendelian tetrads of *LEU2*/*leu2E* heteroalleles (3 Leu+: 1 Leu- or 1 Leu+: 3 Leu-segregation) were initially selected, and then sorted into four classes based on the linkage with flanking markers, *URA3* and/or *HIS4* alleles; GC, Gene conversion; CRA, Crossover associated gene conversion; DCO, double CO; three strands, 3ST, gene conversion associated with incidental CO (schematic figures in Figure 4E middle graph). A previous study showed 40% and 14% of wild-type levels of DSB-I in the *xrs2-228M* and *xrs2-84M* mutants, respectively (Shima et al., 2005). The *xrs2-228M* maintained ~90% of wild-type CO level (CRA and DCO classes). Moreover, decreased level of COs (CRA and DCO) in the *xrs2-84M* mutant (~30%) is much higher than reduced DSB levels (14%) at the locus. These support the idea that CO homeostasis is operating at this locus (Figure 4F), which was not seen in the

physical analysis of this locus in the previous study (Martini et al., 2006). GC frequencies were also reduced in response to decreased DSB levels (Figure 4F), although higher than expected in the *xrs2-228M* (80% to expected 40%) and *xrs2-84M* mutants (65% to expected 14%). These high frequencies of meiotic recombination in the *xrs2-228M* mutant cannot be explained by DSB-I. These might come from an event at DSBs other than DSB-I such as DSB-II.

Reduced levels of meiotic DSBs weaken CO interference

CO interference negatively regulates CO formation to maintain the appropriate number and spacing of COs (Muller, 1916). A previous study on CO interference in response to reduced DSBs (Martini et al., 2006) showed that the interference is maintained when DSB frequencies are reduced. To confirm this, we also analyzed CO interference in *xrs2* mutants using the same data described above. In each interval, the tetrads were classified into three classes with a different combination of flanking markers: parental ditypes (PD), tetra types (TT), and non-parental ditypes (NPD). NPD is a tetrad class with "double" COs involving four chromatids in an interval, whose an expected frequency, NPD_{exp}, is calculated from a frequency of the TT class, which mainly contains a single CO event in the interval (Papazian, 1952). First, we used the Papazian method to examine the ability of a CO to interfere with coincident COs in the interval by determining the ratio of observed NPD (NPD_{obs}) to NPD_{exp} (Figure 5A, Supplementary Tables S2, S3). In the wild type, the ratio of NPD_{obs} to NPD_{exp}, called the NPD ratio, is indicative of interference when the ratio is <1. Indeed, as reported previously (Higashide and Shinohara, 2016; Shinohara et al., 2019), the NPD ratio of seven intervals on chromosome III and VII in the wild type is 0.19–0.55 (Figure 5A; Supplementary Tables S2, S3), confirming CO interference within these intervals. In contrast, we did not detect any NPD tetrads within the *MET13-CYH2* interval after analyzing >1,200 tetrads, indicating the presence of a strong interference in this interval (Figure 5A; Supplementary Tables S2, S3).

We then analyzed tetrads for the *xrs2* mutants. For all *xrs2* mutants, the NPD ratio associated with each interval on chromosomes III and VII was <1 (except for *HML–URA3*) (Figure 5A; Supplementary Tables S2, S3). In all cases, the ratio is statistically significant from one (no interference), showing that the CO interference is maintained in the mutants. Although the NPD ratio at the *HML–URA3* in the *xrs2–314M* was about 1; the number of NPD_{obs} in this interval was too low (1 for wild type, 2 for *xrs2–314M*, and 0 for the other alleles) to draw any significant conclusions. As Papazian's NPD analysis requires an NPD fraction, which we could not obtain for some chromosome III intervals (e.g., *URA3-LEU2*) in *xrs2–84M* because of severe reductions of COs in the mutant. These suggest that CO interference could function even when the number of DSBs was reduced to 20% levels of the wild type. However, as discussed above, this idea depends on the similar DSB distribution along these reporter chromosomes in the *xrs2* mutants to that in the wild type.

When compared with the NPD ratios in various *xrs2* mutants with those in the wild type, we found that the NPD ratios in the *HIS4-MAT*, *CUP2-MET13*, *CYH2-TRP5*, and *TRP5-ADE6* intervals in the *xrs2–84M* mutant (~20% DSBs of wild type) are significantly higher

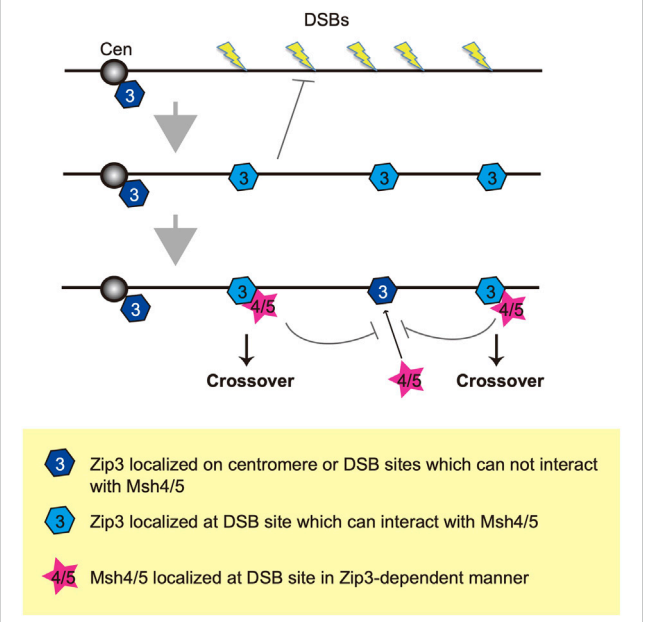

FIGURE 6
A model of two-step selection of CO formation through Zip3 and Msh4-Msh5. Once DSBs are formed on the chromosome, Zip3 may translocate onto roughly selected DSB sites and suppresses additional DSB formation. There are two kinds of modes of Zip3: One is localized at the DSB site and can recruit Msh4-Msh5 (pale blue) and another cannot recruit Msh4-Msh5 (dark blue). Then, the Msh4-Msh5 complex is recruited to the pro-CO site in a Zip3-dependent manner. Zip3 and Msh4-Msh5 suppress additional complex formation in a coordinated manner. Cen indiate a centromere.

than corresponding ratio in wild-type cells (Figure 5A; Supplementary Tables S2, S3). Higher NPD ratios in the mutant relative to the wild type are also observed in the *HIS4-MAT* and *CYH2-TRP5* intervals of the *xrs2–228M* mutant (~65% DSBs) as well as in the *CYH2-TRP5* intervals of the *xrs2–314M* mutant (~80% DSBs). These suggest weakened CO interference when DSB frequencies are reduced by the *xrs2* mutations.

We also analyzed the frequency of double COs in two adjacent intervals using the tetrad data (above) for the coefficient of coincidence (CoC; Figure 5B; Supplementary Table S5). CoC is a ratio of an observed number of tetrads with simultaneous COs in adjacent intervals to an expected number of double crossovers, which is obtained from frequencies of a CO in each interval (Muller, 1916). In the wild type, five adjacent intervals showed a CoC ratio <1 (CoC for *CYH2–TRP5–ADE6* is less than one but not statistically significant). The *xrs2–314M* and *xrs2–228M* mutants exhibited CoC ratios that were <1 for the five intervals. The *xrs2–84M* mutant showed CO interference for four adjacent intervals, but in the *URA3–LEU2–HIS4* interval the CoC was 1.01 (Figure 5B; Supplementary Table S5). This indicated that a ~80% reduction in meiotic DSBs caused a defect in CO interference at *HIS4–LEU2* hotspot on chromosome III, which is an abnormal response of the *xrs2–84M* mutant in CO and NCO formation (Figures 4E, F).

CoCs in the *xrs2* mutants were compared to those in the wild type. In the *xrs2–84M* mutant, CoC ratios are higher in four adjacent intervals, *HML-URA3-LEU2*, *URA3-LEU2-HIS4*, *CUP2-MET13-CYH2*, *MET13-CYH2-TRP5*, and *CYH2-TRP5-ADE6* while lower in one interval, *LEU2-HIS4-MAT*. The *xrs2–228M* mutant shows a

higher CoC ratio in the *LEU2-HIS4-MAT* and *LEU2-HIS4-MAT*, but lower in the *URA3-LEU2-HIS4*. These support the idea that CO interference is weakened when DSB frequencies are largely decreased by the *xrs2* mutations.

Discussion

Here we analyzed meiotic CO formation and the assembly of proteins involved in CO formation in *xrs2* hypomorphic mutants with different levels of DSB formation. The *xrs2–314M* and *xrs2–228M* mutants exhibited 20% and 35% reductions in meiotic DSBs, respectively, but wild-type levels of CO formation and spore viability. This indicated that CO homeostasis functions in the *xrs2* mutant cells, as it does in *spo11* mutants (Martini et al., 2006). In contrast, when DSBs were reduced by ~80%, which was the case in *xrs2–84M* mutant, CO homeostasis weakened. We also described the homeostatic response of the formation of foci containing a ZMM protein, Msh5, but not Zip3 in the *xrs2* mutants. These suggest that CO homeostasis is mediated by Msh5, thus, Msh5-containing MutSγ complex with Msh4.

Foci containing Msh5 exhibit homeostasis in response to reduced DSBs

By analyzing the number of foci containing different meiotic recombination proteins in an *xrs2* mutant with reduced meiotic DSB formation, we found a linear correlation of the number of ensembles containing ZMM/SIC proteins (Zip3, Mer3, and Spo22/Zip4, but not Msh5) as well as Rad51 and Dmc1 (Figure 2B). The steady-state number of these foci is similar among the proteins. If the lifespan of these foci is similar, we expect the same number of ensembles of these proteins. ZMM-focus formation is independent of Rad51/Dmc1-focus formation (Shinohara et al., 2008), although the formation of both Rad51/Dmc1 and ZMM foci requires the formation of ssDNAs at meiotic DSB sites. These suggested that ensembles containing Zip3, Mer3, and Spo22/Zip4 were closely associated with the ssDNA region near Rad51/Dmc1. This is consistent with recent biochemistry and genome-wide mapping of ZMM proteins including Zip3 which bind the DSB sites in addition to chromosome axes (Serrentino et al., 2013; De Muyt et al., 2018).

Although this study revealed the linear relationship of Zip3-focus number to DSB level in the *xrs2* mutants, a previous study showed a non-linear relationship between Zip3 foci and DSBs in *spo11* hypomorphic mutants (Henderson and Keeney, 2004). One critical difference between our study and this previous report was the antibody used to detect Zip3 foci. We used two independent raised polyclonal antibodies against recombinant Zip3 protein generated by our lab (see Materials and Methods) that detected 60.9 ± 8.6 (generated in rabbit) and 60.8 ± 14.5 (generated in rat) foci in wild-type zygotene/pachytene cells. This number is compatible with those reported for Zip3-myc (~60 foci) by two independent groups (Yoon et al., 2016; Hong et al., 2019; Tan et al., 2022). On the other hand, the previous report detected only 35.3 ± 6.2 foci of a Zip3-GFP fusion protein on elongated SCs in wild-type (*ZIP3-GFP*) cells using an antibody against GFP. GFP-tagging of Zip3 may therefore affect the chromosomal localization of Zip3 proteins. Alternatively, an anti-GFP antibody could detect only the subfraction of Zip3 on chromosomes, which is resistant to reduced DSB levels. Indeed, by using our Zip3 antibody, we also found a non-linear response of the Zip3-focus number in the *spo11* hypomorph mutants. A steady-state number of Msh5 foci (~40) is much lower than that of Zip3 and other recombination foci (~60). Given Msh4/5-focus kinetics is similar to those of Rad51/Dmc1 (Zhu et al., 2021 and here), a difference in the life span could not explain the difference in the number of foci, suggesting the presence of a distinct regulatory mechanism to assembly Msh5-ensembles than those of Rad51 and other ZMM proteins.

We propose two distinct homeostatic responses to the assembly of ZMM proteins to DSBs (Figure 6). First, DSB formation and/or associated regulatory mechanisms control the number of ensembles containing ZMM core proteins including Zip3. Second, a subset of Zip3 ensembles might be converted into ensembles with Msh4/Msh5. This second step is also under the control of DSB responses. The double-staining analysis of Zip3 with Msh5 (Figure 3B) supports the presence of two populations of Zip3 foci on meiotic chromosomes. Zip3 foci associated with Msh5 show a homeostatic response to DSBs and become brighter relative to early Zip3 foci (Figure 3A; Supplementary Figure S3E). This might be positive feedback of Zip3-focus formation once colocalized with Msh5. The first step seems to be sensitive to the N-terminal region of Xrs2 with the FHA domain. This region is critical for Tel1 (ATM)-mediated phosphorylation of Hop1-pT318 on meiotic chromosomes in the *rad50S* background (Iwasaki et al., 2016). Tel1 is shown to control a feedback mechanism of meiotic DSB formation (Anderson et al., 2015; Garcia et al., 2015). The *xrs2* mutation-specific effect of Zip3 homeostasis might be related to the Tel1 function, which should be studied in the future.

Msh5 foci show homeostatic response to reduced DSB levels, particularly in the *xrs2–314M* (~80% DSB level) and *xrs2–228M* mutants (~60% DSB level), which also show robust CO homeostasis. This suggests that Msh5, thus, the Msh4-Msh5 complex (MutSγ) is a critical machinery for CO homeostasis. As the Msh4-Msh5 complex stabilized recombination intermediates (Snowden et al., 2004; Cannavo et al., 2020; Kulkarni et al., 2020), it was previously reported that MutSγ recruitment is a critical step in the CO/NCO decision and for CO interference (Bishop and Zickler, 2004; Snowden et al., 2004; Stahl et al., 2004; Shinohara et al., 2008). The MutSγ complex seems to be a key effector for CO control during meiosis. Alternatively, the complex is a downstream readout for the control.

In mouse spermatocytes, MutSγ foci persist longer in late zygotene/early pachytene stages relative to RAD51/DMC1 foci (Moens et al., 2002). Moreover, the number of MSH4-MSH5 foci is less than RAD51/DMC1 foci but is more than MLH1-MLH3 (MutLγ) foci, suggesting the step-wise implementation of ZMM foci for CO formation/control during mouse meiotic prophase I (Reynolds et al., 2013; Qiao et al., 2014). Similarly in *Sordaria*, MSH4 foci appear in early meiotic prophase than MLH1 foci and the number of MSH4 is higher than that of MLH1 (Storlazzi et al., 2010). Interestingly, a recent study showed a chromosomal localization of a tagged version of Mlh1 in the budding yeast and the number of Mlh1 foci is less than ZMM foci in wild type, supporting a regulatory transition from MutSγ to MutLγ is operating in yeast meiosis (Sanchez et al., 2020).

Prior to Msh4-Msh5 assembly, Zip3 is recruited to chromosomes and promotes the assembly of Msh4-Msh5 (Shinohara et al., 2008). We found that 94% of Msh5 foci contained Zip3 foci (Figure 3). A constant Msh5 foci (42-45) level was maintained in each nucleus when CO homeostasis was functioning (Figures 2, 3). The Msh5-Zip3 colocalization frequency was reduced, however, when CO homeostasis was compromised, i.e., in *xrs2–84M* mutant cells. We hypothesize that Zip3-dependent recruitment of Msh4-Msh5 complexes to DSB sites is critical in CO homeostasis and interference. Again, in both mouse spermatocytes and *Sordaria* meiosis, Zip3 orthologues, Rnf212 and Hei10 (and also Mer3/Hfm1 foci) appear earlier than Msh4 foci (Reynolds et al., 2013; Qiao et al., 2014; De Muyt et al., 2018; Dubois et al., 2019). Thus, it is likely that a Zip3-dependent assembly of the Msh4-Msh5 complex in CO formation/control is evolutionarily conserved.

Previous cytological studies on ZMM foci such as Zip3 revealed that Zip3 foci are evenly spaced along chromosome axes (Fung et al., 2004; Zhang et al., 2020). Based on these, the establishment of the CO designation may occur prior to ZMM assembly. Since the number of Msh5 foci maintain on chromosomes when DSB frequencies are reduced, Msh5-mediated CO homeostasis might operate after the CO designation thus, CO interference and/or CO assurances.

In this study, we observed homeostatic responses to ZMM protein to reduced DSBs in a context-dependent manner, which includes a type of mutant, a tag to the protein, and antibodies or a combination of antibodies used for the immuno-staining. Thus, we need a more careful evaluation of the conclusion obtained by cytological analyses.

CO homeostasis varies between a short and a long chromosome

A previous study by Martini et al. (2006) analyzed CO homeostasis on chromosome III (3 intervals), VII (3 intervals), and VIII (2 intervals) in *spo11* mutants and focused on the effect of reduced DSB levels on total COs on all three chromosomes but did not study the chromosome-specific variation of CO homeostasis in detail. In this study, by analyzing one more additional interval in both chromosome III and VII, we not only confirmed "global" CO homeostasis but also examined the chromosome-specific effect on CO homeostasis. In CO homeostasis, the relatively short chromosome III was more sensitive to DSB reductions than the longer chromosome VII (Figure 4C).

In the wild type, five of seven intervals on chromosome III (*URA3–LEU2*, *HIS4–MAT*, *HML–LEU2*, *URA3–HIS4*, and *LEU2–MAT*) were genetically longer than the *MET13–CYH2* interval (12 cM) on chromosome VII (Figure 2B; Supplementary Tables S2, S3). CO frequency associated with the *MET13–CYH2* interval was only mildly affected as DSBs were reduced to ~20% (in the *xrs2–84M* mutant). In contrast, the five intervals on chromosome III showed significant reductions in CO frequencies ($p < 0.001$) in the *xrs2–84M* mutant. This suggested that chromosome III is more sensitive to DSB reductions than chromosome VII. CO homeostasis likely works in a long chromosome better than a short chromosome. Alternatively, given that, together with the two shortest chromosomes I and VI, chromosome III is unique in the regulation of DSB formation (Murakami et al., 2020), rather than chromosome length by itself, the chromosome-specific property may determine the level of CO homeostasis.

We observed reduced and increased CO frequencies in *MET13–CYH2* and *CYH2–TRP5*, respectively, in the three *xrs2* mutants. These intervals previously analyzed in *spo11* hypomorphic mutants (Martini et al., 2006) exhibited similar tendencies. This suggests that different intervals exhibit different sensitivities or responses to reduced frequencies of DSBs, even for intervals on the same chromosome. In addition, we found that the *xrs2–314M* mutant (~65% DSBs) showed weakened CO homeostasis in two intervals that spanned a centromere, *HIS4–MAT* and *TRP5–ADE6* compared to other intervals, which is consistent with the suggestion that centromeres may represent a barrier for CO homeostasis, as has been suggested (Martini et al., 2006).

COs were maintained at the expense of NCO, and reduced level of DSBs weakened CO interference

NCOs tend to be more sensitive to DSB reductions than COs in a manner that is independent of chromosome size. This is particularly seen in the *xrs2–228M* mutant (~65% DSBs), which showed reduced NCO frequencies at 9 loci while maintaining wild-type levels of COs. COs may be maintained at the expense of NCOs, roughly as proposed (Martini et al., 2006). On the other hand, CO and NCO formation showed similar responses to severe reductions in meiotic DSBs (i.e., they did not simply compensate for one another in the case of *xrs2–84M* mutant), suggesting that CO and NCO were controlled through different mechanisms, consistent with previous reports that NCOs differentiate earlier than CO in DSB processing (Allers and Lichten, 2001; Hunter and Kleckner, 2001). Moreover, these suggested that, in CO homeostasis, certain thresholds of DSBs might upregulate meiotic CO formation within each chromosome or genetic interval.

Although CO interference function even when DSBs were reduced by 80% (*xrs2–84M* mutant), we observed CO interference with reduced its strength. Moreover, for the *URA3–LEU2–HIS4* interval on chromosome III, no CO interference was seen in the *xrs2–84M* mutant (Figure 5B). In addition, the non-Mendelian fraction associated with CO (CRA class) at this locus showed reduced CO homeostasis in the *xrs2–84M* mutant (Figure 4F). This suggested that there might be a coordinating mechanism between CO interference and CO homeostasis, as well as DSB formation.

We note a remarkable difference between reductions in the relative ratio of Msh5 foci and CO frequency, which dropped to 38.6% and 73.6% of wild type, respectively, in the *xrs2–84M* mutant (Figure 2B, 4C). One possibility is that reduced DSB frequencies may stimulate ZMM-independent CO formation pathway(s) that are out of CO interference regulation (Sym et al., 1993; Shinohara et al., 2008). SC elongation is required for the downregulation of meiotic DSB formation (Xu et al., 1995; Tung et al., 2000; Carballo et al., 2013; Gray et al., 2013; Rockmill et al., 2013). The completion of SC elongation may provide a signal that there are sufficient DSBs to generate COs and control CO formation. In contrast, incomplete SC elongation may promote additional meiotic DSB formation which may result in the

formation of non-interfering COs (Lee et al., 2021). SC elongation may be involved in CO homeostasis by regulating DSB formation (and non-interfering CO). In the *xrs2–84M* mutant, which had 76% fewer DSBs of the wild type, elongation of Zip1 was severely reduced, whereas CO interference still functions, albeit at reduced effectiveness. This indicated that Zip1 elongation was not critical for CO interference as proposed previously (Zhang et al., 2014).

Data availability statement

The original contributions presented in the study are included in the article/Supplementary Material, further inquiries can be directed to the corresponding author.

Author contributions

MS and AS conceived the study. MS performed all experiments. MS and AS analyzed the data. MS initially wrote the manuscript, MS and AS finalized the paper. All authors listed have made a substantial, direct, and intellectual contribution to the work and approved it for publication.

Funding

This work was supported by a Grant-in-Aid from the JSPS KAKENHI Grant Number; 16H04742, 19H00981 to AS, 19K22402 to MS.

Acknowledgments

We are grateful to N. Kleckner, S. Keeney, and Neil Hunter for helpful discussion and critical reading of the manuscript. We thank S. Umetani, M. Kitamura, A. Okabe, H. Wakabayashi, A. Tokumura, and A. Murakami for their excellent technical assistance. We also thank N. Hunter for providing yeast strains.

Conflict of interest

The authors declare that the research was conducted in the absence of any commercial or financial relationships that could be construed as a potential conflict of interest.

Publisher's note

Supplementary material

The Supplementary Material for this article can be found online at: https://www.frontiersin.org/articles/10.3389/fcell.2023.1170689/full#supplementary-material

SUPPLEMENTARY FIGURE S1
Rad51 focus formation in the *spo11* hypomorph mutants. **(A)** Y-axis showed an average number of Rad51 foci in nuclei in wild type (100%), *spo11-HA*/*spo11-HA* (80%), *spo11-HA*/*spo11-YF* (30%), and *spo11-YF*/*spo11-YF* (0%). Values of the X-axis were referred from Martini *et al.* (Martini et al., 2006). Error bars indicate standard deviations from independent trials (left). The distribution of the number of Rad51 foci in wild-type and *spo11* hypomorph mutants (raw values) is shown. Error bars show medians and interquartile ranges. **(B)** The distributions of the number of Zip3 and Msh5 foci in wild-type and *spo11* hypomorph mutants are shown. Error bars show medians and interquartile ranges. The numbers at the top of the graph indicate the median value. The statistical significance of differences was determined using the Mann-Whitney *U*-test (****$p < 0.0001$). **(C)** The average number of Zip3 and Msh5 foci plotted in each *spo11* mutant strain (left). Values are presented as a ratio relative to the wild type against each relative number of Rad51 foci [i.e., DSBs, **(A)**] in each strain (right).

SUPPLEMENTARY FIGURE S2
Hop1 localization in the BRCT-like domain-deleted *xrs2* mutant Localization of Zip1 (red; rabbit) and Hop1 (green; guinea pig) in wild type, *xrs2-314M*, and *pch2* mutant cells are shown. Scale bar = 2 μm.

SUPPLEMENTARY FIGURE S3
Comparison of focus number of Zip3 and Msh5 in various *xrs2* mutants. **(A)** The number of foci of Zip3 and Msh5 per nucleus in different time points after meiosis entry in wild type, *xrs2-84M*, *xrs2-228M*, and *xrs2-314M*. Error bars show medians and interquartile ranges. **(B)** The number of foci of Zip3 and Msh5 per nucleus from Figure 2B was shown in a scatter dot plot. The number of nuclei analyzed for Figure 2; wild type, *xrs2-84M*, *xrs2-228M*, and *xrs2-314M* are 459, 416, 542, and 339, respectively (Zip3 foci), and 454, 338, 345, and 219, respectively (Msh5 foci). Error bars show medians and interquartile ranges. **(C)** The number of Zip3- and Msh5-foci from co-localization analysis shown in Figure 3 is shown in a scatter dot plot. Error bars show medians and interquartile ranges. **(D)** Kinetics of frequency of Zip3- and Msh5-focus positive nuclei in wild type, *xrs2–228M*, and *xrs2–84M* during meiosis. Error bars show the average and SD. **(E)** The fluorescent signal intensity of Zip3 foci colocalized with or without Msh5 foci was measured and plotted. The *p*-value was calculated with Mann-Whitney *U*-test. Note the number of Zip3 alone foci is smaller than that of Zip3 foci with Msh5 (Figure 3B).

References

Agarwal, S., and Roeder, G. S. (2000). Zip3 provides a link between recombination enzymes and synaptonemal complex proteins. *Cell* 102 (2), 245–255. doi:10.1016/s0092-8674(00)00029-5

Alani, E., Padmore, R., and Kleckner, N. (1990). Analysis of wild-type and rad50 mutants of yeast suggests an intimate relationship between meiotic chromosome synapsis and recombination. *Cell* 61 (3), 419–436. doi:10.1016/0092-8674(90)90524-i

Allers, T., and Lichten, M. (2001). Differential timing and control of noncrossover and crossover recombination during meiosis. *Cell* 106 (1), 47–57. doi:10.1016/s0092-8674(01)00416-0

Anderson, C. M., Oke, A., Yam, P., Zhuge, T., and Fung, J. C. (2015). Reduced crossover interference and increased ZMM-independent recombination in the absence of Tel1/ATM. *PLoS Genet.* 11 (8), e1005478. doi:10.1371/journal.pgen.1005478

Arora, C., Kee, K., Maleki, S., and Keeney, S. (2004). Antiviral protein Ski8 is a direct partner of Spo11 in meiotic DNA break formation, independent of its cytoplasmic role in RNA metabolism. *Mol. Cell* 13 (4), 549–559. doi:10.1016/s1097-2765(04)00063-2

Arora, K., and Corbett, K. D. (2019). The conserved XPF:ERCC1-like Zip2:Spo16 complex controls meiotic crossover formation through structure-specific DNA binding. *Nucleic Acids Res.* 47 (5), 2365–2376. doi:10.1093/nar/gky1273

Bani Ismail, M., Shinohara, M., and Shinohara, A. (2014). Dot1-dependent histone H3K79 methylation promotes the formation of meiotic double-strand breaks in the absence of histone H3K4 methylation in budding yeast. *PLoS One* 9 (5), e96648. doi:10.1371/journal.pone.0096648

Bergerat, A., de Massy, B., Gadelle, D., Varoutas, P. C., Nicolas, A., and Forterre, P. (1997). An atypical topoisomerase II from Archaea with implications for meiotic recombination. *Nature* 386 (6623), 414–417. doi:10.1038/386414a0

Bishop, D. K., Park, D., Xu, L., and Kleckner, N. (1992). DMC1: A meiosis-specific yeast homolog of *E. coli* recA required for recombination, synaptonemal complex formation, and cell cycle progression. *Cell* 69 (3), 439–456. doi:10.1016/0092-8674(92)90446-j

Bishop, D. K. (1994). RecA homologs Dmc1 and Rad51 interact to form multiple nuclear complexes prior to meiotic chromosome synapsis. *Cell* 79 (6), 1081–1092. doi:10.1016/0092-8674(94)90038-8

Bishop, D. K., and Zickler, D. (2004). Early decision; meiotic crossover interference prior to stable strand exchange and synapsis. *Cell* 117 (1), 9–15. doi:10.1016/s0092-8674(04)00297-1

Borner, G. V., Barot, A., and Kleckner, N. (2008). Yeast Pch2 promotes domainal axis organization, timely recombination progression, and arrest of defective recombinosomes during meiosis. *Proc. Natl. Acad. Sci. U. S. A.* 105 (9), 3327–3332. doi:10.1073/pnas.0711864105

Borner, G. V., Kleckner, N., and Hunter, N. (2004). Crossover/noncrossover differentiation, synaptonemal complex formation, and regulatory surveillance at the leptotene/zygotene transition of meiosis. *Cell* 117 (1), 29–45. doi:10.1016/s0092-8674(04)00292-2

Cannavo, E., Sanchez, A., Anand, R., Ranjha, L., Hugener, J., Adam, C., et al.(2020). Regulation of the MLH1-MLH3 endonuclease in meiosis. *Nature* 586 (7830), 618–622. doi:10.1038/s41586-020-2592-2

Carballo, J. A., Panizza, S., Serrentino, M. E., Johnson, A. L., Geymonat, M., Borde, V., et al.(2013). Budding yeast ATM/ATR control meiotic double-strand break (DSB) levels by down-regulating Rec114, an essential component of the DSB-machinery. *PLoS Genet.* 9 (6), e1003545. doi:10.1371/journal.pgen.1003545

Cheng, C. H., Lo, Y. H., Liang, S. S., Ti, S. C., Lin, F. M., Yeh, C. H., et al.(2006). SUMO modifications control assembly of synaptonemal complex and polycomplex in meiosis of *Saccharomyces cerevisiae*. *Genes Dev.* 20 (15), 2067–2081. doi:10.1101/gad.1430406

Claeys Bouuaert, C., Tischfield, S. E., Pu, S., Mimitou, E. P., Arias-Palomo, E., Berger, J. M., et al.(2021). Structural and functional characterization of the Spo11 core complex. *Nat. Struct. Mol. Biol.* 28 (1), 92–102. doi:10.1038/s41594-020-00534-w

Dai, J., Sanchez, A., Adam, C., Ranjha, L., Reginato, G., Chervy, P., et al.(2021). Molecular basis of the dual role of the Mlh1-Mlh3 endonuclease in MMR and in meiotic crossover formation. *Proc. Natl. Acad. Sci. U. S. A.* 118 (23), e2022704118. doi:10.1073/pnas.2022704118

De Muyt, A., Pyatnitskaya, A., Andreani, J., Ranjha, L., Ramus, C., Laureau, R., et al.(2018). A meiotic XPF-ERCC1-like complex recognizes joint molecule recombination intermediates to promote crossover formation. *Genes Dev.* 32 (3-4), 283–296. doi:10.1101/gad.308510.117

Dubois, E., De Muyt, A., Soyer, J. L., Budin, K., Legras, M., Piolot, T., et al.(2019). Building bridges to move recombination complexes. *Proc. Natl. Acad. Sci. U. S. A.* 116 (25), 12400–12409. doi:10.1073/pnas.1901237116

Fung, J. C., Rockmill, B., Odell, M., and Roeder, G. S. (2004). Imposition of crossover interference through the nonrandom distribution of synapsis initiation complexes. *Cell* 116 (6), 795–802. doi:10.1016/s0092-8674(04)00249-1

Garcia, V., Gray, S., Allison, R. M., Cooper, T. J., and Neale, M. J. (2015). Tel1(ATM)-mediated interference suppresses clustered meiotic double-strand-break formation. *Nature* 520 (7545), 114–118. doi:10.1038/nature13993

Gray, S., Allison, R. M., Garcia, V., Goldman, A. S., and Neale, M. J. (2013). Positive regulation of meiotic DNA double-strand break formation by activation of the DNA damage checkpoint kinase Mec1(ATR). *Open Biol.* 3 (7), 130019. doi:10.1098/rsob.130019

Henderson, K. A., and Keeney, S. (2004). Tying synaptonemal complex initiation to the formation and programmed repair of DNA double-strand breaks. *Proc. Natl. Acad. Sci. U. S. A.* 101 (13), 4519–4524. doi:10.1073/pnas.0400843101

Higashide, M., and Shinohara, M. (2016). Budding yeast SLX4 contributes to the appropriate distribution of crossovers and meiotic double-strand break formation on bivalents during meiosis. *G3 (Bethesda)* 6 (7), 2033–2042. doi:10.1534/g3.116.029488

Ho, H. C., and Burgess, S. M. (2011). Pch2 acts through Xrs2 and Tel1/ATM to modulate interhomolog bias and checkpoint function during meiosis. *PLoS Genet.* 7 (11), e1002351. doi:10.1371/journal.pgen.1002351

Hollingsworth, N. M., Ponte, L., and Halsey, C. (1995). MSH5, a novel MutS homolog, facilitates meiotic reciprocal recombination between homologs in *Saccharomyces cerevisiae* but not mismatch repair. *Genes Dev.* 9 (14), 1728–1739. doi:10.1101/gad.9.14.1728

Hong, S., Joo, J. H., Yun, H., Kleckner, N., and Kim, K. P. (2019). Recruitment of Rec8, Pds5 and Rad61/Wapl to meiotic homolog pairing, recombination, axis formation and S-phase. *Nucleic Acids Res.* 47 (22), 11691–11708. doi:10.1093/nar/gkz903

Hunter, N., and Kleckner, N. (2001). The single-end invasion: An asymmetric intermediate at the double-strand break to double-holliday junction transition of meiotic recombination. *Cell* 106 (1), 59–70. doi:10.1016/s0092-8674(01)00430-5

Iwasaki, D., Hayashihara, K., Shima, H., Higashide, M., Terasawa, M., Gasser, S. M., et al.(2016). The MRX complex ensures NHEJ fidelity through multiple pathways including xrs2-FHA-dependent Tel1 activation. *PLoS Genet.* 12 (3), e1005942. doi:10.1371/journal.pgen.1005942

Johzuka, K., and Ogawa, H. (1995). Interaction of Mre11 and Rad50: Two proteins required for DNA repair and meiosis-specific double-strand break formation in *Saccharomyces cerevisiae*. *Genetics* 139 (4), 1521–1532. doi:10.1093/genetics/139.4.1521

Jones, G. H. (1984). The control of chiasma distribution. *Symp. Soc. Exp. Biol.* 38, 293–320.

Kee, K., Protacio, R. U., Arora, C., and Keeney, S. (2004). Spatial organization and dynamics of the association of Rec102 and Rec104 with meiotic chromosomes. *EMBO J.* 23 (8), 1815–1824. doi:10.1038/sj.emboj.7600184

Keeney, S., Giroux, C. N., and Kleckner, N. (1997). Meiosis-specific DNA double-strand breaks are catalyzed by Spo11, a member of a widely conserved protein family. *Cell* 88 (3), 375–384. doi:10.1016/s0092-8674(00)81876-0

Kleckner, N. (2006). Chiasma formation: chromatin/axis interplay and the role(s) of the synaptonemal complex. *Chromosoma* 115 (3), 175–194. doi:10.1007/s00412-006-0055-7

Kulkarni, D. S., Owens, S. N., Honda, M., Ito, M., Yang, Y., Corrigan, M. W., et al.(2020). PCNA activates the MutLγ endonuclease to promote meiotic crossing over. *Nature* 586 (7830), 623–627. doi:10.1038/s41586-020-2645-6

Lee, M. S., Higashide, M. T., Choi, H., Li, K., Hong, S., Lee, K., et al.(2021). The synaptonemal complex central region modulates crossover pathways and feedback control of meiotic double-strand break formation. *Nucleic Acids Res.* 49 (13), 7537–7553. doi:10.1093/nar/gkab566

Maleki, S., Neale, M. J., Arora, C., Henderson, K. A., and Keeney, S. (2007). Interactions between Mei4, Rec114, and other proteins required for meiotic DNA double-strand break formation in *Saccharomyces cerevisiae*. *Chromosoma* 116 (5), 471–486. doi:10.1007/s00412-007-0111-y

Martini, E., Diaz, R. L., Hunter, N., and Keeney, S. (2006). Crossover homeostasis in yeast meiosis. *Cell* 126 (2), 285–295. doi:10.1016/j.cell.2006.05.044

Matsuzaki, K., Shinohara, A., and Shinohara, M. (2008). Forkhead-associated domain of yeast Xrs2, a homolog of human Nbs1, promotes nonhomologous end joining through interaction with a ligase IV partner protein, Lif1. *Genetics* 179 (1), 213–225. doi:10.1534/genetics.107.079236

Matsuzaki, K., Terasawa, M., Iwasaki, D., Higashide, M., and Shinohara, M. (2012). Cyclin-dependent kinase-dependent phosphorylation of Lif1 and Sae2 controls imprecise nonhomologous end joining accompanied by double-strand break resection. *Genes cells.* 17 (6), 473–493. doi:10.1111/j.1365-2443.2012.01602.x

Mimitou, E. P., and Symington, L. S. (2009). DNA end resection: Many nucleases make light work. *DNA Repair (Amst)* 8 (9), 983–995. doi:10.1016/j.dnarep.2009.04.017

Moens, P. B., Kolas, N. K., Tarsounas, M., Marcon, E., Cohen, P. E., and Spyropoulos, B. (2002). The time course and chromosomal localization of recombination-related proteins at meiosis in the mouse are compatible with models that can resolve the early DNA-DNA interactions without reciprocal recombination. *J. Cell Sci.* 115 (8), 1611–1622. doi:10.1242/jcs.115.8.1611

Muller, H. J. (1916). The mechanism of crossing-over. *Am. Nat.* 50, 193–221. doi:10.1086/279534

Murakami, H., Lam, I., Huang, P. C., Song, J., van Overbeek, M., and Keeney, S. (2020). Multilayered mechanisms ensure that short chromosomes recombine in meiosis. *Nature* 582 (7810), 124–128. doi:10.1038/s41586-020-2248-2

Nakagawa, T., Flores-Rozas, H., and Kolodner, R. D. (2001). The MER3 helicase involved in meiotic crossing over is stimulated by single-stranded DNA-binding proteins and unwinds DNA in the 3' to 5' direction. *J. Biol. Chem.* 276 (34), 31487–31493. doi:10.1074/jbc.M104003200

Nakagawa, T., and Ogawa, H. (1999). The *Saccharomyces cerevisiae* MER3 gene, encoding a novel helicase-like protein, is required for crossover control in meiosis. *EMBO J.* 18 (20), 5714–5723. doi:10.1093/emboj/18.20.5714

Nandanan, K. G., Salim, S., Pankajam, A. V., Shinohara, M., Lin, G., Chakraborty, P., et al.(2021). Regulation of Msh4-Msh5 association with meiotic chromosomes in budding yeast. *Genetics* 219 (2), iyab102. doi:10.1093/genetics/iyab102

Nicolas, A., and Rossignol, J. L. (1983). Gene conversion: Point-mutation heterozygosities lower heteroduplex formation. *EMBO J.* 2 (12), 2265–2270. doi:10.1002/j.1460-2075.1983.tb01733.x

Nishant, K. T., Chen, C., Shinohara, M., Shinohara, A., and Alani, E. (2010). Genetic analysis of baker's yeast msh4-msh5 reveals a threshold crossover level for meiotic viability. *Plos Genet.* 6 (8), e1001083. doi:10.1371/journal.pgen.1001083

Novak, J. E., Ross-Macdonald, P. B., and Roeder, G. S. (2001). The budding yeast Msh4 protein functions in chromosome synapsis and the regulation of crossover distribution. *Genetics* 158 (3), 1013–1025. doi:10.1093/genetics/158.3.1013

Padmore, R., Cao, L., and Kleckner, N. (1991). Temporal comparison of recombination and synaptonemal complex formation during meiosis in *S. cerevisiae*. *Cell* 66 (6), 1239–1256. doi:10.1016/0092-8674(91)90046-2

Palmbos, P. L., Daley, J. M., and Wilson, T. E. (2005). Mutations of the Yku80 C terminus and Xrs2 FHA domain specifically block yeast nonhomologous end joining. *Mol. Cell Biol.* 25 (24), 10782–10790. doi:10.1128/MCB.25.24.10782-10790.2005

Pan, J., Sasaki, M., Kniewel, R., Murakami, H., Blitzblau, H. G., Tischfield, S. E., et al.(2011). A hierarchical combination of factors shapes the genome-wide topography of yeast meiotic recombination initiation. *Cell* 144 (5), 719–731. doi:10.1016/j.cell.2011.02.009

Papazian, H. P. (1952). The analysis of tetrad data. *Genetics* 37 (2), 175–188. doi:10.1093/genetics/37.2.175

Perkins, D. D. (1949). Biochemical mutants in the smut fungus ustilago maydis. *Genetics* 34 (5), 607–626. doi:10.1093/genetics/34.5.607

Perry, J., Kleckner, N., and Borner, G. V. (2005). Bioinformatic analyses implicate the collaborating meiotic crossover/chiasma proteins Zip2, Zip3, and Spo22/Zip4 in ubiquitin labeling. *Proc. Natl. Acad. Sci. U. S. A.* 102 (49), 17594–17599. doi:10.1073/pnas.0508581102

Qiao, H., Prasada Rao, H. B., Yang, Y., Fong, J. H., Cloutier, J. M., Deacon, D. C., et al.(2014). Antagonistic roles of ubiquitin ligase HEI10 and SUMO ligase RNF212 regulate meiotic recombination. *Nat. Genet.* 46 (2), 194–199. doi:10.1038/ng.2858

Reynolds, A., Qiao, H., Yang, Y., Chen, J. K., Jackson, N., Biswas, K., et al.(2013). RNF212 is a dosage-sensitive regulator of crossing-over during mammalian meiosis. *Nat. Genet.* 45 (3), 269–278. doi:10.1038/ng.2541

Robert, T., Nore, A., Brun, C., Maffre, C., Crimi, B., Bourbon, H. M., et al.(2016). The TopoVIB-Like protein family is required for meiotic DNA double-strand break formation. *Science* 351 (6276), 943–949. doi:10.1126/science.aad5309

Rockmill, B., Lefrancois, P., Voelkel-Meiman, K., Oke, A., Roeder, G. S., and Fung, J. C. (2013). High throughput sequencing reveals alterations in the recombination signatures with diminishing Spo11 activity. *PLoS Genet.* 9 (10), e1003932. doi:10.1371/journal.pgen.1003932

San-Segundo, P. A., and Roeder, G. S. (1999). Pch2 links chromatin silencing to meiotic checkpoint control. *Cell* 97 (3), 313–324. doi:10.1016/s0092-8674(00)80741-2

Sanchez, A., Adam, C., Rauh, F., Duroc, Y., Ranjha, L., Lombard, B., et al.(2020). Exo1 recruits Cdc5 polo kinase to MutLγ to ensure efficient meiotic crossover formation. *Proc. Natl. Acad. Sci. U. S. A.* 117 (48), 30577–30588. doi:10.1073/pnas.2013012117

Sasanuma, H., Tawaramoto, M. S., Lao, J. P., Hosaka, H., Sanda, E., Suzuki, M., et al.(2013). A new protein complex promoting the assembly of Rad51 filaments. *Nat. Commun.* 4, 1676. doi:10.1038/ncomms2678

Schwacha, A., and Kleckner, N. (1995). Identification of double Holliday junctions as intermediates in meiotic recombination. *Cell* 83 (5), 783–791. doi:10.1016/0092-8674(95)90191-4

Schwacha, A., and Kleckner, N. (1994). Identification of joint molecules that form frequently between homologs but rarely between sister chromatids during yeast meiosis. *Cell* 76 (1), 51–63. doi:10.1016/0092-8674(94)90172-4

Serrentino, M. E., Chaplais, E., Sommermeyer, V., and Borde, V. (2013). Differential association of the conserved SUMO ligase Zip3 with meiotic double-strand break sites reveals regional variations in the outcome of meiotic recombination. *PLoS Genet.* 9 (4), e1003416. doi:10.1371/journal.pgen.1003416

Shima, H., Suzuki, M., and Shinohara, M. (2005). Isolation and characterization of novel xrs2 mutations in *Saccharomyces cerevisiae*. *Genetics* 170 (1), 71–85. doi:10.1534/genetics.104.037580

Shinohara, A., Ogawa, H., and Ogawa, T. (1992). Rad51 protein involved in repair and recombination in *S. cerevisiae* is a RecA-like protein. *Cell* 69 (3), 457–470. doi:10.1016/0092-8674(92)90447-k

Shinohara, M., Bishop, D. K., and Shinohara, A. (2019). Distinct functions in regulation of meiotic crossovers for DNA damage response clamp loader rad24(rad17) and Mec1(ATR) kinase. *Genetics* 213 (4), 1255–1269. doi:10.1534/genetics.119.302427

Shinohara, M., Gasior, S. L., Bishop, D. K., and Shinohara, A. (2000). Tid1/Rdh54 promotes colocalization of Rad51 and Dmc1 during meiotic recombination. *Proc. Natl. Acad. Sci. U. S. A.* 97 (20), 10814–10819. doi:10.1073/pnas.97.20.10814

Shinohara, M., Hayashihara, K., Grubb, J. T., Bishop, D. K., and Shinohara, A. (2015). DNA damage response clamp 9-1-1 promotes assembly of ZMM proteins for formation of crossovers and synaptonemal complex. *J. Cell Sci.* 128 (8), 1494–1506. doi:10.1242/jcs.161554

Shinohara, M., Oh, S. D., Hunter, N., and Shinohara, A. (2008). Crossover assurance and crossover interference are distinctly regulated by the ZMM proteins during yeast meiosis. *Nat. Genet.* 40 (3), 299–309. doi:10.1038/ng.83

Shinohara, M., Sakai, K., Shinohara, A., and Bishop, D. Y. (2003). Crossover interference in *Saccharomyces cerevisiae* requires a TID1/RDH54- and DMC1-dependent pathway. *Genetics* 163 (4), 1273–1286. doi:10.1093/genetics/163.4.1273

Snowden, T., Acharya, S., Butz, C., Berardini, M., and Fishel, R. (2004). hMSH4-hMSH5 recognizes Holliday Junctions and forms a meiosis-specific sliding clamp that embraces homologous chromosomes. *Mol. Cell* 15 (3), 437–451. doi:10.1016/j.molcel.2004.06.040

Stahl, F. W., Foss, H. M., Young, L. S., Borts, R. H., Abdullah, M. F., and Copenhaver, G. P. (2004). Does crossover interference count in *Saccharomyces cerevisiae*? *Genetics* 168 (1), 35–48. doi:10.1534/genetics.104.027789

Storlazzi, A., Gargano, S., Ruprich-Robert, G., Falque, M., David, M., Kleckner, N., et al.(2010). Recombination proteins mediate meiotic spatial chromosome organization and pairing. *Cell* 141 (1), 94–106. doi:10.1016/j.cell.2010.02.041

Sym, M., Engebrecht, J. A., and Roeder, G. S. (1993). ZIP1 is a synaptonemal complex protein required for meiotic chromosome synapsis. *Cell* 72 (3), 365–378. doi:10.1016/0092-8674(93)90114-6

Sym, M., and Roeder, G. S. (1995). Zip1-induced changes in synaptonemal complex structure and polycomplex assembly. *J. Cell Biol.* 128 (4), 455–466. doi:10.1083/jcb.128.4.455

Tan, T., Tan, Y., Wang, Y., Yang, X., Zhai, B., Zhang, S., et al.(2022). Negative supercoils regulate meiotic crossover patterns in budding yeast. *Nucleic Acids Res.* 50 (18), 10418–10435. doi:10.1093/nar/gkac786

Tsubouchi, H., and Ogawa, H. (1998). A novel mre11 mutation impairs processing of double-strand breaks of DNA during both mitosis and meiosis. *Mol. Cell Biol.* 18 (1), 260–268. doi:10.1128/mcb.18.1.260

Tsubouchi, T., Zhao, H., and Roeder, G. S. (2006). The meiosis-specific zip4 protein regulates crossover distribution by promoting synaptonemal complex formation together with zip2. *Dev. Cell* 10 (6), 809–819. doi:10.1016/j.devcel.2006.04.003

Tung, K. S., Hong, E. J., and Roeder, G. S. (2000). The pachytene checkpoint prevents accumulation and phosphorylation of the meiosis-specific transcription factor Ndt80. *Proc. Natl. Acad. Sci. U. S. A.* 97 (22), 12187–12192. doi:10.1073/pnas.220464597

Usui, T., Ohta, T., Oshiumi, H., Tomizawa, J., Ogawa, H., and Ogawa, T. (1998). Complex formation and functional versatility of Mre11 of budding yeast in recombination. *Cell* 95 (5), 705–716. doi:10.1016/s0092-8674(00)81640-2

Wang, S., Liu, Y., Shang, Y., Zhai, B., Yang, X., Kleckner, N., et al.(2019a). Crossover interference, crossover maturation, and human aneuploidy. *Bioessays* 41 (10), e1800221. doi:10.1002/bies.201800221

Wang, S., Veller, C., Sun, F., Ruiz-Herrera, A., Shang, Y., Liu, H., et al.(2019b). Per-nucleus crossover covariation and implications for evolution. *Cell* 177 (2), 326–338. doi:10.1016/j.cell.2019.02.021

White, J. H., Lusnak, K., and Fogel, S. (1985). Mismatch-specific post-meiotic segregation frequency in yeast suggests a heteroduplex recombination intermediate. *Nature* 315 (6017), 350–352. doi:10.1038/315350a0

Xu, L., Ajimura, M., Padmore, R., Klein, C., and Kleckner, N. (1995). NDT80, a meiosis-specific gene required for exit from pachytene in *Saccharomyces cerevisiae*. *Mol. Cell Biol.* 15 (12), 6572–6581. doi:10.1128/mcb.15.12.6572

Yadav, V. K., and Claeys Bouuaert, C. (2021). Mechanism and control of meiotic DNA double-strand break formation in *S. cerevisiae*. *Front. Cell Dev. Biol.* 9, 642737. doi:10.3389/fcell.2021.642737

Yoon, S. W., Lee, M. S., Xaver, M., Zhang, L., Hong, S. G., Kong, Y. J., et al.(2016). Meiotic prophase roles of Rec8 in crossover recombination and chromosome structure. *Nucleic Acids Res.* 44 (19), 9296–9314. doi:10.1093/nar/gkw682

Zhang, L., Espagne, E., de Muyt, A., Zickler, D., and Kleckner, N. E. (2014). Interference-mediated synaptonemal complex formation with embedded crossover designation. *Proc. Natl. Acad. Sci. U. S. A.* 111 (47), E5059–E5068. doi:10.1073/pnas.1416411111

Zhang, Y., Suzuki, T., Li, K., Gothwal, S. K., Shinohara, M., and Shinohara, A. (2020). Genetic interactions of histone modification machinery Set1 and PAF1C with the recombination complex rec114-mer2-mei4 in the formation of meiotic DNA double-strand breaks. *Int. J. Mol. Sci.* 21 (8), 2679. doi:10.3390/ijms21082679

Zhu, Z., Bani Ismail, M., Shinohara, M., and Shinohara, A. (2021). SCF(Cdc4) ubiquitin ligase regulates synaptonemal complex formation during meiosis. *Life Sci. Alliance* 4 (2), e202000933. doi:10.26508/lsa.202000933

Zhu, Z., Mori, S., Oshiumi, H., Matsuzaki, K., Shinohara, M., and Shinohara, A. (2010). Cyclin-dependent kinase promotes formation of the synaptonemal complex in yeast meiosis. *Genes cells.* 15 (10), 1036–1050. doi:10.1111/j.1365-2443.2010.01440.x

frontiers | Frontiers in Cell and Developmental Biology

TYPE Mini Review
PUBLISHED 19 May 2023
DOI 10.3389/fcell.2023.1156766

OPEN ACCESS

EDITED BY
Pedro A San-Segundo,
CSIC-University of Salamanca, Spain

REVIEWED BY
Eugenio Sanchez Moran,
University of Birmingham,
United Kingdom

*CORRESPONDENCE
Arnaud Ronceret,
arnaud.ronceret@ibt.unam.mx

RECEIVED 01 February 2023
ACCEPTED 17 April 2023
PUBLISHED 19 May 2023

CITATION
Rafiei N and Ronceret A (2023), Crossover interference mechanism: New lessons from plants.
Front. Cell Dev. Biol. 11:1156766.
doi: 10.3389/fcell.2023.1156766

Crossover interference mechanism: New lessons from plants

Nahid Rafiei and Arnaud Ronceret*

Plant Molecular Biology Department, Instituto de Biotecnología, Universidad Nacional Autónoma de México (UNAM), Cuernavaca, Mexico

Plants are the source of our understanding of several fundamental biological principles. It is well known that Gregor Mendel discovered the laws of Genetics in peas and that maize was used for the discovery of transposons by Barbara McClintock. Plant models are still useful for the understanding of general key biological concepts. In this article, we will focus on discussing the recent plant studies that have shed new light on the mysterious mechanisms of meiotic crossover (CO) interference, heterochiasmy, obligatory CO, and CO homeostasis. Obligatory CO is necessary for the equilibrated segregation of homologous chromosomes during meiosis. The tight control of the different male and female CO rates (heterochiasmy) enables both the maximization and minimization of genome shuffling. An integrative model can now predict these observed aspects of CO patterning in plants. The mechanism proposed considers the Synaptonemal Complex as a canalizing structure that allows the diffusion of a class I CO limiting factor linearly on synapsed bivalents. The coarsening of this limiting factor along the SC explains the interfering spacing between COs. The model explains the observed coordinated processes between synapsis, CO interference, CO insurance, and CO homeostasis. It also easily explains heterochiasmy just considering the different male and female SC lengths. This mechanism is expected to be conserved in other species.

KEYWORDS

meiotic recombination, crossing-over, interference, synapsis, heterochiasmy, CO insurance, CO homeostasis, HEI10 coarsening model

1 Introduction

1.1 Crossing over interference: a short historical perspective

In sexually reproducing organisms, parental alleles are distributed in the offspring following the laws of segregation defined by Gregor Mendel more than 150 years ago (Mendel, 1866; Birchler, 2015). The chromosomal theory of heredity proposed by Thomas H. Morgan (1926) explains how new chromosomic (genomic) combinations are formed during the meiotic and fertilization processes. During meiosis, new chromosomes are formed using recombination between parental DNA molecules. The junctions between parental chromosomes named crossing-overs correspond to the cytologically observed chiasma defined by Frans A. Janssens (Janssens, 1909) (translated into English by Koszul and Zickler, 2012). Using *Drosophila*, Alfred Sturtevant genetically defined that one CO in a genetic interval reduces the probability of observing another CO in the adjacent interval (Sturtevant, 1913; Sturtevant, 1965), a phenomenon Hermann J. Muller coined 'CO interference' in 1916 (Muller, 1916). John B.S. Haldane explained the genetic mechanism of

interference by the statistical non-Poisson distribution of chiasmata observed in bivalents of various Angiosperms (Haldane, 1931). The correspondence between genetic crossing-overs (CO) and cytological chiasmata was elegantly demonstrated in maize (Creighton and McClintock, 1931; Coe and Kass, 2005). Various models of CO formation have been developed (reviewed in Haber, 2008; Gray and Cohen, 2016; Chuang and Smith, 2023), including various models trying to explain CO interference, ever since Haldane (Berchowitz and Copenhaver, 2010; Sun et al., 2017; Otto and Payseur, 2019; Saito and Colaiácovo, 2019; Chuang and Smith, 2023).

In this minireview, we will discuss what we have recently learned from plants regarding the integrated mechanisms regulating synapsis, CO interference, CO insurance, CO homeostasis, and heterochiasmy.

1.2 An integrated molecular model for CO formation in plants

The meiotic division leads to the reduction by half of the chromosome number in order to balance the fertilization process (Zickler and Kleckner, 2015). Meiosis is one of the most dynamic plant cellular processes (Ronceret and Pawlowski, 2010). It allows, after one step of replication, the equilibrated segregation of homologous chromosomes (meiosis I) followed by the segregation of sister chromatids (meiosis II) to produce four haploid spores (Mercier et al., 2015; Wang and Copenhaver, 2018; Gutierrez-Pinzón et al., 2021; Lloyd, 2023). During meiotic prophase I, homologous chromosomes undergo a genetically regulated process of recombination to create unique new chromosomes from two parental ones. The molecular models for meiotic CO formation of the last 40 years are based on the DNA Double-Strand Breaks (DSBs) Repair model of meiotic recombination proposed by Resnick, 1976 and refined by Szostak et al., 1983. This model explains how two DNA molecules can form a new recombined one using the error-prone repair mechanism of homologous recombination (HR). The basic mechanism of meiotic homologous recombination involves the formation of hundreds of programmed DSBs inflicted to the genome at the beginning of the leptotene stage (de Massy, 2013; Mercier et al., 2015; Yadav and Claeys Bouuaert, 2021). The number of DSBs varies from species to species: 150 to 250 in Arabidopsis (Vignard et al., 2007), 450 to 550 in maize (Pawlowski et al., 2003), and around 400 to 1,500 in hexaploid wheat (Benyahya et al., 2020). These various DSBs are formed in plants by the SPO11 complex containing SPO11-1 (Grelon et al., 2001; Shingu et al., 2012; Sprink and Hartung, 2014; Da Ines et al., 2020; Ku et al., 2020), SPO11-2 (Stacey et al., 2006; Benyahya et al., 2020; Fayos et al., 2020; Sprink and Hartung, 2021; Li et al., 2022; Hyde et al., 2023), MTOPVIB (Fu et al., 2016; Vrielynck et al., 2016; Xue et al., 2019; Jing et al., 2020; Steckenborn et al., 2023), PRD1 (de Muyt et al., 2007; Shi et al., 2021; Wang et al., 2022), PRD2 (de Muyt et al., 2009; Wang C. et al., 2023), PRD3 (de Muyt et al., 2009; Lambing et al., 2022; Wang et al., 2022), and DFO (Zhang et al., 2012). All these DSB factors form a complex where SPO11-1/2 (TOPVIA-like subunit) presents the catalytic transesterase (endonuclease) activity associated with MTOPVIB (TOPVIB-like subunit), underlining that the SPO11 complex conserve the structure of a DNA topoisomerase (Vrielynck et al., 2016; Vrielynck et al., 2021; Wang Y. et al., 2023). In this model, all original DSBs are not necessarily transformed into COs, but all COs are designed from a subset of DSBs (Figure 1). In plants, only a small subset of DSB sites is converted into COs (Mercier et al., 2015). Though in most species studied, the global genomic position of DSBs is randomly distributed along the length of chromosomes (He et al., 2017; Choi et al., 2018), it is known that at smaller scale, there are hotspots of DSBs in open chromatin regions near transcriptional start sites with low nucleosome density in Arabidopsis (He et al., 2017; Choi et al., 2018). It was recently shown that these DSB sites are also silenced to avoid recombination on transcribed genes (Wang et al., 2022). The number of DSBs can finally affect the genomic distribution of CO (Xue et al., 2018). The SPO11 complex is associated with axial elements (AE) of the synaptonemal complex (SC) including the HORMA domain ASY1/PAIR2 (Armstrong et al., 2002; Nonomura et al., 2006; Sanchez-Moran et al., 2007; Cuacos et al., 2021; Wang C. et al., 2023) as well as the ASY3/PAIR3/DSY2 (Wang et al., 2011; Ferdous et al., 2012; Lee et al., 2015) and ASY4 coiled-coil proteins (Chambon et al., 2018), supposably forming the basis of chromatin loops (Vrielynck et al., 2021; Lambing et al., 2022) (Figure 1 Leptotene stage).

The process of meiotic recombination is realized in a context of replicated chromosomes. Each DSB can therefore be repaired by homologous recombination using different undamaged homologous sequences as a repair template. The sites where the identical sister chromatid is used as the repair template form non-CO events (Figure 1). The sites where the DSB repair is processed using either one of the two polymorphic DNA sequences of the homologous chromosomes as the repair template can enter the pathway to form COs (Figure 1). During meiosis, a specific cohesin complex is installed between sister chromatids and contains REC8 instead of SCC1 (Chelysheva et al., 2005; Golubovskaya et al., 2006; Shao et al., 2011) as well as SMC1/3 (Lam et al., 2005; Bolaños-Villegas, 2021), SCC2 (Wang et al., 2020), SCC3 (Chelysheva et al., 2005), CTF7 (Bolaños-Villegas et al., 2013), and PDS5 (Pradillo et al., 2015). The putative helicase MCM8 (Crismani et al., 2013) and the cohesion-like SMC5/6 complex that favors sister chromatin HR repair in somatic cells are also tightly controlled during meiosis to allow the activity of interhomolog HR (Watanabe et al., 2009; Liu et al., 2014; Knoll et al., 2014; Chen et al., 2021; Zhu et al., 2021; Jiang et al., 2022). These DSBs are readily resected 5′ to 3′ by the exonuclease activity of MRE11 to form single-strand overhang 3′ extremities (Puizina et al., 2004; Ji et al., 2013) and allow the liberation of SPO11-bound oligonucleotides (Choi et al., 2018). MRE11 forms a complex with RAD50 (Bleuyard et al., 2004), NBS1 (Akutsu et al., 2007; Waterworth et al., 2007), and COM1 (Uanschou et al., 2007; Ji et al., 2013; Wang et al., 2018). These 3' free single-strand DNA extremities are protected by various RPAs (Chang et al., 2009; Osman et al., 2009; Li et al., 2018; Aklilu et al., 2020), replaced by recA type recombinases RAD51 (Bleuyard et al., 2005; Da Ines et al., 2022; Li et al., 2022), RAD51C (Bleuyard et al., 2005; Jing et al., 2019), XRCC3 (Bleuyard and White, 2004; Zhang et al., 2015), and DMC1 (Couteau et al., 1999; Deng and Wang, 2007; Kurzbauer et al., 2012; Wang et al., 2016; Colas et al., 2019; Szurman-Zubrzycka et al., 2019). BRCA2 directly interacts with RAD51 and DMC1 and could facilitate their loading on the resected end of DSBs (Dray et al., 2006;

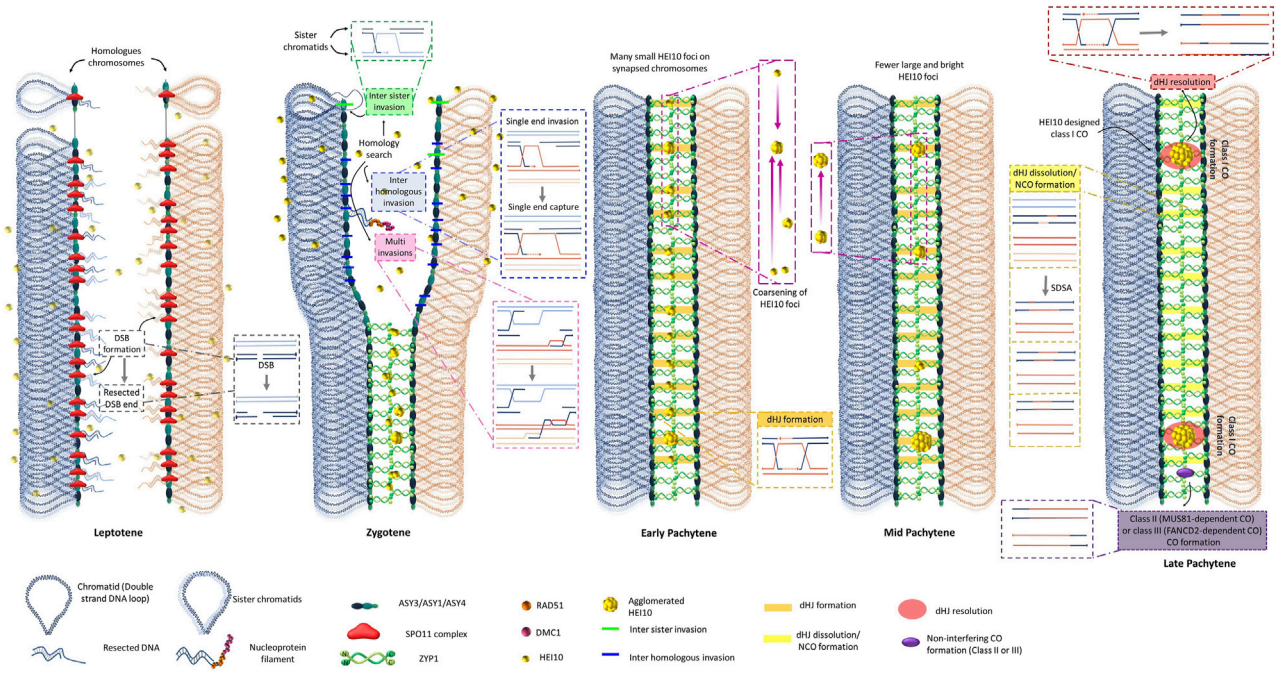

FIGURE 1
An integrated model explaining CO interference. Schematic representation of the formation of CO in just a pair of homologous chromosomes. To simplify, the global arrangement of the chromosome is depicted with two different colors for the homologs (red and blue) and two different tones for sister chromatids (light red and light blue). At this scale, each double-stranded DNA molecule is depicted as a simplifying line. The molecular steps necessary to understand the molecular mechanism of CO formation are depicted in magnified insets, where the 5′ ends of each DNA strand are represented by line with extremities with dots. **In leptotene,** the replicated chromosomes are represented with their important features for meiotic recombination. The axial elements (AE) including ASY1, ASY3, and ASY4 are assembled at the base of the loop of two sister chromatids attached by meiotic cohesins including REC8. Establishment of the proteinaceous axial element is essential to form the Synaptonemal Complex (SC). The formation of tens of DNA **double-strand breaks (DSBs)** for each of the only two homologous chromosomes pictured is processed by the evolutionarily conserved SPO11 complex. DSB ends are resected at either 5′ end to produce 3′ overhang, which are recognized by Rad51 and Dmc1 to generate inter-homologue strand-invasion. The 3′ end can invade either a homolog or a sister chromatid. In addition, multi-invasion of the 3′ tails on a homolog and/or sister chromatid is also possible to find an intact homologous template for HR repair. 3′ tail invasion in the homologous intact molecule generates a displacement loop (D-loop) through single end invasion (SEI). **In zygotene,** multiple SEI are used for homologous chromosome recognition/pairing. The transverse filaments ZYP1 of the synaptonemal complex (SC) start to polymerize at the center of the tripartite SC between two lateral elements. In **early pachytene**, the homologous chromosomes are fully synapsed from telomere to telomere. The SC allows the diffusion in only one dimension of the limiting CO factor HEI10 that can form coarsening recombination nodules explaining interference between CO class I (adapted from Morgan et al., 2021; Durand et al., 2022). In mid pachytene, various recombinant intermediates can be associated with HEI10 foci that progressively form larger agglomerated foci and eliminate the possibility of close CO design, except in the case of non-interfering COs that are not HEI10-dependant. **At the end of pachytene**, most of the chromosomal positions with SEI have not been transformed in CO but are resolved as NCO. At least one and generally few interferent (spaced out) COs are present on each bivalent, except where non-interfering (class II or class III) COs are formed.

Fu et al., 2020). These recombinases have the property to form nucleoprotein filaments that can bring together the single-strand DNA extremities with its specific homologous double-strand DNA molecules in a process known as single-end invasions (SEIs) (review in Emmenecker et al., 2022). Different recombinase subcomplexes exist and have differential functions between inter-sister SEI and interhomolog SEI (Kurzbauer et al., 2012; Pradillo et al., 2012; Su et al., 2017). The main biochemical difference between the Arabidopsis RAD51 and DMC1 recombinases tested *in vitro* is that RAD51 pairing activity seem not to be influenced by Ca^{2+} while DMC1 pairing activity is greatly enhanced in the presence of Ca^{2+} (Kobayashi et al., 2019). The most recently supported model proposes a symmetrical loading of RAD51 and DMC1 homotypic filaments on both DSB ends of a break (Da Ines et al., 2022). Interestingly, the role of the meiotic specific DMC1 seems to attenuate the strand exchange activity of the mitotic and meiotic RAD51 recombinase (Da Ines et al., 2022) (Figure 1 Zygotene stage).

Interhomolog SEI is also promoted during meiosis by axial proteins such as ASY1 (Sanchez-Moran et al., 2007; De Muyt et al., 2009). Other recombinase accessory proteins modulate SEI (review in Emmenecker et al., 2022). For example, RAD54 assists the RAD51 interhomolog repair of meiotic DSB (Hernandez Sanchez-Rebato et al., 2021), while the meiotic specific HOP2 Vignard et al., 2007; Uanschou et al., 2013; Shi et al., 2019, Emmenecker et al., 2022) and MND1 (Kerzendorfer et al., 2006; Lu et al., 2020) form a complex that could assist DMC1 strand invasion (Kang et al., 2015). HOP2 could also prevent illegitimate recombination between non homologous chromosome regions (Farahani-Tafreshi et al., 2022) (Figure 1 Zygotene stages). In rice, HOP2 can directly interact with the ZEP1 SC central component (Shi et al., 2019).

Hundreds of DSB sites allow the formation of the corresponding hundreds of SEI sites along the zygotene homologous chromosomes (Figure 1 Zygotene stage). These multiple sites of SEI connections

(known as joint molecules JMs), involving base pair DNA sequence homology recognition, are usually proposed to explain the mechanism used for the correct association (also known as pairing process) between the homologous chromosomes (Zickler and Kleckner, 1999; Pawlowski et al., 2003; Higgins et al., 2004). Most of these numerous SEIs will not form CO but are proposed to allow the accurate alignment between the right partners not only on a local scale but along the whole chromosome length. The excess of SEIs compared to the restricted final number of COs could therefore explain the accuracy of the pairing process between chromosome bivalents concomitant to synapsis (Gutierrez-Pinzón et al., 2021) (Figure 1 Zygotene stage). The recognized paired interaction zones are stabilized by the zipper-like proteinaceous structure known as the synaptonemal complex (SC). ZYP1 (ZEP1 in rice) is the central element forming a ladder between the two axial elements of the SC and connecting homologs from telomere to telomere (Higgins et al., 2005; Wang et al., 2010; Barakate et al., 2014; Capilla-Pérez et al., 2021; France et al., 2021) (Figure 1 Zygotene stage). The various SEI sites form regions of DNA triple helices known as Displacement-loops (D-loops). Most D-loops do not enter a CO pathway and several anti-recombinase pathways (described later) can dissociate the invading strand from the D-loop and re-anneal with the other DSB end, leading to small patches of hybrid DNA known as non-Crossover (NCO). The dissolved D-loops are proposed to be repaired via the Synthesis-Dependent Strand Annealing (SDSA) model during meiosis (Allers and Lichten, 2001; Puchta, 2005; Vu et al., 2017; Wang and Copenhaver, 2018) (Figure 1 Zygotene and pachytene stages).

For the few D-loops that enter a CO pathway, the invading strand is extended by DNA polymerases that realize a local DNA synthesis using the undamaged strand to copy it (Figure 1 Zygotene stage). The displaced strand of the undamaged DNA molecule hybridizes with the other 3' end of the DSB in a process known as second end capture (Figure 1 Zygotene stage). These joint molecules can interchange part of their homologous strands extending the hybridization zone in a process known as branch migration that leads to the formation of double Holliday junctions (dHJs) (Figure 1 Pachytene stages). The asymmetric resolution of these dHJs can lead to the formation of COs that covalently link new portions of two homologous chromosomes (Szostak et al., 1983).

Two principal classes of CO pathways, one sensitive to interference (class I) and the other insensitive to interference (class II), have been defined in *S. cerevisiae*, animals, and plants (Mercier et al., 2005; Holloway et al., 2008; Gray and Cohen, 2016).

The major pathway (accounting for around 85% of COs in Arabidopsis) is called class I and is subject to CO interference. The formation of the class I CO involves members of the ZMM pathway composed of ZIP4 (Chelysheva et al., 2007; Shen et al., 2012), MER3 (Mercier et al., 2005; Wang et al., 2009), HEI10 (Chelysheva et al., 2012; Wang K. et al., 2012), PTD (Wijeratne et al., 2006; Ren et al., 2019), SHOC1/ZIP2 (Macaisne et al., 2008; Ren et al., 2019), mutS-like MSH4 (Higgins et al., 2004; Zhang et al., 2014b), mutS-like MSH5 (Higgins et al., 2008a; Luo et al., 2013), mutL-like MLH1 (Dion et al., 2007; Liu et al., 2022), and mutL-like MLH3 (Jackson et al., 2006; Colas et al., 2016; Mao et al., 2021). The mut-Lγ resolvase (formed by the MLH1-MLH3 heterodimer of the ZMM complex) can potentially stabilize D-loop structures and mature them as CO (review in Ziolkowski, 2023). This interfering pathway also requires the leading strand DNA polymerase epsilon (Ronceret et al., 2005; Huang et al., 2015; Wang et al., 2022a; Wang et al., 2022b) as well as the potential lagging strand DNA polymerase POLD1 (Wang et al., 2019) and RFC1 factor (Wang Y. et al., 2012) probably necessary for the synthesis steps of HR. This interfering pathway is limited by the HCR1 encoding a Protein Phosphatase X1 that can interact with HEI10, PTD, MSH5, and MLH1 (Nageswaran et al., 2021). In rice, a new plant specific ZMM member named HEIP1 interacting with HEI10, ZIP4, and MSH5 was also identified (Li et al., 2018). In tetraploid wheat, MSH4/MSH5 mutants also demonstrate an 85%–15% proportion of the two CO pathways in wheat species (Desjardins et al., 2020). In hexaploid wheat, the classical Ph1 locus controlling pairing and recombination between homeologous chromosomes, which is very important for breeding strategies, corresponds to a ZIP4 homolog (Rey et al., 2017).

The second minor non-interfering pathway (accounting for 15% of COs in Arabidopsis, around 10% of COs in rice) is called class II and involves the MUS81 protein (Berchowitz et al., 2007; Higgins et al., 2008b; Geuting et al., 2009). The MUS81 complex has a highly controlled endonuclease activity acting on selective DNA structures, such as D-loop and HJ, and can act on several replication and recombination intermediates during mitosis and meiosis depending on its interacting partners and phosphorylation status (Pfander and Matos, 2017). In rice, GEN1, the homolog of the Holliday junction resolvase is necessary for class II CO formation (Wang et al., 2017) while it is not in Arabidopsis (Bauknecht and Kobbe, 2014; Olivier et al., 2016), suggesting that the MUS81 pathways have diverged between dicots and monocots. Compared to Arabidopsis, the MUS81 pathway contributes even less to CO designation in rice (Wang et al., 2017; Mu et al., 2022), suggesting that the weight of the different pathways described in this review probably depend on each species.

In Arabidopsis, a second non-interfering pathway of CO, depending on FANCD2 and parallel to the MUS81 non-interfering CO pathway, contributes to the formation of some type II COs (Kurzbauer et al., 2018). The FANCD2 pathway, but not the MUS81 pathway, affects the distribution of class I CO (Li et al., 2021). In order to avoid confusion, this distinct FANCD2 pathway could be designed as the non-interfering class III CO pathway (Gutierrez-Pinzón et al., 2021).

Various meiotic interhomolog intermediate dissolution pathways (or anti-recombinase pathways) have been identified in Arabidopsis using meiotic mutant suppressor screens restoring fertility. Double mutant and cytological marker analysis have shown that they all reduce specifically the MUS81 dependent non-interfering class II CO pathway. These anti-recombinase pathways act using parallel mechanisms since mutants combining the different pathways lead to additive massive meiotic non-interfering CO formation (Crismani et al., 2012; Girard et al., 2015; Séguéla-Arnaud et al., 2015; Serra et al., 2018; Singh et al., 2023).

The first anti CO pathway requires the RECQ4A and RECQ4B helicase activity homolog to mammal BLM and yeast SGS1 (Hartung et al., 2007; Higgins et al., 2011; Séguéla-Arnaud et al., 2015; Serra et al., 2018). Combine with TOP3α (Hartung et al., 2008) and RMI/BLAP75 (Chelysheva et al., 2008), this complex is known as the RTR complex in plants and is similar to the 'dissolvosome'

BTR complex in mammals and the yeast STR complex (Emmenecker et al., 2022). In Arabidopsis, recq4A mutant suppresses CO dependent on MUS81 activity (Séguéla-Arnaud et al., 2015). The RECQ4A protein is found on recombination intermediates of telomeres during meiosis and could particularly restrict CO class II on these chromosomal regions (Higgins et al., 2011). *Recq4* mutants increase by around three times the number of COs in rice, tomato, and pea (Mieulet et al., 2018). It seems that this RTR complex has functionally diverged between Arabidopsis and tomato (Whitbread et al., 2021).

The second anti CO class II pathway requires FIDGETIN-like AAA-ATPase (FIGL1) (Girard et al., 2015) associated with FLIP (Fernandes et al., 2018). This FIGL1 is an antagonist to the BRAC2 recombinase (Kumar et al., 2019). In rice, the FLIP-like MEICA protein can interact with the TOP3α and MSH7 (Hu et al., 2017), suggesting coordination between the first anti CO pathway at least in rice. MEICA and FIGNL1 both have an anti CO activity affecting class II CO (Zhang et al., 2017; Yang C. et al., 2022). These pathways could also have different strengths in male *versus* female meiosis as observed by the male specific effect of the FIGL mutation in rice (Zhang et al., 2017).

The third anti CO pathway requires the Fanconi Anaemia (FA) pathway comprising the FANCM helicase (Crismani et al., 2012); its cofactors MHF1 and MHF2 (Girard et al., 2015); and the FANCC, FANCE, and FANCF subcomplex (Singh et al., 2023).

It is important to clarify that any of these three parallel anti-recombinase pathways, which substantially increase the number of class II CO, have been shown to abolish CO interference measured genetically. The interpretation of these confounding results is that the large number of class II COs, by decreasing the space between COs, mask the class I spacing mechanism expected to remain unaffected (Crismani et al., 2012; Girard et al., 2015; Séguéla-Arnaud et al., 2017; Fernandes et al., 2018; Li et al., 2021).

Interestingly, in Arabidopsis, FANCD2, FANCM, FIGL1, and RMI1 not only suppress non-interfering CO but also have a role in regulating the distribution of class I CO among chromosomes to insure at least one CO per bivalent (Li et al., 2021). In wheat, it was shown that FANCM not only suppresses class II non-interfering COs but also promotes class I interfering COs and insures at least one CO by bivalent (Desjardins et al., 2022).

It has been proposed that these dissolution pathways leading to NCO could be especially important for multi-invasion complexes formed between more than two DNA molecules that would otherwise lead to aberrant recombination intermediates (Emmenecker et al., 2022; Mu et al., 2022). Whether or not these pathways could be involved in a putative chromatid interference phenomenon (Zhao et al., 1995; Sarens et al., 2021) is still unknown.

In general, the combination of these different pro- and anti- CO pathways leads to the formation of only one or two COs per chromosome arm in plants, fungi, and animals (Otto and Payseur, 2019; Saito and Colaiácovo, 2019; Pazhayam et al., 2021; Tock et al., 2021; Lloyd, 2023).

However, despite the understanding of the molecular factors involved in CO formation in various model species, the mechanism by which COs tend to space out from each other has been debated for more than a century. The other mechanisms of the obligatory CO, CO homeostasis (where the variation of the initial number of recombination intermediate does not affect the final number of COs), and heterochiasmy (where CO rate is different between male and female meiosis) have also gained various insights from recent analysis in plant meiotic models.

1.3 A model of CO interference based on HEI10 coarsening along the SC compartment

Recently, several lines of evidence converged to pinpoint the fundamental role of the localization dynamics of the specific pro-crossover ZMM HEI10 factor on meiotic chromosomes to explain the CO interference phenomenon. HEI10 is a member of a family of RING-finger domain E3 ubiquitin ligase (De Muyt et al., 2014) including Zip3 in *S. cerevisiae* (Agarwal and Roeder, 2000), HEI10 and RNF212 in mammals (Ward et al., 2007; Kong et al., 2008), Vilya in *Drosophila* (Lake et al., 2015) and ZHP-3 in *C. elegans* (Bhalla et al., 2008; Zhang et al., 2018). In Arabidopsis, the expression of HEI10 responds similarly to its overlapping adjacent gene MRD1 to pathogen inoculations via the OZF1 transcription factor (Singh et al., 2022). AtHEI10 is also transcriptionally repressed by a Heat Shock Binding Protein (HSBP) that contributes to the adaptative CO formation in response to change in temperature (Kim et al., 2022) suggesting that HEI10 expression is responding to various environmental factors. In immunolocalization experiments, HEI10 foci show a peculiar pattern with a foci number progressively decreasing from late zygotene to diakinesis with late signal associated with other members of the class I CO such as MLH1 and MLH3 in Arabidopsis and rice (Chelysheva et al., 2012; Wang K. et al., 2012). It was noticed that HEI10 can show either small and faint numerous foci at the beginning of the zygotene stage or large and bright signals at the end of the pachytene stage in rice, Arabidopsis, and wheat meiocytes (Wang Y. et al., 2012; Duroc et al., 2014; Desjardins et al., 2020; Osman et al., 2021). Natural variation in this gene is associated with variation in meiotic recombination rate observed between Arabidopsis ecotypes (Ziolkowski et al., 2017). The dosage of HEI10, reduced in *hei10* heterozygotes or increased in HEI10 overexpression line is a determinant for CO number and the strength of CO interference (Ziolkowski et al., 2017; Serra et al., 2018; Morgan et al., 2021). Using super-resolution SIM track of the HEI10 immunolocalization signal on fully synapsed pachytene bivalents, it was observed that the intensity of HEI10 signal per foci depends on the total number of observed foci per bivalent, with brighter signal when unique foci are present on bivalents (Morgan et al., 2021). During early zygotene, faint HEI10 signals are uniformly distributed along the bivalents (Figure 1. Zygotene stage), the number of HEI10 foci progressively decreases during zygotene and pachytene stages with an aggregation of brighter and larger HEI10 foci at the expense of the fainter and smaller adjacent foci (Figure 1 Zygotene and Pachytene stages). Ultimately by late pachytene, few large bright foci have been spaced out by the mechanism of HEI10 coarsening that has depleted the surrounding HEI10 sites on bivalents (Figure Fig1. Late Pachytene stage). However, by which mechanism HEI10 can coarsen and how it is related to other ubiquitination processes during meiosis require further investigations (Orr et al., 2021; Ren et al., 2021). It is worth underlining that the analysis of pachytene bivalents using electron microscopy had already noticed different sizes and shapes of early (poorly interfering)

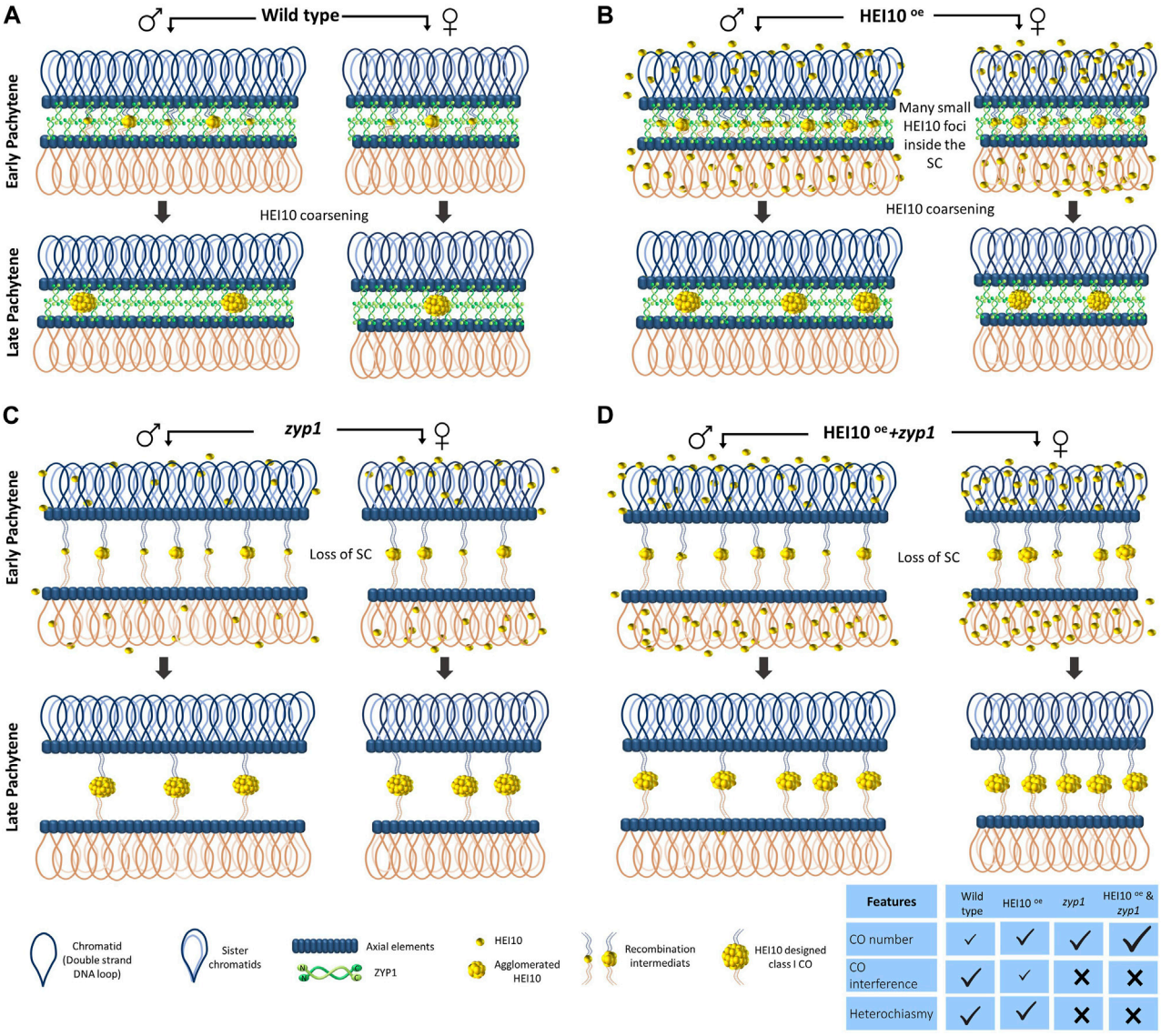

FIGURE 2
Many mechanisms of crossover interference can be explained by the HEI10 coarsening model along the ZYP1 synaptonemal complex structure. Schematic representation of the HEI10 localization at pachytene in *Arabidopsis thaliana* wild type **(A)**, *zyp1* mutant **(B)**, HEI10^{oe} overexpressed line **(C)**, and *zyp1*+ HEI10^{oe} **(D)** adapted from Durand et al., 2022. In wild type, HEI10 proteins are localized into foci. Many small HEI10 foci on synapsed chromosomes appear along the SC. With the progression of the pachytene stages, the number of HEI10 foci gradually decreases and few of them coarsen by agglomerating the smaller foci into the larger ones. Fewer foci are generated in females due to the shorter SC and leads to heterochiasmy **(A)**. In HEI10 OE, the coarsening process occurs as well as wild type and by keeping the heterochiasmy state, CO numbers in both sexes increase while CO interference decreases **(B)**. In the absence of SC, *zyp1*, unlike the presence of SC ones, free diffusion of HEI10 occurs in the nucleoplasm and abolish the competition among foci to absorb the HEI10 and all initial foci grow continuously by capturing the HEI10. Hence, this results in a loss of crossover interference and heterochiasmy but an increase in the CO number **(C)**. As it is expected, the combination HEI10 (OE) and *zyp1* provides larger increases in CO number than *zyp1* and HEI10 OE alone, and CO interference and heterochiasmy are abolished **(D)**.

versus late interfering **'recombination nodules' (RN)** localize along the synaptonemal complex (Anderson and Stack, 2005). Morgan and colleagues proposed a mathematical 'diffusion mediated HEI10 coarsening model' where the SC is seen as a linear structure allowing the diffusion of the HEI10 signal in only one dimension (Morgan et al., 2021). This model convincingly predicts differently tested situations in WT and *hei10* mutant or HEI10^{oe} overexpression line (Morgan et al., 2021) (Figure 2). The model explains very well how the HEI10 recombination nodules become progressively distant from each other. This model also implicitly explains how the mechanism of interference is not affected by the formation of either class II MUS81 dependent CO, nor class III FANCD2 dependent CO, though either of the three pathways can use the same SEI initial recombination intermediates. It also suggests that the remaining SEI sites without HEI10 bright foci are transformed into NCO or non-interfering COs (Figure 1 Pachytene stages).

The coarsening model was initially proposed in *C. elegans*, whose HEI10 homolog ZHP-3 has a similar behavior (Bhalla

et al., 2008; Zhang et al., 2018; Zhang et al., 2021). The SC also seems to have peculiar liquid-crystal properties that can facilitate long range signal transduction (Rog et al., 2017). Whether or not similar properties of the plant SC could help the progressive coarsening of HEI10 remains to be determined in plants.

The situation in mammals could be similar since the HEI10 accumulates at designed CO sites (Qiao et al., 2014). However, in mammals, the interference mechanism might not involve the HEI10 protein itself but rather its antagonist RNF212 SUMO ligase (Qiao et al., 2014; Rao et al., 2017). Indeed, in mammals, RNF212 seems to be the limiting factor for CO class I design since it has sequence variants explaining the recombination rate in human populations (Kong et al., 2008) and shows a sensitive dosage role during mouse meiotic recombination (Reynolds et al., 2013).

1.4 The SC/HEI10 coarsening could also explain the mechanisms of obligatory CO and CO homeostasis

The mechanism by which at least one CO is formed on each bivalent was recognized as essential to segregate the full set of homologous chromosomes during the meiotic reductional division (Darlington and Dark, 1932). This obligate CO was defined by Owen in 1949 (Owen, 1949). This ability to ensure CO (also known as **CO insurance**) on each bivalent can easily be integrated into the HEI10 coarsening model along the SC. The HEI10 coarsening model assumes that if enough HEI10 is deposited on a bivalent, it will produce at least one CO per bivalent explaining CO insurance.

The mechanism of CO homeostasis was defined by Martini et al., 2006 to explain a situation observed in budding yeast where the variation of the number of DSB (i.e., 80% reduction) does not significantly affect the final number of COs. In Arabidopsis, a 30%–40% reduction in DSB number leads to a proportionate though smaller reduction of CO number, affecting their distribution and redirecting them toward the telomeres (Xue et al., 2018). In maize though, it appears that CO homeostasis is somehow limited (Sidhu et al., 2015). Anyway, the coarsening HEI10 model could also account for CO homeostasis if we imagine that a DSB-independent limiting amount of expressed HEI10 per meiocyte limit the final number of the major class I CO. The large excess of DSB and SEI intermediates compared to the final CO number could explain how the bright and large HEI foci designing class I COs might not be affected by a change in the number of DSB and earlier SEI intermediates, as long as the number of these intermediates is at least the same as or exceeds the number of final COs.

1.5 Role of synapsis in interference, obligate CO and heterochiasmy

In species with different CO rates between male and female meiosis (heterochiasmy), the length of SC is particularly different as well. SC length also depends on chromosome size and the SC length is proportional to CO rate (Zickler and Kleckner, 2015).

As already mentioned, the ZYP1 is the central element of the SC. In contrast to the *S cerevisiae*, Zip1 homolog is considered a member of the ZMM pathway that is indispensable for synapsis and CO formation (Sym et al., 1993), the mutation of *zyp1* in Arabidopsis and rice disprupts synapsis but allows the formation of a higher number of COs per meiosis (Wang et al., 2010; Capilla-Pérez et al., 2021; France et al., 2021). It appears that this uncoupling of SC and CO class I formation in plants fortunately allowed the role of the SC in the interference mechanism to be refined. In addition, plants do not have a bone fine pachytene checkpoint leading to apoptosis when bivalents cannot form (De Jaeger-Braet et al., 2022), allowing easier observations of the consequences of the *zyp1* mutation than in animals or budding yeast. In the absence of *zyp1*, the number of COs increases, but interference, obligatory CO, and heterochiasmy are lost (Capilla-Pérez et al., 2021; France et al., 2021). In *zyp1* mutants, the HEI10 foci are still formed despite the loss of the SC and the formation of bright HEI10 signals (Capilla-Pérez et al., 2021), suggesting that the HEI10 diffusion still occurs but in three dimensions in the nucleoplasm, instead of being canalyzed by the SC on each bivalent (Figure 2C). So when synapsis is lost, heterochiasmy is also lost. This data is interpreted as the fact that heterochiasmy does not rely on peculiar regulation of the RH machinery itself except the one imposed by the SC length. It is predicted that all the factors affecting longer SC length will increase CO rate; the one decreasing SC length will decrease CO rate.

The HEI10 coarsening model proposed by Morgan et al., 2021 also reliably accounts for these observed facts in male and female meiosis of Arabidopsis (Durand et al., 2022). The longer male SC can integrate more HEI10 and have a longer distance to space them out, leading to both a higher recombination rate and higher interference (Figure 2B). Finally the HEI10 coarsening model also predicted as well the combination of *zyp1* with HEI10^{oe} situations (Durand et al., 2022; Fozard et al., 2023) (Figure 2D). The situation is also observed in a new separation of function *zyp1* allele (Yang S. et al., 2022). ASY1 also mediates CO insurance and interference (Lambing et al., 2020; Pochon et al., 2022). The effect of ASY1, one of the axial elements of the SC, on CO and interference might also be partly due to the absence of ZYP1 installation in this mutant.

A previous model known as the beam-film model has been extensively proposed to explain the interference mechanism by a redistribution of the mechanical stress that dissipates at the site of CO designation, impeding the formation of another CO nearby (Kleckner et al., 2004; Zhang et al., 2014a; Otto and Payseur, 2019). The beam-film model and the HEI coarsening model are possibly not exclusive and the mechanisms of HEI10 diffusion or coarsening could be influenced by a mechanical stress potentially perceived through SC remodeling (Lambing et al., 2020; Yang C. et al., 2022).

Most of the meiotic studies are still made in male meiocytes but immunolocalization techniques used to analyze female meiocytes have now been developed (Escobar-Guzmán et al., 2015; Gordillo et al., 2020) in order to better understand heterochiasmy and identify the basis of the regulation of the male and female SC length difference.

2 Conclusion

Forty years after the DSB repair model (Szostak et al., 1983), the molecular pathways and factors leading to the formation of CO have

been described in various fungi, animal, and plant models. An integrated model for understanding the CO patterning at the whole genome level remained more difficult to establish. The model reviewed here requires the observed excess of DBS sites for correct pairing between homologs and synapsis. The excess SEI sites are also required for interference and the progressive design of COs along bivalents that lead to the restricted number of final COs. The SEI sites unused to form CO are still repaired and explain the presence of NCO.

In the model reviewed here, which was initially proposed in *C. elegans* by Zhang et al., 2021 as well as in Arabidopsis by Morgan et al., 2021 and refined by Durand et al., 2022 and Fozard et al., 2023, the role of the synaptonemal complex SC, an evolutionary well conserved structure only present during meiosis, is clearly assigned: it allows the HR machinery to work on the bivalent as a unit separated from the rest of the nucleoplasm. This explains how SC is tightly interconnected with the homologous recombination process during meiosis. The SC can therefore restrict the diffusion of important recombination regulators such as HEI10 on a linear basis and explain the observed coordination of mechanisms controlling CO insurance, homeostasis, and interference. In this model, heterochiasmy relies on different SC lengths, as observed cytologically in various species (Zickler and Kleckner, 1999).

Author contributions

NR wrote a draft of the manuscript and realized the figures. AR wrote the manuscript.

Funding

Relevant research in the AR lab was supported by a grant from the Mexican SEP-CONACYT. Ciencia Básica A1-S-8496 to AR. NR received a postdoctoral UNAM-DGAPA fellowship.

Acknowledgments

We acknowledge Patricia Rueda for their technical support and the plant meiotic community for their stimulating discussions. We thank the reviewer for their careful and insightful suggestions, which helped us to improve our manuscript.

Conflict of interest

The authors declare that the research was conducted in the absence of any commercial or financial relationships that could be construed as a potential conflict of interest.

Publisher's note

References

Agarwal, S., and Roeder, G. S. (2000). Zip3 provides a link between recombination enzymes and synaptonemal complex proteins. *Cell* 102 (2), 245–255. PMID: 10943844. doi:10.1016/s0092-8674(00)00029-5

Aklilu, B. B., Peurois, F., Saintomé, C., Culligan, K. M., Kobbe, D., Leasure, C., et al. (2020). Functional diversification of replication protein A paralogs and telomere length maintenance in Arabidopsis. *Genetics* 215 (4), 989–1002. Epub 2020 Jun 12. PMID: 32532801; PMCID: PMC7404240. doi:10.1534/genetics.120.303222

Akutsu, N., Iijima, K., Hinata, T., and Tauchi, H. (2007). Characterization of the plant homolog of Nijmegen breakage syndrome 1: Involvement in DNA repair and recombination. *Biochem. Biophys. Res. Commun.* 353 (2), 394–398. Epub 2006 Dec 13. PMID: 17182003. doi:10.1016/j.bbrc.2006.12.030

Allers, T., and Lichten, M. (2001). Differential timing and control of noncrossover and crossover recombination during meiosis. *Cell* 106 (1), 47–57. PMID: 11461701. doi:10.1016/s0092-8674(01)00416-0

Anderson, L. K., and Stack, S. M. (2005). Recombination nodules in plants. *Cytogenet Genome Res.* 109 (1-3), 198–204. doi:10.1159/000082400

Armstrong, S. J., Caryl, A. P., Jones, G. H., and Franklin, F. C. (2002). Asy1, a protein required for meiotic chromosome synapsis, localizes to axis-associated chromatin in Arabidopsis and Brassica. *J. Cell Sci.* 115 (18), 3645–3655. PMID: 12186950. doi:10.1242/jcs.00048

Barakate, A., Higgins, J. D., Vivera, S., Stephens, J., Perry, R. M., Ramsay, L., et al. (2014). The synaptonemal complex protein ZYP1 is required for imposition of meiotic crossovers in barley. *Plant Cell* 26 (2), 729–740. Epub 2014 Feb 21. PMID: 24563202; PMCID: PMC3967036. doi:10.1105/tpc.113.121269

Bauknecht, M., and Kobbe, D. (2014). AtGEN1 and AtSEND1, two paralogs in Arabidopsis, possess holliday junction resolvase activity. *Plant Physiol.* 166 (1), 202–216. Epub 2014 Jul 18. PMID: 25037209; PMCID: PMC4149707. doi:10.1104/pp.114.237834

Benyahya, F., Nadaud, I., Da Ines, O., Rimbert, H., White, C., and Sourdille, P. (2020). SPO11.2 is essential for programmed double-strand break formation during meiosis in bread wheat (*Triticum aestivum* L). *Plant J.* 104 (1), 30–43. doi:10.1111/tpj.14903

Berchowitz, L. E., and Copenhaver, G. P. (2010). Genetic interference: don't stand so close to me. *Curr. Genomics* 11 (2), 91–102. PMID: 20885817; PMCID: PMC2874225. doi:10.2174/138920210790886835

Berchowitz, L. E., Francis, K. E., Bey, A. L., and Copenhaver, G. P. (2007). The role of AtMUS81 in interference-insensitive crossovers in A. thaliana. *PLoS Genet.* 3 (8), e132. Epub 2007 Jun 26. PMID: 17696612; PMCID: PMC1941751. doi:10.1371/journal.pgen.0030132

Bhalla, N., Wynne, D. J., Jantsch, V., and Dernburg, A. F. (2008). ZHP-3 acts at crossovers to couple meiotic recombination with synaptonemal complex disassembly and bivalent formation in *C. elegans*. *PLoS Genet.* 4 (10), e1000235. doi:10.1371/journal.pgen.1000235

Birchler, J. A. (2015). Mendel, mechanism, models, marketing, and more. *Cell* 163 (1), 9–11. doi:10.1016/j.cell.2015.09.008

Bleuyard, J. Y., Gallego, M. E., Savigny, F., and White, C. I. (2005). Differing requirements for the Arabidopsis Rad51 paralogs in meiosis and DNA repair. *Plant J.* 41 (4), 533–545. PMID: 15686518. doi:10.1111/j.1365-313X.2004.02318.x

Bleuyard, J. Y., Gallego, M. E., and White, C. I. (2004). Meiotic defects in the Arabidopsis rad50 mutant point to conservation of the MRX complex function in early stages of meiotic recombination. *Chromosoma* 113 (4), 197–203. Epub 2004 Aug 10. PMID: 15309561. doi:10.1007/s00412-004-0309-1

Bleuyard, J. Y., and White, C. I. (2004). The Arabidopsis homologue of Xrcc3 plays an essential role in meiosis. *EMBO J.* 23 (2), 439–449. Epub 2004 Jan 15. PMID: 14726957; PMCID: PMC1271761. doi:10.1038/sj.emboj.7600055

Bolaños-Villegas, P., Yang, X., Wang, H. J., Juan, C. T., Chuang, M. H., Makaroff, C. A., et al. (2013). Arabidopsis CHROMOSOME TRANSMISSION FIDELITY 7 (AtCTF7/ECO1) is required for DNA repair, mitosis and meiosis. *Plant J.* 75 (6), 927–940. Epub 2013 Jul 20. PMID: 23750584; PMCID: PMC3824207. doi:10.1111/tpj.12261

Bolaños-Villegas, P. (2021). The role of structural maintenance of chromosomes complexes in meiosis and genome maintenance: Translating biomedical and model plant research into crop breeding opportunities. *Front. Plant Sci.* 12, 659558. PMID: 33868354; PMCID: PMC8044525. doi:10.3389/fpls.2021.659558

Capilla-Pérez, L., Durand, S., Hurel, A., Lian, Q., Chambon, A., Taochy, C., et al. (2021). The synaptonemal complex imposes crossover interference and heterochiasmy in *Arabidopsis*. *Proc. Natl. Acad. Sci. U. S. A.* 118 (12), e2023613118. doi:10.1073/pnas.2023613118

Chambon, A., West, A., Vezon, D., Horlow, C., De Muyt, A., Chelysheva, L., et al. (2018). Identification of ASYNAPTIC4, a component of the meiotic chromosome Axis. *Plant Physiol.* 178 (1), 233–246. Epub 2018 Jul 12. PMID: 30002256; PMCID: PMC6130017. doi:10.1104/pp.17.01725

Chang, Y., Gong, L., Yuan, W., Li, X., Chen, G., Li, X., et al. (2009). Replication protein A (RPA1a) is required for meiotic and somatic DNA repair but is dispensable for DNA replication and homologous recombination in rice. *Plant Physiol.* 151 (4), 2162–2173. Epub 2009 Oct 7. PMID: 19812186; PMCID: PMC2785997. doi:10.1104/pp.109.142877

Chelysheva, L., Diallo, S., Vezon, D., Gendrot, G., Vrielynck, N., Belcram, K., et al. (2005). AtREC8 and AtSCC3 are essential to the monopolar orientation of the kinetochores during meiosis. *J. Cell Sci.* 118 (20), 4621–4632. Epub 2005 Sep 21. PMID: 16176934. doi:10.1242/jcs.02583

Chelysheva, L., Gendrot, G., Vezon, D., Doutriaux, M. P., Mercier, R., and Grelon, M. (2007). Zip4/Spo22 is required for class I CO formation but not for synapsis completion in *Arabidopsis thaliana*. *PLoS Genet.* 3 (5), e83. PMID: 17530928; PMCID: PMC1877879. doi:10.1371/journal.pgen.0030083

Chelysheva, L., Vezon, D., Belcram, K., Gendrot, G., and Grelon, M. (2008). The Arabidopsis BLAP75/Rmi1 homologue plays crucial roles in meiotic double-strand break repair. *PLoS Genet.* 4 (12), e1000309. doi:10.1371/journal.pgen.1000309

Chelysheva, L., Vezon, D., Chambon, A., Gendrot, G., Pereira, L., Lemhemdi, A., et al. (2012). The Arabidopsis HEI10 is a new ZMM protein related to Zip3. *PLoS Genet.* 8 (7), e1002799. Epub 2012 Jul 26. PMID: 22844245; PMCID: PMC3405992. doi:10.1371/journal.pgen.1002799

Chen, H., He, C., Wang, C., Wang, X., Ruan, F., Yan, J., et al. (2021). RAD51 supports DMC1 by inhibiting the SMC5/6 complex during meiosis. *Plant Cell* 33 (8), 2869–2882. PMID: 34009315; PMCID: PMC8408460. doi:10.1093/plcell/koab136

Choi, K., Zhao, X., Tock, A. J., Lambing, C., Underwood, C. J., Hardcastle, T. J., et al. (2018). Nucleosomes and DNA methylation shape meiotic DSB frequency in *Arabidopsis thaliana* transposons and gene regulatory regions. *Genome Res.* 28 (4), 532–546. doi:10.1101/gr.225599.117

Chuang, Y. C., and Smith, G. R. (2023). Meiotic crossover interference: Methods of analysis and mechanisms of action. *Curr. Top. Dev. Biol.* 151, 217–244. Epub 2022 Aug 24. PMID: 36681471. doi:10.1016/bs.ctdb.2022.04.006

Coe, E., and Kass, L. B. (2005). Proof of physical exchange of genes on the chromosomes. *Proc. Natl. Acad. Sci. U. S. A.* 102 (19), 6641–6646. Epub 2005 May 2. PMID: 15867161; PMCID: PMC1100733. doi:10.1073/pnas.0407340102

Colas, I., Barakate, A., Macaulay, M., Schreiber, M., Stephens, J., Vivera, S., et al. (2019). desynaptic5 carries a spontaneous semi-dominant mutation affecting Disrupted Meiotic cDNA 1 in barley. *J. Exp. Bot.* 70 (10), 2683–2698. PMID: 31028386; PMCID: PMC6509107. doi:10.1093/jxb/erz080

Colas, I., Macaulay, M., Higgins, J. D., Phillips, D., Barakate, A., Posch, M., et al. (2016). A spontaneous mutation in MutL-Homolog 3 (HvMLH3) affects synapsis and crossover resolution in the barley desynaptic mutant des10. *New Phytol.* 212 (3), 693–707. doi:10.1111/nph.14061

Couteau, F., Belzile, F., Horlow, C., Grandjean, O., Vezon, D., and Doutriaux, M. P. (1999). Random chromosome segregation without meiotic arrest in both male and female meiocytes of a dmc1 mutant of Arabidopsis. *Plant Cell* 11 (9), 1623–1634. PMID: 10488231; PMCID: PMC144309. doi:10.1105/tpc.11.9.1623

Creighton, H. B., and McClintock, B. A. (1931). A correlation of cytological and genetical crossing-over in zea mays. *Proc. Natl. Acad. Sci. U. S. A.* 17 (8), 492–497. PMID: 16587654; PMCID: PMC1076098. doi:10.1073/pnas.17.8.492

Crismani, W., Girard, C., Froger, N., Pradillo, M., Santos, J. L., Chelysheva, L., et al. (2012). FANCM limits meiotic crossovers. *Science* 336 (6088), 1588–1590. PMID: 22723424. doi:10.1126/science.1220381

Crismani, W., Portemer, V., Froger, N., Chelysheva, L., Horlow, C., Vrielynck, N., et al. (2013). MCM8 is required for a pathway of meiotic double-strand break repair independent of DMC1 in *Arabidopsis thaliana*. *PLoS Genet.* 9 (1), e1003165. Epub 2013 Jan 3. PMID: 23300481; PMCID: PMC3536722. doi:10.1371/journal.pgen.1003165

Cuacos, M., Lambing, C., Pachon-Penalba, M., Osman, K., Armstrong, S. J., Henderson, I. R., et al. (2021). Meiotic chromosome axis remodelling is critical for meiotic recombination in Brassica rapa. *J. Exp. Bot.* 72 (8), 3012–3027. PMID: 33502451; PMCID: PMC8023211. doi:10.1093/jxb/erab035

Da Ines, O., Bazile, J., Gallego, M. E., and White, C. I. (2022). DMC1 attenuates RAD51-mediated recombination in Arabidopsis. *PLoS Genet.* 18 (8), e1010322. PMID: 36007010; PMCID: PMC9451096. doi:10.1371/journal.pgen.1010322

Da Ines, O., Michard, R., Fayos, I., Bastianelli, G., Nicolas, A., Guiderdoni, E., et al. (2020). Bread wheat TaSPO11-1 exhibits evolutionarily conserved function in meiotic recombination across distant plant species. *Plant J.* 103 (6), 2052–2068. Epub 2020 Jul 10. PMID: 32559326. doi:10.1111/tpj.14882

Darlington, C. D., and Dark, S. O. (1932). The origin and behaviour of chiasmata II. Stenobothrus parallelus. *Cytol. (tokyo)* 63, 169–185. doi:10.1508/cytologia.3.169

De Jaeger-Braet, J., Krause, L., Buchholz, A., and Schnittger, A. (2022). Heat stress reveals a specialized variant of the pachytene checkpoint in meiosis of *Arabidopsis thaliana*. *Plant Cell* 34 (1), 433–454. PMID: 34718750; PMCID: PMC8846176. doi:10.1093/plcell/koab257

de Massy, B. (2013). Initiation of meiotic recombination: How and where? Conservation and specificities among eukaryotes. *Annu. Rev. Genet.* 47, 563–599. PMID: 24050176. doi:10.1146/annurev-genet-110711-155423

De Muyt, A., Pereira, L., Vezon, D., Chelysheva, L., Gendrot, G., Chambon, A., et al. (2009). A high throughput genetic screen identifies new early meiotic recombination functions in *Arabidopsis thaliana*. *PLoS Genet.* 5 (9), e1000654. Epub 2009 Sep 18. PMID: 19763177; PMCID: PMC2735182. doi:10.1371/journal.pgen.1000654

De Muyt, A., Vezon, D., Gendrot, G., Gallois, J. L., Stevens, R., and Grelon, M. (2007). AtPRD1 is required for meiotic double strand break formation in *Arabidopsis thaliana*. *EMBO J.* 26 (18), 4126–4137. Epub 2007 Aug 30. PMID: 17762870; PMCID: PMC2230667. doi:10.1038/sj.emboj.7601815

De Muyt, A., Zhang, L., Piolot, T., Kleckner, N., Espagne, E., and Zickler, D. (2014). E3 ligase Hei10: A multifaceted structure-based signaling molecule with roles within and beyond meiosis. *Genes Dev.* 28 (10), 1111–1123. PMID: 24831702; PMCID: PMC4035539. doi:10.1101/gad.240408.114

Deng, Z. Y., and Wang, T. (2007). OsDMC1 is required for homologous pairing in Oryza sativa. *Plant Mol. Biol.* 65 (1-2), 31–42. Epub 2007 Jun 12. PMID: 17562186. doi:10.1007/s11103-007-9195-2

Desjardins, S. D., Ogle, D. E., Ayoub, M. A., Heckmann, S., Henderson, I. R., Edwards, K. J., et al. (2020). *MutS homologue 4* and *MutS homologue 5* maintain the obligate crossover in wheat despite stepwise gene loss following polyploidization. *Plant Physiol.* 183 (4), 1545–1558. Epub 2020 Jun 11. PMID: 32527734; PMCID: PMC7401138. doi:10.1104/pp.20.00534

Desjardins, S. D., Simmonds, J., Guterman, I., Kanyuka, K., Burridge, A. J., Tock, A. J., et al. (2022). FANCM promotes class I interfering crossovers and suppresses class II non-interfering crossovers in wheat meiosis. *Nat. Commun.* 13 (1), 3644. PMID: 35752733; PMCID: PMC9233680. doi:10.1038/s41467-022-31438-6

Dion, E., Li, L., Jean, M., and Belzile, F. (2007). An Arabidopsis MLH1 mutant exhibits reproductive defects and reveals a dual role for this gene in mitotic recombination. *Plant J.* 51 (3), 431–440. PMID: 17559505. doi:10.1111/j.1365-313X.2007.03145.x

Dray, E., Siaud, N., Dubois, E., and Doutriaux, M. P. (2006). Interaction between Arabidopsis Brca2 and its partners Rad51, Dmc1, and Dss1. *Plant Physiol.* 140 (3), 1059–1069. Epub 2006 Jan 13. PMID: 16415210; PMCID: PMC1400560. doi:10.1104/pp.105.075838

Durand, S., Lian, Q., Jing, J., Ernst, M., Grelon, M., Zwicker, D., et al. (2022). Joint control of meiotic crossover patterning by the synaptonemal complex and HEI10 dosage. *Nat. Commun.* 13 (1), 5999. PMID: 36224180; PMCID: PMC9556546. doi:10.1038/s41467-022-33472-w

Duroc, Y., Lemhemdi, A., Larchevêque, C., Hurel, A., Cuacos, M., Cromer, L., et al. (2014). The kinesin AtPSS1 promotes synapsis and is required for proper crossover distribution in meiosis. *PLoS Genet.* 10 (10), e1004674. PMID: 25330379; PMCID: PMC4199493. doi:10.1371/journal.pgen.1004674

Emmenecker, C., Mézard, C., and Kumar, R. (2022). Repair of DNA double-strand breaks in plant meiosis: Role of eukaryotic RecA recombinases and their modulators. *Plant Reprod.* 36, 17–41. Epub ahead of print. PMID: 35641832. doi:10.1007/s00497-022-00443-6

Escobar-Guzmán, R., Rodríguez-Leal, D., Vielle-Calzada, J. P., and Ronceret, A. (2015). Whole-mount immunolocalization to study female meiosis in Arabidopsis. *Nat. Protoc.* 10 (10), 1535–1542. Epub 2015 Sep 10. PMID: 26357009. doi:10.1038/nprot.2015.098

Farahani-Tafreshi, Y., Wei, C., Gan, P., Daradur, J., Riggs, C. D., and Hasenkampf, C. A. (2022). The Arabidopsis HOP2 gene has a role in preventing illegitimate connections between nonhomologous chromosome regions. *Chromosome Res.* 30 (1), 59–75. Epub 2022 Jan 22. PMID: 35064347. doi:10.1007/s10577-021-09681-2

Fayos, I., Meunier, A. C., Vernet, A., Navarro-Sanz, S., Portefaix, M., Lartaud, M., et al. (2020). Assessment of the roles of SPO11-2 and SPO11-4 in meiosis in rice using CRISPR/Cas9 mutagenesis. *J. Exp. Bot.* 71 (22), 7046–7058. PMID: 32842152. doi:10.1093/jxb/eraa391

Ferdous, M., Higgins, J. D., Osman, K., Lambing, C., Roitinger, E., Mechtler, K., et al. (2012). Inter-homolog crossing-over and synapsis in Arabidopsis meiosis are dependent on the chromosome axis protein AtASY3. *PLoS Genet.* 8 (2), e1002507. Epub 2012 Feb 2. PMID: 22319460; PMCID: PMC3271061. doi:10.1371/journal.pgen.1002507

Fernandes, J. B., Duhamel, M., Seguéla-Arnaud, M., Froger, N., Girard, C., Choinard, S., et al. (2018). FIGL1 and its novel partner FLIP form a conserved complex that regulates homologous recombination. *PLoS Genet.* 14 (4), e1007317. PMID: 29608566; PMCID: PMC5897033. doi:10.1371/journal.pgen.1007317

Fozard, J. A., Morgan, C., and Howard, M. (2023). Coarsening dynamics can explain meiotic crossover patterning in both the presence and absence of the synaptonemal complex. *eLife* 12, e79408. doi:10.7554/eLife.79408

France, M. G., Enderle, J., Röhrig, S., Puchta, H., Franklin, F. C. H., and Higgins, J. D. (2021). ZYP1 is required for obligate cross-over formation and cross-over interference in *Arabidopsis*. *Proc. Natl. Acad. Sci. U. S. A.* 118 (14), e2021671118. PMID: 33782125; PMCID: PMC8040812. doi:10.1073/pnas.2021671118

Fu, M., Wang, C., Xue, F., Higgins, J., Chen, M., Zhang, D., et al. (2016). The DNA topoisomerase VI-B subunit OsMTOPVIB is essential for meiotic recombination initiation in rice. *Mol. Plant* 9 (11), 1539–1541. Epub 2016 Jul 28. PMID: 27477684. doi:10.1016/j.molp.2016.07.006

Fu, R., Wang, C., Shen, H., Zhang, J., Higgins, J. D., and Liang, W. (2020). Rice OsBRCA2 is required for DNA double-strand break repair in meiotic cells. *Front. Plant Sci.* 11, 600820. PMID: 33304374; PMCID: PMC7701097. doi:10.3389/fpls.2020.600820

Geuting, V., Kobbe, D., Hartung, F., Dürr, J., Focke, M., and Puchta, H. (2009). Two distinct MUS81-EME1 complexes from Arabidopsis process Holliday junctions. *Plant Physiol.* 150 (2), 1062–1071. Epub 2009 Apr 1. PMID: 19339504; PMCID: PMC2689967. doi:10.1104/pp.109.136846

Girard, C., Chelysheva, L., Choinard, S., Froger, N., Macaisne, N., Lemhemdi, A., et al. (2015). AAA-ATPase FIDGETIN-LIKE 1 and helicase FANCM antagonize meiotic crossovers by distinct mechanisms. *PLoS Genet.* 11 (7), e1005369. doi:10.1371/journal.pgen.1005369

Golubovskaya, I. N., Hamant, O., Timofejeva, L., Wang, C. J., Braun, D., Meeley, R., et al. (2006). Alleles of afd1 dissect REC8 functions during meiotic prophase I. *J. Cell Sci.* 119 (16), 3306–3315. Epub 2006 Jul 25. PMID: 16868028. doi:10.1242/jcs.03054

Gordillo, S. V. G., Escobar-Guzman, R., Rodriguez-Leal, D., Vielle-Calzada, J. P., and Ronceret, A. (2020). Whole-Mount immunolocalization procedure for plant female meiocytes. *Methods Mol. Biol.* 2061, 13–24. PMID: 31583649. doi:10.1007/978-1-4939-9818-0_2

Gray, S., and Cohen, P. E. (2016). Control of meiotic crossovers: From double-strand break formation to designation. *Annu. Rev. Genet.* 23 (50), 175–210. Epub 2016 Sep 14. PMID: 27648641; PMCID: PMC5319444. doi:10.1146/annurev-genet-120215-035111

Grelon, M., Vezon, D., Gendrot, G., and Pelletier, G. (2001). AtSPO11-1 is necessary for efficient meiotic recombination in plants. *EMBO J.* 20 (3), 589–600. PMID: 11157765; PMCID: PMC133473. doi:10.1093/emboj/20.3.589

Gutiérrez Pinzón, Y., González Kise, J. K., Rueda, P., and Ronceret, A. (2021). The Formation of bivalents and the control of plant meiotic recombination. *Front. Plant Sci.* 12, 717423. PMID: 34557215; PMCID: PMC8453087. doi:10.3389/fpls.2021.717423

Haber, J. (2008). "Evolution of models of homologous recombination," in *Recombination and meiosis*. Editors R. Egel and D.-H. Lankenau (Berlin Heidelberg: Springer-Verlag), 1–64. Genome Dyn Stab (3)Published online: 22 December 2007. doi:10.1007/7050_2007_037/

Haldane, J. B. S. (1931). The cytological basis of genetical interference. *Cytologia* 3 (1), 54–65. doi:10.1508/cytologia.3.54

Hartung, F., Suer, S., and Puchta, H. (2007). Two closely related RecQ helicases have antagonistic roles in homologous recombination and DNA repair in *Arabidopsis thaliana*. *Proc. Natl. Acad. Sci. U. S. A.* 104 (47), 18836–18841. doi:10.1073/pnas.0705998104

Hartung, F., Suer, S., Knoll, A., Wurz-Wildersinn, R., and Puchta, H. (2008). Topoisomerase 3alpha and RMI1 suppress somatic crossovers and are essential for resolution of meiotic recombination intermediates in *Arabidopsis thaliana*. *PLoS Genet.* 4 (12), e1000285. doi:10.1371/journal.pgen.1000285

He, Y., Wang, M., Dukowic-Schulze, S., Zhou, A., Tiang, C. L., Shilo, S., et al. (2017). Genomic features shaping the landscape of meiotic double-strand-break hotspots in maize. *Proc. Natl. Acad. Sci. U. S. A.* 114 (46), 12231–12236. Epub 2017 Oct 30. PMID: 29087335; PMCID: PMC5699076. doi:10.1073/pnas.1713225114

Hernandez Sanchez-Rebato, M., Bouatta, A. M., Gallego, M. E., White, C. I., and Da Ines, O. (2021). RAD54 is essential for RAD51-mediated repair of meiotic DSB in Arabidopsis. *PLoS Genet.* 17 (5), e1008919. PMID: 34003859; PMCID: PMC8162660. doi:10.1371/journal.pgen.1008919

Higgins, J. D., Armstrong, S. J., Franklin, F. C., and Jones, G. H. (2004). The Arabidopsis MutS homolog AtMSH4 functions at an early step in recombination: Evidence for two classes of recombination in Arabidopsis. *Genes Dev.* 18 (20), 2557–2570. PMID: 15489296; PMCID: PMC529542. doi:10.1101/gad.317504

Higgins, J. D., Buckling, E. F., Franklin, F. C., and Jones, G. H. (2008a). Expression and functional analysis of AtMUS81 in Arabidopsis meiosis reveals a role in the second pathway of crossing-over. *Plant J.* 54 (1), 152–162. PMID: 18182028. doi:10.1111/j.1365-313X.2008.03403.x

Higgins, J. D., Ferdous, M., Osman, K., and Franklin, F. C. (2011). The RecQ helicase AtRECQ4A is required to remove inter-chromosomal telomeric connections that arise during meiotic recombination in Arabidopsis. *Plant J.* 65 (3), 492–502. Epub 2010 Dec 30. PMID: 21265901. doi:10.1111/j.1365-313X.2010.04438.x

Higgins, J. D., Sanchez-Moran, E., Armstrong, S. J., Jones, G. H., and Franklin, F. C. (2005). The Arabidopsis synaptonemal complex protein ZYP1 is required for chromosome synapsis and normal fidelity of crossing over. *Genes Dev.* 19 (20), 2488–2500. PMID: 16230536; PMCID: PMC1257403. doi:10.1101/gad.354705

Higgins, J. D., Vignard, J., Mercier, R., Pugh, A. G., Franklin, F. C., and Jones, G. H. (2008b). AtMSH5 partners AtMSH4 in the class I meiotic crossover pathway in *Arabidopsis thaliana*, but is not required for synapsis. *Plant J.* 55 (1), 28–39. doi:10.1111/j.1365-313X.2008.03470.x

Holloway, J. K., Booth, J., Edelmann, W., McGowan, C. H., and Cohen, P. E. (2008). MUS81 generates a subset of MLH1-MLH3-independent crossovers in mammalian meiosis. *PLoS Genet.* 4 (9), :e1000186. PMID: 18787696; PMCID: PMC2525838. doi:10.1371/journal.pgen.1000186

Hu, Q., Li, Y., Wang, H., Shen, Y., Zhang, C., Du, G., et al. (2017). Meiotic chromosome association 1 interacts with TOP3α and regulates meiotic recombination in rice. *Plant Cell* 29 (7), 1697–1708. Epub 2017 Jul 10. PMID: 28696221; PMCID: PMC5559755. doi:10.1105/tpc.17.00241

Huang, J., Cheng, Z., Wang, C., Hong, Y., Su, H., Wang, J., et al. (2015). Formation of interference-sensitive meiotic cross-overs requires sufficient DNA leading-strand elongation. *Proc. Natl. Acad. Sci. U. S. A.* 112 (40), 12534–12539. Epub 2015 Sep 21. PMID: 26392549; PMCID: PMC4603498. doi:10.1073/pnas.1507165112

Hyde, L., Osman, K., Winfield, M., Sanchez-Moran, E., Higgins, J. D., Henderson, I. R., et al. (2023). Identification, characterization, and rescue of CRISPR/Cas9 generated wheat SPO11-1 mutants. *Plant Biotechnol. J.* 21 (2), 405–418. Epub 2022 Dec 10. PMID: 36373224; PMCID: PMC9884015. doi:10.1111/pbi.13961

Jackson, N., Sanchez-Moran, E., Buckling, E., Armstrong, S. J., Jones, G. H., and Franklin, F. C. (2006). Reduced meiotic crossovers and delayed prophase I progression in AtMLH3-deficient Arabidopsis. *EMBO J.* 25 (6), 1315–1323. Epub 2006 Feb 9. PMID: 16467846; PMCID: PMC1422170. doi:10.1038/sj.emboj.7600992

Janssens, F. A. (1909). La Thorie de la Chiasmatypie. Nouvelle interprétation des cinèses de maturation. *La Cell.* 25, 389–411.

Ji, J., Tang, D., Wang, M., Li, Y., Zhang, L., Wang, K., et al. (2013). MRE11 is required for homologous synapsis and DSB processing in rice meiosis. *Chromosoma* 122 (5), 363–376. Epub 2013 Jun 22. PMID: 23793712. doi:10.1007/s00412-013-0421-1

Jiang, J., Ou, X., Han, D., He, Z., Liu, S., Mao, N., et al. (2022). A diRNA-protein scaffold module mediates SMC5/6 recruitment in plant DNA repair. *Plant Cell.* 27;34 (10), 3899–3914. doi:10.1093/plcell/koac191

Jing, J., Zhang, T., Wang, Y., Cui, Z., and He, Y. (2019). ZmRAD51C is essential for double-strand break repair and homologous recombination in maize meiosis. *Int. J. Mol. Sci.* 20 (21), 5513. PMID: 31694261; PMCID: PMC6861927. doi:10.3390/ijms20215513

Jing, J. L., Zhang, T., Kao, Y. H., Huang, T. H., Wang, C. R., and He, Y. (2020). *ZmMTOPVIB* enables DNA double-strand break formation and bipolar spindle assembly during maize meiosis. *Plant Physiol.* 184 (4), 1811–1822. Epub 2020 Oct 19. PMID: 33077613; PMCID: PMC7723106. doi:10.1104/pp.20.00933

Kang, H. A., Shin, H. C., Kalantzi, A. S., Toseland, C. P., Kim, H. M., Gruber, S., et al. (2015). Crystal structure of Hop2-Mnd1 and mechanistic insights into its role in meiotic recombination. *Nucleic Acids Res.* 43 (7), 3841–3856. Epub 2015 Mar 3. PMID: 25740648; PMCID: PMC4402518. doi:10.1093/nar/gkv172

Kerzendorfer, C., Vignard, J., Pedrosa-Harand, A., Siwiec, T., Akimcheva, S., Jolivet, S., et al. (2006). The *Arabidopsis thaliana* MND1 homologue plays a key role in meiotic homologous pairing, synapsis and recombination. *J. Cell Sci.* 119 (12), 2486–2496. PMID: 16763194. doi:10.1242/jcs.02967

Kim, J., Park, J., Kim, H., Son, N., Kim, E. J., Kim, J., et al. (2022). Arabidopsis HEAT SHOCK FACTOR BINDING PROTEIN is required to limit meiotic crossovers and HEI10 transcription. *EMBO J.* 41 (14), e109958. Epub 2022 Jun 7. PMID: 35670129; PMCID: PMC9289711. doi:10.15252/embj.2021109958

Kleckner, N., Zickler, D., Jones, G. H., Dekker, J., Padmore, R., Henle, J., et al. (2004). A mechanical basis for chromosome function. *Proc. Natl. Acad. Sci. U. S. A.* 101 (34), 12592–12597. Epub 2004 Aug 6. PMID: 15299144; PMCID: PMC515102. doi:10.1073/pnas.0402724101

Knoll, A., Fauser, F., and Puchta, H. (2014). DNA recombination in somatic plant cells: Mechanisms and evolutionary consequences. *Chromosome Res.* 22 (2), 191–201. PMID: 24788060. doi:10.1007/s10577-014-9415-y

Kobayashi, W., Liu, E., Ishii, H., Matsunaga, S., Schlögelhofer, P., and Kurumizaka, H. (2019). Homologous pairing activities of *Arabidopsis thaliana* RAD51 and DMC1. *J. Biochem.* 165 (3), 289–295. PMID: 30517709. doi:10.1093/jb/mvy105

Kong, A., Thorleifsson, G., Stefansson, H., Masson, G., Helgason, A., Gudbjartsson, D. F., et al. (2008). Sequence variants in the RNF212 gene associate with genome-wide recombination rate. *Science* 319 (5868), 1398–1401. Epub 2008 Jan 31. PMID: 18239089. doi:10.1126/science.1152422

Koszul, R., and Zickler, D. (2012). La theorie de la Chiasmatypie 1909. *Genetics* 191 (2), 319–346. doi:10.1534/genetics.112.139725

Ku, J. C., Ronceret, A., Golubovskaya, I., Lee, D. H., Wang, C., Timofejeva, L., et al. (2020). Dynamic localization of SPO11-1 and conformational changes of meiotic axial elements during recombination initiation of maize meiosis. *PLoS Genet.* 16 (4), e1007881. PMID: 32310948; PMCID: PMC7192515. doi:10.1371/journal.pgen.1007881

Kumar, R., Duhamel, M., Coutant, E., Ben-Nahia, E., and Mercier, R. (2019). Antagonism between BRCA2 and FIGL1 regulates homologous recombination. *Nucleic Acids Res.* 47 (10), 5170–5180. doi:10.1093/nar/gkz225

Kurzbauer, M. T., Pradillo, M., Kerzendorfer, C., Sims, J., Ladurner, R., Oliver, C., et al. (2018). *Arabidopsis thaliana* FANCD2 promotes meiotic crossover formation. *Plant Cell* 30 (2), 415–428. Epub 2018 Jan 19. PMID: 29352063; PMCID: PMC5868695. doi:10.1105/tpc.17.00745

Kurzbauer, M. T., Uanschou, C., Chen, D., and Schlögelhofer, P. (2012). The recombinases DMC1 and RAD51 are functionally and spatially separated during meiosis in Arabidopsis. *Plant Cell* 24 (5), 2058–2070. Epub 2012 May 15. PMID: 22589466; PMCID: PMC3442587. doi:10.1105/tpc.112.098459

Lake, C. M., Nielsen, R. J., Guo, F., Unruh, J. R., Slaughter, B. D., Hawley, R. S., et al. (2015). Vilya, a component of the recombination nodule, is required for meiotic double-strand break formation in *Drosophila*. *Elife.* 4, e08287. doi:10.7554/eLife.08287

Lam, W. S., Yang, X., and Makaroff, C. A. (2005). Characterization of *Arabidopsis thaliana* SMC1 and SMC3: Evidence that AtSMC3 may function beyond chromosome cohesion. *J. Cell Sci.* 118 (14), 3037–3048. Epub 2005 Jun 21. PMID: 15972315. doi:10.1242/jcs.02443

Lambing, C., Kuo, P., Kim, J., Osman, K., Whitbread, A. L., Yang, J., et al. (2022). Differentiated function and localisation of SPO11-1 and PRD3 on the chromosome axis during meiotic DSB formation in *Arabidopsis thaliana*. *PLoS Genet.* 18 (7), e1010298. PMID: 35857772; PMCID: PMC9342770. doi:10.1371/journal.pgen.1010298

Lambing, C., Kuo, P. C., Tock, A. J., Topp, S. D., and Henderson, I. R. (2020). ASY1 acts as a dosage-dependent antagonist of telomere-led recombination and mediates crossover interference in *Arabidopsis*. *Proc. Natl. Acad. Sci. U. S. A.* 117 (24), 13647–13658. Epub 2020 Jun 4. PMID: 32499315; PMCID: PMC7306779. doi:10.1073/pnas.1921055117

Lee, D. H., Kao, Y. H., Ku, J. C., Lin, C. Y., Meeley, R., Jan, Y. S., et al. (2015). The axial element protein DESYNAPTIC2 mediates meiotic double-strand break formation and synaptonemal complex assembly in maize. *Plant Cell* 27 (9), 2516–2529. Epub 2015 Aug 21. PMID: 26296964; PMCID: PMC4815100. doi:10.1105/tpc.15.00434

Li, M., Li, S., He, Y., Wang, Y., Zhang, T., Li, P., et al. (2022). ZmSPO11-2 is critical for meiotic recombination in maize. *Chromosome Res.* 30 (4), 415–428. Epub 2022 Jun 8. PMID: 35674907. doi:10.1007/s10577-022-09694-5

Li, X., Zhang, J., Huang, J., Xu, J., Chen, Z., Copenhaver, G. P., et al. (2021). Regulation of interference-sensitive crossover distribution ensures crossover assurance in *Arabidopsis*. *Proc. Natl. Acad. Sci. U. S. A.* 118 (47), e2107543118. PMID: 34795056; PMCID: PMC8617516. doi:10.1073/pnas.2107543118

Li, Y., Qin, B., Shen, Y., Zhang, F., Liu, C., You, H., et al. (2018). HEIP1 regulates crossover formation during meiosis in rice. *Proc. Natl. Acad. Sci. U. S. A.* 115 (42), 10810–10815. Epub 2018 Oct 1. PMID: 30275327; PMCID: PMC6196533. doi:10.1073/pnas.1807871115

Liu, K., Chen, E., Gu, Z., Dai, B., Wang, A., Zhu, Z., et al. (2022). A retrotransposon insertion in MUTL-HOMOLOG 1 affects wild rice seed set and cultivated rice crossover rate. *Plant Physiol.* 190 (3), 1747–1762. PMID: 35976143; PMCID: PMC9614510. doi:10.1093/plphys/kiac378

Liu, M., Shi, S., Zhang, S., Xu, P., Lai, J., Liu, Y., et al. (2014). SUMO E3 ligase AtMMS21 is required for normal meiosis and gametophyte development in Arabidopsis. *BMC Plant Biol.* 14, 153. PMID: 24893774; PMCID: PMC4189105. doi:10.1186/1471-2229-14-153

Liu, X., Cao, Y., Du, G., Zhang, C., Xu, M., Cheng, Z., et al. (2022). OsRAD51 plays a vital role in promoting homologous recombination in rice meiosis. *Int. J. Mol. Sci.* 23 (17), 9906. PMID: 36077304; PMCID: PMC9456343. doi:10.3390/ijms23179906

Lloyd, A. (2023). Crossover patterning in plants. *Plant Reprod.* 36 (1), 55–72. Epub 2022 Jul 14. PMID: 35834006; PMCID: PMC9957876. doi:10.1007/s00497-022-00445-4

Lu, J., Wang, C., Wang, H., Zheng, H., Bai, W., Lei, D., et al. (2020). *OsMFS1/OsHOP2* complex participates in rice male and female development. *Front. Plant Sci.* 11, 518. PMID: 32499797; PMCID: PMC7243175. doi:10.3389/fpls.2020.00518

Luo, Q., Tang, D., Wang, M., Luo, W., Zhang, L., Qin, B., et al. (2013). The role of OsMSH5 in crossover formation during rice meiosis. *Mol. Plant* 6 (3), 729–742. Epub 2012 Dec 8. PMID: 23220939. doi:10.1093/mp/sss145

Macaisne, N., Novatchkova, M., Peirera, L., Vezon, D., Jolivet, S., Froger, N., et al. (2008). SHOC1, an XPF endonuclease-related protein, is essential for the formation of class I meiotic crossovers. *Curr. Biol.* 18 (18), 1432–1437. doi:10.1016/j.cub.2008.08.041

Mao, B., Zheng, W., Huang, Z., Peng, Y., Shao, Y., Liu, C., et al. (2021). Rice MutLγ, the MLH1-MLH3 heterodimer, participates in the formation of type I crossovers and regulation of embryo sac fertility. *Plant Biotechnol. J.* 19 (7), 1443–1455. Epub 2021 Feb 22. PMID: 33544956; PMCID: PMC8313138. doi:10.1111/pbi.13563

Martini, E., Diaz, R. L., Hunter, N., and Keeney, S. (2006). Crossover homeostasis in yeast meiosis. *Cell* 126 (2), 285–295. PMID: 16873061; PMCID: PMC1949389. doi:10.1016/j.cell.2006.05.044

Mendel, G. (1866). "Experiments in plant hybridization," in *Proceedings of the natural history society of brunn. (Translated by william bateson and corrected by roger blumberg)*. Available at: http://www.mendelweb.org/Mendel.html.

Mercier, R., Jolivet, S., Vezon, D., Huppe, E., Chelysheva, L., Giovanni, M., et al. (2005). Two meiotic crossover classes cohabit in Arabidopsis: One is dependent on MER3,whereas the other one is not. *Curr. Biol.* 15 (8), 692–701. doi:10.1016/j.cub.2005.02.056

Mercier, R., Mézard, C., Jenczewski, E., Macaisne, N., and Grelon, M. (2015). The molecular biology of meiosis in plants. *Annu. Rev. Plant Biol.* 66, 297–327. Epub 2014 Dec 1. PMID: 25494464. doi:10.1146/annurev-arplant-050213-035923

Mieulet, D., Aubert, G., Bres, C., Klein, A., Droc, G., Vieille, E., et al. (2018). Unleashing meiotic crossovers in crops. *Nat. Plants* 4 (12), 1010–1016. Epub 2018 Nov 26. PMID: 30478361. doi:10.1038/s41477-018-0311-x

Morgan, C., Fozard, J. A., Hartley, M., Henderson, I. R., Bomblies, K., and Howard, M. (2021). Diffusion-mediated HEI10 coarsening can explain meiotic crossover positioning in Arabidopsis. *Nat. Commun.* 12 (1), 4674. PMID: 34344879; PMCID: PMC8333306. doi:10.1038/s41467-021-24827-w

Morgan (1926). *The theory of the gene*. Yale University Press. Available at: http://www.esp.org/books/morgan/theory/facsimile/.

Mu, N., Li, Y., Li, S., Shi, W., Shen, Y., Yang, H., et al. (2022). MUS81 is required for atypical recombination intermediate resolution but not crossover designation in rice. *New Phytol.* 237, 2422–2434. Epub ahead of print. PMID: 36495065. doi:10.1111/nph.18668

Muller, H. J. (1916). The mechanism of crossing-over. II. IV. The manner of occurrence of crossing-over. *Am. Nat.* 50, 284–305. doi:10.1086/279541

Nageswaran, D. C., Kim, J., Lambing, C., Kim, J., Park, J., Kim, E. J., et al. (2021). HIGH CROSSOVER RATE1 encodes PROTEIN PHOSPHATASE X1 and restricts meiotic crossovers in Arabidopsis. *Nat. Plants* 7 (4), 452–467. Epub 2021 Apr 12. PMID: 33846593; PMCID: PMC7610654. doi:10.1038/s41477-021-00889-y

Nonomura, K., Nakano, M., Eiguchi, M., Suzuki, T., and Kurata, N. (2006). PAIR2 is essential for homologous chromosome synapsis in rice meiosis I. *J. Cell Sci.* 119 (2), 217–225. PMID: 16410547. doi:10.1242/jcs.02736

Olivier, M., Da Ines, O., Amiard, S., Serra, H., Goubely, C., White, C. I., et al. (2016). The structure-specific endonucleases MUS81 and SEND1 are essential for telomere stability in Arabidopsis. *Plant Cell* 28 (1), 74–86. Epub 2015 Dec 24. PMID: 26704385; PMCID: PMC4746687. doi:10.1105/tpc.15.00898

Orr, J. N., Waugh, R., and Colas, I. (2021). Ubiquitination in plant meiosis: Recent advances and high throughput methods. *Front. Plant Sci.* 12, 667314. PMID: 33897750; PMCID: PMC8058418. doi:10.3389/fpls.2021.667314

Osman, K., Algopishi, U., Higgins, J. D., Henderson, I. R., Edwards, K. J., Franklin, F. C. H., et al. (2021). Distal bias of meiotic crossovers in hexaploid bread wheat reflects spatio-temporal asymmetry of the meiotic program. *Front. Plant Sci.* 12, 631323. PMID: 33679846; PMCID: PMC7928317. doi:10.3389/fpls.2021.631323

Osman, K., Sanchez-Moran, E., Mann, S. C., Jones, G. H., and Franklin, F. C. (2009). Replication protein A (AtRPA1a) is required for class I crossover formation but is dispensable for meiotic DNA break repair. *EMBO J.* 28 (4), 394–404. Epub 2009 Jan 15. PMID: 19153602; PMCID: PMC2646153. doi:10.1038/emboj.2008.295

Otto, S. P., and Payseur, B. A. (2019). Crossover interference: Shedding light on the evolution of recombination. *Annu. Rev. Genet.* 53, 19–44. Epub 2019 Aug 20. PMID: 31430178; PMCID: PMC8715713. doi:10.1146/annurev-genet-040119-093957

Owen, A. R. G. (1949). A possible interpretation of the apparent interference across the centromere found by callan and montalenti in culex pipiens. *Hered. (Edinb)* 3, 357–367. doi:10.1038/hdy.1949.26

Pawlowski, W. P., Golubovskaya, I. N., and Cande, W. Z. (2003). Altered nuclear distribution of recombination protein RAD51 in maize mutants suggests the involvement of RAD51 in meiotic homology recognition. *Plant Cell* 15 (8), 1807–1816. PMID: 12897254; PMCID: PMC167171. doi:10.1105/tpc.012898

Pazhayam, N. M., Turcotte, C. A., and Sekelsky, J. (2021). Meiotic crossover patterning. *Front. Cell Dev. Biol.* 9, 681123. PMID: 34368131; PMCID: PMC8344875. doi:10.3389/fcell.2021.681123

Pfander, B., and Matos, J. (2017). Control of Mus81 nuclease during the cell cycle. *FEBS Lett.* 591 (14), 2048–2056. Epub 2017 Jul 10. PMID: 28640495. doi:10.1002/1873-3468.12727

Pochon, G., Henry, I. M., Yang, C., Lory, N., Fernández-Jiménez, N., Böwer, F., et al. (2022). The Arabidopsis Hop1 homolog ASY1 mediates cross-over assurance and interference. *PNAS Nexus* 2022, pgac302. doi:10.1093/pnasnexus/pgac302

Pradillo, M., Knoll, A., Oliver, C., Varas, J., Corredor, E., Puchta, H., et al. (2015). Involvement of the cohesin cofactor PDS5 (SPO76) during meiosis and DNA repair in *Arabidopsis thaliana*. *Front. Plant Sci.* 1 (6), 1034. PMID: 26648949; PMCID: PMC4664637. doi:10.3389/fpls.2015.01034

Pradillo, M., López, E., Linacero, R., Romero, C., Cuñado, N., Sánchez-Morán, E., et al. (2012). Together yes, but not coupled: New insights into the roles of RAD51 and DMC1 in plant meiotic recombination. *Plant J.* 69 (6), 921–933. Epub 2011 Dec 15. PMID: 22066484. doi:10.1111/j.1365-313X.2011.04845.x

Puchta, H. (2005). The repair of double-strand breaks in plants: Mechanisms and consequences for genome evolution. *J. Exp. Bot.* 56 (409), 1–14. Epub 2004 Nov 22. PMID: 15557293. doi:10.1093/jxb/eri025

Puizina, J., Siroky, J., Mokros, P., Schweizer, D., and Riha, K. (2004). Mre11 deficiency in Arabidopsis is associated with chromosomal instability in somatic cells and Spo11-dependent genome fragmentation during meiosis. *Plant Cell* 16 (8), 1968–1978. Epub 2004 Jul 16. PMID: 15258261; PMCID: PMC519189. doi:10.1105/tpc.104.022749

Qiao, H., Prasada Rao, H. B., Yang, Y., Fong, J. H., Cloutier, J. M., Deacon, D. C., et al. (2014). Antagonistic roles of ubiquitin ligase HEI10 and SUMO ligase RNF212 regulate meiotic recombination. *Nat. Genet.* 46 (2), 194–199. Epub 2014 Jan 5. PMID: 24390283; PMCID: PMC4356240. doi:10.1038/ng.2858

Rao, H. B., Qiao, H., Bhatt, S. K., Bailey, L. R., Tran, H. D., Bourne, S. L., et al. (2017). A SUMO-ubiquitin relay recruits proteasomes to chromosome axes to regulate meiotic recombination. *Science*. 355 (6323), 403–407. Epub 2017 Jan 5. PMID: 28059716; PMCID: PMC5569317. doi:10.1126/science.aaf6407

Ren, L., Zhao, T., Zhao, Y., Du, G., Yang, S., Mu, N., et al. (2021). The E3 ubiquitin ligase DESYNAPSIS1 regulates synapsis and recombination in rice meiosis. *Cell Rep.* 37 (5), 109941. doi:10.1016/j.celrep.2021.109941

Ren, Y., Chen, D., Li, W., Zhou, D., Luo, T., Yuan, G., et al. (2019). OsSHOC1 and OsPTD1 are essential for crossover formation during rice meiosis. *Plant J.* 98 (2), 315–328. Epub 2019 Feb 12. PMID: 30589140. doi:10.1111/tpj.14214

Resnick, M. A. (1976). The repair of double-strand breaks in DNA; a model involving recombination. *J. Theor. Biol.* 59 (1), 97–106. doi:10.1016/s0022-5193(76)80025-2

Rey, M. D., Martín, A. C., Higgins, J., Swarbreck, D., Uauy, C., Shaw, P., et al. (2017). Exploiting the *ZIP4* homologue within the wheat *Ph1* locus has identified two lines exhibiting homoeologous crossover in wheat-wild relative hybrids. *Mol. Breed.* 37 (8), 95. Epub 2017 Jul 18. PMID: 28781573; PMCID: PMC5515957. doi:10.1007/s11032-017-0700-2

Reynolds, A., Qiao, H., Yang, Y., Chen, J. K., Jackson, N., Biswas, K., et al. (2013). RNF212 is a dosage-sensitive regulator of crossing-over during mammalian meiosis. *Nat. Genet.* 45 (3), 269–278. Epub 2013 Feb 10. PMID: 23396135; PMCID: PMC4245152. doi:10.1038/ng.2541

Rog, O., Köhler, S., and Dernburg, A. F. (2017). The synaptonemal complex has liquid crystalline properties and spatially regulates meiotic recombination factors. *Elife* 6, e21455. doi:10.7554/eLife.21455

Ronceret, A., Guilleminot, J., Lincker, F., Gadea-Vacas, J., Delorme, V., Bechtold, N., et al. (2005). Genetic analysis of two Arabidopsis DNA polymerase epsilon subunits during early embryogenesis. *Plant J.* 44 (2), 223–236. doi:10.1111/j.1365-313X.2005.02521.x

Ronceret, A., and Pawlowski, W. P. (2010). Chromosome dynamics in meiotic prophase I in plants. *Cytogenet Genome Res.* 129 (1-3), 173–183. Epub 2010 Jun 10. PMID: 20551605. doi:10.1159/000313656

Saito, T. T., and Colaiácovo, M. P. (2019). Regulation of crossover frequency and distribution during meiotic recombination. *Cold Spring Harb. Symp. Quant. Biol.* 82, 223–234. doi:10.1101/sqb.2017.82.034132

Sanchez-Moran, E., Santos, J. L., Jones, G. H., and Franklin, F. C. (2007). ASY1 mediates AtDMC1-dependent interhomolog recombination during meiosis in Arabidopsis. *Genes Dev.* 21 (17), 2220–2233. PMID: 17785529; PMCID: PMC1950860. doi:10.1101/gad.439007

Sarens, M., Copenhaver, G. P., and De Storme, N. (2021). The role of chromatid interference in determining meiotic crossover patterns. *Front. Plant Sci.* 12, 656691. PMID: 33767725; PMCID: PMC7985435. doi:10.3389/fpls.2021.656691

Séguéla-Arnaud, M., Crismani, W., Larchevêque, C., Mazel, J., Froger, N., Choinard, S., et al. (2015). Multiple mechanisms limit meiotic crossovers: TOP3α and two BLM homologs antagonize crossovers in parallel to FANCM. *Proc. Natl. Acad. Sci. U. S. A.* 112 (15), 4713–4718. Epub 2015 Mar 30. PMID: 25825745; PMCID: PMC4403193. doi:10.1073/pnas.1423107112

Séguéla-Arnaud, M., Choinard, S., Larchevêque, C., Girard, C., Froger, N., Crismani, W., et al. (2017). RMI1 and TOP3α limit meiotic CO formation through their C-terminal domains. *Nucleic Acids Res.* 45 (4), 1860–1871. doi:10.1093/nar/gkw1210

Serra, H., Lambing, C., Griffin, C. H., Topp, S. D., Nageswaran, D. C., Underwood, C. J., et al. (2018). Massive crossover elevation via combination of *HEI10* and *recq4a recq4b* during *Arabidopsis* meiosis. *Proc. Natl. Acad. Sci. U. S. A.* 115 (10), 2437–2442. Epub 2018 Feb 20. PMID: 29463699; PMCID: PMC5877939. doi:10.1073/pnas.1713071115

Shao, T., Tang, D., Wang, K., Wang, M., Che, L., Qin, B., et al. (2011). OsREC8 is essential for chromatid cohesion and metaphase I monopolar orientation in rice meiosis. *Plant Physiol.* 156 (3), 1386–1396. Epub 2011 May 23. PMID: 21606318; PMCID: PMC3135945. doi:10.1104/pp.111.177428

Shen, Y., Tang, D., Wang, K., Wang, M., Huang, J., Luo, W., et al. (2012). ZIP4 in homologous chromosome synapsis and crossover formation in rice meiosis. *J. Cell Sci.* 125 (11), 2581–2591. Epub 2012 Mar 5. PMID: 22393242. doi:10.1242/jcs.090993

Shi, W., Ji, J., Xue, Z., Zhang, F., Miao, Y., Yang, H., et al. (2021). PRD1, a homologous recombination initiation factor, is involved in spindle assembly in rice meiosis. *New Phytol.* 230 (2), 585–600. Epub 2021 Feb 10. PMID: 33421144. doi:10.1111/nph.17178

Shi, W., Tang, D., Shen, Y., Xue, Z., Zhang, F., Zhang, C., et al. (2019). OsHOP2 regulates the maturation of crossovers by promoting homologous pairing and synapsis in rice meiosis. *New Phytol.* 222 (2), 805–819. Epub 2019 Jan 25. PMID: 30584664. doi:10.1111/nph.15664

Shingu, Y., Tokai, T., Agawa, Y., Toyota, K., Ahamed, S., Kawagishi-Kobayashi, M., et al. (2012). The double-stranded break-forming activity of plant SPO11s and a novel rice SPO11 revealed by a Drosophila bioassay. *BMC Mol. Biol.* 13, 1. PMID: 22248237; PMCID: PMC3273433. doi:10.1186/1471-2199-13-1

Sidhu, G. K., Fang, C., Olson, M. A., Falque, M., Martin, O. C., and Pawlowski, W. P. (2015). Recombination patterns in maize reveal limits to crossover homeostasis. *Proc. Natl. Acad. Sci. U. S. A.* 112 (52), 15982–15987. Epub 2015 Dec 14. PMID: 26668366; PMCID: PMC4703008. doi:10.1073/pnas.1514265112

Singh, A., Sharma, A., Singh, N., and Nandi, A. K. (2022). MTO1-RESPONDING DOWN 1 (MRD1) is a transcriptional target of OZF1 for promoting salicylic acid-mediated defense in Arabidopsis. *Plant Cell Rep.* 41 (5), 1319–1328. Epub 2022 Mar 24. PMID: 35325291. doi:10.1007/s00299-022-02861-2

Singh, D. K., Gamboa, R. S., Singh, A. K., Walkemeier, B., Van Leene, J., De Jaeger, G., et al. (2023). The FANCC-FANCE-FANCF complex is evolutionarily conserved and regulates meiotic recombination. *Nucleic Acids Res.* 51, 2516–2528. Epub ahead of print. PMID: 36652992. doi:10.1093/nar/gkac1244

Sprink, T., and Hartung, F. (2021). Heterologous complementation of SPO11-1 and -2 depends on the splicing pattern. *Int. J. Mol. Sci.* 22 (17), 9346. PMID: 34502253; PMCID: PMC8430568. doi:10.3390/ijms22179346

Sprink, T., and Hartung, F. (2014). The splicing fate of plant SPO11 genes. *Front. Plant Sci.* 5, 214. PMID: 25018755; PMCID: PMC4071758. doi:10.3389/fpls.2014.00214

Stacey, N. J., Kuromori, T., Azumi, Y., Roberts, G., Breuer, C., Wada, T., et al. (2006). Arabidopsis SPO11-2 functions with SPO11-1 in meiotic recombination. *Plant J.* 48 (2), 206–216. doi:10.1111/j.1365-313X.2006.02867.x

Steckenborn, S., Cuacos, M., Ayoub, M. A., Feng, C., Schubert, V., Hoffie, I., et al. (2023). The meiotic topoisomerase VI B subunit (MTOPVIB) is essential for meiotic DNA double-strand break formation in barley (Hordeum vulgare L). *Plant Reprod.* 36 (1), 1–15. doi:10.1007/s00497-022-00444-5

Sturtevant (1965). *A history of genetics*. Cold Spring Harbor Laboratory Press. Available at: www.esp.org/books/sturt/history.

Sturtevant, A. H. (1913). The linear arrangement of six sex-linked factors in Drosophila, as shown by their mode of association. *J. Exp. Zool.* 14, 43–59. doi:10.1002/jez.1400140104

Su, H., Cheng, Z., Huang, J., Lin, J., Copenhaver, G. P., Ma, H., et al. (2017). Arabidopsis RAD51, RAD51C and XRCC3 proteins form a complex and facilitate RAD51 localization on chromosomes for meiotic recombination. *PLoS Genet.* 13 (5), e1006827. PMID: 28562599; PMCID: PMC5470734. doi:10.1371/journal.pgen.1006827

Sun, L., Wang, J., Sang, M., Jiang, L., Zhao, B., Cheng, T., et al. (2017). Landscaping crossover interference across a genome. *Trends Plant Sci.* 22 (10), 894–907. Epub 2017 Aug 16. PMID: 28822625. doi:10.1016/j.tplants.2017.06.008

Sym, M., Engebrecht, J. A., and Roeder, G. S. (1993). ZIP1 is a synaptonemal complex protein required for meiotic chromosome synapsis. *Cell* 72 (3), 365–378. PMID: 7916652. doi:10.1016/0092-8674(93)90114-6

Szostak, J. W., Orr-Weaver, T. L., Rothstein, R. J., and Stahl, F. W. (1983). The double-strand-break repair model for recombination. *Cell* 33 (1), 25–35. PMID:6380756. doi:10.1016/0092-8674(83)90331-8

Szurman-Zubrzycka, M., Baran, B., Stolarek-Januszkiewicz, M., Kwaśniewska, J., Szarejko, I., and Gruszka, D. (2019). The *dmc1* mutant allows an insight into the DNA double-strand break repair during meiosis in barley (*Hordeum vulgare* L). *Front. Plant Sci.* 10, 761. doi:10.3389/fpls.2019.00761

Tock, A. J., Holland, D. M., Jiang, W., Osman, K., Sanchez-Moran, E., Higgins, J. D., et al. (2021). Crossover-active regions of the wheat genome are distinguished by DMC1, the chromosome axis, H3K27me3, and signatures of adaptation. *Genome Res.* 31 (9), 1614–1628. Epub 2021 Aug 23. PMID: 34426514; PMCID: PMC8415368. doi:10.1101/gr.273672.120

Uanschou, C., Ronceret, A., Von Harder, M., De Muyt, A., Vezon, D., Pereira, L., et al. (2013). Sufficient amounts of functional HOP2/MND1 complex promote interhomolog DNA repair but are dispensable for intersister DNA repair during meiosis in Arabidopsis. *Plant Cell* 25 (12), 4924–4940. Epub 2013 Dec 20. PMID: 24363313; PMCID: PMC3903996. doi:10.1105/tpc.113.118521

Uanschou, C., Siwiec, T., Pedrosa-Harand, A., Kerzendorfer, C., Sanchez-Moran, E., Novatchkova, M., et al. (2007). A novel plant gene essential for meiosis is related to the human CtIP and the yeast COM1/SAE2 gene. *EMBO J.* 26 (24), 5061–5070. Epub 2007 Nov 15. PMID: 18007598; PMCID: PMC2140101. doi:10.1038/sj.emboj.7601913

Vignard, J., Siwiec, T., Chelysheva, L., Vrielynck, N., Gonord, F., Armstrong, S. J., et al. (2007). The interplay of RecA-related proteins and the MND1-HOP2 complex during meiosis in *Arabidopsis thaliana*. *PLoS Genet.* 3 (10), 1894–1906. Epub 2007 Aug 30. PMID: 17937504; PMCID: PMC2014788. doi:10.1371/journal.pgen.0030176

Vrielynck, N., Chambon, A., Vezon, D., Pereira, L., Chelysheva, L., De Muyt, A., et al. (2016). A DNA topoisomerase VI-like complex initiates meiotic recombination. *Science* 351 (6276), 939–943. PMID: 26917763. doi:10.1126/science.aad5196

Vrielynck, N., Schneider, K., Rodriguez, M., Sims, J., Chambon, A., Hurel, A., et al. (2021). Conservation and divergence of meiotic DNA double strand break forming mechanisms in *Arabidopsis thaliana*. *Nucleic Acids Res.* 49 (17), 9821–9835. PMID: 34458909; PMCID: PMC8464057. doi:10.1093/nar/gkab715

Vu, G. T. H., Cao, H. X., Fauser, F., Reiss, B., Puchta, H., and Schubert, I. (2017). Endogenous sequence patterns predispose the repair modes of CRISPR/Cas9-induced DNA double-stranded breaks in *Arabidopsis thaliana*. *Plant J.* 92 (1), 57–67. Epub 2017 Aug 14. PMID: 28696528. doi:10.1111/tpj.13634

Wang, C., Higgins, J. D., He, Y., Lu, P., Zhang, D., and Liang, W. (2017). Resolvase OsGEN1 mediates DNA repair by homologous recombination. *Plant Physiol.* 173 (2), 1316–1329. Epub 2017 Jan 3. PMID: 28049740; PMCID: PMC5291025. doi:10.1104/pp.16.01726

Wang, C., Huang, J., Li, Y., Zhang, J., He, C., Li, T., et al. (2022b). DNA polymerase epsilon binds histone H3.1-H4 and recruits MORC1 to mediate meiotic heterochromatin condensation. *Proc. Natl. Acad. Sci. U. S. A.* 119 (43), e2213540119. Epub 2022 Oct 19. PMID: 36260743; PMCID: PMC9618065. doi:10.1073/pnas.2213540119

Wang, C., Huang, J., Zhang, J., Wang, H., Han, Y., Copenhaver, G. P., et al. (2019). The largest subunit of DNA polymerase delta is required for normal formation of

meiotic type I crossovers. *Plant Physiol.* 179 (2), 446–459. Epub 2018 Nov 20. PMID: 30459265; PMCID: PMC6426404. doi:10.1104/pp.18.00861

Wang, C., Huang, J., Zhang, J., Yu, Y., Copenhaver, G. P., You, C., et al. (2022a). DNA polymerase epsilon interacts with SUVH2/9 to repress the expression of genes associated with meiotic DSB hotspot in *Arabidopsis*. *Proc. Natl. Acad. Sci. U. S. A.* 119 (41), e2208441119. Epub 2022 Oct 3. PMID: 36191225; PMCID: PMC9564942. doi:10.1073/pnas.2208441119

Wang, C., Qu, S., Zhang, J., Fu, M., Chen, X., and Liang, W. (2023). OsPRD2 is essential for double-strand break formation, but not spindle assembly during rice meiosis. *Front. Plant Sci.* 13, 1122202. PMID: 36714725; PMCID: PMC9880466. doi:10.3389/fpls.2022.1122202

Wang, H., Hu, Q., Tang, D., Liu, X., Du, G., Shen, Y., et al. (2016). OsDMC1 is not required for homologous pairing in rice meiosis. *Plant Physiol.* 171 (1), 230–241. Epub 2016 Mar 9. PMID: 26960731; PMCID: PMC4854709. doi:10.1104/pp.16.00167

Wang, H., Xu, W., Sun, Y., Lian, Q., Wang, C., Yu, C., et al. (2020). The cohesin loader SCC2 contains a PHD finger that is required for meiosis in land plants. *PLoS Genet.* 16 (6), e1008849. PMID: 32516352; PMCID: PMC7304647. doi:10.1371/journal.pgen.1008849

Wang, K., Tang, D., Wang, M., Lu, J., Yu, H., Liu, J., et al. (2009). MER3 is required for normal meiotic crossover formation, but not for presynaptic alignment in rice. *J. Cell Sci.* 122 (12), 2055–2063. Epub 2009 May 26. PMID: 19470578. doi:10.1242/jcs.049080

Wang, K., Wang, M., Tang, D., Shen, Y., Miao, C., Hu, Q., et al. (2012). The role of rice HEI10 in the formation of meiotic crossovers. *PLoS Genet.* 8 (7), e1002809. Epub 2012 Jul 5. PMID: 22792078; PMCID: PMC3390396. doi:10.1371/journal.pgen.1002809

Wang, K., Wang, M., Tang, D., Shen, Y., Qin, B., Li, M., et al. (2011). PAIR3, an axis-associated protein, is essential for the recruitment of recombination elements onto meiotic chromosomes in rice. *Mol. Biol. Cell* 22 (1), 12–19. Epub 2010 Nov 30. PMID: 21119003; PMCID: PMC3016970. doi:10.1091/mbc.E10-08-0667

Wang, M., Wang, K., Tang, D., Wei, C., Li, M., Shen, Y., et al. (2010). The central element protein ZEP1 of the synaptonemal complex regulates the number of crossovers during meiosis in rice. *Plant Cell* 22 (2), 417–430. Epub 2010 Feb 12. PMID: 20154151; PMCID: PMC2845403. doi:10.1105/tpc.109.070789

Wang, Y., Cheng, Z., Huang, J., Shi, Q., Hong, Y., Copenhaver, G. P., et al. (2012). The DNA replication factor RFC1 is required for interference-sensitive meiotic crossovers in *Arabidopsis thaliana*. *PLoS Genet.* 8 (11), e1003039. Epub 2012 Nov 8. PMID: 23144629; PMCID: PMC3493451. doi:10.1371/journal.pgen.1003039

Wang, Y., and Copenhaver, G. P. (2018). Meiotic recombination: Mixing it up in plants. *Annu. Rev. Plant Biol.* 69, 577–609. Epub 2018 Feb 28. PMID: 29489392. doi:10.1146/annurev-arplant-042817-040431

Wang, Y., Jiang, L., Zhang, T., Jing, J., and He, Y. (2018). *ZmCom1* is required for both mitotic and meiotic recombination in maize. *Front. Plant Sci.* 9, 1005. PMID: 30061907; PMCID: PMC6055016. doi:10.3389/fpls.2018.01005

Wang, Y., Li, S. Y., Wang, Y. Z., and He, Y. (2023). ZmASY1 interacts with ZmPRD3 and is crucial for meiotic double-strand break formation in maize. *New Phytol.* 237 (2), 454–470. 18528. Epub 2022 Nov 30. PMID: 36221195. doi:10.1111/nph.18528

Wang, Y., Wang, Y., Zang, J., Chen, H., and He, Y. (2022). ZmPRD1 is essential for double-strand break formation, but is not required for bipolar spindle assembly during maize meiosis. *J. Exp. Bot.* 73 (11), 3386–3400. doi:10.1093/jxb/erac075

Ward, J. O., Reinholdt, L. G., Motley, W. W., Niswander, L. M., Deacon, D. C., Griffin, L. B., et al. (2007). Mutation in mouse hei10, an e3 ubiquitin ligase, disrupts meiotic crossing over. *PLoS Genet.* 3 (8), e139. Epub 2007 Jul 6. PMID: 17784788; PMCID: PMC1959360. doi:10.1371/journal.pgen.0030139

Watanabe, K., Pacher, M., Dukowic, S., Schubert, V., Puchta, H., and Schubert, I. (2009). The STRUCTURAL MAINTENANCE OF CHROMOSOMES 5/6 complex promotes sister chromatid alignment and homologous recombination after DNA damage in *Arabidopsis thaliana*. *Plant Cell* 21 (9), 2688–2699. Epub 2009 Sep 8. PMID: 19737979; PMCID: PMC2768936. doi:10.1105/tpc.108.060525

Waterworth, W. M., Altun, C., Armstrong, S. J., Roberts, N., Dean, P. J., Young, K., et al. (2007). NBS1 is involved in DNA repair and plays a synergistic role with ATM in mediating meiotic homologous recombination in plants. *Plant J.* 52 (1), 41–52. Epub 2007 Aug 2. PMID: 17672843. doi:10.1111/j.1365-313X.2007.03220.x

Whitbread, A. L., Dorn, A., Röhrig, S., and Puchta, H. (2021). Different functional roles of RTR complex factors in DNA repair and meiosis in Arabidopsis and tomato. *Plant J.* 106 (4), 965–977. Epub 2021 Mar 25. PMID: 33619799. doi:10.1111/tpj.15211

Wijeratne, A. J., Chen, C., Zhang, W., Timofejeva, L., and Ma, H. (2006). The *Arabidopsis thaliana* PARTING DANCERS gene encoding a novel protein is required for normal meiotic homologous recombination. *Mol. Biol. Cell* 17 (3), 1331–1343. Epub 2006 Jan 4. PMID: 16394097; PMCID: PMC1382321. doi:10.1091/mbc.e05-09-0902

Xue, M., Wang, J., Jiang, L., Wang, M., Wolfe, S., Pawlowski, W. P., et al. (2018). The number of meiotic double-strand breaks influences crossover distribution in Arabidopsis. *Plant Cell* 30 (10), 2628–2638. Epub 2018 Oct 3. PMID: 30282794; PMCID: PMC6241269. doi:10.1105/tpc.18.00531

Xue, Z., Liu, C., Shi, W., Miao, Y., Shen, Y., Tang, D., et al. (2019). OsMTOPVIB is required for meiotic bipolar spindle assembly. *Proc. Natl. Acad. Sci. U. S. A.* 116 (32), 15967–15972. Epub 2019 Jul 24. PMID: 31341087; PMCID: PMC6689953. doi:10.1073/pnas.1821315116

Yadav, V. K., and Claeys Bouuaert, C. (2021). Mechanism and control of meiotic DNA double-strand break formation in *S. cerevisiae*. *Front. Cell Dev. Biol.* 9, 642737. PMID: 33748134; PMCID: PMC7968521. doi:10.3389/fcell.2021.642737

Yang, C., Sofroni, K., Hamamura, Y., Hu, B., Elbasi, H. T., Balboni, M., et al. (2022). ZYP1-mediated recruitment of PCH2 to the synaptonemal complex remodels the chromosome axis leading to crossover restriction. *Nucleic Acids Res.* 50 (22), 12924–12937. PMID: 36504011; PMCID: PMC9825157. doi:10.1093/nar/gkac1160

Yang, S., Zhang, C., Cao, Y., Du, G., Tang, D., Li, Y., et al. (2022). FIGNL1 inhibits non-homologous chromosome association and crossover formation. *Front. Plant Sci.* 11 (13), 945893. PMID: 35898226; PMCID: PMC9310568. doi:10.3389/fpls.2022.945893

Zhang, B., Wang, M., Tang, D., Li, Y., Xu, M., Gu, M., et al. (2015). XRCC3 is essential for proper double-strand break repair and homologous recombination in rice meiosis. *J. Exp. Bot.* 66 (19), 5713–5725. Epub 2015 Jun 1. PMID: 26034131. doi:10.1093/jxb/erv253

Zhang, C., Song, Y., Cheng, Z. H., Wang, Y. X., Zhu, J., Ma, H., et al. (2012). The *Arabidopsis thaliana* DSB formation (AtDFO) gene is required for meiotic double-strand break formation. *Plant J.* 72 (2), 271–281. Epub 2012 Jul 26. PMID: 22694475. doi:10.1111/j.1365-313X.2012.05075.x

Zhang, L., Köhler, S., Rillo-Bohn, R., and Dernburg, A. F. (2018). A compartmentalized signaling network mediates crossover control in meiosis. *Elife* 7, e30789. PMID: 29521627; PMCID: PMC5906097. doi:10.7554/eLife.30789

Zhang, L., Liang, Z., Hutchinson, J., and Kleckner, N. (2014a). Crossover patterning by the beam-film model: Analysis and implications. *PLoS Genet.* 10 (1), e1004042. PMID: 24497834; PMCID: PMC3907302. doi:10.1371/journal.pgen.1004042

Zhang, L., Stauffer, W., Zwicker, D., and Dernburg, A. F. (2021). *Crossover patterning through kinase-regulated condensation and coarsening of recombination nodules*. bioRxiv 2021.08.26.457865.

Zhang, L., Tang, D., Luo, Q., Chen, X., Wang, H., Li, Y., et al. (2014b). Crossover formation during rice meiosis relies on interaction of OsMSH4 and OsMSH5. *Genetics* 198 (4), 1447–1456. Epub 2014 Oct 2. PMID: 25278554; PMCID: PMC4256764. doi:10.1534/genetics.114.168732

Zhang, P., Zhang, Y., Sun, L., Sinumporn, S., Yang, Z., Sun, B., et al. (2017). The rice AAA-ATPase OsFIGNL1 is essential for male meiosis. *Front. Plant Sci.* 8, 1639. PMID: 29021797; PMCID: PMC5624289. doi:10.3389/fpls.2017.01639

Zhao, H., McPeek, M. S., and Speed, T. P. (1995). Statistical analysis of chromatid interference. *Genetics* 139 (2), 1057–1065. PMID: 7713408; PMCID: PMC1206356. doi:10.1093/genetics/139.2.1057

Zhu, L., Fernández-Jiménez, N., Szymanska-Lejman, M., Pelé, A., Underwood, C. J., Serra, H., et al. (2021). Natural variation identifies SNI1, the SMC5/6 component, as a modifier of meiotic crossover in *Arabidopsis*. *Proc. Natl. Acad. Sci. U. S. A.* 118 (33), e2021970118. PMID: 34385313; PMCID: PMC8379953. doi:10.1073/pnas.2021970118

Zickler, D., and Kleckner, N. (1999). Meiotic chromosomes: Integrating structure and function. *Annu. Rev. Genet.* 33, 603–754. PMID: 10690419. doi:10.1146/annurev.genet.33.1.603

Zickler, D., and Kleckner, N. (2015). Recombination, pairing, and synapsis of homologs during meiosis. *Cold Spring Harb. Perspect. Biol.* 7 (6), a016626. PMID: 25986558; PMCID: PMC4448610. doi:10.1101/cshperspect.a016626

Ziolkowski, P. A., Underwood, C. J., Lambing, C., Martinez-Garcia, M., Lawrence, E. J., Ziolkowska, L., et al. (2017). Natural variation and dosage of the HEI10 meiotic E3 ligase control *Arabidopsis* crossover recombination. *Genes Dev.* 31 (3), 306–317. Epub 2017 Feb 21. PMID: 28223312; PMCID: PMC5358726. doi:10.1101/gad.295501.116

Ziolkowski, P. A. (2023). Why do plants need the ZMM crossover pathway? A snapshot of meiotic recombination from the perspective of interhomolog polymorphism. *Plant Reprod.* 36 (1), 43–54. Epub 2022 Jul 12. PMID: 35819509; PMCID: PMC9958190. doi:10.1007/s00497-022-00446-3

frontiers | Frontiers in Cell and Developmental Biology

TYPE Review
PUBLISHED 12 June 2023
DOI 10.3389/fcell.2023.1191156

OPEN ACCESS

EDITED BY
Pedro A. San-Segundo,
CSIC-University of Salamanca, Spain

REVIEWED BY
Peter Carlton,
Kyoto University, Japan
Sean Burgess,
University of California, Davis,
United States

*CORRESPONDENCE
Joan Blanco,
joan.blanco@uab.cat
Zaida Sarrate,
zaida.sarrate@uab.cat

†These authors have contributed equally to this work and share first authorship

RECEIVED 21 March 2023
ACCEPTED 01 June 2023
PUBLISHED 12 June 2023

CITATION
Solé M, Pascual Á, Anton E, Blanco J and Sarrate Z (2023), The courtship choreography of homologous chromosomes: timing and mechanisms of DSB-independent pairing.
Front. Cell Dev. Biol. 11:1191156.
doi: 10.3389/fcell.2023.1191156

The courtship choreography of homologous chromosomes: timing and mechanisms of DSB-independent pairing

Mireia Solé, Álvaro Pascual, Ester Anton, Joan Blanco*† and Zaida Sarrate*†

Departament de Biologia Cel·lular, Genetics of Male Fertility Group, Unitat de Biologia Cel·lular, Fisiologia i Immunologia, Universitat Autònoma de Barcelona, Barcelona, Spain

Meiosis involves deep changes in the spatial organisation and interactions of chromosomes enabling the two primary functions of this process: increasing genetic diversity and reducing ploidy level. These two functions are ensured by crucial events such as homologous chromosomal pairing, synapsis, recombination and segregation. In most sexually reproducing eukaryotes, homologous chromosome pairing depends on a set of mechanisms, some of them associated with the repair of DNA double-strand breaks (DSBs) induced at the onset of prophase I, and others that operate before DSBs formation. In this article, we will review various strategies utilised by model organisms for DSB-independent pairing. Specifically, we will focus on mechanisms such as chromosome clustering, nuclear and chromosome movements, as well as the involvement of specific proteins, non-coding RNA, and DNA sequences.

KEYWORDS

homologous chromosomes, homologous pairing, chromosome dynamics, meiosis, cell division

Introduction

Meiosis is a process aimed at producing haploid gametes from diploid germ cells. With this purpose, a single round of DNA replication is followed by two consecutive chromosome segregations. Meiosis increases genetic variation via two important mechanisms, namely, independent assortment of homologous chromosomes and genetic recombination. To this end, it is required that, in meiosis I, homologous chromosomes come close together in a process called pairing, synapse via synaptonemal complex (SC) formation (reviewed in Page and Hawley, 2004), recombine (reviewed in Hunter, 2015) and segregate randomly. Although these four processes are conceptually distinct, they are all closely related and take place in a sequential way.

It is widely accepted that the generation of DSBs by the topoisomerase-like transesterase protein Spo11 and the subsequent action of the DNA repair machinery (reviewed by Keeney, 2008; Baudat et al., 2013) induce the physical recognition among homologous DNA sequences. Once DSBs have been formed, the ends are resected to generate 3' single-strand tails, which are loaded with RecA-like proteins, Rad51 and Dmc1. Proteins and DNA form a filament (via a nascent D-loop) able to identify and interact with their corresponding homologous double-strand DNA, that eventually cause the approach and coalignment, at a distance of approximately 400 nm, of specific regions of homologous chromosomes—the

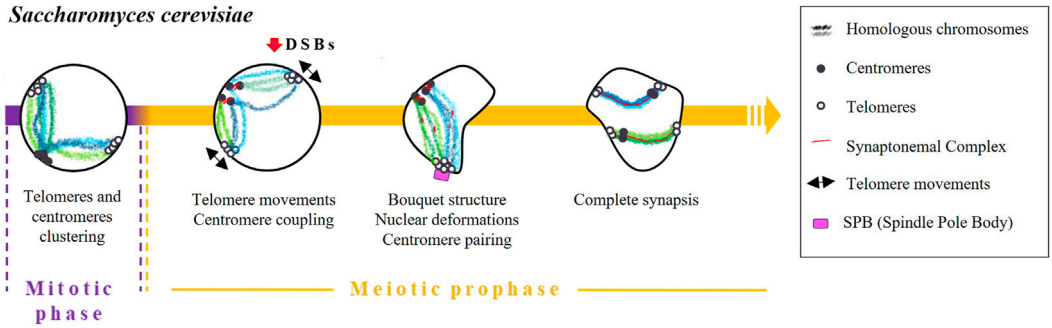

FIGURE 1
Timing and mechanisms of DSB-independent homologous pairing in *Saccharomyces cerevisiae*.

PAIRING (reviewed in Zickler, 2006). It has been suggested that only one of the two generated ends would create this "homology searching tentacle" of DNA and nucleoproteins (Kim et al., 2010). The alignment of the entirety of the homologous chromosomes requires the assembly of SC—the SYNAPSIS (reviewed in Page and Hawley, 2004). Subsequently, the process of RECOMBINATION will move forward through different strand isomerisations leading to crossover and non-crossover products (reviewed in Hunter, 2015; Gray and Cohen, 2016).

Accordingly, in some species the formation and repair of DSBs play an essential role in the processes of pairing and synapsis. In support of this hypothesis, it has been observed in *spo11* mutants a relationship between alterations in the number of DSBs and anomalies in the formation and functionality of the SC (Baudat et al., 2000; Romanienko and Camerini-Otero, 2000; Tesse et al., 2003; Kauppi et al., 2013; Rockmill et al., 2013). Moreover, exogenous DSBs induction partially restores the meiotic defects observed in some of these mutants (Thorne and Byers, 1993; Dernburg et al., 1998; Storlazzi et al., 2003; Tessé et al., 2003).

In contrast, in certain model organisms such as *Drosophila* or *Caenorhabditis*, the involvement of DSBs in the pairing process seems to be dispensable. Moreover, regardless the participation of DSBs, several aspects of the pairing mechanism indicate the existence of alternative pathways that play a role in facilitating the recognition and alignment of homologous chromosomes. For instance, it should be noted that each DSB generates approximately 1 kb of ssDNA that needs to identify and localise its homologous chromatid. A homologous sequence search should be achieved within a short period of time and then held together. This action is not that simple if homologous chromosomes are not previously sharing the same territory. Furthermore, chromosomes contain repetitive sequences, and thus, potential interactions between these pseudo-homologous regions must be avoided or eliminated during the homology search process.

In this article, we review the strategies described in different model organisms that promote homologous pairing throughout mechanisms not related to DSBs formation. It is important to note that the term "pairing" will be used to describe the approximation, association and recognition of homologous chromosomes before the onset of synapsis.

Saccharomyces cerevisiae

The initial stages of homologous pairing in budding yeast are determined by telomere clustering and centromere coupling (Figure 1). In vegetative (mitotic) cells, telomeres are located in a few clusters at the periphery of the nucleus. After the induction of meiosis, telomeres disperse over the nuclear periphery and cluster at the spindle pole body (SPB) (Trelles-Sticken et al., 1999). Meiocytes arrested in premeiotic S-phase have only a few peripheral telomere clusters, suggesting that the resolution of peripheral vegetative telomere clusters occurs at the end of or shortly after premeiotic S-phase (Trelles-Sticken et al., 1999; Trelles-Sticken et al. 2000; Trelles-Sticken et al. 2005). Then, during prophase I, telomeres are distributed in a rim-like pattern (Trelles-Sticken et al., 1999; Trelles-Sticken et al., 2000) and move rapidly (Trelles-Sticken et al., 2005) to create miniclusters that eventually assemble into the large cluster that characterises the bouquet stage (Trelles-Sticken et al., 2005). Once the bouquet is formed, telomeres continue to move rapidly, and the nucleus undergoes oscillating deformations (Trelles-Sticken et al., 2005; Koszul et al., 2008).

Although the molecular mechanisms regulating telomere attachment and clustering during meiosis are not well understood, the presence of the meiotic telomere specific adaptor protein Ndj1/Tam1 appears to be essential for this process (Chua and Roeder, 1997; Conrad et al., 1997). Additionally, it has been observed that telomeres experience an actin-dependent constraint on their mobility during the bouquet stage of meiosis. Cohesin is required to exit the actin polymerisation-dependent telomere clustering and link the SPB to the telomere clustering (Trelles-Sticken et al., 2005).

As soon as pre-meiotic chromosome replication is finished, centromeres undergo homologous and non-homologous pairwise associations, a phenomenon known as "centromere coupling" (Tsubouchi and Roeder, 2005; Obeso and Dawson, 2010). Remarkably, the formation of DSBs and the resulting signalling pathways are not essential for this phenomenon as demonstrated by observation that coupling occurs in mutants lacking the Spo11 protein (Tsubouchi and Roeder, 2005; Obeso and Dawson, 2010). Conversely, the absence of the SC component Zip1 resulted in undetectable centromere coupling, demonstrating the crucial

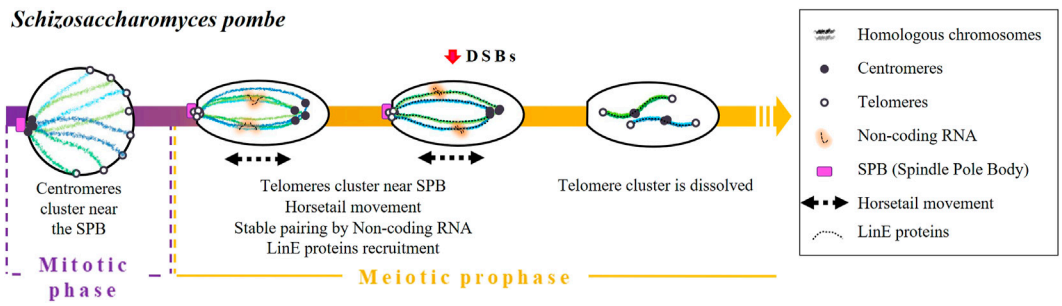

FIGURE 2
Timing and mechanisms of DSB-independent homologous pairing in *Schizosaccharomyces pombe*.

function of this protein in the process (Obeso and Dawson, 2010). Cohesin, on the other hand, is believed to be also required for centromere coupling due to its influence on Zip1 localization rather than its direct participation in the coupling process (Chuong and Dawson, 2010).

Subsequently, as synapsis between homologous chromosomes begins, centromeres seem to transition from centromere coupling to centromere pairing, which involves the specific association of homologous centromeres (Tsubouchi and Roeder, 2005; Storlazzi et al., 2010; Lake et al., 2015).

The cause of centromere coupling is still not fully understood, but some studies have proposed that chromosomes have a partner selection preference dependent on their length (Lefrançois et al., 2016) that may contribute to the effectiveness of homologous pairing in the later stages of meiosis. Besides, it has been suggested that centromere pairing can serve as an alternative mechanism to link achiasmate homologous chromosomes (Dawson et al., 1986). In fact, observations have been made of achiasmatic chromosomes pairing specifically at their centromeres, providing evidence for this alternative pairing mechanism (Kemp et al., 2004; Gladstone et al., 2009; Newnham et al., 2010).

Schizosaccharomyces pombe

Homologous pairing in fission yeast is initiated during the mitotic replication phase and achieved by a combination of different mechanisms acting in an orchestrated way: centromeres and telomeres clustering, nuclear movements, as well as the accumulation of non-coding RNA and the presence of specific cohesins (Chikashige et al., 1994; Ding et al., 1998; Ding et al., 2012; Elkouby et al., 2016; Rubin et al., 2020) (Figure 2). It is worth emphasizing that pairing and synapsis take place normally in *rec12* mutants (*spo11* homolog) (Ding et al., 2012). This observation strongly suggests that both processes are independent of DSBs.

During the mitotic replication phase, the centromeres of *S. pombe* are grouped in association with the SPB (Funabiki et al., 1993; Chikashige et al., 1997). Once meiosis begins, immediately after karyogamy, centromeres detach from SPB and telomeres slide through the nuclear envelope and cluster forming a *bouquet* structure (Chikashige et al., 1994; reviewed in Hiraoka and Dernburg, 2009). It has been established that the loss of telomere-SPB clustering by mutations of telomere binding proteins, such as Taz1 or Rap1 (two proteins involved in telomere maintenance) or by mutations of the Kms1 membrane-bound SPB component, reduces recombination frequencies (Shimanuki et al., 1997; Cooper et al., 1998; Nimmo et al., 1998; Chikashige and Hiraoka, 2001; Kanoh and Ishikawa, 2001).

Then, the nucleus elongates and undergoes a movement called "horsetail". This movement consists of going forward and backward of the cell (Chikashige et al., 1994; Ding et al., 1998) and will eventually allow the achievement of pairing and recombination (Ding et al., 2004). In dynein-disrupted meiotic cells, there is a lack of nuclear movements that end up in paring anomalies (Ding et al., 2004) and low recombination levels (Yamamoto et al., 1999).

In the end, horsetail movements result in stable pairing through the participation of the *sme2* locus. This gene encodes a non-coding RNA required for homologous recognition (Watanabe and Yamamoto, 1994), which is retained at the *sme2* locus by a set of specific proteins (sme2 RNA-associated protein; Smp) (Ding et al., 2016a). It has been proposed that the accumulation of non-coding RNA acts as a recognition marker of DNA sequence homology (Ding et al., 2016b). Indeed, other loci containing genes that encode for long non-coding RNAs have been described as essential for homologous chromosome recognition in different situations. For instance: the X-Inactivation centre encoding the long non-coding RNAs *Xist* in X-chromosome inactivation in mammalian females (Siniscalchi et al., 2022).

Horsetail movements are also associated with the establishment of a SC-like structure between homologous chromosomes formed by the linear elements (LinEs) proteins (Olson et al., 1978; Hirata and Tanaka, 1982; Bähler et al., 1993; Ding et al., 2012), which are evolutionarily related to the axial/lateral elements of the SC. Ellermeier et al. (2005) proposed that the linear element component Rec10 is recruited, which in turn activates Rec12 to perform DNA breaks (Ellermeier et al., 2005). Core LinE proteins (Rec10, Rec25, Rec27, and Mug20) are present only during the horsetail stage except the LinE-binding protein Hop1, which does not disappear even after meiosis I chromosome segregation (Ding et al., 2012). Once movements are finished, telomere clustering dissolves, and homologous chromosomes remain paired (Chikashige et al., 1994; Yamamoto et al., 1999; 2001; Ding et al., 2004).

Finally, Ding et al. (2016a) demonstrated that cohesins also contribute to homologous pairing since it was significantly impaired in *rec8* and *pds5* mutants.

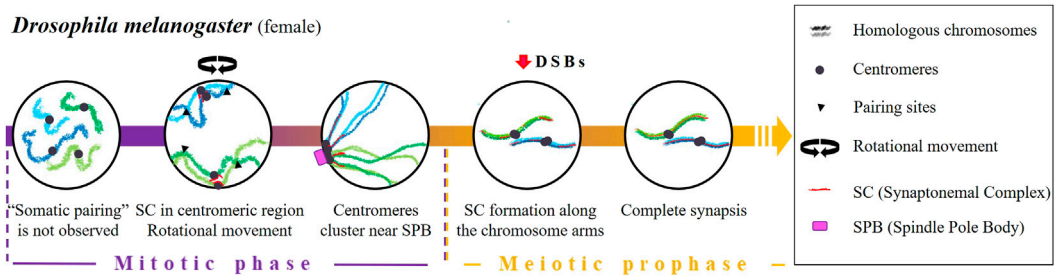

FIGURE 3
Timing and mechanisms of meiotic homologous pairing in *Drosophila melanogaster*.

Drosophila melanogaster

A distinctive feature of *D. melanogaster* is that homologous chromosomes are paired in somatic cells. This feature called "somatic pairing" (Metz, 1916) is frequently observed in Dipterans (Metz, 1916; McKee, 2004; Joyce et al., 2016; King et al., 2019). It has been proposed that somatic pairing initiates at discrete sites ("the button model") along the length of each chromosome (Funabiki et al., 1993; Rowley et al., 2019; Viets et al., 2019). Interestingly, some topologically associated domains (TADs) seem to conduct homologous associations, acting as high affinity pairing sites (Viets et al., 2019). In fact, "buttons" also drive pairing with their homologous sequences even when placed at different positions in the genome (Viets et al., 2019).

Concerning meiotic cells, homologous pairing was thought to be an extension of a supposed pre-existing pairing in premeiotic germ cells (Stevens, 1908; Metz, 1926; Brown and Stack, 1968). However, it was observed that, during the first stages of oogenesis, homologous chromosomes remain unpaired in primordial germ cells [except for the specific repetitive sequences in the ribosomal DNA (rDNA)] (Christophorou et al., 2013; Joyce et al., 2013). Pairing is progressively re-established during the mitotic phase, before the onset of meiosis and the formation of DSBs (Vazquez et al., 2002; McKee et al., 2012), through the bundling of centromeres into clusters (Takeo et al., 2011; Christophorou et al., 2013; Joyce et al., 2013) near the SPB (Zou et al., 2008) and the aggregation of pairing sites (McKee and Karpen, 1990; McKee et al., 1992) (Figure 3).

The mechanisms that lead to centromere clustering before the onset of meiosis are poorly understood. In female *D. melanogaster*, two key factors have been proposed: the presence of SC elements in the centromeric region (Christophorou et al., 2013) and the rotation of the nucleus (Christophorou et al., 2015). Concerning the role of SC elements, two proteins C (3)G and Corona (CONA), which are associated with the transverse filaments and central element of the SC, respectively (Page and Hawley, 2004; Anderson et al., 2005; Page et al., 2008) show a direct relationship between their levels of accumulation in the centromeres of mitotic germ cells and centromere clustering. Homologous pairing is reduced by 30% in *C (3)G* and *Cona* female mutants that also display defective clustering (Christophorou et al., 2013). On the other hand, Christophorou et al., 2015 observed that in female *D. melanogaster,* the rotational movement of the nucleus during mitotic cycles contributes to homologous pairing. In their work, they demonstrate that microtubules, centrosomes, the motor proteins dyneins as well as the Sun and Kash domain transmembrane proteins (which play critical roles in establishing the connection between the nuclear envelope and the cytoskeleton) are required for centromere motion, pairing, clustering and homologous chromosome synapsis.

It is important to mention that the homologous recombination program promoted by DSBs starts shortly after the initiation of SC formation along the chromosome arms (Liu et al., 2002; Mehrotra and McKim, 2006; Lake et al., 2011) and it is not needed for the centromeric aggregation (Takeo et al., 2011). In *Mei-W68* mutants (lacking the enzyme responsible for catalysing DSB formation) and *Mei-P22* mutants (lacking the enzyme that facilitate DSB formation by MEI-W68), which are characterized by the absence of meiotic recombination, a normal SC formation is observed (McKim et al., 1998). However, in the absence of the SC proteins C (3)G and C (2)M, the number of DSBs in oocytes is significantly reduced (Mehrotra and McKim, 2006), suggesting that SC proteins are required for DSB formation.

In male *D. melanogaster*, there is no evidence of a re-establishment of homologous pairing at the transition from mitosis to meiosis. Spermatogenesis completely dispenses with synapsis and recombination; cohesins and lateral elements of the SC are not present (Meyer, 1964; Meyer, 1969; Rasmussen, 1973), and there is a complete lack of crossing over (CO) (Morgan, 1914). Connections between homologous chromosomes, including sex chromosomes, are performed by a surrogate mechanism based on a protein complex consisting of at least two proteins: Stromalin in Meiosis (Snm) and Mod (Mdg4) in Meiosis (MNM) (Thomas et al., 2005; reviewed by McKee et al., 2012). Moreover, sex chromosome pairing is governed by the presence of nucleolar genes (reviewed in McKee, 2009; Tsai and McKee, 2011; McKee et al., 2012), so it has been suggested that rDNA would have a similar function to the pairing centres (PCs) described below in *C. elegans* (Tsai and Mckee, 2011). In support of this idea, it has been observed that an insertion or deletion of rDNA affects sex chromosome pairing and, not only that but, only a few copies of intergenic spacer regions of rDNA are enough to promote pairing (McKee and Karpen, 1990; McKee et al., 1992; McKee, 1996).

Caenorhabditis elegans

The pairing process of *C. elegans* begins at the onset of meiosis by a process that is independent of both DSBs and recombination

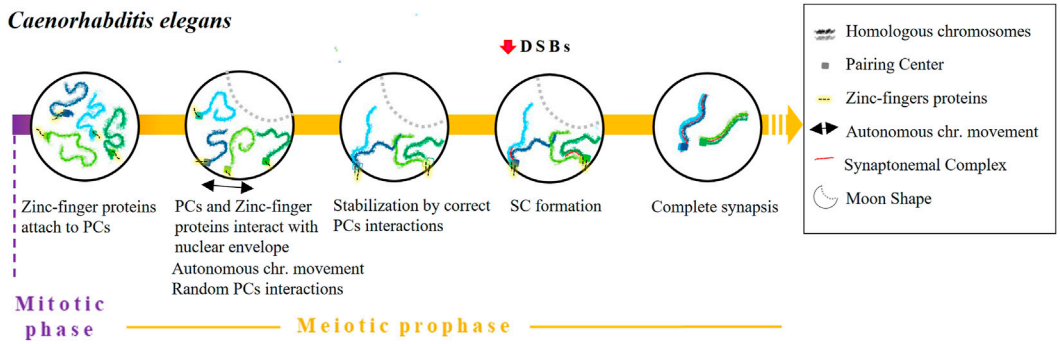

FIGURE 4
Timing and mechanisms of DSB-independent homologous pairing in *Caenorhabditis elegans*.

(Dernburg et al., 1998; McKim et al., 1998) (Figure 4). During the leptotene/zygotene stage, chromatin assumes a half-moon shape (Hirsh et al., 1976) in which the nucleolus locates at the edges (Mlynarczyk-Evans and Villeneuve, 2017). Each chromosome of *C. elegans* contains a single subtelomeric region characterised by repeated DNA sequences widely referred to as Pairing Centres (PC). PCs promote and stabilise pairing and synapsis and are indispensable for accurate homologous segregation (Albertson et al., 1997; MacQueen et al., 2005). Some pieces of evidence indicate that PCs themselves are enough for chromosomes to recognise each other. For instance, pairing and synapsis take place transiently or inefficiently between chromosomes lacking PCs (MacQueen et al., 2005). Moreover, in reciprocal translocation chromosomes that are partly homologous and partly heterologous, pairing always begins in the PC region which is shared by both chromosomes (MacQueen et al., 2005).

Various studies have detailed how PCs promote pairing. First, the alignment of homologous chromosomes is stabilised in a synapse-independent manner (MacQueen et al., 2002; 2005). Indeed, in the absence of synapsis (*syp-1 or syp-2* mutants) transient pairing occurs during the leptotene and zygotene stages (MacQueen et al., 2002; Colaiácovo et al., 2003). We know that a set of zinc-finger proteins encoded in a single gene cluster - HIM-8, ZIM-1, ZIM-2 and ZIM-3—recognise and attach to a specific 12 bp repeat region present in PCs (Phillips et al., 2009). After binding, the resulting complexes interact with SUN-1 to form a bridge that crosses the nuclear envelope in a similar way to how telomeres form a *bouquet* structure. This mechanism is considered a variant of the *bouquet* (Penkner et al., 2009; Sato et al., 2009) although, in this case, the PCs are never completely clustered (Wynne et al., 2012). Afterward, chromosomes move through the nuclear envelope to ease homologous recognition by causing random interactions of PCs until they stabilise with the corresponding homologous PC and the formation of the SC (Baudrimont et al., 2010; Mlynarczyk-Evans and Villeneuve, 2017). SC central element polymerisation typically begins in proximity to PCs, although SC formation can still occur even without the participation of PCs (MacQueen et al., 2005; Hayashi et al., 2010). Importantly, it has been proposed that homologous synapsis is not reliant on recombination, as it occurs normally even in a *C. elegans spo-11* null mutant (Dernburg et al., 1998). Some researchers have proposed that chromosomal dynamics can prevent weak associations between non-homologous chromosomes. This mechanism is thought to be particularly important in cases where there is no stabilisation by PCs (Baudrimont et al., 2010; Wynne et al., 2012). Finally, various proteins have been described as being involved in meiotic prophase chromosome movements, including the meiotic family of serine/threonine protein kinases Polo-like kinases PLK-1 and PLK-2 (Lake et al., 2011), the motor protein dynein, the transmembrane SUN/KASH proteins and the orthologue of mammalian vinculin, DEB-1 (Rohožková et al., 2019). Interestingly, missense mutations in *sun-1* cause pairing defects and non-homologous synapsis (Penkner et al., 2007; Labrador et al., 2013). Moreover, homolog pairing is markedly delayed by dynein knockdown (Sato et al., 2009).

Mus musculus

Some studies have shown that the association of homologous chromosomes in mouse germ cells takes place before the onset of meiosis (Boateng et al., 2013; Solé et al., 2022) or directly at the early leptotene stage (Ishiguro et al., 2014; Scherthan et al., 2014), in both cases before the formation of DSBs. Solé et al. (2022) quantified this process and demonstrated that up to 73.83% of homologous chromosomes are already in contact at premeiotic stages, suggesting the ability of homologous chromosomes to find each other before meiosis.

Boateng et al. (2013) showed that early pairing of homologous chromosomes in mice depends on the presence of SPO11 but not on its catalytic activity. The independence of pairing from SPO11 activity was confirmed later by Ishiguro et al. (2014). They observed pairing of homologous chromosomes in spermatocytes from *spo11* knockout mice, although less frequently than in wild-type spermatocytes, particularly in the early zygotene stage. Ishiguro and others also postulated that cohesins would guide homologous pairing. This idea was based on two observations. First, during the first meiotic prophase, the distribution pattern of cohesins RAD21L and REC8 appeared to be unique along each chromosome but identical in each homolog (Ishiguro et al., 2011). Second, homologous chromosome pairing in mice *rad21l*−/− mutants was impaired, suggesting a relevant role

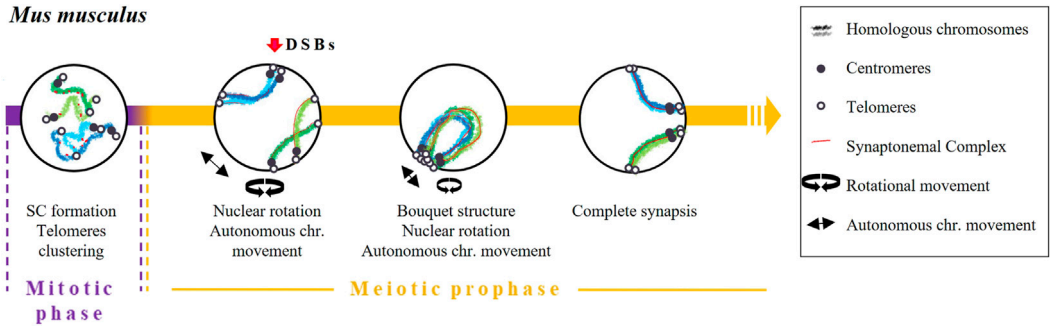

FIGURE 5
Timing and mechanisms of DSB-independent homologous pairing in *Mus musculus*.

for this cohesin in the DSB-independent early pairing. Conversely, homolog pairing was observed in a significant population of *rec8−/−* mice spermatocytes (Ishiguro et al., 2014). Supporting the participation of cohesins, Ding et al. (2016a), Ding et al. (2016b) also observed an alteration of the pairing pattern in *S. pombe* in the absence of Rec8 and Pds5.

The independent pairing of DSBs in mice also appears to be regulated by the expression of certain prophase I genes during spermatogonia proliferation, such as some components of SC and REC8 proteins (Wang et al., 2009; Elkouby et al., 2016) (Figure 5). Rubin et al. (2020) proposed that the expression of SC proteins prior to the onset of meiosis may resemble the expression of transverse filaments and central elements [C (3)G and Corona (CONA), respectively] in *D. melanogaster*. Indeed, Bisig et al. (2012) described an association of telomeres (although not specifically homologous telomeres) and, consequently, of centromeres in type B spermatogonia and pre-leptotene mice spermatocytes. Interestingly, this association was altered in the absence of SYCP3 (Bisig et al., 2012).

Early pairing of homologous chromosomes later became reinforced by the *bouquet* structure formation and chromosome dynamics. This structure facilitates the interaction of different chromosomal interstitial points. In terms of dynamics, a combination of two movements take place during prophase: nuclear rotation and an autonomous movement of the chromosomes (Conrad et al., 2008; Shibuya et al., 2014; Lee et al., 2015; Spindler et al., 2019). When the bouquet structure and chromosome dynamics are altered, a reduction in homologous pairing and synapsis has been observed (Shibuya et al., 2014). Finally, pairing will be completely stabilised through the repair mechanisms of DSBs (recombination) and the formation of the SC (Baudat et al., 2000).

Final remarks

Table 1 summarises the main characteristics of early homologous pairing in the five model organisms reviewed in this work. The clustering of telomeres (or distal regions in the case of *C. elegans*) and/or centromeres appear to be a common mechanism in the early steps of the process. This chromosome disposition would place homologous chromosomes at the same latitude of the nucleus, orienting their chromosome arms and, therefore, helping the alignment of homologous regions for a more efficient homology search. The fact that the clustering occurs at a specific region of the nuclear envelope and before the initiation of chromosomal movements, would prevent the formation of "interlocks" between the chromatin of different chromosomes (images of these knots can be seen in Wang et al., 2009). It should be noted that the clustering of telomeres in the bouquet structure usually occurs near the microtubule organising centre (MTOC; known as the SPB in yeast and fungi, and as the centrosome in *C. elegans* and other metazoans). It suggests that the MTOC could have a role in the *bouquet* structure formation and in causing oscillatory movements (Sawin, 2005; Sato et al., 2009) that ultimately help to promote homologous recognition. Dynamics is another common trait that plays an important role in early homologous pairing. Movements such as nuclear rotation, horsetail movement or the displacement of telomeres through the nuclear envelope have been suggested to have two objectives. It would first help to find those specific elements that facilitate pairing (SC structure, other proteins, RNA and/or DNA) by establishing strong interactions in these regions followed by propagation of pairing along the chromosome, and second, movements would eliminate weak interactions between non-homologous chromosomes. In fact, if there are alterations of proteins involved in chromosomal movement, the frequency of synapsis between heterologous chromosomes increases (Penkner et al., 2009).

Based on the information presented in this review, it becomes evident that the processes of homologous chromosome pairing encompass additional mechanisms before the repair of double-strand breaks (DSBs). Independent DSB repair mechanisms would drive homologous chromosomes to approach, facilitating the search for homology after DSBs formation. In this way, early pairing would prevent the search for homologous sequences in non-homologous chromosomes and, consequently, the formation of unwanted interactions. At the same time, these mechanisms would facilitate the repair of DSBs using the intact homologous duplex as a template.

Overall, it is crucial to shift our understanding of the chromosomal pairing process from being solely driven by recombination to a process promoted by multiple factors that

TABLE 1 Elements involved in early meiotic pairing in different species (Chr.) chromosome, (SC) synaptonemal complex, (PCs) pairing centers. *In *Saccharomyces cerevisiae*, there is a centromere coupling mechanism that involves the proximity of homologous and non-homologous centromeres.

	When does homologous pairing begin?	Does homologous pairing begin before DSBs formation?	Does homologous pairing occur in the absence of DSBs formation or recombination?	Do these elements promote homologous pairing?						
				Centromere clustering	Telomere clustering	Chr. dynamics	SC	DNA sequences	RNA sequences	Cohesin meiotic components
Saccharomyces cerevisiae	Prophase onset	No*	Yes	Yes	Yes	Yes	Yes	No data	No data	Yes
Schizosaccharomyces pombe	Prophase onset	Yes	Yes	Yes	Yes	Yes	No data	No data	Yes (non-coding RNA)	Yes
Drosophila melanogaster	Mitotic phase	Yes	Yes	Yes	No	Yes	Yes	Yes (rDNA, pairing sites)	No data	No data
Caenorhabditis elegans	Prophase onset	Yes	Yes	No (Holocentric chromosomes)	No	Yes	No	Yes (PCs)	No data	No data
Mus musculus	Before prophase	Yes	Yes	Yes	Yes	Yes	Yes	No data	No data	Yes

10.3389/fcell.2023.1191156

overlap in time. A more comprehensive understanding of the factors involved in homologous pairing and how they interact with one another is essential to understand the mechanisms that govern chromosome stability. Future research should aim to identify and characterise these factors.

Author contributions

MS conceived the study, drafted, and edit the article. JB and ZS contributed to the study's conception and design, provided critical feedback on the manuscript, and revised it for important intellectual content. AP and EA participated in the manuscript's critical review and provided valuable feedback for its improvement. All authors contributed to the article and approved the submitted version.

Funding

This study was supported by PI21/00564 (Ministerio de Ciencia e Innovación) and 2021SGR00122 (Generalitat de Catalunya). AP was the recipient of a grant from UAB (PIF/2021).

Acknowledgments

The authors are members of a consolidated research group (2021-SGR-00122) recognized by the Generalitat de Catalunya (Spain). This manuscript has been proofread by Proof-Reading-Service.org.

Conflict of interest

The authors declare that the research was conducted in the absence of any commercial or financial relationships that could be construed as a potential conflict of interest.

Publisher's note

References

Albertson, D. G., Rose, A. M., and Villeneuve, A. M. (1997). *Chromosome organization, mitosis, and meiosis*. New York: Cold Spring Harbor Laboratory Press.

Anderson, L. K., Royer, S. M., Page, S. L., McKim, K. S., Lai, A., Lilly, M. A., et al. (2005). Juxtaposition of C(2)M and the transverse filament protein C(3)G within the central region of Drosophila synaptonemal complex. *Proc. Natl. Acad. Sci. U. S. A.* 102, 4482–4487. doi:10.1073/pnas.0500172102

Bähler, J., Wyler, T., Loidl, J., and Kohli, J. (1993). Unusual nuclear structures in meiotic prophase of fission yeast: A cytological analysis. *J. Cell Biol.* 121 (2), 241–256. doi:10.1083/jcb.121.2.241

Baudat, F., Imai, Y., and de Massy, B. (2013). Meiotic recombination in mammals: Localization and regulation. *Nat. Rev. Genet.* 14 (11), 794–806. doi:10.1038/nrg3573

Baudat, F., Manova, K., Yuen, J. P., Jasin, M., and Keeney, S. (2000). Chromosome synapsis defects and sexually dimorphic meiotic progression in mice lacking Spo11. *Mol. Cell* 6 (5), 989–998. doi:10.1016/s1097-2765(00)00098-8

Baudrimont, A., Penkner, A., Woglar, A., Machacek, T., Wegrostek, C., Gloggnitzer, J., et al. (2010). Leptotene/zygotene chromosome movement via the SUN/KASH protein bridge in *Caenorhabditis elegans*. *PLoS Genet.* 24 (11), e1001219. doi:10.1371/journal.pgen.1001219

Bisig, C. G., Guiraldelli, M. F., Kouznetsova, A., Scherthan, H., Höög, C., Dawson, D. S., et al. (2012). Synaptonemal complex components persist at centromeres and are required for homologous centromere pairing in mouse spermatocytes. *PLoS Genet.* 8 (6), e1002701. doi:10.1371/journal.pgen.1002701

Boateng, K. A., Bellani, M. A., Gregoretti, I. V., Pratto, F., and Camerini-Otero, R. D. (2013). Homologous pairing preceding SPO11-mediated double-strand breaks in mice. *Dev. Cell.* 24, 196–205. doi:10.1016/j.devcel.2012.12.002

Brown, W. V., and Stack, S., M. (1968). Somatic pairing as a regular preliminary to meiosis. *Bull. Torrey Bot. Club* 95, 369–378. doi:10.2307/2483872

Chikashige, Y., Ding, D. Q., Funabiki, H., Haraguchi, T., Mashiko, S., Yanagida, M., et al. (1994). Telomere-led premeiotic chromosome movement in fission yeast. *Science* 264 (5156), 270–273. doi:10.1126/science.8146661

Chikashige, Y., Ding, D. Q., Imai, Y., Yamamoto, M., Haraguchi, T., and Hiraoka, Y. (1997). Meiotic nuclear reorganization: Switching the position of centromeres and telomeres in the fission yeast *Schizosaccharomyces pombe*. *EMBO J.* 16 (1), 193–202. doi:10.1093/emboj/16.1.193

Chikashige, Y., and Hiraoka, Y. (2001). Telomere binding of the Rap1 protein is required for meiosis in fission yeast. *Curr. Biol.* 11, 1618–1623. doi:10.1016/s0960-9822(01)00457-2

Christophorou, N., Rubin, T., Bonnet, I., Piolot, T., Arnaud, M., and Huynh, J. R. (2015). Microtubule-driven nuclear rotations promote meiotic chromosome dynamics. *Nat. Cell Biol.* 17 (11), 1388–1400. doi:10.1038/ncb3249

Christophorou, N., Rubin, T., and Huynh, J. R. (2013). Synaptonemal complex components promote centromere pairing in pre-meiotic germ cells. *PLoS Genet.* 9 (12), e1004012. doi:10.1371/journal.pgen.1004012

Chua, P. R., and Roeder, G. S. (1997). Tam1, a telomere-associated meiotic protein, functions in chromosome synapsis and crossover interference. *Genes & Dev.* 11 (14), 1786–1800. doi:10.1101/gad.11.14.1786

Chuong, H., and Dawson, D. S. (2010). Meiotic cohesin promotes pairing of nonhomologous centromeres in early meiotic prophase. *Mol. Biol. Cell.* 21 (11), 1799–1809. doi:10.1091/mbc.e09-05-0392

Colaiácovo, M. P., MacQueen, A. J., Martinez-Perez, E., McDonald, K., Adamo, A., La Volpe A, Villeneuve, A. M., et al. (2003). Synaptonemal complex assembly in *C. elegans* is dispensable for loading strand-exchange proteins but critical for proper completion of recombination. *Dev. Cell* 5 (3), 463–474. doi:10.1016/s1534-5807(03)00232-6

Conrad, M. N., Dominguez, A. M., and Dresser, M. E. (1997). Ndj1p, a meiotic telomere protein required for normal chromosome synapsis and segregation in yeast. *Sci. (New York, N.Y.)* 276 (5316), 1252–1255. doi:10.1126/science.276.5316.1252

Conrad, M. N., Lee, C. Y., Chao, G., Shinohara, M., Kosaka, H., Shinohara, A., et al. (2008). Rapid telomere movement in meiotic prophase is promoted by NDJ1, MPS3, and CSM4 and is modulated by recombination. *Cell* 133 (7), 1175–1187. doi:10.1016/j.cell.2008.04.047

Cooper, J. P., Watanabe, Y., and Nurse, P. (1998). Fission yeast Taz1 protein is required for meiotic telomere clustering and recombination. *Nature* 23 (6678), 828–831. doi:10.1038/33947

Dawson, D. S., Murray, A. W., and Szostak, J. W. (1986). An alternative pathway for meiotic chromosome segregation in yeast. *Sci. (New York, N.Y.)* 234 (4777), 713–717. doi:10.1126/science.3535068

Dernburg, A. F., McDonald, K., Moulder, G., Barstead, R., Dresser, M., and Villeneuve, A. M. (1998). Meiotic recombination in *C. elegans* initiates by a conserved mechanism and is dispensable for homologous chromosome synapsis. *Cell* 94 (3), 387–398. doi:10.1016/s0092-8674(00)81481-6

Ding, D. Q., Okamasa, K., Yamane, M., Tsutsumi, C., Haraguchi, T., Yamamoto, M., et al. (2012). Meiosis-specific noncoding RNA mediates robust pairing of homologous chromosomes in meiosis. *Science* 336 (6082), 732–736. doi:10.1126/science.1219518

Ding, D. Q., Chikashige, Y., Haraguchi, T., and Hiraoka, Y. (1998). Oscillatory nuclear movement in fission yeast meiotic prophase is driven by astral microtubules, as revealed by continuous observation of chromosomes and microtubules in living cells. *J. Cell Sci.* 111 (6), 701–712. doi:10.1242/jcs.111.6.701

Ding, D. Q., Matsuda, A., Okamasa, K., Nagahama, Y., Haraguchi, T., and Hiraoka, Y. (2016a). Meiotic cohesin-based chromosome structure is essential for homologous chromosome pairing in *Schizosaccharomyces pombe*. *Chromosoma* 125 (2), 205–214. doi:10.1007/s00412-015-0551-8

Ding, D. Q., Okamasa, K., Katou, Y., Oya, E., Nakayama, J. I., Chikashige, Y., et al. (2016b). Chromosome-associated RNA-protein complexes promote pairing of homologous chromosomes during meiosis in *Schizosaccharomyces pombe*. *Nat. Commun.* 10 (1), 5598. doi:10.1038/s41467-019-13609-0

Ding, D. Q., Yamamoto, A., Haraguchi, T., and Hiraoka, Y. (2004). Dynamics of homologous chromosome pairing during meiotic prophase in fission yeast. *Dev. Cell* 6 (3), 329–341. doi:10.1016/s1534-5807(04)00059-0

Elkouby, Y. M., Jamieson-Lucy, A., and Mullins, M. C. (2016). Oocyte polarization is coupled to the chromosomal bouquet, a conserved polarized nuclear configuration in meiosis. *PLoS Biol.* 14 (1), e1002335. doi:10.1371/journal.pbio.1002335

Ellermeier, C., Smith, G. R., and Fox, M. S. (2005). Cohesins are required for meiotic DNA breakage and recombination in *Schizosaccharomyces pombe*. *Proc. Natl. Acad. Sci. U. S. A.* 102 (31), 10952–10957. doi:10.1073/pnas.0504805102

Funabiki, H., Hagan, I., Uzawa, S., and Yanagida, M. (1993). Cell cycle-dependent specific positioning and clustering of centromeres and telomeres in fission yeast. *J. Cell Biol.* 121 (5), 961–976. doi:10.1083/jcb.121.5.961

Gladstone, M. N., Obeso, D., Chuong, H., and Dawson, D. S. (2009). The synaptonemal complex protein Zip1 promotes bi-orientation of centromeres at meiosis I. *PLoS Genet.* 5 (12), e1000771. doi:10.1371/journal.pgen.1000771

Gray, S., and Cohen, P. E. (2016). Control of meiotic crossovers: From double-strand break formation to designation. *Annu. Rev. Genet.* 23 (50), 175–210. doi:10.1146/annurev-genet-120215-035111

Hayashi, M., Mlynarczyk-Evans, S., and Villeneuve, A. M. (2010). The synaptonemal complex shapes the crossover landscape through cooperative assembly, crossover promotion and crossover inhibition during *Caenorhabditis elegans* meiosis. *Genetics* 186, 45–58. doi:10.1534/genetics.110.115501

Hiraoka, Y., and Dernburg, A. F. (2009). The SUN rises on meiotic chromosome dynamics. *Dev. Cell* 17 (5), 598–605. doi:10.1016/j.devcel.2009.10.014

Hirata, A., and Tanaka, K. (1982). Nuclear behavior during conjugation and meiosis in the fission yeast *Schizosaccharomyces pombe*. *J. Gen. Appl. Microbiol.* 28, 263–274. doi:10.2323/jgam.28.263

Hirsh, D., Oppenheim, D., and Klass, M. (1976). Development of the reproductive system of *Caenorhabditis elegans*. *Dev. Biol.* 49, 200–219. doi:10.1016/0012-1606(76)90267-0

Hunter, N. (2015). Meiotic recombination: The essence of heredity. *Cold Spring Harb. Perspect. Biol.* 7, a016618. doi:10.1101/cshperspect.a016618

Ishiguro, K.-I., Kim, J., Shibuya, H., Hernández-Hernández, A., Suzuki, A., Fukagawa, T., et al. (2014). Meiosis-specific cohesin mediates homolog recognition in mouse spermatocytes. *Genes Dev.* 28 (6), 594–607. doi:10.1101/gad.237313.113

Ishiguro, K., Kim, J., Fujiyama-Nakamura, S., Kato, S., and Watanabe, Y. (2011). A new meiosis-specific cohesin complex implicated in the cohesin code for homologous pairing. *EMBO Rep. Mar.* 12 (3), 267–275. doi:10.1038/embor.2011.2

Joyce, E. F., Apostolopoulos, N., Beliveau, B. J., and Wu, C. T. (2013). Germline progenitors escape the widespread phenomenon of homolog pairing during Drosophila development. *PLoS Genet.* 9 (12), e1004013. doi:10.1371/journal.pgen.1004013

Joyce, E. F., Erceg, J., and Wu, C. T. (2016). Pairing and anti-pairing: A balancing act in the diploid genome. *Curr. Opin. Genet. Dev. Apr* 37, 119–128. doi:10.1016/j.gde.2016.03.002

Kanoh, J., and Ishikawa, F. (2001). spRap1 and spRif1, recruited to telomeres by Taz1, are essential for telomere function in fission yeast. *Curr. Biol.* 11 (20), 1624–1630. doi:10.1016/s0960-9822(01)00503-6

Kauppi, L., Barchi, M., Lange, J., Baudat, F., Jasin, M., and Keeney, S. (2013). Numerical constraints and feedback control of double-strand breaks in mouse meiosis. *Genes Dev.* 27 (8), 873–886. doi:10.1101/gad.213652.113

Keeney, S. (2008). Spo11 and the formation of DNA double-strand breaks in meiosis. *Genome Dyn. Stab.* 1 (2), 81–123. doi:10.1007/7050_2007_026

Kemp, B., Boumil, R. M., Stewart, M. N., and Dawson, D. S. (2004). A role for centromere pairing in meiotic chromosome segregation. *Genes & Dev.* 18 (16), 1946–1951. doi:10.1101/gad.1227304

Kim, K. P., Weiner, B. M., Zhang, L., Jordan, A., Dekker, J., and Kleckner, N. (2010). Sister cohesion and structural axis components mediate homolog bias of meiotic recombination. *Cell* 143 (6), 924–937. doi:10.1016/j.cell.2010.11.015

King, T. D., Johnson, J. E., and Bateman, J. R. (2019). Position effects influence transvection in *Drosophila melanogaster*. *Genetics* 213 (4), 1289–1299. doi:10.1534/genetics.119.302583

Koszul, R., Kim, K. P., Prentiss, M., Kleckner, N., and Kameoka, S. (2008). Meiotic chromosomes move by linkage to dynamic actin cables with transduction of force through the nuclear envelope. *Cell* 133 (7), 1188–1201. doi:10.1016/j.cell.2008.04.050

Labrador, L., Barroso, C., Lightfoot, J. W., Müller-Reichert, T., Flibotte, S., Taylor, J., et al. (2013). Chromosome movements promoted by the mitochondrial protein SPD-3 are required for homology search during *Caenorhabditis elegans* meiosis. *PLoS Genet.* 9, e1003497. doi:10.1371/journal.pgen.1003497

Lake, C. M., Nielsen, R. J., and Hawley, R. S. (2011). The Drosophila zinc finger protein trade embargo is required for double strand break formation in meiosis. *PLoS Genet.* 7 (2), e1002005. doi:10.1371/journal.pgen.1002005

Lee, C. Y., Horn, H., Stewart, C. L., Burke, B., Bolcun-Filas, E., Schimenti, J. C., et al. (2015). Mechanism and regulation of rapid telomere prophase movements in mouse meiotic chromosomes. *Cell Rep.* 11, 551–563. doi:10.1016/j.celrep.2015.03.045

Lefrançois, P., Rockmill, B., Xie, P., Roeder, G. S., and Snyder, M. (2016). Multiple pairwise analysis of non-homologous centromere coupling reveals preferential chromosome size-dependent interactions and a role for bouquet formation in establishing the interaction pattern. *PLoS Genet.* 12 (10), e1006347. doi:10.1371/journal.pgen.1006347

Liu, H., Jang, J. K., Kato, N., and McKim, K. S. (2002). mei-P22 encodes a chromosome-associated protein required for the initiation of meiotic recombination in *Drosophila melanogaster*. *Genetics* 162 (1), 245–258. doi:10.1093/genetics/162.1.245

MacQueen, A. J., Colaiácovo, M. P., McDonald, K., and Villeneuve, A. M. (2002). Synapsis-dependent and -independent mechanisms stabilize homolog pairing during meiotic prophase in *C. elegans*. *Genes Dev.* 16 (18), 2428–2442. doi:10.1101/gad.1011602

MacQueen, A. J., Phillips, C. M., Bhalla, N., Weiser, P., Villeneuve, A. M., and Dernburg, A. F. (2005). Chromosome sites play dual roles to establish homologous synapsis during meiosis in *C. elegans*. *Cell* 123 (6), 1037–1050. doi:10.1016/j.cell.2005.09.034

McKee, B. D., Habera, L., and Vrana, J. A. (1992). Evidence that intergenic spacer repeats of *Drosophila melanogaster* rRNA genes function as X-Y pairing sites in male meiosis, and a general model for achiasmatic pairing. *Genet. Oct.* 132 (2), 529–544. doi:10.1093/genetics/132.2.529

McKee, B. D. (2009). Homolog pairing and segregation in Drosophila meiosis. *Genome Dyn.* 5, 56–68. doi:10.1159/000166619

McKee, B. D. (2004). Homologous pairing and chromosome dynamics in meiosis and mitosis. *Biochim. Biophys. Acta* 15 (1-3), 165–180. doi:10.1016/j.bbaexp.2003.11.017

McKee, B. D., and Karpen, G. H. (1990). Drosophila ribosomal RNA genes function as an X-Y pairing site during male meiosis. *Cell* 61 (1), 61–72. doi:10.1016/0092-8674(90)90215-z

McKee, B. D. (1996). The license to pair: Identification of meiotic pairing sites in Drosophila. *Chromosoma. Sep.* 105 (3), 135–141. doi:10.1007/BF02509494

McKee, B. D., Yan, R., and Tsai, J. H. (2012). Meiosis in male Drosophila. *Spermatogenesis* 2 (3), 167–184. doi:10.4161/spmg.21800

McKim, K. S., Green-Marroquin, B. L., Sekelsky, J. J., Chin, G., Steinberg, C., Khodosh, R., et al. (1998). Meiotic synapsis in the absence of recombination. *Science* 279, 876–878. doi:10.1126/science.279.5352.876

Mehrotra, S., and McKim, K. S. (2006). Temporal analysis of meiotic DNA double-strand break formation and repair in Drosophila females. *PLoS Genet.* 2 (11), e200. doi:10.1371/journal.pgen.0020200

Metz, C. W. (1926). Observations on spermatogenesis in Drosophila. *Zellforsch. Mikrosk. Anat.* 4, 1–28. doi:10.1007/bf02628169

Metz, C. W. (1916). Chromosome studies on the Diptera. II. The paired association of chromosomes in the Diptera, and its significance. *J. Exp. Zool.* 21, 213–279. doi:10.1002/jez.1400210204

Meyer, G. F. (1964). A possible correlation between the submicroscopic structure of meiotic chromosomes and crossing over. *Proc. Third Eur. Reg. Conf. Prague* 13, 461462.

Meyer, G. F. (1969). "The fine structure of spermatocyte nuclei of *Drosophila melanogaster*," in *Proceedings of the European regional conference on electron microscopy*. Editors A. L. Houwinck and B. J. Spit (Netherlands: Die Nederlandse Verening voor Electronmicroscopic Delft), 951–954.

Mlynarczyk-Evans, S., and Villeneuve, A. M. (2017). Time-course analysis of early meiotic prophase events informs mechanisms of homolog pairing and synapsis inCaenorhabditis elegans. *Genetics* 207 (1), 103–114. doi:10.1534/genetics.117.204172

Morgan, T. H. (1914). No crossing over in the male of Drosophila of genes in the second and third pairs of chromosomes. *Biol. Bull.* 26, 195–204. doi:10.2307/1536193

Newnham, L., Jordan, P., Rockmill, B., Roeder, G. S., and Hoffmann, E. (2010). The synaptonemal complex protein, Zip1, promotes the segregation of nonexchange chromosomes at meiosis I. *Proc. Natl. Acad. Sci. U. S. A.* 107 (2), 781–785. doi:10.1073/pnas.0913435107

Nimmo, E. R., Pidoux, A. L., Perry, P. E., and Allshire, R. C. (1998). Defective meiosis in telomere-silencing mutants of *Schizosaccharomyces pombe*. *Nature* 392, 825–828. doi:10.1038/33941

Obeso, D., and Dawson, D. S. (2010). Temporal characterization of homology-independent centromere coupling in meiotic prophase. *PloS one* 5 (4), e10336. doi:10.1371/journal.pone.0010336

Olson, L. W., Eden, U., Egel-Mitani, M., and Egel, R. (1978). Asynaptic meiosis in fission yeast? *Hereditas* 89, 189–199. doi:10.1111/j.1601-5223.1978.tb01275.x

Page, S. L., and Hawley, R. S. (2004). The genetics and molecular biology of the synaptonemal complex. *Annu. Rev. Cell Dev. Biol.* 20, 525–558. doi:10.1146/annurev.cellbio.19.111301.155141

Page, S. L., Khetani, R. S., Lake, C. M., Nielsen, R. J., Jeffress, J. K., Warren, W. D., et al. (2008). Corona is required for higher-order assembly of transverse filaments into full-length synaptonemal complex in Drosophila oocytes. *PLoS Genet.* 4 (9), e1000194. doi:10.1371/journal.pgen.1000194

Penkner, A. M., Fridkin, A., Gloggnitzer, J., Baudrimont, A., Machacek, T., Woglar, A., et al. (2009). Meiotic chromosome homology search involves modifications of the nuclear envelope protein Matefin/SUN-1. *Cell* 139 (5), 920–933. doi:10.1016/j.cell.2009.10.045

Penkner, A., Portik-Dobos, Z., Tang, L., Schnabel, R., Novatchkova, M., Jantsch, V., et al. (2007). A conserved function for a *Caenorhabditis elegans* Com1/Sae2/CtIP protein homolog in meiotic recombination. *EMBO J.* 26 (24), 5071–5082. doi:10.1038/sj.emboj.7601916

Phillips, C., Meng, X., Zhang, L., Chretien, J. H., Urnov, F. D., and Dernburg, A. F. (2009). Identification of chromosome sequence motifs that mediate meiotic pairing and synapsis in *C. elegans*. *Nat. Cell Biol.* 11, 934–942. doi:10.1038/ncb1904

Rasmussen, S. W. (1973). Ultrastructural studies of spermatogenesis in *Drosophila melanogaster* Meigen. *Z. fur Zellforsch. Mikrosk. Anat. Austria.* 140 (1), 125–144. doi:10.1007/BF00307062

Rockmill, B., Lefrançois, P., Voelkel-Meiman, K., Oke, A., Roeder, G. S., and Fung, J. C. (2013). High throughput sequencing reveals alterations in the recombination signatures with diminishing Spo11 activity. *PLoS Genet.* 9 (10), e1003932. doi:10.1371/journal.pgen.1003932

Rohožková, J., Hůlková, L., Fukalová, J., Flachs, P., and Hozák, P. (2019). Pairing of homologous chromosomes in *C. elegans* meiosis requires DEB-1 - an orthologue of mammalian vinculin. *Nucleus* 10 (1), 93–115. doi:10.1080/19491034.2019.1602337

Romanienko, P. J., and Camerini-Otero, R. D. (2000). The mouse SPO11 gene is required for meiotic chromosome synapsis. *Mol. Cell* 6, 975–987. doi:10.1016/s1097-2765(00)00097-6

Rowley, M. J., Lyu, X., Rana, V., Ando-Kuri, M., Karns, R., Bosco, G., et al. (2019). Condensin II counteracts cohesin and RNA polymerase II in the establishment of 3D chromatin organization. *Cell Rep.* 26, 2890–2903. doi:10.1016/j.celrep.2019.01.116

Rubin, T., Macaisne, N., and Huynh, J. R. (2020). Mixing and matching chromosomes during female meiosis. *Cells* 9(3), 696. doi:10.3390/cells9030696

Sato, A., Isaac, B., Phillips, C., Rillo, R., Carlton, P. M., Wynne, D., et al. (2009). Cytoskeletal forces span the nuclear envelope to coordinate meiotic chromosome pairing and synapsis. *Cell* 139, 907–919. doi:10.1016/j.cell.2009.10.039

Sawin, K. E. (2005). Meiosis: Organizing microtubule organizers. *Curr. Biol.* 15 (16), R633–R635. doi:10.1016/j.cub.2005.08.001

Scherthan, H., Schöfisch, K., Dell, T., and Illner, D. (2014). Contrasting behavior of heterochromatic and euchromatic chromosome portions and pericentric genome separation in pre-bouquet spermatocytes of hybrid mice. *Chromosoma* 123, 609–624. doi:10.1007/s00412-014-0479-4

Shibuya, H., Ishiguro, K. I., and Watanabe, Y. (2014). The TRF1-binding protein TERB1 promotes chromosome movement and telomere rigidity in meiosis. *Nat. Cell Biol.* 16, 145–156. doi:10.1038/ncb2896

Shimanuki, M., Miki, F., Ding, D. Q., Chikashige, Y., Hiraoka, Y., Horio, T., et al. (1997). A novel fission yeast gene, kms1+, is required for the formation of meiotic prophase-specific nuclear architecture. *Mol. Gen. Genet.* 254, 238–249. doi:10.1007/s004380050412

Siniscalchi, C., Di Palo, A., Russo, A., and Potenza, N. (2022). The lncRNAs at X chromosome inactivation center: Not just a matter of sex dosage compensation. *Int. J. Mol. Sci.* 23 (2), 611. doi:10.3390/ijms23020611

Solé, M., Blanco, J., Gil, D., Valero, O., Cárdenas, B., Fonseka, G., et al. (2022). Time to match; when do homologous chromosomes become closer? *Chromosoma. Dec* 131 (4), 193–205. doi:10.1007/s00412-022-00777-0

Spindler, M. C., Redolfi, J., Helmprobst, F., Kollmannsberger, P., Stigloher, C., and Benavente, R. (2019). Electron tomography of mouse LINC complexes at meiotic telomere attachment sites with and without microtubules. *Commun. Biol.* 2, 376. doi:10.1038/s42003-019-0621-1

Stevens, N. M. (1908). A study of the germ cells of certain Diptera, with reference to the heterochromosomes and the phenomena of synapsis. *J. Exp. Zool.* 5, 359–374. doi:10.1002/jez.1400050304

Storlazzi, A., Gargano, S., Ruprich-Robert, G., Falque, M., David, M., Kleckner, N., et al. (2010). Recombination proteins mediate meiotic spatial chromosome organization and pairing. *Cell.* 141 (1), 94–106. doi:10.1016/j.cell.2010.02.041

Storlazzi, A., Tessé, S., Gargano, S., James, F., Kleckner, N., and Zickler, D. (2003). Meiotic double-strand breaks at the interface of chromosome movement, chromosome remodeling, and reductional division. *Genes Dev.* 17 (21), 2675–2687. doi:10.1101/gad.275203

Takeo, S., Lake, C. M., Morais-de-Sá, E., Sunkel, C. E., and Hawley, R. S. (2011). Synaptonemal complex-dependent centromeric clustering and the initiation of synapsis in Drosophila oocytes. *Curr. Biol.* 21 (21), 1845–1851. doi:10.1016/j.cub.2011.09.044

Tessé, S., Storlazzi, A., Kleckner, N., Gargano, S., and Zickler, D. (2003). Localization and roles of Ski8p protein in Sordaria meiosis and delineation of three mechanistically distinct steps of meiotic homolog juxtaposition. *Proc. Natl. Acad. Sci. U. S. A.* 100 (22), 12865–12870. doi:10.1073/pnas.2034282100

Thomas, S. E., Soltani-Bejnood, M., Roth, P., Dorn, R., Logsdon, J. M., and McKee, B. D. (2005). Identification of two proteins required for conjunction and regular segregation of achiasmate homologs in Drosophila male meiosis. *Cell* 18, 555–568. doi:10.1016/j.cell.2005.08.043

Thorne, L. W., and Byers, B. (1993). Stage-specific effects of X-irradiation on yeast meiosis. *Genetics* 134 (1), 29–42. doi:10.1093/genetics/134.1.29

Trelles-Sticken, E., Adelfalk, C., Loidl, J., and Scherthan, H. (2005). Meiotic telomere clustering requires actin for its formation and cohesin for its resolution. *J. Cell. Biol.* 170 (2), 213–223. doi:10.1083/jcb.200501042

Trelles-Sticken, E., Dresser, M. E., and Scherthan, H. (2000). Meiotic telomere protein Ndj1p is required for meiosis-specific telomere distribution, bouquet formation and efficient homologue pairing. *J. Cell. Biol.* 151 (1), 95–106. doi:10.1083/jcb.151.1.95

Trelles-Sticken, E., Loidl, J., and Scherthan, H. (1999). Bouquet formation in budding yeast: Initiation of recombination is not required for meiotic telomere clustering. *J. Cell. Sci.* 112 (5), 651–658. doi:10.1242/jcs.112.5.651

Tsai, J. H., and McKee, B. D. (2011). Homologous pairing and the role of pairing centers in meiosis. *J. Cell Sci.* 124 (12), 1955–1963. doi:10.1242/jcs.006387

Tsubouchi, T., and Roeder, G. S. (2005). A synaptonemal complex protein promotes homology-independent centromere coupling. *Sci. (New York, N.Y.)* 308 (5723), 870–873. doi:10.1126/science.1108283

Vazquez, J., Belmont, A. S., and Sedat, J. W. (2002). The dynamics of homologous chromosome pairing during male Drosophila meiosis. *Curr. Biol.* 12, 1473–1483. doi:10.1016/s0960-9822(02)01090-4

Viets, K., Sauria, M. E. G., Chernoff, C., Rodriguez Viales, R., Echterling, M., Anderson, C., et al. (2019). Characterization of button loci that promote homologous chromosome pairing and Cell-Type-Specific interchromosomal gene regulation. *Dev. Cell* 51, 341–356. doi:10.1016/j.devcel.2019.09.007

Wang, C. J., Carlton, P. M., Golubovskaya, I. N., and Cande, W. Z. (2009). Interlock formation and coiling of meiotic chromosome axes during synapsis. *Genetics* 183 (3), 905–915. doi:10.1534/genetics.109.108688

Watanabe, Y., and Yamamoto, M. (1994). *S. pombe* mei2+ encodes an RNA-binding protein essential for premeiotic DNA synthesis and meiosis I, which cooperates with a novel RNA species meiRNA. *Cell* 78 (3), 487–498. doi:10.1016/0092-8674(94)90426-x

Wynne, D., Rog, O., Carlton, P. M., and Dernburg, A. F. (2012). Dynein-dependent processive chromosome motions promote homologous pairing in *C. elegans* meiosis. *J. Cell Biol.* 196, 47–64. doi:10.1083/jcb.201106022

Yamamoto, A., Tsutsumi, C., Kojima, H., Oiwa, K., and Hiraoka, Y. (2001). Dynamic behavior of microtubules during dynein-dependent nuclear migrations of meiotic prophase in fission yeast. *Mol. Biol. Cell* 12, 3933–3946. doi:10.1091/mbc.12.12.3933

Yamamoto, A., West, R. R., McIntosh, J. R., and Hiraoka, Y. (1999). A cytoplasmic dynein heavy chain is required for oscillatory nuclear movement of meiotic prophase and efficient meiotic recombination in fission yeast. *J. Cell Biol.* 145 (6), 1233–1249. doi:10.1083/jcb.145.6.1233

Zickler, D. (2006). From early homologue recognition to synaptonemal complex formation. *Chromosoma* 115 (3), 158–174. doi:10.1007/s00412-006-0048-6

Zou, J., Hallen, M. A., Yankel, C. D., and Endow, S. A. (2008). A microtubule-destabilizing kinesin motor regulates spindle length and anchoring in oocytes. *J. Cell Biol.* 180 (3), 459–466. doi:10.1083/jcb.200711031

frontiers | Frontiers in Cell and Developmental Biology

TYPE Original Research
PUBLISHED 21 June 2023
DOI 10.3389/fcell.2023.1144277

OPEN ACCESS

EDITED BY
Mónica Pradillo,
Complutense University of Madrid, Spain

REVIEWED BY
Corentin Claeys Bouuaert,
Université catholique de Louvain, Belgium
Yajie Gu,
University of California, San Diego, United States

*CORRESPONDENCE
Owen R. Davies,
Owen.Davies@ed.ac.uk

RECEIVED 14 January 2023
ACCEPTED 09 June 2023
PUBLISHED 21 June 2023

CITATION
Gurusaran M, Biemans JJ, Wood CW and Davies OR (2023), Molecular insights into LINC complex architecture through the crystal structure of a luminal trimeric coiled-coil domain of SUN1.
Front. Cell Dev. Biol. 11:1144277.
doi: 10.3389/fcell.2023.1144277

Molecular insights into LINC complex architecture through the crystal structure of a luminal trimeric coiled-coil domain of SUN1

Manickam Gurusaran[1], Jelle J. Biemans[1], Christopher W. Wood[2] and Owen R. Davies[1]*

[1]Wellcome Centre for Cell Biology, Institute of Cell Biology, University of Edinburgh, Edinburgh, Scotland, United Kingdom, [2]Institute of Quantitative Biology, Biochemistry and Biotechnology, University of Edinburgh, Edinburgh, Scotland, United Kingdom

The LINC complex, consisting of interacting SUN and KASH proteins, mechanically couples nuclear contents to the cytoskeleton. In meiosis, the LINC complex transmits microtubule-generated forces to chromosome ends, driving the rapid chromosome movements that are necessary for synapsis and crossing over. In somatic cells, it defines nuclear shape and positioning, and has a number of specialised roles, including hearing. Here, we report the X-ray crystal structure of a coiled-coiled domain of SUN1's luminal region, providing an architectural foundation for how SUN1 traverses the nuclear lumen, from the inner nuclear membrane to its interaction with KASH proteins at the outer nuclear membrane. In combination with light and X-ray scattering, molecular dynamics and structure-directed modelling, we present a model of SUN1's entire luminal region. This model highlights inherent flexibility between structured domains, and raises the possibility that domain-swap interactions may establish a LINC complex network for the coordinated transmission of cytoskeletal forces.

KEYWORDS

LINC complex, nuclear envelope, SUN1, KASH5, X-ray crystallography, molecular dynamics, biophysics

Introduction

The Linker of Nucleoskeleton and Cytoskeleton (LINC) complex traverses both inner and outer nuclear membranes to provide physical connections between the cytoskeleton and nuclear contents (Starr and Fridolfsson, 2010) (Figure 1A). The central role of the LINC complex in force transduction is exemplified by its essential function in meiosis. During the first meiotic division, the telomeric ends of chromosomes become tethered to the inner nuclear membrane by the meiotic telomere complex (Shibuya et al., 2015; Dunce et al., 2018b). Here, they bind to the meiotic LINC complex, which transmits microtubule-generated forces to chromosome ends by acting as a transmembrane dynein activating adapter (Horn et al., 2013b; Spindler et al., 2019; Agrawal et al., 2022; Garner et al., 2022). This results in rapid chromosome movements that are thought to facilitate recombination searches and the establishment of homologous chromosome pairs that are necessary for reductive division and crossing over (Shibuya et al., 2014; Lee et al., 2015). Hence, the meiotic LINC complex is required for fertility (Horn et al., 2013b). In addition to meiosis, and other

specialised roles such as in sound perception in the inner ear (Horn et al., 2013a), the LINC complex has generalised functions in determining nuclear structure, shape and position by transmitting active and reactive tension forces to the nuclear lamina and chromatin (Crisp et al., 2006; Luxton et al., 2010; Alam et al., 2015). Hence, the LINC complex is important for cellular life, and its mutations are implicated in laminopathies, including Hutchison-Gilford progeria syndrome and Emery-Dreifuss muscular dystrophy (Mejat and Misteli, 2010; Meinke et al., 2011).

The LINC complex is formed of SUN (Sad1 and UNC84 homology) and KASH (Klarsicht, ANC-1, and Syne homology) proteins (Starr and Fridolfsson, 2010; Meinke and Schirmer, 2015). The SUN protein has an N-terminal nuclear region, crosses the inner nuclear membrane, and then traverses the nuclear lumen (perinuclear space) to position its C-terminal SUN domain immediately below the outer nuclear membrane (Figures 1A, B). Here, it interacts with the eponymous KASH domain, located at the C-terminus of the KASH protein, which then crosses the outer nuclear envelope, and has a large cytoplasmic domain that mediates interactions with the cytoskeleton (Sosa et al., 2012; Wang et al., 2012; Zhou et al., 2012).

The LINC complex is formed by a family of SUN and KASH proteins, which have both generalised and tissue-specific functions. In mammals, there are five SUN proteins (SUN1-5), of which SUN1 and SUN2 are generally expressed and exhibit partial redundancy in nuclear anchorage (Lei et al., 2009; Zhang et al., 2009). SUN1 is essential for meiosis as its disruption in mice leads infertility owing to failure of chromosome synapsis (Ding et al., 2007). Hence, whilst SUN2 is expressed in meiosis and contributes to meiotic telomere attachment (Schmitt et al., 2007; Link et al., 2014), it does not provide redundancy for the meiotic function of SUN1. The remaining SUN proteins, SUN3-5, are specifically expressed in the later stages of spermatogenesis, where they each perform essential roles in sperm head formation (Pasch et al., 2015; Gao et al., 2020; Zhang et al., 2021). There are six mammalian KASH proteins, of which four are Nesprins (Nuclear Envelope Spectrin Repeat proteins). Nesprin-1 and Nesprin-2 are generally expressed, and perform overlapping roles in nuclear anchorage through interactions between their cytoplasmic spectrin-repeat domains and actin (Banerjee et al., 2014; Sakamoto et al., 2017; Zhou et al., 2018). Nesprin-3 is widely expressed are maintains nuclear integrity by interacting with intermediate filaments and microtubules via plectin, BPAG1 and MACF (Wilhelmsen et al., 2005; Ketema and Sonnenberg, 2011). Nesprin-4 is also widely expressed, and functions in microtubule-dependent nuclear positioning by binding to the motor protein kinesin-1 (Roux et al., 2009). It also has an essential role in hearing through a specific function in the outer hair cells of the inner ear (Horn et al., 2013a). KASH5 is a meiosis-specific coiled-coil protein that functions as a dynein activating adapter that transmits microtubule forces to meiotic chromosome and is essential for their synapsis and fertility (Horn et al., 2013b; Agrawal et al., 2022; Garner et al., 2022). The final KASH protein, JAW1/LRMP/IRAG2, interacts with microtubules, and is required to maintain nuclear shape and Golgi structure (Kozono et al., 2018; Okumura et al., 2023). Hence, the combination of five SUN proteins (and their multiple isoforms) and six KASH proteins achieve the widespread, varied and essential functions of the LINC complex in mammals. Owing to the essential roles of SUN1 and KASH5 in meiotic chromosome synapsis and fertility, this study focusses on the meiotic SUN1-KASH5 LINC complex.

The mechanism of force transduction by the LINC complex is inherently defined by its molecular architecture. Structural work has mostly focussed on the SUN-KASH domain interaction that binds together LINC components (Sosa et al., 2012; Wang et al., 2012;

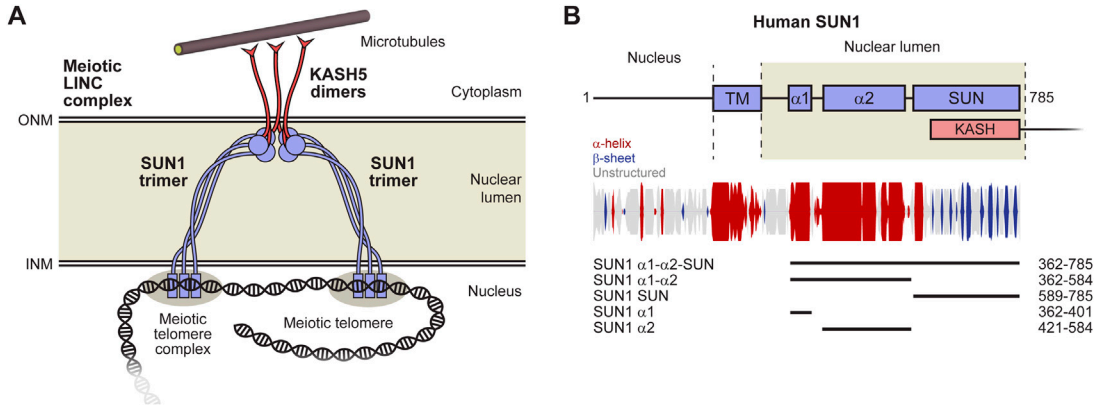

FIGURE 1
The LINC complex. **(A)** The LINC complex consists of interacting SUN and KASH proteins that bind to nuclear and cytoskeletal components, respectively. The luminal region of SUN proteins is thought to consist of a trimeric coiled-coil that bridges between the inner (INM) and outer (ONM) nuclear membranes. SUN trimers terminate in globular domains that interact head-to-head in 6:6 complexes with KASH proteins immediately below the ONM. Whilst we have depicted the LINC complex with a 6:6 stoichiometry, owing to its observation in crystallographic and biochemical studies (Sosa et al., 2012; Wang et al., 2012; Zhou et al., 2012; Cruz et al., 2020; Gurusaran and Davies, 2021), other stoichiometries have been proposed to form in proximity of the ONM *in vivo* (Jahed et al., 2021). Additional components, such as dynein and dynactin, are not depicted to enhance clarity. **(B)** Schematic of the human SUN1 sequence in which its transmembrane (TM) and luminal regions are highlighted. Secondary structure prediction is shown with propensity indicated by peak height (α-helix, red; β-sheet, blue; unstructured, grey) (Drozdetskiy et al., 2015). The principal constructs used in this study are indicated as luminal coiled-coil domains α1 and α2, along with the C-terminal KASH-interacting SUN domain.

Zhou et al., 2012; Cruz et al., 2020; Gurusaran and Davies, 2021). The SUN domain is a globular structure, which upon interaction with KASH domains, forms a trimer preceded by a short coiled-coil (Sosa et al., 2012; Wang et al., 2012; Zhou et al., 2012). Nesprin-1/2/3, Nesprin-4 and KASH5 interact with the SUN domain through a common C-terminal motif and diverse N-terminal interfaces (Cruz et al., 2020; Gurusaran and Davies, 2021). SUN1-KASH complexes are 6:6 structures, formed of two SUN domain trimers associated head-to-head through KASH-mediated interactions, whilst SUN2-KASH complexes form 6:6 and higher order assemblies (Gurusaran and Davies, 2021). Whilst other SUN-KASH complex stoichiometries have been proposed to form *in vivo*, particularly in proximity to the outer nuclear membrane (Jahed et al., 2021), the 6:6 complex is the only structure that has hitherto been observed in crystal structures and in solution (Sosa et al., 2012; Wang et al., 2012; Zhou et al., 2012; Cruz et al., 2020; Gurusaran and Davies, 2021). In absence of KASH-binding, isolated SUN domains remain monomeric, held in autoinhibited complexes by preceding α-helices that otherwise form the SUN-KASH complex coiled-coils (Nie et al., 2016; Jahed et al., 2018a; Jahed et al., 2018b; Xu et al., 2018). There are no structures of cytoplasmic regions of KASH proteins other than short stretches of Nesprin-1/2 (Lim et al., 2021), although we know that KASH5 is a dimer (Agrawal et al., 2022; Garner et al., 2022). There is also a structure of a short nuclear region of SUN1 in a meiotic regulatory complex with SpeedyA-CDK2 (Chen et al., 2021).

The luminal region of SUN proteins upstream of the SUN domain is thought to consist of a long trimeric coiled-coil that passes between nuclear membranes (Jahed et al., 2021). This is based on the short trimeric coiled-coils that emanate from each SUN trimer of the SUN-KASH complex (Sosa et al., 2012; Wang et al., 2012; Zhou et al., 2012), gel filtration and biophysical studies of SUN2 (Jahed et al., 2018b), and the crystal structure of a luminal CC1 trimeric coiled-coil of SUN2 (Nie et al., 2016). The alteration of oligomer state along the LINC complex axis, between SUN trimer, SUN-KASH 6:6 complex and KASH5 dimer, has been proposed to establish a branched LINC complex network suitable for cooperative force transduction (Figure 1A) (Gurusaran and Davies, 2021). Further, the geometry of SUN coiled-coil trimers emanating from SUN-KASH 6:6 complexes suggests that SUN molecules must re-orient from being perpendicular to parallel to the nuclear membrane as they pass through the nuclear lumen (Gurusaran and Davies, 2021). However, the absence of a structure of the full luminal region of a SUN protein has precluded us from visualising how this may occur at the molecular level.

Here, we report the crystal structure of a trimeric coiled-coil domain within the luminal region of SUN1, which lies upstream of a second coiled-coil trimer that corresponds to SUN2's CC1. The two coiled-coils combine in a mutually reinforcing trimer that holds together three SUN domains for KASH-binding and induced head-to-head association. We combine our crystal structure with previous structures of SUN2 CC1 and the autoinhibited SUN domain to build a molecular model of SUN1's entire luminal trimer, which has a length matching that of its solution structure, and which is sufficient to traverse the nuclear lumen. Further, the presence of flexible linkers between the constituent coiled-coils of SUN1 suggest that domain-swap interactions may provide additional branching for force transduction within an integrated LINC complex network.

TABLE 1 Data collection, phasing and refinement statistics.

	SUN1 α1 362–401
PDB accession	8AU0
Data collection	
Space group	$P2_1$
Cell dimensions	
a, *b*, *c* (Å)	33.31, 35.99, 46.10
α, β, γ (°)	90, 104.543, 90
Resolution (Å)	30.31—2.07 (2.11—2.07)*
R_{meas}	0.083 (0.572)
R_{pim}	0.026 (0.287)
$I/\sigma(I)$	8.6 (2.3)
$CC_{1/2}$	0.997 (0.903)
Completeness (spherical) (%)	96.6 (96.4)
Redundancy	3.8 (3.9)
Refinement	
Resolution (Å)	30.31—2.07
UCLA anisotropy (Å)	2.1, 2.1, 2.4
No. reflections	5183
R_{work}/R_{free}	0.2438/0.2551
Cruickshank DPI (Å)	0.25
No. atoms	1,008
Protein	953
Ligand/ion	0
Water	55
B-factors	20.98
Protein	20.81
Ligand/ion	N/A
Water	23.84
R.m.s deviations	
Bond lengths (Å)	0.006
Bond angles (°)	0.790

[a]Values in parentheses are for highest-resolution shell.

Results

Crystal structure of a luminal coiled-coil domain of SUN1

The structure of SUN1's luminal region defines how forces are transduced between the inner and outer nuclear membranes. However, we have hitherto lacked any structural information

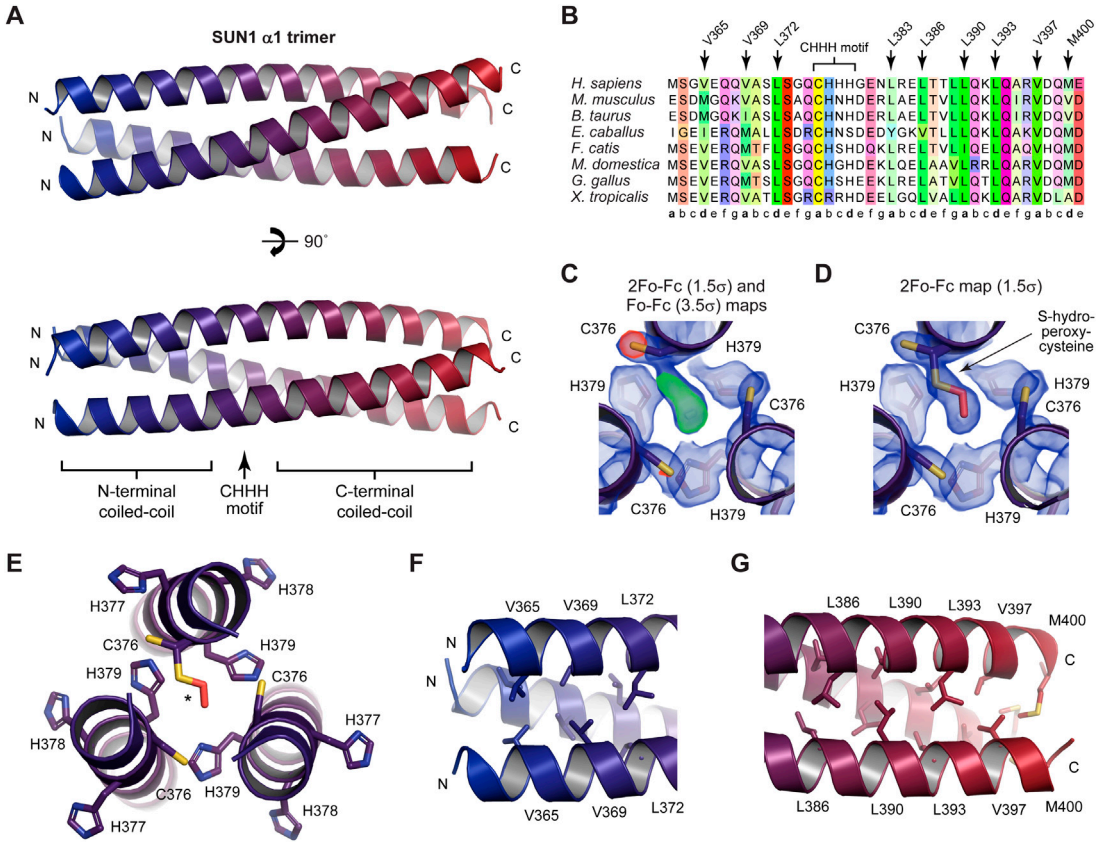

FIGURE 2
Crystal structure of the α1 luminal coiled-coil domain of SUN1. **(A)** Crystal structure of the SUN1 α1 trimeric coiled-coil. The three SUN1 chains (coloured blue to red in an N- to C-terminal direction) are arranged in a parallel configuration, in which a central CHHH motif is continuous with flanking N- and C-terminal coiled-coils. **(B)** Multiple sequence alignment of SUN1 α1, highlighting the central CHHH motif and the amino-acids at 'a' and 'd' heptad positions within the structure. Amino-acids are coloured by chemical properties and according to conservation (Waterhouse et al., 2009). **(C)** 2Fo-Fc map (blue; contoured at 1.5σ) and Fo-Fc difference map (positive difference, green; negative difference, red; contoured at 3.5σ) of the SUN1 α1 structure refined with a reduced cysteine at residue C376 of chain B. **(D)** 2Fo-Fc map (blue; contoured at 1.5σ) of the SUN1 α1 structure in which C376 of chain B was modelled with S-hydroperoxycysteine (2CO) as an alternative conformation of the reduced cysteine residue, refined with relative occupancies of 0.62 and 0.38, respectively. **(E–G)** Structural details of the **(E)** central region encompassing the 376-CHHH-379 motif **(F)** N-terminal coiled-coil formed of heptad residues V365, V369 and L372, and **(G)** C-terminal coiled-coil formed of heptad residues L386, L390, L393, V397 and M400.

regarding the luminal region of SUN1 preceding its KASH-interacting SUN domain. On the basis of conservation and secondary structure prediction (Figure 1B), we identified a 40 amino-acid coiled-coil domain towards the beginning of human SUN1's luminal region (amino-acids 362–401; herein referred to as α1), which was stable in solution following recombinant expression (Supplementary Figure S1). We obtained crystals of SUN1 α1 that diffracted anisotropically to a maximum resolution limit of 2.1 Å, and solved its X-ray crystal structure by molecular replacement of ideal helical fragments using *ARCIMBOLDO_LITE* in 'coiled-coil' mode (Caballero et al., 2018) (Table 1 and Supplementary Figure S2). This revealed a parallel trimeric coiled-coil of approximately 6 nm in length (Figure 2A), in which the "a" and "d" heptad amino-acids are conserved across vertebrates (Figure 2B). Hence, we provide the molecular structure of a trimeric coiled-coiled domain within SUN1's luminal region.

At the centre of the SUN1 α1 coiled-coil structure is a 376-CHHH-379 motif, in which the cysteine residues are at the "a" position of the heptad repeat (Figure 2B) and are oriented away from the coiled-coil axis (Figure 2C). We observed additional electron density for one cysteine of the trimer, which points towards the coiled-coil axis, likely representing an oxidised cysteine residue (Figure 2C). On the basis of the additional density, we modelled this as S-hydroperoxycysteine, as an alternative conformation of the reduced cysteine residue, which refined with relative occupancies of 0.62 and 0.38, respectively (Figures 2D, E). The oxidised C376 residue is packed within the core of the structure, so likely provided additional stability to the coiled-coil, and may have assisted the formation of a robust crystal system suitable for X-ray diffraction. Further, it creates an asymmetry in the structure, explaining the lack of crystallographic three-fold symmetry, with the full trimer constituting the crystal's asymmetric unit.

The central 376-CHHH-379 motif (Figure 2E) is flanked by canonical coiled-coil interfaces. The trimeric coiled-coil on the N-terminal side is formed by heptad amino-acids V365, V369 and L372 (Figure 2F), whilst the coiled-coil on the

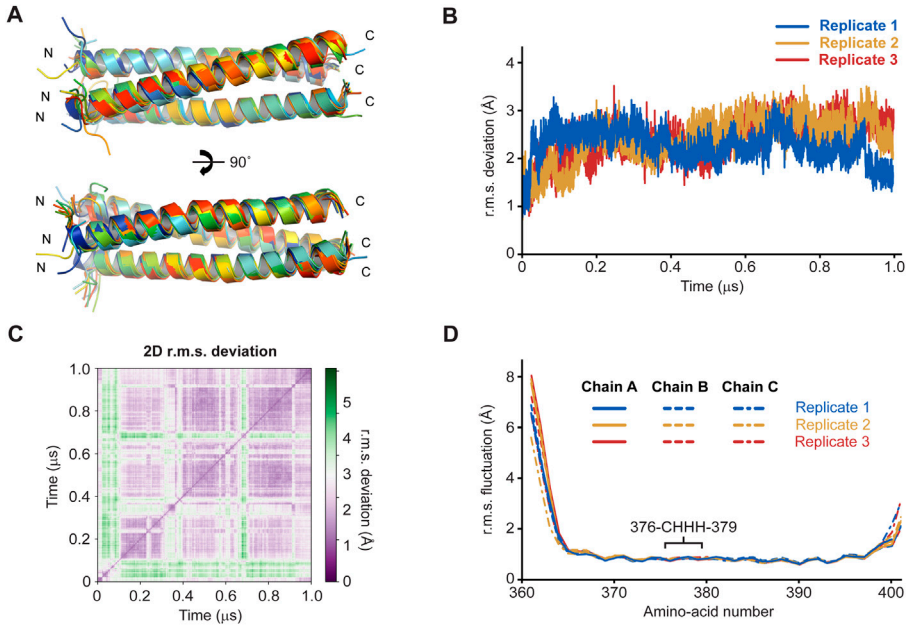

FIGURE 3
Molecular dynamics simulations of the SUN1 α1 structure over 1-μs trajectories at 37°C (n = 3). **(A)** Superimposed SUN1 α1 trimeric coiled-coil structures at 100-ns intervals of a representative trajectory, coloured from blue (0 ns) to red (1 μs). **(B)** Overall r.m.s deviations and **(C)** 2D r.m.s deviations (corresponding to panel A) across 1-μs trajectories (2D r.m.s deviations for the remaining replicates are shown in Supplementary Figure S4). **(D)** Individual amino-acid r.m.s fluctuations following 1-μs trajectories, shown for all chains of the trimer (solid, dashed and dashed/dotted), and indicating the position of the central CHHH motif.

C-terminal side is formed by heptad residues L386, L390, L393, V397 and M400 (Figure 2G). Overall, the structure can be considered as a single trimeric coiled-coil in which the heptad patterns of N-terminal and C-terminal coiled-coil regions are continuous through the intervening "CHHH"-motif region (Figure 2B).

The SUN1 α1 structure is stable during molecular dynamics simulations

We assessed whether the SUN1 α1 trimeric coiled-coil is stable, or could form alternative conformations, through molecular dynamics simulations. The structure was modified to remove the S-hydroperoxycysteine conformation, leaving only reduced C376 residues with full occupancy, and was subjected to molecular dynamics simulations at 37°C. In three replicates of 1-μs simulations in explicit solvent, the structure remained intact and retained its hydrophobic core (Figure 3A). The overall r.m.s deviation was constant throughout the runs, at values of typically between 1.5–3 Å (Figures 3B, C and Supplementary Figure S3. Further, local r.m.s fluctuations were below 1 Å for the coiled-coil α-helices of all chains between amino-acids 365–397, including the central 376-CHHH-379 motif (Figure 3D). The local r.m.s fluctuations had higher values at the N- and C-termini, consistent with splaying apart of helices at the end of the coiled-coil. Notably, these values were greater at N-termini (up to 8 Å) than C-termini (up to 3 Å), consistent with the more extensive coiled-coil on the C-terminal side of the "CHHH"-motif providing greater stability (Figure 3D). Further, α-helical secondary structure was retained throughout the simulations (Supplementary Figure S3). These findings are consistent with the SUN1 α1 crystal structure representing its principle trimeric conformation. Further, as the model contained only reduced C376 amino-acids, these molecular dynamics simulations are consistent with oxidation having occurred as an artefact of crystallisation rather than being a necessary requirement for complex formation.

The SUN1 α1 trimer is stabilised by zinc coordination

We next utilised size-exclusion chromatography multi-angle light scattering (SEC-MALS) to assess the oligomeric state of SUN1 α1 in solution. SEC-MALS analysis of an MBP fusion (used to provide greater molecular mass resolution) confirmed that SUN1 α1 is predominantly trimeric (144 kDa), in keeping with our crystallographic and molecular dynamics analyses (Figure 4A). However, we also observed concentration-dependent dissociation in solution, through a 100 kDa dimeric intermediate, to a 50 kDa monomeric species (Figure 4A).

We wondered whether the unusual properties of consecutive cysteine and histidine residues within the central 376-CHHH-379 motif may contribute to stability of the coiled-coil trimer through metal coordination. Using a spectrophotometric 4-(2-pyridylazo) resorcinol

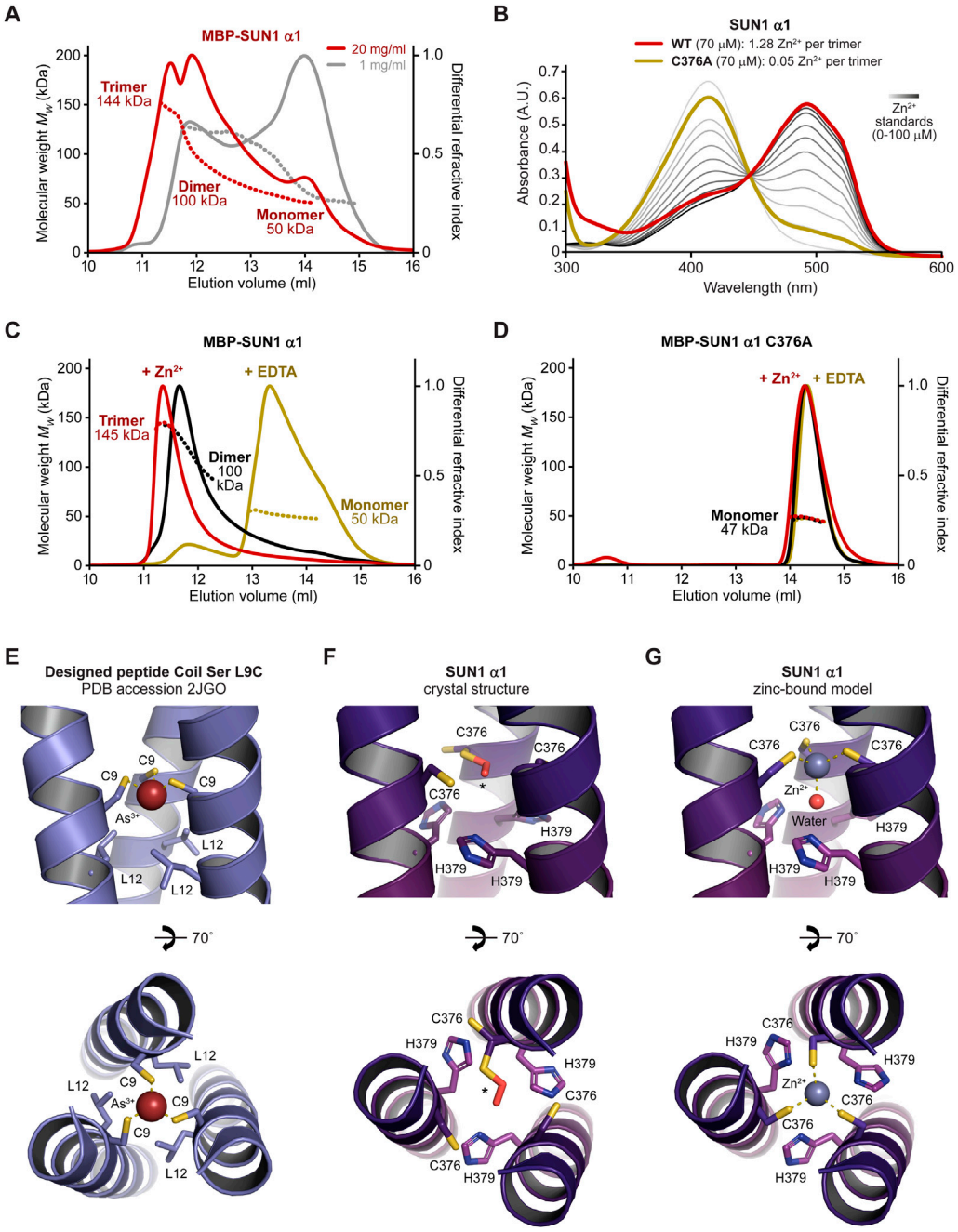

FIGURE 4
The SUN1 α1 trimer is stabilised by zinc coordination. **(A)** SEC-MALS analysis in which differential refractive index (dRI; solid lines) is shown with fitted molecular weights (*Mw*; dashed lines) plotted across elution peaks. MBP-SUN1 α1 is a 144 kDa trimer that dissociates into 100 kDa dimers and 50 kDa monomers (theoretical—148 kDa, 99 kDa and 49 kDa). Data were collected at protein concentrations of 20 mg/mL (red) and 1 mg/mL (grey). **(B)** Spectrophotometric determination of zinc content for wild-type (black; 1.28 Zn^{2+} per trimer) and C376A (red; 0.05 Zn^{2+} per trimer) SUN1 α1, using metallochromic indicator PAR, with zinc standards shown in a gradient from light to dark grey (0–100 μM). **(C and D)** SEC-MALS analysis of **(C)** MBP-SUN1 α1 (20 mg/mL) and **(D)** MBP-SUN1 α1 C376A (5 mg/mL) after purification (black), and after over-night incubation with 2 mM zinc acetate (red) or 10 mM EDTA (yellow). **(C)** MBP-SUN1 α1 is stabilised as a 145 kDa trimer by zinc incubation and is disrupted to a 50 kDa monomer by EDTA. **(D)** MBP-SUN1 α1 C376A is restricted to a 47 kDa monomer in all conditions. **(E)** Structure of designed parallel trimeric coiled-coil Coil Ser L9C bound to arsenic, showing its trigonal coordination by cysteine residues C9 (PDB accession 2JGO; Touw et al., 2007). **(F and G)** SUN1 α1 structure at the central 376-CHHH-379 motif for the **(F)** crystal structure in which one cysteine residue is partially oxidised to S-hydroperoxycysteine and **(G)** modelled structure in which three reduced cysteine residues and a water molecule mediate tetrahedral coordination of a zinc ion.

assay, we detected the presence of a divalent cation bound to SUN1 α1, at a level consistent with one zinc ion per trimer (Figure 4B). Further, the SUN1 α1 trimer was stabilised by addition of zinc prior to SEC-MALS, and was largely disrupted to a monomer by prior incubation with chelating agent EDTA (Figure 4C). We reasoned that zinc-binding likely involves the conserved cysteine residue of the 376-CHHH-

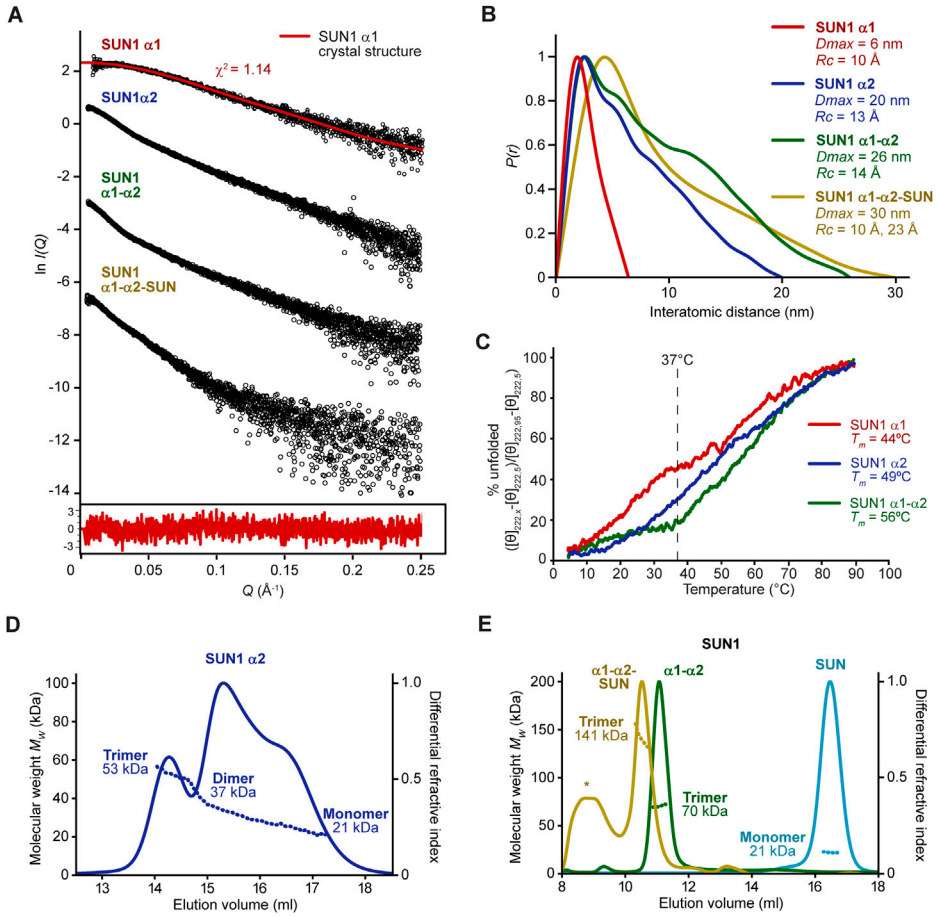

FIGURE 5
The SUN domain is trimerized by α1 and α2 luminal coiled-coils. **(A and B)** SEC-SAXS analysis of SUN1 α1 (red), α2 (blue), α1-α2 (green) and α1-α2-SUN (yellow). **(A)** SAXS scattering data in which the SUN1 α1 scattering cure is overlaid with the theoretical scattering curve of the SUN1 α1 trimeric coiled-coil crystal structure, showing a χ^2 value of 1.14. The residuals for the fit are shown (inset). **(B)** SAXS *P(r)* interatomic distance distributions in which maximum dimensions (*Dmax*) are indicated, along with cross-sectional radii (*Rc*) determined from Guinier analysis (Supplementary Figure S4). **(C)** Thermal denaturation recording the circular dichroism (CD) helical signature at 222 nm between 5°C and 95°C, as % unfolded. Melting temperatures were estimated, as indicated. CD spectra are shown in Supplementary Figure S5. **(D and E)** SEC-MALS analysis. **(D)** SUN1 α2 is a 53 kDa trimer that dissociates into 37 kDa dimers and 21 kDa monomers (theoretical—57 kDa, 38 kDa and 19 kDa). **(E)** SUN1 α1-α2-SUN and α1-α2 are 141 kDa and 70 kDa trimers (theoretical—142 kDa and 75 kDa), whereas the isolated SUN domain is a 21 kDa monomer (theoretical—22 kDa). The additional peak marked with an asterisk in the α1-α2-SUN trace corresponds to a wide range of higher molecular weight species of between 0.2–2.0 MDa, so likely represents a non-specific aggregate.

379 motif (Figure 2B). Accordingly, introduction of point mutation C376A eliminated zinc-binding and blocked trimerization, restricting SUN1 α1 to a monomer (Figures 4B, D). Hence, our data suggest that SUN1 α1 trimer is stabilised in solution by zinc-binding to cysteine residue C376.

How can we rationalise stabilisation of the SUN1 α1 trimer by zinc-binding? We observed several cases in the literature in which metal ions are located along the three-fold axis of trimeric coiled-coils (Touw et al., 2007; Zastrow and Pecoraro, 2014; Cristie-David and Marsh, 2019). In one case, arsenic was trigonally coordinated by symmetric cysteine residues (PDB accession 2JGO; Figure 4E), and it was speculated that zinc could be tetrahedrally coordinated through the same arrangement of cysteine residues with water acting as a fourth exogenous ligand (Touw et al., 2007). We reasoned that this coordination pattern may explain zinc-binding by SUN1 α1. Hence, we built a zinc-bound model by changing the rotamer state of cysteine residues to that of metal-bound structures, and positioning zinc and water along the three-fold axis (Figures 4F, G). In the resultant energy-minimised model, the bond lengths and angles between zinc and its cysteine and water ligands closely match those of tetrahedral geometry (Figure 4G). Further, H379 residues of the 376-CHHH-379 motif have a suitable location to complete tetrahedral binding of the water molecule (Figure 4G). Thus, we propose that tetrahedral coordination of zinc by cysteine and water ligands provides the structural basis for stabilisation of the SUN1 α1 trimer by zinc-binding.

SUN1's α1 and α2 coiled-coil domains mutually reinforce its trimerization

What is the role of SUN1's α1 trimeric coiled-coil within its wider luminal structure? We utilised SEC-MALS and size-exclusion

chromatography small-angle X-ray scattering (SEC-SAXS) to determine the oligomeric states and structures formed by SUN1 luminal constructs in solution, alongside circular dichroism (CD) to assess their helicity and thermal stability.

The SUN1 α1 trimer showed SAXS data and corresponding real-space *P(r)* pair-distance distribution function indicating an elongated molecule of approximately 6 nm in length (Figures 5A, B and Supplementary Figure S4A). This matches the 6 nm length of the SUN1 α1 crystal structure. Further, Guinier analysis indicated a cross-sectional radius of 10 Å (Supplementary Figure S4B). We previously established that dimeric coiled-coils have Guinier cross-sectional radii of 8–9 Å, whereas four-helical coiled-coils have cross-sectional radii of 10–14 Å (Dunce et al., 2018a; Dunne and Davies, 2019; Sanchez-Saez et al., 2020; Dunce et al., 2021). Hence, a 10 Å cross-sectional radius is consistent with SUN1 α1 being a trimeric coiled-coil. Finally, the SAXS scattering curve was closely fitted by the SUN1 α1 trimeric coiled-coil structure (χ^2 = 1.14; Figure 5A). Further, in agreement with our SEC-MALS data indicating concentration-dependent dissociation (Figure 4A), CD showed that SUN1 α1 underwent gradual non-cooperative unfolding, retaining only 55% of its α-helical structure at 37°C, with an arbitrary melting temperature of 44°C (Figure 5C and Supplementary Figure S5). Hence, our combined SEC-MALS, SEC-SAXS and CD data indicate that whilst the SUN1 α1 crystal structure represents the *bona fide* trimeric solution state, it has the propensity to dissociate and unfold at low protein concentrations and high temperatures, consistent with a low micromolar affinity.

We wondered whether the α1 coiled-coil domain may be afforded additional stability by downstream coiled-coils within SUN1's luminal region. On the basis of conservation and secondary structure prediction (Figure 2B), we identified a second luminal coiled-coil domain (amino-acids 421–584; herein referred to as α2), which was stable in solution following recombinant expression (Supplementary Figure S1). This SUN1 α2 coiled-coil domain includes a region of sequence similarity (less than 20% sequence identity) with SUN2's CC1 trimeric coiled-coil (Nie et al., 2016), and is separated from the α1 coiled-coil domain by a predicted unstructured sequence of 22 amino-acids (Figure 2B). SEC-MALS analysis of SUN1 α2 revealed a trimeric structure (53 kDa) that underwent dissociation, through a 37 kDa dimeric intermediate, to a 21 kDa monomer (Figure 5D). SEC-SAXS analysis of the trimer indicated maximum dimensions and cross-sectional radius compatible with it forming a trimeric coiled-coil (Figures 5A,B and Supplementary Figures S4C, D). Further, CD showed a gradual non-cooperative pattern of unfolding, retaining approximately 70% of its α-helical structure at 37°C, with an arbitrary melting temperature of 49°C (Figure 5C and Supplementary Figure S5). Thus, α1 and α2 luminal coiled-coil domains similarly form trimers that dissociate, so are predicted to be dynamic in solution and potentially within their cellular context.

We next tested how the α1 and α2 coiled-coils behave together when joined by the intervening 22 amino-acid sequence (amino-acids 362–584; herein referred to as α1-α2). SUN1 α1-α2 was soluble following recombinant expression (Supplementary Figure S1), and SEC-MALS analysis showed that it forms a stable trimer, with no dissociation to lower oligomeric species (Figure 5E). Further, CD showed cooperative unfolding, with retention of over 80% of its α-helical structure at 37°C, and a melting temperature of 56°C (Figure 5C and Supplementary Figure S5). It is unlikely that the intervening 22 amino-acid linker mediates formation of a single continuous α1-α2 trimeric coiled-coil as its sequence, which includes four glycine and three proline residues, is strongly predicted to be unstructured. Instead, we propose that α1 and α2 coiled-coil domains are flexibly linked, mutually reinforcing their trimeric structure, and thereby stabilising trimerization of the whole luminal coiled-coil region. This is supported by its SEC-SAXS dimensions, which are consistent with a linear arrangement of α1 and α2 trimeric coiled-coils (Figures 5A,B and Supplementary Figure S4E, F). Finally, we analysed SUN1's entire structured luminal domain (amino-acids 362–785; herein referred to as α1-α2-SUN), confirming that the stable and non-dissociating trimeric structure was retained upon inclusion of its C-terminal SUN domain (Figure 5E). Hence, SUN1's α1 and α2 domains have mutually reinforcing trimeric coiled-coil structures that combine to hold together three SUN domains at the end of a luminal trimer.

Molecular model for the SUN1 luminal structure

To integrate our findings with those of previous studies, we built a structure-directed model of SUN1's luminal region using a local installation of *Alphafold2* multimer (Evans et al., 2021; Jumper et al., 2021) in which we could direct its use of structural templates. We specified the use of our SUN1 α1 structure (PDB accession 8AU0), the SUN2 CC1 structure (PDB accession 5ED9; Nie et al., 2016) and the autoinhibited SUN domain structure (PDB accession 5YWZ; Xu et al., 2018) as templates for modelling SUN1's α1, α2 and SUN domains. The resultant trimeric models of SUN1's luminal region (amino-acids 326–785) were consistent, with high pLDDT and low PAE scores in structured regions. The pLDDT score is the per-residue confidence in the local surrounding structure within each chain, whereas PAE is predicted aligned error between distant regions within and between chains of multimers (Evans et al., 2021; Jumper et al., 2021). We selected the top-ranked model, and extended its unstructured linkers to present this in a 'relaxed' linear state (Figure 6 and Supplementary Figure S6). In the model, the first 33 amino-acids (after the transmembrane region) are unstructured, consistent with their poor conservation, lack of secondary structure prediction and presence of four proline residues (Figure 1B). The subsequent α1 trimer structure is linked to a modelled α2 trimer by a 22 amino-acid unstructured/flexible linker, in keeping with our previous analysis. The α2 trimeric coiled-coil is continuous with helices at the beginning of the SUN domains, which are maintained in autoinhibited conformations, in three-fold symmetry, oriented away from the coiled-coil axis (Figure 6). Whilst this model must be considered as a prediction, it provides a molecularly plausible explanation for the architecture of SUN1 within the nuclear lumen. Further, it allows a means for estimating the maximum length that could be bridged by SUN1 molecules. The α1 and α2 structures are approximately 6 nm and 20 nm long, matching the lengths determined by SEC-SAXS analysis (Figures 5A, B and Supplementary Figures S4A–D). The two flexible linkers can vary in length between approximately 8–12 nm and 6–8 nm, depending on whether they are relaxed or at full stretch. Hence, we predict relaxed lengths of up to 32 nm for

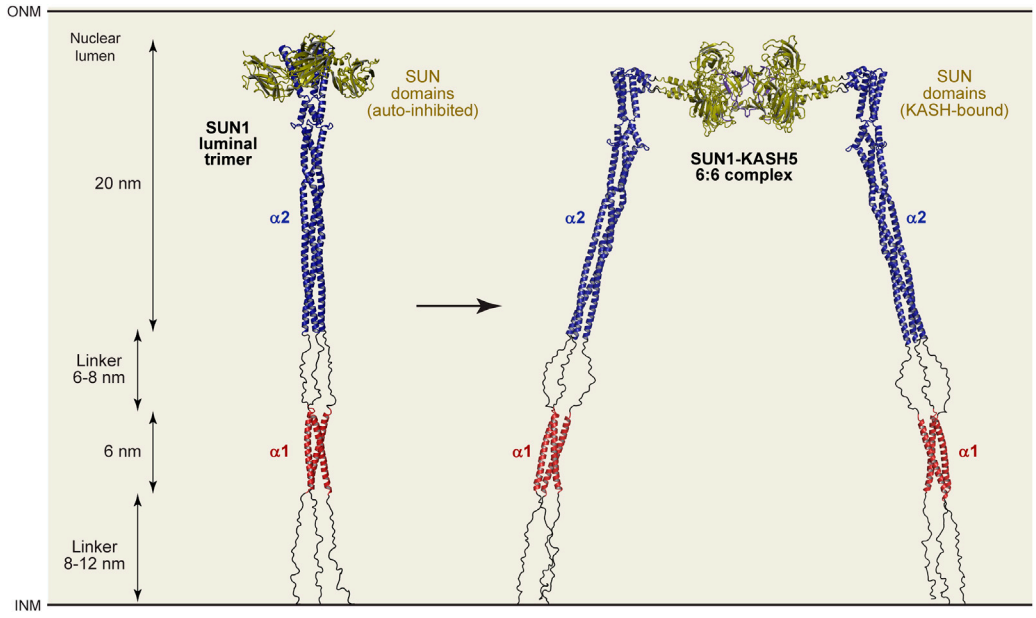

FIGURE 6
Structure-directed models of luminal SUN1 and SUN1-KASH5 complexes. Models of the SUN1 luminal trimer (left) and the SUN1-KASH5 luminal 6:6 complex (right), based on structures and Alphafold2 multimer models generated using specified templates. Modelling details are shown in Supplementary Figures S6-S8. The structured regions of both conformations have lengths of 6 nm and 20 nm, whereas intervening linkers may adopt relaxed linear (as shown) or stretched conformations, varying between lengths of 8-12 nm and 6-8 nm. Hence, the overall length of the SUN1 luminal trimer and SUN1-KASH5 6:6 complex is predicted to vary between 40-46 nm depending on the magnitude and direction of applied tension forces. For comparison, Alphafold2 multimer predictions of the SUN1 trimer without the use of templates, the full 6:6 complex using templates, and the core 6:6 complex without templates, are shown in Supplementary Figures S9A-I, respectively.

both α1-α2 and α1-α2-SUN constructs (which lack the first flexible linker), matching the 26 nm and 30 nm lengths determined by SEC-SAXS analysis (Figures 5A, B and Supplementary Figures S4E–H). Hence, our molecular model for the SUN1 luminal trimer agrees with its experimentally determined dimensions. In total, the full SUN1 luminal trimer is predicted to be between 40–46 nm (Figure 6), depending on tension forces, consistent with the nuclear luminal width (Watson, 1955).

Molecular model for the luminal meiotic LINC complex

Finally, we used the same technique to build a model of the entire luminal region of the SUN1-KASH5 meiotic LINC complex. We first modelled a SUN1 α2-SUN complex (amino-acids 421–785), with SUN domains in trimeric conformation, using as structural templates the SUN2 CC1 crystal structure (PDB accession 5ED9; Nie et al., 2016) and the SUN1-KASH5 structure (PDB accession 6R2I; Gurusaran and Davies, 2021), but not autoinhibited SUN domains. As previously, models were consistent, with high pLDDT and low PAE scores within structured regions (Supplementary Figure S7). We combined this model with the SUN1-KASH5 6:6 core structure (PDB accession 6R2I; Gurusaran and Davies, 2021), and the N-terminal region of the previous SUN1 luminal trimer model, to model the entire SUN1-KASH5 luminal 6:6 complex (Figure 6 and Supplementary Figure S8). In this model, SUN domains adopt their trimeric KASH-bound conformation, in a "flower-like" arrangement of SUN domains around the coiled-coil stem. Interestingly, α2 and SUN domains are joined by a short flexible linker, which corresponds to a helix-loop-helix turn of the autoinhibited conformation. Hence, the SUN1-KASH5 interface is flexibly oriented relative to the coiled-coil, providing an explanation for how SUN1 transitions from being perpendicular to parallel to the nuclear membrane for KASH-binding. Further even with a 90° bend between α2 and SUN domains, this structure is approximately the same length as the SUN1 luminal trimer, so is also predicted to stretch between 40–46 nm, in keeping with the width of the nuclear lumen (Watson, 1955). Thus, we conclude by presenting a model of the luminal region of the meiotic LINC complex (Figure 6), demonstrating how all existing structural information can be integrated into a molecularly plausible structure that fulfils the necessary geometrical requirements for force transduction between inner and outer nuclear membranes within a 6:6 head-to-head LINC complex assembly.

Discussion

The LINC complex operates over a cellular scale, bridging between the cytoskeleton and nuclear contents across lengths of potentially hundreds of nanometres, but is formed principally of coiled-coils that are less than 2 nm in width. Hence, the LINC complex falls within a "grey area" of biology, in which the scale of its full assembly is too large for high resolution methods, but its smallest dimensions require higher resolutions than can be achieved by

cellular microscopy (Joseph et al., 2017; Goodsell et al., 2020). Thus, to understand its structure requires an integrative approach in which we combine high-resolution structures of domains *in silico* to obtain models that explain its molecular structure at a biological scale. We have integrated our crystal structure of SUN1's luminal α1 coiled-coil domain with previous structures and biophysical data to build molecular models of luminal SUN1 and the LINC complex at a scale relevant to the nuclear luminal width (Watson, 1955). Thus, we have provided the first full molecular model of the luminal architecture of the LINC complex.

The SUN1 α1 trimer was stabilised by zinc-binding, which we modelled as tetrahedral coordination involving C376 residues, in keeping with previous metal-bound trimeric coiled-coil structures (Touw et al., 2007; Zastrow and Pecoraro, 2014; Cristie-David and Marsh, 2019). However, the zinc-bound trimer demonstrated a propensity for dissociation in solution, and incubation with exogenous zinc was required to enhance its stability. Further, the crystal structure lacked bound zinc, but included a partially oxidised cysteine residue, which seemingly provided an alternative means for structural stabilisation. Thus, the SUN1 α1 trimer appears to be dynamic, raising the possibility that its assembly could be regulated by the availability of zinc, or another divalent cation, within the nuclear lumen. Further, the nature of the central 376-CHHH-379 motif suggests that cysteine oxidation, disulphide formation and protonation could also affect assembly. Indeed, zinc-binding and cysteine oxidation are mutually exclusive, so oxidation could provide a means for irreversibly blocking zinc-induced trimerization. Similarly, disulphide bond formation between C376 residues could stabilise a dimeric conformation. Such regulatory mechanisms have previously been proposed based on observations that SUN2's luminal trimer is disrupted by low pH and calcium, (Jahed et al., 2018b), the SUN-KASH interaction is enhanced by calcium (Majumder et al., 2022), and that SUN1 trimers may be linked together by inter-molecular disulphide bond formation (Lu et al., 2008). Nevertheless, the biological roles of zinc-binding and other hypothesised mechanisms remain unknown, and must be determined experimentally *in vivo*.

An important prediction from our structure-directed models is that SUN1's luminal region consists of three structural units separated by flexible linkers. The α1, α2 and SUN domains are formed by approximately 87% of the 460 amino-acid luminal region, with remaining amino-acids forming flexible linkers. The first linker of 33 amino-acids bridges from the transmembrane region to the α1 coiled-coil, the second linker of 22 amino-acids connects this to the α2 coiled-coil, and then the final linker of 5 amino-acids joins this to the initial coiled-coil of the SUN domain (this linker is absent in the autoinhibited SUN domain conformation). Their flexible nature is indicated by amino-acid composition (including a large proportion of glycine and proline residues), lack of predicted secondary structure and structured-directed *Alphafold2* models. The presence of these flexible linkers suggests that SUN1 does not form a continuous rod-like coiled-coil between nuclear membranes. Instead, it likely forms a string of linked rigid structural units with conformational freedom to move relative to one another within the lumen (Figure 7), in agreement with previously proposed models (Jahed et al., 2021). Our model is based on the SUN-KASH complex having a 6:6 stoichiometry as this is the only oligomeric state that has been observed in crystal structures and in solution (Sosa et al., 2012; Wang et al., 2012; Zhou et al., 2012; Cruz et al., 2020; Gurusaran and Davies, 2021). Nevertheless, our model of the SUN1 luminal region is compatible with other SUN-KASH stoichiometries, such as 3:3 or larger oligomers, which could potentially form in proximity of the outer nuclear membrane *in vivo* (Jahed et al., 2021).

What is the benefit of SUN1's luminal region consisting of linked coiled-coil domains rather than forming a single continuous coiled-coil? Firstly, the presence of intervening flexible linkers may facilitate coiled-coil folding by overcoming the topological challenge of coiling chains of up to 300 amino-acids around each another. Secondly, conformational freedom between coiled-coil and SUN domains provides a simple explanation for how SUN1 can reorient from perpendicular to parallel to the nuclear membrane as it crosses the nuclear lumen to form SUN-KASH 6:6 complexes (Gurusaran and Davies, 2021). Indeed, the change in helical angulation could be achieved by a single 90° bend in one linker (as shown in the model), or through progressive angulation at each linked step (Figure 7). Finally, linked coiled-coil domains could in principle adapt to changing tension forces, adopting conformations that are more angled or perpendicular to the nuclear membrane in response to forces in these directions. Importantly, our models demonstrate that flexible linkers must be largely stretched for LINC complexes to reach across nuclear widths of >40 nm (Watson, 1955). This is consistent with the need for flexible linkers to bear tension during force transduction by the LINC complex.

We observed that the SUN1 α1 and α2 coiled-coil domains are dissociating oligomers that form stable trimers when joined by their intervening linker. It was previously shown that SUN2's CC1 coiled-coil domain (corresponding to α2) with subsequent SUN domain also dissociates (Nie et al., 2016; Jahed et al., 2018b), whereas its full luminal region forms a stable trimer (Sosa et al., 2012). Hence our findings may be conserved in SUN2, in which the predicted coiled-coil upstream of CC1 may have a stabilising role analogous to SUN1's α1 domain. The presence of flexibly linked discrete coiled-coil domains raises the possibility of domain-swap interactions in which α1 and α2 sequences may form coiled-coil structures with chains from different SUN1 molecules (Figure 7). This is unlikely to occur in solution as the proximity of tethered sequences greatly favours the formation of coiled-coils between the same chains. However, we speculate that it may occur *in vivo* if SUN1 molecules are present at a sufficiently high local concentration for upstream interactions to occur with similar likelihood between chains of the same or distinct downstream trimers. This has two potentially beneficial consequences. Firstly, dissociation and reassociation with different chains may overcome tangles that could develop as the luminal structure adapts to altering tension forces and structural changes. Secondly, domain-swap interactions may facilitate force propagation by providing branch sites within the LINC complex axis. Hence, they may contribute to the force integration and distribution provided by oligomer state alteration between KASH5 dimers, SUN1-KASH5 6:6 complexes and SUN1 trimers (Gurusaran and Davies, 2021; Garner et al., 2022), disulphide bond formation between SUN1 trimers (Lu et al., 2008), and other higher-order interactions between SUN proteins (Jahed et al., 2018a), to facilitate force transduction through a branched LINC complex network. This model is consistent with

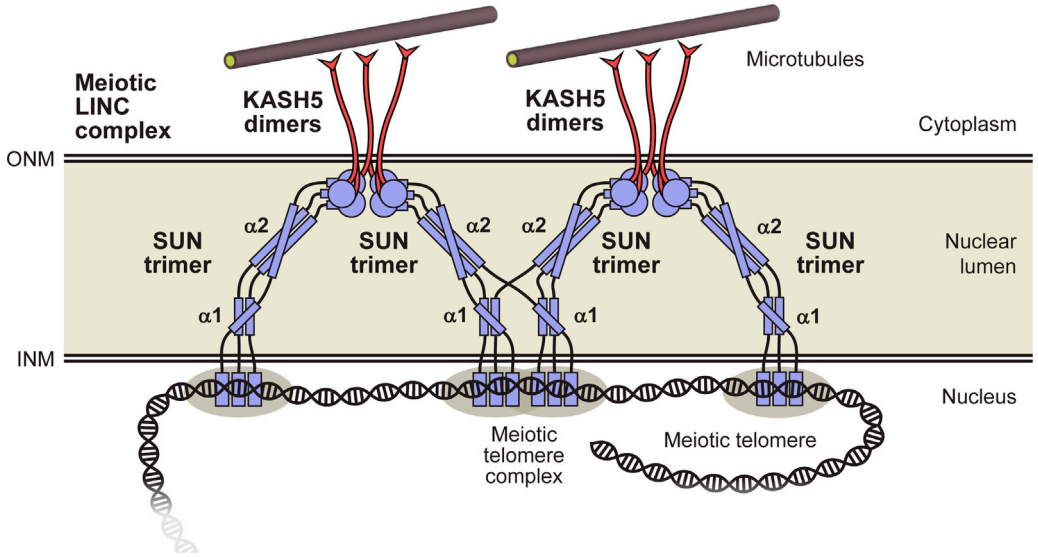

FIGURE 7
Model for the luminal structure of SUN1 within the meiotic LINC complex. The luminal region of SUN1 consists of α1 and α2 trimeric coiled-coil domains, and a C-terminal globular SUN domain that interact head-to-head within 6:6 complexes with KASH5 proteins. These discrete domains are linked together, and to the transmembrane region (at the INM), by flexible unstructured sequences. These intervening flexible linkers provide the possibility for domain-swap interactions between adjacent 6:6 LINC complexes that my contribute to branching within a force-transducing meiotic LINC complex network. Additional components, such as dynein and dynactin, are not depicted to enhance clarity.

the observation that SUN1's luminal domain has been shown to form oligomers that are larger than trimers upon expression in cellular systems (Hennen et al., 2018).

Here, we have used the example of the meiotic LINC complex to illustrate the structure-function relationships inherent in LINC complex architecture. Indeed, the transmission of microtubule-generated forces to achieve the meiotic chromosome movements exemplifies the challenges of LINC-mediated force transduction and the necessity for adaptivity, load bearing and distribution by SUN1's luminal structure (Ding et al., 2007; Horn et al., 2013b). Nevertheless, the LINC complex has several other specialised roles such as in hearing (Horn et al., 2013a), and is essential for nuclear structure, shape and positioning (Crisp et al., 2006; Luxton et al., 2010; Alam et al., 2015; Kozono et al., 2018). Hence, the molecular models for luminal SUN1 and LINC complex architecture presented herein should be directly applicable to the generalised and specialised functions of the LINC complex in its many and varied cellular roles.

Materials and methods

Recombinant protein expression and purification

Sequences corresponding to human SUN1 (amino-acids 362–401, 421–584, 362–584, 362–785; Uniprot accession O94901) were cloned into pMAT11 vectors (Peranen et al., 1996) for expression as TEV-cleavable N-terminal His-MBP- fusion proteins. Constructs were expressed in BL21 (DE3) cells (Novagen®) in 2xYT media, induced with 0.5 mM IPTG for 16 h at 25°C. Cells were lysed by sonication in 20 mM Tris pH 8, 500 mM KCl, and fusion proteins were purified from clarified lysate through consecutive Ni-NTA (Qiagen), amylose (NEB) and HiTrap Q HP (Cytiva) ion exchange chromatography. Affinity tags were removed by incubation with TEV protease and cleaved samples were purified by HiTrap Q HP ion exchange chromatography and size exclusion chromatography (HiLoad™ 16/600 Superdex 200, Cytiva) in 20 mM HEPES pH 7.5, 150 mM KCl, 2 mM DTT. Protein samples were concentrated using Pall 10 kDa Microsep™ Advance centrifugal devices, except for SUN1 362–401 where Pall 3 kDa Microsep™ Advance centrifugal devices were used, and were stored at −80°C following flash-freezing in liquid nitrogen. Protein samples were analysed by SDS-PAGE with Coomassie staining, and concentrations were determined by UV spectroscopy using a Cary 60 UV spectrophotometer (Agilent) with extinction coefficients and molecular weights calculated by ProtParam (http://web.expasy.org/protparam/).

Crystallisation and structure solution of SUN1 α1

SUN1 362–401 protein crystals were obtained through vapour diffusion in sitting drops, by mixing 100 nL of protein at 3.5 mg/mL with 100 nL of crystallisation solution (0.09 M Sodium nitrate, 0.09 M Disodium phosphate, 0.09 M Ammonium sulfate, 0.1 M imidazole pH 6.5, 0.1 M MES (acid), 37.5% MPD (racemic), 37.5% PEG 1K, 37.5% PEG 3350) and equilibrating at 20°C for 10–20 days. Crystals were flash frozen in liquid nitrogen. X-ray diffraction data were collected at 0.9795 Å, 100 K, as 2000 consecutive 0.10° frames of 0.040 s exposure on an Eiger2 XE 16 M detector at beamline I04 of the Diamond Light Source synchrotron facility (Oxfordshire, United Kingdom) on 12/

05/2019. Data were processed using *AutoPROC* (Vonrhein, 2011), in which indexing, integration, scaling were performed by XDS (Kabsch, 2010) and Aimless (Evans, 2011). Crystals belong to monoclinic spacegroup $P2_1$ (cell dimensions a = 31.31 Å, b = 35.99 Å, c = 46.10 Å, α = 90°, β = 104.54°, γ = 90°), with a SUN1 trimer in the asymmetric unit. Data were corrected for anisotropy using the UCLA diffraction anisotropy server (https://services.mbi.ucla.edu/anisoscale/) (Strong et al., 2006), imposing anisotropic limits of 2.4 Å, 2.1 Å, 2.1 Å, with principal components of 19.50 $Å^2$, −9.18 $Å^2$ and −10.31 $Å^2$. Structure solution was achieved through fragment-based molecular replacement using *ARCIMBOLDO_LITE* (Rodriguez et al., 2009), in which six helices of 18 amino acids were placed by *PHASER* (McCoy et al., 2007) and extended by tracing in *SHELXE* utilising its coiled-coil mode (Caballero et al., 2018). A correct solution was identified by a *SHELXE* correlation coefficient of 52.9%. Model building was performed through iterative re-building by *PHENIX* Autobuild (Adams et al., 2010) and manual building in *Coot* (Emsley et al., 2010). Additional density was observed for cysteine residue C376 of chain B, which was modelled as alternative conformations of a reduced cysteine and peroxysulfenic acid (2CO), which refined to occupancies of 0.38 and 0.62, respectively. The structure was refined using *PHENIX* refine (Adams et al., 2010), using isotropic atomic displacement parameters, against anisotropy-corrected 2.07 Å data, to R and R_{free} values of 0.2438 and 0.2551 respectively, with 100% of residues within the favoured regions of the Ramachandran plot (0 outliers), clashscore of 6.38 and overall *MolProbity* score of 1.35 (Chen et al., 2010). The final SUN1 model was analysed using the *Online_DPI* webserver (http://cluster.physics.iisc.ernet.in/dpi) to determine a Cruikshank diffraction precision index (DPI) of 0.25 Å (Kumar et al., 2015).

Molecular dynamics

Molecular dynamics (MD) simulations were performed using *AMBER* ff19SB and OPC forcefields (Case et al., 2022) in *OpenMM* (Eastman et al., 2017), run locally on NVIDIA GeForce RTX 3090 GPU cards through a Google Colab notebook that was modified from the "Making-it-rain" cloud-based MD notebook (Arantes et al., 2021). The SUN1 trimer was placed in a water box 10 Å larger than the structure, and was neutralised at a KCl concentration of 150 mM, by *AMBER* tleap (Case et al., 2022). The structure was equilibrated for 200 ps, and then run for 1 μs at 310 K and 1 bar pressure, using periodic boundary conditions, with the Langevin Middle Integrator and MonteCarlo Barostat, with integration times of 2 fs The run was repeated three times. MD trajectories were analysed using *pytraj* (Roe and Cheatham, 2013; Hai Nguyen et al., 2016).

Size-exclusion chromatography multi-angle light scattering (SEC-MALS)

The absolute molar masses of SUN1 protein samples were determined by multi-angle light scattering coupled with size exclusion chromatography (SEC-MALS). SUN1 protein samples at > 5 mg/mL (unless otherwise stated) were loaded onto a Superdex™ 200 Increase 10/300 GL size exclusion chromatography column (Cytiva) in 20 mM HEPES pH 7.5, 150 mM KCl, 2 mM DTT, at 0.5 mL/min, in line with a DAWN® HELEOS™ II MALS detector (Wyatt Technology) and an Optilab® T-rEX™ differential refractometer (Wyatt Technology). For induction and disruption of zinc-binding, samples were pre-incubated with 2 mM zinc acetate or 10 mM EDTA overnight prior to analysis. Differential refractive index and light scattering data were collected and analysed using ASTRA® 6 software (Wyatt Technology). Molecular weights and estimated errors were calculated across eluted peaks by extrapolation from Zimm plots using a dn/dc value of 0.1850 mL/g.

Spectrophotometric determination of zinc content

The presence of zinc in protein samples was determined through a spectrophotometric method using the metallochromic indicator 4-(2-pyridylazo) resorcinol (PAR) (Sabel et al., 2009). Protein samples at 70 μM, corresponding to SUN1 α1 wild-type and C376A, were digested with 0.6 μg/μL proteinase K (NEB) at 60°C for 1 h. Of the supernatant, 10 μL of each protein digestion was added to 80 μL of 50 μM 4-(2-pyridylazo)-resorcinol (PAR) in 20 mM Tris, pH 8.0, 150 mM KCl, incubated for 5 min at room temperature, and UV absorbance spectra were recorded between 600 and 300 nm (Varian Cary 60 spectrophotometer). Zinc concentrations were estimated from the ratio between absorbance at 492 and 414 nm, plotted on a line of best fit obtained from analysis of 0–100 μM zinc acetate standards.

Size-exclusion chromatography small-angle X-ray scattering (SEC-SAXS)

SEC-SAXS experiments were performed at beamline B21 of the Diamond Light Source synchrotron facility (Oxfordshire, United Kingdom). Protein samples at concentrations >5 mg/mL were loaded onto a Superdex™ 200 Increase 10/300 GL size exclusion chromatography column (Cytiva) in 20 mM HEPES pH 7.5, 150 mM KCl at 0.5 mL/min using an Agilent 1200 HPLC system. The column outlet was fed into the experimental cell, and SAXS data were recorded at 12.4 keV, detector distance 4.014 m, in 3.0 s frames. Data were subtracted and averaged, and analysed for Guinier region *Rg* and cross-sectional *Rg* (*Rc*) using *ScÅtter* 4.0 (http://www.bioisis.net), and *P(r)* distributions were fitted using *PRIMUS* (Konarev et al., 2003). Crystal structures and models were fitted to experimental data using *CRYSOL* (Svergun and Koch, 1995).

Circular dichroism (CD) spectroscopy

Far UV circular dichroism (CD) spectroscopy data were collected on a Chirascan VX CD spectrometer (School of Chemistry, University of Edinburgh). CD spectra were recorded in 10 mM Na_2HPO_4/NaH_2PO_4 pH 7.5, 150 mM NaF, at protein concentrations between 0.1–0.3 mg/mL, using a 0.5 mm pathlength quartz cuvette (Applied Photophysics), at 0.2 nm intervals between 260 and 185 nm at 4°C. Spectra were averaged across three accumulations, corrected for buffer signal, smoothed and converted to mean residue ellipticity ([θ])

(x1,000 deg. cm^2. $dmol^{-1}$. $residue^{-1}$). CD thermal denaturation was performed in 10 mM Na_2HPO_4/NaH_2PO_4 pH 7.5, 150 mM NaF, at protein concentrations between 0.1–0.3 mg/mL, using a 0.5 mm pathlength quartz cuvette (Applied Photophysics). Data were recorded at 222 nm, between 4°C and 95°C, at 0.5°C intervals with ramping rate of 2°C per minute, and were converted to mean residue ellipticity ($[\theta_{222}]$) and plotted as % unfolded ($[\theta]_{222,x}$-$[\theta]_{222,5}$)/($[\theta]_{222,95}$-$[\theta]_{222,5}$). Melting temperatures (Tm) were estimated as the points at which samples are 50% unfolded.

SUN1 and SUN1-KASH5 luminal structural modelling

Models were generated using a local installation of *Alphafold2* v2.2.2 (Jumper et al., 2021). This installation was modified to control the use of templates from the PDB and allow additional templates from newly solved crystal structures. Models of the SUN1 luminal trimer (amino-acids 326–785) were generated through the multimer pipeline (Evans et al., 2021), using PDB structures 5YWZ (Xu et al., 2018), 5ED9 (Nie et al., 2016) and the newly reported α1 crystal structure 8AU0, as the sole templates. The constituent α1 and α2-SUN domains of the resultant model were re-positioned in line, and their intervening linkers were re-modelled in "relaxed" linear conformations. For the model of the meiotic SUN1-KASH5 luminal LINC complex, the α2-SUN trimer (amino-acids 421–785) was first modelled in trimeric SUN domain conformation by the *Alphafold2* multimer pipeline (Evans et al., 2021; Jumper et al., 2021), using PDB structures 5ED9 (Nie et al., 2016) and 6R2I (Gurusaran and Davies, 2021) as the sole templates. The SUN domain trimer of the resultant structure was replaced with one KASH5-bound trimer of the SUN1-KASH5 6:6 core complex structure (PDB accession 6R2I; Gurusaran and Davies, 2021), with re-modelling of the intervening flexible linkers. The structure was combined with the α1 domain flanked by flexible linkers of the previous SUN1 luminal trimer model, and was replicated for the second KASH5-bound trimer of the complex, to achieve a full model of the SUN1-KASH5 luminal 6:6 structure. *Alphafold2* multimer modelling data were analysed using modules from the ColabFold notebook (Mirdita et al., 2022). Models were edited, combined and flexible linkers were remodelled using the *PyMOL* Molecular Graphics System, Version 2.0.4 Schrödinger, LLC, and *Coot* (Emsley et al., 2010).

Protein sequence and structure analysis

Multiple sequence alignments were generated using *Jalview* (Waterhouse et al., 2009), and molecular structure images were generated using the *PyMOL* Molecular Graphics System, Version 2.0.4 Schrödinger, LLC.

Statistics and reproducibility

All biochemical and biophysical experiments were repeated at least three times with separately prepared recombinant protein material. Molecular dynamics simulations were performed in triplicate by repeating every step of the simulation from the same structural model.

Data availability statement

Crystallographic structure factors and atomic co-ordinates have been deposited in the Protein Data Bank (PDB) under accession number 8AU0, and corresponding raw diffraction images have been deposited at https://proteindiffraction.org/.

Author contributions

MG crystallised SUN1 and performed biophysical experiments. CW and OD performed molecular dynamics simulations. JB and OD performed *Alphafold2* modelling. OD solved the SUN1 crystal structure, analysed data, designed experiments and wrote the manuscript. All authors contributed to the article and approved the submitted version.

Funding

This work was supported by a Wellcome Senior Research Fellowship to OD. (Grant Number 219413/Z/19/Z), and a core grant to the Wellcome Centre for Cell Biology (203,149). CW is supported by an Engineering and Physical Sciences Research Council Fellowship (EP/S003002/1) and by the Wellcome-Trust University of Edinburgh Institutional Strategic Support Fund ISSF3.

Acknowledgments

We thank Diamond Light Source and the staff of beamlines I04 and B21 (proposals mx18598 and sm21777).

Conflict of interest

The authors declare that the research was conducted in the absence of any commercial or financial relationships that could be construed as a potential conflict of interest.

Publisher's note

Supplementary material

The Supplementary Material for this article can be found online at: https://www.frontiersin.org/articles/10.3389/fcell.2023.1144277/full#supplementary-material

References

Adams, P. D., Afonine, P. V., Bunkoczi, G., Chen, V. B., Davis, I. W., Echols, N., et al. (2010). Phenix: A comprehensive python-based system for macromolecular structure solution. *Acta Crystallogr. D. Biol. Crystallogr.* 66, 213–221. doi:10.1107/S0907444909052925

Agrawal, R., Gillies, J. P., Zang, J. L., Zhang, J., Garrott, S. R., Shibuya, H., et al. (2022). The KASH5 protein involved in meiotic chromosomal movements is a novel dynein activating adaptor. *bioRxiv*, 11. doi:10.7554/elife.78201

Alam, S. G., Lovett, D., Kim, D. I., Roux, K. J., Dickinson, R. B., and Lele, T. P. (2015). The nucleus is an intracellular propagator of tensile forces in NIH 3T3 fibroblasts. *J. Cell. Sci.* 128, 1901–1911. doi:10.1242/jcs.161703

Arantes, P. R., Poleto, M. D., Pedebos, C., and Ligabue-Braun, R. (2021). Making it rain: Cloud-based molecular simulations for everyone. *J. Chem. Inf. Model.* 61, 4852–4856. doi:10.1021/acs.jcim.1c00998

Banerjee, I., Zhang, J., Moore-Morris, T., Pfeiffer, E., Buchholz, K. S., Liu, A., et al. (2014). Targeted ablation of nesprin 1 and nesprin 2 from murine myocardium results in cardiomyopathy, altered nuclear morphology and inhibition of the biomechanical gene response. *PLoS Genet.* 10, e1004114. doi:10.1371/journal.pgen.1004114

Caballero, I., Sammito, M., Millan, C., Lebedev, A., Soler, N., and Uson, I. (2018). ARCIMBOLDO on coiled coils. *Acta Crystallogr. D. Struct. Biol.* 74, 194–204. doi:10.1107/S2059798317017582

Case, D. A., Belfon, K., Ben-Shalom, I. Y., Berryman, J. T., Brozell, S. R., Cerutti, D. S., et al. (2022). *Amber 2022*.

Chen, V. B., Arendall, W. B., Headd, J. J., Keedy, D. A., Immormino, R. M., Kapral, G. J., et al. (2010). MolProbity: All-atom structure validation for macromolecular crystallography. *Acta Crystallogr. Sect. D-Biological Crystallogr.* 66, 12–21. doi:10.1107/S0907444909042073

Chen, Y., Wang, Y., Chen, J., Zuo, W., Fan, Y., Huang, S., et al. (2021). The SUN1-SPDYA interaction plays an essential role in meiosis prophase I. *Nat. Commun.* 12, 3176. doi:10.1038/s41467-021-23550-w

Crisp, M., Liu, Q., Roux, K., Rattner, J. B., Shanahan, C., Burke, B., et al. (2006). Coupling of the nucleus and cytoplasm: Role of the LINC complex. *J. Cell. Biol.* 172, 41–53. doi:10.1083/jcb.200509124

Cristie-David, A. S., and Marsh, E. N. G. (2019). Metal-dependent assembly of a protein nano-cage. *Protein Sci.* 28, 1620–1629. doi:10.1002/pro.3676

Cruz, V. E., Esra Demircioglu, F., and Schwartz, T. U. (2020). Structural analysis of different LINC complexes reveals distinct binding modes. *J. Mol. Biol.* 432, 6028–6041. doi:10.1016/j.jmb.2020.09.019

Ding, X., Xu, R., Yu, J., Xu, T., Zhuang, Y., and Han, M. (2007). SUN1 is required for telomere attachment to nuclear envelope and gametogenesis in mice. *Dev. Cell.* 12, 863–872. doi:10.1016/j.devcel.2007.03.018

Drozdetskiy, A., Cole, C., Procter, J., and Barton, G. J. (2015). JPred4: A protein secondary structure prediction server. *Nucleic Acids Res.* 43, W389–W394. doi:10.1093/nar/gkv332

Dunce, J. M., Dunne, O. M., Ratcliff, M., Millan, C., Madgwick, S., Uson, I., et al. (2018a). Structural basis of meiotic chromosome synapsis through SYCP1 self-assembly. *Nat. Struct. Mol. Biol.* 25, 557–569. doi:10.1038/s41594-018-0078-9

Dunce, J. M., Milburn, A. E., Gurusaran, M., Da Cruz, I., Sen, L. T., Benavente, R., et al. (2018b). Structural basis of meiotic telomere attachment to the nuclear envelope by MAJIN-TERB2-TERB1. *Nat. Commun.* 9, 5355. doi:10.1038/s41467-018-07794-7

Dunce, J. M., Salmon, L. J., and Davies, O. R. (2021). Structural basis of meiotic chromosome synaptic elongation through hierarchical fibrous assembly of SYCE2-TEX12. *Nat. Struct. Mol. Biol.* 28, 681–693. doi:10.1038/s41594-021-00636-z

Dunne, O. M., and Davies, O. R. (2019). A molecular model for self-assembly of the synaptonemal complex protein SYCE3. *J. Biol. Chem.* 294, 9260–9275. doi:10.1074/jbc.RA119.008404

Eastman, P., Swails, J., Chodera, J. D., Mcgibbon, R. T., Zhao, Y., Beauchamp, K. A., et al. (2017). OpenMM 7: Rapid development of high performance algorithms for molecular dynamics. *PLoS Comput. Biol.* 13, e1005659. doi:10.1371/journal.pcbi.1005659

Emsley, P., Lohkamp, B., Scott, W. G., and Cowtan, K. (2010). Features and development of Coot. *Acta Crystallogr. D. Biol. Crystallogr.* 66, 486–501. doi:10.1107/S0907444910007493

Evans, P. R. (2011). An introduction to data reduction: Space-group determination, scaling and intensity statistics. *Acta Crystallogr. D. Biol. Crystallogr.* 67, 282–292. doi:10.1107/S090744491003982X

Evans, R., O'Neill, M., Pritzel, A., Antropova, N., Senior, A., Green, T., et al. (2021). *Protein complex prediction with AlphaFold-Multimer*. Cold Spring Harbor Laboratory. bioRxiv.

Gao, Q., Khan, R., Yu, C., Alsheimer, M., Jiang, X., Ma, H., et al. (2020). The testis-specific LINC component SUN3 is essential for sperm head shaping during mouse spermiogenesis. *J. Biol. Chem.* 295, 6289–6298. doi:10.1074/jbc.RA119.012375

Garner, K. E. L., Salter, A., Lau, C. K., Gurusaran, M., Villemant, C., Granger, E. P., et al. (2022). The meiotic LINC complex component KASH5 is an activating adaptor for cytoplasmic dynein. *bioRxiv*.

Goodsell, D. S., Olson, A. J., and Forli, S. (2020). Art and science of the cellular mesoscale. *Trends Biochem. Sci.* 45, 472–483. doi:10.1016/j.tibs.2020.02.010

Gurusaran, M., and Davies, O. R. (2021). A molecular mechanism for LINC complex branching by structurally diverse SUN-KASH 6:6 assemblies. *Elife* 10, e60175. doi:10.7554/eLife.60175

Hai Nguyen, D. R. R., Jason, S., and David., A. (2016). *Pytraj: Interactive data analysis for molecular dynamics simulations*.

Hennen, J., Saunders, C. A., Mueller, J. D., and Luxton, G. W. G. (2018). Fluorescence fluctuation spectroscopy reveals differential SUN protein oligomerization in living cells. *Mol. Biol. Cell.* 29, 1003–1011. doi:10.1091/mbc.E17-04-0233

Horn, H. F., Brownstein, Z., Lenz, D. R., Shivatzki, S., Dror, A. A., Dagan-Rosenfeld, O., et al. (2013a). The LINC complex is essential for hearing. *J. Clin. Investig.* 123, 740–750. doi:10.1172/JCI66911

Horn, H. F., Kim, D. I., Wright, G. D., Wong, E. S., Stewart, C. L., Burke, B., et al. (2013b). A mammalian KASH domain protein coupling meiotic chromosomes to the cytoskeleton. *J. Cell. Biol.* 202, 1023–1039. doi:10.1083/jcb.201304004

Jahed, Z., Domkam, N., Ornowski, J., Yerima, G., and Mofrad, M. R. K. (2021). Molecular models of LINC complex assembly at the nuclear envelope. *J. Cell. Sci.* 134, jcs258194. doi:10.1242/jcs.258194

Jahed, Z., Fadavi, D., Vu, U. T., Asgari, E., Luxton, G. W. G., and Mofrad, M. R. K. (2018a). Molecular insights into the mechanisms of SUN1 oligomerization in the nuclear envelope. *Biophys. J.* 114, 1190–1203. doi:10.1016/j.bpj.2018.01.015

Jahed, Z., Vu, U. T., Fadavi, D., Ke, H., Rathish, A., Kim, S. C. J., et al. (2018b). A molecular model for LINC complex regulation: Activation of SUN2 for KASH binding. *Mol. Biol. Cell.* 29, 2012–2023. doi:10.1091/mbc.E18-04-0266

Joseph, A. P., Polles, G., Alber, F., and Topf, M. (2017). Integrative modelling of cellular assemblies. *Curr. Opin. Struct. Biol.* 46, 102–109. doi:10.1016/j.sbi.2017.07.001

Jumper, J., Evans, R., Pritzel, A., Green, T., Figurnov, M., Ronneberger, O., et al. (2021). Highly accurate protein structure prediction with AlphaFold. *Nature* 596, 583–589. doi:10.1038/s41586-021-03819-2

Kabsch, W. (2010). Xds. *Acta Crystallogr. D. Biol. Crystallogr.* 66, 125–132. doi:10.1107/S0907444909047337

Ketema, M., and Sonnenberg, A. (2011). Nesprin-3: A versatile connector between the nucleus and the cytoskeleton. *Biochem. Soc. Trans.* 39, 1719–1724. doi:10.1042/BST20110669

Konarev, P. V., Sokolova, A. V., Koch, M. H. J., and Svergun, D. I. (2003). Primus - a Windows-PC based system for small-angle scattering data analysis. *J. Appl. Cryst.* 36, 1277–1282. doi:10.1107/s0021889803012779

Kozono, T., Tadahira, K., Okumura, W., Itai, N., Tamura-Nakano, M., Dohi, T., et al. (2018). Jaw1/LRMP has a role in maintaining nuclear shape via interaction with SUN proteins. *J. Biochem.* 164, 303–311. doi:10.1093/jb/mvy053

Kumar, K. D., Gurusaran, M., Satheesh, S., Radha, P., Pavithra, S., Thulaa Tharshan, K., et al. (2015). Online_DPI: A web server to calculate the diffraction precision index for a protein structure. *J. Appl. Crystallogr.* 48, 939–942. doi:10.1107/s1600576715006287

Lee, C. Y., Horn, H. F., Stewart, C. L., Burke, B., Bolcun-Filas, E., Schimenti, J. C., et al. (2015). Mechanism and regulation of rapid telomere prophase movements in mouse meiotic chromosomes. *Cell. Rep.* 11, 551–563. doi:10.1016/j.celrep.2015.03.045

Lei, K., Zhang, X., Ding, X., Guo, X., Chen, M., Zhu, B., et al. (2009). SUN1 and SUN2 play critical but partially redundant roles in anchoring nuclei in skeletal muscle cells in mice. *Proc. Natl. Acad. Sci. U. S. A.* 106, 10207–10212. doi:10.1073/pnas.0812037106

Lim, S. M., Cruz, V. E., Antoku, S., Gundersen, G. G., and Schwartz, T. U. (2021). Structures of FHOD1-Nesprin1/2 complexes reveal alternate binding modes for the FH3 domain of formins. *Structure* 29, 540–552 e5. doi:10.1016/j.str.2020.12.013

Link, J., Leubner, M., Schmitt, J., Gob, E., Benavente, R., Jeang, K. T., et al. (2014). Analysis of meiosis in SUN1 deficient mice reveals a distinct role of SUN2 in mammalian meiotic LINC complex formation and function. *PLoS Genet.* 10, e1004099. doi:10.1371/journal.pgen.1004099

Lu, W., Gotzmann, J., Sironi, L., Jaeger, V. M., Schneider, M., Luke, Y., et al. (2008). Sun1 forms immobile macromolecular assemblies at the nuclear envelope. *Biochim. Biophys. Acta* 1783, 2415–2426. doi:10.1016/j.bbamcr.2008.09.001

Luxton, G. W., Gomes, E. R., Folker, E. S., Vintinner, E., and Gundersen, G. G. (2010). Linear arrays of nuclear envelope proteins harness retrograde actin flow for nuclear movement. *Science* 329, 956–959. doi:10.1126/science.1189072

Majumder, S., Hsu, Y. Y., Moghimianavval, H., Andreas, M., Giessen, T. W., Luxton, G. W. G., et al. (2022). *In vitro* synthesis and reconstitution using mammalian cell-free lysates enables the systematic study of the regulation of LINC complex assembly. *Biochemistry* 61, 1495–1507. doi:10.1021/acs.biochem.2c00118

Mccoy, A. J., Grosse-Kunstleve, R. W., Adams, P. D., Winn, M. D., Storoni, L. C., and Read, R. J. (2007). Phaser crystallographic software. *J. Appl. Crystallogr.* 40, 658–674. doi:10.1107/S0021889807021206

Meinke, P., Nguyen, T. D., and Wehnert, M. S. (2011). The LINC complex and human disease. *Biochem. Soc. Trans.* 39, 1693–1697. doi:10.1042/BST20110658

Meinke, P., and Schirmer, E. C. (2015). LINC'ing form and function at the nuclear envelope. *FEBS Lett.* 589, 2514–2521. doi:10.1016/j.febslet.2015.06.011

Mejat, A., and Misteli, T. (2010). LINC complexes in health and disease. *Nucleus* 1, 40–52. doi:10.4161/nucl.1.1.10530

Mirdita, M., Schutze, K., Moriwaki, Y., Heo, L., Ovchinnikov, S., and Steinegger, M. (2022). ColabFold: Making protein folding accessible to all. *Nat. Methods* 19, 679–682. doi:10.1038/s41592-022-01488-1

Nie, S., Ke, H., Gao, F., Ren, J., Wang, M., Huo, L., et al. (2016). Coiled-coil domains of SUN proteins as intrinsic dynamic regulators. *Structure* 24, 80–91. doi:10.1016/j.str.2015.10.024

Okumura, W., Tadahira, K., Kozono, T., Tamura-Nakano, M., Sato, H., Matsui, H., et al. (2023). Jaw1/LRMP is associated with the maintenance of Golgi ribbon structure. *J. Biochem.* 173, 383–392. doi:10.1093/jb/mvad004

Pasch, E., Link, J., Beck, C., Scheuerle, S., and Alsheimer, M. (2015). The LINC complex component Sun4 plays a crucial role in sperm head formation and fertility. *Biol. Open* 4, 1792–1802. doi:10.1242/bio.015768

Peranen, J., Rikkonen, M., Hyvonen, M., and Kaariainen, L. (1996). T7 vectors with modified T7lac promoter for expression of proteins in *Escherichia coli*. *Anal. Biochem.* 236, 371–373. doi:10.1006/abio.1996.0187

Rodriguez, D. D., Grosse, C., Himmel, S., Gonzalez, C., de Ilarduya, I. M., Becker, S., et al. (2009). Crystallographic *ab initio* protein structure solution below atomic resolution. *Nat. Methods* 6, 651–653. doi:10.1038/nmeth.1365

Roe, D. R., and Cheatham, T. E., 3R. D. (2013). PTRAJ and CPPTRAJ: Software for processing and analysis of molecular dynamics trajectory data. *J. Chem. Theory Comput.* 9, 3084–3095. doi:10.1021/ct400341p

Roux, K. J., Crisp, M. L., Liu, Q., Kim, D., Kozlov, S., Stewart, C. L., et al. (2009). Nesprin 4 is an outer nuclear membrane protein that can induce kinesin-mediated cell polarization. *Proc. Natl. Acad. Sci. U. S. A.* 106, 2194–2199. doi:10.1073/pnas.0808602106

Sabel, C. E., Shepherd, J. L., and Siemann, S. (2009). A direct spectrophotometric method for the simultaneous determination of zinc and cobalt in metalloproteins using 4-(2-pyridylazo)resorcinol. *Anal. Biochem.* 391, 74–76. doi:10.1016/j.ab.2009.05.007

Sakamoto, N., Ogawa, M., Sadamoto, K., Takeuchi, M., and Kataoka, N. (2017). Mechanical role of nesprin-1-mediated nucleus-actin filament binding in cyclic stretch-induced fibroblast elongation. *Cell. Mol. Bioeng.* 10, 327–338. doi:10.1007/s12195-017-0487-6

Sanchez-Saez, F., Gomez, H. L., Dunne, O. M., Gallego-Paramo, C., Felipe-Medina, N., Sanchez-Martin, M., et al. (2020). Meiotic chromosome synapsis depends on multivalent SYCE1-SIX6OS1 interactions that are disrupted in cases of human infertility. *Sci. Adv.* 6, eabb1660. doi:10.1126/sciadv.abb1660

Schmitt, J., Benavente, R., Hodzic, D., Hoog, C., Stewart, C. L., and Alsheimer, M. (2007). Transmembrane protein Sun2 is involved in tethering mammalian meiotic telomeres to the nuclear envelope. *Proc. Natl. Acad. Sci. U. S. A.* 104, 7426–7431. doi:10.1073/pnas.0609198104

Shibuya, H., Hernandez-Hernandez, A., Morimoto, A., Negishi, L., Hoog, C., and Watanabe, Y. (2015). MAJIN links telomeric DNA to the nuclear membrane by exchanging telomere cap. *Cell.* 163, 1252–1266. doi:10.1016/j.cell.2015.10.030

Shibuya, H., Morimoto, A., and Watanabe, Y. (2014). The dissection of meiotic chromosome movement in mice using an *in vivo* electroporation technique. *PLoS Genet.* 10, e1004821. doi:10.1371/journal.pgen.1004821

Sosa, B. A., Rothballer, A., Kutay, U., and Schwartz, T. U. (2012). LINC complexes form by binding of three KASH peptides to domain interfaces of trimeric SUN proteins. *Cell.* 149, 1035–1047. doi:10.1016/j.cell.2012.03.046

Spindler, M. C., Redolfi, J., Helmprobst, F., Kollmannsberger, P., Stigloher, C., and Benavente, R. (2019). Electron tomography of mouse LINC complexes at meiotic telomere attachment sites with and without microtubules. *Commun. Biol.* 2, 376. doi:10.1038/s42003-019-0621-1

Starr, D. A., and Fridolfsson, H. N. (2010). Interactions between nuclei and the cytoskeleton are mediated by SUN-KASH nuclear-envelope bridges. *Annu. Rev. Cell. Dev. Biol.* 26, 421–444. doi:10.1146/annurev-cellbio-100109-104037

Strong, M., Sawaya, M. R., Wang, S., Phillips, M., Cascio, D., and Eisenberg, D. (2006). Toward the structural genomics of complexes: Crystal structure of a PE/PPE protein complex from *Mycobacterium tuberculosis*. *Proc. Natl. Acad. Sci. U. S. A.* 103, 8060–8065. doi:10.1073/pnas.0602606103

Svergun, D. I., and Koch, M. H. J. (1995). Crysol – A program to evaluate X-ray solution scattering of biological macromolecules from atomic coordinates. *J. Appl. Cryst.* 28, 768–773. doi:10.1107/s0021889895007047

Touw, D. S., Nordman, C. E., Stuckey, J. A., and Pecoraro, V. L. (2007). Identifying important structural characteristics of arsenic resistance proteins by using designed three-stranded coiled coils. *Proc. Natl. Acad. Sci. U. S. A.* 104, 11969–11974. doi:10.1073/pnas.0701979104

Wang, W., Shi, Z., Jiao, S., Chen, C., Wang, H., Liu, G., et al. (2012). Structural insights into SUN-KASH complexes across the nuclear envelope. *Cell. Res.* 22, 1440–1452. doi:10.1038/cr.2012.126

Waterhouse, A. M., Procter, J. B., Martin, D. M., Clamp, M., and Barton, G. J. (2009). Jalview Version 2--a multiple sequence alignment editor and analysis workbench. *Bioinformatics* 25, 1189–1191. doi:10.1093/bioinformatics/btp033

Watson, M. L. (1955). The nuclear envelope; its structure and relation to cytoplasmic membranes. *J. Biophys. Biochem. Cytol.* 1, 257–270. doi:10.1083/jcb.1.3.257

Wilhelmsen, K., Litjens, S. H., Kuikman, I., Tshimbalanga, N., Janssen, H., van Den Bout, I., et al. (2005). Nesprin-3, a novel outer nuclear membrane protein, associates with the cytoskeletal linker protein plectin. *J. Cell. Biol.* 171, 799–810. doi:10.1083/jcb.200506083

Xu, Y., Li, W., Ke, H., and Feng, W. (2018). Structural conservation of the autoinhibitory domain in SUN proteins. *Biochem. Biophys. Res. Commun.* 496, 1337–1343. doi:10.1016/j.bbrc.2018.02.015

Zastrow, M. L., and Pecoraro, V. L. (2014). Designing hydrolytic zinc metalloenzymes. *Biochemistry* 53, 957–978. doi:10.1021/bi4016617

Zhang, X., Lei, K., Yuan, X., Wu, X., Zhuang, Y., Xu, T., et al. (2009). SUN1/2 and Syne/Nesprin-1/2 complexes connect centrosome to the nucleus during neurogenesis and neuronal migration in mice. *Neuron* 64, 173–187. doi:10.1016/j.neuron.2009.08.018

Zhang, Y., Yang, L., Huang, L., Liu, G., Nie, X., Zhang, X., et al. (2021). SUN5 interacting with Nesprin3 plays an essential role in sperm head-to-tail linkage: Research on Sun5 gene knockout mice. *Front. Cell. Dev. Biol.* 9, 684826. doi:10.3389/fcell.2021.684826

Zhou, C., Rao, L., Shanahan, C. M., and Zhang, Q. (2018). Nesprin-1/2: Roles in nuclear envelope organisation, myogenesis and muscle disease. *Biochem. Soc. Trans.* 46, 311–320. doi:10.1042/BST20170149

Zhou, Z., du, X., Cai, Z., Song, X., Zhang, H., Mizuno, T., et al. (2012). Structure of Sad1-UNC84 homology (SUN) domain defines features of molecular bridge in nuclear envelope. *J. Biol. Chem.* 287, 5317–5326. doi:10.1074/jbc.M111.304543

frontiers | Frontiers in Cell and Developmental Biology

TYPE Perspective
PUBLISHED 13 November 2023
DOI 10.3389/fcell.2023.1278571

OPEN ACCESS

EDITED BY
Ricardo Benavente,
Julius Maximilian University of Würzburg, Germany

REVIEWED BY
María Teresa Parra,
Universidad Autónoma de Madrid, Spain
Marcia Manterola,
University of Chile, Chile

*CORRESPONDENCE
Alfonso Fernández-Álvarez,
alfonso.fernandez.alvarez@csic.es

RECEIVED 16 August 2023
ACCEPTED 01 November 2023
PUBLISHED 13 November 2023

CITATION
Fernández-Álvarez A (2023), Beyond tradition: exploring the non-canonical functions of telomeres in meiosis. *Front. Cell Dev. Biol.* 11:1278571. doi: 10.3389/fcell.2023.1278571

Beyond tradition: exploring the non-canonical functions of telomeres in meiosis

Alfonso Fernández-Álvarez *

Institute of Functional Biology and Genomics (IBFG), Consejo Superior de Investigaciones Científicas (CSIC), University of Salamanca, Salamanca, Spain

The telomere bouquet is a specific chromosomal configuration that forms during meiosis at the zygotene stage, when telomeres cluster together at the nuclear envelope. This clustering allows cytoskeleton-induced movements to be transmitted to the chromosomes, thereby facilitating homologous chromosome search and pairing. However, loss of the bouquet results in more severe meiotic defects than can be attributed solely to recombination problems, suggesting that the bouquet's full function remains elusive. Despite its transient nature and the challenges in performing *in vivo* analyses, information is emerging that points to a remarkable suite of non-canonical functions carried out by the bouquet. Here, we describe how new approaches in quantitative cell biology can contribute to establishing the molecular basis of the full function and plasticity of the bouquet, and thus generate a comprehensive picture of the telomeric control of meiosis.

KEYWORDS

telomeres, bouquet, meiosis, gametogenesis, yeast, chromosome dynamics, centromere

1 Introduction

The genetic diversity of gametes is facilitated by DNA recombination between homologous chromosomes during meiosis (Petronczki et al., 2003; Hunter, 2015; Zickler and Kleckner, 2015). Strong nuclear movements driven by cytoskeleton motors play a central role in promoting the search and pairing of homologous chromosomes within the nucleoplasm. These movements increase the likelihood of homologous chromosomes meeting and also destabilize interactions between non-homologous chromosomes (Yamamoto et al., 1999; Scherthan et al., 2007; Koszul et al., 2008; Baudrimont et al., 2010; Wynne et al., 2012; Woglar and Jantsch, 2014; Christophorou et al., 2015; Lee et al., 2015; Chacon et al., 2016). For nuclear motion to be transmitted to the chromosomes efficiently, the chromosomes must stay associated with the nuclear envelope (NE). In meiosis, specific associations between telomeres and the NE during the zygotene stage lead to the formation of dynamic clusters of telomeres that are visible through live imaging as groups of telomeres in motion (Chikashige et al., 1994; Klutstein and Cooper, 2014; Mytlis et al., 2023). In some species, these telomere clusters concentrate near a specific region of the NE, often close to the centrosome, resulting in a chromosomal configuration resembling a bouquet of flowers with the telomeres forming the gathered stems. This distinctive meiotic-specific arrangement is thus called the telomere bouquet (Scherthan, 2001). The formation of telomere clusters at the NE, including the telomere bouquet, has been observed in Opisthokonts (fungi and animals) and in plants (Zickler and Kleckner, 2016), suggesting that the origin of telomere bouquet formation is likely contemporaneous with the emergence of the meiotic DNA recombination program in the early evolution of eukaryotes.

For many years, telomere bouquet formation was believed only to facilitate the pairing and subsequent recombination of homologous chromosomes. It was assumed that chromosomes passively followed nuclear movements, with the telomere bouquet acting merely as a spreader of motion. However, loss of the bouquet results in severe defects in meiotic progression that cannot be fully explained by its canonical role (Tomita and Cooper, 2007; Klutstein et al., 2015; Katsumata et al., 2016; Moiseeva et al., 2017). The complete function of the telomere bouquet has remained a mystery, due primarily to the challenge of manipulating and visualizing its transient nature in most eukaryotes (Scherthan, 2001; Fernandez-Alvarez and Cooper, 2017). Advances in quantitative cell biology, coupled with the availability of predictive models and new unsupervised tools based on deep learning for data analysis, now offer opportunities to explore meiotic chromosomal dynamics at high spatial and temporal resolutions. Using these techniques, previously undetectable patterns in telomeric movements have been identified and modelled, providing insights into their biological relevance. From the huge volume of information being generated through these approaches, it is becoming evident that the formation of the telomere clusters in meiosis and the nuclear movements are not random or stochastic. Hence, these recent advances offer exciting opportunities to better understand the molecular basis of the telomeric control of gametogenesis.

2 Assembly and disassembly of the telomere bouquet: key to ensuring faithful gametogenesis

The assembly of the telomere bouquet during meiosis coincides with the initiation of the nuclear movements (Yoshida et al., 2013). However, the nuclear movements seem to end before bouquet disassembly (Ruan et al., 2015; Moiseeva et al., 2017). Two components are required for the formation and dissolution of telomere–NE associations: specific telomere bouquet proteins that strengthen the interaction with the NE and promote telomere clustering; and NE proteins that facilitate the interaction with the telomeres, the most common of which is the linker of nucleoskeleton and cytoskeleton (LINC) complex (Hiraoka and Dernburg, 2009; Sosa et al., 2012; Burke, 2018).

The proteins responsible for the meiotic telomere–NE associations are mostly meiotic-specific and have been identified in various organisms: TERB1, TERB2, and MAJIN in mice (da Cruz et al., 2020; Shibuya et al., 2015; Shibuya et al., 2014; Daniel et al., 2014); HIM-8, ZIM-1, ZIM-2, ZIM-3, and MLJ-1 in *Caenorhabditis elegans* (Phillips et al., 2005; Phillips and Dernburg, 2006; Phillips et al., 2009; Kim et al., 2023); Ndj1 and Csm4 in *Saccharomyces cerevisiae* (Conrad et al., 1997; Trelles-Sticken et al., 2000; Conrad et al., 2007; Conrad et al., 2008; Kosaka et al., 2008; Wanat et al., 2008); and Bqt1 and Bqt2 in *Schizosaccharomyces pombe* (Chikashige et al., 2006). However, the sequences of these proteins are not conserved between vertebrates and other metazoans, or even among fungal species. This suggests not only that the proteins responsible for telomere-NE associations have undergone significant turnover during evolution but also that different protein sequences can facilitate the interaction between telomeres and the NE and support bouquet formation. The variability in these protein sequences poses a challenge to the identification of these components in other model organisms that exhibit bouquet formation, such as *Arabidopsis thaliana*.

Telomere bouquet proteins are typically recruited at the telomeres thanks to their direct interaction with shelterin complex (formed by telomere-specific proteins associate with arrays of DNA repeats that protects chromosome ends), which form a protein bridge that connects the telomeres to the LINC complex (de Lange, 2005; Conrad et al., 2007; Hiraoka and Dernburg, 2009; Starr and Fridolfsson, 2010; Rao et al., 2011; Rubin et al., 2020). The LINC complex, which is highly conserved in evolution, plays a crucial role in mediating nuclear movements. The complex consists of a Sad1/UNC-84 (SUN)-domain protein and a Klarsicht, ANC-1, Syne Homology (KASH)-domain protein, both of which interact in the space between the inner and outer nuclear membranes (Hiraoka and Dernburg, 2009). Several studies have demonstrated physical interactions between telomere bouquet proteins (e.g., TERB1/2, Ndj1, and Bqt1) and SUN-domain proteins (e.g., SUN-1/2 in mice, Mps3 in *S. cerevisiae* and Sad1 in *S. pombe*) (Chikashige et al., 2006; Conrad et al., 2007; Conrad et al., 2008; Shibuya et al., 2014). By contrast, the KASH-domain proteins, which are not as highly conserved during evolution as the SUN-domain proteins, interact with cytoskeleton motors in the cytoplasm. Together, these interactions form an intricate network that underpins the orchestration of nuclear movements during meiosis.

Studies in yeast and nematodes have highlighted a strong association between defects in telomere bouquet disassembly and the phosphorylation status of the SUN-domain protein. In budding yeast, the phosphorylation state of Mps3 plays a crucial role in the duration of telomere–NE associations; meiosis-specific phosphorylation introduces negative charges in the luminal region of Mps3, which regulate its localization on the NE for meiotic chromosome motion (Prasada Rao et al., 2021). Phosphorylation of the SUN-domain protein in *C. elegans,* SUN-1, is regulated by the widely conserved kinases CDK-1, PLK-2 and CHK-2 (Penkner et al., 2009; Sato et al., 2009; Labella et al., 2011; Woglar et al., 2013; Prasada Rao et al., 2021). In addition, posttranslational modifications of foundational telomere proteins, such as Rap1, may affect their interaction with telomere bouquet proteins; in fission yeast, phosphorylation of Rap1, together with its intrinsic negative charge, control the assembly and disassembly of the bouquet, these features are important for forming interactions with its binding partners Bqt1 and Bqt2 (Amelina et al., 2015).

3 Cytoskeleton dynamics in telomere bouquet assembly and disassembly

Actin and dynein are highly conserved motor proteins that have a crucial role in generating forces for nuclear movements during the telomere bouquet stage across various species (Yamamoto et al., 1999; Miki et al., 2002; Koszul et al., 2008; Wynne et al., 2012; Link and Jantsch, 2019). However, the duration, trajectory, and morphology of these nuclear movements vary significantly between species (Rubin et al., 2020; Kim et al., 2022; Sole et al., 2023). For instance, in *S. cerevisiae*, the nuclear membrane undergoes deformations presumably related to rapid telomere-led

movements, in which telomeres move in clusters (Hayashi et al., 1998; Scherthan et al., 2007; Conrad et al., 2008). By contrast, in the fission yeast *S. pombe*, the entire nucleus oscillates between the cell poles while the telomeres remain grouped beneath the spindle pole body (SPB), the centrosome equivalent in yeast. This type of movements is commonly referred to as horsetail nuclear movements (Chikashige et al., 1994; Chikashige et al., 2006). Similarly, metazoans demonstrate diverse chromosome morphologies during the telomere bouquet stage: in *C. elegans*, for example, chromatin adopts a crescent shape while being pushed by the nucleolus to one side of the nucleus (Rog and Dernburg, 2013; Rog and Dernburg, 2015; Link and Jantsch, 2019). Conversely, in *Drosophila melanogaster* and mice, characteristic movements involve microtubule-driven chromosomal rotations (Cooley and Theurkauf, 1994; Shibuya et al., 2014). The molecular reasons for the variety of movement types observed in different organisms remain poorly understood. The number of chromosomes could potentially play a role in determining the type of movement. For instance, species with low number of chromosomes, such as fission yeast, may require a more vigorous type of movement. Other factors that could potentially influence movement patterns include the presence of the synaptonemal complex (SC), a structure transiently formed during meiosis to facilitate recombination between homologous chromosomes (Page and Hawley, 2004). Organisms lacking the SC, like *S. pombe* or the ciliate *Tetrahymena thermophila* (Loidl, 2021), may need to employ different dynamics for the movement of their chromosomes compared to organisms with the SC.

The elimination of either actin or dynein, depending on the species, results in the cessation of nuclear movements, which subsequently impedes telomere motions (Miki et al., 2002; Koszul et al., 2008; Wynne et al., 2012). This in turn blocks DNA pairing and recombination, leading to defective chromosome segregation and reduced gamete viability. A meiosis-specific microtubule organizing centre has been identified in certain species, such as *S. pombe* (Saito et al., 2005; Tanaka et al., 2005; Funaya et al., 2012). This microtubule organizing centre, Hrs1, reinforces the dynamic movement of microtubules that is required to pull the SPB back and forth. Loss of Hrs1 results in a slowdown of nuclear movements and, eventually, disassembly of the telomere bouquet.

The formation of the telomere bouquet involves the action of cytoskeleton forces, which cluster the telomeres at specific regions of the NE. In fission yeast, telomere clustering relies on various microtubule motors, kinesins, microtubules and a meiosis-specific microtubule-organizing center named telocentrosome (Yoshida et al., 2013). In particular, the telocentrosome plays a pivotal role in the formation of the telomere bouquet by facilitating the recruitment of the gamma tubulin complex and the movement of telomeres along the NE, from their interphase position, to the SPB (Yoshida et al., 2013). Interestingly, similar structures involving cilia are conserved in zebrafish and mice. These cilia promote the formation of the telomere bouquet by generating microtubule arrays that accumulate at specific regions of the NE (Mytlis et al., 2022).

By contrast, the disassembly of the bouquet appears to be independent of the nuclear movements (Ruan et al., 2015; Moiseeva et al., 2017), suggesting that it occurs after these movements have ended. It is likely that the disassembly of the bouquet is dependent on the completion of other DNA events during meiosis.

4 The multifaceted nature of the telomere bouquet

Several studies–particularly in fission yeast, where live imaging allows for a more detailed analysis–have revealed unexpected functions of the telomere bouquet. For instance, the Cooper and Yamamoto labs have shown that the absence of bouquet formation compromises the formation of spindle microtubules, which are crucial for chromosome segregation (Tomita and Cooper, 2007; Katsumata et al., 2016). Elimination of telomere bouquet proteins such as Bqt1 or Bqt2 leads to defects in spindle formation and thus to aberrant chromosome segregation. These defects are associated with problems in the localized NE disassembly, a process that necessitates the proximity of telomeres to create a hole in the NE for the insertion of the duplicated SPBs. This stage of NE disassembly beneath the SPB is analogous to the NE breakdown stage observed in mammals (Fernández-Álvarez et al., 2016) (Figure 1). The proximity of telomeres to the NE likely triggers a modification in the SUN-domain protein, Sad1, in *S. pombe*, leading to the reorganization of Sad1 to form a ring, which in turn promotes local NE disassembly and SPB insertion (Fernández-Álvarez et al., 2016; Bestul et al., 2017).

The formation of the telomere bouquet controls another crucial function in the meiotic program: centromere reassembly. During meiosis, centromeres must be disassembled in preparation for specialized chromosome segregation in the first round of nuclear division. During bouquet formation, a microenvironment is created around the SPB that is characterized by the proximity of centromeres and telomeres, resulting in the transfer of heterochromatin factors from the telomeres to the centromeres (Klutstein et al., 2015; Hou et al., 2021).

Moreover, the Hiraoka and Tomita labs discovered that defects in DNA replication and repair prolong the duration of nuclear movements and the telomere bouquet stage in fission yeast (Ruan et al., 2015; Moiseeva et al., 2017). This finding indicates that bouquet assembly and disassembly are coordinated with crucial chromosomal events. Furthermore, we have found that DNA repair may affect not only the duration of the bouquet but also the behaviour of telomeric movements during meiosis. Specifically, persistent DNA damage alters the trajectory of telomeres during the horsetail movement, likely facilitating DNA repair between homologous chromosomes to ensure accurate meiotic progression (Leon-Perinan and Fernandez-Alvarez, 2020; Leon-Perinan and Fernandez-Alvarez, 2021).

5 Alternative conformations of the telomere bouquet and their evolutionary significance

In addition to being studied extensively in Opisthokonts, telomere bouquet formation has been identified in species of the Chloroplastida and Alveolata groups, indicating its likely evolution from the origin of eukaryotes along with the meiotic program

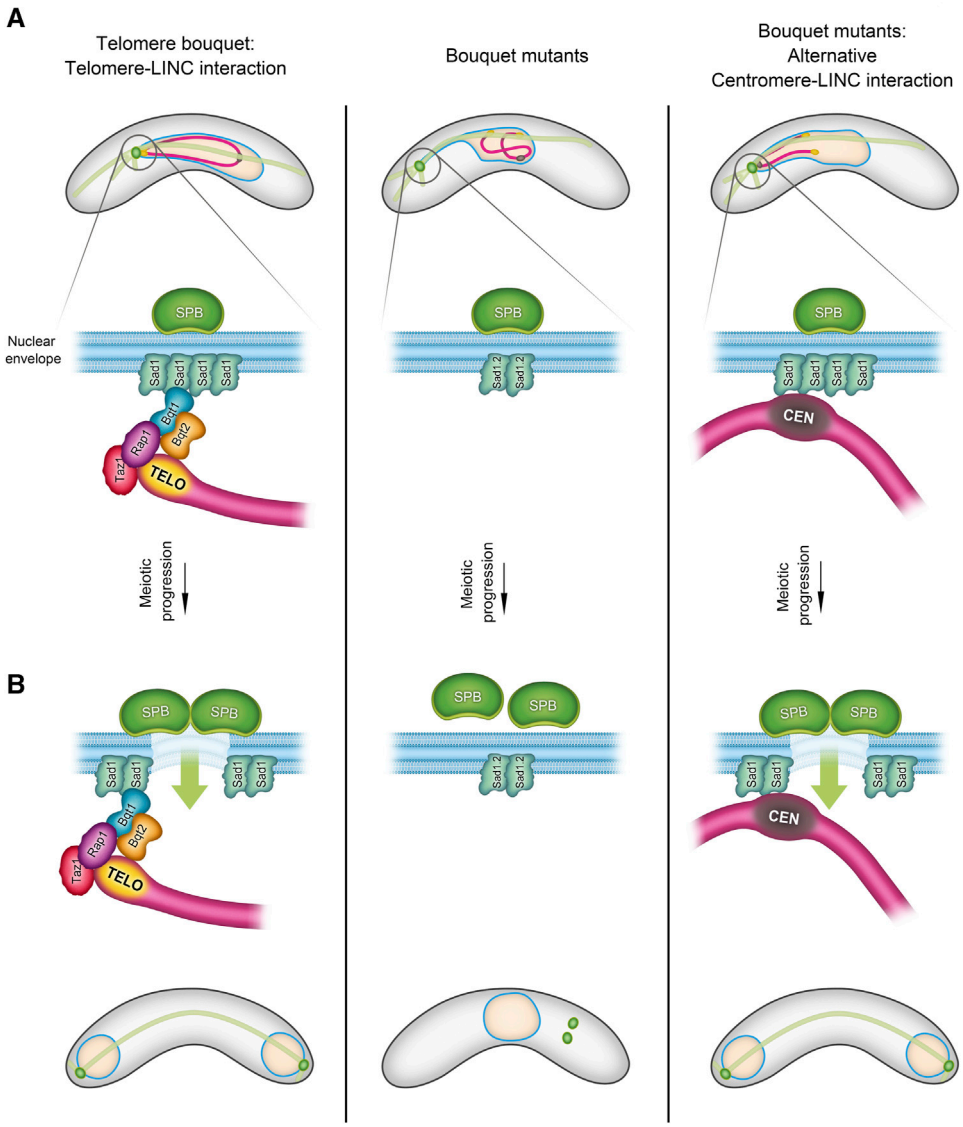

FIGURE 1
Telomere-Centromere interchange during the bouquet formation stage in *S. pombe*. During the bouquet stage, there is an exchangeability between telomeres and centromeres in their role of facilitating the SPB insertion into the nuclear envelope (NE). The schematic in **(A)** illustrates three scenarios of chromosome-LINC interactions in fission yeast: 1) in normal telomere bouquet formation (left), telomere-LINC interaction enables chromosomes to follow the SPB movements through the interaction of the telomere bouquet protein Bqt1 with the SUN-domain protein, Sad1. 2) In bouquet mutants (right), where *bqt1* and/or *bqt2* are deleted, interaction between telomeres and Sad1 is disrupted. However, centromeres are capable of contacting Sad1, forming an alternative "centromere" bouquet conformation. 3) The middle panel shows a combined scenario, *bouquet*Δ in conjunction with the Sad1.2 allele, resulting in the inhibition of both telomere-LINC and centromere-LINC interactions. In **(B)**, the left panel depicts the triggering of partial NE disassembly by telomere-LINC interaction, facilitating the SPB insertion into the NE and spindle formation. This signalling can also be controlled by the centromeres (right). Lack of interaction between telomeres/centromeres and the LINC complex disrupts the SPB insertion process, thereby compromising spindle formation (middle panel) (more information in (Fennell et al., 2015; Fernández-Álvarez et al., 2016).

(Scherthan, 2001; Zickler and Kleckner, 2016; Hurel et al., 2018). Although bouquet formation is conserved in evolution, it displays some conformational plasticity, which has led to variations in the number and distribution of telomere clusters along the NE that in turn result in differences in chromosome polarization and the trajectories of telomere movements between species (Rubin et al., 2020; Sole et al., 2023). Notably, two common variations involve the diversity of the meiosis-specific telomere protein sequences that support telomere-NE associations (Rubin et al., 2020; Kim et al., 2022) and the unexpected interchangeability between telomeres and centromeres. In certain scenarios, a so-called centromere bouquet can replace the telomere bouquet (Stewart and Dawson, 2008; Loidl et al., 2012; Fennell et al., 2015) (Figure 1).

As described above, loss of the telomere bouquet in fission yeast causes severe defects in local NE disassembly and, consequently, in the SPB insertion into the NE and spindle formation (Tomita and Cooper, 2007; Pineda-Santaella and Fernández-Álvarez, 2019; Pineda-Santaella et al., 2021). However, approximately 50% of bouquet-mutant cells can form normal spindles by using centromeres in prophase to create a bouquet-like structure

(Fennell et al., 2015) (Figure 1). Given that centromeres and telomeres represent distinct chromosomal regions, the common features that support this capacity for substitution have yet to be uncovered. The molecular bases that underpin this interchangeability are intriguing, given that telomeres and centromeres do not commonly share functions.

In the protist *T. thermophila*, the nucleus undergoes substantial stretching in meiotic prophase, with chromosomes adopting a bouquet-like arrangement in which telomeres and centromeres attach to opposite poles of the nucleus. Centromere clustering was found to be more important than telomere clustering for homologous pairing, suggesting that centromere clustering may have been the primordial mechanism for chromosome pairing (Tian et al., 2020). In *D. melanogaster*, it is the centromeres rather than the telomeres that support the formation of the bouquet (Rubin et al., 2020). It remains an enigma as to why telomeres perform this function in certain organisms while centromeres assume this role in others. This intriguing and unconventional nature of these occurrences raises the question of whether it is of significance whether it is telomeres or centromeres carrying out these functions.

Another question that we are currently exploring is how to cluster telomeres at the NE without the highly conserved LINC complex. Whereas the sequence of telomere bouquet proteins may be highly divergent between species, the presence of the LINC complex–which has a crucial role in transmitting movement to the chromosomes–has remained highly conserved since the origin of eukaryotes. We have found that in some Basidiomycota fungi, such as the pathogen *Ustilago maydis*, all the machinery of the meiotic recombination program and the telomeric proteins (e.g., Taz1 and Rap1) are conserved (Kojic et al., 2013), but the LINC complex is missing. This raises questions about which elements are essential for bouquet formation and which have undergone more turnover throughout evolution. Finding the answers to these questions will help us to determine whether meiotic chromosome movements and the formation of the telomere bouquet have driven the evolution of the meiotic program.

6 New imaging techniques provide insights into telomere motion

Both the canonical and non-canonical functions of the telomere bouquet are closely related to the chromosomal conformations during this stage. The canonical function involves transmitting forces generated in the cytoplasm through the movement of the telomere clusters along the NE (Scherthan, 2001; Zickler and Kleckner, 2016; Mytlis et al., 2023). By contrast, the non-canonical functions of the bouquet as a regulator of meiotic spindle formation or centromere assembly require the telomeres to be in close proximity to the NE. This is so that the localized NE disassembly can be triggered, which is necessary for proper spindle formation (Tomita and Cooper, 2007; Fernández-Álvarez et al., 2016), or to create the microenvironment that supports centromere reassembly during meiotic prophase (Klutstein et al., 2015; Hou et al., 2021). We have observed that telomere trajectories along the NE during bouquet stage in fission yeast are not stochastic but instead follow movement patterns that are imperceptible by direct human observation but are computationally identifiable and mathematically predictable (Leon-Perinan and Fernandez-Alvarez, 2021). Hence, telomere movements along the NE change trajectory and velocity in response to specific chromosomal events, such as DNA repair. Tracking this behaviour in detail is key to understanding the functions of telomere clustering and to uncovering new connections to meiosis.

Many studies have investigated recognizable chromosome movement patterns using tracking schemes to monitor chromosome behaviour in organisms such as *S. cerevisiae* (Scherthan et al., 2007; Conrad et al., 2008; Gonzalez-Arranz et al., 2020), *C. elegans* (Baudrimont et al., 2010; Wynne et al., 2012; Labrador et al., 2013; Woglar and Jantsch, 2014; Rog and Dernburg, 2015) and *S. pombe* (Ding et al., 2004; Chacon et al., 2016; Moiseeva et al., 2017). Time-lapse fluorescence microscopy is commonly used to follow the movements of particles, including proteins like dynein, as well as chromosomal loci (Mine-Hattab and Rothstein, 2012; Ananthanarayanan et al., 2013). Methods such as mean square displacement, velocity measurements, and automatic and cross-correlation analyses have been used to evaluate long-range spatiotemporal patterns, generating a high volume of information about chromosome dynamics at specific loci (Mine-Hattab and Chiolo, 2020). For example, these approaches have been used in budding yeast to identify and characterize rotational meiotic movements that result from both nuclear rotation and individual chromosome movements (Lee et al., 2015). Studies in human cells have shown that chromosome end motion is both highly heterogeneous and inversely related to telomere length (Wang et al., 2008) and that telomeres display intermittent accumulations in specific local niches that depend on their exposure to different types of stress (Benelli and Weiss, 2022). One of the most relevant findings in recent years is the observation that upon exposure to DNA-damaging agents, telomeres are more likely to move away from their sites on the NE. These discoveries demonstrate that a combination of factors, including the release of chromatin-NE tethering, internal chromatin connections, and microtubule dynamics, work together to mobilize the genome in response to DNA damage (Therizols et al., 2006; Mine-Hattab and Rothstein, 2012; Lawrimore et al., 2017; Mine-Hattab and Chiolo, 2020).

These findings, together with the optimization of model organisms for visualizing chromosome dynamics, such as zebrafish (Blokhina et al., 2019; Imai et al., 2021; Mytlis et al., 2022; Mytlis et al., 2023) and *Arabidopsis thaliana* (Hurel et al., 2018), are paving the way for exciting new research opportunities in this field.

However, these types of techniques have limitations arising from their time-ensemble nature (Mine-Hattab and Chiolo, 2020). For example, different modes of motion can produce the same mean square displacement curves or velocity distributions, since trajectories that are effectively different can nevertheless produce identical distribution summaries. This means that specific patterns of chromosome movements, particularly those not yet linked to a known biological process, cannot be easily identified. Hence, complementary strategies to explore chromosome dynamics are being developed. For example, novel imaging techniques with a low signal-to-noise ratio offer exciting prospects for further investigations into homologous pairing (Nozaki et al., 2021).

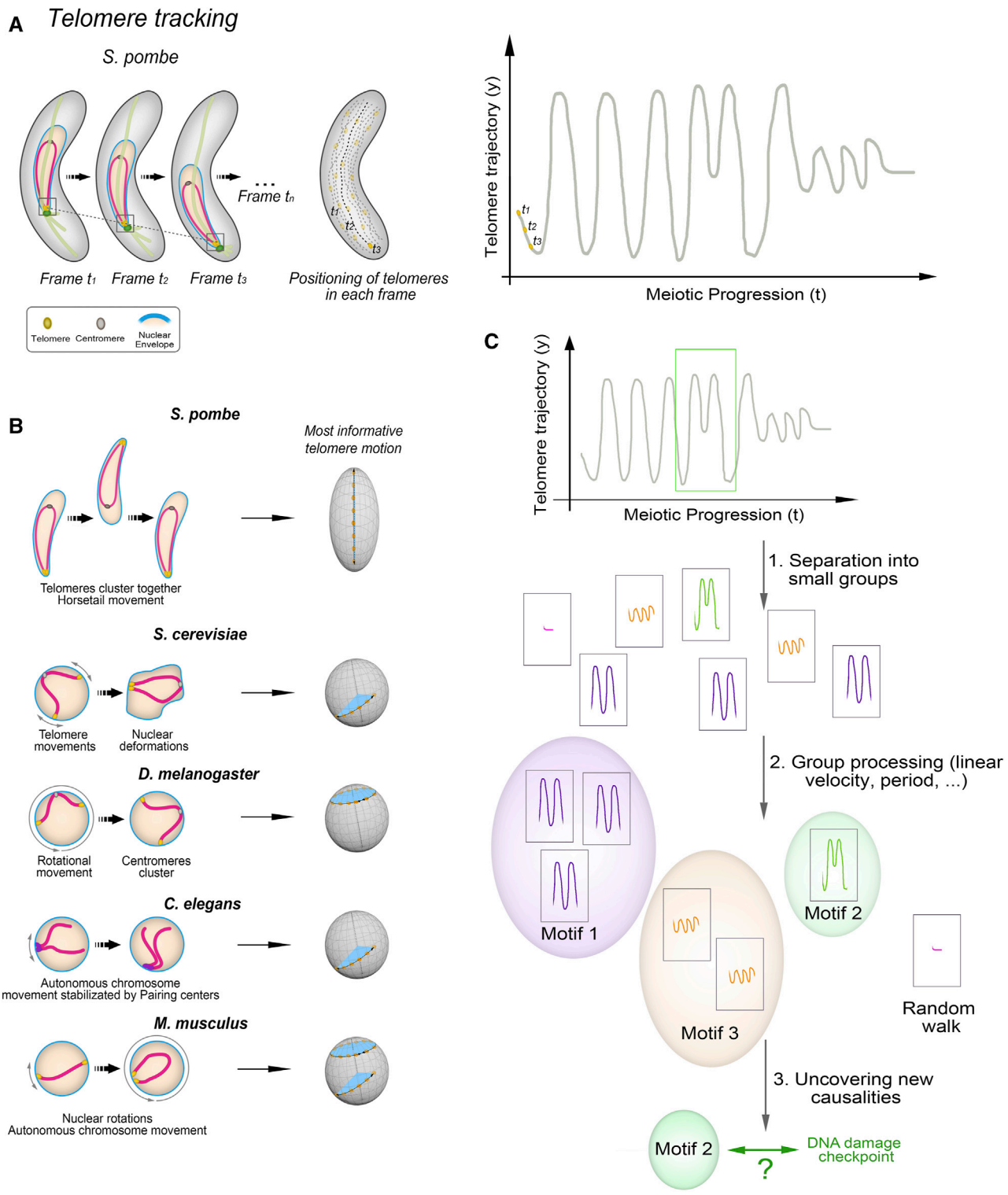

FIGURE 2
Unveiling Telomere Movement Patterns in Fission Yeast and Prospects for Cross-Species Applications **(A)** Illustration depicting the process employed to analyze telomere positioning in fission yeast. Quantification and tracking of telomere positioning, representation of telomere motion in the *y*-axis, the most informative in case of *S. pombe*. **(B)** Zygotene-stage telomere movements exhibit distinct characteristics across species. Linear movements covering short distances along the nuclear envelope (NE) are observed in *S. cerevisiae* and *C. elegans*, while *D. melanogaster* displays rotational movements. *M. musculus* displays both types. **(C)** Outline of the process used to identify telomere movement patterns. Key steps involve determining the primary axis of movement—such as the *y*-axis for fission yeast's oscillatory motion—tracking trajectories via *in vivo* telomere labelling, segmenting time intervals, and clustering based on various variables like linear/angular velocity and period. Comparisons between wild-type and mutant strains unveil the presence or absence of 'motifs' and their distribution throughout prophase.

Correlative conventional and PALM (photoactivated localization microscopy) imaging enhances our capacity to analyse the mobility and time-averaged nanoscopic structural characteristics of locus-specific chromatin with single-molecule sensitivity (Mehra et al., 2022). Using point-spread-function engineering and deep-learning-based image analysis, we can now conduct live imaging of telomere diffusion (Naor et al., 2022).

7 Harnessing data mining and causality analysis for predictive modelling

A major limitation in developing a predictive model is the need for large sample sizes. Data mining and time-window approaches offer solutions to some of these limitations. For example, researchers are now automatically creating synthetic variations of chromosome movements during the telomere bouquet stage based on wild-type and mutant datasets. The creation of *in silico* versions of budding yeast strains and their analysis using experimental data and simulations have revealed important information about the active motion of telomeres and the biological implications of the bouquet (Penfold et al., 2012; Marshall and Fung, 2016; Marshall and Fung, 2019; Navarro et al., 2022). For example, this approach has revealed that active telomere forces can increase the selectivity of chromosome pairing (Marshall and Fung, 2019). Complementary approaches are using segment-discovery libraries, like segclust2d and segmenTier, and matrix profile calculations to extract information about chromosome movement from time-lapse experiments. At the same time, causality analysis algorithms, such as Peter-Clark algorithm, variable-lag transfer entropy and variable-lag Granger causality, can be used to identify whether changes in one variable (e.g., chromosome morphology) affect another variable (e.g., chromosome movement) (Leon-Perinan and Fernandez-Alvarez, 2021). As these algorithms help to establish causal relationships, they provide valuable information for understanding the mechanisms and regulation of chromosome dynamics during meiotic prophase in various organisms.

8 Summary

The telomere bouquet is conserved in eukaryotes and has both canonical and non-canonical functions. Its canonical functions involve transmitting the forces generated in the cytoplasm to promote the chromosome movements needed to facilitate homologous pairing, while its non-canonical functions include regulating meiotic spindle formation, meiotic centromere assembly and DNA events such as replication and repair. New techniques–including time-lapse fluorescence microscopy, tracking schemes, and data mining–are now enabling researchers to circumvent the limitations of previous experimental approaches. These techniques have been used to identify patterns of chromosome movement, such as rotational meiotic movements, and modifications to the trajectory of chromosomes in response to DNA events (Figure 2). Combining these techniques with causality analysis algorithms and other advances in quantitative cell biology, such as low-signal-to-noise imaging and deep-learning-based analysis, offers opportunities to explore chromosomal motion at even higher spatial and temporal resolutions. These techniques offer new insights into homologous pairing and nanoscopic structural features of chromatin.

Data availability statement

The raw data supporting the conclusion of this article will be made available by the authors, without undue reservation.

Author contributions

AF-Á: Conceptualization, Funding acquisition, Investigation, Writing–original draft, Writing–review and editing.

Funding

The author(s) declare financial support was received for the research, authorship, and/or publication of this article. This work was supported by PID 2021-127232NB-I00 funded by the MCIN/AEI/10.13039/501100011033 and by the "FEDER, Una manera de hacer Europa", awarded to AF-Á. The Institute of Functional Biology and Genomics (IBFG) has received funding through the program "Escalera de Excelencia" of the Regional Government of Castile and Leon (ref.: CLU-2017-03) and co-financed by the P.O. FEDER of Castilla and León 14–20, and the Internationalization Project "CL-EI-2021-08-IBFG Unit of Excellence" of the Spanish National Research Council (CSIC), funded by the Regional Government of Castile and Leon and co-financed by the European Regional Development Fund (ERDF Europe drives our growth).

Acknowledgments

We thank Julie Cooper for critical comments on the manuscript, and to Victor Carranco for his contribution to figure design.

Conflict of interest

The author declares that the research was conducted in the absence of any commercial or financial relationships that could be construed as a potential conflict of interest.

Publisher's note

References

Amelina, H., Subramaniam, S., Moiseeva, V., Armstrong, C. A., Pearson, S. R., and Tomita, K. (2015). Telomere protein Rap1 is a charge resistant scaffolding protein in chromosomal bouquet formation. *BMC Biol.* 13, 37. doi:10.1186/s12915-015-0149-x

Ananthanarayanan, V., Schattat, M., Vogel, S. K., Krull, A., Pavin, N., and Tolic-Norrelykke, I. M. (2013). Dynein motion switches from diffusive to directed upon cortical anchoring. *Cell* 153 (7), 1526–1536. doi:10.1016/j.cell.2013.05.020

Baudrimont, A., Penkner, A., Woglar, A., Machacek, T., Wegrostek, C., Gloggnitzer, J., et al. (2010). Leptotene/zygotene chromosome movement via the SUN/KASH protein bridge in *Caenorhabditis elegans*. *PLoS Genet.* 6 (11), e1001219. doi:10.1371/journal.pgen.1001219

Benelli, R., and Weiss, M. (2022). Probing local chromatin dynamics by tracking telomeres. *Biophys. J.* 121 (14), 2684–2692. doi:10.1016/j.bpj.2022.06.020

Bestul, A. J., Yu, Z., Unruh, J. R., and Jaspersen, S. L. (2017). Molecular model of fission yeast centrosome assembly determined by superresolution imaging. *J. Cell Biol.* 216 (8), 2409–2424. doi:10.1083/jcb.201701041

Blokhina, Y. P., Nguyen, A. D., Draper, B. W., and Burgess, S. M. (2019). The telomere bouquet is a hub where meiotic double-strand breaks, synapsis, and stable homolog juxtaposition are coordinated in the zebrafish, *Danio rerio*. *PLoS Genet.* 15 (1), e1007730. doi:10.1371/journal.pgen.1007730

Burke, B. (2018). LINC complexes as regulators of meiosis. *Curr. Opin. Cell Biol.* 52, 22–29. doi:10.1016/j.ceb.2018.01.005

Chacon, M. R., Delivani, P., and Tolic, I. M. (2016). Meiotic nuclear oscillations are necessary to avoid excessive chromosome associations. *Cell Rep.* 17 (6), 1632–1645. doi:10.1016/j.celrep.2016.10.014

Chikashige, Y., Ding, D. Q., Funabiki, H., Haraguchi, T., Mashiko, S., Yanagida, M., et al. (1994). Telomere-led premeiotic chromosome movement in fission yeast. *Science* 264 (5156), 270–273. doi:10.1126/science.8146661

Chikashige, Y., Tsutsumi, C., Yamane, M., Okamasa, K., Haraguchi, T., and Hiraoka, Y. (2006). Meiotic proteins Bqt1 and Bqt2 tether telomeres to form the bouquet arrangement of chromosomes. *Cell* 125 (1), 59–69. doi:10.1016/j.cell.2006.01.048

Christophorou, N., Rubin, T., Bonnet, I., Piolot, T., Arnaud, M., and Huynh, J. R. (2015). Microtubule-driven nuclear rotations promote meiotic chromosome dynamics. *Nat. Cell Biol.* 17 (11), 1388–1400. doi:10.1038/ncb3249

Conrad, M. N., Dominguez, A. M., and Dresser, M. E. (1997). Ndj1p, a meiotic telomere protein required for normal chromosome synapsis and segregation in yeast. *Science* 276 (5316), 1252–1255. doi:10.1126/science.276.5316.1252

Conrad, M. N., Lee, C. Y., Wilkerson, J. L., and Dresser, M. E. (2007). MPS3 mediates meiotic bouquet formation in *Saccharomyces cerevisiae*. *Proc. Natl. Acad. Sci. U. S. A.* 104 (21), 8863–8868. doi:10.1073/pnas.0606165104

Conrad, M. N., Lee, C. Y., Chao, G., Shinohara, M., Kosaka, H., Shinohara, A., et al. (2008). Rapid telomere movement in meiotic prophase is promoted by NDJ1, MPS3, and CSM4 and is modulated by recombination. *Cell* 133 (7), 1175–1187. doi:10.1016/j.cell.2008.04.047

Cooley, L., and Theurkauf, W. E. (1994). Cytoskeletal functions during Drosophila oogenesis. *Science* 266 (5185), 590–596. doi:10.1126/science.7939713

da Cruz, I., Brochier-Armanet, C., and Benavente, R. (2020). The TERB1-TERB2-MAJIN complex of mouse meiotic telomeres dates back to the common ancestor of metazoans. *BMC Evol. Biol.* 20 (1), 55. doi:10.1186/s12862-020-01612-9

Daniel, K., Trankner, D., Wojtasz, L., Shibuya, H., Watanabe, Y., Alsheimer, M., et al. (2014). Mouse CCDC79 (TERB1) is a meiosis-specific telomere associated protein. *BMC Cell Biol.* 15, 17. doi:10.1186/1471-2121-15-17

de Lange, T. (2005). Shelterin: the protein complex that shapes and safeguards human telomeres. *Genes Dev.* 19 (18), 2100–2110. doi:10.1101/gad.1346005

Ding, D. Q., Yamamoto, A., Haraguchi, T., and Hiraoka, Y. (2004). Dynamics of homologous chromosome pairing during meiotic prophase in fission yeast. *Dev. Cell* 6 (3), 329–341. doi:10.1016/s1534-5807(04)00059-0

Fennell, A., Fernández-álvarez, A., Tomita, K., and Cooper, J. P. (2015). Telomeres and centromeres have interchangeable roles in promoting meiotic spindle formation. *J. Cell Biol.* 208 (4), 415–428. doi:10.1083/jcb.201409058

Fernandez-Alvarez, A., and Cooper, J. P. (2017). Chromosomes orchestrate their own liberation: nuclear envelope disassembly. *Trends Cell Biol.* 27 (4), 255–265. doi:10.1016/j.tcb.2016.11.005

Fernández-Álvarez, A., Bez, C., O'Toole, E. T., Morphew, M., and Cooper, J. P. (2016). Mitotic nuclear envelope breakdown and spindle nucleation are controlled by interphase contacts between centromeres and the nuclear envelope. *Dev. Cell* 39 (5), 544–559. doi:10.1016/j.devcel.2016.10.021

Funaya, C., Samarasinghe, S., Pruggnaller, S., Ohta, M., Connolly, Y., Muller, J., et al. (2012). Transient structure associated with the spindle pole body directs meiotic microtubule reorganization in *S. pombe*. *Curr. Biol.* 22 (7), 562–574. doi:10.1016/j.cub.2012.02.042

Gonzalez-Arranz, S., Gardner, J. M., Yu, Z., Patel, N. J., Heldrich, J., Santos, B., et al. (2020). SWR1-Independent association of H2A.Z to the LINC complex promotes meiotic chromosome motion. *Front. Cell Dev. Biol.* 8, 594092. doi:10.3389/fcell.2020.594092

Hayashi, A., Ogawa, H., Kohno, K., Gasser, S. M., and Hiraoka, Y. (1998). Meiotic behaviours of chromosomes and microtubules in budding yeast: relocalization of centromeres and telomeres during meiotic prophase. *Genes cells.* 3 (9), 587–601. doi:10.1046/j.1365-2443.1998.00215.x

Hiraoka, Y., and Dernburg, A. F. (2009). The SUN rises on meiotic chromosome dynamics. *Dev. Cell* 17 (5), 598–605. doi:10.1016/j.devcel.2009.10.014

Hou, H., Kyriacou, E., Thadani, R., Klutstein, M., Chapman, J. H., and Cooper, J. P. (2021). Centromeres are dismantled by foundational meiotic proteins Spo11 and Rec8. *Nature* 591 (7851), 671–676. doi:10.1038/s41586-021-03279-8

Hunter, N. (2015). Meiotic recombination: the essence of heredity. *Cold Spring Harb. Perspect. Biol.* 7 (12), a016618. doi:10.1101/cshperspect.a016618

Hurel, A., Phillips, D., Vrielynck, N., Mezard, C., Grelon, M., and Christophorou, N. (2018). A cytological approach to studying meiotic recombination and chromosome dynamics in *Arabidopsis thaliana* male meiocytes in three dimensions. *Plant J.* 95 (2), 385–396. doi:10.1111/tpj.13942

Imai, Y., Olaya, I., Sakai, N., and Burgess, S. M. (2021). Meiotic chromosome dynamics in zebrafish. *Front. Cell Dev. Biol.* 9, 757445. doi:10.3389/fcell.2021.757445

Katsumata, K., Hirayasu, A., Miyoshi, J., Nishi, E., Ichikawa, K., Tateho, K., et al. (2016). A Taz1-and microtubule-dependent regulatory relationship between telomere and centromere positions in bouquet formation secures proper meiotic divisions. *PLoS Genet.* 12 (9), e1006304. doi:10.1371/journal.pgen.1006304

Kim, H. J., Liu, C., and Dernburg, A. F. (2022). How and why chromosomes interact with the cytoskeleton during meiosis. *Genes (Basel).* 13 (5), 901. doi:10.3390/genes13050901

Kim, H. J., Liu, C., Zhang, L., and Dernburg, A. F. (2023). MJL-1 is a nuclear envelope protein required for homologous chromosome pairing and regulation of synapsis during meiosis in *C. elegans*. *Sci. Adv.* 9 (6), eadd1453. doi:10.1126/sciadv.add1453

Klutstein, M., and Cooper, J. P. (2014). The Chromosomal Courtship Dance-homolog pairing in early meiosis. *Curr. Opin. Cell Biol.* 26, 123–131. doi:10.1016/j.ceb.2013.12.004

Klutstein, M., Fennell, A., Fernandez-Alvarez, A., and Cooper, J. P. (2015). The telomere bouquet regulates meiotic centromere assembly. *Nat. Cell Biol.* 17 (4), 458–469. doi:10.1038/ncb3132

Kojic, M., Sutherland, J. H., Perez-Martin, J., and Holloman, W. K. (2013). Initiation of meiotic recombination in Ustilago maydis. *Genetics* 195 (4), 1231–1240. doi:10.1534/genetics.113.156752

Kosaka, H., Shinohara, M., and Shinohara, A. (2008). Csm4-dependent telomere movement on nuclear envelope promotes meiotic recombination. *PLoS Genet.* 4 (9), e1000196. doi:10.1371/journal.pgen.1000196

Koszul, R., Kim, K. P., Prentiss, M., Kleckner, N., and Kameoka, S. (2008). Meiotic chromosomes move by linkage to dynamic actin cables with transduction of force through the nuclear envelope. *Cell* 133 (7), 1188–1201. doi:10.1016/j.cell.2008.04.050

Labella, S., Woglar, A., Jantsch, V., and Zetka, M. (2011). Polo kinases establish links between meiotic chromosomes and cytoskeletal forces essential for homolog pairing. *Dev. Cell* 21 (5), 948–958. doi:10.1016/j.devcel.2011.07.011

Labrador, L., Barroso, C., Lightfoot, J., Muller-Reichert, T., Flibotte, S., Taylor, J., et al. (2013). Chromosome movements promoted by the mitochondrial protein SPD-3 are required for homology search during *Caenorhabditis elegans* meiosis. *PLoS Genet.* 9 (5), e1003497. doi:10.1371/journal.pgen.1003497

Lawrimore, J., Barry, T. M., Barry, R. M., York, A. C., Friedman, B., Cook, D. M., et al. (2017). Microtubule dynamics drive enhanced chromatin motion and mobilize telomeres in response to DNA damage. *Mol. Biol. Cell* 28 (12), 1701–1711. doi:10.1091/mbc.E16-12-0846

Lee, C. Y., Horn, H. F., Stewart, C. L., Burke, B., Bolcun-Filas, E., Schimenti, J. C., et al. (2015). Mechanism and regulation of rapid telomere prophase movements in mouse meiotic chromosomes. *Cell Rep.* 11 (4), 551–563. doi:10.1016/j.celrep.2015.03.045

Leon-Perinan, D., and Fernandez-Alvarez, A. (2021). ChroMo, an application for unsupervised analysis of chromosome movements in meiosis. *Cells* 10 (8), 2013. doi:10.3390/cells10082013

Leon-Perinan, D., and Fernandez-Alvarez, A. (2020). Identification of a meiosis-specific chromosome movement pattern induced by persistent DNA damage. *bioRxiv*. doi:10.1101/2020.07.23.218016

Link, J., and Jantsch, V. (2019). Meiotic chromosomes in motion: a perspective from *Mus musculus* and *Caenorhabditis elegans*. *Chromosoma* 128 (3), 317–330. doi:10.1007/s00412-019-00698-5

Loidl, J., Lukaszewicz, A., Howard-Till, R. A., and Koestler, T. (2012). The Tetrahymena meiotic chromosome bouquet is organized by centromeres and promotes interhomolog recombination. *J. Cell Sci.* 125 (Pt 23), 5873–5880. doi:10.1242/jcs.112664

Loidl, J. (2021). Tetrahymena meiosis: simple yet ingenious. *PLoS Genet.* 17 (7), e1009627. doi:10.1371/journal.pgen.1009627

Marshall, W. F., and Fung, J. C. (2016). Modeling meiotic chromosome pairing: nuclear envelope attachment, telomere-led active random motion, and anomalous diffusion. *Phys. Biol.* 13 (2), 026003. doi:10.1088/1478-3975/13/2/026003

Marshall, W. F., and Fung, J. C. (2019). Modeling meiotic chromosome pairing: a tug of war between telomere forces and a pairing-based Brownian ratchet leads to increased pairing fidelity. *Phys. Biol.* 16 (4), 046005. doi:10.1088/1478-3975/ab15a7

Mehra, D., Adhikari, S., Banerjee, C., and Puchner, E. M. (2022). Characterizing locus specific chromatin structure and dynamics with correlative conventional and super-resolution imaging in living cells. *Nucleic Acids Res.* 50 (13), e78. doi:10.1093/nar/gkac314

Miki, F., Okazaki, K., Shimanuki, M., Yamamoto, A., Hiraoka, Y., and Niwa, O. (2002). The 14-kDa dynein light chain-family protein Dlc1 is required for regular oscillatory nuclear movement and efficient recombination during meiotic prophase in fission yeast. *Mol. Biol. Cell* 13 (3), 930–946. doi:10.1091/mbc.01-11-0543

Mine-Hattab, J., and Chiolo, I. (2020). Complex chromatin motions for DNA repair. *Front. Genet.* 11, 800. doi:10.3389/fgene.2020.00800

Mine-Hattab, J., and Rothstein, R. (2012). Increased chromosome mobility facilitates homology search during recombination. *Nat. Cell Biol.* 14 (5), 510–517. doi:10.1038/ncb2472

Moiseeva, V., Amelina, H., Collopy, L. C., Armstrong, C. A., Pearson, S. R., and Tomita, K. (2017). The telomere bouquet facilitates meiotic prophase progression and exit in fission yeast. *Cell Discov.* 3, 17041. doi:10.1038/celldisc.2017.41

Mytlis, A., Kumar, V., Qiu, T., Deis, R., Hart, N., Levy, K., et al. (2022). Control of meiotic chromosomal bouquet and germ cell morphogenesis by the zygotene cilium. *Science* 376 (6599), eabh3104. doi:10.1126/science.abh3104

Mytlis, A., Levy, K., and Elkouby, Y. M. (2023). The many faces of the bouquet centrosome MTOC in meiosis and germ cell development. *Curr. Opin. Cell Biol.* 81, 102158. doi:10.1016/j.ceb.2023.102158

Naor, T., Nogin, Y., Nehme, E., Ferdman, B., Weiss, L. E., Alalouf, O., et al. (2022). Quantifying cell-cycle-dependent chromatin dynamics during interphase by live 3D tracking. *iScience* 25 (5), 104197. doi:10.1016/j.isci.2022.104197

Navarro, E. J., Marshall, W. F., and Fung, J. C. (2022). Modeling cell biological features of meiotic chromosome pairing to study interlock resolution. *PLoS Comput. Biol.* 18 (6), e1010252. doi:10.1371/journal.pcbi.1010252

Nozaki, T., Chang, F., Weiner, B., and Kleckner, N. (2021). High temporal resolution 3D live-cell imaging of budding yeast meiosis defines discontinuous actin/telomere-mediated chromosome motion, correlated nuclear envelope deformation and actin filament dynamics. *Front. Cell Dev. Biol.* 9, 687132. doi:10.3389/fcell.2021.687132

Page, S. L., and Hawley, R. S. (2004). The genetics and molecular biology of the synaptonemal complex. *Annu. Rev. Cell Dev. Biol.* 20, 525–558. doi:10.1146/annurev.cellbio.19.111301.155141

Penfold, C. A., Brown, P. E., Lawrence, N. D., and Goldman, A. S. (2012). Modeling meiotic chromosomes indicates a size dependent contribution of telomere clustering and chromosome rigidity to homologue juxtaposition. *PLoS Comput. Biol.* 8 (5), e1002496. doi:10.1371/journal.pcbi.1002496

Penkner, A. M., Fridkin, A., Gloggnitzer, J., Baudrimont, A., Machacek, T., Woglar, A., et al. (2009). Meiotic chromosome homology search involves modifications of the nuclear envelope protein Matefin/SUN-1. *Cell* 139 (5), 920–933. doi:10.1016/j.cell.2009.10.045

Petronczki, M., Siomos, M. F., and Nasmyth, K. (2003). Un menage a quatre: the molecular biology of chromosome segregation in meiosis. *Cell* 112 (4), 423–440. doi:10.1016/s0092-8674(03)00083-7

Phillips, C. M., and Dernburg, A. F. (2006). A family of zinc-finger proteins is required for chromosome-specific pairing and synapsis during meiosis in *C. elegans*. *Dev. Cell* 11 (6), 817–829. doi:10.1016/j.devcel.2006.09.020

Phillips, C. M., Wong, C., Bhalla, N., Carlton, P. M., Weiser, P., Meneely, P. M., et al. (2005). HIM-8 binds to the X chromosome pairing center and mediates chromosome-specific meiotic synapsis. *Cell* 123 (6), 1051–1063. doi:10.1016/j.cell.2005.09.035

Phillips, C. M., Meng, X., Zhang, L., Chretien, J. H., Urnov, F. D., and Dernburg, A. F. (2009). Identification of chromosome sequence motifs that mediate meiotic pairing and synapsis in *C. elegans*. *Nat. Cell Biol.* 11 (8), 934–942. doi:10.1038/ncb1904

Pineda-Santaella, A., and Fernández-Álvarez, A. (2019). Spindle assembly without spindle pole body insertion into the nuclear envelope in fission yeast meiosis. *Chromosoma* 128 (3), 267–277. doi:10.1007/s00412-019-00710-y

Pineda-Santaella, A., Fernandez-Castillo, N., Jimenez-Martin, A., Macias-Cabeza, M. D. C., Sanchez-Gomez, A., and Fernandez-Alvarez, A. (2021). Loss of kinesin-8 improves the robustness of the self-assembled spindle in *Schizosaccharomyces pombe*. *J. Cell Sci.* 134 (16), jcs253799. doi:10.1242/jcs.253799

Prasada Rao, H. B., Sato, T., Challa, K., Fujita, Y., Shinohara, M., and Shinohara, A. (2021). Phosphorylation of luminal region of the SUN-domain protein Mps3 promotes nuclear envelope localization during meiosis. *Elife* 10, e63119. doi:10.7554/eLife.63119

Rao, H. B., Shinohara, M., and Shinohara, A. (2011). Mps3 SUN domain is important for chromosome motion and juxtaposition of homologous chromosomes during meiosis. *Genes cells.* 16 (11), 1081–1096. doi:10.1111/j.1365-2443.2011.01554.x

Rog, O., and Dernburg, A. F. (2013). Chromosome pairing and synapsis during *Caenorhabditis elegans* meiosis. *Curr. Opin. Cell Biol.* 25 (3), 349–356. doi:10.1016/j.ceb.2013.03.003

Rog, O., and Dernburg, A. F. (2015). Direct visualization reveals kinetics of meiotic chromosome synapsis. *Cell Rep.* 10 (10), 1639–1645. doi:10.1016/j.celrep.2015.02.032

Ruan, K., Yamamoto, T. G., Asakawa, H., Chikashige, Y., Masukata, H., Haraguchi, T., et al. (2015). Meiotic nuclear movements in fission yeast are regulated by the transcription factor Mei4 downstream of a Cds1-dependent replication checkpoint pathway. *Genes cells.* 20 (3), 160–172. doi:10.1111/gtc.12207

Rubin, T., Macaisne, N., and Huynh, J. R. (2020). Mixing and matching chromosomes during female meiosis. *Cells* 9 (3), 696. doi:10.3390/cells9030696

Saito, T. T., Tougan, T., Okuzaki, D., Kasama, T., and Nojima, H. (2005). Mcp6, a meiosis-specific coiled-coil protein of *Schizosaccharomyces pombe*, localizes to the spindle pole body and is required for horsetail movement and recombination. *J. Cell Sci.* 118 (Pt 2), 447–459. doi:10.1242/jcs.01629

Sato, A., Isaac, B., Phillips, C. M., Rillo, R., Carlton, P. M., Wynne, D. J., et al. (2009). Cytoskeletal forces span the nuclear envelope to coordinate meiotic chromosome pairing and synapsis. *Cell* 139 (5), 907–919. doi:10.1016/j.cell.2009.10.039

Scherthan, H., Wang, H., Adelfalk, C., White, E. J., Cowan, C., Cande, W. Z., et al. (2007). Chromosome mobility during meiotic prophase in *Saccharomyces cerevisiae*. *Proc. Natl. Acad. Sci. U. S. A.* 104 (43), 16934–16939. doi:10.1073/pnas.0704860104

Scherthan, H. (2001). A bouquet makes ends meet. *Nat. Rev. Mol. Cell Biol.* 2 (8), 621–627. doi:10.1038/35085086

Shibuya, H., Ishiguro, K., and Watanabe, Y. (2014). The TRF1-binding protein TERB1 promotes chromosome movement and telomere rigidity in meiosis. *Nat. Cell Biol.* 16 (2), 145–156. doi:10.1038/ncb2896

Shibuya, H., Hernandez-Hernandez, A., Morimoto, A., Negishi, L., Hoog, C., and Watanabe, Y. (2015). MAJIN links telomeric DNA to the nuclear membrane by exchanging telomere cap. *Cell* 163 (5), 1252–1266. doi:10.1016/j.cell.2015.10.030

Sole, M., Pascual, A., Anton, E., Blanco, J., and Sarrate, Z. (2023). The courtship choreography of homologous chromosomes: timing and mechanisms of DSB-independent pairing. *Front. Cell Dev. Biol.* 11, 1191156. doi:10.3389/fcell.2023.1191156

Sosa, B. A., Rothballer, A., Kutay, U., and Schwartz, T. U. (2012). LINC complexes form by binding of three KASH peptides to domain interfaces of trimeric SUN proteins. *Cell* 149 (5), 1035–1047. doi:10.1016/j.cell.2012.03.046

Starr, D. A., and Fridolfsson, H. N. (2010). Interactions between nuclei and the cytoskeleton are mediated by SUN-KASH nuclear-envelope bridges. *Annu. Rev. Cell Dev. Biol.* 26, 421–444. doi:10.1146/annurev-cellbio-100109-104037

Stewart, M. N., and Dawson, D. S. (2008). Changing partners: moving from non-homologous to homologous centromere pairing in meiosis. *Trends Genet.* 24 (11), 564–573. doi:10.1016/j.tig.2008.08.006

Tanaka, K., Kohda, T., Yamashita, A., Nonaka, N., and Yamamoto, M. (2005). Hrs1p/Mcp6p on the meiotic SPB organizes astral microtubule arrays for oscillatory nuclear movement. *Curr. Biol.* 15 (16), 1479–1486. doi:10.1016/j.cub.2005.07.058

Therizols, P., Fairhead, C., Cabal, G. G., Genovesio, A., Olivo-Marin, J. C., Dujon, B., et al. (2006). Telomere tethering at the nuclear periphery is essential for efficient DNA double strand break repair in subtelomeric region. *J. Cell Biol.* 172 (2), 189–199. doi:10.1083/jcb.200505159

Tian, M., Agreiter, C., and Loidl, J. (2020). Spatial constraints on chromosomes are instrumental to meiotic pairing. *J. Cell Sci.* 133 (22), jcs253724. doi:10.1242/jcs.253724

Tomita, K., and Cooper, J. P. (2007). The telomere bouquet controls the meiotic spindle. *Cell* 130 (1), 113–126. doi:10.1016/j.cell.2007.05.024

Trelles-Sticken, E., Dresser, M. E., and Scherthan, H. (2000). Meiotic telomere protein Ndj1p is required for meiosis-specific telomere distribution, bouquet formation and efficient homologue pairing. *J. Cell Biol.* 151 (1), 95–106. doi:10.1083/jcb.151.1.95

Wanat, J. J., Kim, K. P., Koszul, R., Zanders, S., Weiner, B., Kleckner, N., et al. (2008). Csm4, in collaboration with Ndj1, mediates telomere-led chromosome dynamics and recombination during yeast meiosis. *PLoS Genet.* 4 (9), e1000188. doi:10.1371/journal.pgen.1000188

Wang, X., Kam, Z., Carlton, P. M., Xu, L., Sedat, J. W., and Blackburn, E. H. (2008). Rapid telomere motions in live human cells analyzed by highly time-resolved microscopy. *Epigenetics Chromatin* 1 (1), 4. doi:10.1186/1756-8935-1-4

Woglar, A., and Jantsch, V. (2014). Chromosome movement in meiosis I prophase of *Caenorhabditis elegans*. *Chromosoma* 123 (1-2), 15–24. doi:10.1007/s00412-013-0436-7

Woglar, A., Daryabeigi, A., Adamo, A., Habacher, C., Machacek, T., La Volpe, A., et al. (2013). Matefin/SUN-1 phosphorylation is part of a surveillance mechanism to coordinate chromosome synapsis and recombination with meiotic progression and chromosome movement. *PLoS Genet.* 9 (3), e1003335. doi:10.1371/journal.pgen.1003335

Wynne, D. J., Rog, O., Carlton, P. M., and Dernburg, A. F. (2012). Dynein-dependent processive chromosome motions promote homologous pairing in *C. elegans* meiosis. *J. Cell Biol.* 196 (1), 47–64. doi:10.1083/jcb.201106022

Yamamoto, A., West, R. R., McIntosh, J. R., and Hiraoka, Y. (1999). A cytoplasmic dynein heavy chain is required for oscillatory nuclear movement of meiotic prophase and efficient meiotic recombination in fission yeast. *J. Cell Biol.* 145 (6), 1233–1249. doi:10.1083/jcb.145.6.1233

Yoshida, M., Katsuyama, S., Tateho, K., Nakamura, H., Miyoshi, J., Ohba, T., et al. (2013). Microtubule-organizing center formation at telomeres induces meiotic telomere clustering. *J. Cell Biol.* 200 (4), 385–395. doi:10.1083/jcb.201207168

Zickler, D., and Kleckner, N. (2015). Recombination, pairing, and synapsis of homologs during meiosis. *Cold Spring Harb. Perspect. Biol.* 7 (6), a016626. doi:10.1101/cshperspect.a016626

Zickler, D., and Kleckner, N. (2016). A few of our favorite things: pairing, the bouquet, crossover interference and evolution of meiosis. *Semin. Cell Dev. Biol.* 54, 135–148. doi:10.1016/j.semcdb.2016.02.024

frontiers | Frontiers in Cell and Developmental Biology

TYPE Original Research
PUBLISHED 04 December 2023
DOI 10.3389/fcell.2023.1285695

OPEN ACCESS

EDITED BY
Alexei Arnaoutov,
Eunice Kennedy Shriver National Institute of Child Health and Human Development (NIH), United States

REVIEWED BY
Inna Lermontova,
Leibniz Institute of Plant Genetics and Crop Plant Research (IPK), Germany
Christopher Makaroff,
Miami University, United States
Olivier Da Ines,
Institut de Génétique, Reproduction & Développement (iGReD), France

*CORRESPONDENCE
Mónica Pradillo,
pradillo@bio.ucm.es

RECEIVED 30 August 2023
ACCEPTED 21 November 2023
PUBLISHED 04 December 2023

CITATION
Fernández-Jiménez N, Martinez-Garcia M, Varas J, Gil-Dones F, Santos JL and Pradillo M (2023), The scaffold nucleoporins SAR1 and SAR3 are essential for proper meiotic progression in *Arabidopsis thaliana*.
Front. Cell Dev. Biol. 11:1285695.
doi: 10.3389/fcell.2023.1285695

The scaffold nucleoporins SAR1 and SAR3 are essential for proper meiotic progression in *Arabidopsis thaliana*

Nadia Fernández-Jiménez[1], Marina Martinez-Garcia[2], Javier Varas[3], Félix Gil-Dones[1], Juan Luis Santos[1] and Mónica Pradillo[1]*

[1]Department of Genetics, Physiology and Microbiology, Faculty of Biological Sciences, Universidad Complutense de Madrid, Madrid, Spain, [2]Department of Biotechnology-Plant Biology, School of Agricultural, Food and Biosystems Engineering, Universidad Politécnica de Madrid, Madrid, Spain, [3]GlaxoSmithKline Spain, Madrid, Spain

Nuclear Pore Complexes (NPCs) are embedded in the nuclear envelope (NE), regulating macromolecule transport and physically interacting with chromatin. The NE undergoes dramatic breakdown and reformation during plant cell division. In addition, this structure has a specific meiotic function, anchoring and positioning telomeres to facilitate the pairing of homologous chromosomes. To elucidate a possible function of the structural components of the NPCs in meiosis, we have characterized several Arabidopsis lines with mutations in genes encoding nucleoporins belonging to the outer ring complex. Plants defective for either SUPPRESSOR OF AUXIN RESISTANCE1 (SAR1, also called NUP160) or SAR3 (NUP96) present condensation abnormalities and SPO11-dependent chromosome fragmentation in a fraction of meiocytes, which is increased in the double mutant *sar1 sar3*. We also observed these meiotic defects in mutants deficient in the outer ring complex protein HOS1, but not in mutants affected in other components of this complex. Furthermore, our findings may suggest defects in the structure of NPCs in *sar1* and a potential link between the meiotic role of this nucleoporin and a component of the RUBylation pathway. These results provide the first insights in plants into the role of nucleoporins in meiotic chromosome behavior.

KEYWORDS

Arabidopsis, meiosis, nuclear pore complex, NUP96, NUP160, SAR1, SAR3

Introduction

The nuclear pore complex (NPC) is one of the largest non-polymeric protein complexes in eukaryotic cells (Knockenhauer and Schwartz, 2016). The main function of the NPC is to mediate the selective nucleocytoplasmic transport of macromolecules while allowing the free diffusion of molecules smaller than 40 kDa (Raíces and D'Angelo, 2012; Meier et al., 2017). Most of the proteins forming the NPCs, known as nucleoporins, are evolutionarily conserved, as well as the octagonal symmetry of these complexes (Gall, 1967; Hoelz et al., 2011; Lin and Hoelz, 2019). The NPC is organized in different subcomplexes composed of more than 30 different nucleoporins (Tamura and Hara-Nishimura, 2013; Li and Gu, 2020). In addition to their main role as trafficking channels, NPCs also act as hubs

for relevant processes such as chromatin organization, gene transcription, replication stress resolution or DNA repair (Blobel, 1985; Beck and Hurt, 2017; Lamm et al., 2021). In these cases, NPCs could act as membrane-bound sliding platforms to associate the underlying chromatin with other protein complexes localized in the nucleus (Strambio-De-Castilla et al., 2010; Raices and D'Angelo, 2012).

The overall organization of the NPCs is highly conserved among evolutionarily distant eukaryotes, although there is a significant variability in the composition of nucleoporins (Fiserova et al., 2009; Tamura et al., 2011; 2013; Fernandez-Martinez and Rout, 2021). Nucleoporins assemble into different subcomplexes forming the inner, outer, and membrane rings. Moreover, the central channel is filled by phenylalanine-glycine-rich (FG) nucleoporins, and a nuclear basket and cytoplasmic filaments are anchored to the nuclear and cytoplasmic outer rings, respectively (Alber et al., 2007; Beck and Hurt, 2017; Meier et al., 2017). The outer ring complex nucleoporins form Y-shaped complexes, and accordingly, this NPC module is also known as the Y-complex (Stuwe et al., 2015). This complex is also called NUP107-160 in plants and vertebrates and Nup84 (or Nup84-Nup133) in yeast (Lutzmann et al., 2002; Walther et al., 2003; Meier et al., 2017; Nordeen et al., 2020). The outer ring complex plays essential roles in NPC assembly, microtubule polymerization at kinetochores, and DNA repair (Walther et al., 2003; Nagai et al., 2008; Mishra et al., 2010). In *Arabidopsis thaliana*, members of this complex are involved in flowering time regulation, abiotic stress and immune responses, as well as in hormone signaling (Gu, 2018; Zhang A. et al., 2020; Cheng et al., 2020; Nie et al., 2023). In this species, defective mutants for members of this complex, such as *nup160* and *nup96*, were identified in a screening for suppression of auxin resistance phenotypes. For this reason, these mutants are also called *suppressor of auxin resistance1* (*sar1*) and *sar3*, respectively, and exhibit pleiotropic growth defects including an early flowering phenotype (Cernac et al., 1997; Parry et al., 2006; Wiermer et al., 2012).

Meiosis is a specialized cell division required to generate haploid gametes from diploid parent cells. During early prophase I, homologous chromosomes pair, synapse and exchange genetic information. These processes are facilitated by the movement of telomeres along the nuclear envelope (NE) (Koszul and Kleckner, 2009). The transmission of cytoplasmic forces to telomeres is mediated by the LINC (LInker of the Nucleoskeleton and Cytoskeleton) complexes (Starr, 2009; Klutstein and Cooper, 2014). These complexes consist of SUN and KASH proteins that span the inner and outer nuclear membranes (INM and ONM), connecting nuclear and cytoplasmic structures. Disrupting the function of the LINC complex impairs chromosome movements, leading to defects in synapsis and meiotic recombination (Ding et al., 2007; Murphy et al., 2014; Varas et al., 2015; Zhang F. et al., 2020). This role for LINC complexes seems to be conserved in yeast, animals, and plants (Burke, 2018). It has been suggested that LINC complexes and NPCs could be functionally related. Indeed, in HeLa cells SUN1 interacts with NPCs being important for their distribution (Liu et al., 2007). However, studies showing a possible meiotic function for NPCs are scarce and mostly focused on yeast. Several of these studies have associated the function of certain nucleoporins with kinetochores and chromosome segregation (Yang et al., 2015; Hattersley et al., 2016; 2022). In *Saccharomyces cerevisiae*, the nuclear basket nucleoporins Nup2 and Nup60 transiently detach from the NPC core during the first meiotic division and promote chromosome dynamics during meiosis (Chu et al., 2017; Komachi and Burgess, 2022; King et al., 2023). Until now, no work in plants has linked NPCs to chromatin organization and chromosome behavior during meiosis. In this regard, it is important to note that in contrast to the situation in yeast, in plants, the NE breaks down to allow the connection between the chromosomes and the cytoplasmic spindle (Meier et al., 2017).

In this study, we focus on the meiotic role of nucleoporins belonging to the outer ring complex of the NPC, in particular NUP160 (SAR1) and NUP96 (SAR3). Analysis of the meiotic process in pollen mother cells (PMCs) has revealed that SAR1 and SAR3 are essential for ensuring proper chromatin condensation and meiotic repair of double-strand breaks (DSBs). Additionally, the findings may suggest that SAR1 is important for preserving the integrity of NPCs in prophase I and that its meiotic function could be linked to that of AXR1, a subunit of the RUB1 activating enzyme, which regulates the protein degradation activity of SKP1-CULLIN1-F-BOX (SCF) complexes. Our work provides, for the first time, important insights into the function of NPCs in plant meiosis.

Materials and methods

Plant material and growth conditions

All plants used in this study were *Arabidopsis thaliana* (L.) Heynh, Columbia (Col-0) accession. Mutant lines were obtained from the European Arabidopsis Stock Centre: *sar1-4* (SALK_126801), *sar3-4* (SALK_117966), *hos1-3* (SALK_069312), *nup85-2* (SALK_113274), and *seh1-1* (SALK_022717). Double mutants were built using: *spo11-1-5* (SALK_009440) (Pradillo et al., 2007), and *axr1-31* (SALK_013238) (Martínez-García et al., 2020). Seeds were sown on soil directly or after transfer from MS plates (Murashige and Skoog, 1962). Plants were grown under long-day conditions (16 h light/8 h dark) at 19°C. Homozygous plants were identified by PCR screening using primers listed in Supplementary Table S1.

Cytogenetic analyses

Fixation of flower buds and spreading of male meiocytes were performed according to Ross et al. (1996). The fluorescent *in situ* hybridization (FISH) technique was carried out as described by Sanchez-Moran et al. (2001) with minor modifications. The DNA probes used in the analysis of chromosomal configurations at metaphase I were 45S rDNA (pTa71; Gerlach and Bedbrook, 1979) and 5S rDNA (pCT4.2; Campell et al., 1992). At least three plants of each genotype were analyzed. To analyze pollen grains, we used fresh material and transferred anthers to a 1% solution of carmine in 45% acetic acid, we heated the slide slowly over an alcohol burner (~30 s) and used the squash method. A Nikon Eclipse E400 phase-contrast microscope with a Nikon DMX-12005-E400 digital camera were used for image acquisition.

To detect meiotic recombination proteins, we performed the spreading technique described by Armstrong et al. (2009) with the modifications included in Varas and Pradillo (2018). To detect histone modifications and NE proteins, we applied the squash technique detailed in Oliver et al. (2013). Information about the dilution and source of primary antibodies is included in Supplementary Table S2. The secondary antibodies used were anti-rabbit Alexa Fluor 555-conjugated (Invitrogen, Molecular probes; 1:500), anti-rat Alexa Fluor 555-conjugated (Invitrogen, Molecular probes; 1:500), anti-mouse FITC-conjugated (Agrisera; 1:100), and anti-rabbit FITC-conjugated (Merck; 1:50). Cells were imaged using an Olympus BX61 epifluorescence microscope with an Olympus DP71 digital camera. Quantification of foci was performed using ImageJ. We scored all images blind to genotype.

RNA FISH

To evaluate mRNA nuclear accumulation, we followed the protocol described in Parry (2014) using samples from roots and flower buds. The samples were incubated with a Cy3 labelled oligo(dT) probe. For quantification, we compared pixel intensity between the nucleus and the cytoplasm (ImageJ) and calculated the fold change (ratio nucleus/cytoplasm) in each cell respect to Col-0. Cells from at least three different slides were analyzed for each tissue.

Statistical analyses

Microsoft Office Excel and GraphPad Prism were used for data organization and statistical analysis, respectively. Mann-Whitney *U* test and one-way ANOVA with *post hoc* Tukey test were performed to compare independent samples. Fisher's Exact test and Chi-square test were used to compare frequencies.

Results

Mutants defective in outer ring complex nucleoporins show abnormal male meiosis

The mutants analyzed in this study were previously characterized by Cernac et al. (1997) and Parry et al. (2006). These authors revealed that *sar1* and *sar3* show a pleiotropic phenotype with early flowering, dwarfism, and abnormal auxin response. These mutants also have altered expression of certain defense genes and nuclear mRNA accumulation (Meier and Brkljacic, 2009; Wiermer et al., 2012). In addition, the pleiotropic defects in the single mutants were exacerbated in the double mutant *sar1 sar3*, suggesting the disruption of an NPC specific function associated to the loss of several subunits (Parry et al., 2006). The reduced production of seeds in these plants was attributed to their developmental defects and abnormal inflorescences (Parry et al., 2006).

In this work, we have confirmed the fertility defects in *sar1* and *sar3* (Supplementary Figure S1) and observed that this phenotype is aggravated in the double mutant *sar1 sar3*, which is completely sterile. In addition, this double mutant has viability problems, as only 2% of *sar1 sar3* double mutant plants were obtained in the offspring of double heterozygous plants. The detailed cytological characterization of pollen mother cells (PMCs) that we conducted in these mutants revealed that these fertility defects are due to abnormalities during meiosis. In the single mutants *sar1* and *sar3*, most of the meiocytes were apparently indistinguishable from the control: homologous chromosomes were associated along their entire length in pachynema; five bivalents, with no alterations in chromosome condensation, were observed at metaphase I; and chromosomes and sister-chromatids segregated correctly at anaphase I and II, respectively, giving rise to balanced tetrads with the same amount of genetic material in each nucleus (Supplementary Figure S2). However, alterations in chromatin condensation and chromosome fragmentation appeared at different stages corresponding to both meiotic divisions in a percentage of meiocytes (*sar1*: 13.52%, n = 636; *sar3*: 19.08%, n = 1,373). No anomalies were observed at leptonema, but from zygonema onwards some PMCs showed aberrant chromatin condensation. In metaphase I, entangled bivalents were observed and segregation problems, as well as chromosome fragments, were detected in both meiosis I and II. All these defects led to the formation of tetrads and polyads with differentially condensed and unbalanced nuclei (Figure 1A). Abnormal meiocytes were not limited to specific flower buds or anthers but appeared alongside populations of normal cells (Figure 1B; Supplementary Figure S1). The percentage of abnormal meiocytes was much higher in the double mutant (57.02%, n = 114) than in the single mutants, which also differed from each other (Figure 1C; Supplementary Tables S3, S4). In addition, the proportion of meiocytes with chromosomal fragmentation was increased in the double mutant compared to the single mutants (Supplementary Table S5).

In order to elucidate whether these defects were a consequence of the alteration of any component of the outer ring complex, we analyzed other mutants defective for this subunit. HIGH EXPRESSION OF OSMOTICALLY RESPONSIVE GENES1 (HOS1) functions in the regulation of flowering through controlling the protein level of CONSTANT, like SAR1 and SAR3 (Cheng et al., 2020; Li et al., 2020). The cytological analysis of male meiosis in *hos1* revealed the same type of alterations as those observed in *sar1* and *sar3* mutants (Supplementary Figure S2). Problems in chromatin condensation and chromosomal fragmentation were detected, although meiocytes without any abnormalities could also be observed. Interestingly, these meiotic alterations do not appear when other components of the outer ring, such as NUP85 (n = 166) or SEH1 (n = 36), are absent (Supplementary Figure S2). Both *sar1* (mutant in which we detected meiosis abnormalities) and *nup85* (mutant in which we did not detect any meiosis abnormalities) show mRNA accumulation in the nucleus, not only in root cells, but also in flower bud cells (Supplementary Figure S3). Therefore, these results show that the different outer ring components are not equally important during meiosis, and that the meiotic defects do not appear to arise as a consequence of the mRNA accumulation.

Synapsis and chiasma frequency, as well as the pattern of certain epigenetic marks, are normal in most *sar1* meiocytes

In order to conduct a more exhaustive study of the meiotic process, the *sar1* mutant was chosen as representative of the meiotic problems observed in the outer ring complex mutants. Since the

10.3389/fcell.2023.1285695

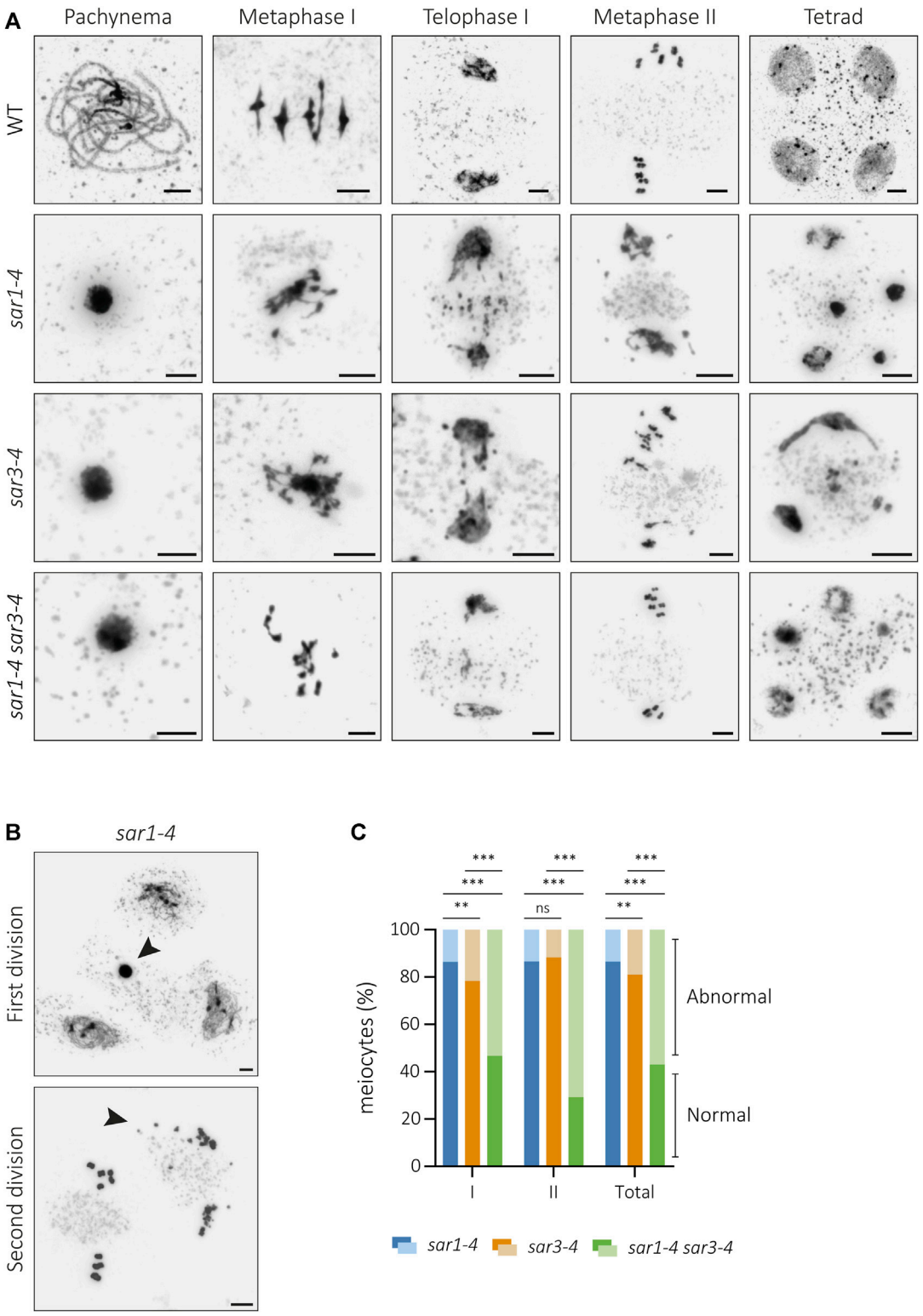

FIGURE 1
Cytological analysis of meiotic defects in *sar* mutants. **(A)** Chromosome spreads of male meiocytes from WT, *sar1-4, sar3-4* and the double mutant *sar1-4 sar3-4*. Mutants show hypercondensed meiocytes at pachynema, entangled chromosomes at metaphase I, chromosome fragments and unbalanced segregations at telophase I, unbalanced nuclei and chromosome fragments at metaphase II, and polyads with nuclei displaying unevenly condensed chromatin. **(B)** Examples from *sar1-4* showing abnormal meiocytes (arrowheads) surrounded by normal meiocytes in both meiotic divisions. **(C)** Proportion of abnormal and normal meiocytes in *sar1-4, sar3-4* and the double mutant *sar1-4 sar3-4*. Fisher's exact test was performed to analyze differences between mutants (*p*-value: ns–non-significant, $*p < 0.05$, $**p < 0.01$, $***p < 0.001$). I: Meiosis I; II: Meiosis II. Scale bars = 5 µm.

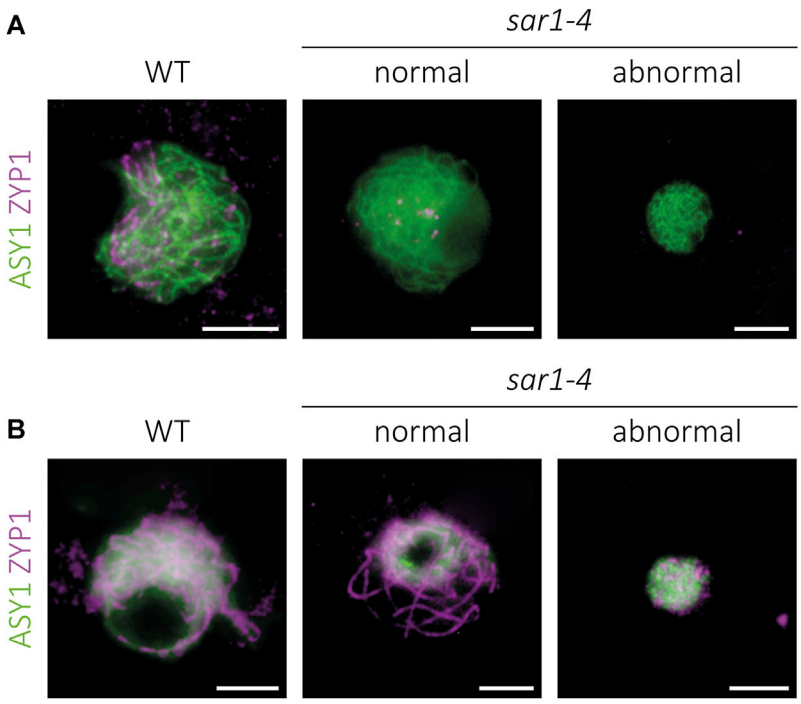

FIGURE 2
Immunolocalization of meiotic chromosome axes and synaptonemal complex in *sar1-4*. Squash preparations of male meiocytes showing the meiotic chromosome axis protein ASY1 (green) and the synaptonemal complex transverse filament protein ZYP1 (magenta). **(A)** Zygonema. Chromosome axes appear to be normal despite condensation defects in *sar1-4*. **(B)** Pachynema. Although full synapsis is observed in normal-looking *sar1-4* meiocytes, ZYP1 forms numerous chromosomic aberrant aggregates in hypercondensed *sar1-4* meiocytes, revealing problems in synaptonemal complex formation in these cells. Scale bars = 5 μm.

meiotic problems began to be detected in zygonema-pachynema, we carried out an analysis of the synaptonemal complex (SC) formation by immunolocalization of ASY1 (protein associated to the axial/lateral element) and ZYP1 (transverse filament protein) on prophase I chromosome spreads (Armstrong et al., 2002; Higgins et al., 2005). We also detected two cell populations with respect to SC formation. In all meiocytes in which the chromosome morphology was indistinguishable to the WT (Supplementary Figure S2), the pattern corresponding to the ASY1+ZYP1 proteins revealed normal behavior: bright linear signals of ASY1 in the unsynapsed regions during zygonema and short stretches of ZYP1 that extended until full synapsis at pachynema (Figure 2; Supplementary Figure S4). In the case of meiocytes with extreme chromosomal condensation, we observed a continuous ASY1 signal in zygonema, despite the small size of these nuclei (Figure 2A). However, in these abnormal meiocytes we could not detect a continuous ZYP1 signal, observing only some aggregates without a defined pattern (Figure 2B). Thus, chromosomal axes appear to form correctly in *sar1* meiocytes, and although synapsis is normal in most *sar1* meiocytes, some have problems achieving synapsis.

To determine whether, despite not detecting problems in synapsis and bivalent formation, there is any defect in meiotic recombination in normal-looking meiocytes in *sar1*, the frequency of chiasmata per cell at metaphase I was analyzed. To facilitate the interpretation of bivalent morphology and the localization of chiasmata, we performed 45S and 5S rDNA FISH (Sanchez-Moran et al., 2001) (Figure 3A). This analysis could not be applied to meiocytes with aberrant chromatin condensation, although we observed an arrangement of the FISH signals indicating some level of pairing, since homologous chromosomes were close together in the nucleus and presented some co-orientation at metaphase I (Figure 3B). The mean cell chiasma frequency in the WT was 10.20 ± 0.14 (n = 69), with a range of variation from 8 to 13. In *sar1* no significant differences were found with respect to this value, since the mean was 10.07 ± 0.21 (n = 43), varying from 7 to 14 (U = 1,393; p = 0.579) (Figure 3C).

Histone post-translational modifications are thought to play a pivotal role in chromosome condensation during meiosis (Fuchs et al., 2006; Xu et al., 2009). To test whether there was any variation in the epigenetic pattern of abnormally condensed meiocytes, we immunolocalized histone modifications associated to euchromatin and heterochromatin, as well as a modification specific of the chromosomal condensation process. Specifically, we analyzed the pattern corresponding to H3K4me3 (euchromatin-specific methylation), H3K9me2 (heterochromatin-specific methylation), and H3S10ph (phosphorylation associated to chromosome condensation) (Supplementary Figure S5). H3K4me3 is observed in all chromosomal regions except pericentromeric heterochromatin (Oliver et al., 2013). No variations from the WT were detected in *sar1* prophase I meiocytes. In the case of *sar1* hypercondensed meiocytes, H3K4me3 also had a similar pattern, appearing in most of the chromatin area. On the other hand, H3K9me2, which is restricted to pericentromeric regions throughout meiosis (Oliver et al., 2013), showed no variations in *sar1* meiocytes compared to WT, since signals were always observed in the chromocenters or

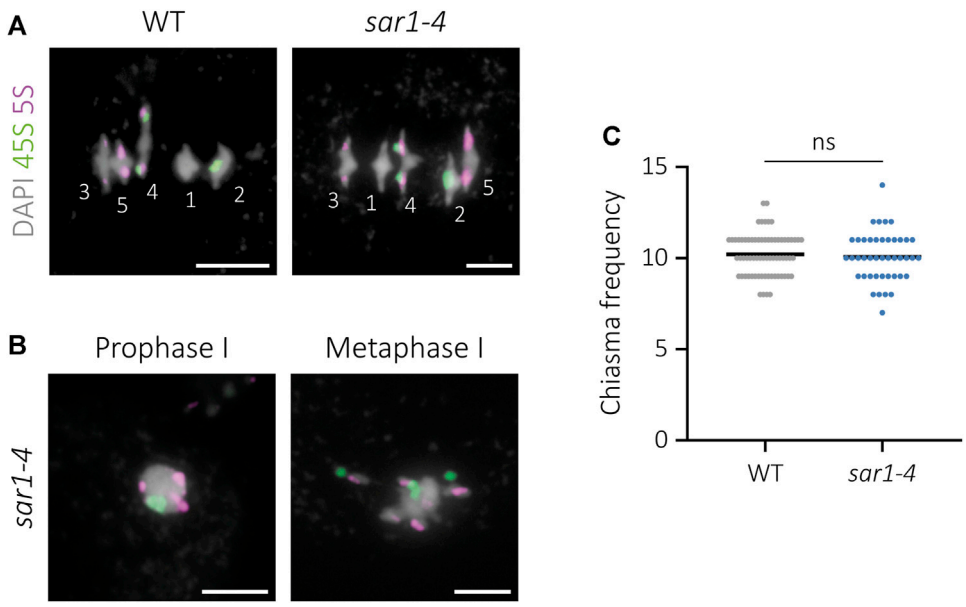

FIGURE 3
Cytological analysis of chiasma frequency in *sar1-4*. 45S rDNA (green) and 5S rDNA (magenta) probes were used for chromosome identification. DAPI is showed in gray. **(A)** WT and normal-looking *sar1-4* meiocytes at metaphase I. Numbers identify each bivalent. **(B)** Abnormal *sar1-4* meiocytes. The position of the FISH signals indicates pairing in prophase I and some co-orientation of homologous chromosomes in metaphase I. **(C)** Quantification of chiasma frequency per cell in WT and *sar1-4* (see the text for more details). Scale bars = 5 μm.

brightest DAPI regions. Surprisingly, no changes were observed in the H3S10ph pattern either. This mark appears in Arabidopsis from diplonema onwards, a stage in which the chromatin is more condensed (Oliver et al., 2013). We could expect the presence of this modification in *sar1* meiocytes with hypercondensation. However, no signal corresponding to this epigenetic mark was detected despite chromatin compaction. Therefore, the condensation abnormalities observed in *sar1* meiocytes are not due to alterations in these histone modifications, at least at the cytological level.

Chromosomal fragmentation defects observed in *sar1* are SPO11-dependent

Analysis of PMCs from *sar1* plants revealed fragmented chromosomes from anaphase I onwards in a percentage of meiocytes, leading to the formation of polyads containing microspores with unequal amounts of DNA (Figure 1). To ascertain whether DSBs formed by SPO11 could be the source of the chromosome fragmentation observed in SAR1-deficient plants, we generated *sar1 spo11-1* double mutants. Meiosis in *spo11* mutants is characterized by the presence of ten univalents at metaphase I, which segregate randomly during anaphase I (Grelon et al., 2001). In the absence of either SPO11-1 or SPO11-2, no DSBs occur at the onset of meiosis, therefore the integrity of the chromosomes in *spo11* mutants is intact.

The meiotic phenotype of the double mutant *sar1 spo11-1* was very similar to that observed in the *spo11-1* single mutant, and no formation of SC or bivalents was detected. Ten univalents were invariably observed at metaphase I (n = 42) and no evidence of chromosomal fragmentation was found in any of the successive stages of meiosis (Figure 4A). Therefore, *sar1* chromosomal fragmentation problems are caused by the failure to repair SPO11-induced DSBs.

Detailed analysis of *sar1 spo11-1* PMCs revealed that although chromosomal fragmentation disappears, this double mutant still shows alterations in chromatin condensation (Figure 4B). In fact, the percentage of abnormal meiocytes (with alterations in chromatin condensation and/or chromosome fragmentation) during the first division did not vary significantly from that observed in the *sar1* single mutant (Figure 4C; Supplementary Table S6). In contrast, we detected a reduction in the frequency of abnormal meiocytes observed during the second division in the double mutant. The differences become apparent at the second division because at this division most of the abnormal meiocytes quantified in the *sar1* single mutant have chromosomal breaks, whereas at the first division most of the abnormal *sar1* meiocytes have chromatin condensation problems. Therefore, the chromosome condensation abnormalities observed in the *sar1* single mutant do not appear to arise from a specific meiotic alteration or at least from defects in the processing of DSBs. There is no evidence to suggest that hypercondensation has a pre-meiotic nature, as we did not identify any issues with chromatin condensation in somatic cells (Supplementary Figure S5). Furthermore, as mentioned before, all the observed leptotene meiocytes appeared to be normal-looking.

γH2AX and RAD51 foci are significantly reduced in hypercondensed *sar1* meiocytes

To further examine the meiotic homologous recombination (HR) process in *sar1* meiocytes, we detected phosphorylated

10.3389/fcell.2023.1285695

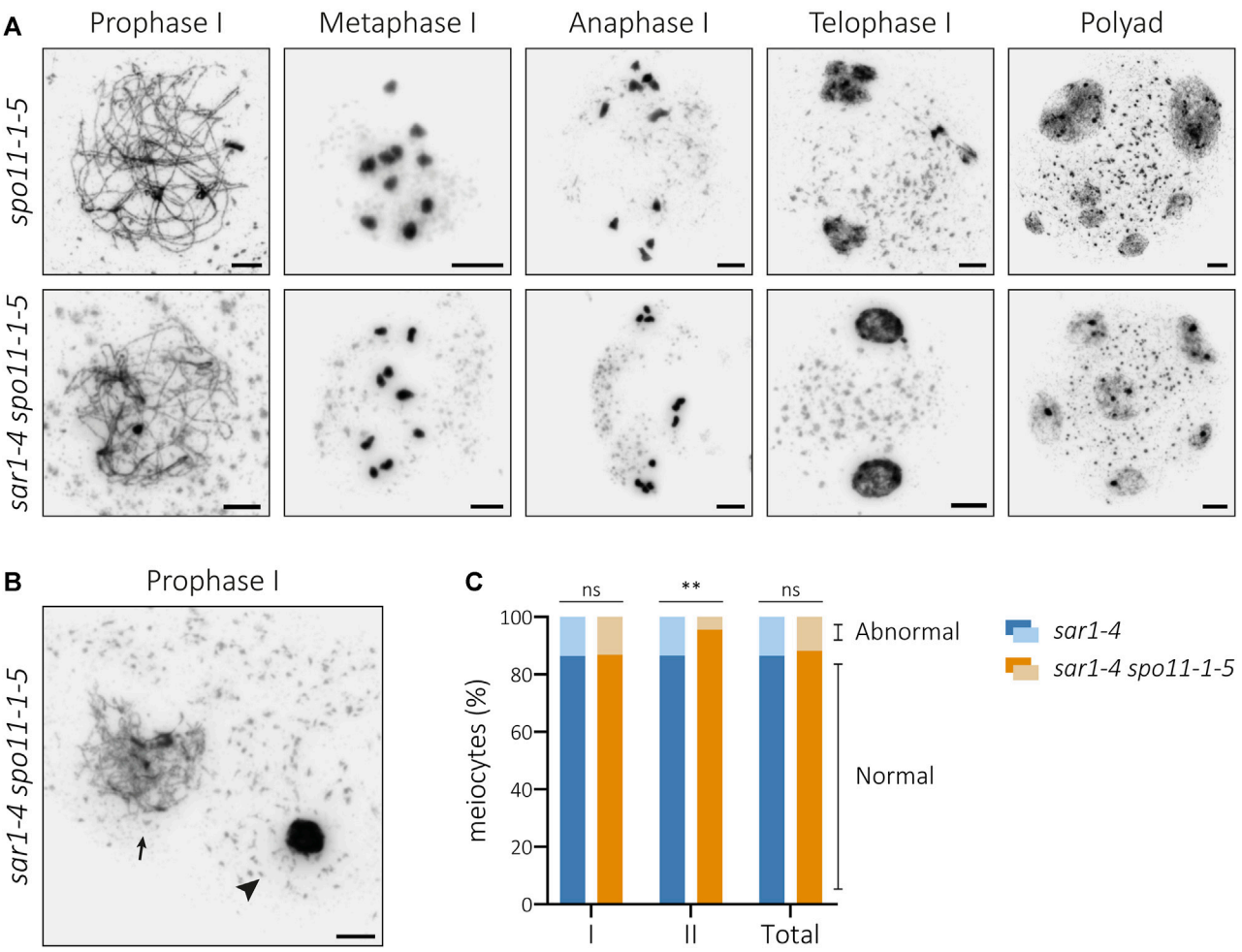

FIGURE 4
Cytological analysis of PMCs from the double mutant *sar1-4 spo11-1-5*. **(A)** Chromosome spreads of male meiocytes in *spo11-1-5* and *sar1-4 spo11-1-5*. Homologous chromosomes fail to undergo synapsis and ten univalents are observed at metaphase I in both mutants. The presence of univalents leads to mis-segregations of chromosomes at anaphase I, unbalanced nuclei during second meiotic division and polyads. **(B)** Example of hypercondensed (arrowhead) and normal-looking (arrow) meiocyte in the double mutant *sar1-4 spo11-1-5*. **(C)** Proportion of abnormal and normal meiocytes in *sar1-4* (blue) and *sar1-4 spo11-1-5* (orange). Fisher's exact test was performed to analyze differences between the mutants (*p*-value: ns—non-significant, *$p < 0.05$, **$p < 0.01$, ***$p < 0.001$). I: Meiosis I; II: Meiosis II. Scale bars = 5 μm.

histone H2AX (γH2AX) and RAD51 foci by immunolocalization. γH2AX is deposited at DNA damage sites and is commonly used as a DSB-marker (Lowndes and Toh, 2005), and the recombinase RAD51 is loaded on ssDNA during meiotic recombination (Kurzbauer et al., 2012). The number of foci corresponding to both proteins was quantified in both normal appearing and hypercondensed *sar1* meiocytes (Figure 5; Supplementary Figure S6). We used ASY1 protein as a prophase I progression marker (Armstrong et al., 2002).

The number of γH2AX foci in *sar1* normal-looking meiocytes (196.61 ± 6.76; n = 46) was comparable as that observed in WT meiocytes (200.04 ± 6.02; n = 47), whereas we detected a significant reduction in the number of γH2AX foci in *sar1* hypercondensed meiocytes (66,00 ± 10,96; n = 15) (Figures 5A, B; Supplementary Table S7). The results for the quantification of the number of RAD51 foci were very similar, as no differences were found between normal-looking *sar1* (152.71 ± 7.49; n = 14) and WT meiocytes (149.42 ± 7.03; n = 36), whereas the number of RAD51 foci was drastically reduced in *sar1* hypercondensed cells (44.8 ± 5.03; n = 5) (Figures 5C, D; Supplementary Table S7). These results confirm that the meiotic recombination process, in line with the results obtained for synapsis, is severely compromised in *sar1* hypercondensed meiocytes.

Nuclear envelope distribution of NPCs is altered in abnormal *sar1* meiocytes

Since the absence of the outer ring complex nucleoporins may compromise the integrity of the NPCs, we decided to analyze the distribution of these complexes, as well as that of the LINC complexes in the NE of *sar1* meiocytes. For the study of LINC complexes, we applied an immunolocalization to detect SUN proteins (Figure 6; Supplementary Figure S7). In WT meiocytes these proteins present a distribution pattern along the entire NE during prophase I, disappearing at the end of this stage (n = 107). In

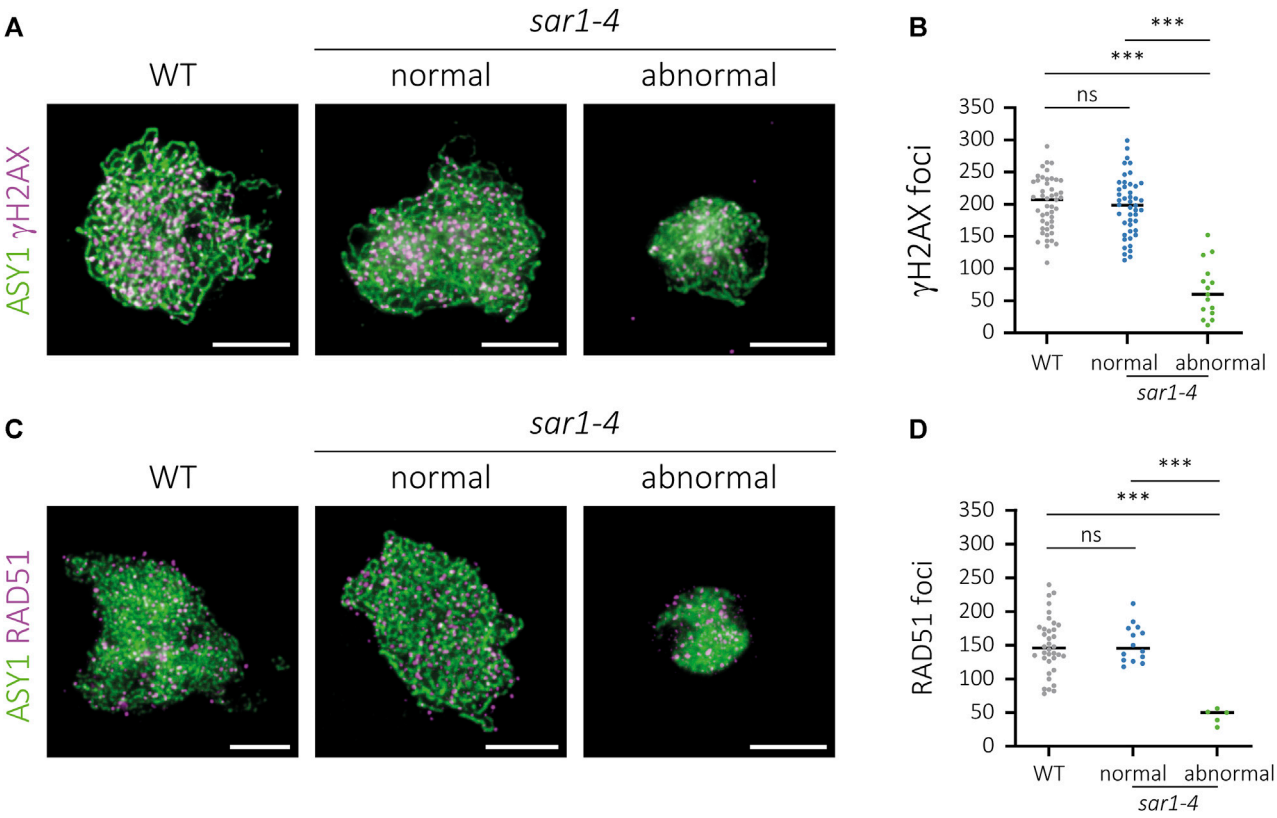

FIGURE 5
Immunolocalization of γH2AX and RAD51 in *sar1-4*. Chromosome spreads of male meiocytes showing γH2AX (magenta) and the recombinase RAD51 (magenta). ASY1 (green) has been used as a cytological marker to identify the meiotic chromosome axes. **(A)** WT, normal-looking and hypercondensed *sar1-4* zygotene cells showing ASY1 (green) and γH2AX foci (magenta). **(B)** Quantification of γH2AX foci in zygotene cells. **(C)** WT, normal-looking and hypercondensed *sar1-4* zygotene cells showing ASY1 (green) and RAD51 foci (magenta). **(D)** Quantification of RAD51 foci in zygotene cells. One-way ANOVA with a Tukey's *post hoc* test was performed in both cases (*p*-value: ns—non-significant, *p* *** < 0.001). Scale bars = 5 μm.

the case of *sar1*, no differences were found in the pattern of these proteins with respect to WT, with a continuous signal also appearing around the entire NE, both in normal-looking meiocytes (n = 25) and in hypercondensed meiocytes (n = 9). As expected, we observed a reduction of the NE surface in the latter, in line with their hypercondensed chromatin state. Thus, the distribution of LINC complexes is apparently not affected by the absence of a structural nucleoporin.

Regarding NPCs, in WT cells the distribution pattern is similar to that of the LINC complexes, with a signal appearing along the entire NE during prophase I (Figure 6). We confirmed that normal-looking *sar1* meiocytes (n = 103) do not display variations in the distribution pattern of NPCs with respect to WT meiocytes (n = 83). However, in *sar1* hypercondensed meiocytes, no trace of the signal corresponding to NPCs was detected at any location in the nucleus (n = 76), revealing that these cells present severe structural abnormalities in the NPCs.

The interplay between SAR1 and AXR1

Nucleoporins SAR1 and SAR3 are called by these names because they were firstly identified in a screening for suppression of the *axr1* resistance to auxin phenotype (Cernac et al., 1997; Parry et al., 2006). The *axr1* mutation produces a dramatic effect on plant morphology (Lincoln et al., 1990) and, interestingly, meiotic defects consisting of abnormal synapsis at prophase I, univalents at metaphase I, unequal chromosome segregation at anaphase I, and unbalanced tetrads or polyads (Jahns et al., 2014). The origin of these meiotic abnormalities is poorly understood, although it has been suggested that they could be related to the protein modifications associated to the RUBylation pathway (Jahns et al., 2014).

Since mutations in either *SAR1* or *SAR3* suppress most aspects of the phenotype conferred by *axr1* (Cernac et al., 1997; Parry et al., 2006; Supplementary Figure S8), we wondered if this suppression also affects *axr1* meiotic defects. To find out if this was the case, we generated the double mutant *sar1 axr1* and analyzed its meiotic phenotype. The results showed that the characteristic meiotic problems associated with *axr1* disappear in *sar1 axr1* (Figure 7A). In the double mutant, we observed full synapsis at pachynema, five bivalents at metaphase I, equal distribution of chromosomes during both meiotic divisions, and balanced tetrads. This means that in the double mutant the asynaptic phenotype of *axr1* disappears, as well as the problems in bivalent formation.

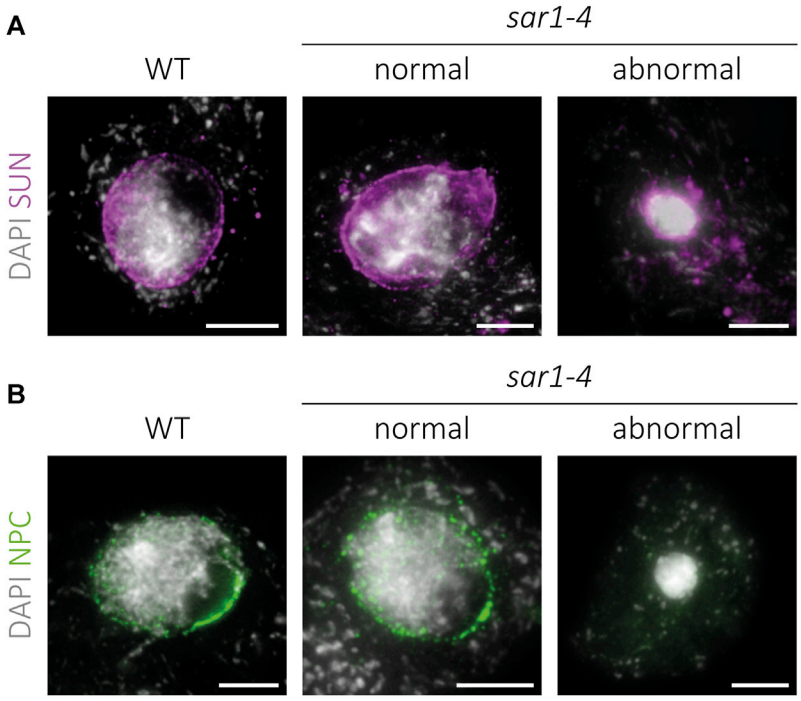

FIGURE 6
Immunolocalization of SUN proteins and NPCs in *sar1-4*. Squash preparations of WT, normal-looking and hypercondensed *sar1-4* zygotene cells. **(A)** SUN proteins (magenta) combined with DAPI (gray). A continuous signal around the entire NE is present in both normal-looking and hypercondensed *sar1-4* meiocytes, as well as in the WT. **(B)** NPCs (green) combined with DAPI (gray). Normal-looking *sar1-4* meiocytes are indistinguishable from WT cells, whereas in hypercondensed *sar1-4* meiocytes NPCs appear to be absent. Scale bars = 5 μm.

To analyze the different chromosome configurations in more detail, the FISH technique was applied (Supplementary Figure S8). In WT meiocytes most of the bivalents are closed (ring bivalents), with at least one chiasma in each arm (76.2%; n = 69), and the same occurs in *sar1* (85.5%; n = 43), in which no univalents are detected either. In *axr1* most of the bivalents are open (rod bivalents), without chiasmata in one of the arms (47.2%; n = 72), although there are also closed bivalents (24.2%) and univalents (28.6%). In the double mutant *sar1 axr1,* most bivalents appeared in closed configuration (70.4%; n = 50), recovering the WT phenotype (p = 0.155). Obligatory chiasma formation is almost restored in this double mutant, as univalents disappear. We detected only 4% of the cells with a single pair of univalents (2/50). To further analyze recombination events, we conducted an immunolocalization to detect MLH1, a marker of most crossovers in Arabidopsis (Jackson et al., 2006). This analysis showed no significant differences between the WT (8.09 ± 0.40), *sar1* (8.03 ± 0.38), and *sar1 axr1* (8.42 ± 0.25) (F = 0.469, p = 0.627) concerning MLH1 foci (Supplementary Figure S8).

Regarding to the presence of abnormal meiocytes, in the double mutant *sar1 axr1* there was a decrease in the percentage of these meiocytes, as well as in *sar1 spo11* (Figures 7B, C). We observed fewer abnormal meiocytes than in the *sar1* single mutant in the first meiotic division, although the difference between both mutants was not significant. The reduction was statistically significant in the second meiotic division (Supplementary Table S8). Furthermore, in *sar1 axr1*, the proportion of hypercondensed meiocytes was higher than that of fragmented meiocytes in the second division, in contrast to the *sar1* single mutant (Supplementary Table S5).

Discussion

The results of this work have revealed that some of the structural nucleoporins that belong to the outer ring complex of the NPC are necessary for proper meiosis progression. Several of the nucleoporin-defective mutants of this complex show a pleiotropic phenotype, including developmental deficiencies and reduced fertility (Cernac et al., 1997; Parry et al., 2006). We have demonstrated that the semi-sterile phenotype is due to failures in meiosis, highlighting the importance of the NPCs in this cell division.

SAR1 and SAR3, as well as HOS1, are necessary to ensure the proper progression of meiosis

The cytological analysis of PMCs in *sar* mutants has determined the presence of abnormal meiocytes, both in first and second division. The altered meiotic phenotype is characterized by the presence of cells with extreme chromatin condensation, especially during the first division, in addition to the appearance of chromosomal fragments from anaphase I onwards, which generates unbalanced tetrads and even polyads at the end of meiosis. These abnormal meiocytes appear along with others in which meiosis is properly achieved. The percentage of meiocytes with alterations varies between the mutants *sar1* and *sar3* and increases considerably in the double mutant *sar1 sar3* (Figure 1), which might suggest a certain degree of independence in their functions. In the double mutant, problems in vegetative development and fertility are

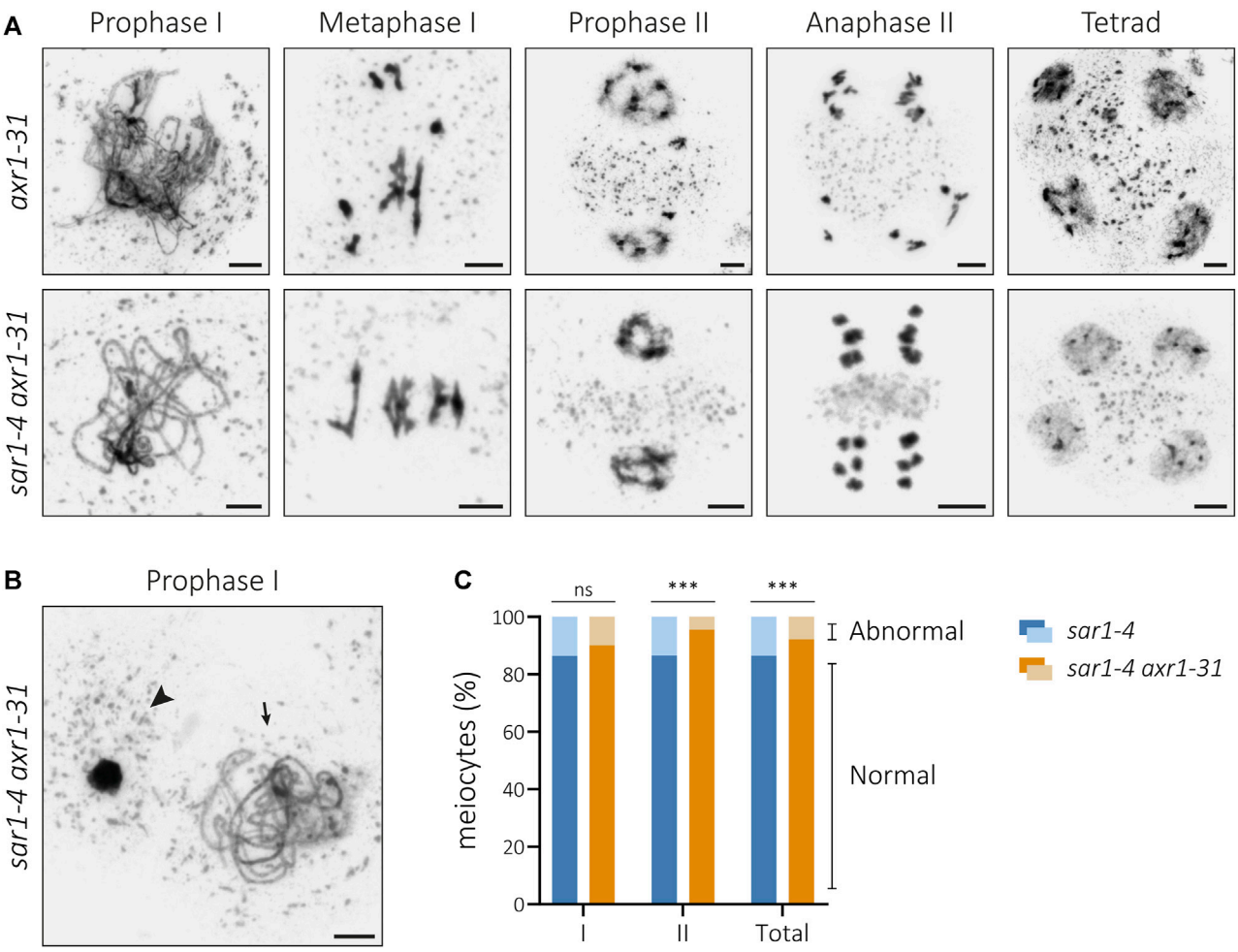

FIGURE 7
Cytological analysis of PMCs from the double mutant *sar1-4 axr1-31*. **(A)** Chromosome spreads of male meiocytes in *axr1-31* and *sar1-4 axr1-31*. The single mutant *axr1-31* shows defects in synapsis, presence of univalents at metaphase I, unbalanced nuclei during the second meiotic division, and tetrads with micronuclei. These meiotic defects are suppressed in the double mutant *sar1-4 axr1-31*. **(B)** Example of hypercondensed (arrowhead) and normal-looking (arrow) meiocyte in the double mutant *sar1-4 axr1-31*. **(C)** Proportion of abnormal and normal meiocytes in *sar1-4* (blue) and *sar1-4 axr1-31* (orange). Fisher's exact test was performed to analyze differences between the mutants (*p*-value: ns–non-significant, ***$p < 0.001$). I: Meiosis I; II: Meiosis II. Scale bars = 5 μm.

also exacerbated respect to the single mutants, suggesting that the loss of both nucleoporins produce a severe defect in NPC function (Parry et al., 2006). We also found similar meiotic alterations in *hos1* (Supplementary Figure S2). HOS1 is an outer ring complex nucleoporin that functions as an E3 ubiquitin ligase preventing precocious flowering. Interestingly, SAR1 and SAR3 also contribute to flowering time regulation by ensuring the stability and association of HOS1 with the NPC (Cheng et al., 2020; Li et al., 2020). It is possible that these nucleoporins affect a common regulatory mechanism between flowering and meiosis, since we have not detected meiotic problems in other mutants defective in the outer ring complex (*nup85*, *seh1*), which, unlike the previous ones, do not exhibit a significant flowering phenotype (Li and Gu, 2020). These mutations also do not aggravate the somatic abnormalities observed in *sar1*, suggesting some functional diversity between these nucleoporins that belong to the same NPC subcomplex (Wiermer et al., 2012; Parry, 2014). On the other hand, an accumulation of polyadenylated mRNA was found in all outer ring complex mutants in which RNA export was analyzed (Parry, 2015). Therefore, the observed meiotic alterations do not seem to be related to this mRNA accumulation (Supplementary Figure S3). It is likely that these nucleoporins do not only function in the context of NPCs. Indeed, NPCs undergo large-scale structural rearrangements during cell division and, for example, the nuclear basket transiently dissociate from the NPC core during meiosis in budding yeast (King et al., 2023). It is not known whether something similar occurs in Arabidopsis, but in any case, HOS1, apart from its E3-ubiquitin ligase activity, is associated with chromatin to influence gene expression in this species (Lazaro et al., 2012; Jung et al., 2014). In the case of SAR1 and SAR3, no such association has been confirmed. Further experiments will be required to confirm whether the meiotic functions of these nucleoporins are related to their structural function within the NPC.

sar1 and *sar3* present abnormalities in mRNA accumulation or nuclear morphology in all somatic cells (Cernac et al., 1997; Parry et al., 2006; Parry, 2014). However, they only show meiotic alterations in a percentage of meiocytes. Although there is no

clear explanation for this result, it is possible that in some meiocytes other nucleoporins cannot supply the function of SAR proteins. Alternatively, it could be a timing problem, with defects occurring in meiocytes in which meiosis is slower. In any case, the presence of normal-looking meiocytes together with abnormal meiocytes has been described in other mutants. For example, mutations in *BQT1,* a gene encoding a protein that tether telomeres to the spindle-pole body during prophase I, affect spindle formation in about half of meiotic cells in fission yeasts (Klutstein et al., 2015). In Arabidopsis, mutants lacking JASON, a protein essential for proper spindle orientation, or NSE2, a protein belonging to the SMC5/6 complex, generate normal and unreduced meiotic products (Erilova et al., 2009; De Storme and Geelen, 2011; Yang et al., 2021). Mutants affected in *CYCA2* genes or *CYCB3;1* also show alterations in a fraction of meiocytes (Bulankova et al., 2013).

The suppression of chromosome fragmentation in *sar1 spo11* has evidenced that fragments produced by the absence of the nucleoporin are generated by the inability to properly repair the recombination intermediates formed from meiotic DSBs (Figure 4). These defects in DNA repair may be due to failures in the recruitment of proteins involved in the early stages of HR, as evidenced by a reduction in the number of γH2AX and RAD51 foci (Figure 5). Another possibility is that, due to the absence of the nucleoporin, HR proceeds more slowly in some meiocytes and this triggers failures in the repair of DSBs. In any case, despite these problems in HR, the chromosome axes seem to form correctly, even in the abnormal meiocytes, according to the results obtained for ASY1. However, the process of synapsis is compromised (Figure 2). The absence of synapsis is most likely caused by problems in DNA homology search during DSB repair, which is a prerequisite for the progression of synapsis (Osman et al., 2011). In addition, the entangled chromosomes observed at metaphase I in *sar1*, *sar3*, and *hos1* (Figures 1, 3; Supplementary Figure S2) are reminiscent of those observed in recombination-defective mutants such as *rad51*, *xrcc3*, *rad51c* or *mnd1* (Kerzendorfer et al., 2006; Pradillo et al., 2012; 2014). Interestingly, SUMOylation in plants, as well as in yeast, appears to be linked to the NPC, and SUMOylated proteins accumulate in mutants defective for NUA (structural component of the nuclear basket) and SAR1 (Muthuswamy and Meier, 2011). In fission yeast, the Y-complex nucleoporin Nup132 is involved in the regulation of SUMOylation during meiosis, and mutants deficient for this nucleoporin exhibit upregulated SUMOylated proteins including Pim1, Top1, and Top2 (Yang et al., 2023). Hyper-SUMOylation of Top2 alters meiotic chromosome architecture (Li et al., 2013). In Arabidopsis, *topII* mutants show condensation defects, entangled chromosomes, and high levels of DNA fragmentation (Martinez-Garcia et al., 2018). It is tempting to speculate that the meiotic phenotype observed in Arabidopsis Y-complex deficient mutants is somehow related to alterations in the SUMOylation of proteins with meiotic function.

Distribution of NPCs is altered in hypercondensed meiocytes

The excessive chromatin condensation observed in *sar1* does not seem to originate from the problems in HR, as it does not disappear in the *sar1 spo11* double mutant (Figure 4). These abnormally condensed meiocytes have a morphology similar to that of cells undergoing cell death. This process is characterized by cell shrinkage, chromatin condensation, and DNA fragmentation (Kerr et al.,1972; Reape et al., 2008). Hendzel et al. (1998) pointed out that during cell death, chromatin condensation is not an active process associated with histone phosphorylation as occurs in mitosis or meiosis (Houben et al., 1999; Manzanero et al., 2000; Oliver et al., 2013). In this case, condensation would be the result of the degradation of euchromatin, nuclear matrix and lamin, in addition to the aggregation of heterochromatin. However, we have not detected appreciable variations in euchromatin- or heterochromatin-specific epigenetic marks in the abnormally condensed cells, at least at the cytological level, as variations at the molecular level cannot be ruled out (Supplementary Figure S5). Chromosome condensation problems in meiosis have been described in mutants defective for the condensin complex (Siddiqui et al., 2003; Smith et al., 2014) or *mmd1* (*male meiocyte death1*) mutants (Yang et al., 2003; Wang et al., 2016). Nevertheless, unlike *sar* mutants, these mutants do not show any defects in the appearance of chromosomes during early prophase I and present chromatin decondensation at later stages (Yang et al., 2003; Smith et al., 2014).

The altered distribution of NPCs in the NE could be the source of the problems in chromatin compaction, since in abnormally condensed meiocytes there is no defined pattern for NPCs, unlike in normal-looking meiocytes (Figure 6). This phenotype reveals the importance of SAR1 in the structure of NPCs. The absence of signal corresponding to NPCs in these meiocytes is not due to NE disintegration, as the signal corresponding to SUN proteins is observed around the chromatin. Perhaps the apparent collapse of NPCs could have some reversibility, and this explains why meiotic changes only occur in a percentage of cells. Indeed, in HeLa cells depletion of the Nup107-160 complex results in nuclei with a continuous NE but no NPCs, although the defect in NPC assembly could be reversed by adding Nup107-160 complex containing fractions (Walther et al., 2003). In addition, depletion of this complex also induces cell death following a spindle checkpoint-dependent delay during mitosis (Rieder and Maiato, 2004; Zuccolo et al., 2007). In plants, the spindle checkpoint is not as tightly regulated as in yeast or animals, and it could even not function or be much relaxed during meiosis (Komaki and Schnittger, 2016). In this sense, mutants with severe recombination problems can complete meiosis, although no gamete is functional (Wijnker and Schnittger, 2013). In *sar* mutants the hypercondensed meiocytes appear to progress through meiosis, giving rise to the masses of entangled chromosomes observed at metaphase I (Figure 1). This is of particular interest because studying meiosis in these mutants may provide information on the possible meiotic function of these nucleoporins that cannot be obtained from studies using other model organisms.

SAR1, AXR1, and the auxin response

AXR1 is a component of the RUBylation pathway targeting, among others, cullin proteins (Mergner and Schwechheimer, 2014).

axr1 plants display auxin-related growth defects that are suppressed by eliminating the function of SAR1 or SAR3 (Cernac et al., 1997; Parry et al., 2006). In the present work, we have shown that the *sar1* mutation also reverses the altered meiotic phenotype of *axr1*, which is completely different from that of *sar1* (Jahns et al., 2014). In *sar1 axr1* the synapsis problems disappear and the formation of the obligatory chiasma, required for bivalent formation, is restored (Figure 7). In the case of the somatic phenotype, it has been suggested that sar mutants delay the nuclear import of Aux/IAA negative regulators, thus ameliorating the defect in *axr1*, which initially inhibits auxin gene expression (Parry et al., 2006). The reversal of the *axr1* meiotic phenotype in *sar1 axr1* may also be explained in this way. On the other hand, neither *sar1* nor *sar3* exhibit auxin hypersensitivity, revealing a complex relationship between the NPC and the auxin response (Parry et al., 2006; Robles et al., 2012). Surprisingly, there are no studies showing a clear link between auxins and meiosis. This deserves further investigation in the future.

Alternatively, the reversal of the meiotic phenotype in *sar1 axr1* might be related to the RUBylation pathway. It has been suggested that AXR1 functions during meiotic recombination through the activation of a CRL4 (CULLIN RING LIGASE4) complex involved in the ubiquitylation of specific protein targets, since a *cul4* mutant exhibit a meiotic phenotype reminiscent of that observed in *axr1* (Jahns et al., 2014). Curiously, the SUMO and ubiquitin-proteasome systems function coordinately in meiotic chromosome organization and the regulation of meiotic recombination in mouse (Prasada Rao et al., 2017). The presence of upregulated SUMOylated proteins in *sar1* may somehow compensate for the lack of CRL4 activity in *axr1*. Further analyses will be required to connect the function of these post-translational modifications to the NPCs.

Concluding remarks

During meiosis, LINC complexes contribute to promote telomere-driven chromosome movement at prophase I and this function is highly conserved in evolution (Kim et al., 2022). Strikingly, these complexes are also required for the distribution of NPCs in the NE (Liu et al., 2007). Surprisingly, few studies have analyzed the distribution of NPCs in plants, although they appear to have a non-homogeneous distribution during the early stages of meiosis (Holm, 1977; Zickler and Kleckner, 1998; Cowan et al., 2002). Similarly, little is known about how NPCs can influence chromosome behavior during meiosis. This study reveals a meiotic role for SAR1 and SAR3, scaffold nucleoporins belonging to the outer ring complex, in plant meiosis. These findings will lead to new lines of research to better understand how NE organization is modulated in the dynamic chromosome events during meiosis and the specific function of NPCs in this type of cell division.

Data availability statement

The original contributions presented in the study are included in the article/Supplementary Material, further inquiries can be directed to the corresponding author.

Author contributions

NF-J: Conceptualization, Data curation, Formal Analysis, Investigation, Methodology, Writing–original draft, Writing–review and editing. MM-G: Data curation, Formal Analysis, Investigation, Writing–review and editing. JV: Conceptualization, Investigation, Writing–review and editing. FG-D: Data curation, Investigation, Writing–review and editing. JS: Formal Analysis, Writing–review and editing. MP: Conceptualization, Formal Analysis, Funding acquisition, Supervision, Writing–original draft, Writing–review and editing.

Funding

The author(s) declare financial support was received for the research, authorship, and/or publication of this article. This research was supported by the Ministry of Science and Innovation (PID2020-118038GB-I00/AEI/10.13039/501100011033) to MP and by the PhD fellow funded by the FPU program of Spanish Ministry of Education (FPU16/02772) to NF-J. MP also acknowledges the current support of the European Union (TED2021-131852B-I00/AEI/10.13039/501100011033/Unión Europea NextGenerationEU/PRTR).

Acknowledgments

We thank B. Martín and M. C. Moreno for excellent technical assistance, Prof. C. Franklin (University of Birmingham, United Kingdom) for anti-RAD51, anti-MLH1, anti-ASY1, and anti-ZYP1 antibodies, and Spanish Meiosis Community and members of the COST Action n° CA 16212 "INDEPTH" for helpful discussions about this research.

Conflict of interest

Author JV was employed by GlaxoSmithKline Spain.

The remaining authors declare that the research was conducted in the absence of any commercial or financial relationships that could be construed as a potential conflict of interest.

The reviewer ODI declared a past coauthorship with the author MP to the handling editor.

Publisher's note

Supplementary material

The Supplementary Material for this article can be found online at: https://www.frontiersin.org/articles/10.3389/fcell.2023.1285695/full#supplementary-material

References

Alber, F., Dokudovskaya, S., Veenhoff, L. M., Zhang, W., Kipper, J., Devos, D., et al. (2007). The molecular architecture of the nuclear pore complex. *Nature* 450, 695–701. doi:10.1038/nature06405

Armstrong, S. J., Caryl, A. P., Jones, G. H., and Franklin, F. C. H. (2002). Asy1, a protein required for meiotic chromosome synapsis, localizes to axis-associated chromatin in *Arabidopsis* and *Brassica*. *J. Cell Sci.* 115, 3645–3655. doi:10.1242/jcs.00048

Armstrong, S. J., Sanchez-Moran, E., Chris, F., and Franklin, H. (2009). Cytological Analysis of *Arabidopsis thaliana* meiotic chromosomes. *Methods Mol. Biol.* 558, 131–145. doi:10.1007/978-1-60761-103-5_9

Beck, M., and Hurt, E. (2017). The nuclear pore complex: understanding its function through structural insight. *Nat. Rev. Mol. Cell Biol.* 18, 73–89. doi:10.1038/nrm.2016.147

Blobel, G. (1985). Gene gating: a hypothesis. *Proc. Natl. Acad. Sci.* 82, 8527–8529. doi:10.1073/pnas.82.24.8527

Bulankova, P., Akimcheva, S., Fellner, N., and Riha, K. (2013). Identification of *Arabidopsis* meiotic cyclins reveals functional diversification among plant cyclin Genes. *PLoS Genet.* 9, e1003508. doi:10.1371/journal.pgen.1003508

Burke, B. (2018). LINC complexes as regulators of meiosis. *Curr. Opin. Cell Biol.* 52, 22–29. doi:10.1016/j.ceb.2018.01.005

Campell, B. R., Song, Y., Posch, T. E., Cullis, C. A., and Town, C. D. (1992). Sequence and organization of 5S ribosomal RNA-encoding genes of *Arabidopsis thaliana*. *Gene* 112, 225–228. doi:10.1016/0378-1119(92)90380-8

Cernac, A., Lincoln, C., Lammer, D., and Estelle, M. (1997). The SAR1 gene of Arabidopsis acts downstream of the AXR1 gene in auxin response. *Development* 124, 1583–1591. doi:10.1242/dev.124.8.1583

Cheng, Z., Zhang, X., Huang, P., Huang, G., Zhu, J., Chen, F., et al. (2020). NUP96 and HOS1 are mutually stabilized and gate constans protein level, conferring long-day photoperiodic flowering regulation in Arabidopsis. *Plant Cell* 32, 374–391. doi:10.1105/tpc.19.00661

Chu, D. B., Gromova, T., Newman, T. A. C., and Burgess, S. M. (2017). The nucleoporin Nup2 contains a meiotic-autonomous region that promotes the dynamic chromosome events of meiosis. *Genetics* 206, 1319–1337. doi:10.1534/genetics.116.194555

Cowan, C. R., Carlton, P. M., and Cande, W. Z. (2002). Reorganization and polarization of the meiotic bouquet-stage cell can be uncoupled from telomere clustering. *J. Cell Sci.* 115, 3757–3766. doi:10.1242/jcs.00054

De Storme, N., and Geelen, D. (2011). The Arabidopsis mutant *jason* produces unreduced first division restitution male gametes through a parallel/fused spindle mechanism in meiosis II. *Plant Physiol.* 155, 1403–1415. doi:10.1104/pp.110.170415

Ding, X., Xu, R., Yu, J., Xu, T., Zhuang, Y., and Han, M. (2007). SUN1 is required for telomere attachment to nuclear envelope and gametogenesis in mice. *Dev. Cell* 12, 863–872. doi:10.1016/j.devcel.2007.03.018

Erilova, A., Brownfield, L., Exner, V., Rosa, M., Twell, D., Scheid, O. M., et al. (2009). Imprinting of the Polycomb group gene *MEDEA* serves as a ploidy sensor in Arabidopsis. *PLoS Genet.* 5, e1000663. doi:10.1371/journal.pgen.1000663

Fernandez-Martinez, J., and Rout, M. P. (2021). One ring to rule them all? structural and functional diversity in the nuclear pore complex. *Trends biochem. Sci.* 46, 595–607. doi:10.1016/j.tibs.2021.01.003

Fiserova, J., Kiseleva, E., and Goldberg, M. W. (2009). Nuclear envelope and nuclear pore complex structure and organization in tobacco BY-2 cells. *Plant J.* 59, 243–255. doi:10.1111/j.1365-313X.2009.03865.x

Fuchs, J., Demidov, D., Houben, A., and Schubert, I. (2006). Chromosomal histone modification patterns - from conservation to diversity. *Trends Plant Sci.* 11, 199–208. doi:10.1016/j.tplants.2006.02.008

Gall, J. G. (1967). Octagonal nuclear pores. *J. Cell Biol.* 32, 391–399. doi:10.1083/jcb.32.2.391

Gerlach, W. L., and Bedbrook, J. R. (1979). Cloning and characterization of ribosomal RNA genes from wheat and barley. *Nucleic Acids Res.* 7, 1869–1885. doi:10.1093/nar/7.7.1869

Grelon, M., Vezon, D., Gendrot, G., and Pelletier, G. (2001). *AtSPO11-1* is necessary for efficient meiotic recombination in plants. *EMBO J.* 20, 589–600. doi:10.1093/emboj/20.3.589

Gu, Y. (2018). The nuclear pore complex: a strategic platform for regulating cell signaling. *New Phytol.* 219, 25–30. doi:10.1111/nph.14756

Hattersley, N., Cheerambathur, D., Moyle, M., Stefanutti, M., Richardson, A., Lee, K. Y., et al. (2016). A nucleoporin docks protein phosphatase 1 to direct meiotic chromosome segregation and nuclear assembly. *Dev. Cell* 38, 463–477. doi:10.1016/j.devcel.2016.08.006

Hattersley, N., Schlientz, A. J., Prevo, B., Oegema, K., and Desai, A. (2022). MEL-28/ELYS and CENP-C coordinately control outer kinetochore assembly and meiotic chromosome-microtubule interactions. *Curr. Biol.* 32, 2563–2571.e4. doi:10.1016/j.cub.2022.04.046

Hendzel, M. J., Nishioka, W. K., Raymond, Y., Allis, C. D., Bazett-Jones, D. P., and Th'ng, J. P. H. (1998). Chromatin condensation is not associated with apoptosis. *J. Biol. Chem.* 273, 24470–24478. doi:10.1074/jbc.273.38.24470

Higgins, J. D., Sanchez-Moran, E., Armstrong, S. J., Jones, G. H., and Franklin, F. C. H. (2005). The Arabidopsis synaptonemal complex protein ZYP1 is required for chromosome synapsis and normal fidelity of crossing over. *Genes Dev.* 19, 2488–2500. doi:10.1101/gad.354705

Hoelz, A., Debler, E. W., and Blobel, G. (2011). The Structure of the nuclear pore complex. *Annu. Rev. Biochem.* 80, 613–643. doi:10.1146/annurev-biochem-060109-151030

Holm, P. B. (1977). Three-dimensional reconstruction of chromosome pairing during the zygotene stage of meiosis in *Lilium longiflorum* (Thunb.). *Carlsb. Res. Commun.* 42, 103–151. doi:10.1007/bf02906489

Houben, A., Wako, T., Furushima-Shimogawara, R., Presting, G., Künzel, G., Schubert, I., et al. (1999). Short communication: the cell cycle dependent phosphorylation of histone H3 is correlated with the condensation of plant mitotic chromosomes. *Plant J.* 18, 675–679. doi:10.1046/j.1365-313X.1999.00496.x

Jackson, N., Sanchez-Moran, E., Buckling, E., Armstrong, S. J., Jones, G. H., and Franklin, F. C. H. (2006). Reduced meiotic crossovers and delayed prophase I progression in AtMLH3-deficient *Arabidopsis*. *EMBO J.* 25, 1315–1323. doi:10.1038/sj.emboj.7600992

Jahns, M. T., Vezon, D., Chambon, A., Pereira, L., Falque, M., Martin, O. C., et al. (2014). Crossover localisation is regulated by the neddylation posttranslational regulatory pathway. *PLoS Biol.* 12, e1001930. doi:10.1371/journal.pbio.1001930

Jung, J. H., Lee, H. J., Park, M. J., and Park, C. M. (2014). Beyond ubiquitination: proteolytic and nonproteolytic roles of HOS1. *Trends Plant Sci.* 19, 538–545. doi:10.1016/j.tplants.2014.03.012

Kerr, J. F. R., Wyllie, A. H., and Currie, A. R. (1972). Apoptosis: a basic biological phenomenon with wideranging implications in tissue kinetics. *Br. J. Cancer* 26, 239–257. doi:10.1038/bjc.1972.33

Kerzendorfer, C., Vignard, J., Pedrosa-Harand, A., Siwiec, T., Akimcheva, S., Jolivet, S., et al. (2006). The *Arabidopsis thaliana MND1* homologue plays a key role in meiotic homologous pairing, synapsis and recombination. *J. Cell Sci.* 119, 2486–2496. doi:10.1242/jcs.02967

Kim, H. J., Liu, C., and Dernburg, A. F. (2022). How and why chromosomes interact with the cytoskeleton during meiosis. *Genes (Basel).* 13, 901. doi:10.3390/genes13050901

King, G. A., Wettstein, R., Varberg, J. M., Chetlapalli, K., Walsh, M. E., Gillet, L. C. J., et al. (2023). Meiotic nuclear pore complex remodeling provides key insights into nuclear basket organization. *J. Cell Biol.* 222, e202204039. doi:10.1083/jcb.202204039

Klutstein, M., and Cooper, J. P. (2014). The chromosomal courtship dance-homolog pairing in early meiosis. *Curr. Opin. Cell Biol.* 26, 123–131. doi:10.1016/j.ceb.2013.12.004

Klutstein, M., Fennell, A., Fernández-Álvarez, A., and Cooper, J. P. (2015). The telomere bouquet regulates meiotic centromere assembly. *Nat. Cell Biol.* 17, 458–469. doi:10.1038/ncb3132

Knockenhauer, K. E., and Schwartz, T. U. (2016). The nuclear pore complex as a flexible and dynamic gate. *Cell* 164, 1162–1171. doi:10.1016/j.cell.2016.01.034

Komachi, K., and Burgess, S. M. (2022). The Nup2 meiotic-autonomous region relieves inhibition of Nup60 to promote progression of meiosis and sporulation in *Saccharomyces cerevisiae*. *Genetics* 221, iyac045. doi:10.1093/genetics/iyac045

Komaki, S., and Schnittger, A. (2016). The spindle checkpoint in plants — a green variation over a conserved theme? *Curr. Opin. Plant Biol.* 34, 84–91. doi:10.1016/j.pbi.2016.10.008

Koszul, R., and Kleckner, N. (2009). Dynamic chromosome movements during meiosis: a way to eliminate unwanted connections? *Trends Cell Biol.* 19, 716–724. doi:10.1016/j.tcb.2009.09.007

Kurzbauer, M. T., Uanschou, C., Chen, D., and Schlögelhofer, P. (2012). The recombinases DMC1 and RAD51 are functionally and spatially separated during meiosis in *Arabidopsis*. *Plant Cell* 24, 2058–2070. doi:10.1105/tpc.112.098459

Lamm, N., Rogers, S., and Cesare, A. J. (2021). Chromatin mobility and relocation in DNA repair. *Trends Cell Biol.* 31, 843–855. doi:10.1016/j.tcb.2021.06.002

Lazaro, A., Valverde, F., Pineiro, M., and Jarillo, J. A. (2012). The *Arabidopsis* E3 ubiquitin ligase HOS1 negatively regulates CONSTANS abundance in the photoperiodic control of flowering. *Plant Cell* 24, 982–999. doi:10.1105/tpc.110.081885

Li, C., Liu, L., Teo, Z. W. N., Shen, L., and Yu, H. (2020). Nucleoporin 160 regulates flowering through anchoring HOS1 for destabilizing CO in *Arabidopsis*. *Plant Commun.* 1, 100033. doi:10.1016/j.xplc.2020.100033

Li, X., and Gu, Y. (2020). Structural and functional insight into the nuclear pore complex and nuclear transport receptors in plant stress signaling. *Curr. Opin. Plant Biol.* 58, 60–68. doi:10.1016/j.pbi.2020.10.006

Li, X. M., Yu, C., Wang, Z. W., Zhang, Y. L., Liu, X. M., Zhou, D., et al. (2013). DNA topoisomerase II is dispensable for oocyte meiotic resumption but is essential for

meiotic chromosome condensation and separation in mice. *Biol. Reprod.* 89, 118–211. doi:10.1095/biolreprod.113.110692

Lin, D. H., and Hoelz, A. (2019). The structure of the nuclear pore complex (An Update). *Annu. Rev. Biochem.* 88, 725–783. doi:10.1146/annurev-biochem-062917-011901

Lincoln, C., Britton, J. H., and Estelle, M. (1990). Growth and development of the *axr1* mutants of *Arabidopsis*. *Plant Cell* 2, 1071–1080. doi:10.1105/tpc.2.11.1071

Liu, Q., Pante, N., Misteli, T., Elsagga, M., Crisp, M., Hodzic, D., et al. (2007). Functional association of Sun1 with nuclear pore complexes. *J. Cell Biol.* 178, 785–798. doi:10.1083/jcb.200704108

Lowndes, N. F., and Toh, G. W.-L. (2005). DNA repair: the importance of phosphorylating histone H2AX. *Curr. Biol.* 15, R99–R102. doi:10.1016/j.cub.2005.01.029

Lutzmann, M., Kunze, R., Buerer, A., Aebi, U., and Hurt, E. (2002). Modular self-assembly of a Y-shaped multiprotein complex from seven nucleoporins. *EMBO J.* 21, 387–397. doi:10.1093/emboj/21.3.387

Manzanero, S., Arana, P., Puertas, M. J., and Houben, A. (2000). The chromosomal distribution of phosphorylated histone H3 differs between plants and animals at meiosis. *Chromosoma* 109, 308–317. doi:10.1007/s004120000087

Martinez-Garcia, M., Fernández-Jiménez, N., Santos, J. L., and Pradillo, M. (2020). Duplication and divergence: new insights into AXR1 and AXL functions in DNA repair and meiosis. *Sci. Rep.* 10, 8860–8913. doi:10.1038/s41598-020-65734-2

Martinez-Garcia, M., Schubert, V., Osman, K., Darbyshire, A., Sanchez-Moran, E., Franklin, F. C. H., et al. (2018). TOP II and chromosome movement help remove interlocks between entangled chromosomes during meiosis. *J. Cell Biol.* 217, 4070–4079. doi:10.1083/jcb.201803019

Meier, I., and Brkljacic, J. (2009). The nuclear pore and plant development. *Curr. Opin. Plant Biol.* 12, 87–95. doi:10.1016/j.pbi.2008.09.001

Meier, I., Richards, E. J., and Evans, D. E. (2017). Cell biology of the plant nucleus. *Annu. Rev. Plant Biol.* 68, 139–172. doi:10.1146/annurev-arplant-042916-041115

Mergner, J., and Schwechheimer, C. (2014). The NEDD8 modification pathway in plants. *Front. Plant Sci.* 5, 103. doi:10.3389/fpls.2014.00103

Mishra, R. K., Chakraborty, P., Arnaoutov, A., Fontoura, B. M. A., and Dasso, M. (2010). The Nup107-160 complex and γ-TuRC regulate microtubule polymerization at kinetochores. *Nat. Cell Biol.* 12, 164–169. doi:10.1038/ncb2016

Murashige, T., and Skoog, F. (1962). A revised medium for rapid growth and bio assays with Tobacco tissue cultures. *Physiol. Plant.* 15, 473–497. doi:10.1111/j.1399-3054.1962.tb08052.x

Murphy, S. P., Gumber, H. K., Mao, Y., and Bass, H. W. (2014). A dynamic meiotic SUN belt includes the zygotene-stage telomere bouquet and is disrupted in chromosome segregation mutants of maize (*Zea mays* L.). *Front. Plant Sci.* 5, 314–411. doi:10.3389/fpls.2014.00314

Muthuswamy, S., and Meier, I. (2011). Genetic and environmental changes in SUMO homeostasis lead to nuclear mRNA retention in plants. *Planta* 233, 201–208. doi:10.1007/s00425-010-1278-7

Nagai, S., Dubrana, K., Tsai-Pflugfelder, M., Davidson, M. B., Roberts, T. M., Brown, G. W., et al. (2008). Functional targeting of DNA damage to a nuclear pore-associated SUMO-dependent ubiquitin ligase. *Science* 322, 597–602. doi:10.1126/science.1162790

Nie, Y., Li, Y., Liu, M., Ma, B., Sui, X., Chen, J., et al. (2023). The nucleoporin NUP160 and NUP96 regulate nucleocytoplasmic export of mRNAs and participate in ethylene signaling and response in Arabidopsis. *Plant Cell Rep.* 42, 549–559. doi:10.1007/s00299-022-02976-6

Nordeen, S. A., Turman, D. L., and Schwartz, T. U. (2020). Yeast Nup84-Nup133 complex structure details flexibility and reveals conservation of the membrane anchoring ALPS motif. *Nat. Commun.* 11, 6060–6112. doi:10.1038/s41467-020-19885-5

Oliver, C., Pradillo, M., Corredor, E., and Cuñado, N. (2013). The dynamics of histone H3 modifications is species-specific in plant meiosis. *Planta* 238, 23–33. doi:10.1007/s00425-013-1885-1

Osman, K., Higgins, J. D., Sanchez-Moran, E., Armstrong, S. J., and Franklin, F. C. H. (2011). Pathways to meiotic recombination in *Arabidopsis thaliana*. *New Phytol.* 190, 523–544. doi:10.1111/j.1469-8137.2011.03665.x

Parry, G. (2014). Components of the *Arabidopsis* nuclear pore complex play multiple diverse roles in control of plant growth. *J. Exp. Bot.* 65, 6057–6067. doi:10.1093/jxb/eru346

Parry, G. (2015). The plant nuclear envelope and regulation of gene expression. *J. Exp. Bot.* 66, 1673–1685. doi:10.1093/jxb/erv023

Parry, G., Ward, S., Cernac, A., Dharmasiri, S., and Estelle, M. (2006). The *Arabidopsis* SUPPRESSOR OF AUXIN RESISTANCE proteins are nucleoporins with an important role in hormone signaling and development. *Plant Cell* 18, 1590–1603. doi:10.1105/tpc.106.041566

Pradillo, M., López, E., Linacero, R., Romero, C., Cuñado, N., Sanchez-Moran, E., et al. (2012). Together yes, but not coupled: new insights into the roles of RAD51 and DMC1 in plant meiotic recombination. *Plant J.* 69, 921–933. doi:10.1111/j.1365-313X.2011.04845.x

Pradillo, M., López, E., Romero, C., Sanchez-Moran, E., Cuñado, N., and Santos, J. L. (2007). An analysis of univalent segregation in meiotic mutants of *Arabidopsis thaliana*: a possible role for synaptonemal complex. *Genetics* 175, 505–511. doi:10.1534/genetics.106.067595

Pradillo, M., Varas, J., Oliver, C., and Santos, J. L. (2014). On the role of *AtDMC1*, *AtRAD51* and its paralogs during *Arabidopsis* meiosis. *Front. Plant Sci.* 5, 23. doi:10.3389/fpls.2014.00023

Prasada Rao, H. B. D., Qiao, H., Bhatt, S. K., Bailey, L. R. J., Tran, H. D., Bourne, S. L., et al. (2017). A SUMO-ubiquitin relay recruits proteasomes to chromosome axes to regulate meiotic recombination. *Science* 355, 403–407. doi:10.1126/science.aaf6407

Raices, M., and D'Angelo, M. A. (2012). Nuclear pore complex composition: a new regulator of tissue-specific and developmental functions. *Nat. Rev. Mol. Cell Biol.* 13, 687–699. doi:10.1038/nrm3461

Reape, T. J., Molony, E. M., and McCabe, P. F. (2008). Programmed cell death in plants: distinguishing between different modes. *J. Exp. Bot.* 59, 435–444. doi:10.1093/jxb/erm258

Rieder, C. L., and Maiato, H. (2004). Stuck in division or passing through: what happens when cells cannot satisfy the spindle assembly checkpoint. *Dev. Cell* 7, 637–651. doi:10.1016/j.devcel.2004.09.002

Robles, L. M., Deslauriers, S. D., Alvarez, A. A., and Larsen, P. B. (2012). A loss-of-function mutation in the nucleoporin AtNUP160 indicates that normal auxin signalling is required for a proper ethylene response in *Arabidopsis*. *J. Exp. Bot.* 63, 2231–2241. doi:10.1093/jxb/err424

Ross, K. J., Fransz, P., and Jones, G. H. (1996). A light microscopic atlas of meiosis in *Arabidopsis thaliana*. *Chromosom. Res.* 4, 507–516. doi:10.1007/BF02261778

Sanchez-Moran, E. S., Armstrong, S. J., Santos, J. L., Franklin, F. C. H., and Jones, G. H. (2001). Chiasma formation in *Arabidopsis thaliana* accession Wassileskija and in two meiotic mutants. *Chromosom. Res.* 9, 121–128. doi:10.1023/A:1009278902994

Siddiqui, N. U., Stronghill, P. E., Dengler, R. E., Hasenkampf, C. A., and Riggs, C. D. (2003). Mutations in *Arabidopsis* condensin genes disrupt embryogenesis, meristem organization and segregation of homologous chromosomes during meiosis. *Development* 130, 3283–3295. doi:10.1242/dev.00542

Smith, S. J., Osman, K., and Franklin, F. C. H. (2014). The condensin complexes play distinct roles to ensure normal chromosome morphogenesis during meiotic division in Arabidopsis. *Plant J.* 80, 255–268. doi:10.1111/tpj.12628

Starr, D. A. (2009). A nuclear-envelope bridge positions nuclei and moves chromosomes. *J. Cell Sci.* 122, 577–586. doi:10.1242/jcs.037622

Strambio-De-Castillia, C., Niepel, M., and Rout, M. P. (2010). The nuclear pore complex: bridging nuclear transport and gene regulation. *Nat. Rev. Mol. Cell Biol.* 11, 490–501. doi:10.1038/nrm2928

Stuwe, T., Correia, A. R., Lin, D. H., Paduch, M., Lu, V. T., Kossiakoff, A. A., et al. (2015). Nuclear pores. Architecture of the nuclear pore complex coat. *Sci. (80-.)* 347, 1148–1152. doi:10.1126/science.aaa4136

Tamura, K., Fukao, Y., Iwamoto, M., Haraguchi, T., and Hara-Nishimura, I. (2011). Identification and characterization of nuclear pore complex components in *Arabidopsis thaliana*. *Plant Cell* 22, 4084–4097. doi:10.1105/tpc.110.079947

Tamura, K., and Hara-Nishimura, I. (2013). The molecular architecture of the plant nuclear pore complex. *J. Exp. Bot.* 64, 823–832. doi:10.1093/jxb/ers258

Varas, J., Graumann, K., Osman, K., Pradillo, M., Evans, D. E., Santos, J. L., et al. (2015). Absence of SUN1 and SUN2 proteins in *Arabidopsis thaliana* leads to a delay in meiotic progression and defects in synapsis and recombination. *Plant J.* 81, 329–346. doi:10.1111/tpj.12730

Varas, J., and Pradillo, M. (2018). Immunolabeling protocols for studying meiosis in plant mutants defective for nuclear envelope components. *Methods Mol. Biol.* 1840, 237–247. doi:10.1007/978-1-4939-8691-0_17

Walther, T. C., Alves, A., Pickersgill, H., Loïodice, I., Hetzer, M., Galy, V., et al. (2003). The conserved Nup107-160 complex is critical for nuclear pore complex assembly. *Cell* 113, 195–206. doi:10.1016/S0092-8674(03)00235-6

Wang, J., Niu, B., Huang, J., Wang, H., Yang, X., Dong, A., et al. (2016). The PHD finger protein MMD1/DUET ensures the progression of male meiotic chromosome condensation and directly regulates the expression of the condensin gene *CAP-D3*. *Plant Cell* 28, 1894–1909. doi:10.1105/tpc.16.00040

Wiermer, M., Cheng, Y. T., Imkampe, J., Li, M., Wang, D., Lipka, V., et al. (2012). Putative members of the Arabidopsis Nup107-160 nuclear pore sub-complex contribute to pathogen defense. *Plant J.* 70, 796–808. doi:10.1111/j.1365-313X.2012.04928.x

Wijnker, E., and Schnittger, A. (2013). Control of the meiotic cell division program in plants. *Plant Reprod.* 26, 143–158. doi:10.1007/s00497-013-0223-x

Xu, D., Bai, J., Duan, Q., Costa, M., and Dai, W. (2009). Covalent modifications of histones during mitosis and meiosis. *Cell Cycle* 8, 3688–3694. doi:10.4161/cc.8.22.9908

Yang, F., Fernández-Jiménez, N., Tučková, M., Vrána, J., Cápal, P., Díaz, M., et al. (2021). Defects in meiotic chromosome segregation lead to unreduced male gametes in

Arabidopsis SMC5/6 complex mutants. *Plant Cell* 33, 3104–3119. doi:10.1093/plcell/koab178

Yang, H., Asakawa, H., Li, F., Haraguchi, T., Shih, H., and Hiraoka, Y. (2023). A nuclear pore complex-associated regulation of SUMOylation in meiosis. *Genes Cells* 28, 188–201. doi:10.1111/gtc.13003

Yang, H. J., Asakawa, H., Haraguchi, T., and Hiraoka, Y. (2015). Nup132 modulates meiotic spindle attachment in fission yeast by regulating kinetochore assembly. *J. Cell Biol.* 211, 295–308. doi:10.1083/jcb.201501035

Yang, X., Makaroff, C. A., and Ma, H. (2003). The Arabidopsis *MALE MEIOCYTE DEATH1* gene encodes a PHD-finger protein that is required for male meiosis. *Plant Cell* 15, 1281–1295. doi:10.1105/tpc.010447

Zhang, A., Wang, S., Kim, J., Yan, J., Yan, X., Pang, Q., et al. (2020a). Nuclear pore complex components have temperature-influenced roles in plant growth and immunity. *Plant Cell Environ.* 43, 1452–1466. doi:10.1111/pce.13741

Zhang, F., Ma, L., Zhang, C., Du, G., Shen, Y., Tang, D., et al. (2020b). The SUNdomain proteins OsSUN1 and OsSUN2 play critical but partially redundant roles in meiosis. *Plant Physiol.* 183, 1517–1530. doi:10.1104/pp.20.00140

Zickler, D., and Kleckner, N. (1998). The leptotene-zygotene transition of meiosis. *Annu. Rev. Genet.* 32, 619–697. doi:10.1146/annurev.genet.32.1.619

Zuccolo, M., Alves, A., Galy, V., Bolhy, S., Formstecher, E., Racine, V., et al. (2007). The human Nup107-160 nuclear pore subcomplex contributes to proper kinetochore functions. *EMBO J.* 26, 1853–1864. doi:10.1038/sj.emboj.7601642

Frontiers in
Cell and Developmental Biology

Explores the fundamental biological processes of life, covering intracellular and extracellular dynamics.

The world's most cited developmental biology journal, advancing our understanding of the fundamental processes of life. It explores a wide spectrum of cell and developmental biology, covering intracellular and extracellular dynamics.

Discover the latest Research Topics

See more →

Frontiers

Avenue du Tribunal-Fédéral 34
1005 Lausanne, Switzerland
frontiersin.org

Contact us

+41 (0)21 510 17 00
frontiersin.org/about/contact